NASA/CR—1999–208923

National Aeronautics and Space Administration (NASA)/ American Society for Engineering Education (ASEE) Summer Faculty Fellowship Program – 1998

Volume 1

Richard B. Bannero, Editor
University of Houston
Houston, Texas

Donn G. Sickorez, Editor
University Programs Office
Lyndon B. Johnson Space Center
Houston, Texas

National Aeronautics and
Space Administration

Lyndon B. Johnson Space Center

Prepared for Lyndon B. Johnson Space Center
under Grant NAG-9-867

May 1999

Available from:

NASA Center for AeroSpace Information
7121 Standard Drive
Hanover, MD 21076-1320
301-621-0390

National Technical Information Service
5285 Port Royal Road
Springfield, VA 22161
703-605-6000

PREFACE

The 1997 Johnson Space Center (JSC) National Aeronautics and Space Administration (NASA)/ American Society for Engineering Education (ASEE) Summer Faculty Fellowship Program was conducted by the University of Houston and JSC. The 10-week program was operated under the auspices of the ASEE. The program at JSC, as well as the programs at other NASA Centers, was funded by the Office of University Affairs, NASA Headquarters, Washington, D.C. The objectives of the program, which began in 1965 at JSC and in 1964 nationally, are:

1. To further the professional knowledge of qualified engineering and science faculty members.

2. To stimulate an exchange of ideas between participants and NASA.

3. To enrich and refresh the research and teaching activities of participants' institutions.

4. To contribute to the research objectives of the NASA Centers.

Each faculty fellow spent at least 10 weeks at JSC engaged in a research project commensurate with his/her interests and background and worked in collaboration with a NASA/JSC colleague. This document is a compilation of the final reports on the research projects done by the faculty fellows during the summer of 1998. Volume I contains the first reports, and volume 2 contains the remaining reports.

1998 SFFP RESEARCH TOPICS

Electronic Systems for Spacecraft Vehicles: Required EDA Tools	Rafic Bachnak
Calcium Solubility and Cation Exchange Properties in Zeoponic Soil	Raymond E. Beiersdorfer
Petrology and Geochemistry of a Mg- and Al-rich Orthopyroxenite Xenoliths in the EETA79001 Shergottite: Implications for Mars Crustal Evolution	John L. Berkley
Ellington Field: A Short History, 1917-1963	Erik D. Carlson
A Study of Mars Dust Environment Simulation at NASA Johnson Space Center Energy Systems Test Area Resource Conversion Test Facility	Yuan-Liang Albert Chen
Numerical Investigation of the ARMSEF ARC-Jet	Carey F Cox
Instrumentation and Methods to Measure Dynamic Forces During Exercise Using the Horizontal Exercise Machine	Fernando Figueroa
Surveying Biomass Burning and Smoke Palls from the NASA-Mir Missions (1996-1998)	Marvin E. Glasser
Coss Lesson Creation Process	R. Stephen Harper
Safety Analysis of Soybean Processing for Advanced Life Support	Dawn L Hentges
Metrics of a Paradigm for Intelligent Control	Henry Hexmoor
Reliability Models and Attributable Risk	Richard D. Jarvinen
Mathematics Foundation for Plane Covering using Hexagons	Gordon G. Johnson
Dynamic Altitude Simulation System Performance Modeling	Leo J. LaFrance
A Study of Aberrant Glycosylation in Simulated Microgravity Using Laser Induced Autoflorescence and Flow Cytometry	B. DeSales Lawless
Prediction of Fatigue Crack Growth Using Regularized Numerical Models	Andrew J. Meade, Jr.
Archean Age Fossils from Northwestern Australia (-3.3 to 3.5 GA, Warrawoona Group, Towers Formation)	Penny A. Morris-Smith
Virtual Manufacturing Techniques Designed and Applied to Manufacturing Activities in the Manufacturing Integration and Technology Branch	Charles Shearrow
Influence of High Aspect Ratio Vessel Cell Culture on TNF-Alpha, Insulin Secretion and Glucose Homeostasis in Pancreatic Islet of Langerhans from Wistar Furth Rats	Brian W. Tobin
Changes in Body Inertia During Bed Rest Studies	Beth A. Todd
Establishing a Distance Learning Plan for International Space Station (ISS) Interactive Video Education Events (IVEE)	Clint Wallington
Lesson Plan Prototype for International Space Station's Interactive Video Education Events	Thomas Zigon
Support for Astronaut's View of Mexican/Central American Fires and On-line Earth Observations Training Manual	Charles F. Kaminski
Computer Aided Modeling to Determine the Effectiveness of Resistive Exercise as Countermeasures for Bone Mineral Density Loss	Benjamin M. Murphy
Hydroponics Database and Handbook for the Advanced Life Support Test Bed	Allen J. Nash
Signal Processing System for Pressure Rate Data of the Auxiliary Power Units on the Space Shuttle	Monica R. Sharpnack
Nutritional Aspects of Crew Members' Cardiovascular Health Indicated by Dietary Lipids	Marcelle A. Thurston
Spectroscopic Properties of Metamorphosed Mafic Rocks: Remote Sensing Applications on Mars	Trevor G. Graff
Crystal Chemistry of Melanite Garnet	Dawn Marie Nguyen

CONTENTS

CONTENTS
(continued)

(1)
IN-23

ELECTRONIC SYSTEMS FOR SPACECRAFT VEHICLES: REQUIRED EDA TOOLS

Final Report
NASA/ASEE Summer Faculty Fellowship Program -- 1998
Johnson Space Center

Prepared by:	Rafic Bachnak, Ph.D.
Academic Rank:	Associate Professor
University & Department:	Northwestern State University Industrial & Engineering Technology Williamson Hall Natchitoches, LA 71458

NASA/JSC	
Directorate:	Engineering
Division:	Manufacturing, Materials, & Process Technology
Branch:	Manufacturing Services Branch
JSC Colleague:	Rhonda Moore
Date Submitted:	August 7, 1998
Contract Number:	NAG 9-867

ABSTRACT

The continuous increase in complexity of electronic systems is making the design and manufacturing of such systems more challenging than ever before. As a result, designers are finding it impossible to design efficient systems without the use of sophisticated Electronic Design Automation (EDA) tools. These tools offer integrated simulation of the electrical, mechanical, and manufacturing functions and lead to a correct by design methodology. This report identifies the EDA tools that would be needed to design, analyze, simulate, and evaluate electronic systems for spacecraft vehicles. In addition, the report presents recommendations to enhance the current JSC electronic design capabilities. This includes cost information and a discussion as to the impact, both positive and negative, of implementing the recommendations.

INTRODUCTION

The continuous increase in complexity of electronic systems is making the design and manufacturing of such systems more challenging than ever before. As a result, designers find it impossible to design efficient systems without the use of sophisticated Electronic Design Automation (EDA) tools. These tools, which provide integrated simulation of the electrical, mechanical, and manufacturing functions, result in reducing development time, decreasing cost, and improving product quality. The elements of an EDA system may be grouped as follows:

- Entry tools: they include schematic capture, block diagram and state diagram entry tools, Hardware Description Language (HDL) editors, and system level design methods.
- Simulation tools: they include analog and digital simulators, timing simulators, HDL simulators, signal integrity analysis, electromagnetic interference, thermal analysis, vibration and fatigue analysis, and faults analysis.
- Synthesis tools: they include HDL entry and simulation and behavioral languages.
- Printed Circuit Board (PCB) tools: they include layout editors, routing tools, and design rule checkers.
- Field Programmable Gate Array (FPGA) tools: they include design entry, simulation, placement, and optimization.

In general, it is impossible for any one EDA vendor to provide the leading edge tool for every design case. While some EDA companies, such as Mentor Graphics, Viewlogic, VeriBest, and Cadence, offer a wide range of software tools that support most of the design functions listed above, other vendors offer point solutions specialized in handling a few of the design tasks. Therefore, an organization must carefully determine its design needs and identify the tools that satisfy them. These tools must be compatible, otherwise, this introduces a number of complications that slow down the design process. These complications include the following:

- Difficulty moving files between tools
- Possible errors may be introduced during file transfers
- Errors found during simulation must be corrected back in the original design tool
- Waste of time learning, managing, and maintaining multiple tools

The rest of this report is organized as follows. First, the latest trends in EDA are summarized. Second, the required EDA tools for designing electronic systems for spacecraft vehicles are identified and compared to the existing tools at JSC. Finally, recommendations to enhance the electronic design capabilities at JSC are presented.

EDA INDUSTRY TRENDS

A new "predict and prevent" paradigm is replacing the old "find and fix" design approach [1]. The goal is to make sure that the design is completely correct before the manufacturing and testing stages. With this approach, the design begins with a virtual prototype and ends with full design verification. The major components of this new approach are briefly described below.

Concurrent Design

Designers have realized that to achieve high productivity the processes used are as important as the tools employed. In recent years, organizations have been moving toward more concurrent design methodologies. A major advantage of concurrent design is that it brings together team members from different disciplines, allowing for the interaction between electrical, mechanical, and manufacturing engineers. This results in early detection of design flaws and leads to fewer design changes, a reduction in time to market, and the improvement in overall quality.

System Level Design

Electronic System Level (ESL) tools describe the system at a high abstraction level. In this case, the functionality of the product is captured independently of its implementation, allowing quick analysis of various architectural implementations. It is predicted that a System Level Design Language (SLDL) will be available by the end of 2000 [2]. The language will have the capabilities to describe system requirements prior to partitioning into hardware (HW) and software (SW) and will facilitate HW/SW co-design.

Virtual Prototyping

While hardware prototyping may still be necessary at some point in the development cycle, taking full advantage of software simulation can significantly improve the overall design process. A virtual prototype is used to guarantee that the system's operation and performance meet the initial system requirements, by graphically simulating the operation using a model that best matches reality. In addition to the fact that virtual prototype iterations are easier and cheaper than hardware prototype iterations, this approach reduces the time required for software and hardware integration.

Design Verification

While testing is performed after the manufacturing of a product to detect defects introduced during the manufacturing process, verification is performed during the design process to verify that the design meets the specifications [3]. In the case of embedded systems, the trend is to perform co-verification (concurrent verification of hardware and software). The major reason for this is the need for early identification of problems. Hardware designers, for example, can take the code that the software engineers have

developed and use it to test the hardware with real software. Despite the advantages of co-verification, sophisticated tools are still unavailable [5].

Design for Test (DFT)

DFT represents a set of rules and methods that can be added to the design in order to make it easier to test a product. These additional rules and methods do not add any functionality to the product but reduce the testing time at manufacturing. Some DFT tools are available, however, they don't offer a comprehensive solution to the DFT problem [6]. It is expected that these tools will be readily available within the next five years.

Fault Simulation

Fault simulation is used after the circuit has been designed to determine if there are any flaws in the product. The purpose is to run tests with specific flaws inserted as inputs. The output is compared to the output of fault-free outputs to determine if the faults are detected. A detection rate of 100% means that the test pattern was able to detect every possible fault. In general, a detection rate of 95% or greater is acceptable. Fault simulation tools are available but only with few EDA tools.

Design For Manufacturing (DFM)

These tools allow addressing manufacturing aspects such as layout, fabrication, assembly, and testing of a product early in the design process. A parts list, for example, may be examined to discover any problems affecting manufacturing.

OTHER HOT EDA AREAS

Synthesis is still a major topic of interest to EDA vendors and users [7]. Other areas which have been receiving considerable attention in the last two years include Web-based and Windows-based EDA tools.

Synthesis

Synthesis consists of translating functional descriptions into actual circuit implementations, using various vender technologies. This may include several designs with price, performance, and options. The major synthesis tool is an HDL (VHDL or Verilog). Compared to schematic capture, HDL delivers designs that are easier to produce, faster to verify, readily reused in other projects, and portable across Programmable Logic Devices (PLD) vendors.

Web-Based EDA

The latest trend in EDA is Web-based tools. One of the major advantages of web-based tools is that the Internet supports multi-site access to a single design project. This provides better communication, faster access to design data, and easier design team

management. Although the Internet offers a foundation to build the next generation of EDA tools, major issues such as data security should be resolved before that becomes a reality.

Windows NT-Based EDA Tools

The improvement of computing power of Personal Computers (PCs) has enhanced the performance of these systems. As a result, EDA vendors have been looking at Windows NT as a feasible alternative to the UNIX-based platform [8-10] and many of them have introduced Windows-based EDA tools in the last two years (see Table 1). In addition, major EDA users such as Intel and Chrysler have already moved their entire design environment to NT-based EDA. While Unix remains the undisputed leader in the EDA industry, according to Collett International (a consulting firm), Dataquest (another consulting firm) predicts that platforms running Windows NT will become the primary platforms by the year 2001.

EDA TOOLS FOR SPACECRAFT ELECTRONIC SYSTEMS

Based on meetings I had with several designers at JSC and my own views, I concluded that the EDA tools required to design the electronic systems for spacecraft vehicles should be able to:

- Perform electrical, mechanical, and manufacturing simulation in a concurrent design environment
- Perform system level design and simulation including virtual prototyping, hardware/software co-design, and high-level synthesis (behavioral and HDL)
- Support rapid prototyping
- Perform mixed-signal (analog and digital) design and simulation
- Analyze various design levels, from chips to complete systems
- Run on a Windows NT platform (the majority of tools) – at JSC

Using the above criteria and the information in Table 1, the list of required EDA tools for designing electronic systems for spacecraft vehicles is shown in Table 2, under the column labeled "Required/Desired Tools".

Table 1. - WINDOWS NT-BASED EDA TOOLS AND SOME MAJOR VENDORS

EDA Category	EDA Tool	Company Name
Electronic Design	**Schematic Capture** (schematics using libraries of parts)	ACCEL; Capilano Computing Systems; Interactive Image Technologies, Ltd.; Mentor Graphics; MicroCode; MyCAD; OrCAD; Protel; Synario; Tanner; VeriBest; Viewlogic
	Design Entry (circuit design using HDL, symbolic libraries, etc.)	HP EEsof; Mentor Graphics; MyCAD; OrCAD; Synario; Synplicity; Tanner; VeriBest; Viewlogic
	System Level Design (the design is at the behavioral level where functionality is described without considering the implementation details)	Chronology HP EEsof VeriBest Viewlogic
	Virtual Prototyping (hardware and software virtual prototyping of complete systems)	Mentor Graphics Synopsys
	Hardware/Software Co-design	Cadence; HP EEsof; Mentor Graphics
	Logic Synthesis (transforms logic descriptions into gate- chip-level implementations)	Altera; Accolade Design; Cadence Exemplar; Mentor Graphics; OrCAD; Synopsys; Synplicity; VeriBest; Viewlogic
	RTL Synthesis (allow describing a design by the transfer of information from one register to another – Register Transfer Level)	Accolade Design Automation; Intusoft; Mentor Graphics; MyCAD OrCAD; Synplicity; VeriBest; Viewlogic
	Verilog Simulation (simulation using the Verilog code)	HP EEsof; Cadence; Mentor Graphics; Simucad; Synario Design Automation; VeriBest; Viewlogic
	VHDL Simulation (simulation using the VHDL code)	Accolade Design; HP EEsof; Mentor Graphics; MyCAD; OrCAD; Synario; VeriBest; Viewlogic
	Design for Test	Mentor Graphics; Synopsys; Viewlogic Systems
	Design Verification	Synopsys
	Fault Simulation (allows simulation of defects in the circuit)	Intusoft; Mentor Graphics; Simucad; Viewlogic
	Digital Simulation (logic simulation, timing analysis, waveform display, etc.)	Interactive Image Technologies, Ltd.; Intusoft; Mentor Graphics; MicroCode; MyCAD; OrCAD; Synario; Tanner; VeriBest; Viewlogic
	Analog Simulation (simulation of analog circuits)	HP EEsof; Interactive Image Technologies, Ltd.; Intusoft; Mentor Graphics; MicroCode; MyCAD; OrCAD; Tanner; VeriBest

Table 1. - CONTINUED

EDA Category	EDA Tool	Company Name
PLD	**FPGA Design and Analysis** (libraries, place and route, analysis)	Accolade Design Automation; Altera; GateField Corporation; HP EEsof; Mentor Graphics; Minc; MyCAD; OrCAD; Protel; QuickLogic; Synario; Synopsys; Synplicity, Inc.; Tanner; VeriBest, Inc.; Viewlogic Systems
PCB	**Design and Layout** (Design, placement, and routing of PCB circuits)	ACCEL; Cadence; HP EEsof; Interactive Image Technologies, Ltd.; Mentor Graphics; MyCAD; OrCAD; Tanner; VeriBest, Inc.; Zuken-Redac
	Signal Integrity Analysis	HP EEsof; Hyperlynx; Mentor Graphics; VeriBest; Viewlogic
	Thermal Analysis	Dynamic Soft Analysis, Inc.; Mentor Graphics; VeriBest
	Timing Analysis	Mentor Graphics; Viewlogic
	Electromagnetic Analysis	Cadence; Hyperlynx; Mentor Graphics; Viewlogic
	Mechanical Analysis (vibration and fatigue)	Mentor Graphics; VeriBest
	Reliability Analysis	Mentor Graphics
	Virtual Prototyping	Hyperlynx; Mentor Graphics; Viewlogic
Misc	**Analog Design and Simulation** (design, analysis, and verification of analog circuits from low to high frequencies)	HP EEsof; Interactive Image Technologies, Ltd.; Intusoft; Mentor Graphics; MicroCode; OrCAD; Synario; VeriBest; Viewlogic
	DSP Toolset	HP EEsof; Hyperception; Mentor Graphics; Synopsys
	Libraries and Models	ACCEL; Chronology; Duet Technologies; HP EEsof; Hyperlynx Interactive Image Technologies, Ltd.; Intusoft; Mentor Graphics; OrCAD; Synopsys; VeriBest; Viewlogic
	Mixed-Signal Design & Simulation (analog and Digital circuits)	ACCEL; HP EEsof; Interactive Image Technologies, Ltd.; Intusoft; Mentor Graphics; MicroCode; OrCAD; Tanner; VeriBest; Viewlogic
	RF Design and Simulation	HP EEsof; Cadence; Intusoft
	Design for Manufacturing	Mentor Graphics
	Mechanical Design	Parametric Technology, Structural Dynamic Research, Dassault Systems, etc.
	Wire Harness Design	Linius; Mentor Graphics
	Web-Based EDA Tools	Viewlogic; QuickLogic

CURRENT DESIGN CAPABILITIES AT JSC

To assess the current JSC electronic design capabilities, I met with designers in EM, EV, and ER. All the individuals were very helpful and exhibited a high level of dedication and professionalism. It was obvious to me that JSC has made major improvements to its design capabilities in the last two years. Three of these improvements are standardizing the EDA tools, acquiring new software, and moving (partially) to a Windows NT-based environment.

The tools that are presently available or being purchased include OrCAD Capture (OrCAD, Inc.), OrCAD Express (OrCAD, Inc.), OrCAD Layout (OrCAD, Inc.), OrCAD PSpice (OrCAD, Inc.), Signal Processing Workstation (Cadence), Matlab and associated toolboxes (The Mathworks Group), MAX+PLUS II (Altera), Dr. Spice (Duetsh Research), Labview (National Instruments), Mathcad (Mathsoft), Mathematica (Wolfram Research), RF Board Designer Pro (HP EEsof), AutoCAD (Autodesk), and Pro/E (Parametric Technology). The column labeled "Existing/Planned Tools" in Table 2 summarizes the current capabilities.

As can be seen here, the major EDA vendor at JSC is OrCAD. OrCAD has a number of products that handle many of the required design functions. Express, for example, combines chip- and board- level design and includes support for developing FPGAs, Complex Programmable Logic Devices (CPLDs), and PCBs. It offers mixed schematic and VHDL design entry, VHDL simulation and synthesis and is integrated with place and route tools from Actel, Altera, Lattice, Lucent, Vantis, and Xilinx. Another product, OrCAD PSpice, integrates the design entry, PCB layout, and PLD design products with the PSpice analog and mixed-signal simulation products. Furthermore, OrCAD has plans to integrate the synthesis engine from Exampler's Leonardo Spectrum tool into its next upgrade of OrCAD Express design environment by the end of 1998. This will allow OrCAD to have better FPGA synthesis and optimization features tuned to the process from a number of PLD vendors.

Despite all of this, there are still very important functions that OrCAD does not address. Some of these functions are essential to enhance the electronic design capabilities at JSC.

RECOMMENDATIONS

Given that it is almost impossible for any one EDA vendor to provide the leading edge tool for every design case, users are left to choose the set of EDA tools that satisfy their requirements and is able to transform their design ideas into reality. Considering the capabilities of EDA vendors (see Table 1) and the required tools for designing electronic

Table 2. - SUMMARY OF REQUIRED, EXISTING, AND NEEDED EDA TOOLS

EDA Category	EDA Tool	Required/ Desired Tools	Existing/ Planned Tools	Needed/ Desired Tools
Design	Schematic Capture	X	X	
	Design Entry	X	X	
	System Level Design	X	X	X
	Virtual Prototyping	X		X
	Hardware/Software Co-design	X	X	X
	Logic Synthesis	X	X	
	RTL Synthesis	X	X	
	Verilog/VHDL Simulation	X	X	
	Design for Test	X		X
	Design Verification	X		X
	Fault Simulation	X		X
	Digital Simulation	X	X	
	Analog Simulation	X	X	
PLD	FPGA Design and Analysis	X	X	
PCB	Design and Layout	X	X	
	Signal Integrity Analysis	X		X
	Thermal Analysis	X		X
	Timing Analysis	X		X
	Electromagnetic Analysis	X		X
	Mechanical Analysis	X		X
	Reliability Analysis	X		X
	Virtual Prototyping	X		X
Misc	Analog Design and Simulation	X	X	
	DSP Toolset	X	X	
	Libraries and Models	X	X	
	Mixed-Signal Design	X	X	
	RF Design and Simulation	X	X	
	Design for Manufacturing	X		X
	Mechanical Design	X	X	
	Wire Harness Design	X	X	X
	Web-Based EDA Tools	X		X

systems for spacecraft vehicles (see Table 2), it seems that JSC can select one of the following two approaches:

1. Adopt the software that will offer the majority of the design functions required at JSC. In this case, one of the following vendors may be selected (selection criteria must be defined): Mentor Graphics, Viewlogic, or VeriBest. Some of the issues that must be addressed in this case include cost, training, and length of time required to move to the new environment. In general, this choice will be more expensive (in terms of equipment) but will lead to reaching a higher level of design capabilities faster.

2. Keep OrCAD as the main EDA vendor and supplement it with available (must be compatible with OrCAD) software. This approach will take longer to reach a high level of design capabilities since many of the available tools do not interface with OrCAD.

In the event the latter approach is chosen, enhancing the design capabilities can be implemented in two phases. Phase 1 involves acquiring currently available tools (that interface with OrCAD) as shown in Table 3. Phase 2 involves acquiring the tools listed in Table 4. These tools are currently either incompatible with OrCAD, unavailable to run on Windows NT, or are still being developed.

Table 3. - RECOMMENDED AVAILABLE EDA TOOLS

EDA Category	**EDA Tool**	**Product**	**Cost**	**Company**
PCB	Signal Integrity Analysis	HyperSuite v4.6[1]	$9,995	Hyperlynx
	Thermal Analysis	BETAsoft-Board-WIN-Trc[1]	$9,000	Dynamic Soft Analysis
	Electromagnetic Analysis	HyperSuite v4.6[1]	$9,995	Hyperlynx
	Reliability Analysis	Analysis System A[2]	$7,695	Relex Software
	Virtual Prototyping	HyperSuite v4.6[1]	$9,995	Hyperlynx
Misc	Wire Harness Design	Logical Cable[3] <u>or</u> Embassy[3]	$20,000 $25,000	Mentor Graphics Linius

[1] interfaces with OrCAD
[2] interfaces with BETAsoft
[3] interfaces with Pro/E

The following is a short description of the recommended tools in Table 3.

<u>BETAsoft Board</u>: A software package, which interfaces with OrCAD, for analyzing the thermal properties of PCB. It reveals the board temperature and gradients, component and junction temperature, and the amount they exceed their respective limits.

<u>Analysis System A</u>: A reliability prediction software which interfaces with BETAsoft. It evaluates reliability of both mechanical and electrical parts.

<u>HyperSuite v4.6</u>: An integrated package, which interfaces with OrCAD, containing LineSim, LineSim EMC, BoardSim, and BoardSim EMC for both pre- and post-layout signal integrity and EMC analysis.

<u>Logical Cable or Embassy</u>: Both software packages interface with Pro/E. They have the capabilities for system interconnect and wire harness design.

Table 4. - RECOMMENDED FUTURE EDA TOOLS

EDA Category	EDA Tool	Not Developed Enough Yet – Should Be Available Within 5 Years	Currently Unavailable with OrCAD
Design	System Level Design	X	X
	Virtual Prototyping	X	X
	Hardware/Software Co-design		X
	Design for Test	X	X
	Design Verification	X	X
	Fault Simulation		X
PCB	Timing analysis		X
	Mechanical Analysis		X
Misc	Design for Manufacturing		X
	Web-Based EDA Tools	X	X

CONCLUSION

The continuous increase in complexity of electronic systems is making the design and manufacturing of such systems more challenging than ever before. In addition, a new "predict and prevent" paradigm is replacing the old "find and fix" design approach. As a result, designers find it impossible to design efficient systems without the use of sophisticated EDA tools and methods.

JSC has made major enhancements to its electronic design capabilities during the last two years. Three of these enhancements are standardizing the EDA tools, acquiring new software, and moving (partially) to a Windows NT-based environment. To bring the electronic design capabilities at JSC to a higher level, additional steps must be taken. JSC may select one of two approaches: 1. adopt a new EDA suite of tools capable of handling most of the required design functions, or 2. acquire additional tools that interface with existing ones. The advantage of the first approach is that JSC capabilities may be brought up to the required level within two years. The advantage of the second approach, which will take longer to reach the same level of design does not require a major shift in the current procedures.

REFERENCES

[1] Charles Small, "Focus report: high-speed PCB and MCM design," Integrated System Design, March 1997.

[2] Steven Schulz, "The new system-level design language," Integrated System Design, July 1998.

[3] Dean Drako and Paul Cohen, "HDL verification coverage," Integrated System Design, June 1998.

[4] David Park, "Dive into system level hardware/software co-design," Electronic Design, June 22, 1998.

[5] Cheryl Ajluni, "HW/SW co-design and co-verification come of age," Electronic Design, June 22, 1998.

[6] Daniel Holden, "Focus report: design-for-test tools," Integrated System Design, September 1997.

[7] Steven Schulz, "EDA platform: what really happened at DAC?," Integrated System Design, August 1998.

[8] James Lee and John Miklosz, "EDA platform benchmark: simulation," Integrated System Design, March 1998.

[9] Jonah McLead, "The plight of Unix: is it a lost cause?," Integrated System Design, June 1998.

[10] Carolyn Mathas, "Focus report: Windows EDA tools," Integrated System Design, October 1997.

CALCIUM SOLUBILITY AND CATION EXCHANGE PROPERTIES IN ZEOPONIC SOIL

/ 2 /
IN-46

Final Report

NASA/ASEE Summer Faculty Fellowship Program - 1998

Johnson Space Center

Prepared by:	Raymond E. Beiersdorfer, Ph.D.
Academic Rank:	Associate Professor
University & Department:	Youngstown State University Department of Geology Youngstown, Ohio 44555

NASA/JSC

Directorate:	Space and Life Sciences
Division:	Earth Science and Solar System Exploration
Branch:	Planetary Science
JSC Colleague:	Douglas W. Ming, Ph.D.
Date Submitted:	August 24, 1998
Contract Number:	NAG 9-867

ABSTRACT

An important aspect of a regenerative life support system at a Lunar or Martian outpost is the ability to produce food. Essential plant nutrients, as well as a solid support substrate, can be provided by: 1) treated Lunar or Martian regolith; 2) a synthetic soil or 3) some combination of both. A synthetic soil, composed of ammonium- and potassium-saturated clinoptilolite (a zeolite mineral) and apatite, can provide slow-release fertilization of plants via dissolution and ion-exchange reactions. Previous equilibrium studies (Beiersdorfer, 1997) on mixtures of synthetic hydroxyapatite and saturated-clinoptilolite indicate that the concentrations of macro-nutrients such as ammonium, phosphorous, potassium, magnesium, and calcium are a function of the ratio of clinoptilolite to apatite in the sample and to the ratio of potassium to ammonium on the exchange sites in the clinoptilolite. Potassium, ammonium, phosphorous and magnesium are available to plants at sufficient levels. However, calcium is deficient, due to the high degree of calcium adsorption by the clinoptilolite. Based on a series of batch-equilibration experiments, this calcium deficiency can be reduced by 1) treating the clinoptilolite with $CaNO_3$ or 2) adding a second Ca-bearing mineral (calcite, dolomite or wollastonite) to the soil. Treating the Cp with CaNO3 results in increased Ca in solution, decreased P in solution and decreased NH4 in solution. Concentrations of K were not effected by the CaNO3 treatment. Additions of Cal, Dol and Wol changed the concentrations of Ca and P in solution in a systematic fashion. Cal has the greatest effect, Dol the least and Wol is intermediate. The changes are consistent with changes expected for a common ion effect with Ca. Higher concentrations of Ca in solution with added Cal, Dol or Wol do not result in changes in K or NH4 concentrations.

INTRODUCTION

An important aspect of a regenerative life support system at a Lunar or Martian outpost will be the ability to utilize plants to produce food and convert carbon dioxide into oxygen. Plant growth systems will most likely utilize the local regolith, in combination with synthetic soil-additives to provide essential plant nutrients as well as a solid support substrate. A zeolite-apatite (zeoponic) mixture has the potential to serve as a synthetic soil-additive for plant growth during long duration space missions. The zeoponic mixture can provide slow release fertilization of essential plant nutrients through dissolution and ion-exchange reactions. The zeoponic material investigated in this study was developed by the National Aeronautics and Space Administration (NASA) and is composed of mixtures of synthetic nutrient-substituted hydroxyapatite and naturally-occurring Wyoming clinoptilolite (a zeolite mineral) that has been saturated with ammonium or potassium. As a 1997 NASA-ASEE Summer Faculty Fellow (Beiersdorfer, 1997) I performed equilibrium studies of the dissolution and ion-exchange properties of mixtures of synthetic nutrient-substituted hydroxyapatite and naturally-occurring Wyoming clinoptilolite saturated with ammonium or potassium. This work indicates that the concentrations of macro-nutrients such as ammonium, phosphorous, potassium, magnesium, and calcium are a function of the ratio of clinoptilolite to apatite in the sample and to the ratio of potassium to ammonium on the exchange sites in the clinoptilolite. The summer 1997 work also indicates that potassium, ammonium, phosphorous and magnesium are available to plants at sufficient levels. However, calcium is deficient, due to the high degree of calcium adsorption by the clinoptilolite. The goals of this study are to: determine if calcium can be increased in solution by 1) treating the clinoptilolite with CaNO3 or 2) adding a second Ca-bearing mineral (calcite, dolomite or wollastonite) to the soil by performing a series of batch-equilibration experiments.

MATERIALS AND METHODS

Starting Materials

The starting materials consist of clinoptilolite (Cp) mined from the Green River Formation in Sweetwater County, Wyoming, a synthetic apatite (Ap) (H062896s) developed at NASA's Johnson Space Center Advanced Life Support Laboratory, calcite (Cal) from Montana (D. J. Minerals M-61), Dolomite (Dol) (Baker Grandol Regular # 4) and Wollastonite (Wol) from the NYCO mine, New York State. All materials were sieved and the 0.5 to 1.0 sieve fraction was used. Two series of batch-equilibration experiments were performed. The first experiment (samples 1 - 15) was to determine the effect of treating the K- and NH4- saturated Cp with CaNO3 solution prior to combining it with Ap and Dol in a zeoponic soil. The second experiment (samples 16 - 72) studied the effects of adding Cal, Dol or Wol on apatite dissolution and ion-exchange.

CaNO3 Treatment of Clinoptilolite

The effects of treating the Cp with CaNO3 solution on apatite dissolution and ion-exchange was determined by combining 0.9 gm K-saturated Cp, 0.9 g NH4-saturated Cp, 0.45 g Ap and 0.25 g Dol with 100 ml of de-ionized water in a 125 ml Erlenmeyer flask. Both the K-saturated Cp and NH4-saturated Cp were treated for four hours in CaNO3 solution of 0, 0.05, 0.1, 0.5 or 1.0 N concentrations. CaNO3 treatments were performed by John Gruener, Hernandez Engineering at the JSC Advanced Life Support Laboratory in Building 31. In each case the total solid was 2.5 grams resulting in a constant fluid-solid ratio of 40

ml/g. Each flask was capped with a foam stopper to allow free exchange with atmospheric CO2 and was placed on an orbital shaker set at 90 rpm and 25° C. Samples were removed at 500 hours and were filtered through a #42 Whatman filter. Each treatment was replicated three times. Concentrations of P, NH4, K, Mg and Ca as well as pH and electrical conductivity were measured. Potassium, magnesium and calcium concentrations were determined by flame atomic absorption spectrometry. Phosphorous was determined using a ascorbic-acid, molybdophosphate-blue colorimetric method (Olsen and Sommers, 1982). Ammonium, pH and electrical conductivity were measured using conventional probes.

Addition of Calcite, Dolomite or Wollastonite

The effects of adding Cal, Dol or Wol on apatite dissolution and ion-exchange was determined by combining varying amounts of Cal, Dol or Wol to K-saturated Cp, NH4-saturated Cp, apatite and 100 ml of de-ionized water in a 125 ml Erlenmeyer flask. The Cp to Ap ratio was held constant at 4:1 and the K to NH4 ratio was held constant at 1:1. The amount of the third mineral (Cal, Dol or Wol) was varied at 0, 5, 10, 15, 20, 25 and 50 weight %. For example, a sample with 20 weight % Cal consisted of 0.500 g of Cal, 0.000 g of Dol, 0.000 g of Wol, 0.800 g of K-saturated clinoptilolite, 0.800 g of NH4-saturated clinoptilolite and 0.400 g of apatite. In each case the total solid was 2.5 grams resulting in a constant fluid-solid ratio of 40 ml/g. Each flask was capped with a foam stopper to allow free exchange with atmospheric CO2 and was placed on an orbital shaker set at 90 rpm and 25° C. Samples were removed at 500 hours and were filtered through a #42 Whatman filter. Each treatment was replicated three times. Concentrations of P, NH4, K, Mg and Ca as well as pH and electrical conductivity were measured using the same methods listed above.

RESULTS AND DISCUSSION

CaNO3 Treatment of Clinoptilolite

Chemical equilibria among clinoptilolite, apatite and water will be dominated by the dissolution of apatite and subsequent ion exchange between Ca and K or NH4 on exchange sites in the clinoptilolite. According to Allen et al. (1993) these reactions can be represented as:

$$Ca_5\left(PO_4\right)_3OH + 3H_2O \Leftrightarrow 5Ca^{2+} + 3HPO_4^{2-} + 4OH^- \text{ and}$$

$$\left(K^+\right)_x - Cp - \left(NH_4^+\right)_y + Ca^{2+} \Leftrightarrow Ca^{2+} - Cp + \left(K^+\right)_x + \left(NH_4^+\right)_y$$

where x,y = 2,0; 1,1; or 0,2. The first reaction represents a simplified dissolution of hydroxyapatite ignoring the trace micronutrients present. The second reaction represents the adsorption of Ca by clinoptilolite which results in the shifting of both reactions to the right. Prior treatment of the Cp with CaNO3 will result in Ca replacing K or NH4 on some exchange sites in the clinoptilolite. The result of this treatment should be a reduction in the cation exchange of Ca for K or NH4 and a reduction of the dissolution of the apatite. This can be documented by reduced concentrations of K, NH4, and P and increased concentration of Ca with an increase in the concentration of the CaNO3 treatment solution. The measured solution pH, ionic strength, and phosphorous, ammonium, potassium, magnesium and calcium concentrations after 500 hours of shaking time for samples

undergoing CaNO3 treatment of clinoptilolite of various concentrations are shown in Table one. Ionic strength was calculated from measured conductivity using the empirical relationship of Griffin and Jurinak (1973) where

Ionic Strength (moles/liter) = 0.0127 Electrical Conductivity (decisiemens/meter).

TABLE 1: SOLUTION pH, IONIC STRENGTH, P, Ca, Mg, K AND NH_4 CONCENTRATIONS AFTER 500 HOURS SHAKING TIME FOR CaNO3-TREATED ZEOPONIC SOILS

No.	[CaNO3] N	pH	I.S. mmol/L	P ppm	Ca ppm	Mg ppm	K ppm	NH4 ppm
1	0.00	8.2	3.64	35.7	0.68	1.41	20.5	37.1
2	0.00	8.3	3.71	35.1	0.68	1.97	29.3	37.3
3	0.00	8.3	3.72	35.1	0.68	1.56	21.6	37.3
4	0.05	8.3	3.37	18.8	0.86	1.49	19.8	32.6
5	0.05	8.2	3.44	18.9	0.97	1.13	20.4	32.9
6	0.05	8.3	3.42	20.2	1.00	1.34	18.6	32.2
7	0.10	8.2	3.21	14.9	1.19	1.28	19.1	30.4
8	0.10	8.2	3.30	14.4	1.19	1.22	19.6	30.4
9	0.10	8.2	3.26	14.7	1.14	1.28	19.1	30.3
10	0.50	8.1	2.92	7.7	1.76	1.28	18.1	25.4
11	0.50	8.2	3.01	7.6	1.81	1.56	18.5	25.6
12	0.50	8.2	2.98	7.7	1.91	1.44	18.5	25.4
13	1.00	8.1	2.84	6.1	2.38	1.51	17.8	23.7
14	1.00	8.1	2.88	5.8	2.50	1.62	17.6	23.8
15	1.00	8.1	2.78	6.8	2.32	1.31	19.3	22.9

The measured solution phosphorous, calcium, magnesium, ammonium, and potassium concentrations as a function of the concentration of CaNO3 in the treatment solution are shown in figures 1 to 5. In each figure the horizontal axis represents the concentration of CaNO3 in the treatment solution and the vertical axis represents the solution concentration in ppm. As illustrated in figure 1 P concentration decreases systematically from an average value of 35.3 ppm with no CaNO3 treatment to an average value of 6.2 ppm with treatment of 1 N CaNO3 solution. The reduction in P represents reduced dissolution of apatite due to a reduction in the Ca cation exchange "driving mechanism." The reduction in the Ca cation exchange (or possibly Ca self-exchange of apatite derived Ca for CaNO3 derived Ca) also results in increased Ca levels with increased concentration of CaNO3 in the treatment solution as shown in figure 2. Magnesium concentrations are shown in figure 3. They range from 1.13 ppm to 1.97 ppm and do not show any systematic variation with concentration of CaNO3 in the treatment solution. Ammonium concentrations are illustrated in figure 4 and show a strong correlation with the concentration of CaNO3 in the treatment solution. NH4 decreases systematically from an average value of 37.2 ppm with no CaNO3 treatment to an average value of 23.5 ppm with treatment of 1 N CaNO3 solution. Potassium concentrations are shown in figure 5. With the exception of one possible outlier value (29.3) they range from 17.7 ppm to 21.6 ppm and do not show a systematic variation with concentration of CaNO3 in the treatment solution. This strong correlation of NH4 and lack of a correlation of K most likely reflects the higher ion selectivity of K over NH4 in clinoptilolite (Ames, 1960).

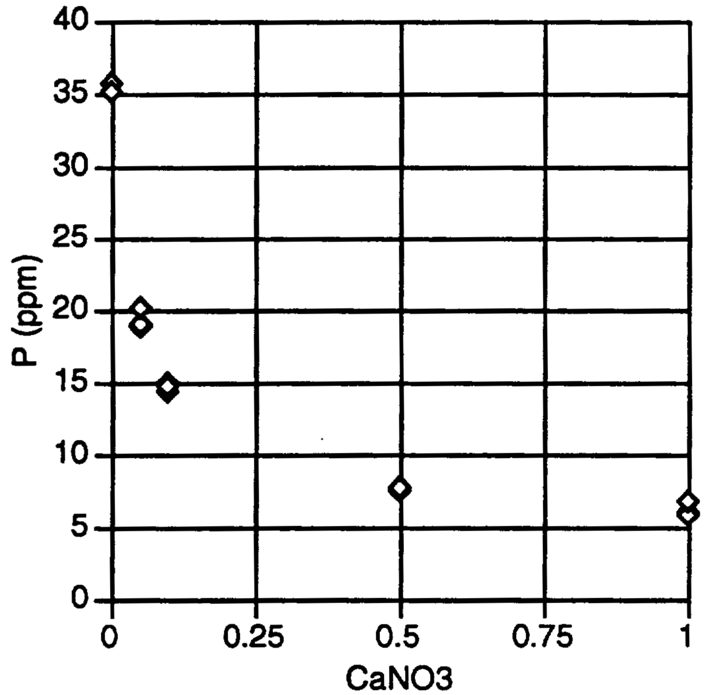

Figure 1: Solution P Concentration as a Function of CaNO3 Treatment of the Clinoptilolite

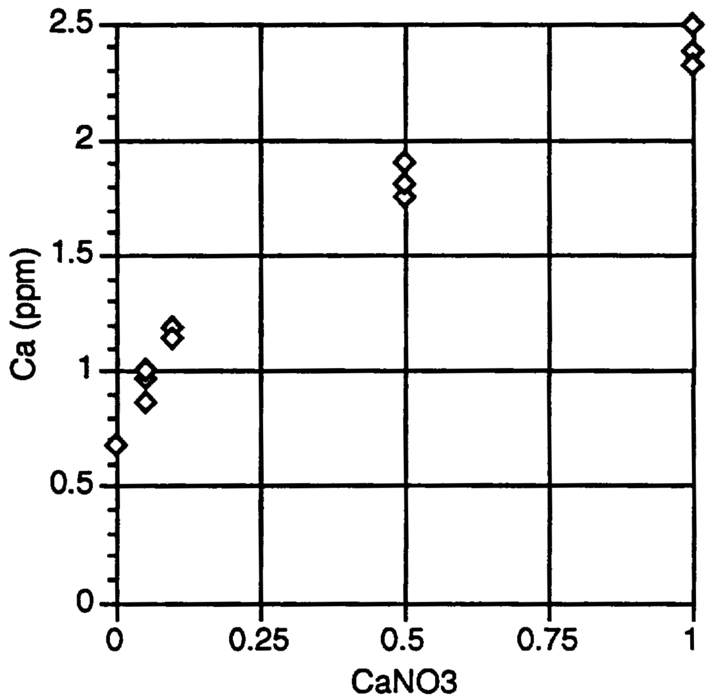

Figure 2: Solution Ca Concentration as a Function of CaNO3 Treatment of the Clinoptilolite

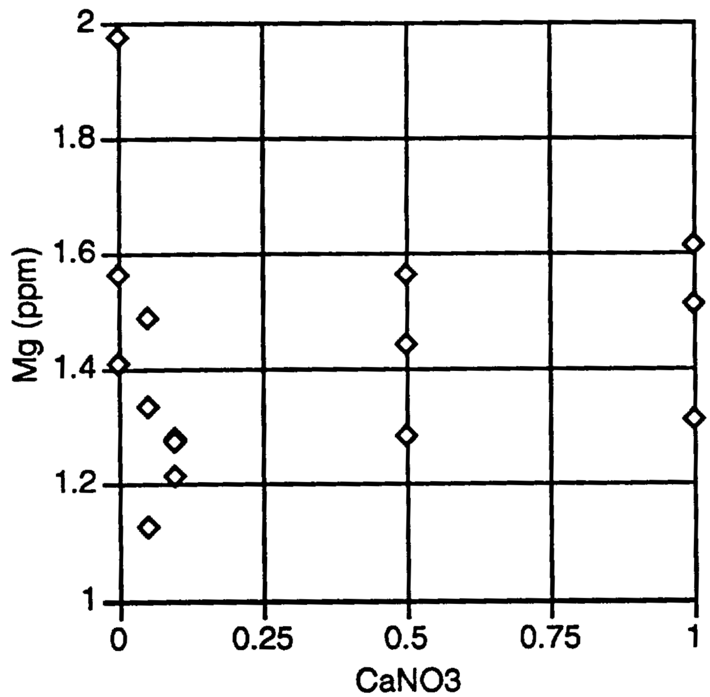

Figure 3: Solution Mg Concentration as a Function of CaNO3 Treatment of the Clinoptilolite

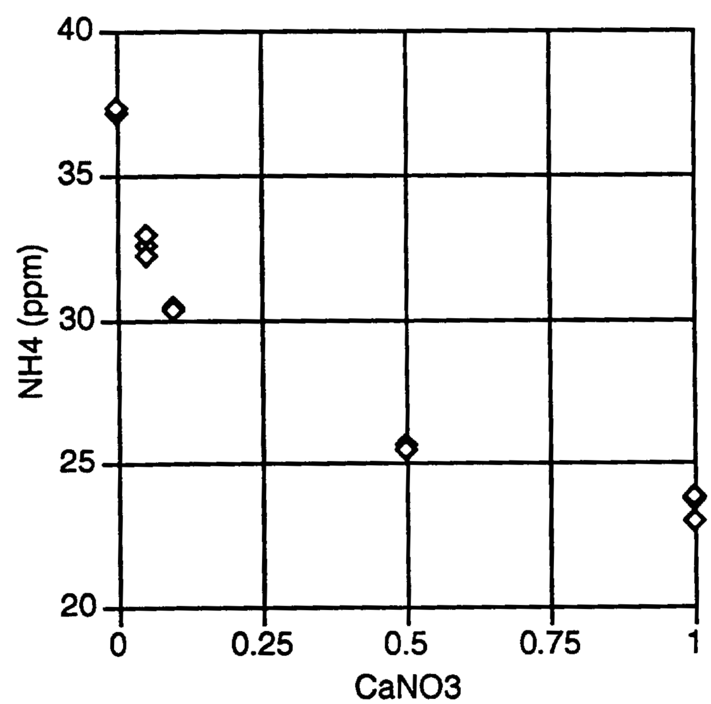

Figure 4: Solution NH4 Concentration as a Function of CaNO3 Treatment of the Clinoptilolite

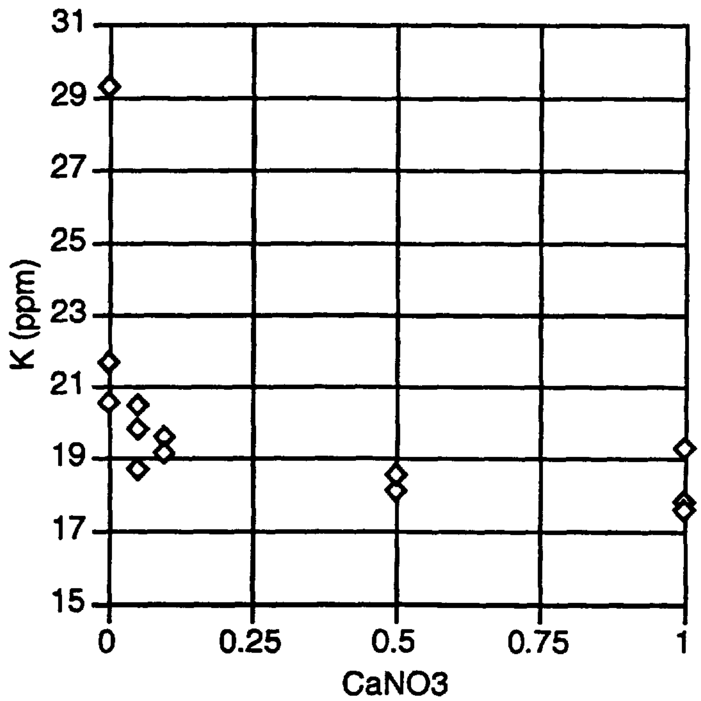

Figure 5: Solution K Concentration as a Function of CaNO3 Treatment of the Clinoptilolite

Addition of Calcite, Dolomite or Wollastonite

Addition of a second calcium bearing mineral to the Ap plus Cp mixture should result in higher concentrations of Ca in solution. Additionally, the solubility of a salt (e.g. Ap) is diminished by the presence of one of its own ions in solution (i.e. Ca) by what is called the "common-ion effect" (Krauskopf and Bird, 1995). Moreover, the presence of ions in solution not present in the salt tend to make the salt more soluble (op. cit.). The addition of calcite ($CaCO_3$) and wollastonite ($CaSiO_3$) should increase the concentration of Ca in solution and should also lower the amount of P in solution due to the common ion effect on Ap dissolution. The addition of dolomite ($CaMg(CO_3)_2$) should increase the concentrations of Ca and Mg in solution. The net change in the dissolution of apatite due to the addition of Dol will be a sum of the off-setting effects of calcium's common-ion effect and magnesium's propensity to increase the solubility of the Ap. The increased concentration of Ca (and Mg for Dol) in solution may result in increased cation exchange in the Cp resulting in increased K or NH_4 in solution. The measured solution pH, ionic strength, and phosphorous, ammonium, potassium, magnesium and calcium concentrations after 500 hours of shaking time for samples containing various amounts of Cal, Dol or Wol are shown in Table two. Ionic strength was calculated in the same manner as in Table one.

The measured solution phosphorous, calcium, magnesium, ammonium, and potassium concentrations as a function of weight percent of added Cal, Dol or Wol are shown in figures 6 to 10. In each figure the horizontal axis represents the weight percent of added Cal, Dol and Wol and the vertical axis represents the solution concentration in ppm. As illustrated in figure 6 P concentration decreases systematically with added Cal, Dol and Wol. The reduction in P represents reduced dissolution of apatite due to the common ion effect of additional Ca in solution. For all of the weight percents studied (5, 10, 15, 20,

TABLE 2: SOLUTION pH, IONIC STRENGTH, P, Ca, Mg, K AND NH_4 CONCENTRATIONS AFTER 500 HOURS SHAKING TIME FOR ZEOPONIC SOILS INCLUDING CALCITE, DOLOMITE OR WOLLASTONITE

No.	Min	Wt %	pH	I.S. mmol/L	P ppm	Ca ppm	Mg ppm	K ppm	NH4 ppm
16	none	0	8.0	3.90	151.4	0.55	1.33	23.3	36.4
17	none	0	8.0	3.92	149.3	0.47	1.32	24.2	36.1
18	none	0	8.0	3.91	150.7	0.53	1.32	23.3	36.5
19	Cal	5	8.2	3.90	109.0	0.60	1.23	25.7	37.1
20	Cal	5	8.2	3.94	97.7	0.65	1.30	25.1	37.6
21	Cal	5	8.2	3.91	100.5	0.72	1.40	25.0	37.1
22	Cal	10	8.3	3.96	82.4	0.82	1.40	27.1	38.5
23	Cal	10	8.2	4.01	89.5	0.71	1.36	26.5	38.5
24	Cal	10	8.2	3.92	82.4	0.93	1.25	24.2	38.8
25	Cal	15	8.3	4.06	58.4	1.01	1.54	25.7	39.6
26	Cal	15	8.3	3.87	75.7	0.77	1.27	23.8	36.1
27	Cal	15	8.3	3.95	67.9	1.00	1.42	23.9	38.1
28	Cal	20	8.3	3.95	49.5	1.17	1.45	24.1	38.1
29	Cal	20	8.2	3.99	54.6	1.20	1.50	26.2	38.4
30	Cal	20	8.4	4.08	45.9	1.10	1.46	26.5	39.0
31	Cal	25	8.4	4.08	38.6	1.35	1.50	26.6	39.6
32	Cal	25	8.4	3.99	42.6	1.31	1.58	25.4	38.4
33	Cal	25	8.4	4.10	35.7	1.31	1.55	28.1	40.1
34	Cal	50	8.5	3.77	13.9	2.41	1.59	26.6	36.8
35	Cal	50	8.5	3.76	15.4	2.58	1.57	25.0	36.7
36	Cal	50	8.5	3.73	15.6	2.43	1.53	26.7	35.9
37	Dol	5	8.0	3.89	137.5	0.49	1.38	25.9	38.9
38	Dol	5	8.0	4.03	138.9	0.49	1.51	26.0	39.0
39	Dol	5	8.0	4.04	141.7	0.62	1.56	25.5	38.3
40	Dol	10	8.1	3.87	124.2	0.65	1.61	25.0	38.1
41	Dol	10	8.0	3.87	131.2	0.58	1.57	25.5	38.0
42	Dol	10	8.0	3.75	117.9	0.53	1.35	26.3	36.5
43	Dol	15	8.1	3.81	119.8	0.65	1.59	24.6	38.0
44	Dol	15	8.0	3.82	122.2	0.58	1.57	24.5	37.8
45	Dol	15	8.1	3.87	117.0	0.62	1.66	25.3	38.7
46	Dol	20	8.1	3.82	117.9	0.65	1.65	24.1	38.0
47	Dol	20	8.1	3.76	112.3	0.69	1.66	24.7	38.3
48	Dol	20	8.1	3.66	115.8	0.62	1.62	23.3	37.5
49	Dol	25	8.2	3.71	97.0	0.65	1.80	26.1	37.7
50	Dol	25	8.1	3.73	101.2	0.69	1.80	24.5	37.5
51	Dol	25	8.2	3.63	97.7	0.71	1.65	23.9	37.2
52	Dol	50	8.2	3.28	66.3	0.81	2.22	23.0	33.3
53	Dol	50	8.3	3.33	70.5	0.76	2.08	23.3	33.3
54	Dol	50	8.2	3.33	64.9	0.81	2.03	23.0	33.3
55	Wol	5	8.1	4.09	135.5	0.83	1.41	26.4	40.1
56	Wol	5	8.1	4.03	133.5	0.71	1.33	24.9	39.2
57	Wol	5	8.0	3.84	121.3	0.65	1.09	25.0	38.1
58	Wol	10	8.2	4.04	111.8	0.88	1.40	26.1	39.0
59	Wol	10	8.1	3.99	108.4	0.90	1.34	25.5	38.9
60	Wol	10	8.1	3.95	113.9	0.90	1.32	26.1	39.2
61	Wol	15	8.2	3.77	90.9	0.95	1.30	24.6	38.9
62	Wol	15	8.2	3.78	100.3	0.90	1.29	26.1	39.2
63	Wol	15	8.3	3.84	91.5	0.93	1.32	25.6	40.6
64	Wol	20	8.3	3.63	88.7	0.81	1.18	24.7	39.0
65	Wol	20	8.3	3.67	78.2	1.07	1.12	23.4	40.5
66	Wol	20	8.3	3.71	84.3	1.00	1.22	25.5	40.0
67	Wol	25	8.3	3.72	73.2	1.17	1.33	25.8	39.7
68	Wol	25	8.3	3.71	71.8	1.12	1.20	24.9	39.5
69	Wol	25	8.3	3.64	75.9	1.00	1.18	23.2	37.8
70	Wol	50	8.4	3.33	43.1	1.55	1.15	24.5	34.9
71	Wol	50	8.4	3.33	41.7	1.60	1.11	22.9	35.2
72	Wol	50	8.4	3.43	41.7	1.88	1.17	24.7	35.9

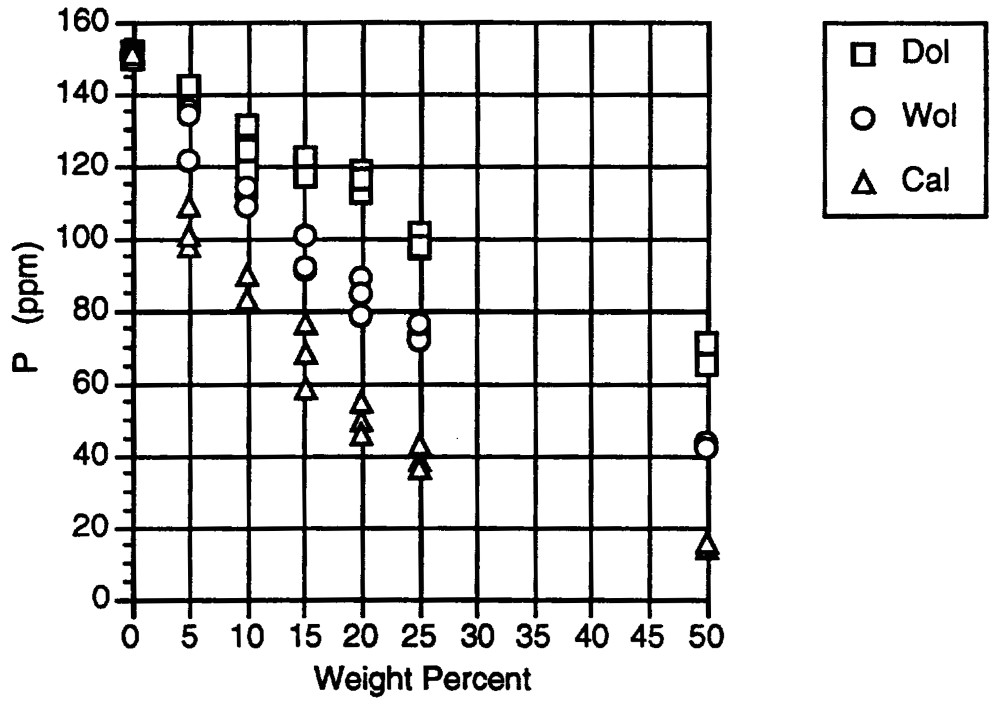

Figure 6: Solution P Concentration as a Function of Weight Percent Calcite, Dolomite or Wollastonite

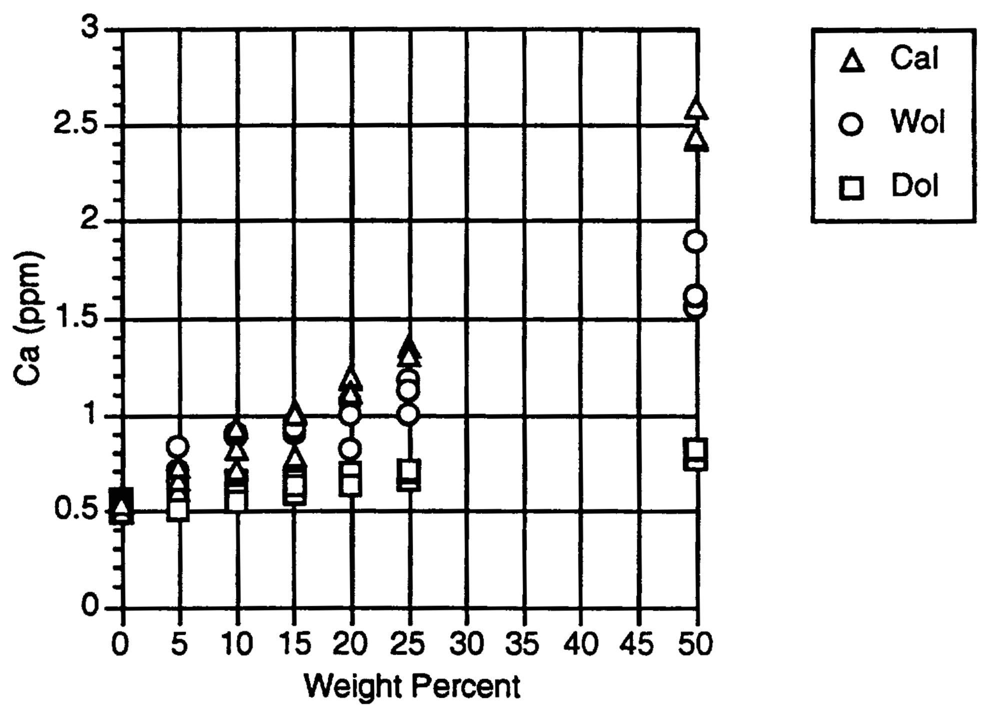

Figure 7: Solution Ca Concentration as a Function of Weight Percent Calcite, Dolomite or Wollastonite

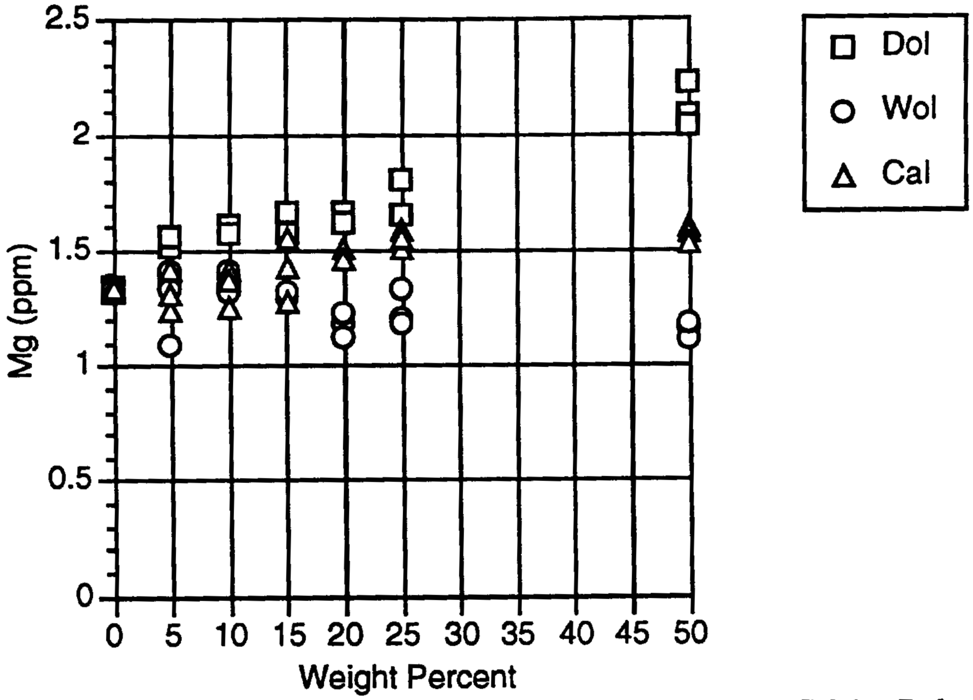

Figure 8: Solution Mg Concentration as a Function of Weight Percent Calcite, Dolomite or Wollastonite

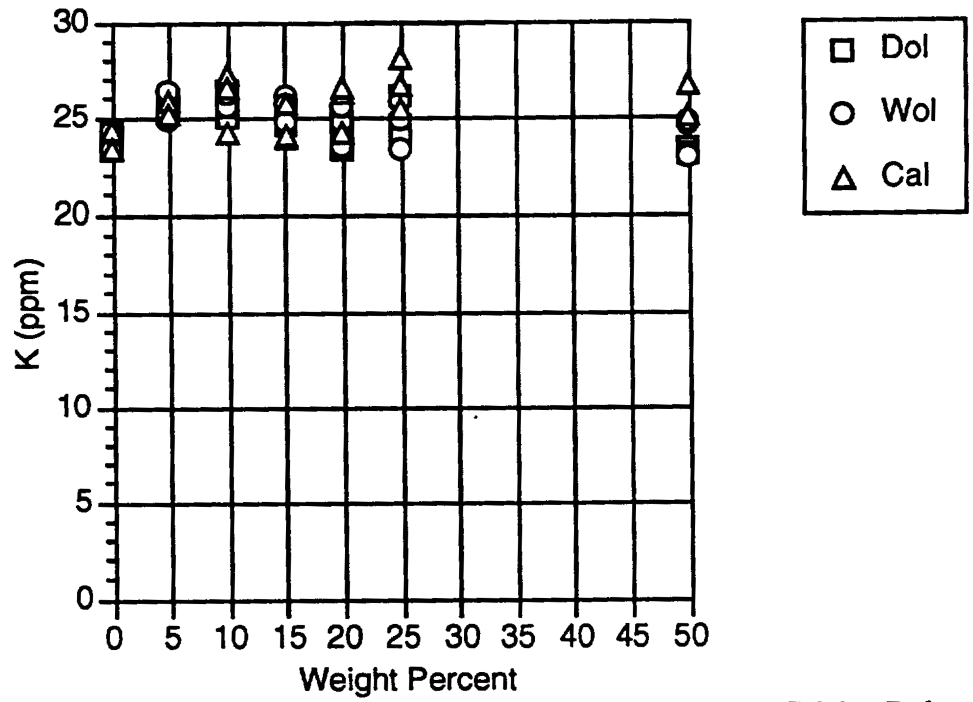

Figure 9: Solution K Concentration as a Function of Weight Percent Calcite, Dolomite or Wollastonite

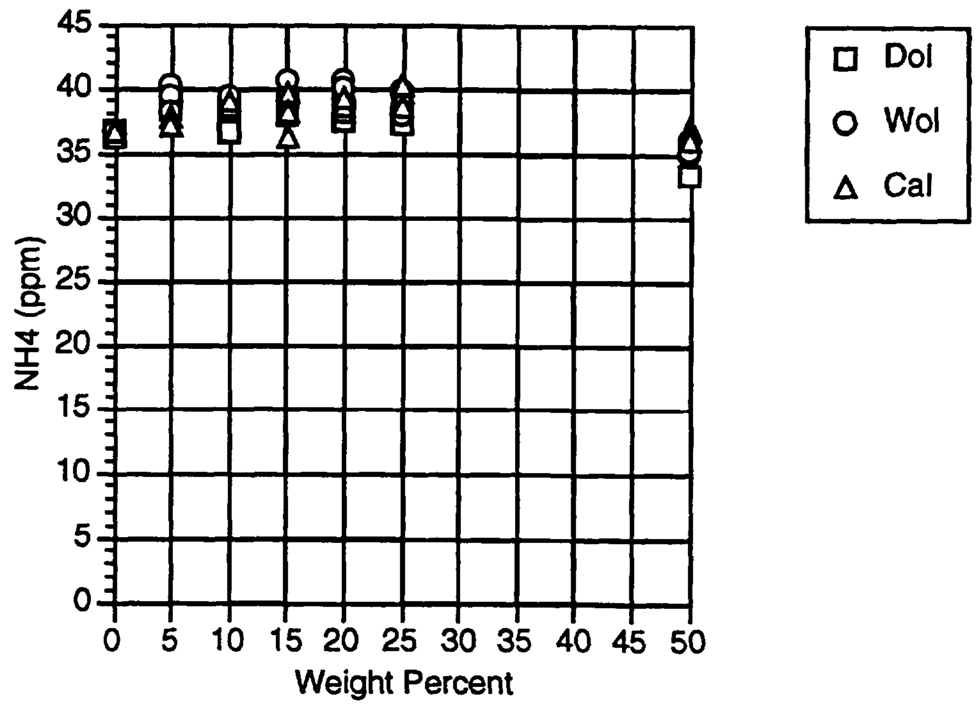

Figure 10: Solution NH4 Concentration as a Function of Weight Percent Calcite, Dolomite or Wollastonite

25, 50) the addition of Cal resulted in the largest reduction of P concentration from the average of 150.5 ppm with no added Cal, Dol or Wol. The addition of Dol had the least effect and Wol had an intermediate effect. . Calcium concentrations are shown in figure 7. Ca concentration increases systematically with added Cal, Dol and Wol. Similar to the P data, Cal has the greatest effect and Dol the least. Magnesium concentrations are shown in figure 8. and do not show any systematic variation with added Cal or Wol. Adding Dol, an Mg-bearing mineral does result in higher concentrations of Mg in solution. Potassium and Ammonium concentrations are shown in figures 9 and 10 respectively. With the exception of the 50 weight percent samples, K and NH4 do not change in concentration with added Cal, Dol or Wol.

CONCLUSIONS

The goal of this research was to determine the effects on Ca solubility and cation exchange in a zeoponic mixture due to: 1) treating the Cp with CaNO3 after saturating it with K or NH4 and 2) adding a second Ca-bearing mineral, Cal, Dol or Wol. Treating the Cp with CaNO3 results in increased Ca in solution, decreased P in solution and decreased NH4 in solution. Concentrations of K were not effected by the CaNO3 treatment. The increased Ca and decreased P is due to a lessening of the Ca cation exchange driven driving force on Ap dissolution. The decrease in NH4 indicates that the CaNO3 treatment is able to replace NH4 with Ca on some of the Cp exchange site. The lack of any change in K concentrations suggests that the CaNO3 treatment is not effective for K due to Cp's higher ion selectivity for K.

Addition of Cal, Dol and Wol change the concentrations of Ca and P in solution in a systematic fashion. Cal has the greatest effect, Dol the least and Wol is intermediate. The changes are consistent with changes expected for the common ion effect. The fact that Wol

has a greater effect than Dol, although it is less soluble than Dol, could be due to the common ion effect of Ca in Dol being partially offset by the increased Mg in solution. The higher concentrations in Ca in solution with added Cal, Dol or Wol do not result in changes in K or NH4 concentrations. This could be due to two offsetting factors canceling each other out. The expected increased cation exchange of Ca for K or NH4 could be negated by the smaller volumes of K- and NH4-saturated Cp in the sample. However, for these two effects to exactly cancel each other out would be fortuitous. The samples with 50 weight percent Cal, Dol or Wol have the lowest concentrations of K and NH4 in solution, most likely due to the smaller amount of K- and NH4-saturated Cp in these sample.

REFERENCES CITED

Allen, E. R., Hossner, L. R., Ming, D. W. and Henninger, D. L., 1993, Solubility and cation exchange in phosphate rock and saturated clinoptilolite mixtures, Soil Science Society of America Journal, v. 57, p. 1368 - 1374

Ames, L. L., Jr., 1960, Cation sieve properties of clinoptilolite. American Mineralogist, v.45, p. 689 - 700

Beiersdorfer, R. E., 1997, Solubility and cation exchange properties of synthetic apatite and clinoptilolite mixtures, in Hyman, W. A. and Sickorez, D. G., eds. NASA Contractor Report NAG-931, NASA/ASEE Summer Faculty Fellowship Program - 1997, p. 1.1 - 1.12

Griffin, R. A. and Jurinak, J. J., 1973, Estimation of acidity coefficients from the electrical conductivity of natural aquatic systems and soil extracts, Soil Science v. 116, p. 26 - 30

Krauskopf, K. B. and Bird, D. K., 1995, Introduction to Geochemistry, 3rd edition, McGraw-Hill, New York, 647 p.

Olsen, S. R. and Sommers, L. E., 1982, Phosphorous, in Page, A. L., Miller, R. H. and Keeney, D. R., eds., Methods of Soils Analysis, Part 2, Chemical and Microbiological Properties, second edition, p. 413 - 414

(3)
, p. 46

Petrology and Geochemistry of a Mg- and Al-rich Orthopyroxenite Xenolith in the EETA79001 Shergottite: Implications for Mars Crustal Evolution

Final Report

NASA/ASEE Summer Faculty Fellowship Program - 1998

Johnson Space Center

Prepared by:	**John L. Berkley, Ph.D.**
Academic Rank:	**Associate Professor**
University and Department:	**SUNY, College at Fredonia**

NASA/JSC

Directorate:	**Space and Life Sciences**
Division:	**Earth Science & Solar System Exploration**
Branch:	**Planetary Science**
JSC Colleague:	**John H. Jones, Ph.D.**
Date Submitted:	**August 11, 1998**
Contract Number:	**344-31-20-18 (Igneous Meteorites)**

ABSTRACT

EETA79001 is a Mars meteorite (SNC) consisting of multiple rock types, including two basalt types, olivine and pyroxene xenocrysts and ultramafic xenoliths. This study is focused on the petrology and geochemistry of one orthopyroxenite xenolith in PTS ,68, designated X-1. It consists of chemically homogeneous orthopyroxene cores with exceptionally high Mg/Fe (mg#=85) and Al. Cores are permeated by minute high-Si+Al glassy inclusions, some with augite microlites. Magnesian core areas are mantled by more Fe-rich orthopyroxene rims grading to pigeonite away from cores. The xenolith is transected by cross-cutting shear planes, some of pre-incorporation origin. Major and minor element composition and variation suggest that core areas are primarily igneous, crystallized from a high temperature mafic melt. However, nearly constant mg# across cores suggest metamorphic equilibration. Si+Al inclusions may result from, among other processes, exsolution of feldspathic material during subsolidus cooling, or may be solid materials (alkali feldspar) poikilitically enclosed by growing igneous orthopyroxene crystals. Late reaction with more fractionated melts produced Fe-rich mantles, the whole assemblage later cut by tectonic micro-shear planes.

Raw electron microprobe data produced during this study are available on request from the author.

INTRODUCTION

Currently, twelve achondrite meteorites are classified as SNC (Shergottite-Nakhlite-Chassignite) meteorites. Isotopic signatures combined with petrologic evidence point to an origin for SNC meteorites as impact ejected samples from the planet Mars. The Antarctic meteorite EETA79001 is classified as a basaltic shergottite, but contains a complex mix of rock types including two basalt types and various mafic xenocrysts and ultramafic xenoliths. The basalts are designated Lithology A (Lith-A) and Lithology B (Lith-B), the latter being slightly more iron-rich and significantly coarser grained than Lith-A. These basalt fractions are in sharp planar contact, with Lith-B probably representing a large xenolith within Lith-A. Lith-A also contains ultramafic xenoliths and olivine and pyroxene xenocrysts (absent in lith-B), mostly large (up to 5 mm dia.) solitary olivine and orthpyroxene grains.

The principal subject of this study is a single orthopyroxenite xenolith within Lith-A, designated by the author as Xenolith-1 (X-1), in section EETA79001,68. Three large olivine xenocrysts (X-2,3,4) also occur in this thin section. McSween and Jarosewich (1983) have established a compelling petrogenetic relationship between the xenocrysts in EETA79001 and lherzolitic shergottites (e.g., ALHA77005 and LEW88516). However, X-1 is unique among previously described orthopyroxene (opx) assemblages in EETA79001 in having higher Mg/Mg+Fe (mg#) and average Al in core areas. In addition, core areas are permeated by minute high-Si+Al melt inclusions, some with high-Ca clinopyroxene crystallites and other minerals, a feature unknown in previously described xenocrysts in EETA79001.

This research was principally conducted using the Cameca SX-100 electron microbe facility in Building 31, directed by Dr. Gordon McKay. Dr. Vincent Yang assisted in calibrating standards and otherwise preparing the machine for analysis. Operating conditions typically were 15 kV accelerating voltage, 20 nanoamps sample current, with 20 second point counts per element. One session was run with 10 kV accelerating voltage in an attempt to avoid or limit fluorescence of melt inclusions during core opx analysis.

PETROGRAPHY

General

The X-1 xenolith measures approximately 3 x 2 mm. It is primarily composed of magnesian orthopyroxene "core areas"(mg#=85) enveloped by more iron-rich orthopyroxene and pigeonite crystals. Petrographic interpretation is complicated by pervasive shear planes and fractures which have disrupted the original fabric of the rock. However, in rare areas unaffected by mechanical strain, cores show thin rims of more FeO-rich opx which grade outward to pigeonite. On back scattered electron (BSE) images core areas stand out prominently as dark areas surrounded by brightly reflecting, more Fe-rich pyroxenes.

Core areas display high concentrations of tiny (avg. 2 μm dia.) rounded melt inclusions. Most inclusions contain high-Si+Al glass with no apparent crystalline phases. Some inclusions show a faint preferred orientation possibly crystallographically controlled. Rare inclusions have

high-Ca clinopyroxene (augite) crystallites on their margins in addition to glass. Rare complex inclusions occur in more iron rich orthopyroxene areas (but not in pigeonite) that contain high-Si+Al glass enclosing various combinations of Ca phosphate, augite, and high-Ni pyrrhotite ($(Fe,Ni)_{1-x}S$).

One large (100 μm) diameter cubic chromite grain occurs imbedded within pigeonite. This chromite grain has elevated Cr and Mg compared to Lith-A Cr-spinel (mostly Cr-rich titanomagnetite). Smaller chromite grains occur adjacent to the olivine grain described below.

One large (500μm) olivine grain (Fo_{67}) also occurs associated with pigeonite. Its low core mg# suggests lack of equilibrium with core orthopyroxene. Thus, it may represent an independent olivine xenocryst tectonically injected into the xenolith, or if cogenetic with core opx, may have re-equilibrated with a late fractionated liquid.

Pyroxene Relations

Electron microprobe traverses show that mg# is virtually constant across core areas (Fig. 1), although Al_2O_3 varies between about 0.7 to 1.4 weight percent (avg. 0.9). Some variation may result from beam fluorescence of ubiquitous high-Si+Al inclusions despite care to avoid them. Other minor elements (e.g., Ni, Mn, Ti) show no significant variation within cores, except that Cr shows some positive correlation with Al (Fig. 2).

All opx core margins that are not cut off by shear planes show a fairly abrupt transformation to more iron-rich orthopyroxene (Fig. 1) which forms thin rims not exceeding about 200-300 μm. FeO-enriched rims give way to progressively more Ca- and Fe-rich pigeonite further from core margins (Fig. 3). Similar zoning occurs in orthopyroxene xenocrysts analyzed in PTS ,439, although opx cores are less Mg-rich (max. mg#=82) than X-1. Pigeonite constitutes the dominant modal silicate mineral in the X-1 xenolith.

High-Silica Inclusions

Mg-rich core areas contain numerous and ubiquitous tiny inclusions of high-Si+Al glass, most measuring no more than 2-3μm in diameter. Glass in these inclusions typically has about 70 wt.% SiO_2, 20 wt.% Al_2O_3 and less than 5 wt.% each of MgO, CaO, and FeO. Total alkalis are very low, generally much lower than 2.0 wt.%. Thus, although "feldspathic" in composition, no feldspar microlites were observed in the inclusions, probably because of a deficiency in alkalis and Ca. Rare inclusions in core areas, however, contain augite that may have crystallized from the inclusion. Augite compositions (Fig. 4) corrected for "others" components (Lindsley, 1983) show that most are too FeO-rich to be in equilibrium with the host opx, and also show intragranular compositional inhomogeneity.

High-silica inclusions are not present in non-core areas, even in Fe-enriched opx rims. This suggests that the formation of rims either destroyed pre-existing inclusions, or inclusions never existed there. It is likely that whatever process produced the inclusions was restricted to, and controlled by the formation of core areas alone. On the other hand, some fairly large (10-25 :m) inclusions occur in FeO-rich opx rim areas. Invariably, in addition to Si+Al-rich glass, these

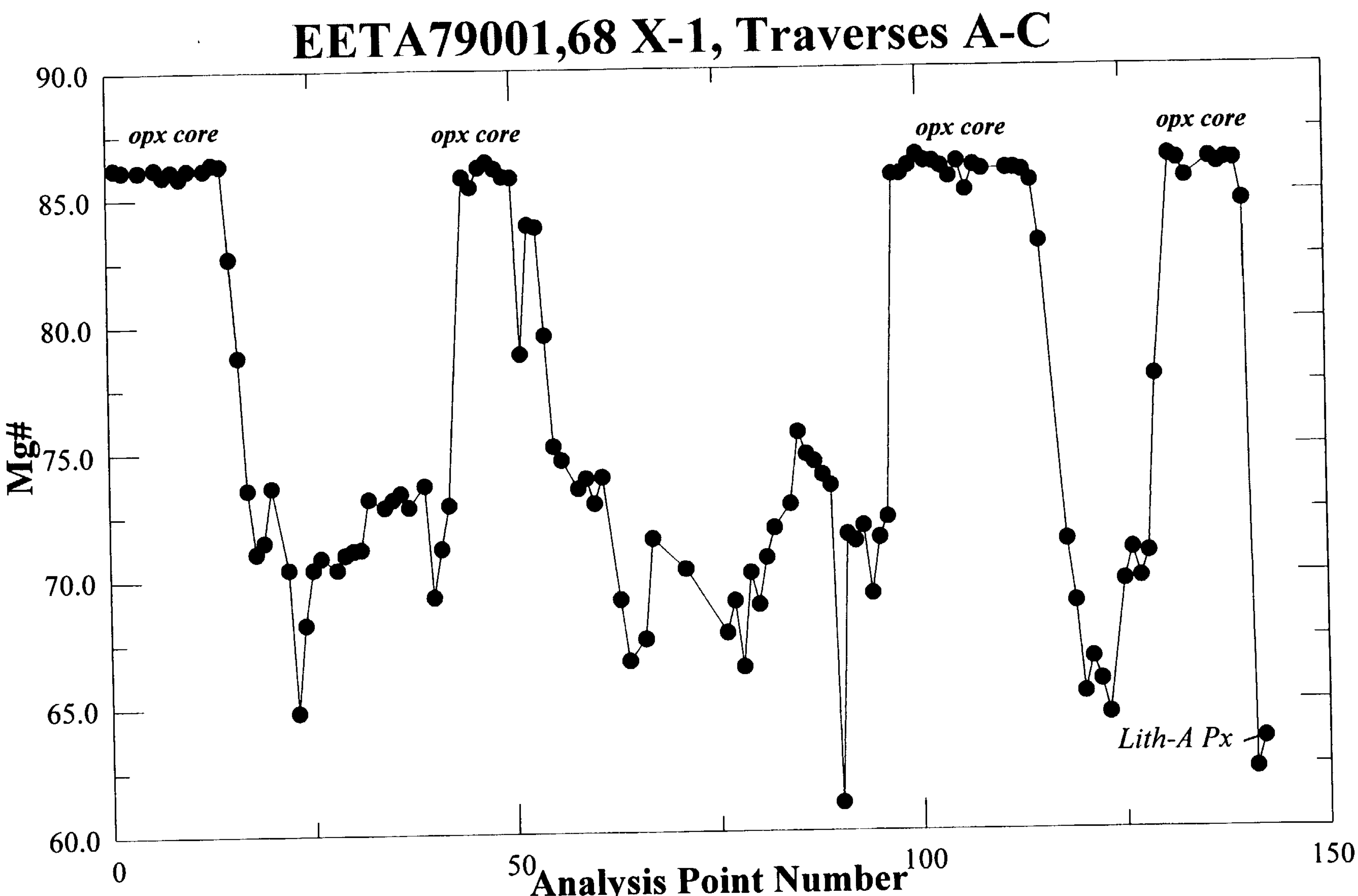

Fig. 1. Combined automated microprobe traverses across opx cores and intervening pyroxenes.

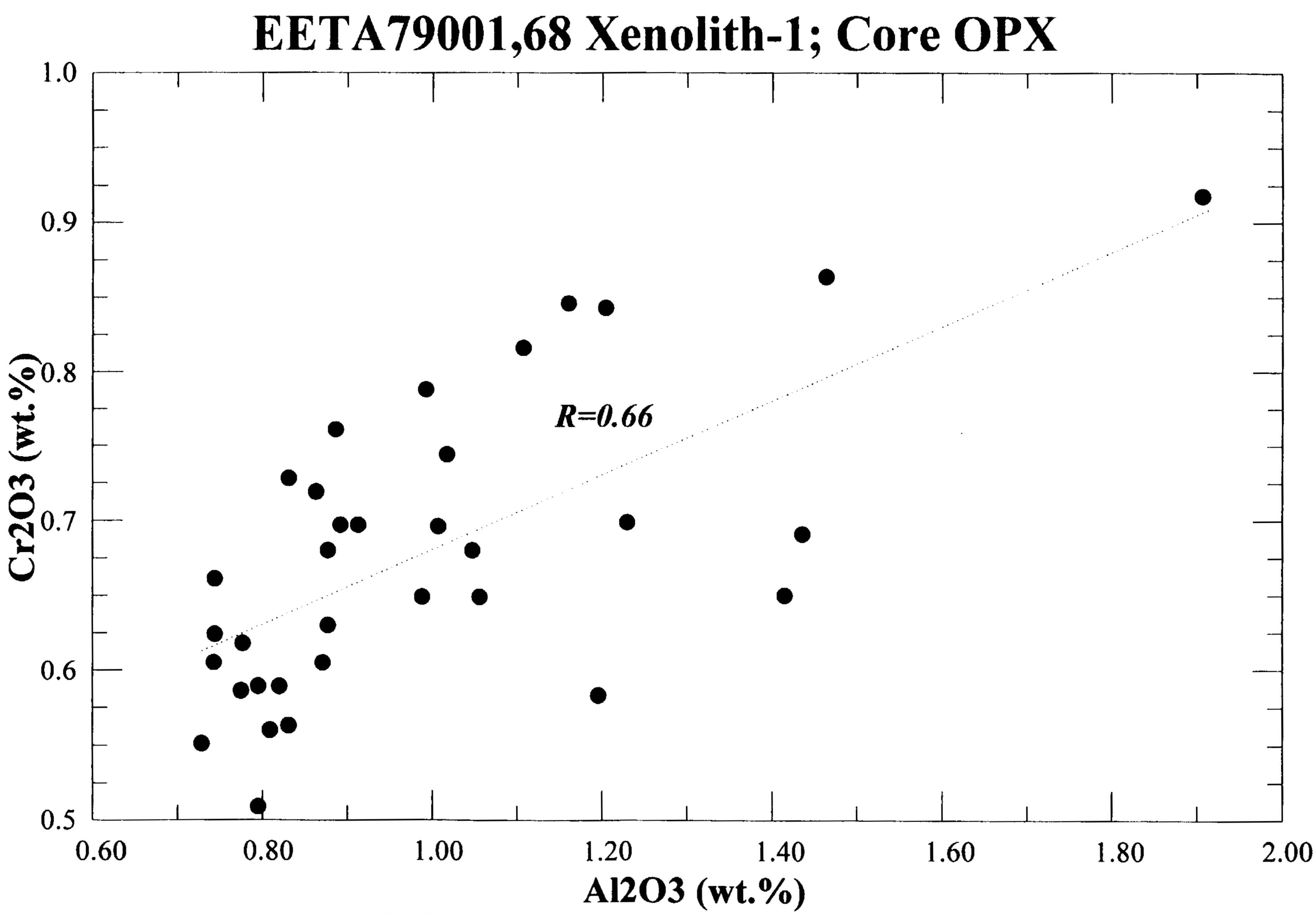

Fig. 2. Correlation and variation of Cr and Al in core opx grains.

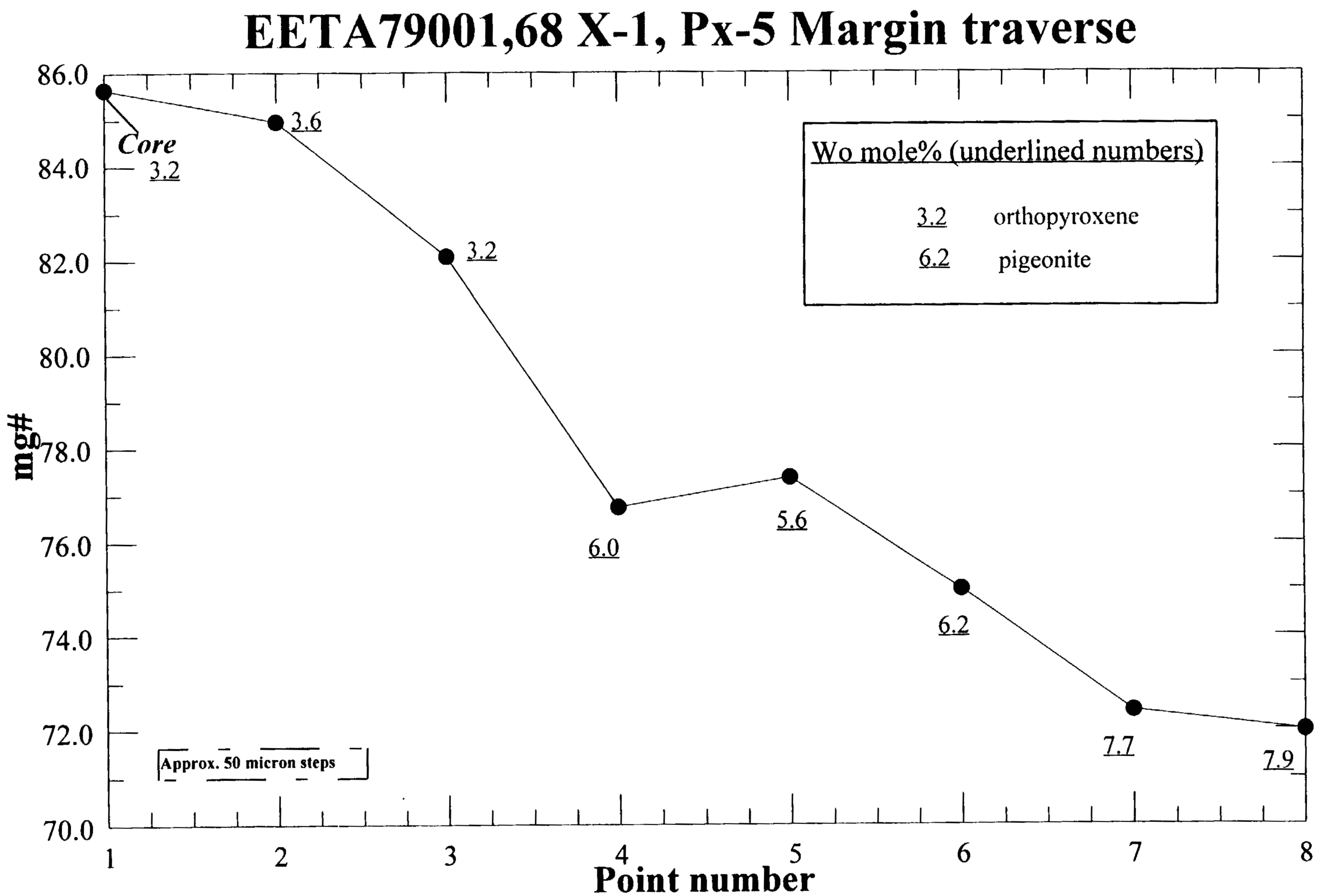

Fig. 3. Microprobe traverse from core opx margin through opx rim to pigeonite envelope.

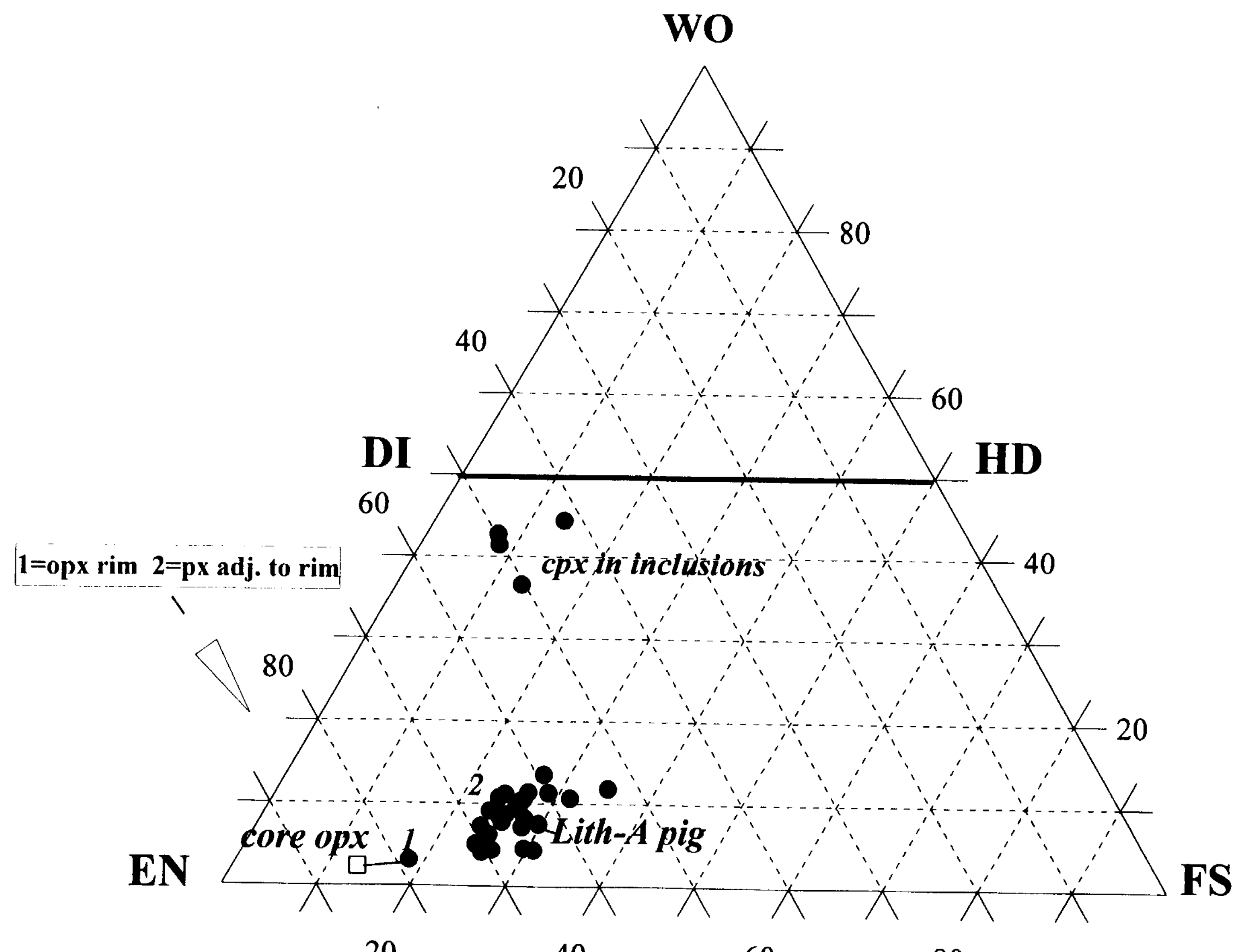

Fig. 4. Pyroxene quadrilateral showing Xenolith-1 compostions in terms of molecular components.

inclusions contain various combinations of calcium phosphate, augite, and high-Ni pyrrhotite. The pyrrhotite contains about 2.5 wt.% Ni, either dissolved in its structure or as micro-intergrowths of pentlandite [$(Fe,Ni)_9S_8$], although no lamellae were observed in BSE images. One of these inclusions contains glass with a true plagioclase composition (maskelynite), although others resemble glass compositions in core areas.

Tectonic Strain

Silicate minerals in the xenolith are cut by an extensive system of straight or gently curved knife-edge shear traces. These, in turn, are crosscut by coarse, irregular fractures. Sharp edged linear shear planes apparently stop at the contact with Lith-A basalt, suggesting that X-1 experienced tectonic strain prior to incorporation into Lith-A. In fact, some incursions of Lith-A material into the xenolith show evidence of intruding along zones of weakness provided by pre-existing shear planes. Because these early shear planes crosscut all pyroxene phases (Mg-opx cores, Fe-opx rims, pigeonite) but do not cross Lith-A, it is very unlikely that reaction with Lith-A caused the extreme iron enrichment zoning around the cores. Additionally, Mg-cores in direct contact with Lith-A show no zoning whatsoever. Therefore, iron-enrichment along margins apparently occurred prior to incorporation into Lith-A.

Irregular, relatively gaping fractures crosscut the sharp edged internal fractures and continue into the surrounding Lith-A basalt. These fractures probably originated in a more recent impact-induced shock event. In addition, many silicate grains show micro-shear lateral displacement, undulatory extinction, and minor brecciation of likely shock origin.

DISCUSSION

Origin of Orthopyroxene Cores

Orthopyroxene cores in X-1 are enriched in Mg/Fe and Al compared to previously reported opx xenocrysts from EETA79001. Compared to opx megacrysts in 79001,439 analyzed in this study, X-1 opx is also enriched in Ca (Fig. 5).

Meteoritic enstatite normally contains little Al, but the C3 carbonaceous chondrite Allende contains enstatite with up to 7.5 wt.% Al_2O_3 (Fuchs, 1969). Al_2O_3 in enstatites from terrestrial pelitic (Al-rich) metamorphic assemblages may exceed 8 wt.%. Thus, the elevated Al in X-1, although high compared to other EETA79001 opx xenocrysts, is not particularly high compared to potential opx Al values.

Terrestrial opx with relatively high Ca (Bushveld type) contain between 0.9 and 1.32 wt.% CaO. Mean CaO in X-1 opx cores (1.8 wt.%; 3.4 mole% Wo) is comparable or higher,.

In general, core opx compositions are consistent with a relatively high temperature of formation. Support for this contention comes primarily from the unusually high Mg/Fe, but is supported by high Al and Ca, as well. The solubility of alumina in opx in the spinel stability region (applicable to X-1) is not pressure sensitive, but *is* positively affected by temperature (Anastasiou and Seifert, 1972).

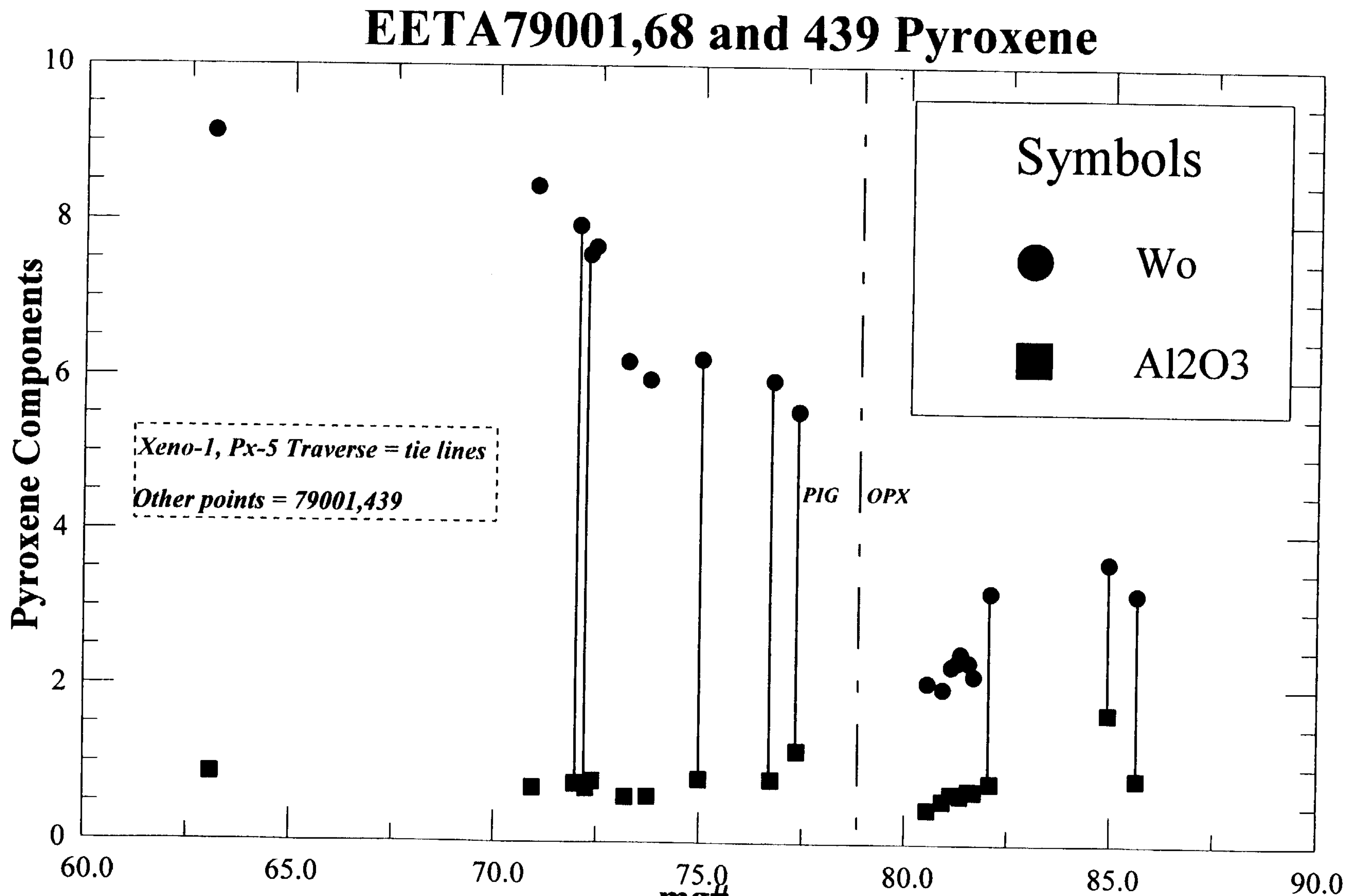

Fig. 5. Traverse as in Fig. 3. Comparison of ,439 and ,68 pyroxene (tie lines), Ca (as Wo) and Al variation vs. mg#.

CaO in opx is well known to increase with increasing temperature of formation in igneous systems (e.g., Lindsley, 1983). An attempt to calculate an equilibrium temperature between melt inclusion augite and enclosing opx in X-1 using the method of Lindsley (1983) gave a temperature of somewhat less than 1200°C. Although suspect because of a lack of homogeneity within augite grains, this temperature — albeit excessively high — is consistent with high-Ca opx core compositions in a general sense. Compared to the SNC orthopyroxenite ALHA84001, X-1 opx is more aluminous and has higher Ca and mg#, suggesting a higher formation temperature for X-1 (Fig. 6).

The ultimate origin of X-1 core opx — igneous versus metamorphic — is difficult to assess. Texturally, grain contacts that could give clues to thermal adjustment during subsolidus annealing are virtually non-existent due to tectonic shearing and extensive iron-rich margins. Orthopyroxene cores never occur in direct granular contact with each other.

However, compositional factors may offer clues. Although virtually invariant, mg# suggests a high degree of equilibration, but minor elements show significant variation, particularly alumina (Figs. 2 and 6). The correlation of Cr variability with Al (Fig. 2) suggests that Al variability is not due solely to microprobe beam fluorescence of subsurface high-Si+Al inclusions. In addition, Wo content varies among superior opx analyses from about 3.0 to 4.3 mole%. Extensive metamorphic annealing would be expected to homogenize the values of minor elements, yet some variability persists in opx cores. Thus, the ultimate origin of opx cores was probably igneous as deduced for opx in ALHA84001 (Berkley and Boynton, 1993; Mittlefehldt and Lindstrom, 1994). On the other hand, calculation of a hypothetical parent melt composition for opx cores using experimental distribution coefficients from Longi and Pan (1989) result in a melt that is unrealistically enriched in MgO and Al_2O_3. This suggests that, for whatever reason, the current core compositions do not reflect original igneous characteristics.

The gradual zoning from more FeO-rich opx to pigeonite surrounding opx cores probably represents late reaction with lower temperature silicate differentiates. As noted above, textural evidence suggests that this event occurred prior to incorporation in Lith-A basalt.

Origin of High-Si+Al Inclusions

The origin of the pervasive, minute inclusions in opx cores is enigmatic. Hypotheses for their origin include: (1) droplets of igneous melt incorporated into cores during crystallization; (2) partial melts derived from heating of opx; (3) exsolution products, and (4) poikilitically-enclosed materilas. These ideas are discussed in turn below.

1- Melt inclusions occurring in mafic silicate minerals commonly occur as fairly widely dispersed features, although exceptions exist. Roedder (1984) has noted "swarms" of small melt+gas or solely gas inclusions in meteoritic olivine, but these are restricted to annealed defect structures. They are not all pervasive as in the present case. Additionally, inclusion compositions (Si+Al ~90%) are distinctly non-magmatic and unlikely to represent equilibrium liquids with highly magnesian opx cores. The majority of inclusions contain no obvious crystallization products whose appearance would fractionate the melts from early magmatic compositions. Also, crystallization of opx on inclusion walls would not produce the observed high silica and alumina in the inclusion glass.

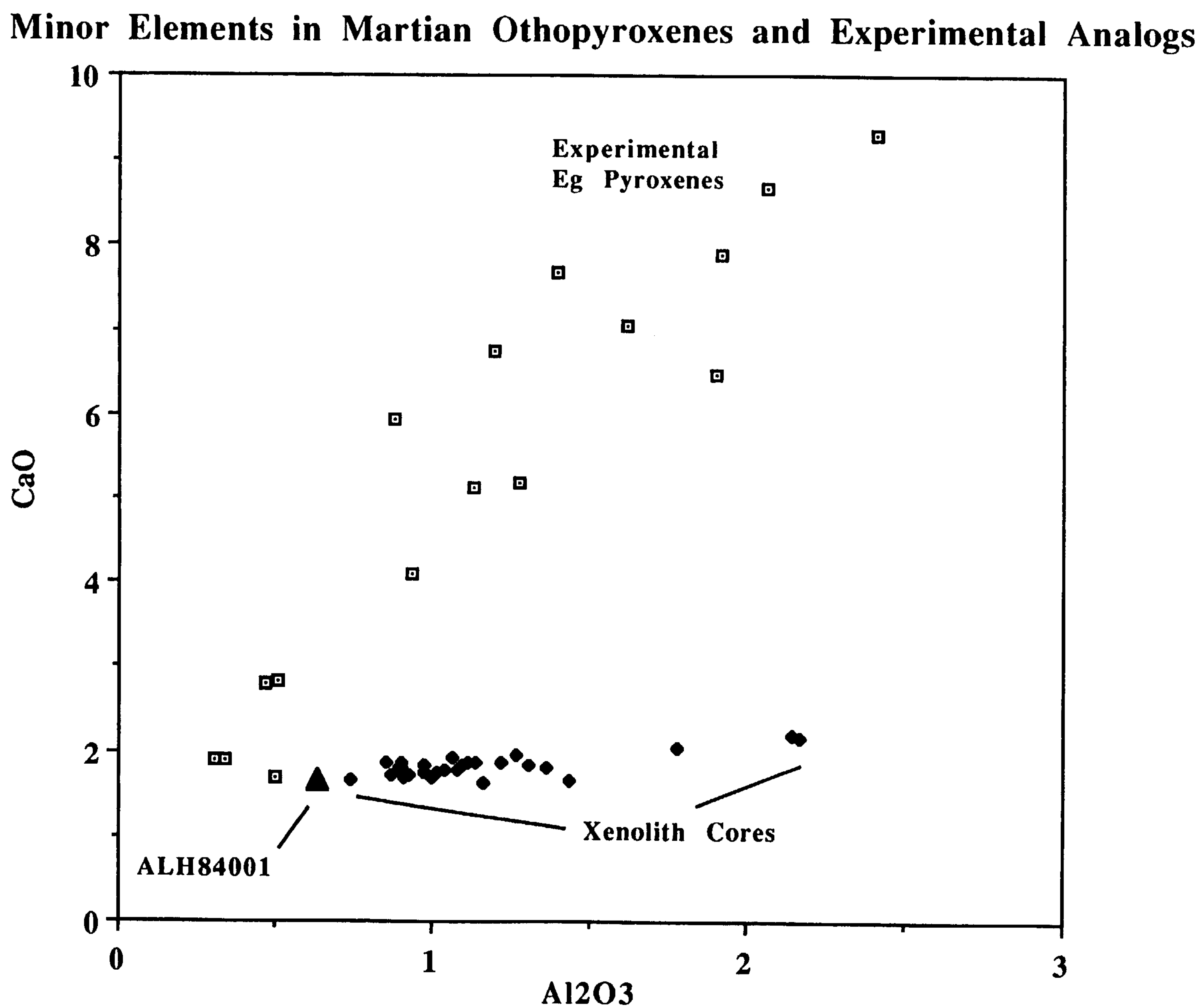

Figure 6. CaO and Al2O3 in EET79001A opx xenolith cores, ALH84001 opx, and experimental (Eg) low-Ca pyroxenes.

2- Partial melts from mafic silicate crystalline aggregates (e.g., mantle peridotite) are generally restricted to silicate boundaries where surface free energies are at a maximum. The production of melts from the interior crystals, except from severe defect structures, would not be expected. In addition, experimental studies (Huebner and Turnock, 1980)) show that a partial melt in equilibrium with magnesian orthopyroxene would have a high-Ca clinopyroxene composition with forsterite+augite+opx on the liquidus at 1 atm. pressure. Iinclusion compositions in this study more closely resemble feldspars.

3- Orthopyroxene megacrysts in aluminous natural systems, like anorthosite complexes, have been described having plagioclase exsolution lamellae parallel to (100) (e.g., Emslie, 1975). Some melt inclusion domains in core opx grains show weak preferred orientation parallel to the c crystallographic direction. Although not true feldspar compositions, they are "feldspathic" in having elevated Si+Al, although lacking sufficient alkalies and Ca to stabilize stoichiometric feldspar. If inclusions, in fact, represent exsolution products, they may result from an attempt by the opx cores to expell excess Al during subsolidus cooling. At least one "large" pyrrhotite-bearing inclusion from an iron-rich opx area has maskelynite glass with a true plagioclase composition.

4- Inclusions may represent solid materials poikilitically enclosed during igneous crystallization of opx grains. Glass compositions have Si/Al ratios similar to alkali feldspars, although low alkali abundances of inclusions are difficult to explain. Alkalis may have been lost during shock metamorphism in the same event that converted the feldspars to glass (maskelynitization). This model helps explain why inclusion are not found in FeO-rich margins (margins formed after primary igneous inclosure of inclusions), but requires a magma capable of crystallizing tiny alkali feldspars coincident with opx crystallization.

Implication of Ni-bearing Pyrrhotite

Pyrrhotite is well known to crystallize as an early, high temperature liquidus phase in mafic silicate magmas. Although its stability range extends to <300°C, its upper limit is over 1,100°C (Jensen, 1942; Kullerud, 1962). Experimental data shows that Ni content is neither temperature nor pressure dependent, but a function of a_{Ni} in the system. However, it may be significant that pyrrhotite occurs alone in X-1, because at progressively lower temperatures binary pairs become increasingly stable (Kullerud, 1962). In any event, the occurrence of pyrrhotite (and absence of pyrite and other Fe-Ni sulfides) is consistent with other evidence pointing to a relatively high temperature of origin.

Summary and Conclusions

The large orthopyroxenite xenolith (X-1) in pts EETA79001,68 shows evidence of a complex history including igneous crystallization, subsolidus modification, and later tectonic alteration either by orogenic tectonism, impact metamorphism or both. This xenolith is important because it has the highest mg# of any mafic silicate ever encountered in a sample from Mars. However, the interpretation of its origin is hampered by features that suggest the influence of both igneous and metamorphic processes. For example, although Mg/Fe is virtually invariable in

opx cores indicative of metamorphic equilibration, Al and Ca show variation more readily explained by igneous models. How the high-Si+Al inclusions fit into the story remains paradoxical. More work is needed to work out details and to solve remaining questions: (1) Origin of high-Mg and Al contents in opx cores; (2) origin of "feldspathic" inclusions in opx cores; (3) process involved in the production of Fe-enriched pyroxene mantles around opx cores; and (4) detailed delineation of post-crystallization metamorphic and tectonic processes and events. Neverthe less, a hypothetical history of the X-1 orthopyroxenite is presented below:

1. Igneous crystallization of opx cores from a relatively high-T, aluminous mafic magma at depth in the Martian crust. Si+Al-rich inclusions form during sustained subsolidus cooling, or as igneous inclusions;
2. Later reaction of cores with fractioned melts, in one or more events;
3. Production of sharp micro-shear planes, probably during multiple events;
4. Incorporation of the xenolith in Lithology-A basalt;
5. Late impact-related shock producing irregular fractures that cross-cut all other features.

REFERENCES

Anastasiou, P. and Seifert, F., 1972. "Solid Solubilty of Al_2O_3 in Enstatite at High Temperatures and 1-5 Kbar Water Pressure," *Contr. Min. Pet,.* Vol. 34, pp. 272-287.

Berkley, J. L. and Boynton, N. J., 1992. "Minor/Major Element Variation Within and Among Diogenite and Howardite Orthopyroxenite Groups," *Meteoritics*, Vol. 27, pp. 27, pp. 387-394.

Emslie, R. F., 1975. "Pyroxene Megacrysts from Anorthositic Rocks: New Clues to the Sources and Evolution of the Parent Magmas," *Can. Min.*, Vol. 13, pp. 138-145.

Fuchs, L. H., 1969. "Occurrences of Cordierite and Aluminous Orthoenstatite in the Allende Meteorite," *Amer. Min.*, Vol. 54, pp. 1645-1653.

Huebner, J. S. and Turnock, A. C., 1980. "The Melting Relations at 1 bar of Pyroxenes Composed Largely of Ca-, Mg-, and Fe-bearing Components," *Amer. Min.* Vol. 65, pp. 225-271.

Jensen, E., 1942. "Pyrrhotite: Melting Relations and Composition," *Amer. J. Sci.*, Vol. 240, pp. 695-709.

Kullerud, G., 1962. "The Ni-S system and Related Minerals," *J. Petrol.*, Vol. 3, pp. 126-175.

Lindsley, D., 1983. "Pyroxene Thermometry," *Amer. Min.*, Vol. 68, pp. 477-493.

Longi, J. and Pan, V., 1989. "The Parent Magmas of the SNC Meteorites," *Proceedings of the 19th Lunar and Planetary Science Conference,* Lunar and Planetary Institute, Houston, pp. 451-464.

McSween, H. Y. Jr. and Jarosewich, E., 1983. "Petrogenesis of the EETA79001 Meteorite: Multiple Magma Pulses on the Shergottite Parent Body," *Geochim. Cosmochim. Acta*, Vol. 47, pp. 1501-1513.

Mittlefehldt, D. and Lindstrom, M. M., 1994. "ALH84001: Comparison with Other Martian Meteorites and Yamato 75032-Type and Lew88xxx Ferroan Diogenites (abs.)," *NIPR Sym. Antarctic Meteorites, 19th*, National Inst. Polar Res., Tokyo, pp. 179-182.

Roedder, E., 1984. "Fluid Inclusions," in *Reviews in Mineralogy*, Vol. 12, Amer. Min. Soc., pp.644.

(4)
IN-99

Ellington Field: A Short History, 1917-1963

Oral History With Joseph Algranti

Johnson Space Center Oral History Project: An Evaluation

Final Report

NASA/ASEE Summer Faculty Fellowship Program-1998

Johnson Space Center

Prepared by:	Erik D. Carlson, Ph.D.
Academic rank:	Visiting Professor
University and Department:	Texas Wesleyan University Department of History Forth Worth, Texas 76105

NASA/JSC

Directorate:	Information Systems
JSC Colleague:	William A. Larsen
Position:	Assistant to Director
Date Submitted:	August 14, 1998
Contract:	NAG 9-867

OUTLINE

I. Acknowledgments

II. Foundations of U.S. Army Aviation

III. U.S. Army Aviation in Texas

IV. Biography of Lt. Eric Lamar Ellington

V. Biography of Lt. Hugh M. Kelly

VI. Ellington's Fatal Crash in San Diego

VII. World War I and the Establishment of Ellington Field

VIII. Ellington Field During the 1920s

IX. Ellington Field Closes

X. World War II and Ellington Field

XI. Ellington Air Force Base in the Post-1945 Period

XII. Ellington Field and Johnson Space Center

XIII. Conclusions

ABSTRACT

My 1998 NASA/ASEE Summer Faculty Fellowship comprised two separate assignments: one to study the history of Ellington Field, the other to evaluate the Johnson Space Center Oral History Project (JSCOHP). This final report gives a summary of my article-length history of Ellington Field, from it inception as a U.S. Army training base to its present commercial/private status. The full-length article will be published in 1999 in the NASA STI Report Series. This final report also presents my assessment of the methodology, administration, and continuing value of the JSCOHP, which is a series of recorded interviews with former and long-time JSC employees begun in 1997 to capture the experience of key participants in the human space program.

INTRODUCTION

The research and writing of this article was completed during a NASA/ASEE Summer Faculty Fellowship at the Johnson Space Center in the summer of 1998, and based upon archival sources available in the Houston area and web pages on the Internet. This research will be published as an article in the NASA STI Report Series. For publication information please contact Sue McDonald in JSC Publications in Building 12.

SUMMARY

In 1907 United States Army aviation began with the formation of the aeronautical division of the Signal Corps. With the purchase of a Wright Flyer the next year, the U.S. Army began test flying the aircraft at Fort Myers, Virginia. Soon the U.S. Army had aviation schools in College Park, Maryland; Augusta, Georgia; and Palm Beach, Florida. Because of the of rudimental aeronautical knowledge and the lack of funds to keep aircraft properly maintained, being an army pilot was a dangerous occupation.

Army aviators flew Wright and Curtiss pusher and grasscutter aircraft, which looked more like powered kites than airplanes. In 1913, many feared that growing troubles in Mexico might overflow into the United States. In response, president William Howard Taft ordered the U.S. Army to guard the Texas-Mexico border. The U.S. Second Infantry Division was sent to Texas and it encamped near Texas City, Texas. Along with infantry and artillery came aviators. For the first time in American history, however, a squadron of combat-level aircraft was formed at the encampment. This unit was designated the First Aero Squadron. Two members of the newly formed unit were Lt. Eric L. Ellington and Lt. Hugh M. Kelly. Within weeks, the problems in Mexico subsided, and the army left Texas. The First Aero Squadron, though, was transferred to North Island at San Diego, California. On the morning of November 24, 1913, Lt. Ellington and Lt. Kelly took their Wright Flyer up for a training mission. Minutes after takeoff, the plane plummeted out of control into the beach at North Island, killing both pilots.

In April of 1917, the United States entered the First World War. In response to the great need for combat pilots, the U.S. Army established training bases throughout the nation. In September of 1917, twenty-five miles south of Houston on the coastal plains of Texas, the U.S. Army built a training base named for aviation pioneer Eric L. Ellington. Ellington Field was an advanced training base where pilots learned to fly Curtiss JN-4 and DH-4 De Haviland aircraft. The field also served as an aerial navigation and gunnery school. With the end of the war in November of 1918, Ellington Field remained open for two years as a reserve training center maintained by a small caretaker staff.

Within three years, the federal government began the process of dismantling the remaining structures at Ellington for auction. In 1923, in the midst of demolition, Ellington Field received a reprieve. Officials from the United States Army approved the formation of a Texas National Guard aviation unit at Ellington Field. The new unit was designated the 111th Observation Squadron. From 1923 to 1928, the 111th Observation Squadron trained pilots and flew readiness missions from the airfield. In 1928 the city of Houston built a modern airport. Municipal Field (now Houston Hobby) opened by the first of the year. By this time, Ellington Field was in poor shape with little federal support. The Texas National Guard, impressed with

the new facilities and the close proximity of the airport to Houston, moved the 111th Observation Squadron. The field was dealt a death blow when a fire scorched it in 1928. All that remained at Ellington were concrete foundations and the water tower.

In 1939 Europe and Asia were torn apart by a war. By 1940 the United States, though still a neutral country, began a national defense program. Congress allocated enough funds to build several air bases for training and coastal defense purposes. After nine months of construction, a new Ellington Field arose on the site of the old base. In December 1941 the Japanese attacked Pearl Harbor, plunging the United States into a two-front world war. During the war, instructors at Ellington Field trained pilots, navigators, and bombardiers. With the cessation of hostilities in September of 1945, the need for bases such as Ellington Field was greatly diminished. At first it was planned that Ellington Field remain an active duty base; however, it was deactivated in 1946, to be only partially reopened as a reserve base.

With the passage of the National Security Act and the establishment of an independent United States Air Force, Ellington Field was renamed Ellington Air Force Base (AFB). As tensions rose between the United States and Soviet Union, the need a for large peacetime military became more apparent. In 1949 Ellington AFB was reopened with the only radar-navigator school in the United States. Throughout this period the 3605th Navigator Training Wing trained hundreds of radar-navigators in TB-25s and T-34s. The 3605th was transferred from Ellington AFB in 1959 and control of the facility was shifted to the Continental Air Command (CONAC). Under the Continental Air Command, the 446th Troop Carrier Wing flew C-119 cargo aircraft.

In 1961 the National Aeronautics and Space Administration (NASA) planned to open a facility to be the headquarters for the Manned Spacecraft Program. After several political battles, NASA chose Houston as the site for its new facility. While the Manned Spacecraft Center (MSC), now Johnson Space Center, was under construction, NASA leased out space and facilities at Ellington Air Force Base. After the completion of the MSC, NASA used Ellington AFB for astronaut readiness and lunar landing training. In 1976 Ellington AFB was permanently deactivated, and eight years later the city of Houston purchased the facility for commercial and general aviation purposes. Despite this privatization, NASA is still a major lessee at Ellington Field.

REFERENCES

Ellington Air Force Base Fact Sheets, 1960-1961, History Office, Ellington Field, Houston Texas.

Houston Chronicle, 1917-1963.

Dethloff, Henry C. *Suddenly Tomorrow Came: A History of the Johnson Space Center (Washington: NASA, 1993).*

Hennessey, Juilette. *U.S. Army Air Arm, 1861-1917* (Washington DC: Office of Air Force History, 1985).

The Johnson Space Center Oral History Project: An Evaluation

By Erik D. Carlson, Ph.D.

Introduction

In 1993 the Johnson Space Center (JSC) History Office (JSCHO) was eliminated due to budgetary considerations. Throughout JSCHO's existence it collected and housed historical documents and promoted the writing of JSC history. When the JSCHO was shut down, the collection was transferred to three sites: the JSC STI Center, JSC History Archive at Rice University, and the National Archives and Records Administration (NARA) in Forth Worth, Texas.[1]

In 1997, JSC Director George Abbey decided that it would be beneficial to collect and preserve the early history of JSC, which was being lost through employee retirement and death, through an oral history project. Out of this conviction grew the Johnson Space Center Oral History Project (JSCOHP). Mr. Abbey selected fifty-three key JSC employees to interview, ranging from astronauts to administrators. Eventually the original interview list was expanded to sixty-eight employees. Signal Corporation was contracted to create an oral history methodology, to collect previous interviews, conduct new interviews, and create an oral history database.

The following report is an evaluation of the Johnson Space Center Oral History Project's methodology based upon my use of the *Research Guidebook: Johnson Space Center Oral History Project* in interviewing Joseph Algranti, my attending intern/staff meetings and conversations with JSCOHP staff and interns, and my three years of cumulative experience in the study of oral history methodology and conducting interviews.

Administration

On an administrative level the JSCOHP is in good hands. Michelle Kelly, Carol Butler, and Summer Bergen developed an impressive research methodology. Because Signal Corporation is involved in the project on a contractual basis, the possibility of employee turnover is a concern. Just this summer (1998), Michelle Kelly left Signal to return to graduate school. The possible loss of key researchers such as Miss Butler and Miss Bergen for any reason would be a major set back to JSCOHP. For this reason, an in-house JSC oral history project has the advantage of employee stability.

[1] Information on the Johnson Space Center History Office was gleaned from notes taken from several informal conversations with William A. Larsen, Assistant to the Director For Information, JSC-NASA.

Selection of Interns

In 1997, Signal Corporation used five colleges interns to help conduct research for oral history interviews. In 1998 eight interns were involved in the project. Since the Johnson Space Center is a facility where engineers and scientists develop technology to conduct space exploration, only trained personnel are used in this mission. Likewise, the writing of history is complex and should be written by only those trained in the historical method. The interns in the JSCOHP are all likable and capable young men and woman. They range in academic level, degree, and research experience. One complaint, however, made by Miss Butler and Miss Bergen was that they had to teach each intern how to conduct historical research. The JSCOHP should employ as summer interns only graduate-level students in history, political science, and English. The use of these well trained graduate-level students would eliminate the need to train incoming summer interns.

Training of Interns

The JSCOHP research manual is excellent, and will guide the interns in the collection of all primary and secondary sources necessary for the preparation of interviews. JSCOHP interns should also use the WORLDCAT/FIRST SEARCH database to be comprehensive in their research. In June of 1998 JSCOHP staff were unaware of this database, which is now available through Internet at the JSC STI Center.

The required reading list for interns should be standardized. All interns should read the same books or articles. If an intern is focusing on one program or period in JSC history, create a specialized reading list. An article by Alex Soojung-Kim Pang, "Oral History and the History of Science: A Review Essay with Speculations," *IJOH* (November, 1989), was not included in the guidebook's bibliography. This is an excellent overview on conducting oral history with scientists and engineers, and should be standard reading for both staff and interns.

Research procedure

If the purpose of the JSCHPO remains the same, the research time necessary for each interview (three weeks) is acceptable. If the program is expanded again, with a full-time staff of only two and the help of summer interns, a three-week research time per target is too long. On this time frame the project could take years to complete.

A set of five to ten standardized historiographical questions, which each interview target would be asked, is necessary to establish JSC within a historical context. These questions can be constructed along the line of programs, projects, divisions, etc. These questions should reflect major policy shifts, changes in JSC administration, technological changes, and the like. This type of historiographical information is **vital** to future historians of JSC.

Evolution of Oral History

During the first half of the twentieth century, historians of American history had little use for modern oral history. These historians studied events where the participants were long dead and inaccessible to the interview process. Scholars relied on primary sources: diaries, letters, documents, memos, and newspapers to reconstruct the past.

Yet oral history was not just the product of post-1960s America. During the New Deal, the Works Progress Administration (WPA) Writer's Project conducted oral history interviews with the last living link to 19th century American slavery. With America's participation in World War II, the United States military sponsored an extensive history program to document its role in the conflict. Many times these government historians relied on oral interviews of combat soldiers to assist in the reconstruction of past events. In the 1960s the writing of history began to evolve. This change, which continues to this writing, shifted the focus of historical writing from distant times to recent events, and from a leadership perspective to the point of view of the everyday person. With these methodological changes, historians now had event participants alive and readily accessible.

In the 1970s and 1980s, oral history as a genre became very popular in the United States. Cataclysmic events such as war, economic depression, and social upheaval were appealing topics for oral historians. In particular military oral history has become a hot commodity in local bookstores. By early 1980s, oral historians such as Donald Knox and Studs Terkel had become household names. [2]

Value of Oral History

Traditionally academic historians have viewed oral history with skepticism. Because oral history transcripts are secondary sources, many scholars saw this source as too impressionistic. This view, however, is not shared by all academic historians. Military and social historians have come to value the oral history transcript as an insightful source. Oral history interviews are best when researched and conducted by a scholar or someone who has a background of the topic. A qualified researcher can query the interviewee on controversial issues, little known events, key players, and sensitive topics. Valuable oral history is that which clarifies matters in the historical record and provides memorable and colorful stories. Misdirected oral history is of little value to the academic historian, becoming at best an interesting historical curiosity.

A historian can not write history based upon oral history alone. This history would be impressionistic at best. Scholarly history must be written with archival sources balanced with a small blend of secondary materials. Oral history is an uncertain secondary source and must be used with caution. Oral history transcripts can suffer from an interviewee's bad memory, bias, or outright falsehoods.

Value of JSCOHP

A historical researcher will view the JSCOHP files as an impressive array of bibliographical and biographical information. For a good researcher, however, the JSCOHP materials is great starting point, but not an end! The value of the JSCOHP's work is in the recorded transcripts, not the bibliographical and biographical files. The program must stress the interview, not the accumulation of mounds of biographical material which is ultimately accessible to any competent researcher.

---

[2] This section is drawn from the author's experiences in the classroom and out in the field, conversations with other oral historians, and the like. For textbooks on oral history methodology, please see Thad Sitton et al, *Oral History: A Guide For Teachers* and James Hoopes' *Oral History: An Introduction for Students.*

Recommendations

1. Finish the Johnson Space Center Oral History Project. Use the oral transcripts and the bibliographical and biographical files to create an impressive JSC history website for media and research purposes. If future expansion is approved, research time could be reduced to two weeks (eight-hour days) per target.

2. Reopen the JSC History Office. The JSCOHP research results are important from a short term public relations standpoint, but unsatisfactory from the perspective of the academic historian. The money allocated for the JSCOHP could be better spent on the resurrection of the History Office to conduct and manage of the writing of scholarly JSC history. In addition to a staff historian, the Office should employ a publications manager who has experience in writing and editing both scholarly and popular works. The Johnson Space Center has a rich, but untapped history. Two topics—for example, the Space Shuttle Orbiter Office and the Lunar Receiving Laboratory—are waiting for historical analysis. This does not mean an end to oral history; on the contrary, oral histories would still be conducted by the JSC historian, but not on the intensity level found with the JSCOHP.[3]

REFERENCES

Hoopes, James. *Oral History: An Introduction for Students* (Chapel Hill: University of North Carolina Press, 1979)

Sitton, Thad, et. al. *Oral History: A Guide for Teachers and Others.* (Austin: The University of Texas, 1983).

---

[3] Thanks to William A. Larsen, Sue McDonald, Laura Gross, Dr. Roger Launius, and Dr. Deborah Douglas for their help.

A Study of Mars Dust Environment Simulation at NASA Johnson Space Center Energy Systems Test Area Resource Conversion Test Facility

5

IN-09

Final Report

NASA/ASEE Summer Faculty Fellowship Program - 1998

Johnson Space center

Prepared by:	Yuan-Liang Albert Chen, Ph.D.
Academic Rank:	Associate Professor
University & Department:	Oklahoma Baptist University
	Department of Physics
	Shawnee, Oklahoma 74802

NASA/JSC

Directorate:	Engineering
Division:	Energy System
Branch:	Energy System Test
JSC Colleague:	Joseph Cook
Date Submitted:	August 7, 1998
Contract Number:	NAG 9-867

ABSTRACT

The dust environment on Mars is planned to be simulated in a 20 foot thermal-vacuum chamber at the Johnson Space Center, Energy Systems Test Area Resource Conversion Test Facility in Houston, Texas. This vacuum chamber will be used to perform tests and study the interactions between the dust in Martian air and ISPP hardware.

This project is to research, theorize, quantify, and document the Mars dust/wind environment needed for the 20 foot simulation chamber. This simulation work is to support the safety, endurance, and cost reduction of the hardware for the future missions.

The Martian dust environment conditions is discussed. Two issues of Martian dust, (1) Dust Contamination related hazards, and (2) Dust Charging caused electrical hazards, are of our interest. The different methods of dust particles measurement are given. The design trade off and feasibility were studied.

A glass bell jar system is used to evaluate various concepts for the Mars dust/wind environment simulation. It was observed that the external dust source injection is the best method to introduce the dust into the simulation system. The dust concentration of 30 mg/m^3 should be employed for preparing for the worst possible Martian atmosphere condition in the future.

Two approaches thermal-panel shroud for the hardware conditioning are discussed. It is suggested the wind tunnel approach be used to study the dust charging characteristics then to be apply to the close-system cyclone approach. For the operation cost reduction purpose, a dehumidified ambient air could be used to replace the expensive CO_2 mixture for some tests.

Introduction

The purpose of in-situ propellant production (ISPP) for the Mars mission is to develop new technology to produce propellant on Mars for the return phase of the mission. This could reduce the total launch mass of the spacecraft and reduce the cost of Mars Sample Return (MSR) mission significantly.

To utilize the Martian resources for propellant production, a thorough understanding of Martian air and the interactions between ISPP hardware and Martian environment is essential. At NASA Johnson Space Center's Energy Test Area Resource Conversion Test Facility in Houston, Texas, a 20 foot diameter thermal vacuum chamber is being used to perform these tests and study the interactions between the dust in Martian air and ISPP hardware. This simulation will support the safety, endurance, and cost reduction of the hardware for the future missions.

Dust Environment on Mars

Martian atmosphere has a density close to 0.02 kg/m^3 and an average dust concentration of 1 mg/m^3 suspended in the Martian air.[1] This is equivalent to 13.4 times the amount of dust in normal air in manufacturing plants on Earth, which is a concentration of 4.59 mg/m^3 dust out of 1.23 kg/m^3 Earth's air.[2] The local dust cyclone on Mars has a dust loading of 30 mg/m^3, which is 402 times of dust in normal air in manufacturing plants. This will cause a major impact on the ISPP hardware reliability and long term operation.

On the Martian surface, dust plays a major role in almost all of the surface interactions considered.[3] The main issues of Martian dust impact of our interesting are (1) Dust Contamination related hazards, and (2) Dust Charging caused electrical hazards.[4]

The dust particles contaminate hardware equipment. The ability of equipment to resist the effects of dust particles which may penetrate into cracks, crevices, bearings, and joints has to be tested and ascertained. Dust particles precipitated onto the power generation system will degrade the solar panels resulting in system power loss.[5, 6]

The extremely dry Martian atmosphere and high surface resistivity provide an ideal condition of triboelectric charging.[7, 8] The Martian dust particles interact with surface and between each other will charge the dust particles and the articles that move on the Martian surface. Kolecki and Landis at NASA Lewis Research Center reported that a 350 volts was observed in their WAE experiment.[9] It is also believed that an article moving on Mars may charge more strongly than the wheel did in the laboratory. Pathfinder wheel charging was observed that nearly independent of the rotation speed and wheel slip. It is suggested that charge generation may have resulted from triboelectric effects in the dust when compacted by the wheel.

Martian air is also believed dominated by Paschen's breakdown.[10] The estimated Paschen's discharging voltage for the Martian environment is about 100 volts. As charged dust particles settle, the charge on individual particles is concentrated. This can result in

very high charge densities in dust particles which have a low level of charge on individual particles.[11] The dust particles with a resistivity in the range above 10^{12} ohm-m are capable to produce high electric potential and cause electrical hazards.

To date, the detail of Martian dust particles charging characteristics is not known. A well controlled Martian dust/wind environment simulation is needed to access their impacts.

Different Methods of Dust Particles Measurement

Introduction

The measurement of Martian dust particles properties plays a central roll in the Martian environment simulation. The parameters of Martian dust particles needed in the simulated environment are: the concentration of dust, the speed of dust flow, the speed of Martian air flow, the size distribution, the rate of dust particles precipitation, and the dust particles charging characteristics.

The following instruments represent the dust particles measuring devices of different concepts and using different physical property of dust particles. The instruments listed here are narrowed to those have a potential application in the Martian environment, and most are commercially available. The measuring concepts are discussed briefly, and trade of each instrument are given.

Methods of Dust Particles Measurement

The measurement methods are classified by the physical properties that utilized by the instrument as :

(1) Inertial/Mechanical Analyzer
(2) Electrical Analyzer
(3) Optical Counter
(4) Quartz Crystal Sensor System (Quartz Crystal Microbalance)
(5) Static/Capacitor Charge Detector
(6) Filter Sampling

Inertial/ Mechanical Analyzer

The Inertial/Mechanical Analyzers[12] are the aerodynamic diameter classification devices and divided into three categories. These are centrifuges, inertial impactors, and cyclones. Centrifuge analyzer uses a rapidly spinning body through which an air sample is flowing at a constant controlled rate. A very high centrifugal force can be applied to the particles of interest which causes the size-separating mechanically. These type devices collect dust particles in a size-dependent manner. Samples of particulate matter are then available for subsequent detector for further analyses. The physical/mechanical complication makes it very vulnerable to dust contamination.

Electrical Analyzer

Electrical analyzer[13] is a device collects the dust particles during measurement and through a diffuse charging or corona charging process to charge the dust particles. The mobility of a dust particles in an electric field is a function of particle size. The particle size may be measured by determining the electric mobility of an unknown particle in a known electric field and compare with a calibrated data base of particles with an equal electric mobility. It is very powerful to detect small size dust particles in the range of 0.01 - 0.5 micron.[7] It is a rapid response detector and good for in-situ measurement. The cost of this type instrument is fairly high. The recharging of a charged dust particle for detection process could be a problem for our purpose. The typical application of this detector is for fine particles size distribution below the range of the optical counter.

Optical Counter (Light Scattering Counter)

Optical counter employs the light scattering by small particles in the flow and detects the Doppler shift of light from these moving particles. The frequency shifting corresponds to particle speed and the amplitude of scattered light relates to the size of particles. Laser Doppler Anemometer (LDA)[14] is one typical optical counter which uses a laser light source.

This type device has a very good frequency response, no probe blockage, and simple signal interpretation. It can't be used for a continuous sampling without disturbing the flow system and is well suited to hostile, or highly dynamic flow environment. It is a relatively expensive and technically complicated technique. It also requires optical access to the flow field. This counter measures the speed of particles suspended in the flow which scattered the light, not flow speed. For dust speed measurement in Martian air simulation, this type counter is the best method. However, a careful design for optical access window is needed.

Quartz Crystal Sensor System (QCSS)

A Quartz Crystal Sensor System is a device to utilize the property of the changing of oscillating frequency of a quartz crystal due to mass loading on the crystal surface. The resonant frequency decreases in direct proportion to the mass of the adhering particles on the crystal. In some field, this device is referred as **Quartz Crystal Microbalance (QCM)**.

The QCSS uses two similar quartz crystal discs. The two crystals are selected such that their characteristic resonant frequency are matched. These two quartz crystals will produce a low frequency beat when the two slightly different frequency are mixed together. One crystal opens to the dust environment and faces up to collect the dust particles. The other is sealed from the dust. When dust particles accumulated onto and adhered to the surface of the opened quartz crystal, the resonant frequency will decrease

slightly. This will cause the beat frequency to increase. The quality of dust particles is then determined by the pre-calibrated beat-mass relationship.

The QCSS has been used in the field of aerosol measurement and referred as Piezoelectric Sensor. In the aerosol measurement, the aerosol sample is drawn into the QCSS chamber by a pump and passed through a corona discharge needle. The corona precipitator is used to charge the dust particles and deposit the charged particles onto the quartz crystal surface. This type detector is equipped with a mechanism for wiping the dust particles off the sensor when the accumulated mass exceeds an overload limit of the instrument.

During the Pathfinder mission, a quartz crystal microbalance was used to measure the mass of dust that falls on the rover's solar array. The crystal facing the sky was coated with a thin layer of adhesive to which dust will adhere. The mass of settled dust will change the crystal oscillation frequency slightly. The QCM monitors the difference in frequency (beat frequency) between the two crystals and relates the beat frequency change to pre-calibrated mass loading. The QCM sensor is very sensitive and accurate. It is capable to measure the mass loading in the nanogram range. The adhesive surface of the opened crystal doesn't have a mean to remove the settled dust particles. After dust accumulates beyond the designed limit, the results from the QCM won't be reliable. This will limit the instrument's useable life time.

QCSS is very sensitive, reliable and readily available. It is very good for measuring mass concentration, precipitation rate, and some size distribution information. QCSS is not capable to measure the speed of air flow and dust speed.

For our purpose, the method(s) to be used to deposit the dust particle onto the quartz crystal surface is crucial. The corona charging method is better than the adhesive surface method, since the dust particles settled on the opened crystal surface can be removed easily. For a long term Martian environment simulation, the instrument has to have a long useable life span. The problem of the corona charging method is mainly involved the charging characteristics of Martian dust. A further study is needed in this area.

Capacitor Charge Detector (CCD)

The dust particles moving in the Martian dry environment will be charged due to triboelectric effect. When the charged particle passes through a capacitor, a small voltage is induced on the capacitor. This induced voltage is proportional to the charge that the particle carried. By using a pair cylindrical capacitors with a fixed distance, the speed of particle can be determined. The correlation between the charge amount and property of the particle can be utilized to measure the size and mass of the particle.

This type detector has been widely used in space dust particles environment to measure the velocity, flux, and mass distribution of interplanetary dust particles. The same design concept is used in the van de Graaf dust particles accelerator for discrete dust particle detection.

For the purpose of Martian dust particles measurement environment, the particles stream flows through the capacitor system continuously with a fairly low speed (in the m/s range). Some of the measuring setups are different from the discrete dust particles

measurement system used in the interplanetary environment. For the interplanetary dust particle, the particle that passes through the capacitors will induce a voltage pulse on each capacitor, but the Martian dust particles stream will cause a constant voltage jump on the capacitors. A grid is placed in front of the first capacitor. The grid is connected to a electronic switch which controls the grounding and takes some of the charges away from the Martian dust particles stream that flow through the capacitors. This grounding will produce a negative voltage surge on the capacitors when the less charged particles stream pass through. The negative surge signals from the two fixed distance capacitors will be used to measure the speed of the particle stream. The capacitor voltage surging characteristics is related to the property of Martian dust particles which can be applied to the size and mass distribution measurements of the Martian dust particles.

This type detector is simple, inexpensive, reliable and can be built fairly fast since many circuitry designs are available. By varying the orientation of CCD, the vector quantity of the dust stream flow can be measured. These data are very valuable for numerical modeling. The physical size of this detector can be very small, a matrix of detectors integrated into system monitoring would help to gain a better understanding and control of the simulated Martian environment. The problems associated with the capacitor charge detector are (1) the charging and discharging characteristics of dust particles are not well known, (2) the correlation between the size, mass and charge of Martian dust particles are needed. At present time, there is not much information (no information !) in this area, (3) the cylindrical shape of the capacitors will complicate the dust decontamination of the CCD. (4) there is no commercially available CCD for our purposes, we have to develop our own CCD.

The CCD has many disadvantages, however, overcoming these difficulties and solving the problems will help a great deal of understanding the charging characteristics of Martian dust particles. These characteristics are very important issues for the hardware certification and safety of the ISPP project as well. CCD can measure the concentration of dust, the speed of dust flow, the size distribution, the rate of dust particles precipitation, and the dust particle charge.

Filter Sampling

Filter sampling[15] involves passing a flow sufficiently near a surface such that dust particles make contact and are retained by the surface. The dust particles are captured by filters when air passing through. The dust mass is measured by weighting the filter after exposure. It is necessary to accurately measure the volume of air from which the particles are removed. With the mass data from weighting and air volume, the concentration of dust can be obtained. The multiple filters with different pores may be used to classify the size distribution of dust particles. This method is simple but cumbersome. It is not recommended to employ this method for dust concentration monitoring inside the 20 foot subsystem chamber which complicates the sampling and operation process.

To prevent dust particles from damaging the vacuum pump, the multiple filters system is a necessity. The dust lost in the vacuum pumping is important information. It can be used for the dust re-supply to the system.

Conclusion

There is no one single device readily available for all the parameters that needed for Martian dust environment simulation. The best instrument for Martian dust environment simulation purpose is the optical counter along with a Pitot tube for flow speed measurement. This combination will cover the measurement of the dust concentration, the speed of dust flow, the speed of Martian air flow, and the size distribution. The rate of dust particles precipitation, and the dust particles charging characteristics have to be measured with an additional instrument like the QCM or CCD.

Bell Jar Experiments

Introduction

To test the design concepts for Martian Dust Environment, a 30" bell jar system with vacuum pump, Baratron Digital Vacuum Gauge, and other necessary peripherals was constructed. The Bell Jar has a 18" OD, 30" height and average thickness of 3/16". The total volume is 0.107450 m^3 . We are looking for (1) the best method to reproduce the Martian dust environment in a confined volume, (2) the best method to produce cyclone inside the bell jar, (3) dust particles impact on vacuum pump, (4) dust particles charging property, and (5) the areodynamic property of low pressure air with dust particles. To prepare for the worst possible situation, we selected the dust concentration of 30 mg/m^3 in the bell jar which is the dust concentration of a local cyclone dust loading on Mars. The ambient air is used to reduced the experiment cost and possible hazards. The dust used for this work is Carbondale Red Clay (CRC),[16] a fire clay mined in Carbondale, California. Like most fire clays, CRC consists mainly of disordered kaolinite, contaminated with quartz, and chlorite. Similar to semectites, koalinite are a naturally occurring mineral mass that are recognized for being fine grained particles that are fairly uniform in size and shape.

Procedures and Results

(1) A 4" computer cooling fan was used along with strings taped to the pre-selected rods for flow field indicator purpose. The fan speed increased at a lower air pressure as expected. The flow indicators stop moving at about 15 Torr. The flow field showed that there was a strong turbulant along the rods and the top the bell jar.

(2) A Trisonic Reedy motor with a 6 by 4 propeller replaced the small cooling fan. It produced a satisfied air flow at even 4 Torr. The propeller was tried at 10K, 13K, 18K, and 20K rpm. At 20K rpm, 7 Torr, the visiable dust on the ramped tray was still not ejected into the airflow. The air pressure was increased gradually to observe the "dust lifting" by propeller. The dust on the tray started to move into air at 220 Torr. This indicated that a stronger fan/propeller is

needed for fan-dust-lifting at 7 Torr. The probem of cooling the fan motor during longer runs needs to be addressed.

(3) The home made Pitot Tube was attached to the Baratron Gauge for flow speed measurement. A ball valve with a flexiable tubing attached was used as dust injection port. The other end of the ball valve linked to a stainless steel tubing which goes to the top center of bell jar for spreading dust. By momentarily open the ball valve to draw a pre-measured dust from a small container, the dust was injected into bell jar successfully. It was very quick and fairly even. The Pitot tube mearured the flow speed showing 15 m/s, 14 m/s, and 11.5 m/s with different fan speeds at 7 Torr. The dust aflot in the air was visible. The precipitated dust on the surface of the instrument inside the bell jar was significant. The filter in front of the vacuum pump has accumulate a large amount of dust. Within about 29 minutes, most the dust particles in the air became invisible. This partially due to the thin air inside the bell jar and a strong Earth's gravity pull.

(4) A simple electrometer attached to a large metal sheet to increase the capacitance was placed inside the bell jar for dust charge detection. This is a very simple charge detector and is not capable to perform the voltage measurement. Due to the grounding problem, the result is not satisfactory. We observed some charges detected by the electrometer after the bell jar's metal protective cover cage was removed. A better grounding and a voltage measurement device is needed.

Conclusion

To shorten the experiment time and protect the fan motor from over heating, a 300 mg/m^3 dust concentration was introduced. The air injected through the ball valve is the method to use to inject dust particles into the simulation system. The fan/propeller with a higher rpm is needed to produce the 30 m/s wind speed local cyclone. A better charge detector is needed for the voltage measurement. There are a few experiments can be performed in bell jar, for instant, the dust preciptation rate, the dust measuring detector testing, and the dust charge detector testing. It is highly recommanded that a scaled test article and new concepts be tested in this bell jar before implimentation inside the 20 foot chamber.

Recommandations and Conclusion

For Martian temperature simulation, a 6' x 6' x 9' thermo-panel shroud is being constructed and placed inside the 20 foot chamber. All the hardware testing will be conducted inside this shroud under simulated Martian environment. The dust environment should be setup and monitored in this shroud. There are two approaches to utilize this facility. First, close the shroud, setup local cyclone inside the shroud. Second, open two

sides of the shroud, use the steam-ejector system for vavuum pumps, make it into a wind tunnel type instrument.

The following concepts learned from bell jar are suggested to apply to the subsystem chamber.

(1) Use a dust concentration of 30 mg/ m^3 to prepare for the worst possible dust loading by local cyclone.

(2) Utilize the ball valve to inject the dust from the upper stream of the flow.

(3) To shorten the running time and reduce the cost, a proportionaly higher dust concentration for the Martian environment simulation to investigate the dust contamination hazards to hardware.

(4) A "differential pumping" scheme may be feasible to apply to the thermo-pannel shroud interior to help maintain the Martian air concentration needed.

(5) The preciptation monitor, air flow monitor, dust speed monitor, and dust charge monitor should be placed inside the shroud; the dust concentration monitor and air composition monitor may be used outside the subsystem chamber through a sampling pump that draws simulated air sample from the center of the shroud.

(6) Use two high rpm ac motors with adequate cooling to produce the local cyclone inside the shroud.

(7) Special precaution to all the groundings for all the matels and test articles inside test chamber.

(8) Cover the ground surface pannels with a simulated Martian dirt to form a high resistance ground surface. This will prevent the dust particles discharge through the metal ground and change the dust particle's charging characteristics.

For the first approach, a multiple filters is needed to keep the mechanical pump protection from dust particles contamination. The second approach might encounter the following problems.

(1) For the thermo-panels to cool down the fast cross flow to a satisfied temperature, either a pre-cooling system at upper stream, or a much higher flow rate of cooling agency in the thermo-pannel is needed.

(2) Under the extemely low temperature (140 K), the subsystem chamber vacuum seals may need special care.

(3) A full scale Martian environment simulation for long duration can be quite

expensive, especially, using the steam-ejector vacuum system, to refurbish the simulated Martian air (for both CO_2 and dust particles) in the system could be very costly.

The first approach seems to have lower operation cost and conditions are more close to the bell jar's close-system concept. The second approach has more available information from the related wind turnel experiments and easier to measure the dust characteristics through the steady and less tubulent flow. A dehumidified ambient air can be used to substitude the expensive CO_2 mixture to reduce the running cost. The dust charging could be observed more effectively by using the second approach.

More research works are needed in following areas: (1) continue to work on bell jar Martian environment simulation and use it as a breadboard test facility, (2) numerical simulation of the two-phase flow in the 20 foot subsystem chamber, (3) numerical and experimental study of dust particle charging characteristics, (4) dust removal technology, and (5) setup a routine numerical simulation facilities at NASA's ESTA to help the research and testing work on site.

References

1. D. I. Kaplan, Environment of Mars, 1988, NASA Technical Memorandum 100470, p.2-11, (1988)

2. A.Eugene, A. Avallane, and T. Baumeister, Sources and Control of Air Pollution, Mark's Standard Handbook for Mechanical Engineers, 9th Edition, p. 18-12.

3. J. Kolecki, and G. Hillard, Overview of Mars System-Environment Interactions, 27th AIAA Plasmadynamics and Lasers Conference, June 17-20, 1996, New Orleans, LA.

4. J. C. Kolecki, G. B. Hillard, and D. C. Ferguson, Electrical System/Environment Interactions on the Planet Mars, Sand and Dust on Mars, NASA CP-10074, p. 34 (1991).

5. J. Appelbaum, and G. Landis, Photovoltaic Arrays for Martian Surface Power, NASA TM-105827 (1992).

6. G. R. Olheoft, Magnetic and Electrical Properties of Martian Particles, Sand and Dust on Mars, NASA CP-10074, p. 44 (1991).

7. J. R. Gaiser, M. E. Perez-Davis, Effects of Martian Dust on Power System Components, Sand and Dust on Mars, NASA CP-10074, p.18 (1991).

8. D. D. Sentman, Electrostatic Fields in a Dust Martian Environment, Sand and Dust on Mars, NASA CP-10074, p. 53 (1991).

9. M. Siebert, and J. Kolecki, Electrostatic Charging of the Pathfinder Rover, AIAA 96-0486, 34th Aerospace Sciences Mtg & Exhibit, Jan 15-18, 1996, Reno, NV.

10. R. N. Leach, Effect of Pressure on Electrostatic Processes on Mars, Sand and Dust on Mars, NASA CP-10074, p. 36 (1991).

11. Jean Cross, Hazards and Problems in: Electrostatics: Principles, Problems and Applications, Adam Hilger, Bristol, Dublin, Ireland, p365 (1987).

12. D. Laudgren, Inertial Classification in: Aerosol Measurement,University Presses of Florida, Gainesville (1979).

13. D. Laudgren, Elctrical Aerosol Analyzer in: Aerosol Measurement,University Presses of Florida, Gainesville (1979).

14. R. S. Figiola, and D. E. Beasley, Pressure and Velocity Measurements in: Introduction to FluidMechanics, John Wiley & Sons, New York, 1992.

15. C. Bruce, and L. Hall, Chapter 3 in: Measuring Aerosol Density Using Nephelometry and Dosimetry, Center for Atmospheric Sciences, New Mexico State University, Las Cruces, New Mexico, 1987.

16. B. R. White, B. M. Lacchia, R. Greeley, and R. N. Leach, The behavior of Dust in a Simulated Martian Environment, *Journal of Geophysical Research: Planets* Vol. 102, No. E99, November 25, 1997.

NUMERICAL INVESTIGATION OF THE ARMSEF ARC-JET

6
IN-37

Final Report

NASA/ASEE Summer Faculty Fellowship Program - 1998

Johnson Space Center

Prepared by:	Carey F. Cox
Academic Rank:	Assistant Professor
University & Department:	Lamar University Department of Mechanical Engineering Beaumont, TX 77710-0028

NASA/JSC

Directorate:	Engineering
Division:	Structures and Mechanics
Branch:	Thermal
JSC Colleague:	Carl D. Scott, Ph.D.
Date Submitted:	August 21, 1998
Contract Number:	NAG 9-867

ABSTRACT

The NASA/JSC 10 MW Atmospheric Reentry Materials and Structures Evaluation Facility (ARMSEF) is used for the development and evaluation of thermal protection systems for manned reentry vehicles. In an effort at better understanding the flow characteristics of an arc-jet wind tunnel and hence the correlation between simulation and actual flight conditions, preliminary numerical analyses have been made. Difficulties in defining inlet boundary conditions to the plenum chamber, where there is very little usable experimental data, are discussed. Two different boundary conditions for the plenum, a straight profile and parabolic profile, are employed to describe the conditions in this very important flow defining region. Comparisons are made to experimental data with the results showing that some type of parabolic or step profile is needed to adequately resolve the strong core flow that is present in the nozzle and plume region. Recommendations are made regarding future efforts in analyzing this challenging flow field.

INTRODUCTION

The arc-heated wind tunnels comprising the NASA/JSC 10 MW Atmospheric Reentry Materials and Structures Evaluation Facility (ARMSEF) are important experimental tools in the evaluation of thermal protection systems (TPS) for space vehicles designed for atmospheric reentry. However, experimental analyses do not always provide a clear, detailed and accurate simulation. In order to be able to accurately correlate experimental data with actual flight conditions, knowledge of the arc-jet flow field is essential. In particular, desired properties include, temperature, chemical composition, velocity, density and pressure, as well as surface heat flux, most of which are difficult to measure. Compounding these difficulties is the non-uniformity of flow across the test section due to wall effects, and a non-equilibrium expansion of gases in the nozzle which is not present in the free stream under actual flight conditions. Computational analysis used in conjunction with experimental data can provide a clearer insight into the simulation and subsequently better tools for the design and analysis of thermal protection systems.

Arc-Jet Facility

There are two test positions, TP1 and TP2, comprising the ARMSEF facility, both consisting of an arc heater column or constrictor, plenum settling chamber, converging-diverging nozzle and test chamber with diffuser. The gas mixture, consisting of nitrogen and oxygen, is injected throughout the heater column, heated by the arc, settles in the plenum and is expanded through the nozzle. Table 1 shows dimensional and operational

	TP1	TP2
Chamber diameter, ft.	10	8
Diffuser diameter (length), ft.	4.9 (46)	3.6 (20)
Nozzle diameter, up to, in.	40	25
Arc heater power, MW	10	5
Mass flow rate, lb/s	0.03-1.5	0.03-0.35

Table 1: Arc-Jet Characteristics

characteristics for the two test positions. Common to both are the diameters of the plenum chamber, throat and constrictor which are 4 in., 2.25 in. and 1.5 in., respectively. It should be pointed out that the constrictor is actually smaller than the throat. For further information on the ARMSEF facility, the reader is encouraged to read the paper by Rochelle, et. al., 1983.

Flow Description

Flow in the arc-jet is very physically intriguing and difficult to model, encompassing several different flow and thermodynamic regimes. The flow-field is basically composed of a core and wall region, with viscous flow dominating the relatively cool wall region and inviscid, compressible flow dominating the high temperature core. Starting in the constrictor the flow can be assumed to be fully developed pipe flow under near equilibrium conditions, with radiation from the high temperature arc dominating the heat transfer. Strong gradients arise in the plenum, where the flow should be subsonic, well mixed and under high pressure and chemical non-equilibrium conditions. Thermochemical non-equilibrium with multiple temperatures and a strongly developing boundary layer characterize flow in the nozzle, where the flow undergoes a rapid expansion to supersonic/hypersonic velocities. Nozzle wall flow may or may not be turbulent. Flow in the plume region should be frozen, with mixing with the chamber gas occurring in the shear layer. An excellent review on arc-jet flow characteristics is given in Sharma, et. al., 1996.

COMPUTATIONAL ANALYSIS

Preliminary computations of flow in the TP2 arc-jet wind tunnel were made in an attempt at better understanding the flow characteristics. Numerical analysis is very dependent on boundary and initial conditions. In particular, for arc-jet flow, boundary conditions in the plenum are the primary determinants for the nozzle flow-field. Unfortunately, due to the harsh operating environment, there is a dearth of usable data describing the plenum of the ARMSEF arc-jet. Thus the focus for this research primarily became the search for appropriate inlet boundary conditions for the plenum.

Geometry

The physical domain was discretized via a 3-block, axisymmetric, structured grid of the latter half of the plenum chamber, nozzle and plume region. Figure 1 shows blocks 1 (145x57) and 2 (89x57) of the computational grid for the plenum, nozzle and nozzle extension, while Figure 2 shows the entire computational domain, including block 3 (73x93), the test section.

Plenum Boundary Conditions

Accurate numerical simulations require a good definition of boundary and initial conditions. Unfortunately, there is very little useful experimental data describing the flow inside the plenum chamber. Researchers at NASA-JSC took spectral radiation measurements optically through special windows installed into the plenum chamber at four radial locations spaced 1.27 cm apart beginning in the center (Mack, et.al., 1996). These spectra were

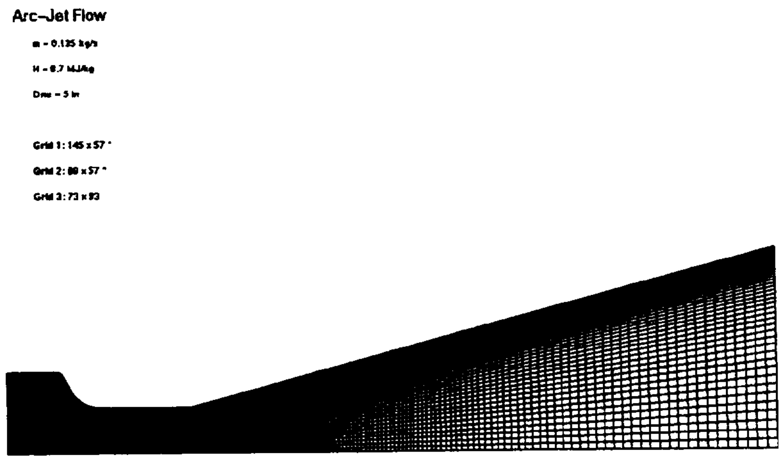

Figure 1: Grid for Plenum and Nozzle

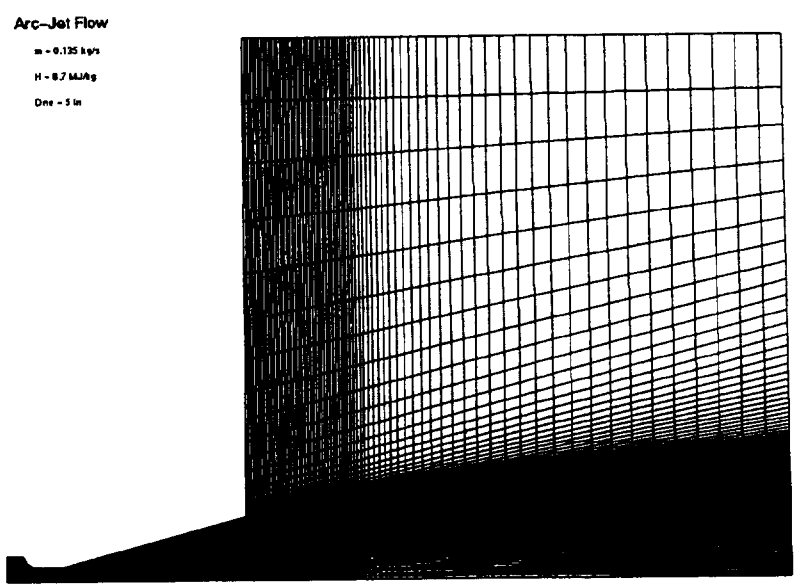

Figure 2: Grid for Entire Computational Domain

reduced to vibrational, rotational and electronic temperatures, giving rough parabolic temperature profiles with the highest temperatures occurring at the centerline, as one would expect. Tunnel operating conditions for this test were, total enthalpy, 8.7 MJ/kg, mass flow rate, 0.135 kg/s, and measured plenum pressure, 0.95 atm.

Due to the lack of information, basic assumptions about the flow profile in the plenum chamber had to be made, with two specific cases tried. The first and easiest, was to assume a straight profile for all properties, with pressure, total enthalpy, and mass flow rate given from the experimental results above. This will be designated the SP boundary condition in the following. Assuming equilibrium conditions, the complete thermodynamic state is defined as a function of the two state variables, pressure and enthalpy.

The second case assumes a parabolic profile for properties in the plenum except pressure which is kept constant and is defined as the PP boundary condition. The equations for density and velocity as functions of radial distance are

$$\rho(r) = \rho_{min} + \left(\frac{r}{R}\right)^2 \Delta\rho,$$

and

$$U(r) = U_{max}\left[1 - \left(\frac{r}{R}\right)^2\right].$$

The resulting profiles from the above equations were integrated to insure that the mass flow rate and total enthalpy for the test case were satisfied, i.e.

$$\dot{m} = \int_0^R \rho U dA,$$

and

$$\dot{m}H_T = \int_0^R \rho U \left(e_o + \frac{p}{\rho}\right) dA.$$

The coefficients were determined iteratively, with the total energy, e_o, determined using a chemical equilibrium solver, CHEMEQ (Cox and Cinnella, 1993), and are $\rho_{\text{min}} = 0.4\ kg/m^3$, $\Delta\rho = 0.6\ kg/m^3$ and $U_{max} = 560\ m/s$. Figures 3 and 4 show the density and velocity profiles for the PP boundary condition.

RESULTS

Results were obtained using the General Aerodynamic Simulation Program, GASP, on the Cray J90 at NASA/JSC. A non-equilibrium air model employing 11 species and 47

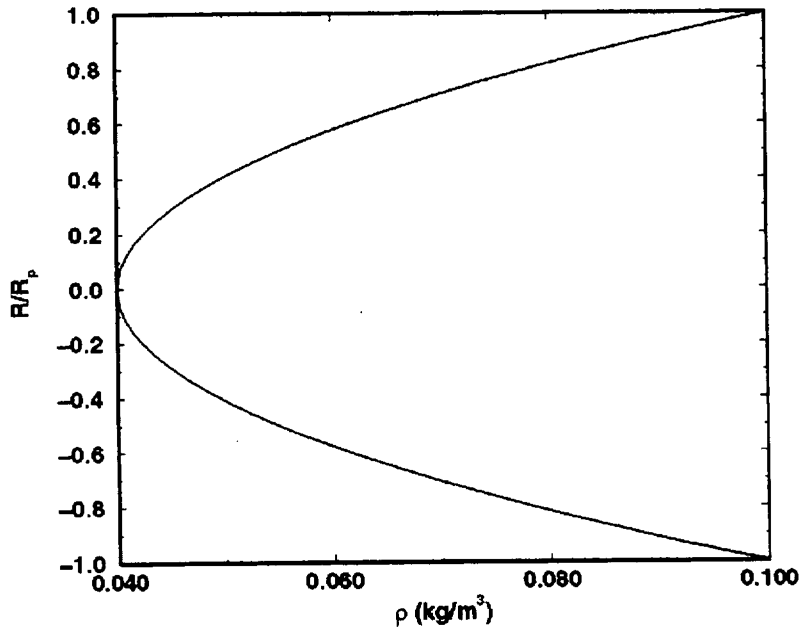

Figure 3: Density Profile Boundary Condition

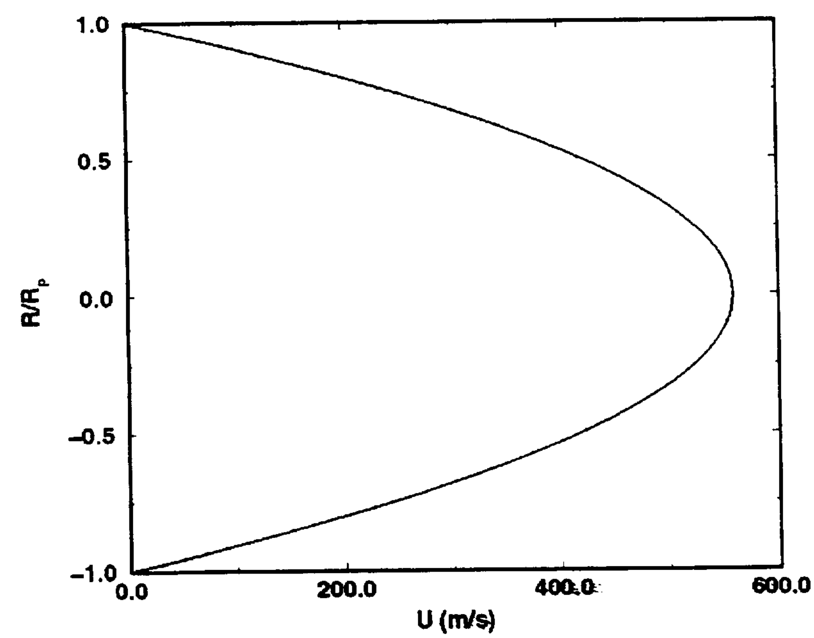

Figure 4: Velocity Profile Boundary Condition

reactions was used for the chemistry, with thermodynamic equilibrium assumed for both cases. The flow was assumed to be laminar with a constant wall temperature of 500 K and radiation effects were considered negligible. Third-order spatial accuracy was employed for all solutions. Comparisons were made of the results for both the straight and parabolic profile boundary conditions with experimental results (Bouslog, Caram and Pham, 1996). Although there were many test runs executed and presented, due to a lack of time, numerical analyses were made only for the test conditions corresponding to the plenum conditions given previously and test data taken at a location 8 in. downstream of a nozzle exit of diameter, 10in.

In order to be consistent with the experimental data, heat fluxes were computed from the numerical solutions using the following curve-fit relating heat flux, q, and stagnation enthalpy, h_o,

$$q = \frac{h_o}{K}\left(\frac{p_o}{R_{eff}}\right)^{1/2},$$

where $R_{eff} = 0.153\ m$ is the effective spherical radius for a flat-faced probe and $K = 89,309$ is a constant given for air mixtures (Bouslog, Caram and Pham, 1996). Stagnation pressure is computed from

$$p_o = p + C_{p_{max}}\left(\frac{1}{2}\rho_\infty U_\infty^2\right),$$

where,

$$C_{p_{max}} = f(\gamma, M_\infty) = \frac{2}{\gamma M_\infty^2}\left\{\left[\frac{(\gamma+1)^2 M_\infty^2}{4\gamma M_\infty^2 - 2(\gamma-1)}\right]^{\gamma/(\gamma-1)}\left[\frac{1-\gamma+2\gamma M_\infty^2}{\gamma+1}\right] - 1\right\},$$

is the maximum pressure coefficient for hypersonic flows (Anderson, 1989).

Figure 5 compares the pressure distribution for the SP boundary condition with the experimental results, with both plotted along the radial direction normalized to the exit radius. Glitches in the computed results appearing at a normalized radius of 1.7 are due to use of the relation for maximum pressure coefficient at low Mach numbers, for which it is not applicable. Though showing some similarity, predicted pressures are roughly twice the measured values and as such the SP boundary is not a good choice. This is further amplified when looking at the heat flux profiles in Figure 6 where it can be seen that there is little qualitative matching. The pressure profile for the PP Boundary condition can be seen in Figure 7 to give a much better match with the experimental data. Equally exciting results can be seen for the heat flux distribution plotted in Figure 8 and while not a perfect

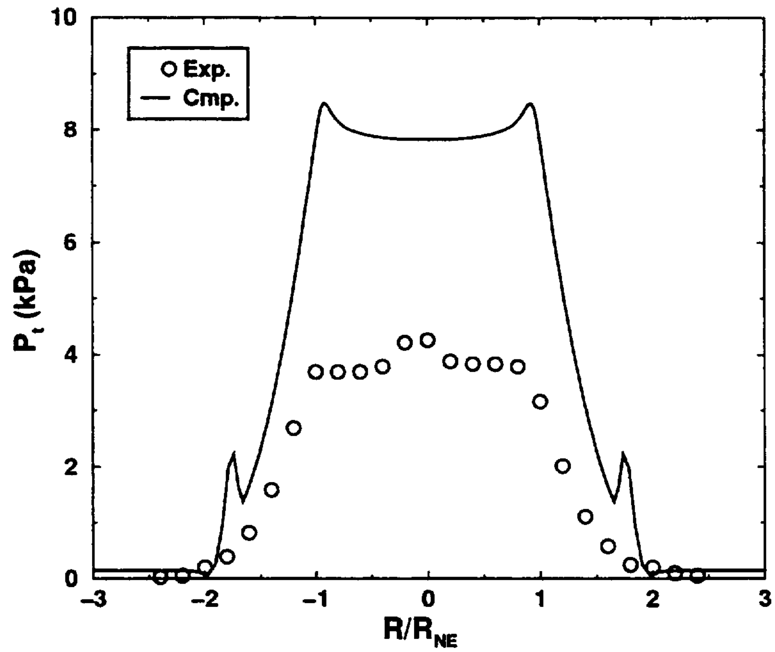

Figure 5: Pressure Distribution for the Straight Profile Boundary Condition

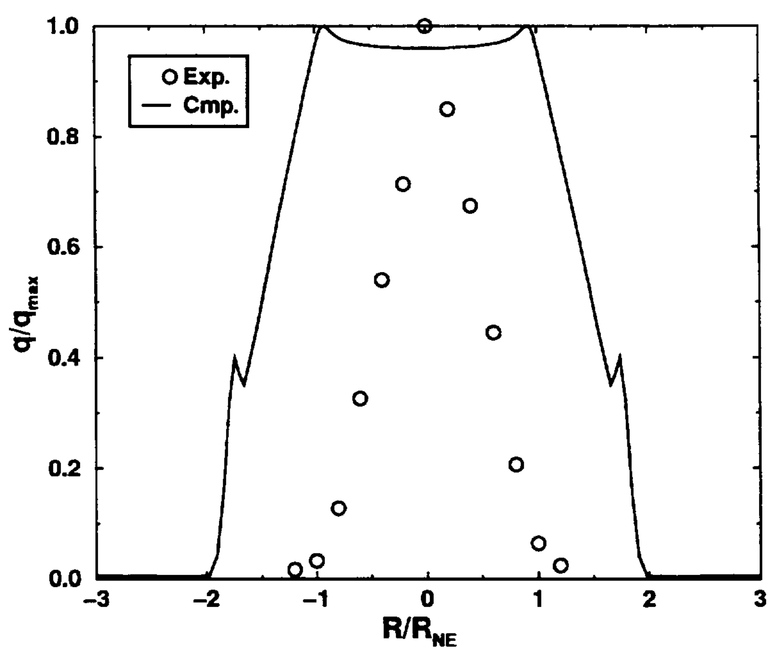

Figure 6: Heat Flux Distribution for the Straight Profile Boundary Condition

quantitative match, computed values are roughly twice that of experimental values (not shown), qualitatively the PP boundary condition is a much better match. This indicates the presence of a strong core flow beginning in the plenum. Further evidence of this artifact is reflected by the pressure contours shown in Figure 9, where the shear layer, expansion fans and inviscid core are readily visible.

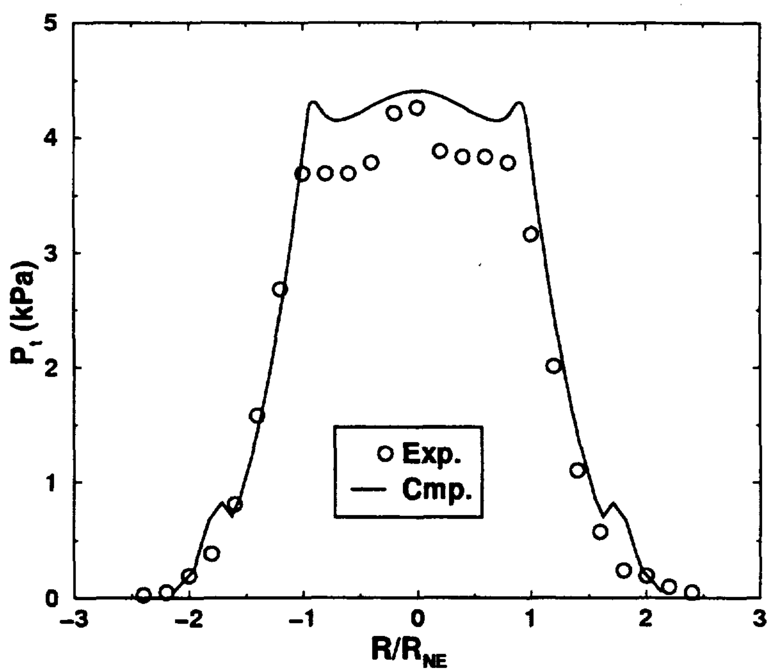

Figure 7: Pressure Distribution for the Parabolic Profile Boundary Condition

CONCLUSIONS

The results presented above are just preliminary, and there is a lot of work left to be done. The straight profile boundary condition, while providing a good starting point for the initial testing of the problem setup, does not provide an accurate depiction of the flow in the test chamber. Although not a perfect match, the parabolic profile boundary condition results show an adequate qualitative agreement with the experimental data. From the results, both experimental and computational, there is an indication of a strong core flow, which is perhaps an artifact of the smaller diameter constrictor. This begs the question of whether the plenum is truly a settling chamber where thorough mixing is occurring or is it basically functioning as a nozzle. Might some type of step profile be a better choice for a boundary condition?

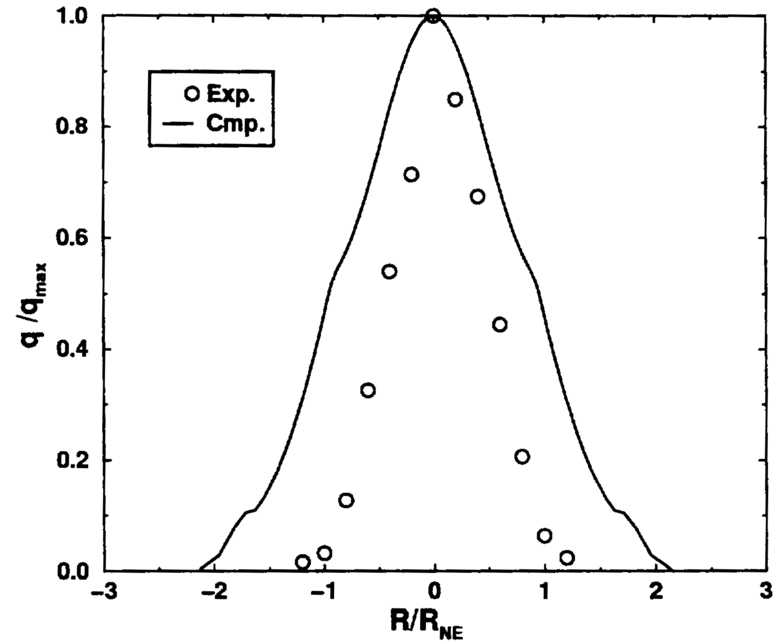

Figure 8: Heat Flux Distribution for the Parabolic Profile Boundary Condition

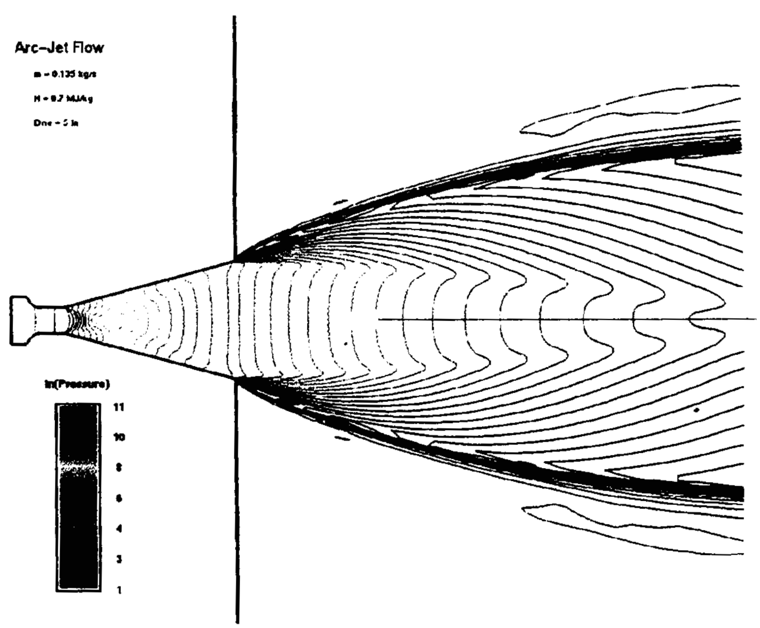

Figure 9: Pressure Contours for the Parabolic Profile Boundary Condition

FUTURE WORK

Further effort needs to be made in determining the plenum conditions, as these dictate the free-stream flow in the test chamber. One fairly quick investigation would involve simply readjusting the parabolic profile boundary conditions or even trying a step profile boundary condition. Another effort that should be made is modeling the flow into the plenum from the constrictor. Finally, one could hope for more experimental data describing the plenum, in particular more detailed velocity, temperature and pressure profiles. As the present investigation only involved non-equilibrium chemistry, with the thermodynamic state assumed to be in equilibrium, further effort should be made to determine the effects of thermodynamic non-equilibrium on the flow field. Along those lines, the effects of wall catalysis should also be investigated as these effects could have a substantial impact on the displacement thickness of the boundary layer and hence the inviscid core footprint, which so predominates the flow.

REFERENCES

Anderson, J. D., *Hypersonic and High Temperature Gas Dynamics*, pg. 54, McGraw Hill, New York, 1989.

Bouslog, S. A., Caram, J. M., and Pham, V. T., "Catalytic Characteristics of Shuttle High-Temperature TPS Materials," AIAA Paper No. 96-0610, presented at the 34th Aerospace Sciences Meeting, Reno, NV, 1996.

Cox, C. and Cinnella P., "A General Solution Procedure for Flows in Local Chemical Equilibrium," *AIAA Journal*, Vol. 32, No. 3, pp. 519-527, March 1994.

Mack, L. H., Rob, M. A., Arepalli, S., Scott, C. D., Milhoan, J. D., and Laux, C. O., "Radial Spectral Measurements in the Plenum Region of an Arc Jet Wind Tunnel," AIAA Paper No. 96-1897, presented at the 31st AIAA Thermophysics Conference, New Orleans, 1996.

Rochelle, W. C., Battley H. H., Grimaud, J. E., Tillian, D. J., Murray, L. P., Lueke, W. J., and Heaton, T. M., "Orbiter TPS Development and Certification Testing at the NASA/JSC 10 MW Atmospheric Reentry Materials and Structures Evaluation Facility," AIAA Paper No. 83-0147, presented at the AIAA 21st Aerospace Sciences Meeting, Reno, NV, 1983.

Sharma, S. P., Park, C. C., Newfield, M., Balboni, J., Scott, C. D., Arepalli, S., and Taunk, J., "Arcjet Flow Characterization," AIAA Paper No. 96-0612, presented at the 34th Aerospace Sciences Meeting, Reno, NV, 1996.

INSTRUMENTATION AND METHODS TO MEASURE DYNAMIC FORCES DURING EXERCISE USING THE HORIZONTAL EXERCISE MACHINE

(4

111-54

Final Report
NASA/ASEE Summer Faculty Fellowship Program--1998
Johnson Space Center

Prepared By: Fernando Figueroa, Ph.D.

Academic Rank: Associate Professor

College and Department: Tulane University
Department of Mechanical Engineering
New Orleans, LA 70118

NASA/JSC

Directorate: Space and Life Sciences

Division: Medical Sciences

Branch: Life Sciences Research Laboratories

JSC Colleague: Linda C. Shackelford, M.D.

Date Submitted: August 31, 1998

Contract Number: NAG 9-867

ABSTRACT

It is hypothesized that bone loss experienced by astronauts in zero gravity conditions may be curtailed by appropriate exercise. According to Wolf's law, bone regenerates when muscles produce stresses by pulling on the bone during daily activity and/or exercise on Earth. To use this theory to prevent or decrease bone loss, one needs to quantify musculoskeletal loads and relate them to bone density changes. In the context of the space program, it is desirable to determine musculoskeletal loads during exercise so that one may make similar measurements on Earth and in space. In this manner, load measurements on Earth may be used as reference to generate similar loads during exercise in space.

A research project to investigate the effects of high-resistive exercise to decrease bone density loss under zero-gravity conditions is being carried out in Life Sciences Research Laboratories at NASA JSC. The project consists of a bed-rest study whereby subjects remain in horizontal position for seventeen weeks. During the study, a subset of those subjects executes a regime of resistive exercises in the horizontal exercise machine (HEM). The HEM was designed so that subjects remain horizontal wile exercising to minimize gravity loading even during exercise. Bone density of each subject is measured throughout the duration of their participation. The objective of the study is to determine if the resistive exercises are effective in diminishing or eliminating bone loss.

My participation in this project relates to instrumentation, measurement, and processing of signals from displacement sensors (optical encoders) and load-cells. Measurement of displacements will be used to determine the motion of the body during exercise, and load measurements will be used (along with displacement data) to determine forces and torques exerted on each section of the body during exercise. Further, I have assisted in specifying new sensors to be added to the HEM and to a new prototype resistive exercise machine called the Interim Resistive Exercise Device (IRED). New load cells and encoders should be mounted in these devices to obtain more complete kineto-dynamic information.

This report includes a description of the instrumentation that was built to perform measurements in the HEM and the IRED, along with the software that was developed to collect the measurements. It also includes examples of measurements taken in the HEM. Finally, a plan is laid out that describes how these measurements may be used to determine forces exerted by muscles for each exercise

INTRODUCTION

It has been determined that astronauts loose bone from the trabecular regions during space flight [1]. This loss is significant even when the permanence in zero-g conditions is as short as two weeks. Because of absence of gravitational forces, it is hypothesized that the reason for bone loss is the decrease of muscle pull activity on the bone during normal daily chores and during exercise (Wolfe's Law). Therefore, one way to quantify bone remodeling activity is to determine the loading history on the bone. One may generate bone loading history during exercise on earth to determine the types of loads required for bone maintenance, and use this data as a template for musculoskeletal loads that must be generated in space.

The Life Sciences Research Laboratories at NASA JSC is carrying out a research project to try to quantify the role of high-resistive exercises on the maintenance of bone density under zero-gravity conditions. The project consists of a bed-rest study whereby subjects remain in horizontal position for seventeen weeks. During the study, a subset of those subjects executes a regime of resistive exercises in the horizontal exercise machine (HEM). The HEM was designed so that subjects remain horizontal wile exercising to minimize gravity loading even during exercise. Bone density of each subject is measured throughout the duration of their participation. The objective of the study is to determine if the resistive exercises are effective in diminishing or eliminating bone loss.

This report describes the instrumentation, measurement, and processing of signals from displacement sensors (optical encoders) and load-cells. Measurement of displacements will be used to determine the motion of the body during exercise, and load measurements will be used (along with displacement data) to determine forces and torques exerted on each section of the body during exercise. Beyond the measurements performed with sensors already installed, I have assisted in specifying new sensors to be added to the HEM and to a new prototype resistive exercise machine called the Interim Resistive Exercise Device (IRED). New load cells and encoders should be mounted in these devices to obtain more complete kineto-dynamic information.

This report includes a description of the instrumentation specified, mounted, and operated to perform measurements in the HEM and the IRED, along with the software that was developed to collect the measurements. It also includes examples of measurements taken in the HEM and the IRED. Finally, a methodology is laid out to use these measurements to describe the motion and eventually to determine forces exerted by muscles during each exercise.

THE HORIZONTAL EXERCISE MACHINE (HEM)

This machine consists of a sliding platform where the individual lies horizontally to perform the exercises. It also includes a system of pulleys and cables to lift weights from two towers located at the extremes of the machine (See Figure 1). These

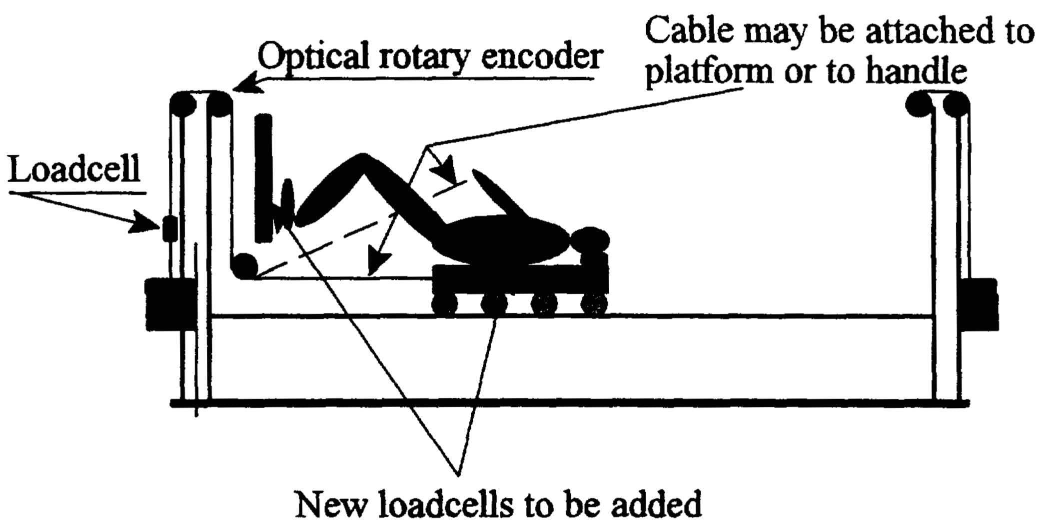

Figure 1 Horizontal Exercise Machine

weights generate the resistance in each exercise. The platform may be allowed to move with the cable attached to it to perform leg exercises such as bench-press or heel raises; or it may be fixed to perform exercises involving the arms such as biceps curls.

Exercises

The exercise regime includes the following exercises:

1. Bench press
2. Heel raises
3. Biceps curls
4. Triceps curls
5. Rowing
6. Vertical row
7. Squats
8. Knee raises

9. Back extensions
10. Hip abduction

From these, measurements were taken for three exercises:
1. Bench press
2. Heel raises
3. Biceps curls

Sensors and Measurements

Two sensors were installed in the HEM: an optical encoder to measure displacement of the cable attached to the weights, and a loadcell to measure the instantaneous force in the cable.

Encoder

The encoder used is manufactured by Dynapar Corporation, model E15-0360-B304, with a resolution of 360 lines/revolution. In order to decode the pulses generated by the encoder, a decoder box was designed and built (see Figure 2). The signals from the encoder go through the decoder box where they are converted into a 16-bit number indicating the rotational displacement of the encoder shaft. These bits are connected directly to the data acquisition (DAQ) system to be read by the program. A few digital lines from the DAQ system are used to control the operation in the decoder box. One line is used to reset the counter, another to enable operation, and another to select which eight-bit portion of the number is to be passed to the DAQ system.

A second decoder box was also built to decode simultaneously two encoders (see Figure 3). This box is intended for the IRED to monitor displacement of each of its two cables.

DECODER ELECTRONIC BOX

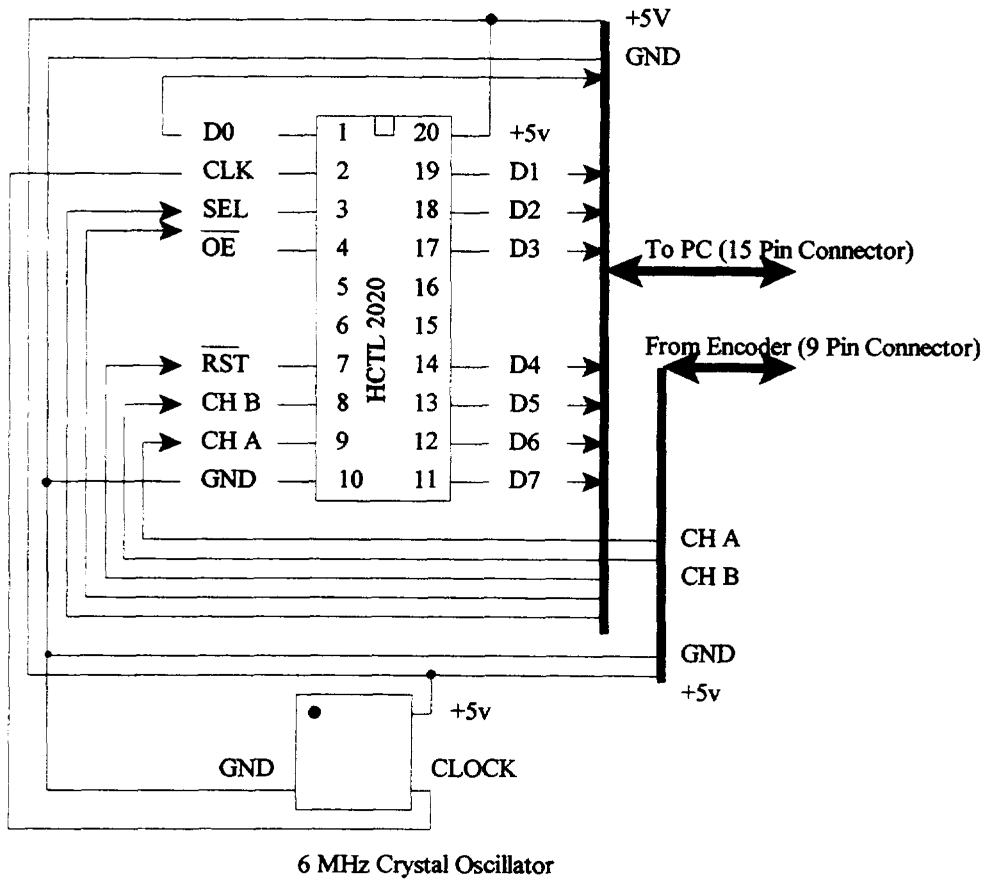

Fernando Figueroa
May 11, 1998

Figure 2 Decoder box electronics.

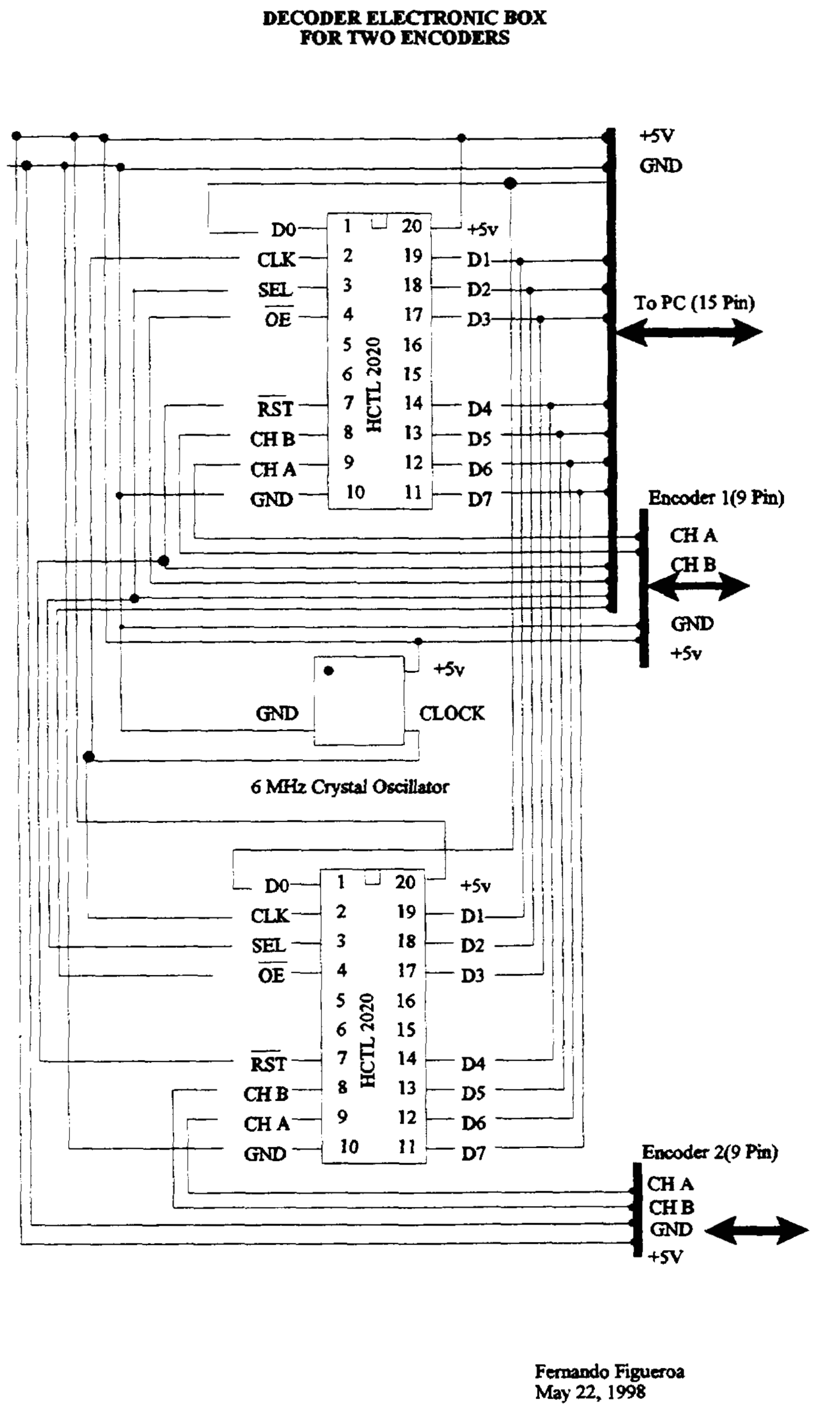

Figure 3 Decoder box electronics for two encoders.

Loadcell

The loadcell used is manufactured by EntranCorporation, and it has 1000 lb of load capacity.

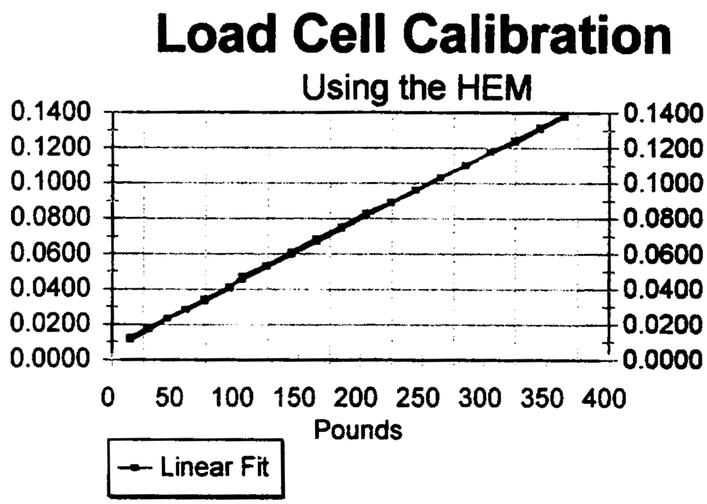

Figure 4 Calibration for subject 2

Calibration

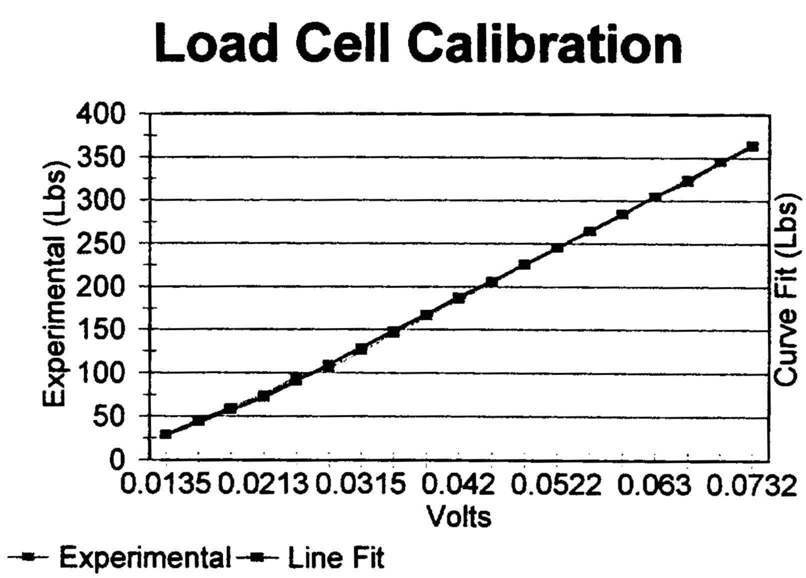

Figure 5 Calibration for loadcell U4288

The load cell mounted on the HEM was calibrated twice. The first calibration was used to perform measurements on Subject 2. The second calibration was used to perform the rest of the measurements. Figures 2 and 3 show the calibration curves. The linear fit in each case has the following parameters.

Calibration 1: the resulting linear fit was as follows.

$$pounds = 2769.6 \bullet volts - 20.20$$

Std. Error = 3.6 pounds.

Calibration 2: the resulting linear fit was as follows.

Loadcell M165472, s/n U4288, connected to CH1 of the 1100 Module.

$$pounds = 5601.5 \bullet volts - 47.5$$

Std. Error = 2.9 pounds.

Loadcell M165473, s/n U4289, connected to CH0 of the 1100 Module.

$$pounds = 5682.1 \bullet volts - 57.1$$

Std. Error = 3.9 pounds.

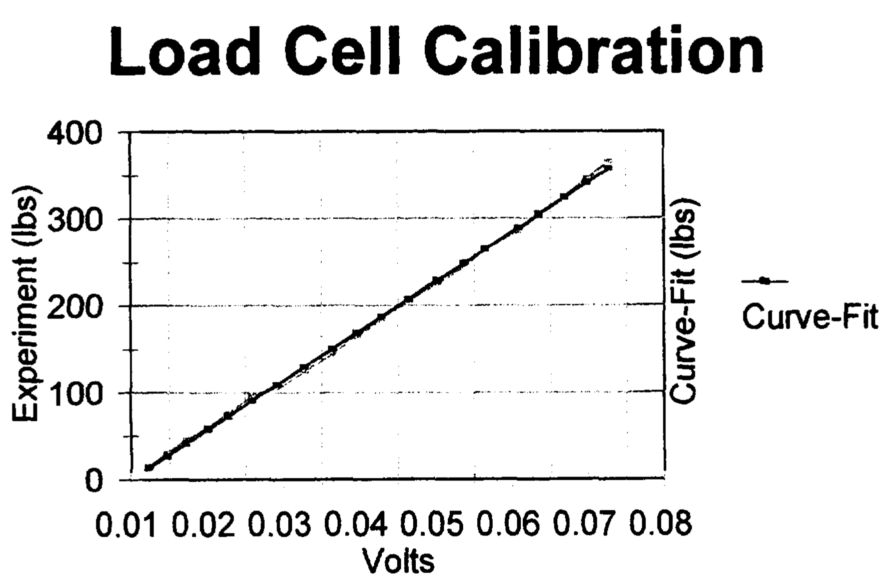

Figure 6 Calibration for loadcell U4289

Kinematic Analysis

The measurements taken during exercise are used to determine the kinematics of motion of each section of the individual. During my residence at NASA, the following kinematic solution for the bench-press exercise was developed.

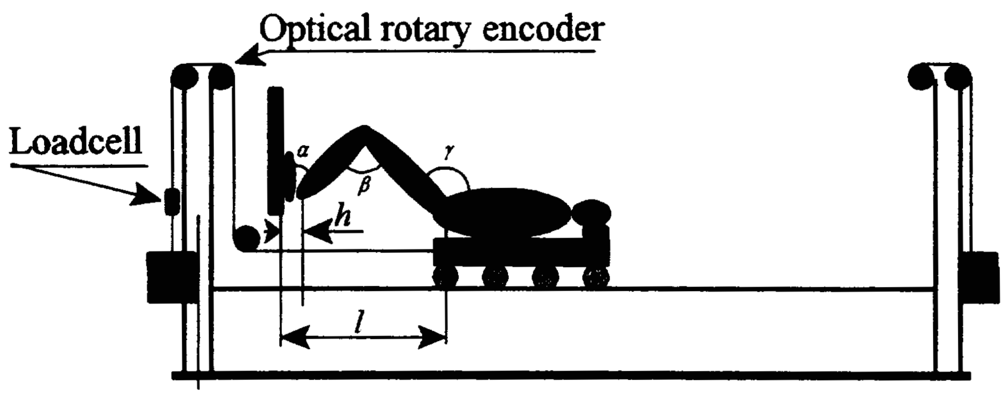

Figure 7 Measurements for the kinematic analysis

Based on the schematic shown in Figure 7, the following triangular figure shows all dimensions needed for the kinematic solution associated with the bench-press exercise.

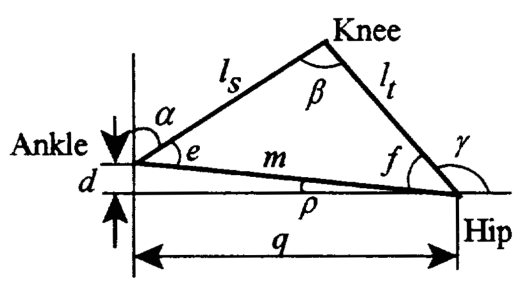

Figure 8 Parameters for the kinematic analysis

From Figures 7 and 8:

$q = l - h$

The value for d is always constant. l_s and l_t are the lengths of the shank and thigh respectively. From initial conditions, the initial value of l can be determined.

$$d = l_t \sin\gamma - l_s \cos\alpha$$

$l_0 = l_s \sin\alpha + h - l_t \cos\gamma$ Where l_0 is the initial value of l.

After motion begins, $l = l_0 + x$, where x is the cable travel. Cable travel can be calculated as follows.

The decoder chip increments the resolution of the encoder by four. Therefore, the overall resolution of the angular displacement is OR=1,440 counts/rev, or OR=229.1831 counts/radian. The total angle rotated as measured by the encoder is $\theta = \frac{\text{count}}{\text{OR}}$, and so $x = r \cdot \theta$ or $x = 1.5 \cdot \frac{2\pi}{1440} \cdot count$. Where *count* is the decoder count value.

Now that the value of l can be calculated during motion, angles α, β, and γ can be calculated as follows.

$$\rho = A\tan(\tfrac{d}{q})$$
$$m = \sqrt{d^2 + q^2}$$
$$\cos\beta = \frac{l_s^2 + l_t^2 - m^2}{2 l_s l_t}$$
$$\sin f = \frac{l_s}{m}\sin\beta$$
$$\sin e = \frac{l_t}{m}\sin\beta$$
$$\alpha = \frac{\pi}{2} - e + \rho$$
$$\gamma = \pi - f - \rho$$

Dynamic Analysis

To determine forces on the trunk-and-head, thigh, shank, and foot, additional force measurements are needed, or special assumptions must be made. We are focusing on a two dimensional analysis only. For an analysis in three dimensions,

even more measurements would be needed to describe the motion outside the sagittal plane.

To complete the dynamic analysis in two dimensions, additional sensors have been purchased and will be installed. These sensors will measure support forces by the translating platform and by the foot plate.

Further analysis to determine forces exerted by individual muscles or groups of muscles will require the use of optimization methods and/or assumptions regarding the sharing of forces among muscles. The following procedure may be used for this purpose: (1) Use Newton-Euler Equations of Motion of each body segment to determine a set of equations that relate the forces exerted by muscles on the segment bone and forces and torques applied by other bone neighboring sections at joints and contact points; this set of equations is indeterminate, meaning that there will be more unknowns than equations [2,3,4,5,6,7,8]. (2) Generate additional equations using optimization methods (optmize a criteria function) [9,2], heuristic knowledge about muscle activity during portions of an exercise [7], muscle force sharing indicated by muscle, tendon, and moment arm[10], and other methods. Verification of the results could be done using EMG measurements

THE INTERIM RESISTIVE EXERCISE DEVICE (IRED)

This device is very similar to the HEM except that the resistance is generated by a collection of flexible disks. The IRED is a prototype machine for space, that is why it uses elastic deformation as the source of resistance rather than weight. Given that this machine is new, Dr. Shackelford suggested to measure the forces on the cables during exercise. This means we needed to modify slightly the software developed for the HEM to handle two loadcells instead of one. In addition, both loadcells were re-calibrated using the HEM weights.

The measurements taken showed that the force settings in the IRED were not very accurate, and were different on each side. Meaning that if one thought to be pulling a force of 100 lbs., it may have been more or less by a significant amount (possibly 5 to 10 lbs.). In fact, it seems to be a good idea to have such measurement system on the IRED, augmented by sensors that measure cable displacement so as to have a more accurate description of the exercises being performed (know more precisely the forces and motion).

DATA ACQUISITION AND PROCESSING SOFTWARE

The data acquisition system used was acquired from National Instruments and is

very flexible in terms of applicability and expandability. It consists of a chassis (SXI-1000) with two modules (SCXI-1200 and SCXI-1100). The system can sample analog signals at speeds up to 100,000 samples/sec. However, since we are also acquiring digital signals from the encoder, the speed is greatly reduced. Nevertheless, it was possible to acquire and save data at speeds of up to 150 samples/sec. This speed was sufficient for our application.

The software developed consists of two programs. One to read the sensors and save the information in the hard disk, and the other to read the data from the hard disk, process it, and display it. The programs were developed in the LabView environment from National Instruments.

Data Acquisition

The program to read the sensor data is easily modified to increment the number of analog sensors that can be used. Figure 9 shows the window displaying the input parameters necessary to run it. Input regarding details of the exercise are used to create an appropriate filename. Input regarding the details of the data acquisition such as speed and signal size, are used to optimize the resolution and to scale the numbers when read back from the disk. Input regarding the channels used are set to a default and can be modified if more than one analog signal is being read. For example, to acquire data from the IRED, a second analog input channel was used by simply modifying the description of the channels in the *channels* control box.

The program to read sensor data first calibrates the analog inputs by measuring the zero-offset. This value is latter used to compensate the values read and make them more accurate. Then it proceeds to initialize the data acquisition operation, and to read sequentially data from the encoder and from the analog sensors. The encoder is read 8-bits at a time as per the specifications of the chip that provides the count value. Finally, the data is streamed to the hard disk to be stored. The data is stored exactly as read from the data acquisition system (raw). Along with the data, all relevant parameters to interpret the data are saved (scales, offsets, speed, etc.) so that it may be used by the next program which processes the raw data.

The front panel of the program to read the data stored previously in disk is shown in Figure 10. This program reads the sensor data along with all other data acquisition parameters, processes the data, and displays it using the appropriate units. The cable displacement data is to be used by the kinematic analysis equations as described earlier. The force data is to be used by the dynamic analysis, but as indicated, more development is needed to carry out the dynamic analysis.

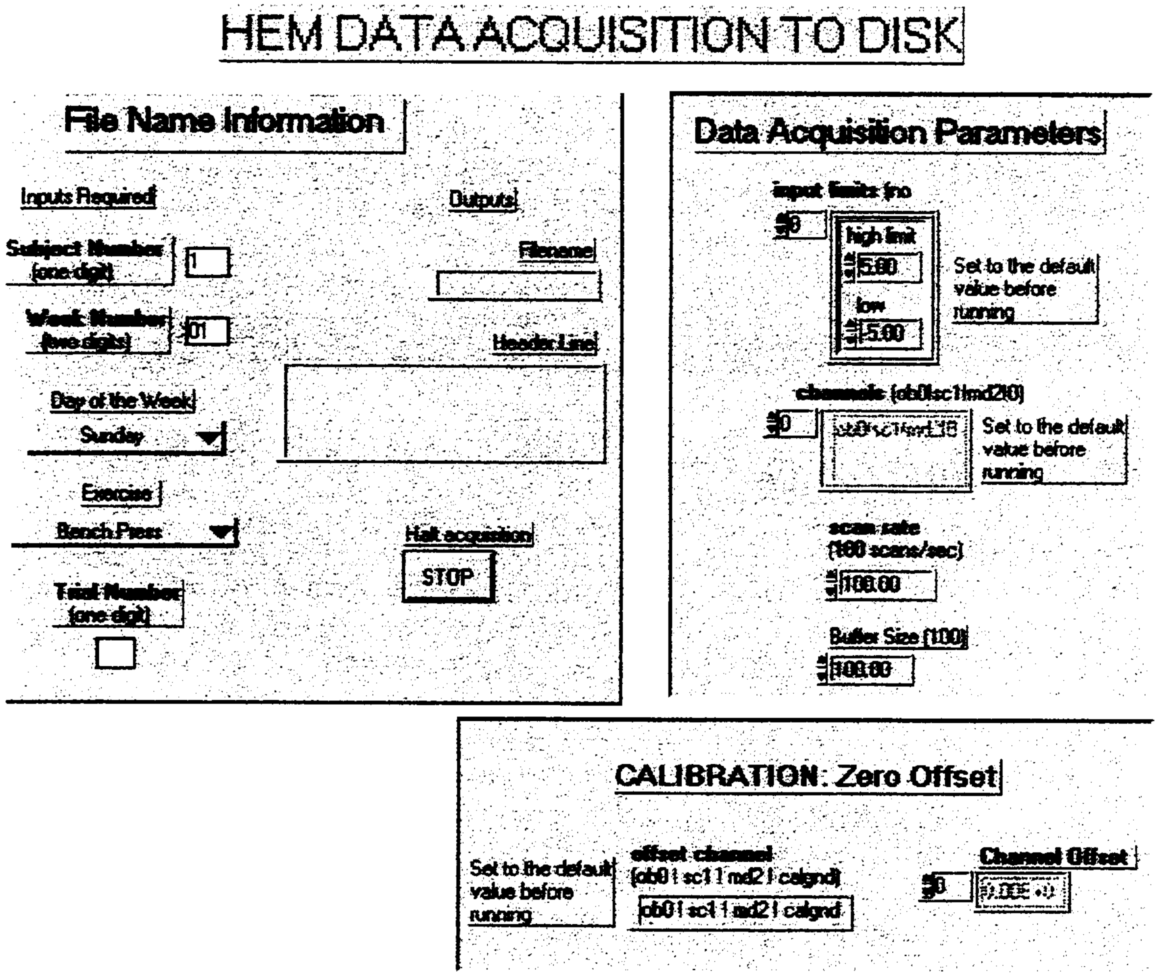

Figure 9 Data acquisition of force and cable displacement from the HEM.

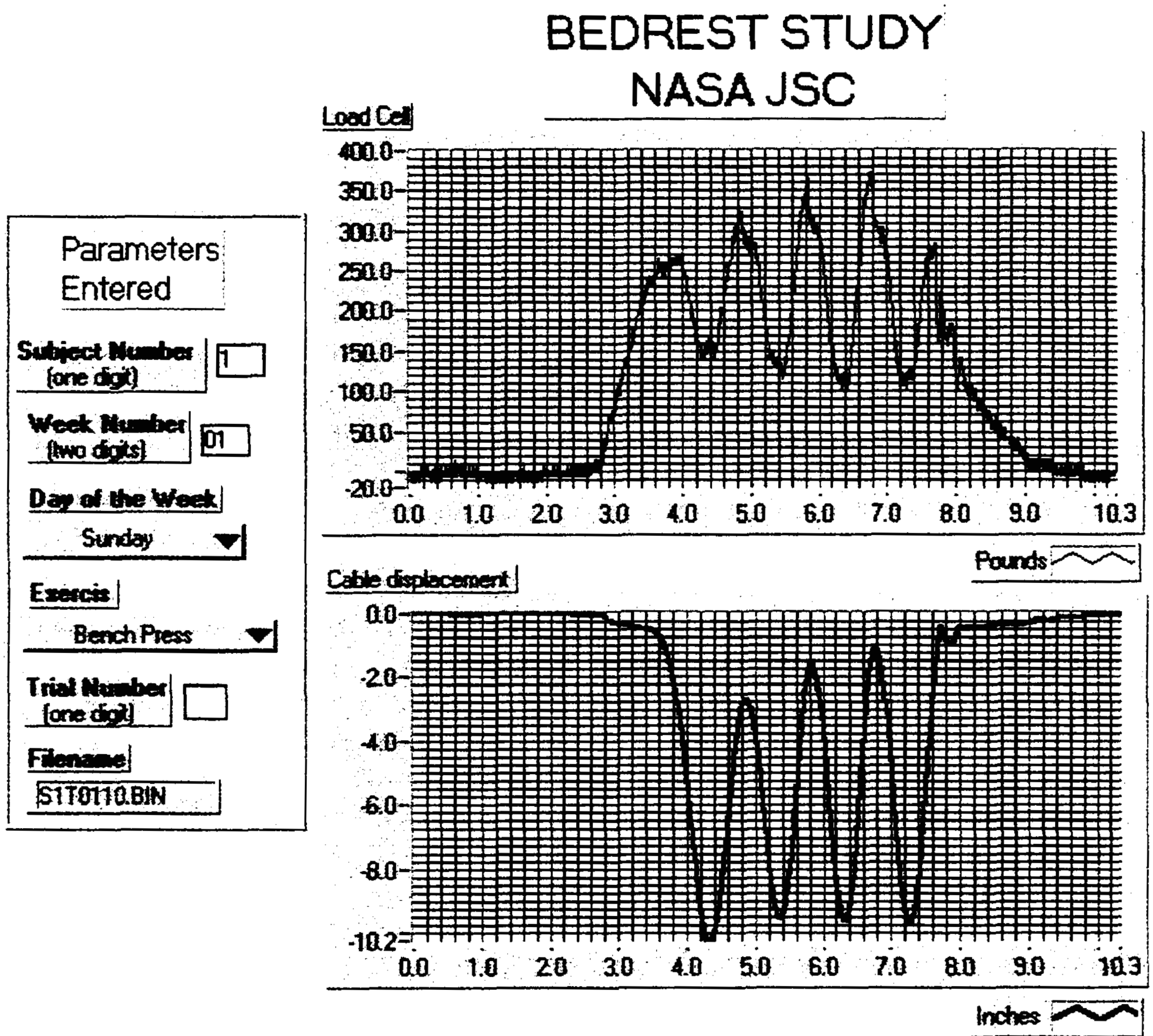

Figure 10 Panel showing data read from the hard disk and processed to display in correct units.

PENDING TASKS

The pending tasks to determine musculoskeletal forces include:

1. Use kinematic equations to determine angular velocity and acceleration of each body section, and the acceleration of the center of mass.
2. Use the Newton-Euler equations of motion and other optimization and heuristic equations to determine forces exerted by particular muscles.
3. Provide musculoskeletal forces and points of application for input to a finite element analysis of the bone.

CONCLUSIONS AND RECOMMENDATIONS

A Horizontal Exercise Machine (HEM) and an Interim Resistive Excercise Device (IRED) were partially instrumented to measure forces and displacements during exercise. The measurements are to be used to perform kinematic and dynamic analysis on various body members. The instrumentation consists of force and displacement sensors, a data acquisition system, and software. Data acquisition was carried out on individuals participating in a bedrest study (HEM) and on others who followed an exercise regime to test the IRED. The software and hardware performed as planned and data has been stored in disks. The kinematic solution equations have been developed for a bench-press exercise, and all the data exists to develop solutions for the heel raise exercise. A procedure to determine forces has been outlined, but it is indicated that additional sensors are needed and methods beyond Newton-Euler must be applied. These additional methods include optimization and euristic techniques. Once the forces exerted by individual muscles are determined, they will be used as input to a finite element analysis model currently being developed by Dr. Beth A Todd [11] who also works with NASA Colleague Dr. Shackelford.

REFERENCES

1. Oganov, V.S., Grigoriev, A.I., Voronin, L.I., Rakhmanov, A.S., Bakulin, A.V., Schneider, V., LeBlanc, A. "Bone mineral density in cosmonauts after 4.5-6 month long flights aboard Orbital Station Mir". *Aerospace and Environmental Medicine*. 5,6:20-24, 1992.

2. Redfield, R., and Hull, M. L. (1986A). Prediction of pedal forces in bicycling using optimization methods. *J. Biomechanics*, Vol. 19, No. 7, pp. 523-540.

3. Anderson, F. C., Ziegler, J. M., Pandy M. G., and Whalen, R. T. (1993), Numerical computation of optimal controls for large-scale musculoskeletal systems. Advances in Bioengineering, ASME Winter Annual Meeting. BED-Vol. 26, pp. 519-522.

4. Yang, Y., Yahia, L. H., and Feldman, A. G. (1993). A versatile dynamic model of human arm. Advances in Bioengineering, ASME Winter Annual Meeting. BED-Vol. 26, pp. 527-529.

5. Abdel-Rahman, E., and Hefzy, M. S.(1993). Three-Dimensional dynamic modeling of the tibio-femoral joint. Advances in Bioengineering, ASME Winter Annual Meeting. BED-Vol. 26, pp. 315-318.

6. Ericson, M. O., Ekholm, J., Svensson, O., and Nisell, R. (1985). The forces of ankle joint structures during ergometer cycling. *J. of the American Orthopaedic Foot and Ankle Soc.*, Vol. 6, No. 3, pp. 135-142.

7. Harrison, R. N., Lees, A., McCullagh, P. J. J., and Rowe, W. B. (1986). A bioengineering analysis of human muscle and joint forces in the lower limbs during running. *J. of Sports Sciences*, Vol. 4, pp. 201-218.

8. Figueroa, J. Fernando "Loading, electromyograph, and motion during exercise", Final Report, NASA/ASEE Summer Faculty Fellowship Program, Eds: Hyman, W.A. and Goldstein, S.H., 1993, NASA CR-188271, pp. 11-1-11-11.

9. Seireg, A., and Arvikar, R. J. (1973). A mathematical model for evaluation of forces in lower extremities of the musculo-skeletal system. J. Biomechanics, Vol. 6, pp. 313-326.

10. Hoy, M. G., Zajac, F. E., and Gordon, M. E. (1990). A musculoskeletal model of the human lower extremity: the effect of muscle, tendon, and moment arm on the moment-angle relationship of musculotendon actuators at the hip, knee, and ankle. J. Biomechanics, Vol. 23, No. 2, pp. 157-169.

11. Todd, Beth A., "Finite Element Modeling of the Lower Extremities," Final Report, NASA/ASEE Summer Faculty Fellowship Program, Eds: Bannerot, R., 1994, NASA CR-?, pp. 29-1-29-?.

SURVEYING BIOMASS BURNING AND SMOKE PALLS FROM THE NASA-MIR MISSIONS (1996-1998)

Final Report

NASA/ASEE Summer Faculty Fellowship Program - 1998

Johnson Space Center

Prepared by:	Marvin E. Glasser
Academic Rank:	Professor
University & Department:	University of Nebraska at Kearney Department of Physics & Phys. Sci. Kearney, Nebraska 68849

NASA/JSC

Directorate:	Space and Life Sciences
Division:	Earth Science & Solar System Exploration
Office:	Earth Science
JSC Colleague:	Kamlesh Lulla, Ph.D.
Date Submitted:	August 5, 1998
Contract Number	NAG 9-867

Surveying Biomass Burning and Smoke Palls from the NASA-Mir missions (1996-1998)

Kamlesh Lulla and Marvin Glasser*
Office of Earth Sciences
NASA/Johnson Space Center
Houston, Texas 77058

ABSTRACT

A survey of the photography taken by cosmonauts and astronauts from the Mir station during the NASA-Mir mission was undertaken in order to understand the global spatial patterns of biomass burning events and their associated smoke palls. These NASA-Mir photographs provided spatial and temporal profiles of these dynamic and vital environmental phenomena. The information extracted from the photographic data has the potential to be integrated into the current atmospheric and environmental models to refine their predictive capabilities. In this photo-essay, we provide the results of survey of the NASA-Mir documentation of biomass burning and smoke palls.

Background

The Earth's global physical and ecological environments are changing vigorously and rapidly (Botkin et al, 1989). Major scientific concerns about global environmental changes are that they are occurring during man's period of planetary stewardship and that these changes are most likely the result of man-stimulated modifications of Earth's environment. The extrapolated rate of present environmental change is more rapid than any known from the geological record, including the great waves of biological extinction found at some major geological era boundaries (reference).

Global biomass burning is an increasingly important agent of contemporary environmental change. Prior to the 19th-20th centuries, biomass burning in savannas, dry-wet tropical, and Asian lowland dipterocarp forests was both a traditional practice with a relatively low-level biological impact and a natural event of occasionally episodic proportions.

Biomass burning provides a significant input into the overall atmospheric budget of particulate and trace gases. Andrasko et al. (1990) report that global deforestation and

biomass burning contribute perhaps 15% of the current anthropogenic emissions of greenhouse gases. Because of this, the amount of data being collected and published on the scale of tropical biomass burning is increasing (Booth, 1989; Connors et al., 1986; Helfert, 1983-90; Helfert & Lulla, 1989a; 1989b; Pereira & Setzer, 1986). Nevertheless the geographical distribution and temporal frequency of biomass burning in traditional savanna management and in conversion of tropical moist forests to agricultural and grazing uses in South/Southeast Asia, Indonesia, Africa, and Latin America is not well understood. Confidence in modeling atmospheric, hydrologic, and ecological changes connected with large-scale, repetitive, biomass burning is inhibited by a lack of basic geographic, temporal, chemical, and physical data.

In order for global change models to be of predictive and real value, confirmatory data on spatial and temporal patterns of these processes is essential. Our objective in this study is to delineate and map the occurrence of biomass burning and smoke palls observed globally using the Earth-viewing photography from the NASA-Mir missions spanning a time frame from March 1996 to June 1998 (Fig. 1). The determination of the spatial extent of biomass burning and associated smoke palls may help provide confident quantitative determinations of their environmental impact.

NASA-Mir Mission Timelines

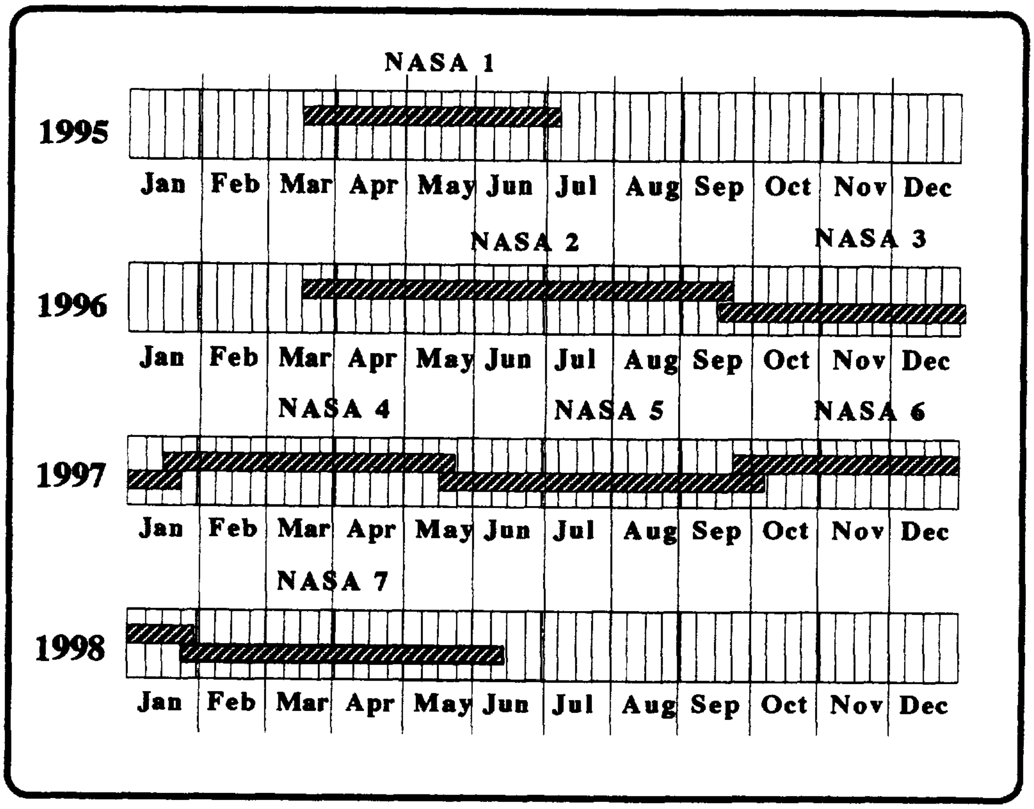

NASA #	Astronaut	Flight Up	Start Date	Flight down	End Date	Days
NASA 1	Thagard	Soyuz TM21	14-Mar-95	STS-71	7-Jul-95	115
NASA 2	Lucid	STS-76	22-Mar-96	STS-79	26-Sept-96	137
NASA 3	Blaha	STS-76	16-Sep-96	STS-81	22-Jan-97	128
NASA 4	Linenger	STS-81	12-Jan-97	STS-84	24-May-97	113
NASA 5	Foale	STS-84	15-May-97	STS-86	6-Oct-97	144
NASA 6	Wolfe	STS-86	25-Sep-97	STS-89	31-Jan-98	128
NASA 7	Thomas	STS-89	22-Jan-98	STS-91	12-June-98	141
					TOTAL	906

Fig. 1 Timelines and designations for the NASA-Mir missions are provided in tabular form. The graphical representation indicates mission timelines to the nearest week.

Documentation of Smoke Palls and Biomass Burning Using the NASA-Mir missions Photography

The documentation of dynamic phenomena of Earth processes observed during manned space flights remains the cornerstone of the NASA-Mir Earth Sciences program, as it was with the earlier Mercury, Gemini, Apollo, Skylab and Space Shuttle Earth observations programs. Details on the camera systems and videographic systems used during these space flights have been addressed in Amsbury & Bremer (1989) and Lulla & Helfert (1989).

Large-scale biomass burning in South Asia, Africa and Madagascar, Indonesia, portions of Australia, and the Americas, has been documented in both unmanned satellite imagery and NASA space photography seasonally and episodically, especially since the late 1970's. Photography from the earlier space flights (Mercury, Gemini, Apollo) is less useful as the early photography is composed of more oblique views proportionally than is characteristic of the Space Shuttle (1981-1990) photography (Helfert et al., 1990; Lulla et al., 1989).

Additionally, based on our earlier review (Lulla, 1990) of all frames in the entire length-of-record (1961-1990) global photography database, we recognize that the large-scale environmental changes in the global tropics of the 1960's were not as generally pronounced or as severe in degree those observable from space in the 1980's.

Database Used in This Study

The NASA-Mir missions have provided American astronauts the most continuous observation opportunity yet available for photography of global environmental changes. During the 115 day NASA 1mission in 1995 and the continuous coverage between March 22, 1996 and June 12, 1998, Fig. 2, the astronauts took more than 22,000 photos, See Evans et al. Of these photos, 460 exhibited smoke plumes and smoke palls characteristic of biomass burning. The period of the Mir missions documented three major wildfire episodes each of which equaled or exceeded the intensity of earlier occurrences of fire recorded for those regions and produced smoke palls on the scale of those observed in the 1980's in the Amazon.

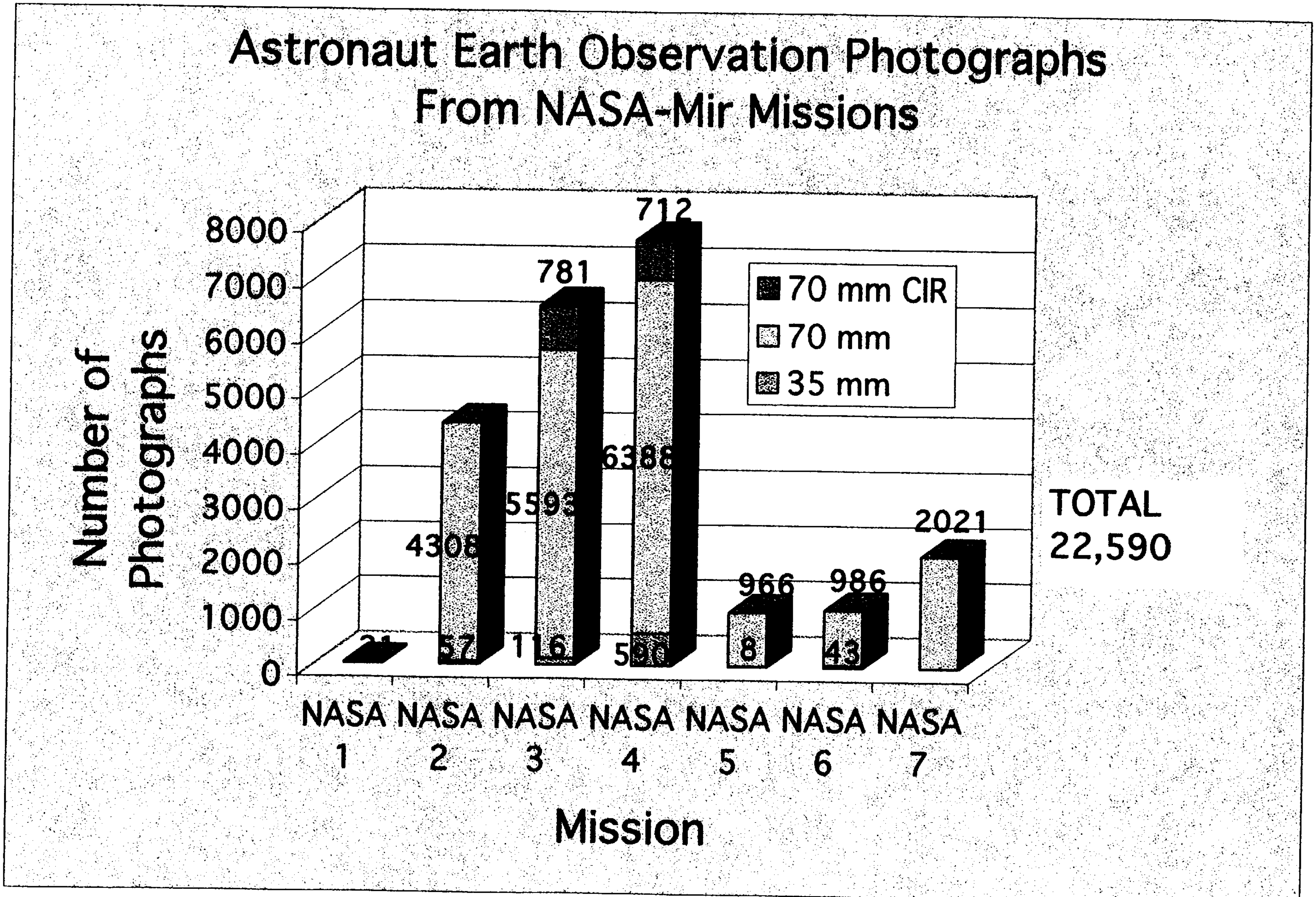

Fig. 2 Distribution of astronaut Earth observation photos taken from the NASA-Mir missions by mission and by film type.

Each photo from the Mir missions was visually scanned and interpreted to determine the presence of smoke. The date and time information from over 450 photos, which were observed to contain smoke from wild fires, were entered into a program that computed the location of the Mir station for that time. Fig. 3 is a map of locations of 433 photographs whose coordinates could be accurately determined. Circles represent clusters of photos of smoke in a given region. Each circle may represent up to 40 photos. The number associated with the individual circles indicates the NASA mission during which the photos were taken. The color code denotes the 3-month period in which the photo was taken, starting with blue for January through March. The extent of the smoke palls associated with the fire episodes in the Indonesia and Mexico-Central America fires have been sketched on the map using TOMS (Total Ozone Mapping Satellite) remote sensing data. Andrew Thomas, who took photos on the NASA 7 mission, remarked on the lack of opportunity to acquire photos of fires burning in the Amazon basin during his missions because of persistent cloud cover.

One significant feature of the map is the known association of wildfires with the spring season in the Northern Hemisphere. Green circles, representing the April through June period and the associated high incidence of smoke in Southern Russia, Northern Mongolia and in Mexico-Central America. Another important feature is the size scale of smoke palls associated with wildfires in Indonesia and Mexico-Central America.

The unique capabilities of astronaut photography to detect smoke from fires have been documented by Glasser and Lulla (1998). The NASA-Mir photographic evidence of smoke includes some particularly notable wildfire episodes that produced smoke palls covering major continental regions. Three record-setting wildfire episodes during the NASA-Mir missions were in Indonesia, Southern Russia- Northern Mongolia and Mexico-Central America. The episodes produced continental scale smoke palls that have major implications for global impact on atmospheric and environmental conditions. The photographic evidence of the smoke palls for each of these cases is presented in the following sections along with information on the factors involved in producing the wildfires and the effects associated with the wildfires.

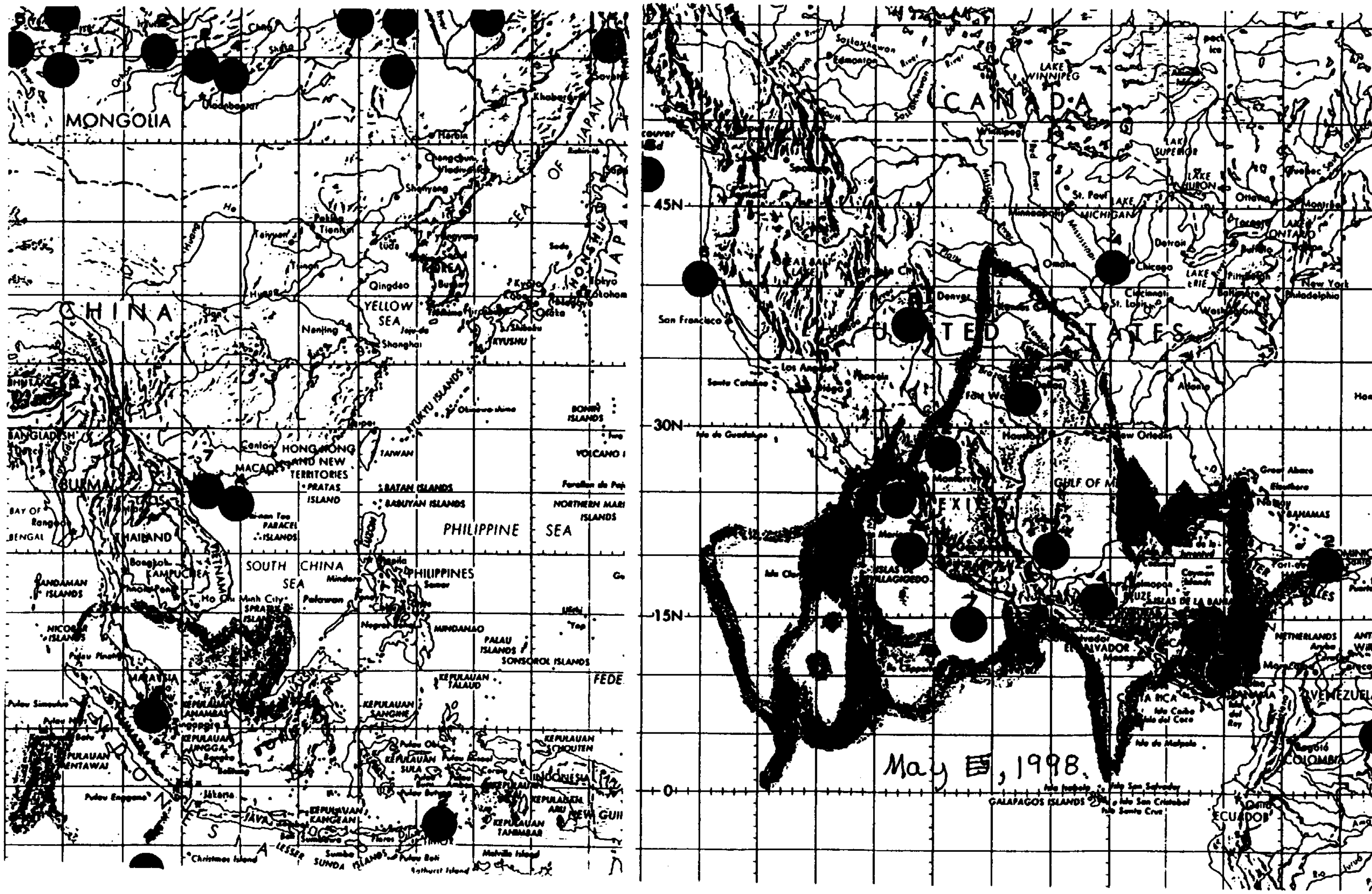

Fig. 3 Global distribution of 433 biomass burning photos from the 22,590 Earth observation photos from the NASA-Mir missions. Each dot represents a cluster of up to 40 photos. The color code represents the time period as indicated and the number above the circles indicates the particular NASA-Mir mission that took the photos. The colored regions are taken from TOMS readings of smoke concentrations in the Indonesia and Mexico-Central America biomass burning episodes in July of 1997 and May of 1998 respectively.

Indonesia

Continental scale smoke palls from wildfires occurred in Indonesia and Southeast Asia starting in the spring of 1997. The fires and associated smoke were identifiable from Satellite imagery such as AVHRR (Advanced Very High Resolution Radaometer), TOMS and from astronaut photography on the Mir station and the Space Shuttle Mission, STS-86. Astronauts aboard these missions reported that they were unable to see the land and ocean surfaces of the Indonesian archipelago and its mainland neighbors such as Malaysia (Fig. 3). Air quality monitors in Singapore and Malaysia recorded record levels of smoke particulate. Burning, whether to clear agricultural land of refuse or forested lands for other uses, has been a way of life in the region for millennia. For many rural people fire is the only tool they have to prepare their land for subsistence crops. For other people it is a way to clear forested land for plantations or other uses. Ever increasing pressures from population growth in the region and special meteorological factors were important factors that distinguished the 1997 fire season from previous fire events. Previously, major wildfires occurred in 1982-83, 1987, 1991 and 1994 in connection with the El Niño weather event associated with the irregular ENSO (El Niño Southern Oscillation) weather cycle.

The El Niño event, which meteorologists had predicted would occur during 1997, was more intense and persistent than usual. It was comparable to the 1982-83 event, which also experienced dramatic inter-regional smoke palls. The El Niño weather cycle characteristically brings drought to the Australiasian region early in the year, but in 1982 and 1997 it persisted into the following year, related to the late onset of the wet season of the monsoon cycle which normally dramatically reduces fire occurrence after September. In Indonesia, the early onset of the dry season and persistence of the drought led to extreme water shortages, crop failures and famine. Slash-and-burn farmers and foresters took advantage of the dry conditions to clear land that had been too wet to be burned successfully during the previous two years. In addition to the usual intentional fires, there were many wildfires that resulted from fires that had gone out of control, escaping into forests and tree plantations. The weakened trade winds and an upper level inversion caused by a persistent high pressure system over the region were contributing factors in producing the unprecedented thick smog layer. Much of the smoke that was produced occurred when water tables dropped and allowed deep smoldering fires to burn in the organic soils and peat-lands of coastal regions in Sumatra and Kalimantan. An astronaut photo from the NASA 4 mission shows the early stages of formation of the smoke pall produced by fires in Sumatra early in the fire episode of Indonesia which grew in intensity from March to September in 1997, Fig. 4.

Fig. 4 This photograph, S86E5995, from the ESC (Electronic Still Camera), was taken by astronauts on the STS086 mission which served as the transition between NASA 5 and NASA 6 on the Mir station. The view is over the west coast of Sumatra on September 27, 1997.

Mexico-Central America

It is clear from Fig. 4 that wildfires ranged widely over Mexico and Central America during the NASA 7 mission. Andrew Thomas, the last American astronaut aboard the Mir station, photographed smoke from these fires. Astronaut photos captured the development of the fires from when they began in April of 1998 through the peak of the episode in May. Factors responsible for these wildfires are very similar to those involved in the fires in Indonesia and other tropical regions undergoing rapid deforestation. Fires in Mexico and Central America are the result of both small and large landowners clearing vegetation and waste materials, and from land being cleared of forests. In the dry conditions of the 1997-1998 El Niño year, fires escaped into forested areas, in wetter years these vegetation types do not usually burn spontaneously. Virtually all fires in this region were related to human activities.

The smoke pall from fires in Mexico-Central America extended into the southern states of the US. Not only are smoke episodes within countries becoming common, but visible transport of smoke across international boundaries has become a global issue as well. Smoke from fires in Mexico and Central America during the 1998 burning season is shown moving over the Gulf of Mexico and Florida from the NASA 7 mission (Fig. 5).

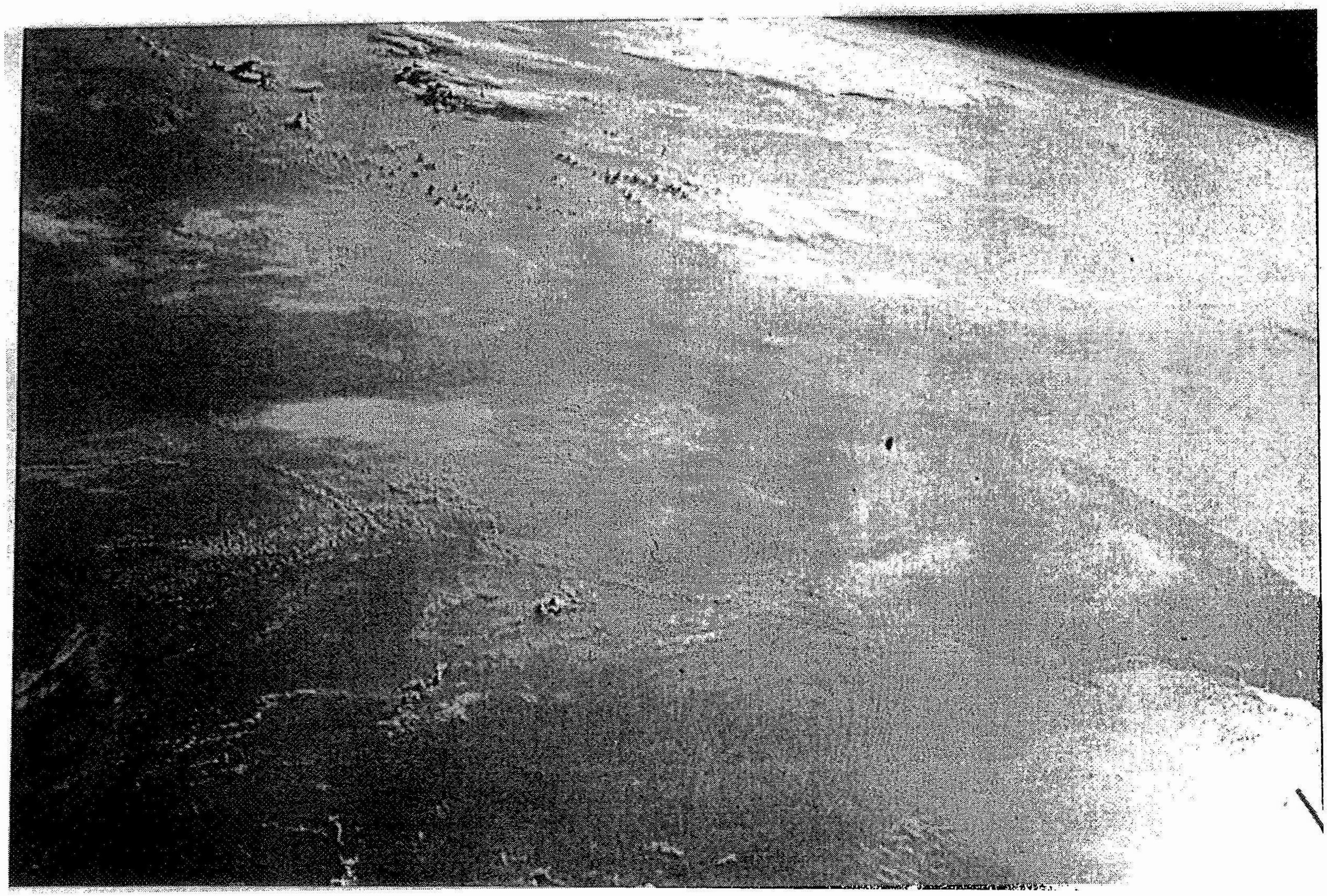

Fig. 5 This photographh, NASA 7-725-022, from the last NASA-Mir mission views the smoke pall over the Gulf of Mexico produced by fires in Mexico-Central America. The view is toward the East where the smoke pall covers the Gulf of Mexico and the peninsula of Florida and extends along the Eastern Atrlantic seaboard. The photo was taken in mid May 1998 near the peak of the export of smoke.

Russia - Mongolia

At the start of the NASA 2 mission in March 1996, the central regions of Asia, including Southern Russia, Northern Mongolia and to a lesser extent, Northeastern China, were experiencing wildfires. Since the spring of 1996 was following the unusually dry winter of 1995-96, the taiga forest zones and steppe (grassland) vegetation were tinder dry going into the usual spring burning season. In combination, these fires produced regional burning on a scale unprecedented in the recollections of fire officials in these areas. Both Russia, Mongolia were hampered in their efforts to suppress wildfires because of the economic constraints. Fig. 6 provides an example of astronaut photographs of smoke from wildfires in Northern Mongolia. NASA-Mir astronauts also observed extensive fires during the burning season in the spring of the following year. Cloud seeding was used in several cases to augment precipitation in an effort to help in suppressing fires. Space technology in the form of NOAA AVHRR imagery was utilized throughout the episode and proved to be invaluable in monitoring the location and progress of fires and in observing the weather conditions that impact on the spread of wildfires. While astronaut photos are valuable in assessing the occurrence and extent of smoke from fires, the information is only available after the mission is completed and the film is returned for processing.

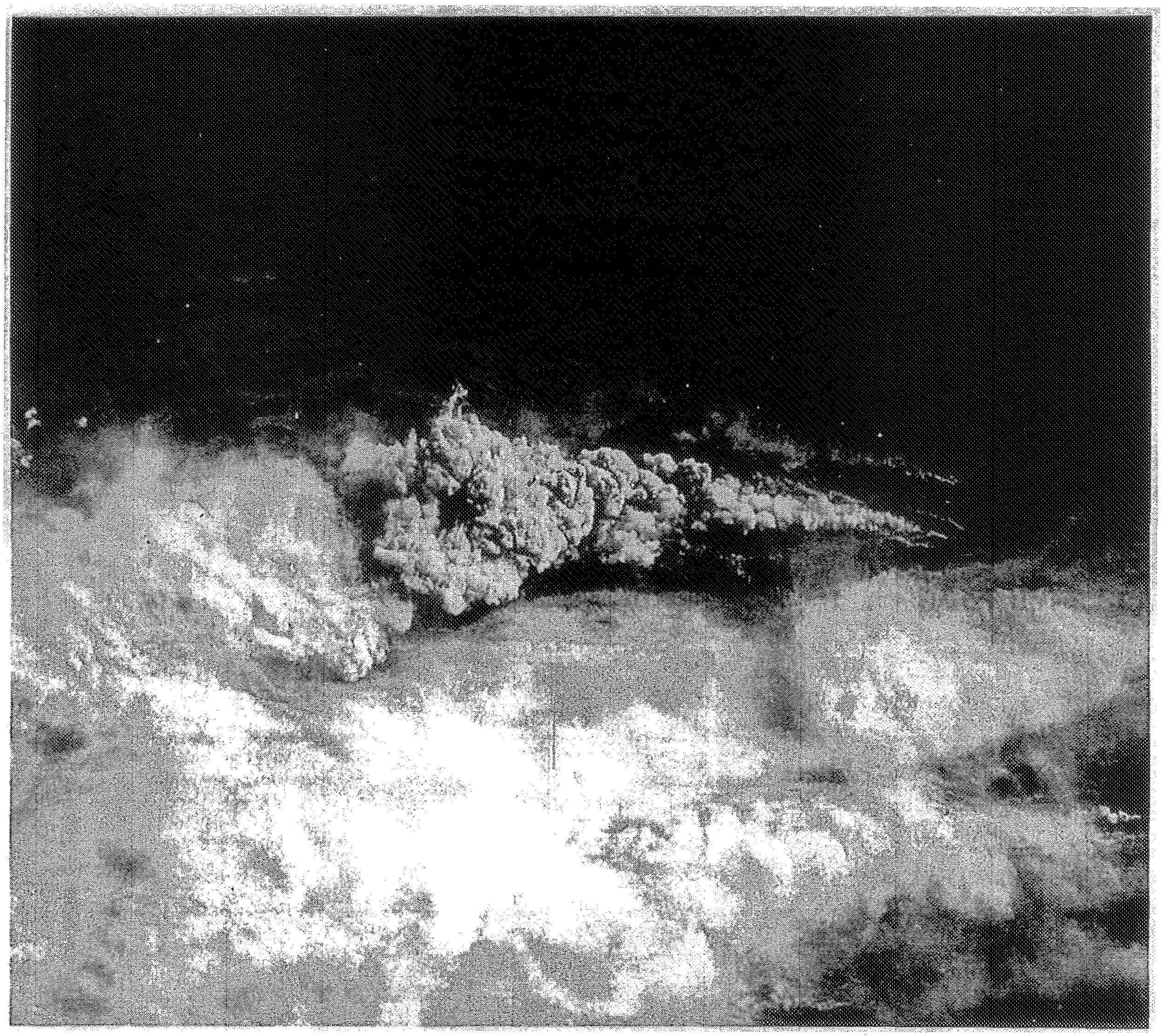

Fig. 6 In April 1996, Mongolian forest fires raged out of control for more than three weeks. This photo, NM21-735-062, shows smoke from several large fires.

Conclusion

Earth photography from the NASA-Mir missions has produced an unprecedented 2-year global survey of biomass burning and the associated smoke palls. The photographic record produced by the NASA-Mir missions captured biomass burning episodes of major proportions in three regions, Indonesia, Russia-Mongolia, and Mexico-Central America. The continental scale smoke palls observed in two of these events extends the range of large scale smoke palls and smoke transport and complements observations by astronauts in the 1980's of smoke palls in the Amazon basin. The importance of these large smoke pall episodes can not be ignored because of the significant impact that the burning and smoke have on human health and safety, transportation, deforestation, biodiversity, erosion, water quality, atmospheric chemistry, and even global climate.

The experience of the NASA-Mir missions points toward the importance of future earth observations on long duration missions by astronauts on the International Space Station (ISS). The presence of a high quality window with greater transmisivity will enhance the range of sensors used to monitor environmental change on the earth. Also, the use of near real-time digital imaging by astronauts on the International Space Station will be an invaluable additional tool for detection of wildfires with the potential to aid in the monitoring and control of biomass burning.

Andrasko, K., D. R. Ahuja, and D. A. Tirpak, 1990. Policy options for managing biomass burning to mitigate global climate change. *Abstr., Chapman Conf on Global Biomass Burning: Atmospheric Climatic and Biospheric Implications.* 19-23 Mar 1990. Williamsburg, Virginia. No page numbers.

Booth, W., 1989. Monitoring the fate of the forests from space. *Science*, 243: 1429-1429.

Botkin, D., M. Caswell, J. Estes, and A. Orio. 1989. *Changing The Global Environment-Perspectives on Human Involvement.* Academic Press, Inc., New York. 495 p.

Glasser, M. E., and Lulla, K. P. 1998. *Evidence of Change in the Boreal Forests Using NASA Astronaut Photography: The Case for International Space Station Earth Observations.* Proceedings, 27th International Symposium on Remote Sensing of Environment. 8-12 Jun 1998. Tromso, Norway. 282-287

Helfert, M., and Lulla, K. P. 1990. Mapping Continental-Scale Biomass Burning and Smoke Palls over the Amazon Basin as Observed from the Space Shuttle. *Photogrammetric Engineering and Remote Sensing*, 56. 1367-1373.

Lulla, K., C. Evans, D. Amsbury, J. Wilkinson, K. Willis, J. Caruana, C. O'Neill, S. Runco, D. McLaughlin, M. Gaunce, M. F. McKay, and M. Trenchard. 1996. *Environmental Geosciences*, 3, 1. 40-44.

(9)
IN-53

COSS LESSON CREATION PROCESS

Final Report

NASA/ASEE Summer Faculty Fellowship Program - 1998

Johnson Space Center

Prepared by: R. Stephen Harper

Academic Rank: Assistant Professor

University & Department: Carroll College
Department of Mathematics, Engineering,
Physics and Computer Science
Helena, Montana 59625

NASA/JSC

Directorate: Mission Operations Directorate

Division: Space Flight Training Division

JSC Colleague: Frank E. Hughes

Date Submitted: August 6, 1998

Grant Number: NAG 9-867

ABSTRACT

COSS (Crew On-Orbit System Support) is changing. Designed as computer based in-flight refresher training, it is getting good reviews and the demands on the product can be expected to increase. Last year, the lessons were written using Authorware, which had a number of limitations. The most important one was that the navigation and the layout functions were both in one package that was not easy to learn. The lesson creator had to be good at both programming and design. There were also a number of other problems, as detailed in my report last year.

This year the COSS unit made the switch to embrace modularity. The navigation function is handled by a player that was custom-written using Delphi. The layout pages are now standard HTML files that can be created using any number of products. This new system gives new flexibility and unties the process from one product (and one company). The player can be re-written by a programmer without affecting the lesson pages. It is also now possible for anybody with a word-processor to make part of the HTML lesson pages and to use many of the new commercially available tools that are being designed for web pages.

This summer I created a computer-based training (CBT) lesson on the IBM ThinkPad 760 ED and 760XD laptop computers that should fly on the International Space Station. I also examined the COSS system, the new player and the other new software products.

INTRODUCTION

COSS (Crew On-Orbit System Support) is maturing. It has already taken training further that it's ever gone before – literally. Astronaut training traditionally has been mostly preflight at designated sites with specialized facilities. This has several disadvantages when the astronauts live in different countries and when longer space missions dictate that training happens months in advance of the actual deployment. Starting with Shannon Lucid, NASA has developed and tested COSS and has sent it with each astronaut visitor aboard the Mir. A laptop computer uses a set of specially prepared CDs and videotapes. The on-board training software is getting rave reviews, and the demand for it can be expected to increase.

Last summer, I developed a computer-based training (CBT) refresher course for an experiment on Interferometer Protein Crystal Growth. (This flight product was sent to the Mir last fall as part of LDM6.) I then analyzed the advantages/shortcomings of Authorware (the production software) and the template created and used by COSS for creating computer courses.

Authorware, while it works well, has several limitations. While the text, graphics and video are developed and refined using any of a number of commercial products, the navigation and the layout of the pages themselves has to be created in Authorware. Also, changing the layout is difficult to do. In other words, the player function and the layout function are tied together in one product. Furthermore, some expertise is required to master Authorware. In reality, a developer has to be a programmer and a design artist rolled into one. Being tied to one product is not a good idea in a rapidly changing computer world.

This year the COSS unit made the switch to modularity. The new driver, called *ASAP Player*, is a custom made player (created using Delphi) that only has to be created once. The layout pages are now standard HTML files -- the files that are used on the Internet and created using any of the many HTML creation tools available.

Now people in the lesson production team can use the software tools that they prefer without impacting the others. Designer skills, not computer skills, can now be paramount for lesson production.

This summer I created a CBT lesson on the IBM ThinkPad 760ED and 760XD laptop computers that should fly on the International Space Station. I also examined the COSS system, the *ASAP Player*, and the other new software -- Flash and Dreamweaver.

The new COSS system works much better and has much more flexibility. It makes the move toward needing more designer skills and less programmer skills. It also moves toward making it possible for the PI to create text and graphics that can be used directly in lessons.

LAST YEAR: AUTHORWARE

Authorware, a standard for computer pages authoring, is very good for putting text and pictures together on a screen along with digital video. If one wants to create a linear book on a computer screen, it is the tool for the job. However, if one wants to be

interactive, it gets more difficult. Problems include: skipping around, video control, menus, optional pages, numbering pages and navigation.

Since Authorware is a difficult product for a beginner to use, the COSS lab has created a good template. The Authorware template was the key to the whole computer based training (CBT) process. The template made lesson creation a lot easier by hiding a lot from the programmer. It also made the "look and feel" similar in various COSS lessons. There are still a number of problems (as noted in my report last year) for a new-comer using the template.

To make it readily useable, the Authorware template needed several fixed structures. For example, the template fixed the names of the sections for each lesson -- "Overview", "Hardware", "Setup", "Nominal operations", "video", etc. Unfortunately, not all of those topics were applicable for every lesson. (Andy Thomas said in one lesson he got "very upset" when he saw the video section, turned there and there were no videos available for that lesson.)

The template also required consistent placement of navigation icons, page numbers, and titles. The price was flexibility.

Most of the problems are inherent in Authorware because of the absence of a usable array setup for titles and variables. Much must therefore be hardcoded. This affected section and page titles which had to copied into 5 different places. Lack of arrays impacted: frame and icon titles for the section, icon titles for the pages, sections listed on the Sections Menu drop down menu list, check marks in front of the items in this list, a sections list created after the right mouse button is pushed, check marks in front of the items in that list, a content map that lists all the sections and pages, section names in hot text, arrows in front of section names if a user has visited that section, and page names in hot text, to mention a few. In fact almost all the programmer's variables in the template (variables that have to be individually changed depending on the Frame) could be solved by a page array.

THIS YEAR: MODULARITY

COSS gets positive feedback from the astronauts who use the lessons, but the expectations are growing. To meet demand, the hardware, software and processes must keep changing.

Since work on many of the Stealth Lab lessons starts only 3 months before launch, there are a lot of last minute activities and last minute changes. It becomes even more imperative that the computer products not only be easily changed but even modifiable by a person other than the original creator. The software tools are critical.

This year the COSS unit made the switch to modularity. The new CBT runtime engine is a custom made player (created using Delphi) called *ASAP Player* that only has to be created once. The new pages, the order of the pages and the page structure is now easy to modify separately from the player software.

The improvement is both in functionality (*ASAP Player* has some options that Authorware doesn't) and in modularity. Modularity is important because the technology changes so fast. The custom-built ASAP lesson player links each page to an HTML file, so the player software is now separate from the page creation software.

It is now possible to change out any or all the creation tools:

- the lesson player (the custom written Delphi player)
- HTML page development software (such as Dream Weaver or almost any word processor these days)
- ActiveX tools (such as Active Movie)
- Video capture software (such as VidCapture)
- Video editing and compressing software (such as Premiere)
- the graphic generator (such as PaintShop)
- Photo editing software (such as Photoshop)
- animation or movie creation software (such as Director or Flash)
- scanning software (such as Deskscan)

This allows progress in each area.

With the new modular system, people can still create using the old products and learn the new ones when time is available. For example, people who know Director well can still use it to create animation, while others are using Flash. Since my lesson on the 760ED/XD required 8 different software products, this is no small consideration.

Last year Authorware demanded dual personality programmer/designers. This year a programmer may still modify the *ASAP Player* occasionally, but most of the work will be done by page designers. In other words, you can now get good designers and, without having to train them in the computer programming, let them use their designer skills right away.

COSS PROCESS

Learning the lesson's software components (Photoshop, Premier, Dreamweaver, etc.) takes a while, and it is easy to focus on the learning and forget the reason for it: to create a lesson. Here are some helpful pieces to learn to create a CBT for the first time:

- I personally like an overview of the whole process – not just the computer pieces, but the lesson progression and "who keeps the latest info" about the experiment and how do I find out in a timely manner.
- There are a few "fixed" rules to help the lesson player. In the same directory as the player (*ASAP Player.exe*), you create a sub-directory called *DATA* that holds all the html, graphic and video files. You also need a sub-sub-directory called *ASAP Data* that holds files the player needs. Inside the *ASAP Data* directory, you will need to change these 3 files to specifically reflect your lesson: *Startscreen.htm*, *Glossary2* and *Credits.rtf*. In the same directory as the player (outside *Data* directory), you need 2 files: *MAP.SAP* gives the section and page titles, while *ASAP.INI* gives directions on where to go when the user clicks on the page title. You can edit these files with Notepad or any word processor that creates text-only files.
- The text in a lesson is nice. The pictures are even more important and the video is crucial. Therefore, having the lesson creator be present for the video shoot is critical. In fact, creating a shoot list ahead of time is important. When possible, each scene should have a pan in to see details and give an idea of their general location. I think it would be very helpful to video tape a 30

second overview of all the equipment and pieces, and a 30 second overview of all the procedures.

- Observe the astronaut training to see which parts are particularly difficult and need underscoring in the COSS lesson.
- This year I knew that video could be created solely for my COSS lesson. This made it much easier. Having the intention to create 15 second video chunks shaped the video session. In particular, it allowed recording whole small scenes (sound and motion together) and repeating from different angles with all the sound recorded as "15 second sound bites". For the most part, each entire scene was used without internal editing. Occasionally, the unedited video from one take was put together with the unedited sound from another take. The time savings from not needing to edit individual sentences more than repaid the extra shooting time.

Photos are still custom made for a particular page and a particular size. As the variety of available computers grows, there is room for a good tool that can deal with the many pictures in a handy way. This could be similar to the treatment of text in HTML that is now scalable using relative terms instead of always being a pre-determined absolute size.

Currently, COSS creates computer lessons from material prepared by an experiment's Principle Investigator (or the trainers). The PI completes all the materials and communicates the important parts to put in the lesson. The new Delphi-based template makes it possible for PIs to create their own HTML files with text and pictures, without having to become computer experts. Now the COSS lab can edit and add video, save time and end up with a better product.

DELPHI-CREATED LESSON PLAYER

The COSS-created custom ASAP lesson Player has a number of very nice features. It acts like the WWW (World Wide Web) so people familiar with that technology are comfortable. It also makes it easier to put out lessons over the web.

Navigation is more straight forward -- the front and back arrows are not in the way, and the user can use them to jump from page to page. On successive clicks of the arrow, if the last page in a section is being read, it closes the section (removes the page list), then opens the next section (displays that page list), then opens the first page (links to the HTML file for that page). Mostly, users can use the section listing that is always present to figure out where they are in the lesson and what comes next.

The player puts a red dot in front of the page currently being displayed, and puts blue dots in front of all pages that have been visited. This is a nice feature.

There is a second lesson player for a quality-check Review. This does not affect the lesson and only makes a couple of changes in the session. It puts the words "For Review Only" in red letters at the bottom left of the screen and also adds a comment choice into the Tools menu. This very nice feature lets a lesson reviewer make comments (in a separate file) about the lesson. The reviewer can also select and drag text from the lesson pages and make suggested changes to the text. The comment file can be sent to the

lesson creator. The author can look at the suggestions and cut and paste changes into the lesson itself.

Many of the problems with Authorware have disappeared with the modularization of the navigation function and the layout function. For example, the section names are now easily changed. There need not be a video section if the lesson does not have video. In fact, the author picks all the section names. Navigation is simplified and the author can put in jumps anywhere on the page. The player mostly keeps track of the current location so that page numbers are not needed (although the author can put them in). Page titles can go anywhere or be left off entirely. Most importantly, with HTML frames, the page can be divided, subdivided or re-united depending on the material being presented and the user's choices.

However, there are a few nuisances.

The 3 files inside the *ASAP Player* directory that the lesson creator must modify could be put in a separate directory (the "*Change Me*" folder) or at least re-named so that they appear at the beginning of the directory listing. The file *credits* could be made into an HTML file instead of an RTF (Rich Text Format) file, for consistency with the other pages. This also allows inserting movies into the credits.

While the lesson section listing is helpful for navigation, it does have a few annoying problems. Some sections have only one page. It would be nice if clicking on the section title automatically opened the only page.

When a person double clicks on the section title, the page list displays. If the double click is on the plus sign in front of the section title, it appears that nothing happens. (Actually the plus sign turns to a minus sign, the page list displays and then immediately disappears as the minus sign turns back into a plus sign.) There is a similar behavior problem in Windows Explorer, but it makes more sense to simply display the page list.

There are two arrows pointing left ("back" in our culture). The straight left arrow navigates pages, while the curvy one over the word "Back" returns to the previous page visited. The tool tip for the former says "Go to previous page" and for the latter "Go back". It might make more sense to say "Go back in History" or "Go back in time" or "Return to whence you came".

There is a help menu but the "How to use this lesson" section has not been written yet. It should include instructions for all the tools such as e-mail, Find, Glossary, Gouge Sheet (take notes), Print Screen and Comments.

Help should also have notes on re-sizing the display and the problems that it may cause. (The user can always stop the lesson, exit and re-start with the pre-set size.) Other topics should include how to close (exit), how to use video controls, how to use the section list (with the strange box holding the + or - sign), how to zoom with the right mouse button, and the presence of the wonderful blue and red circles.

Before displaying the lesson, the special Review player might start right away with an explanation about the Comment section, how to select and drag text and even how to mail the comment file to the reviewer.

Likewise, the regular player's startup screen itself could have a button for explanations for beginners.

There is no red nor blue dot when a user follows a link from inside a page and jumps to a different section without using the player 's section listing for navigation.

Print Screen is a nice option, but it would also be nice to have a Print This Whole Page option.

Some improvements to the player could include the ability to keep track of what was covered in a previous session. (Maybe a black dot could note pages visited in prior times.) It could even figure a % of the total pages that have been visited. Some lesson author may want to create some on-line testing. This section may want to use the history feature to correlate questions missed on the test with unread sections.

DREAMWEAVER

After creating the lesson text in Microsoft Word and using the *Save As HTML* option, I used Dreamweaver to set up the frames for the page that incorporated the text. Dreamweaver has several nice features.

Creating HTML frames lets one easily split up the page (& rejoin when necessary) to provide flexibility to mix and match these pieces:

- title sections (with buttons to jump to certain anchors on the page)
- graphics sections (with buttons to change the picture)
- video sections
- text sections

Dreamweaver has video options to play video in both Explorer and Netscape, and makes jumping (links) to another page very easy. It even has a nice spellchecker.

Dreamweaver readily links in Flash animation files. Flash saves space using vector graphics instead of bit map photos and gives the user "Zoom in" capabilities where the hot areas -- areas that are linked to other pages -- are resized appropriately.

Flash does have some problems (e.g. some animation does not work until a final product is created, "tween" creates nice motion but is awkward to use, and the mask does not work in draft mode), but it is a nice animation product.

However, Dreamweaver could be more helpful in reminding the user of the difference between frames and framesets.

Like most HTML products, Dreamweaver wants a picture with a specified size, resolution, number of colors, etc. It would be nice to be able to adjust that on the fly. The designer must set the text and pictures on the page but since they are absolute sizes, the user can resize the window -- which destroys the spacing since the graphics and text don't resize. Fortunately, most users use full screen rendering and don't adjust the window size. It would be nice if, when the user changes the window size, the text and the titles were still proportionate. Now HTML, and not just hardware, creates display problems.

Since the Delphi lesson player is set to 800 by 600 to fit a lap top computer screen, I would open the Delphi player, then on top of it place the Dreamweaver window for creating the lesson. If I resized the Dreamweaver window to exactly match the size of the player window, I could open lesson pages that were the same size the reader would get. This was very helpful for placement of text and pictures and seeing how much would fit on a screen.

Creating Dreamweaver templates allowed me to use a standard layout that already had frames named. I had one template with 3 frames named *Title*, *Text* and *Video* with some of the basics filled in -- including place holder information such as title, pre-set

jump-to-anchor buttons and video controls. This made frame reference names easy to remember and helped me have consistent frame borders and fonts for titles and text.

FUTURE

With the Delphi lesson player, COSS has made a major improvement in its CBT system.

Since Principle Investigators are not always physically at JSC, it is possible for idea originators to create their own training lessons for distribution using the World Wide Web using standard word-processing and embedded pictures (all saved as an HTML files).

Many new components are being built for the Internet by the commercial community that can be immediately integrated into the COSS process. For example, to make the Delphi player run on any machine instead of just Windows machines with Explorer as the Browser, the player can be re-written in Java and nothing has to be done to any other parts of the lessons. (Or, maybe Delphi will offer the option to recompile in Java.) This will become more important as more people take advantage of computer based training on diverse computers.

The new products that come out will undoubtedly have a focus to be useable on the Web. That makes the new COSS system a direct beneficiary of these improvements. In particular, as new Virtual Environment (VE) products come out for low-end machines, it now becomes possible for high-end PCs to use these products. Previously, except for very simple renderings, VE was the domain of very expensive computers.

Also, this new modularity makes it possible for the COSS lab to build small tools to help with current needs -- without having to build a huge integrated project that has all the tools that they need. There are a number of tools that would be helpful.

For example, the lab needs a way to play several different videos one after another without the user having to do anything. In the 760ED/XD lesson, several repair sections demonstrated opening the computer and removing the CD drive. Each page then had a unique video scene and most of them followed with a demonstration of replacing the CD drive. The video portions became mix and match. HTML does not handle this scenario well. Currently, one must program a Java script to deal with these choices. A Java tool that would create HTML pages with Java script embedded would be nice.

Creating tools can be a small-size project involving writing a small driver in Delphi or Java. There could be a set of these smaller tools created and used as needed. As soon as there is a commercial available product that is better than one of these tools, the lab can easily switch, will not have to re-write any lesson, and has lost very little in terms of investment time into the now-obsolete tool.

An installation/registration tool could install the player, check the products needed (browser, ActiveX, Flash driver, etc.) and down load and register them.

Eventually arrays, a real problem in Authorware, will be needed in the new process as lessons get very long and developers need to avoid the problem of individually naming hundreds of HTML pages. Delphi can deal with arrays, and so can Java. Some more tools to handle these problems could be in the offing.

COSS currently is designed for building "refresher" courses. The new WWW capabilities open up many possibilities for world wide use in lots of training and testing roles for a relatively cheap cost.

Now all the parts of the lesson building are modular. Even more important, they are lined up to take advantage of current commercial development thrusts.

(10)

IN-54

SAFETY ANALYSIS OF SOYBEAN PROCESSING FOR ADVANCED LIFE SUPPORT

Final Report

NASA/ASEE Summer Faculty Fellowship Program - 1998

Johnson Space Center

Prepared by:	Dawn L. Hentges
Academic Rank:	Assistant Professor
University & Department:	Bowling Green State University Department of Family and Consumer Sciences Bowling Green, Ohio 43403

NASA/JSC

Directorate:	Space and Life Sciences
Division:	Flight Crew Support
Branch:	Flight Systems
JSC Colleague:	Charles T. Bourland, Ph.D
Date Submitted:	August 6, 1998
Grant Number:	NAG9-867

ABSTRACT

Soybeans (cv. Hoyt) is one of the crops planned for food production within the Advanced Life Support System Integration Testbed (ALSSIT), a proposed habitat simulation for long duration lunar/Mars missions. Soybeans may be processed into a variety of food products, including soymilk, tofu, and tempeh. Due to the closed environmental system and importance of crew health maintenance, food safety is a primary concern on long duration space missions. Identification of the food safety hazards and critical control points associated with the closed ALSSIT system is essential for the development of safe food processing techniques and equipment. A Hazard Analysis Critical Control Point (HACCP) model was developed to reflect proposed production and processing protocols for ALSSIT soybeans. Soybean processing was placed in the type III risk category. During the processing of ALSSIT-grown soybeans, critical control points were identified to control microbiological hazards, particularly mycotoxins, and chemical hazards from antinutrients. Critical limits were suggested at each CCP. Food safety recommendations regarding the hazards and risks associated with growing, harvesting, and processing soybeans; biomass management; and use of multifunctional equipment were made in consideration of the limitations and restraints of the closed ALSSIT.

INTRODUCTION

In order to support NASA's goal of continued exploration and future colonization of the moon and Mars, a food system is being developed to provide Advanced Life Support (ALS) for long duration missions. A proposed habitat simulation for long duration lunar/Mars missions is the Advanced Life Support System Integration Testbed (ALSSIT). This structure has interconnecting modules in which all life support systems (air, water, waste, and food) will be recycled. Plants are an integral part of this closed environment. The proposed ALSSIT configuration includes two biomass production chambers, a life support chamber, a habitation chamber, a laboratory chamber, an utilities distribution module, an airlock, a transhabitation module, and an interconnecting tunnel. Because of weight/volume restrictions and prolonged periods between earth resupply shipments, some of the foods consumed on these missions are being proposed to be grown, processed, and prepared in space.

Hazard Analysis Critical Control Point

Hazard Analysis Critical Control Point (HACCP) is a system designed to ensure safety of the food supply from production through consumption. Biological, physical, and chemical hazards associated with growing, harvesting, processing, distribution, marketing, preparation, and consumption are identified and assessed for severity and degree of risk. Critical control points (CCP) are identified and monitored in the process where loss of control could result in an unacceptable food safety risk. When noncompliance of critical limits at a CCP occurs, adjustments are made to maintain control. Effective records must be kept, and the HACCP system vertified to ensure that it is working correctly. HACCP does not apply to food quality, fraud, or aesthetics unless these affect food safety.

Objectives

Safety analyses, using a Hazard Analysis Critical Control Point (HACCP) approach, were conducted for ALS soybean processing. The objectives of this project were to:

1. Develop food processing flow diagrams.
2. Assess hazards and risk associated with growing, harvesting, and processing soybeans; biomass management; and use of multifunctional equipment in the closed system.
3. Determine critical control points (CCP) required to control the identified hazards.
4. Establish critical limits that must be met at each identified CCP.

METHODS

Food processing flow diagrams were designed by reviewing accepted industry and proposed ALS food processing protocols. Hazard analysis and establishment of critical control points and critical limits were accomplished by conducting a comprehensive literature search and communication with scientists in the fields of agriculture, food science, microbiology, water recycling, and waste management.

FOOD SAFETY ANALYSIS

Description Of The Food

Soybeans (*Glycine max* L. cv. Hoyt) is one of the crops proposed to be grown as part of an Advanced Life Support of long duration missions. The cropping system for ALSSIT-produced soybeans is being developed at the NASA Kennedy Space Center and Utah State University. In the Biomass Production Chamber, soybeans will be grown

using recirculating nutrient (hydroponic) film culture with controlled pH, electrical conductivity, temperature, humidity, and atmospheric carbon dioxide partial pressures (Wheeler et al, 1996). The soybeans will be harvested at 70 days maturity (Bugbee, 1998). Inedible biomass will be directed to the waste recovery system. Since quantities of each crop produced will be sufficient to meet menu needs during the subsequent crop growing period, the amount of storage space required for raw crops and processed foods will be minimal. During this short storage period utilizing a first in-first out (FIFO) rotational system, the potential for growth of pathogenic and spoilage microorganisms should be minimized if proper storage conditions are maintained.

Soybeans will primarily be processed into soymilk, tofu, and tempeh for the ALSSIT diet. Soymilk is a water extract of soybeans that can be used in the ALSSIT as a beverage and food ingredient. Tofu is a soybean curd made from soymilk. It may be eaten with or without further heat processing. Tempeh is a mold fermentation product of whole soybeans. Heat processing of tempeh, customary before consumption, will reduce or eliminate contaminating pathogens. Okara (soymilk residue) and soy hulls are byproducts of soybean processing that can be dried, finely ground, and added to food products for nutritional supplementation.

Soybean processing produces a large amount of whey and waste water. During a recent ALSSIT protype soymilk machine test, the water used to clean the soybeans contained 36.5 mg/L inorganic carbon, 70.5 mg/L total organic carbon, and 452.5 mg/L total solids (Vodovotz et al, 1998). Guu et al (1997) reported that soybean soaking water contains about 0.08% (w/w) crude proteins, 0.2% (w/w) carbohydrates, and up to 10,000 ppm chemical oxygen demand (COD). This wash and soaking water must be treated before it can be reused as drinking water. Soluble peptides, glucose, fructose, oligosaccharides, and ash could be obtained by concentrating the waste water using nanofiltration or reverse osmosis (Guu et al, 1997; Matsubara et al, 1996).

Identifying The Intended Use And Consumers Of The Food

Integration of soybeans into the food system will reduce the dependency on resupply creating greater autonomy for the ALSSIT. In the primarily crop-based diet, soymilk will be used as a beverage and ingredient for food preparation. Tofu and tempeh will provide a good source of protein, vitamins, and minerals and may be used as a meat substitute. Due to the closed environmental system and importance of crew health maintenance, food safety is a primary concern. A nominal four person crew is planned for Mars missions. Although automated as much as possible, the crew will be responsible for the production, harvesting, processing, storage, and preparation of food.

Verifying The Process Flow Diagram In The Operation It Is Meant To Represent.

The processing protocols for the soybean crop system in the ALSSIT are currently being developed. Multifunctional and specific use equipment are being designed to operate under the minimal space and energy requirements of the chamber, the partial gravity environment on Mars, to facilitate cleaning and sanitation, ease of maintenance, and safety. Although storage parameters for the soybeans and processed products were primarily designed to reduce or prevent pathogenic microorganism growth, these conditions should also decrease spoilage or quality changes. The food safety analysis, developed as part of this project, will have to be reviewed and modified to reflect the actual processes once established.

To maximize space utilization of the interconnecting tunnel, multifunctional equipment will be used for processing various crops into food products and ingredients. The equipment should be cleaned and sanitized between crops to prevent cross-contamination. Besides concerns about microbial contaminants, some food components elicit sensitivity reactions in certain individuals, e.g. soybean allergy and gluten intolerance. To prevent development of sensitivies to food product dust and mold spores, masks should be worn during harvest through milling processing steps. Although most foods processed and prepared in the ALSSIT will be heated before consumption, care should be taken to segregate raw crop operations from later stages of food processing. The equipment arrangement should facilitate the processing flow diagrams which are described later and increase work efficiency

HAZARDS OF SOYBEAN PROCESSING

Biological Hazards

Although a few bacteria and yeasts are present, the predominant microflora on soybeans are molds, such as *Aspergillus*, *Rhizopus*, *Penicillium*, *Alternaria*, *Cladosporium*, *Helminthosporium*, *Mucor*, and *Fusarium*.. Some mold species can produce mycotoxins which are hightly toxic and potentially carcinogenic. Possible mycotoxins that may be found on soybeans include: aflatoxin, sterigmatocystin, penicillic acid, zearalenone, deoxynivalenol (DON), diacetoxyscirpenol (DAS), T-2 toxin, ochratoxin, patulin, itrinin, griseofulvin, alternariol, altenuene, and altertoxin (Bullerman, 1979; Jacobsen et al, 1995). Since mycotoxins are secondary fungal metabolites, the presence of toxinogenic molds does not automatically mean that mycotoxins are present. Since mycotoxins are quite stable to heat and other food processing procedures, it is crucial to prevent their formation. Moisture and temperature are important factors affecting mycotoxin production. In general, mycotoxins are not produced on soybeans below 13.5-14.5% moisture (Moorman, 1990). The minimum water activity necessary for aflatoxin B_1 production in soybeans is 0.865 (Fernandez Pinto et al, 1991). The optimum temperature for aflatoxin B_1 and ochratoxin production in soybeans is 25 C (Fernandez Pinto et al, 1991) and 30 C (Jay, 1992), respectively. If mycotoxins exceed the FDA Defect Action Level of 20 ppb aflatoxin, the soybeans should be destroyed and care taken during biomass recovery to prevent aflatoxin contamination of the environment, or the contaminated soybeans should be treated with ammonia, methylamine, sodium hydroxide, sodium bisulfite, UV radiation, hydrogen peroxide, or ozone to inactivate the aflatoxin (Diener, 1981; Goldblatt, 1968; Jay, 1992; Maeba et al, 1988). Genetic breeding can produce seeds that have barriers to mold which would significantly reduce mycotoxin contamination.

Soymilk and tofu are rich in nutrients and provide an excellent growth medium for microorganisms. Heat treatment of the bean slurry effectively reduces vegetative bacterial cells but does not sterilize the product. For example, soybeans soaked over night with 10^6 organisms/g decreased to less than 10^2/g after heating (Szabo et al, 1989). Refrigeration of soymilk is necessary to prevent growth of psychrotropic bacteria, such as *Listeria*, *Yersinia*, and *Escherichia coli*, present due to cross-contamination from equipment and handling. Even though the cook step in tofu production also reduces microorganisms, poor sanitation and not following good manufacturing practices increases the microbial count in the final product. Microbial testing of 153 tofu samples in Canada found that more than 45% were contaminated with $> 10^6$ psychrotrophs, more than 35% with $> 10^3$ coliforms, and also contaminated with *Staphyloccus aureus* , and *Yersinia enterocolitica* (Szabo et al, 1989). In 1982, 87 people developed yersiniosis in Seattle, Washington after eating tofu (Aulisio et al, 1983).

During soaking of the dehulled soybeans for tempeh production, growth of resident lactic acid bacteria lowers the pH of the soaking water. The pH is not low enough, however, to prevent growth of pathogenic microorganisms (Ashenafi and Busse, 1989; Hachmeister and Fung, 1993). Enterbacteriaceae, *S. aureus* , total aerobic bacteria, lactic acid bacteria, coliforms and yeasts can grow in naturally acidified soak water during tempeh production (Ashenafi and Busse, 1989, 1991). Addition of acid, such as acetic or lactic acids, to the soaking water will lower the pH (pH 4.0-5.0) sufficiently to inhibit pathogen growth; however, a pH below pH 3.5 will inhibit the growth of the *Rhizopus* inoculum (Liu, 1997). During incubation, fungal fermentation raises the pH to 6-7 permitting growth of contaminating microorganisms (Hachmeister and Fung, 1993). After boiling, the microbiological population of tempeh depends largely on sanitation and handling procedures occurring in subsequent processing steps. *Bacillus cereus*, *S. aureus*, *Clostridium botulinum*, *Listeria*, *Salmonella*, and *E. coli* have been isolated in tempeh (Ashenafi, 1991; Ashenafi and Busse, 1991; Samson et al, 1987; Tanaka et al, 1985). "Typically tempeh is considered relatively safe because of *Rhizopus* properties, the presence of lactic acid bacteria, the incubation under microaerobic conditions, and the customary heating prior to consumption" (Hachmeister and Fung, 1993).

Chemical Hazards

Soybeans contain antinutritional factors, such as trypsin inhibitors, lectins, goitrogens, and phytate, which may cause health concerns and decrease their biological value. Lectins, also called heamagglutinin, occur naturally at high levels in all legume seeds. It can destroy the epithelia of the gastrointestinal tract; interfere with cell mitosis; damage kidney, liver, and heart; and agglutinate red blood cells. Lectins can be reduced by moist heat (Jones, 1992; Paredes-Lopez and Harry, 1989). Goitrogens, also present in soybeans, may cause thyroid cancer and goiter by interfering with iodine metabolism and thyroid function. Cooking and freezing can reduce the amount of goitrogens in soybeans (Jones, 1992). The health effects of goitrogen are also decreased when there is an adequate supply of iodine in the diet (Jones, 1992). Phytates, located in the cotyledons, decrease protein solubility and bind minerals, such as calcium, magnesium, iron, and zinc, reducing their bioavailability. This creates particular concern in the ALSSIT due to the limited diet. Increased phytase activity during soaking and fermentation reduces the phytate content in soybeans.

Soybeans contain two trypsin inhibitors, Bowman-Birk and Kunitz, which can cause pancreatic hypertrophy, hyperplasia, adenoma, and growth depression. Whole soybeans and tofu contain 16.7-27.2 mg/g and 0.6 mg/g trypsin inhibitors, respectively (Anderson and Wolf, 1995). During soybean processing, trypsin inhibitors are reduced by soaking, dehulling, cooking, and fermenting (Paredes-Lopez and Harry, 1989). To maximize the protein efficiency ratio, thermal processing of soymilk at 100 C for 14 minutes or 30 minutes should be sufficient to inactivate 80% and 90% of the trypsin inhibitors, respectfully (Hackler et al, 1965). Overheating the soymilk to completely destroy the trypsin inhibitors will destroy amino acids, particularly cystine, making it a limiting amino acid in the product (Hackler et al, 1965; Liu, 1997). During moist heating, the Bowman-Birk trypsin inhibitor is inactivated before the Kunitz trypsin inhibitor (Dipietro and Liener, 1989). Since disulfide bonds contribute to the structural integrity of trypsin inhibitors, increasing the pH (Wallace et al, 1971) or adding a reducing agent, such as cysteine (Lei et al, 1981), decreases the heating time necessary to inactivate trypsin inhibitors in soymilk. Genetic breeding can also eliminate the Kunitz trypsin inhibitor in soybeans (Liu, 1997).

In the closed environment of the ALSSIT, concentration of volatiles released into the atmosphere during soybean processing is an air quality concern. Quantification of volatiles emitted using SoyaCow™, a prototype soymilk machine which performs the grinding and steam cooking steps of soymilk production, revealed that ethanol, acetaldehyde, methanol, hexanal, propanal, acetone, and carbon disulfide would exceed the Spacecraft Maximum Allowable Concentrations (SMAC, 1995) for a 180 day mission (Vodovotz et al, 1998). Other food processing procedures occurring in the ALSSIT during this time period may also contribute volatiles. A scrubbing method to periodically remove these volatiles is necessary to maintain acceptable air quality. By using high efficiency air filters, airborne microbial contamination, such as mold spores, could almost be eliminated.

Physical Hazards

Soy pods not properly removed during seed cleaning and metal fragments from equipment breakdown are the primary physical hazards occurring at low risk in production of soymilk, tofu, and tempeh from soybeans.

SOYBEAN PROCESSING PROTOCOLS

Conventional soybean processing methodologies (Liu, 1997; Vodovotz, et al, 1998) were adapted to reflect proposed processing protocols for ALSSIT-grown soybeans. A process flow diagram for soymilk, tofu, and tempeh is shown in Figure 1. Using the definitions from the National Advisory Committee on Microbiological Criteria for Foods (1992), three potential hazards were identified for processing of ALSSIT-produced soybeans into soymilk, tofu, and tempeh: Hazard D--The product is subject to recontamination after processing before packing; Hazard E--There is substantial potential for abusive handling in distribution or in consumer handling that could render the product harmful when consumed; and for some uses of soymilk and tofu, Hazard F--There is no terminal heat process after packaging or when cooked in the home. These hazards place soybeans in the type III risk category. During the processing of ALSSIT-grown soybeans, critical control points were identified at the crop dryer, seed cleaner, steam cook (soymilk), cook (tofu, tempeh), incubate (tempeh), label and date (soymilk, tofu, tempeh), and storage (soybeans, soymilk, tofu, tempeh) steps.

Soybeans

Production Soybeans will be grown in a recirculating nutrient hydroponic system. Soybeans may become contaminated during production by *Bacillus cereus* and molds. *B. cereus* is an aerobic, sporeforming rod that is normally present in soil, dust, and water and produces enterotoxins. It poses a high risk of a mild hazard. Soybeans may also be contaminated with molds that produce mycotoxins. Molds offer a variable risk of a severe hazard.

Harvest To shorten time in the Biomass Production Chamber, soybean pods are harvested at 70 days maturity while containing a 20-30% moisture content (Bugbee, 1998). The same hazards exist as in soybean production. The crop should be observed for mold growth, and moldy grain should be isolated, tested for mycotoxins, and treated, if necessary, as decribed under seed cleaner. Inedible biomass will be directed to the waste recovery system.

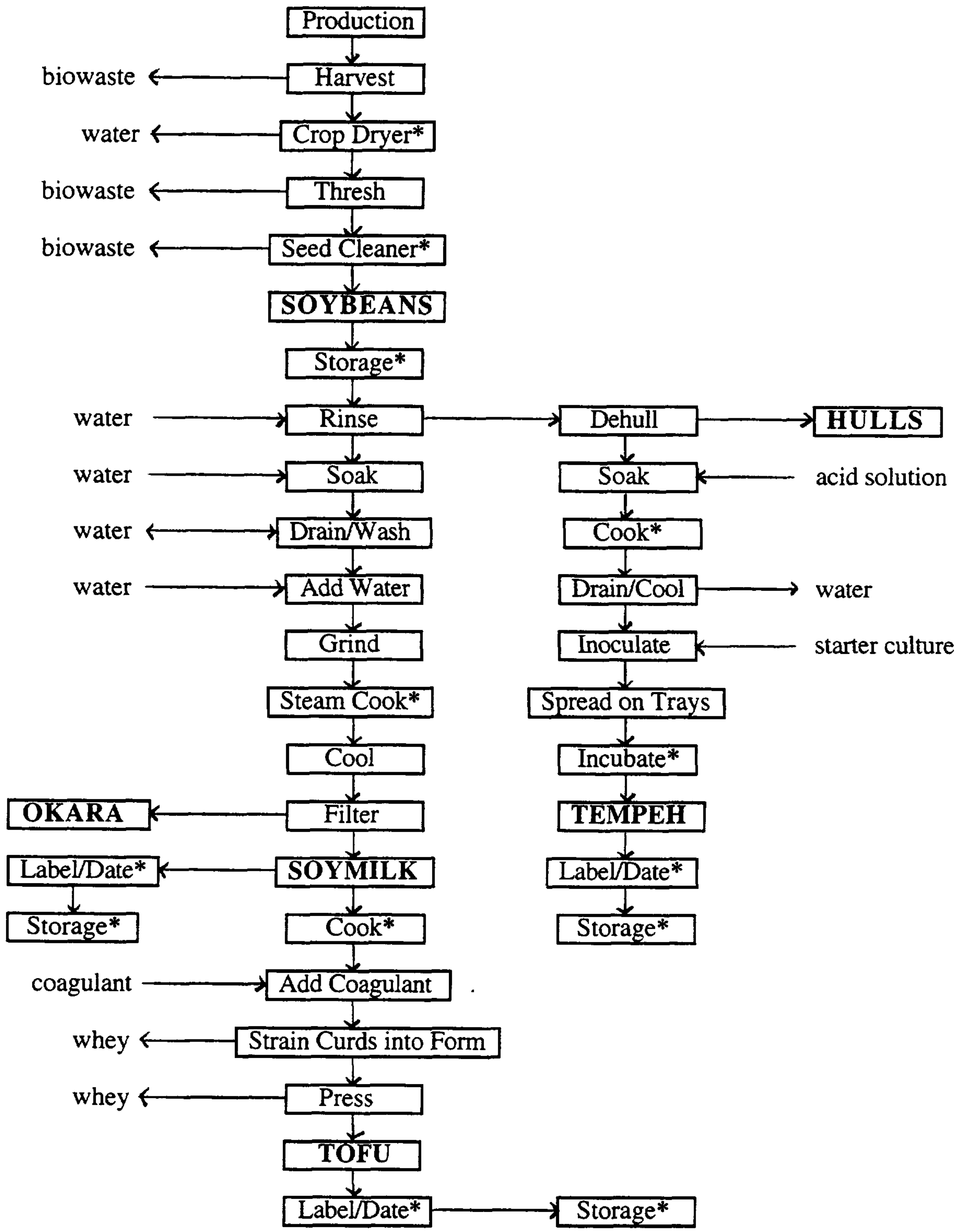

Figure 1.- Process Flow Diagram For Soymilk, Tofu, And Tempeh
* Critical Control Point

Crop Dryer* After soybean pods are harvested, they should be dried as soon as possible to prevent microbial growth. The soybeans should be dried to 10-13% moisture content (Erickson, 1995; Vieira et al, 1994) to reduce microbial growth, mycotoxin production, and germination. Molds offer a variable risk of a severe hazard. In general, mycotoxins are not produced on soybeans below 13.5-14.5% moisture (Moorman, 1990). Moisture content of the soybeans should be monitored. The crop dryer should be cleaned and sanitized to prevent cross-contamination.

Thresh During threshing, the soybean seeds are separated from the pods. Inedible biomass will be directed to the waste recovery system. Careful handling of the soybeans is necessary to prevent splitting and breakage which could promote enzymatic activity and heat damage during storage (Erickson, 1995). The thresher should be cleaned and sanitized to prevent cross-contamination.

Seed Cleaner* The seed cleaner will remove the pods from soybean seeds. The cleaned seeds should be visually inspected to ensure complete removal of pods, which may become a physical hazard if consumed. The soybean seeds should also be tested for mycotoxins. If they exceed the FDA Defect Action Level of 20 ppb aflatoxin, the soybeans should be destroyed and care taken during biomass recovery to prevent aflatoxin contamination of the environment, or the contaminated soybeans should be treated with ammonia, methylamine, sodium hydroxide, hydrogen peroxide, or ozone to inactivate the aflatoxin (Diener, 1981; Goldblatt, 1968; Jay, 1992; Maeba et al, 1988). Molds offer a variable risk of a severe hazard. The seed cleaner should be cleaned and sanitized to prevent cross-contamination.

Storage* The soybeans should be stored in a cool bin that is ventilated to prevent hot spots, moisture accumulation, microbial growth, and mycotoxin formation. These situations offer variable risk of mild to severe hazards. Since most food processing procedures are not effective in reducing mycotoxins, it is crucial to prevent mold contamination and growth. Moisture content of the soybeans should be monitored. Care should be taken to prevent adulteration of the soybeans with other crops. The storage bins should be cleaned and sanitized to prevent cross-contamination.

Rinse Before further food processing, the soybeans should be rinsed with potable water to remove chaff and reduce surface bacterial counts.

Soymilk

Soak The soybeans should be soaked in potable water for 7-8 hours at room temperature. During soaking, trypsin inhibitors are leached into the soaking medium, and phytate is hydrolyzed by phytase. Conditions are favorable for growth of microflora present on the soybeans. If soaking time is extensive, sprouting and fermentation may occur. The containers should be cleaned and sanitized to prevent cross-contamination.

Drain/Wash The hydrated soybeans should be drained and thoroughly rinsed with potable water. The soaking water, containing leached antinutrients, should be discarded.

Add Water Enough 35-40 C potable water should be added to the soybeans for a final volume of 2.25 liters. Soymilk is a water extract of soybeans.

Grind The soybeans and water will be ground at 10,000 rpm for one minute into a slurry. The mill should be cleaned and sanitized to prevent cross-contamination.

Steam Cook* SoyaCow™ (ProSoya, Inc., Ottawa, Canada), a prototype soymilk machine, is currently being tested for ALSSIT which will perform the grinding and steam cooking steps of soymilk production (Vodovotz et al, 1998). To maximize the protein efficiency ratio, thermal processing of soymilk at 100 C for 14 minutes or 30 minutes should be sufficient to inactivate 80% and 90% of trypsin inhibitors, respectfully (Hackler et al, 1965). In the SoyaCow™, the bean slurry is steam cooked at 95 C for 60 minutes. Even though this temperature is 5 C lower than above, the cooking time seems extensive. Overheating of the soymilk will destroy amino acids, particularly cystine, making it a limiting amino acid in the product (Hackler et al, 1965; Liu, 1997). Steam cook is the only "kill" step during soymilk processing that will destroy pathogenic microorganisms and antinutritional factors present in the product. Time and temperature must be monitored. In the remaining processing steps, sanitary procedures need to be closely followed to prevent recontamination which could offer variable risk of mild to severe hazards. When cleaning the SoyaCow™, use of highly alkaline detergents will ease removal of the heated protein residue on the internal surfaces.

Cool For easier handling, the soybean slurry should be allowed to cool for 30 minutes before further processing.

Filter Using cheesecloth, the soybean slurry will be filtered, and the soymilk filtrate collected in a clean and sanitized container. The remaining insoluble residue is called okara. Okara is rich in fiber and high quality protein. It may be dried, ground, and added to various foods for nutritional supplementation (Chan and Ma, 1998) or may be used to grow secondary food sources, such as mushroom mycelia (Cheung, 1997).

Label and Date* The soymilk should be poured into clean and sanitized containers. Because potential pathogenic contaminants, such as *Listeria, Yersinia, and E. coli* which offer variable risk of mild to life threatening hazards, may grow at refrigeration temperatures, the containers should be labeled and dated to help ensure first in-first out (FIFO) product rotation. This will decrease time for microbial growth and help minimize spoilage waste.

Storage* Microbial testing indicated no detectable *Salmonella*, *Staphylococci*, coliform, or aerobic bacteria in the fresh soymilk produced in the SoyaCow™ (Vodovotz et al, 1997). This soymilk, however, is not sterile and must be refrigerated. Due to its high water activity and neutral pH of 6.7 (Vodovotz et al, 1998), soymilk needs to be stored at 4.4 C or below to decrease growth of microorganisms. Pasteurization of the soymilk at 75 C for 15 seconds will extend the shelf life at 4 C storage to seven days (Kwok and Niranjan, 1995). The storage area should be cleaned and sanitized to prevent cross-contamination.

Tofu

Cook* Soymilk should be cooked at 100 C for 10 minutes in order to denature the soy proteins in preparation for coagulation, destroy vegetative bacteria, improve nutritonal quality, and reduce beany flavor (Liu, 1997). Time and temperature must be monitored. In the remaining processing steps, sanitary procedures need to be followed to prevent microbial recontamination which could offer variable risk of mild to severe hazards. When cleaning the equipment, use of highly alkaline detergents will ease removal of the heated protein residue.

Add Coagulant Soy curds are formed with the addition of a coagulant, such as calcium sulfate, magnesium chloride, or glucono-δ-lactone. The amount of coagulant should be monitored to prevent accidental addition of toxic levels.

Strain Curds into Form The soy curds should be strained into a clean and sanitized form. The whey is sent to the waste recovery system.

Press The curds in the form are pressed for at least 30 minutes to remove excess whey. The tofu should be cut into pieces, placed in clean and sanitized containers, and covered with whey or potable water. The remaining whey will be sent to the waste recovery system. The press should be cleaned and sanitized to prevent cross-contamination.

Label and Date* Because potential pathogenic contaminants, such as *Listeria, Yersinia, and E. coli* which offer variable risk of mild to life threatening hazards, may grow at refrigeration temperatures, the containers should be labeled and dated to help ensure first in-first out (FIFO) product rotation. This will decrease time for microbial growth and help minimize spoilage waste.

Storage* Because tofu has a 75% moisture content and a relatively high pH of 5.8-6.2 (Liu, 1997), refrigeration at 7 C or less is necessary to decrease microbial growth. Tofu covered in cold water may be stored for up to seven days. Using 0.5% acetic acid or 0.15% potassium sorbate and 0.5% acetic acid solution to cover the tofu will help control microbial growth and permit storage up to 23 days at 11-15 C (Liu, 1997). If used, amounts of the chemicals should be monitored to prevent accidental addition of toxic levels. The storage area should be cleaned and sanitized to prevent cross-contamination.

<u>Tempeh</u>

Dehull Soybeans should be soaked in potable water 8-10 hours at room temperature to loosen the hulls (testae). If soaking time is extensive, sprouting and fermentation may occur. The hulls should be rubbed off and strained from the water. The hulls, which are a good source of fiber and have the highest concentration of iron relative to other seed components (Levine et al, 1982), may be finely ground and added to various foods for nutritional supplementation (Johnson et al, 1985). Dehulling the soybeans is necessary to promote adequate tempeh mold growth (Liu, 1997). The dehulled soybeans should then be drained and rinsed to reduce surface bacteria and leached antinutrients. Although yet to be designed, a dehuller and "floater" separator equipment are planned for the ALSSIT interconnecting tunnel. Soaking the soybeans to facilitate hull removal produces large amounts of waste water and provides conditions which promote bacterial growth. An alternative method would be to heat condition the soybeans, crack the seeds between rollers, and separate the cotyledons and hulls by aspiration (air classifier). If whole soybeans are preferred, this procedure may not be appropriate since the cotyledons are broken into pieces. All of the equipment should be cleaned and sanitized to prevent cross-contamination.

Soak The dehulled soybeans should be soaked in potable water an additional 10-14 hours at room tempeature. If soaking time is extensive, sprouting may occur. During soaking, bacterial fermentation produces acids that lowers the pH of the soaking water preventing growth of undesirable bacteria, such as *Staphylococcus aureus* (Ashenafi and Busse, 1992). To accelerate this acidification, lactic acid ($\leq$ 0.5%) or acetic acid ($\leq$ 0.25%) should

be added to the soaking water (Hachmeister and Fung, 1993). The amount of acid added should be monitored. Tempeh mold growth is inhibited below pH 3.5 (Hachmeister and Fung, 1993; Liu, 1997). Soaking the seeds also facilitates mycelial penetration during the last step of tempeh production.

Cook* The soybeans should be cooked at 100 C for 30-60 minutes in the soaking water (Ashenafi and Busse, 1989; Hachmeister and Fung, 1993; Shurtleff and Aoyagei, 1979). "Partial cooking is necessary to destroy contaminating bacteria that could interfere with fermentation, to destroy antinutritional factors, such as trypsin inhibitors, and to release some of the nutrients required for mold growth" (Hachmeister and Fung, 1993). Thermal processing should be sufficient to inactivate 80% and 90% of trypsin inhibitors in the soybeans. Overheating will destroy amino acids, particularly cystine, making it a limiting amino acid in the product (Hackler et al, 1965; Liu, 1997). Time and temperature must be monitored. The equipment should be cleaned and sanitized to prevent cross-contamination.

Drain/Cool The cooked soybeans should be drained while still hot, spread on a clean and sanitized tray, and allowed to cool to 37 C. Higher temperatures may kill the mold inoculum or increase the incubation time required for sufficient mycelial growth.

Inoculate The cooled, cooked soybeans should be mixed with a commercial starter culture containing sporangiospores of *Rhizopus* spp, usually *Rhizopus oligosporus*, to get a final inoculation level of 10^6/100 g cooked beans (Ashenafi and Busse, 1989; Wang et al, 1975). Too little inoculum will increase the fermentation time which may permit growth of contaminating bacteria. The starter culture should be microbiologically tested to ensure that it is not contaminated with pathogens which would elicit a moderate risk of a mild to severe hazard. Pure starter cultures of *R. oligosporus* have a shelf life of one year at 4 C (Medwid and Grant, 1984).

Spread on Perforated Trays The inoculated soybeans should be spread in a 2-3 cm deep layer on sanitized perforated trays and covered with perforated plastic sheets to create a microaerobic environment (Hachmeister and Fung, 1993). The fermentation container should prevent moisture loss yet allow oxygen diffusion to promote growth and metabolic activity of *R. oligosporus* (Beuchat, 1984). Too much oxygen will encourage sporulation and darkening of the mycelium (Hachmeister and Fung, 1993).

Incubate The inoculated soybeans should be incubated at 30-38 C for 20-24 hours until the beans are tightly bound together by white mycelia. Time and temperature must be monitored. Fermentation above 42 C may cause the soybeans to dry out suppressing mold growth (Hachmeister and Fung, 1993). During fermentation, the pH of the soybeans rises from 5.0 to 7.6 (Jay, 1992; Liu, 1997) due to release of ammonia as amino acids are hydrolyzed (Paredes-Lopez and Harry, 1989). "*Rhizopus oligosporus* produces an antibacterial agent which prevents growth of contaminating bacteria during fermentation" (Wang et al, 1969).

Label and Date* The tempeh should be put into clean and sanitized containers. The containers should be labeled and dated to help ensure first in-first out (FIFO) product rotation. This will decrease time for microbial growth which could provide variable risk of mild to severe hazards and help minimize spoilage waste. Since tempeh is customarily cooked before consumption, pathogenic bacteria will be destroyed; however, heat stable toxins, such as *S. aureus* toxin, may remain in the cooked product.

Storage* Fresh tempeh must be consumed within one day of preparation because the ammonia produced from degradation of soy proteins and mold mycelia will make it inedible (Beuchat, 1984). Drying, frying, freezing (14 weeks), blanching, steaming, and canning (10 weeks) can increase the shelf life of tempeh (Hachmeister and Fung, 1993). The storage area should be cleaned and sanitized to prevent cross-contamination.

RECOMMENDATIONS FOR FURTHER RESEARCH

1. Review and revise the food safety analysis plan as the crop production and food processing procedures are further developed.
2. Continue evaluation of possible food sanitizers in the Bio-Plex. Determine the minimal levels of sanitizer and exposure times required to appropriately reduce microbial populations on the raw crops, processed products, and food equipment.

REFERENCES

Anderson, R. and Wolf, W. 1995. Compositional changes in trypsin inhibitors, phytic acid, saponins, and isoflavones related to soybean processing. The Journal of Nutrition, 125(3 supplement):5815.

Ashenafi, M. 1991. Growth of *Listeria monocytogenes* in fermenting tempeh made of various beans and its inhibition by *Lactobacillus plantarum.* Food Microbiology, 8(4):303.

Ashenafi, M. and Busse, M. 1989. Inhibitory effect of *Lactobacillus plantarum* on *Salmonella infantis, Enterobacter aerogenes,* and *Escherichia coli* during tempeh fermentation. Journal of Food Protection, 52(3):169.

Ashenafi, M. and Busse, M. 1991. Growth of *Bacilllus cereus* in fermenting tempeh made from various beans and its inhibition by *Lactobacillus plantarum*.. Journal of Applied Bacteriology, 70(4):329.

Ashenafi, M. and Busse, M. 1991. The microflora of soak water during tempeh production from various beans. Journal of Applied Bacteriology, 70(4):334.

Ashenafi, M. and Busse, M. 1992. Growth of *Staphylococcus aureus* in fermenting tempeh made from various beans and its inhibition by *Lactobacillus plantarum*.. International Journal of Food Science and Technology, 27(1):81.

Aulisio, C.C.G., Sanfield, J.T., Weagent, S.D., and Hill, W.E. 1983. Yersiniosis associated with tofu consumption: Serological, biochemical, and pathogenicity studies of *Yersinia ennterocolitica* isolates. Journal of Food Protection. 46:226.

Beuchat, L.R. 1984. Fermented soybean foods. Food Technology, 38(6):64.

Bugbee, B. July 31, 1998. Personal Communication. Crop Physiologist, Utah State University, Logan, Utah.

Bullerman, L.B. 1979. Significance of mycotoxins to food safety and human health. Journal of Food Protection, 42:65.

Chan, W.M. and Ma, C.Y. 1998. Enzyme modification of protein from soymilk residue (okara). Paper presented at the Annual Institute of Food Technologists Meeting, Atlanta, Georgia, June 21, Book of Abstracts, p. 38.

Cheung, P.C.-K. 1997. Chemical evaluation of some lesser known edible mushroom mycelia produced in submerged culture from soymilk waste. Food Chemistry, 60:61.

Diener, U.L. 1981. Unwanted biological substances in foods: Aflatoxins. In Ayres, J.C. and Kirschman, J.C. (Ed.) "Impact of Toxicology on Food Processing," AVI: Westport, Connecticut, pp. 122-150.

Dipietro, C.M. and Liener, I.E. 1989. Soybean protease inhibitors in foods. Journal of Food Science. 54(3):606.

Erickson, D.R. 1995. "Practical Handbook of Soybean Processing and Utilization." AOCS Press: Champaign, Illinois and United Soybean Board: St. Louis, Missouri, p.45.

Fernandez Pinto, V.E., Vaamonde, G., and Montani, M. 1991. Influence of water activity, temperature and incubation time on the accumulation of aflatoxin B_1 in soybeans. Food Microbiology, 8:195.

Goldblatt, L.A. 1968. Aflatoxin and its control. Economic Botany, 22:51.

Guu, Y., Chiu, C., and Young, J.. 1997. Processing of soybean soaking water with a NF-RO membrane system and lactic acid fermentation of retained solutes. Journal of Agricultural and Food Chemistry, 45(10):4096.

Hachmeister, K.A. and Fung, Daniel Y.C. 1993. Tempeh: A mold-modified indigenous fermented food made from soybeans and/or cereal grains. Critical Reviews in Microbiology, 19(3):137.

Hackler, L.R., Van Buren, J.P., Streinkraus, K.H., El Rawi, I. and Hand, D.B. 1965. Effect of heat treatment on nutritive value of soymilk protein fed to weanling rats. Journal of Food Science, 30:723.

Jacobsen, B.J., Harlin, K.S., Swanson, S.P., Lambert, R.J., Beasley, V.R., Sinclair, J.B., and Wei, L.S. 1995. Occurrence of fungi and mycotoxins associated with field mold damaged soybeans in the midwest. Plant Disease, 79(1):86.

Jay, J.M. 1992. "Modern Food Microbiology," 4th ed. Van Nostrand Reinhold: New York, p. 146.

Johnson, C.D., Berry, M.F., and Weaver, C.M. 1985. Soybean hulls as an iron source for bread enrichment. Journal of Food Science. 50:1275.

Johnson, L.A., Deyoe, C.W., Hoover, W.J., and Schwenke, J.R. 1980. Inactivation of trypsin inhibitors in aqueous soybean extracts by direct steam infusion. Cereal Chemistry, 57(6):376.

Jones, J.M. 1992. "Food Safety," Eagan Press: St. Paul, Minnesota. pp. 77, 78,146.

Kwok, K. and Niranjan, K. 1995. Review: Effect of thermal processing on soymilk. International Journal of Food Science and Technology, 30:263.

Levine, S.E., Weaver, C.M., and Kirleis, A.W. 1982. Accumulation of selected trace elements in hydroponically grown soybeans and distribution of the elements in processed soybean fractions. Journal of Food Science, 47:1283.

Liu, K. 1997. "Soybeans Chemistry, Technology, and Utilization." Chapman & Hall: New York.

Maeba, H., Takamoto, Y., Kamimura, M., and Miura, T. 1988. Destruction and detoxification of aflatoxins with ozone. Journal of Food Science. 53:667.

Matsubara, Y., Iwasaki, K., Nakajima, M., Nabetani, H., and Nakao, S. 1996. Recovery of oligosaccharides from steamed soybean waste water if tofu processing by reverse osmosis and nanofiltration membranes. Bioscience, Biotechnology, and Biochemistry, 60(3):421.

Medwid, R.D. and Grant, D.W. 1984. Germination of *Rhizopus oligosporus* sporangiospores. Applied Environmental Microbiology, 48:1067.

Moorman, M. 1990. Mycotoxins and food safety. Dairy, Food, and Environmental Sanitation, 10(4):207.

Mulyowidarsok, R.K., Fleet, G.H., and Buckle, K.A. 1990. Association of bacteria with the fungal fermentation of soybean tempe. Journal of Applied Bacteriology, 68:43.

National Advisory Committee on Microbiological Criteria for Foods. 1992. Hazard Analysis and Critical Control Point System. International Journal of Food Microbiology, 16:1.

Paredes-Lopez, O. and Harry, G.I. 1989. Changes in selected chemical and antinutritional components during tempeh preparation using fresh and hardened common beans. Journal of Food Science, 54(4):968.

Samson, R.A., Van Kooij, J.A., and DeBoer E. 1987. Microbiological quality of commercial tempeh in The Netherlands. J. Food Protection. 50:92.

Shurtleff, W. and Aoyagei, A. 1979. "The Book of Tempeh," Harper and Row: New York.

Spacecraft Maximum Allowable Concentration for Airborne Contaminants (SMAC). 1995. NASA-JSC 20584.

Szabo, R.A., Jarvis, G.A., and Weiss, K.F. 1989. A research note: Microbiological quality of tofu and related products in Canada. Journal of Food Protection, 52(10):727.

Tanaka, N., Kovats, S.K., Guggisberg, J.A., Meske, L.M., and Doyle, M.P. 1985. Evaluation of the microbiological safety of tempeh made from unacidified soybeans. Journal of Food Protection. 48:438.

Vieira, C.P., Vieria, R.D., and Paschoalick, J.H.N. 1994. Effects of mechanical damage during soybean seed processing on physiological seed quality and storage potential. Seed Science and Technology, 22(3):581.

Vodovotz, Y., Bourland, C.T., and Rappole, C.L. 1998. Assessment of a prototype soy-milk machine for use in an enclosed chamber. Manuscript submitted to Advances in Space Research.

Wallace, G.M., Bannatyne, W.R., and Khaleque, A. 1971. Studies on the processing and properties of soymilk II. Effect of processing conditions on the trypsin inhibitor activity and the digestibility in vitro of proteins in various soymilk preparations. Journal of the Science of Food and Agriculture, 22:526.

Wang, H.L., Swain, E.W., and Hesseltine, C.W. 1975. Mass production of *Rhizopus oligosporus* spores and their application in tempeh fermentation. Journal of Food Science. 40:168.

Wang, H.L., Ruttle, D.I., and Hesseltine, C.W. 1969. Antibacterial compound from a soybean product fermented from *Rhizopus olligosporus* . Proceedings of the Society of Experimental Biology and Medicine, 131:579.

Wheeler, R.M., Mackowiak, C.L., Sager, J.C., Knott, W.M., and Berry, W.L. 1996. Proximate composition of CELSS crops grown in NASA's biomass production chamber. Advances in Space Research, 18(4/5):43.

METRICS OF A PARADIGM FOR INTELLIGENT CONTROL

(11) IN-63

Final Report

NASA/ASEE Summer Faculty Fellowship Program- 1998

Johnson Space Center

Prepared by:	Henry Hexmoor, Ph.D.
Academic Rank:	Assistant Professor
University & Department:	University of North Dakota Department of Computer Science Grand Forks, ND 58202

NASA/JSC

Directorate:	Engineering
Division:	Automation, Robotics, and Simulation
Branch:	Intelligent System
JSC Colleague:	Tom Pendleton
Date Submitted:	August 7, 1998
Contract Number:	NAG 9-867

ABSTRACT

We present metrics for quantifying organizational structures of complex control systems intended for controlling long-lived robotic or other autonomous applications commonly found in space applications. Such advanced control systems are often called integration platforms or agent architectures. Reported metrics span concerns about time, resources, software engineering, and complexities in the world.

1. INTRODUCTION

Complex autonomous systems are artificial organisms that share many of the properties of living organisms. They have a physiology and basic self-preservation mechanisms. They have built-in capabilities and biases. These capabilities include patterns of interactions in the world governed in part by a body of encoded deterministic knowledge and algorithms. A class of these organisms might be endowed with heuristics and programs that can assimilate and generate new patterns of behavior. Latter can be considered to be cognitive functions.

Lets agree that that there is a cognitively appropriate level for situation assessment and response generation. Our sense of appropriateness includes timeliness, avoiding negative consequences, and purposefulness. It is the type of know-how and processes for using them that dictate appropriateness. We call the loci and organization of know-how architecture of organism. Furthermore, we think of this architecture roughly as a mammalian brain made up of spinal cord, brain stem, and forebrain. For a number of years, researchers in AI and robotics have used software structures called architectures, [Hexmoor, et al, 97. Kortenkamp, et al, 98, Arkin, 98]. Gat in [Gat, 98] presented a history of a three-tiered architectures. He argues that separation of control software into layers has mostly to do with internal states. Internal state refers to recording what is true in the world. The three layers are identified by characteristics of (a) little or no state is maintained, world interactions are as responsive as they can be without imposing hard-real-time requirement, all failures are detected, (b) states are based on past and world interactions governed by this layers are somewhat slow, (c) states are based on future and world interactions are slow. These properties are common in many applications. However, we don't believe them to be the distinguishing characteristics.

Let's examine the issue of maintaining state in an architecture. In AI, keeping state means maintaining an internal model of the world. Clearly, describing map of an environment is providing an internal model of the world. Checking value of a parameter in the world before acting is also internal modeling. Combining a few observations to decide on an abstract notion is also internal modeling. Therefore, a state is using any variable that either stands in direct correspondence with an external entity in the world or any variables storing relationships among entities in the world. A related notion is abstract knowledge. Perhaps we can choose to reserve abstract states when we maintain a model of the world whereas concrete states can be used in behavior-based approaches. Another related notion is acting either based on immediate information in the world, memory of the past, or anticipations of the future. Acting without history is known as a Markovian process. Let's consider acting with memory of the past as historic and acting with future anticipations as anticipatory.

According to [Arkin 98], when our knowledge of a domain is limited and environmental uncertainties are not adequately predictable, a behavior-based approach is preferred over a system that uses internal model of the environment, call latter knowledge-based approach. Of course we may choose to model everything in a behavior-based approach. However, when the systems being modeled have well known knowledge we may choose to model them using world models and model-based reasoning. Appropriately used, knowledge based approach provides economy and accuracy. Nontrivial systems may need to model a variety of situations from the predictable and procedural to the unpredictable and unknown. This often leads us to building hybrid systems that have both a behavior-based and knowledge-based components.

1.1 Metrics

In software engineering, a metric is defined as "a quantitative measure of the degree to which a system, component, or process possesses a given attribute" [IEEE]. What is required for a metric is to devise an objective cost either for the entire system or specific parts of it. Subsequently, this cost can be measured against features, modes, or modules of a software. It is our aim to develop three types of metrics for control system: (a) architectural features, (b) operating modes, and (c) knowledge engineering and design.

Lets agree that imposing any structure incurs a cost in development, maintenance, and operation of the system, say S. The system lacking that structure is assumed to be inefficient and let's measure cost of this inefficiency as C. If C is

larger than S, it is beneficial to consider the structure. The inefficiency itself can be measured by subtracting system cost with and without the feature. I.e., C = system cost with feature - system cost without feature. Let's consider N as the nominal cost of development, maintenance, or operation. We will consider the ratio (C-S)/N as the metric that measure merit of a given architectural feature.

Operating computationally generously versus frugally, navigating conservatively versus experimentally are philosophical principles or stylistic decomposition in running a software commonly referred as 'mode'. Lets agree on a default mode of operation with cost DC for the entire system or a particular component of the system and another mode of operation with C. |C-DC|/DC can be considered to be a mode metric. We will examine modes of handling resources, and planning.

Given a framework such as 3T, software engineers and application developers need metrics (i.e., guidelines) for designing cohesive yet decoupled code modules. Lets consider maximum/capacity cost of a module or a component of the module at run-time as CC and expected cost as EC. (MC-EC)/MC can be considered to be KE metric. If EC is larger than MC, then the module or component need to be decomposed to be handled more efficiently. If EC reflects the upper limit of expectation, this metric will reflect a sort of a the safety margin. We will examine metrics for latency, interruptibility/autonomy, state/memory, and fault-detection.

In the remaining parts of this report, we outline parts of a canonical control system that resemble 3T. 3T provides three layers for planning, reaction, and a layer for interfacing the previous two layers called sequencer. We use the concept of organizational principle of layering from 3T but interpret contents of each layer somewhat liberally. We ask the reader, to think of 3T implementations as a subset of capabilities that can be modeled in a 3 layer system. For instance, see [Hexmoor, 96] for another 3 layer system that is closer to human brain layers. Our intent is to overlook shortcomings with specific 3T implementations. Our discussions will liberally apply to all these systems. In various places we analyze functionalities, data from applications, or metrics from NASA testbeds that quantify existing system capabilities and substantiate new requirements. The organization of our canonical system roughly outlines anatomy of an autonomous agent.

2. RELATED WORK

[Hanks, et al 1993] discuss the merits of testbeds and benchmarks for revealing values of agent design concepts. These issues mostly revolved around reactiveness versus planned behavior. They argued about inconclusiveness of experiments but that generalizations and interpretations are left to researchers. Our approach offers generalized metrics and uses benchmarks for discussion and instantiation.

[Mali and Mukerjee 1998] define behaviors and tasks, and present concepts for comparing behaviors along dimensions of power, span, task space, usefulness, flexibility, and scalability. Their comparative metrics become guides for knowledge engineering behaviors at appropriate levels along their dimension of analysis. [Mali 1998] goes further and defines goals, environments, and markers. Mali sketches that more complex goals are achieved by adding markers or making behavior sets complex by adding coupling among behaviors. He argues that reactivity and planning do not have to be considered orthagonal but are related along how well the agent treats complexity of the world. With that he implies that there is a spectrum of ways to interact with the world. A knowledge engineer can change the behavior sets or markers to gain more or less reactivity. We agree with Mali's points. However, this does not invalidate multi-layered architectures since they provide concurrent means of interaction with the world. To use Mali's terms, his analysis provides a framework for designing behavior systems that address reactivity along spatial dimension. Hybrid systems are addressing spatial as well as temporal dimensions of interacting with the world.

MissionLab [MacKenzie and Arkin 1998] is a platform for editing where behaviors and the mission for multiagent system are specified apart from agent architecture. Flexibly, users select architectures to instantiate the mission This is a highly desirable feature that relieves the burden of coding missions in agent systems from the start. Although they have not done this, we believe metrics can be incorporated into

architecture instantiations for measuring the effect of architectural principles.

[Brown, et al 1998] preset metrics for interface agents. Their metrics in the areas of adaptivity, autonomy, collaboration, and robustness are ratios measuring system's actual level of appropriate output over maximum expected appropriate output. These measures consider the overall system but do not target effect of specific system design/architecture. In contrast to objective metrics defined here, ours are relative.

New Millennium Remote Agent (NMRA) is a control system developed at NASA Ames for autonomous control of unmanned spacecraft missions. NMRA has three major modules. It models mission know-how at a layer they call Executive. This layer models parts of the system as if it is modeling hardware. It provides programming mechanisms for resource management and temporally tight action execution. The Executive interacts with a deductive Model-based Identification and Recovery (MIR) module that given a target state and probability distribution on the current state generates a recovery sequence of actions using planning techniques. The third NMRA module is a planning and scheduling (PS) module that plans missions and modifies existing plans. NMRA's Executive is very similar to 3T's sequencer. PS and MIR form cognitive functioning in NMRA. [so what?]

3. KNOWLEDGE ORGANIZATION AND MODELING

Just as object-oriented programming paradigm is a more intuitive paradigm for modeling physical and mental concepts in the world, we posit that organisms provide a more intuitive model for software architectures of autonomous control systems. Evolution has provided biological organisms multiple mechanisms for survival and coping in the world. Control of many regulatory systems reside in different part of a human nervous system such as the cerebellum or the spinal cord. The reasons for distribution of control in organisms is beyond the scope of this report. Perhaps, distribution of control provide a diffusion of attention. This decentralization in organisms might be responsible for greater autonomy. We will use this distribution analogically and discuss our control systems in rough parallel.

Let's consider a few metrics for architectural features. Assume a corridor of 2 units wide by 4 units long and we want a robot to travel the length of this corridor. Every other corridor grid become occupied every other unit of time. Assume all movements between grids to take one unit of action and one unit of time. Let cost for travel be the number of actions plus number of time units elapsed between start and end of travel. Imagine the fastest robot (robot 1) that sees the front grid occupied, moves to the other side of corridor, moves forward one unit, switches to the other side of corridor, and so on. This robot would have been on move constantly for 7 grid movements in 7 units of time for a 14 unit cost. If the robot takes two units of time to execute on one move (robot 2), the front obstacles (occupied grids) would clear and it would take 3 actions in 6 units of time for a total cost of 9 units. If the robot is even slower and takes 4 units of time to perform an action (robot 3) it would take 3 actions and 12 units time for a total of 15 units. Robot 2 has the smallest cost and is the most timely. Both too fast and too slow reactions can be more costly. Naturally, it is difficult to decide the right level of reactivity from the start. We can measure each robot reaction level against the optimal (in this case 9 units) for a relative value or metric of comparison. Imagine a robot that is capable of generating responses like either one of the earlier robots 1-3. This would be like having a multi-layer (or multi-function) robot with behaviors of each type being generated at separate layer (function). However, the robot needs to decide on its behavior layer (function) based on a heuristic. Let's assume this heuristic to cost 1 unit. Therefore, the multi-layeredness (multi-functionality) feature can be measured as (C+1 - 9) / 9 where C is cost of each of the non-optimal plans. For instance, the most reactive plan with cost of 14 yields 6/9, i.e., the most reactive approach is 33% less effective. In general, assume the optimal cost is N , the overhead of deciding which level should generate the response is O and cost of each non-optimal plan is C. (C+O-N)/N is the metric that measures relative merit in using a system without the feature the produces optimality. We can call it the *timeliness metric* as a feature metric.

The general principle for this metric is shown in Figure 1. Assume, for a given system reaction time is constant. So the horizontal axis depicts

systems with differing reaction time. For a given system and environment, there is a reaction constant that minimizes system cost.

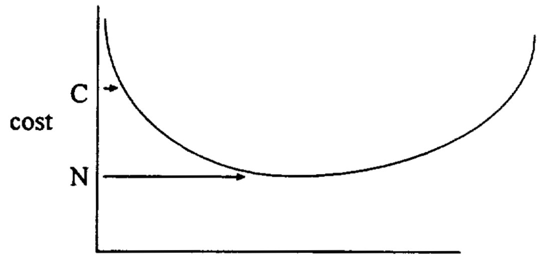

Figure 1

Let's consider a corridor similar to above example. This time think of the corridor to be 3 units wide and it gets occupied in order from left to right and sequentially progressing forward with 2 time units in the corners and 1 time unit in the middle. If we start with our agile robot that starts in a corner and sees it occupied and then moves to middle, forward one unit, left or right one unit (left will be OK but right will be a bad decision since it will be blocked and it has to return to the middle. If it took a left turn, it would have 5 movements and 5 time units for a cost of 10 but with a right choice, there will be 7 movements in 7 time units for a cost of 14 units. If the robot were able to predict the right corner being occupied and that prediction cost 1 unit, (14+1-10)/10 ratio show a 50% merit for including a feature for predicting consequence of grid occupation pattern. Assume the optimal plan costs N, cost of non-optimal system is C, and overhead of prediction is O. (C+O-N)/N is a metric we call the *purposefulness metric* as a feature metric.

The general principle for this metric is shown in Figure 2. Purposefulness reduces system cost but too much purposefulness does not reduce cost.

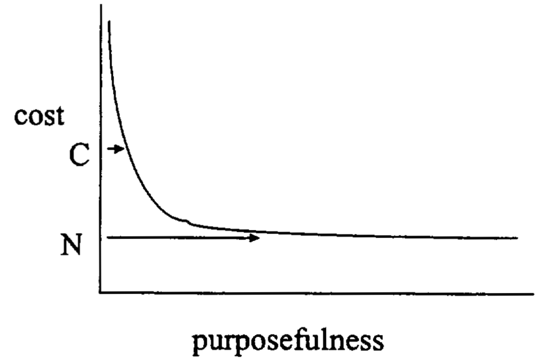

Figure 2

The word "autonomy" implies self-governance. A system is autonomous if it independently controls itself. Although autonomous control is desirable, it is human nature to think that we need the ability to intervene. In the labs we take pleasure designing creatures that are autonomous but in arenas where it is very critical, the ability to access and selectively change system behavior is highly desirable. This implies architectural hooks into the loci of control, e.g., decision making about controlled, automatics, or reflexive actions. In its most general form, it might be desirable to modify knowledge, memory, or operation of decision making processes. However, we limit our interest of interruption firstly to automatic system's ability for *suppression* and *supersede* of what the system decides at certain levels of granularity. Suppression is cessation of an ongoing behavior. Supersede is replacement of execution of one behavior over another. This type of interruption is asynchronous and the performed in a supervisory manner. The system has no expectations. Such a system will be obedient of its masters and we will call it auto-obide or autobide for short. An autobide can be measured as to how fast it responds to an authorized interruption. Let's assume an active behavior to be interrupted is a feedback loop generating impulse inputs with frequency of f; i.e., every f units of time, the feedback loop issues an impulse input. We can measure suppression rate in how many f units it takes before the feedback loop stops. We keep in mind that some feedback loops cannot end immediately and must end gradually. Supersede can be measured in terms of f units as well. Bringing up a new behavior might have to be gradual and it will affect the behavior replacement time. Lets denote the cost of system's lethargy to respond to interrupts as L (can be decomposed to cost per f) and the

computational overhead of quickly responding to the overhead as O. With N as the nominal cost of system operation, (L-O)/N is the *interruption metric*. This is a mode metric. The second type of interruption we consider is cooperative. In this type of control, system expects to be interrupted. We will not discuss this issue further in this report. For an example of the interruption metric, consider a conveyor belt delivering widgets at a constant speed and a robot arm pushes the widgets off the conveyor belt onto a bucket. The bucket location is mostly constant until it is full and a person replaces the bucket. The new location of the bucket may be different than the previous location. We expect the robot be able to react to new bucket location quickly. We can think of bucket replacement as an interruption. If the robot is not quick, widgets will be pushed onto floor which incurs a cleanup cost. However, the robot's more frequent monitoring of bucket location also adds to the cost. Interruption metric can be used to decide the utility of the more interruptible mode.

The general principle for this metric is shown in Figure 3. Reducing delay is often incurs constant cost and cost due to delays is linearly proportional to interrupt response delay.

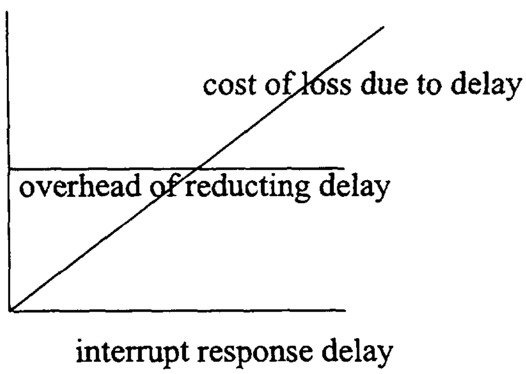

Figure 3

31 Modeling bodies or devices

At this level, bodies or devices are controlled by hard and inflexible mechanisms. We consider what is represented to be modeling the circuitry of the organisms and not its knowledge.

Inputs at this level are raw data from sensors and triggers to start a control system. Output at this level are reports to other parts of the system and control data sent to actuators. What is encoded at this level might be open or closed loop feedback systems with the world. Other parts of the system can be considered to be supervisory to this level. In anthropomorphic terms, what is encoded can is closely tied to physiology and not normally altered. For instance, reflexes, automatic behaviors, skills, habits are modeled.

In regards to system abilities to model a system, we consider measuring the system ability to model control loops. These might be open loops like for modeling reflexes and some automatic behaviors, or closed loop found mostly in automatics behaviors, skills, and habits. 3T distinguishes modules at this level as blocks and events.

At this level, we want the system to provide the fastest execution time possible. If we assume a central loop, as in 3T's skill manager loop, there will be a cycle execution time. Let's call this time *latency*. This is an architectural parameter that determines how fast we determine execution. Let's assume in 3T that two behaviors request the same resource. The resource can only be available to one behavior at a time and the rate of request is faster than latency. Assume the loop time is L, we have N behavior requesting attention every F units of time each. Furthermore, we can assume that behaviors are sequential. With L > L/N > F,

- the first behavior will be L/N units late,
- the second behavior which is expected to start when the first behavior finished will be late by L/N + |L/N -F|,
- similarly, the third behavior will be 2N + |L/N - 2F| units late, and so on. Finally,
- the Nth behavior will be (N-1)L/N + |L/N - (N-1)F| units late.

For the Nth behavior not to be late, let's set delay equal 0 and solve for L. This gives us L = (N-1) F. For example, imagine N= 10 behaviors, and F = 10 msec. L < 900 msec. So if L = 1 sec we will have delays. We will consider (L-(N-1)F)/L a *latency metric*. This is a KE metric. This is a KE metric. If we assumed behaviors need concurrent execution, behavior delays will be L/N, 2L/N, …, (N-1)L/N. In either case, we observe accumulation of lateness in responding to requests as time goes by.

The general principle for this metric is shown in Figure 4.

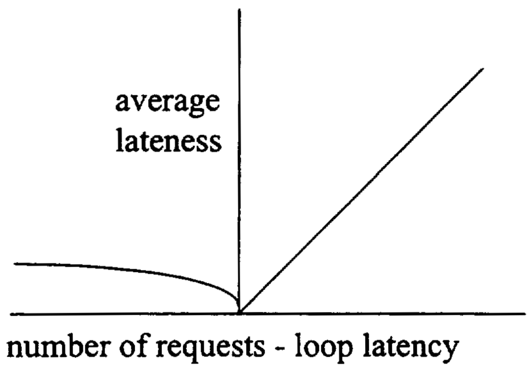

Figure 4

If latency becomes a problem, our solution is twofold: (a) decentralization of the task at the top level loop to other loop, (b) adding another run of the program which is horizontal decomposition of the problem. In a separate data structure, we can record requests for resources and a dedicated process can process this data structure at a much faster rate than the original loop. We will refer to this data structure as RDS. Let's consider the functions of a top level loop. It looks at all active behaviors. Among the active behaviors, the highest priority that has not clobbered others is selected for consideration and its request and control data for a resource are extracted and put onto RDS. Lets call the status of behaviors as triggered. Concurrent with top level loop, RDS loop examines resource request and determines compatibility among requests. If a resource can be used concurrently by the current input impulses and input impulses from the past, RDS will send it a signal which we will discuss in a little while. The corresponding behaviors are given the status of fired. The resulting impulse from compatible inputs and past inputs must fit into resources execution trapezoid. The resource is either ramping up, coasting or ramping down. All instantaneous inputs are added and past through a smoothing filter so it will be compatible with resource usage. Once inputs are issued to the resource, the behaviors is given a status of the executed and a number is returned proportional to the level of level of input it contributed to the final execution impulse.

RDS loop might determine conflict between two request for a resource and deny execution. At this level we will use priority of a behavior to resolve conflicts among request. Special conflict indices can be developed in the behavior level that might account for resolution of resource contention.

RDS loop can make use of an observer function that records patterns of resource usage and predicts frequently occurring patterns. This might be considered in input adding signals.

Consider a variation to the previous analysis with $L > F > L/N$,

- the first behavior will be L/N units late,
- the second behavior which is expected to start when the first behavior finished will be early by F - L/N. We cannot assume the system will hang on until it is time for the behavior to be processed. So the loop will proceed to the next behavior.
- similarly, the third behavior is early by 2(F-L/N) units. At this rate all subsequent tasks will be early and wont be executed until the next cycle. However, in the next cycle, the second task which has been waiting a long time will be late by L - L/N - F.
- this is the most severe lateness since other behaviors will be caught up. If this is to be small, equate it to 0 and we get $L = FN/(N-1)$. The latency metric is then $(L - (FN/(N-1)))/L$.

There is a variation to the previous analysis with $L+(L/N) > F > L > L/N$,

- the first behavior will be L/N units late,
- the second behavior which is expected to start when the first behavior finished will be early by F - L/N. As before we skip it until the next loop.
- in the next loop, the second behavior will be L + L/N - F late.
- The delay for the second and subsequent behaviors is very small and will not pose a problem.

As we discussed in introduction, [Gat 98] tell us that a major distinction between layers of 3T is the kinds of "state" it maintains. By state he means internal representations of the environment. We have examined a few 3T applications and found that at the skills layer, some robotic applications maintain a type of short term memory that might be considered to be muscle memory. For instance, in robotic applications we may design behaviors that rely on memory of target coordinates for visual cues or navigation. What is represented internally and can be considered to be (a) reference signals to feedback loops, or (b) invariants in the top level

loop of this layer. This memory is often short-lived. We can present the life of such a memory in terms of impulse inputs of the feedback loop for which the signal (state) stays constant, F. Surely, another design principle might be to avoid such memories. In a given domain and with a behavior design we can contrast systems with memory versus without. Subtract costs of operation and divide by cost of system without memory for an index of difference between the designs. We can call this the *history metric*. This is a mode metric. An example would be contrasting navigation using a map and without. The environment and tasks will affect that outcome.

Should the organism be cognizant of its own ineffectiveness or abnormalities in its environment? If things are very wrong, very little might be possible. The organism might be able to execute a nesting maneuver until the situation improves or it can think of a situation. The latter would be a cognitive act and would require reasoning. At this layer, we expect to notice large divergence in feedback loops or detection of abnormalities. The ratio of time difference between existence of a fault and time it is detected over time span of operation can be a KE metric called *fault-detection metric*.

3. Modeling knowledge and knowledge use

At this level, organisms operate based on (a) algorithms and knowledge that we consider innate, and (b) processes for generating response, reactions and assimilation to the external world. In addition to being an expressible environment for knowledge, we expect the processes at this level to allow for varying levels of monitoring. We also expect adaptability and learning, interruption, and knowledge augmentation. The knowledge engineering principle for encoding knowledge at this level is that (a) unlike the previous layer, the knowledge models a non-reflexive process, and (b) no reasoning takes place over action consequences which is a characteristic of a behavior-based reactive agent.

The knowledge is provided by engineers. Model of an organism's knowledge may include reactive plans. Unlike the previous level, concerns at this level are not hard real-time. Such systems are expected to react to external events and long chains of execution are avoided. Encoded knowledge is typically in the form of a conditional plan. Input to this level comes from (a) situations perceived out of data in the bodily level, and (b) new commitments to goals or constraints. Output of this system is (a) status of achievement of goals, (b) choice of or input to bodily feedback loops.

This level is very similar to the previous with regard to internal representations. In most applications, sometimes there is a need to remember previous actions or conditions. This memory is also short-lived. An example is navigating based on a map. We can present the life of such a memory in terms of ratio F/N where F is number of RAP cycles during which memory of previous conditions or actions are needed. Similar to previous level, we can call this the *history metric* as a mode metric. we can contrast systems with memory versus without. Note that this level and the previous one are similar with regards to Gat's distinction of state.

3.2.1 The language tool

A language that has been used corresponding to this level of 3T is RAPs. A RAP is either a primitive RAP and not further decomposable or a disjunct of one or methods. Each method is a *context* followed by an expression of *tasks* separated by operators *parallel, sequence, unordered, and one-of.* RAPs allows temporal constraints to synchronize tasks and monitors to watch for external events. Each task is a RAP. RAPs also allow for assertion of facts. The disjunction of RAPS into methods make them equivalents to horn-clauses which is a subset of first order predicate logic. As in Prolog, RAPs are good rule production languages. Thus RAPs is a good language for representing knowledge and a good knowledge engineering tool.

Although we won't offer a complete list of attributes of interest with these languages, we consider them to include: (a) temporal expressivity, (b) runtime concurrency control, (c) runtime event listening, (d) commitment completeness, (e) real-time extendibility, (f) friendly GUI, and (g) non-determinism.

Temporal expressivity refers to ability to express constraints among tasks both in absolute time, and in relative time. In addition to commonsense notion of concurrency control, we expect the ability to start processes and monitoring processes asynchronously. Runtime event

handling is the ability to react to external events. Commitment completeness refers to the ability to suspend and resume tasks and a sense or perseverance to accomplish the tasks. Real-time extendibility is the ability to encode more knowledge and make it available to the system while the system is running. Friendly GUI is obvious. Non-determinism is modeling the notion of randomness in selecting tasks. RAPs is fairly adequate in all respects except perhaps real-time extendibility.

The structure of RAPs is well suited for encoding a conditional plan but no provision is made for adaptation or learning. By learning at this level we have in mind associations between sensing and acting much in the sense of connectionist or genetic approaches to behavioral learning. Most generally in RAPs, situations are encoded in contexts and actions are in primitive RAPs. As a RAP is expanded for execution, further situations are examined for action selection. The tree structure of situations and actions is not immediately suitable for the style of learning we described. One of two thins has to happen. Either a mechanism needs to be developed to linearize RAP structures into pairs of situations and actions or a new variants of old learning paradigms need to be developed to operate within exiting RAP structures.

We have not offered any metrics for language comparison. Any metric would be either a language feature or a knowledge engineering principle for design.

3.2.2 Behavior Design

Design of each RAP module can be critiqued with regard to knowledge engineering concerns for coupling and cohesion. Specifically, metrics developed in [Mali and Mukerjee 1998] can be applied to RAP design. For reference, we include their list of metrics: power, modularity, flexibility, usefulness, span, and scalability. Their metrics compared two behaviors in relative terms. Each behavior is a triple of <situation, action, consequence>. One behavior can be more powerful than another if the situation of the first behavior is more general and it s consequence is at least as broad as the second. This is extended to comparison between behavior sets. They gave a theorem that if one behavior set is more powerful than another, then it is more flexible, useful, and modular. If we can loosely apply this to RAP system, we can design more powerful RAPs.

Reusable resources--

In this section we are concerned with design of behaviors that account for using a shared resource. Specifically, we will examine design of two behaviors that share a single resource. Let's have a behavior F for navigating in the direction the robot is facing while following a moving target. A second behavior C uses the vision system to look for objects that are closer and smaller for obstacle avoidance. Let's assume the vision system can only process the target in about 5 feet away and 4 feet in height. The vision system cannot see 3 feet or smaller objects any closer than 3 feet. When the vision system is maintaining the target in view, robot cannot attend to nearby objects. Behaviors F and C must share the vision system by time sharing it. Let the minimum frequency for maintaining target in view be denoted by ft and minimum frequency for avoiding nearby objects by fo. If the vision system has capacity C. Assume the switching cost between two visual tasks be negligible. If C is less than ft+fo we need a more powerful vision system. Otherwise, we can measure the ability of the system for sharing the vision system. The best scenario is that fo and ft are met. If the actual frequencies are marked as fo' and ft', we can measure the shortcoming as $|fo-fo'| + |ft-ft'|$. We suggest dividing this value by C to as a metric for measuring adequacy of sharing the vision resource. Let's call the general form of this mode metric as *resource-sharing metric*.

3.3 Modeling cognitive functions

We will limit our considerations to several special specific functionalities. A high level ability is planning and learning.

Input at this level is either provided by the user in the form of goals, priorities, states, deadlines, and events or internally as the system interacts with the world. Outputs at this level are status to user, delegation of tasks to lower levels, and parameters for guidance to lower level functions.

3.3.1 Planning

Planning is a cognitive function for building or extending a plan. A plan is a path through a problem space that dictates ordering of goals or

action execution. As such a plan is a knowledge that can be modeled as we discussed in the previous section. However, planning knowledge is knowledge about plans and goals and it is considered to be at a higher cognitive level. Planning in realistic environments often involves incomplete information, interference from the environment, and imperfections in the agent's ability to complete tasks. In the context of changing world, a planner has the choice of commitment to details. The program responsible to carry out a plan is said to be execution a plan. This is often closely tied to coming up with alterations to the original plan when it fails.

Incomplete information—

In the following, we will present an analysis of planning that considers incomplete information. Let's consider a problem with incomplete information and contrast reactive versus deliberative approaches to planning. Having incomplete information might be due to (a) inadequate or unreliable sensing and perception, or (b) lack of knowledge about interactions between goals and actions.

Incomplete information can be due to lack of knowledge about interaction among goals. Imagine a grid of 5 by 5 and imagine the robot starting at the center and has the 4 goals of visiting 4 corners of the grid. It can move horizontally or vertically and each unit of action A moves it one grid location. If the robot does not know that its 4 goals are highly related. It might go to each goal and return to center of grid adding up to 24A. If it knew that it can continue from the first goal to the second without returning to the center and so on, it would take it 12A. The knowledge of interaction among goals saved it 50% work. Although this example is simplistic, it motivates the metrics we need. Let C1 be the plan cost with incomplete knowledge. Let C2 be the cost of a plan considering incomplete knowledge. $|C1-C2|/\min(C1, C2)$ would be *incomplete knowledge metric*. This is a mode metric.

To motivate the problem of incomplete information due to sensing, imagine three boxes that need to be closed. There are three object, denoted by Oi, that are randomly placed in the three boxes. We want to close objects in their respective boxes. So there is problem with prematurely closing a box, trapping an object that belongs in another box. Let's assume cost of moving objects between boxes is negligible. Let's denote cost of closing a box as Di. Let cost of undoing action, i.e,, opening a box due to premature closure as Ui. Let S1 denote cost of sensing rapidly. Assume S1 is a fast form of sensing and can only determine location of a given object. E.g., Q: where is object2, A: box1. Let S2 denote cost of a complete form of sensing and it returns locations of all objects.

Now imagine all boxes are open at the start and all three objects are in box 1. One scenario for closing boxes will proceed as S1D1S1U1D1D2S1U1D1D3. Objects 2 and 3 are trapped in box1 and need to be retrieved. We think of this approach as "reactive" and will name it such. In contrast, another course of action could have been S2D1D2D3. We consider this approach as "deliberative" and will call it such.

If we extend this problem to N boxes the cost of new problem would be NS1 + ND1 + D2+D3+...+ DN + (N-1)U versus S2+D1D2...DN. If all Di cost the same, say one unit, this simplifies to: NS1+ (2N-1) + (N-1)U or N(S1+2+U) - 1 - U versus S2+N. We can consider U and ratio of S2 to S1 as free variables and contrast costs of two plans. We have considered the worst case scenario of having all objects in box1. On the average case of objects being randomly placed in boxes, less undoing is needed. Let I (a ratio less than 1) reflect the rate of undoing and the cost of reactive approach is more realistically reflected by NS1+ N + (N-1)I + (N-1)(1-I)U.

If undoing is cheap and S2 is very expensive, reactive approach is more attractive since cost of such plans are lower. Otherwise, deliberative approach wins. In highly critical situations, U might be enormously high which promotes a deliberative approach. The agent might have a mental attitude to minimize undoing, as a principle. When there is a desire for avoiding undoing, U can be inflated artificially to reflect that. In our benchmark example, the metric would be (NS1+(N-1)(I +U-IU)-S2)/(NS1+ N + (N-1)I + (N-1)(1-I)U)

The general principle for this metric is shown in Figure 5.

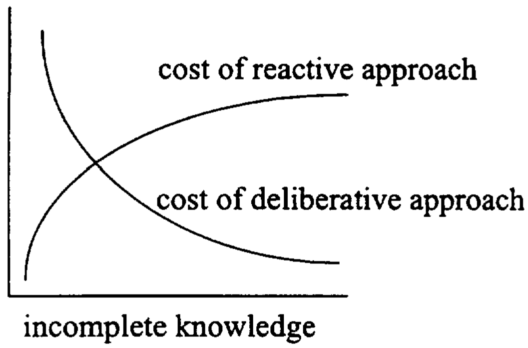

Figure 5

Other agents--

Let's consider a problem with other agents interfering and contrast reactive versus deliberative approaches to planning. Other agents may (a) help bring about desired situations, or (b) pose problems in accomplishing goals.

Let's consider interference from other agents where other agents cause problems. In the grid world, other agents may provide obstacle on a grid location on arcs between goals. This will cause the robot to take a detour. In the worst case, any obstacle on the path will cost 4 added units of action. This would not affect the reactive approach. In the deliberative approach, in the worst case, it will take 8 moves which is the same as reactive approach. Taking the cost difference yields 0. Similar to incomplete knowledge we suggest a metric for the system's ability to recognize correct strategy to deal with other agents *other agents.* This is a mode metric.

Let's consider interference from other agents where other agents inadvertently help. Suppose, as box1 is closed someone opens it up. If this was faster than S1, our agent can only get to repeatedly close box1 and do nothing else. Otherwise, in the reactive approach this might be considered welcome since less undoing has to take place. Let R1 be the ratio of time between changes by the other agent to S1 sensing the change. Let R2 be the ratio of time between changes by the other agent to S2 sensing the change. The plan cost in the reactive approach will be NS1+ N + (N-1) R1 + (N-1) (1-R1)U. In deliberative case, the agent may have to repair the undoings, resulting in cost of S2 + N + (N-1)R2 + (N-1) (1-R2)U. The metric yields (NS1+ (N-1) R1 - (N-1) R1U - S2 - (N-1)R2 + (N-1)R2U) / (NS1+ N + (N-1) R1 + (N-1) (1-R1)U).

Clumsy agent—

Let's consider a problem with our agent to be clumsy and not accomplish the task well so it has to be redone and contrast reactive versus deliberative approaches to planning. Being clumsy decreases performance in both our benchmarks.

In the grid world, imagine the agent taking more than one unit of action to move between adjacent grids. Let C (>1) be the multiplier of extra work that it takes to move. Furthermore, let's assume it only affects the deliberative case costing 4+8C. The difference in costs is 24-4-8C = 20-8C. Using a *clumsiness metrics* we will have (20-8C)/24. This is a mode metric.

In the boxes benchmark, let C (> 1) reflect the rate of redoing a task. In reactive case the cost is now be NS1+ N + (N-1) C + (N-1)U. In deliberative case, the cost is S2 + N + (N-1)C. The metric yields (NS1 + (N-1)U - S2) / (NS1+ N + (N-1) C + (N-1)U).

Consumable Resources--

In the following we will illustrate that deliberately accounting for consumable resources pays off. Let's assume that we have a grid of 3 by 3 marked 1-9, 9 different objects that appear randomly, a robot arm that can place objects in their respective locations. We assume cost of sensing is negligible. The arm can carry 1-3 objects at a time. Lets assume cost of carry one object is one unit and cost of carrying 2 objects is 1+U and cost of carrying 3 objects is 1+2U. Assume U < 1. The arm will only carry multiple objects only if they are in neighboring grid locations. The arm can wait until 3 objects show up before taking action. This manner of using the arm is treating the arm as a resource that can be used more efficiently. It cannot wait until all objects how up and then pick neighbor objects. In the most reactive scenario, an object shows up and the arm places it in its location. Lets consider 9 units of work associated with the reactive approach. If with luck, always neighbors of 2 show up, the work is 5+4U. If with luck, always neighbors of 3 show up, the work is 3+ 6U. If U = ½, then the work is 7 and 6 units respectively. This is considerable saving over purely reactive scenario. The savings are 22% and 33%. Let's say we can measure the cost a plan with most frugal resource usage F, a plan with the most

liberal resource usage L. A *resource-usage metric* would be (L-F)/F. This is a mode metric.

Forethought--

Often our perceptions are of things yet to come. Using these forward looking perceptions, actions can be more carefully selected. For example, image a grid of 4 by 4 and we want to move on the grids of outer edge. In the corners we can turn smoothly C or come to a stop and turn 90 degrees CC which is more costly. Straight move costs are A per grid. If we can see two squares ahead we can choose the smooth turn otherwise we are stuck with 90 degree turns. Let's consider a mode metric we can call *forethought metric* where we subcontract the costs of travel with and without prediction divided by the lower cost of travel. The extra cost of looking two squares ahead instead of one is P. The metric is 8A + 4CC - (8A + 4C + 15P)/(8A + 4CC). With CC = 2C and P = 1/5, the ratio is 1/16.

3.3.2 Learning:

In this section , we consider learning as a cognitive function for modifying knowledge and performance. An important element of learning is being able to ascertain current state of knowledge or performance. Metrics we have been discussing are useful in this determination. For a system that learns there are additional metrics to judge the process of learning. Learning curve is a plot of system performance or knowledge attainment over time and it is used to judge the merit of learning algorithm.

Knowledge migration—

Lets envision the ability to transfer knowledge from one layer to another. Let the cost of system operating with knowledge prior to transfer be C1 and after the transfer be C2 and cost of transfer be O. (O+C2 -C1)/C1 would be a metric for transfer. For example in a grid of 5 by 5, we can assume the system to plan steps for travel; between start and goal positions in terms of grid step movements. Let p1 be the cost of coming up with plan to travel between start and goal. Let p2 be the cost of matching and retrieving that planning is not required but the cost of caching the plan is o, then p1+o-p2/p1 is the metric.

4. SUMMARY AND CONCLUSION

This work was motivated by an examination of need for architectural features in complex autonomous control systems. This work has developed a framework for metrics to quantify these features and help in selection and design of these systems. Metrics provided in this report span concerns about time, resources, software engineering, and complexities in the world.

We have discussed three types of metrics. The first type gives us a measure a trade off for a feature and gives percentage of gain for the feature. We compare overhead of having a feature versus cost incurred by absence of the feature. These features are architectural. We presented two such features that motivated layers in 3T we called purposefulness and timeliness metrics.

The second type of metric measures the effectiveness of one mode of operation over another mode. When the system is capable of operating in multiple modes, these metrics help decide the best mode of operation. The mode we examined were on incomplete knowledge, clumsiness, other agent, consumable resource management, forethought, reusable resources, and a type of learning. Note that we can could examine these issues with metrics of first type. We chose these for illustrations of the 2nd type of metric.

The third type of metric measures a point of decision making in designing an application. These metrics are used by application developers and knowledge engineers in designing their modules. We offered latency, interruptibility/autonomy, state/memory, fault- and detection metrics. A few of these metrics are considered software engineering or knowledge engineering metrics.

Undoubtedly, many other metrics can be designed. For instance, metrics for level of parallelism, modularity and granularity of behaviors, fault-tolerance, run-time flexibility are few of the ones we will consider for further development.

REFERENCES

R. Arkin, 1998. **Behavior-Based Robotics**, MIT Press.

S. Brown, E. Santos, S. Banks, M. Oxley, 1998. Using Explicit Requirements for Interface Agent User Model Correction, International Conference on Autonomous Agents (Agents '98).

E. Gat, 1998. Three-Layer Architectures, D. Kortankamp, P. Bonasso, R. Murphy (eds), 1998. **Artificial Intelligence and Mobile Robots**, MIT Press.

S. Hanks, M. Pollack, P. Cohen, 1993. Benchmarks, Testbeds, Controlled Experimentation, and the Design of Agent Architectures, AI magazine 14(4): 17-42, MIT press.

H. Hexmoor, 1996. Learning Routines, In Agent theories, architectures and languages, M. Wooldrige, J. Mueller, and Milind Tambe (editors), Springer Verlag.

H. Hexmoor, D. Kortenkamp, I. Horswill, 1997. Software architectures for hardware agents, **J. of Experimental and Theoretical AI**, 9, Taylor and Francis.

IEEE, IEEE Standards Catalog, 1993.

A. Mali 1998. Tradeoffs in Making the Behavior-based Robotic Systems Goal-Directed, IEEE International Conference on Robotics and Automation, Belgium.

A. Mali and A. Mukerjee, 1998. Metrics for Evaluation of Behavior-based Robotic Systems, IEEE International Conference on Robotics and Automation, Belgium.

D.C. MacKenzie, R.C. Arkin, 1998. Evaluating the Usability of Robot Programming Toolsets, The International Journal of Robotics Research, 17(4):381-401.

K. Konolige, 1997. COLBERT: A language for Reactive control in Saphira, Proceedings of German Conference in AI, Germany.

D. Kortankamp, P. Bonasso, R. Murphy (eds), 1998. **Artificial Intelligence and Mobile Robots**, MIT Press.

R. Simmons and D. Apfelbaum, 1998. A Task Description Language for Robot Control, IROS '98.

(12)
/N-65

RELIABILITY MODELS AND ATTRIBUTABLE RISK

Final Report

NASA/ASEE Summer Faculty Fellowship Program—1998

Johnson Space Center

Prepared by:	**Richard D. Jarvinen, Ph.D.**
Academic Rank:	**Professor**
University and Department:	**Winona State University** **The Minnesota State Universities** **Department of Mathematics and Statistics** **Winona, Minnesota 55987**

NASA/JSC

Directorate:	**Safety, Reliability, and Quality Assurance Office**
Division:	**Technology Division**
JSC Colleague:	**Richard P. Heydorn, Ph.D.**
Date Submitted:	**August 7, 1998**
Contract Number:	**NAG 9-867**

ABSTRACT

The intention of this report is to bring a developing and extremely useful statistical methodology to greater attention within the Safety, Reliability, and Quality Assurance Office of the NASA Johnson Space Center. The statistical methods in this exposition are found under the heading of attributable risk. Recently the Safety, Reliability, and Quality Assurance Office at the Johnson Space Center has supported efforts to introduce methods of medical research statistics dealing with the survivability of people to bear on the problems of aerospace that deal with the reliability of component hardware used in the NASA space program. This report, which describes several study designs for which attributable risk is used, is in concert with the latter goals. The report identifies areas of active research in attributable risk while briefly describing much of what has been developed in the theory of attributable risk. The report, which largely is a report on a report, attempts to recast the medical setting and language commonly found in descriptions of attributable risk into the setting and language of the space program and its component hardware.

ACKNOWLEDGEMENTS

The author, while a NASA-ASEE 1998 Summer Faculty Fellow, continues an appointment as a Visiting Scientist at the Mayo Clinic in Rochester, Minnesota. In the latter connection he has a research association with the authors of [2], and is presently working to develop the theory of attributable risk to accommodate censored data, thereby extending the theory found in [2].

First, then, this report is designed for the most part to help bring the application of attributable risk as found in [2] to NASA and the Johnson Space Center. The step taken here to do so is by couching the medical research context and language found in [2] in the context and language of hardware component reliability and risk assessment as those pertain to the NASA space program and the concerns of the Safety, Reliability, and Quality Assurance Office, Technology Division, of the Johnson Space Center. Second, new software to carry out the methods of attributable risk carried in [2] is to become available to the author and applied by him to forthcoming NASA data sets. The NASA data to which attributable risk and related software are planned to be applied deal with the reliability of certain thruster valves on the Space Shuttle, with quantified data representing aspects that influence Space Shuttle landings, with causal variables that contribute to gas path occurrences in one or more of the six joints of the revised solid rocket motor nozzle of the Space Shuttle, and with data that pertains to the guidance mechanism of the Space Shuttle.

The author acknowledges the work of the authors of [2], especially Dr. W. Michael O'Fallon, Professor of Biostatistics, Chair, Department of Health Sciences Research, The Mayo Clinic, for his helpfulness. The author also acknowledges the sage advice of Dr. Richard P. Heydorn of the Safety, Reliability, and Quality Assurance Office, Technology Division, of the NASA Johnson Space Center for his valuable insights and suggestions, and for his vision to perceive the usefulness of the theory of attributable risk at the NASA Johnson Space Center. For the most part this report is a report on the Technical Report [2]. With the emergence of the NASA data and the availability of the related software, applications of attributable risk for the benefit of NASA is an expectation.

INTRODUCTION

Attributable risk statements provide valuable statistical information which are readily understandable. In settings such as for the analysis of the reliability of hardware components, they provide statistical profiles that help one to cleanly assess the extent to which a certain factor/exposure contributes to a certain failure/damage. They allow for statements about populations of hardware in contrast to statements restricted to an individual piece of hardware relative to its specific characteristics. When many causal variables are known to lead to failure, attributable risk helps one to decide where first dollars should be spent to most

dramatically reduce failures and increase safety. Said another way, attributable risk gages the extent to which each of perhaps many risk factors influences a specific failure.

Credit has been given to Levin (1953) for introducing the notion of attributable risk. He did so within a medical research statistical setting in which he attempted to quantify the percentage of lung cancer cases that were attributable to smoking. He found the figure to be between 56 and 92 percent, and stated that somewhere between half and almost all cases of lung cancer could be eliminated if smoking would cease...*provided* that smoking is truly a causative agent for lung cancer. We are reminded that correlation and causation can be independent.

The focus on attributable risk in this report is in the context of aerospace and the NASA space program. As such, we are interested here in the reliability of hardware components in contrast, but analogous, to the survivability of people. We pursue attributable risk for the purpose of assessing what percentage of failures of a certain hardware component is attributable to a certain risk factor.

ATTRIBUTABLE RISK

Introduction

In the literature one finds other names for attributable risk, which we symbolize as AR. These include the terms population attributable risk and etiologic fraction, EF. We make quick mention that etiology is the science of causes and origins. AR, as an entity *per se*, is a percent. As a percent it tells us, within a population of hardware components all possessing a certain failure, what percentage is due to exposure to a certain risk factor, F. In the latter context, categorical statements of the following kind are typical: A certain failure occurs in 3% of the Space Shuttle flights while 80% of those occurrences are attributed to a certain identified risk factor. Providing greater detail or refinements, we might alternatively communicate: A certain failure/damage, D, occurs in 3% of Space Shuttle missions, and, of the many factors that are known to lead to this failure, there is a 95% certainty that 80% $\pm$ 2% of the failures are attributed to the specific risk factor, F. Here, the 95% is the confidence level and the 2% is the accuracy of the point estimate of 80%.

A word of caution: There is a similar concept known as attributable fraction, AF, which is defined as the proportion of failures in a population of components that all have the same risk factor exposure. See [1, 4]. Lending further contrast, in the AR setting one begins with a population all having the same failure. In the AF setting,

one begins with a population all having the same risk factor exposure. This paper is not about the notion of attributable fraction. It is about attributable risk.

The Concept, Notation, and Equivalent Expressions

In [2] it is said that the concept of AR is deceptively simple. The simplicity lies in the kind of information it provides per se. Aspects, as we will indicate, associated with this concept have not been easy to develop.

But going on for the moment, specifically, AR is the percentage of those failed/damaged hardware components in a population which have the failure/damage, D, due to being exposed to risk factor, F. For example, suppose there are 100 damaged hardware components—all of which have the same type of damage, D—but there would have been only 17 if no one of these 100 components possessed the risk factor, F. Thus, 83 components underwent the damage due to the risk factor. There are 83 excess cases of failure or damage due to the risk factor. The attributable risk, the AR-value, is 83%.

Another way to think of AR is as the fraction

$$\frac{I^*}{I}$$

expressed as a percentage, where I^* is the number of pieces of damaged hardware with the risk factor within the total population of I damaged hardware components. Again, it is a specific category or type of damage that we have in mind.

We use the following notations for:

1. the probability of damage/failure, D: $P(D)$

2. the probability of the risk factor, F: $P(F)$

3. the probability of damage, granted the presence of the risk factor: $P(D|F)$

4. the probability of damage, granted the absence of the risk factor: $P(D|\overline{F})$

5. the probability of the factor, granted the presence of damage: $P(F|D)$

6. the probability of the factor, granted the absence of damage: $P(F|\overline{D})$

7. **the relative risk:** $RR = \dfrac{P(D|F)}{P(D|\overline{F})}$

Note that if $RR > 1$, then the risk factor contributes to damage rather than the opposite.

Note that I is approximately $N\,P(D)$ where N is the number of hardware components in the population and $P(D)$ is the probability of failure/damage. Hence, I^* is approximately $N\,P(D) - N\,P(D|\overline{F})$. Consequentially,

$$\text{(1)} \qquad AR = \frac{I^*}{I} = \frac{P(D) - P(D|\overline{F})}{P(D)}$$

And one can show, using conditional probability statements, that AR can also be expressed as in (2) and (3) below:

$$\text{(2)} \qquad AR = \frac{P(F)(RR-1)}{P(F)(RR-1)+1} \qquad \text{(Levin, circa 1953)}$$

$$\text{(3)} \qquad AR = \frac{P(F|D)(RR-1)}{RR} \qquad \text{(Mietinen, 1974)}$$

Relationships among the variables in (2) and (3) are seen in the following two families of graphs found in [2].

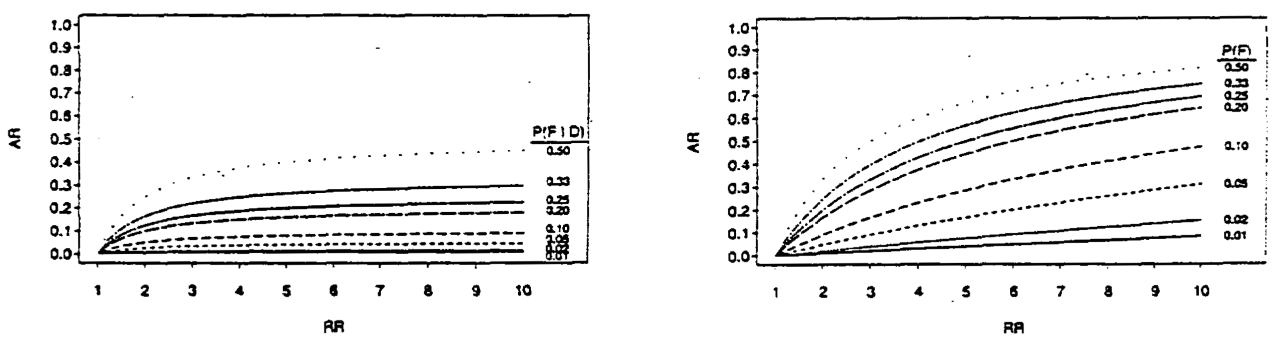

Figure 1: Relationship between RR and AR as a function of 1) prevalence of risk factor, P(F) and 2) prevalence of risk factor among diseased P(F | D).

Hypothesis Testing

From (2) we see that

$$(4)\quad AR = 0 \Leftrightarrow P(F) = 0 \; or \; RR = 1$$

Thus, tests of hypotheses involving attributable risk can be equivalently done by testing hypotheses involving relative risk. The latter topic is adequately explored within the literature.

Distributions

Characterizations that have been difficult to obtain since the introduction of the concept of attributable risk are revealed in the statement made in 1974 by the accomplished statistician Miettinen: "The sampling variability of the [above] estimators poses a rather challenging problem. No results are available." Rising to the challenge, Walters, in the mid 1970's, established that the AR estimators have approximately Gaussian (normal) distributions if the sample sizes are large enough.

DESIGNS

The following study designs are of a general nature. Each gives a context in which attributable risk assessments can be made. In the appropriate setting, each has the potential for important application in the NASA space program.

Design 1

The context here is that a single random sample has been drawn from a population of hardware components and then observed for a period of time. The following notation accompanies this model.

N = **size of the sample of hardware components**
$m_1 = a + b$ = **the number of components exposed to the risk factor**
a = **number of components that fail/become damaged**
$m_2 = c + d$ = **number of components not exposed to the risk factor**
c = **number of components that fail and are not exposed to the risk factor**

			Damage		
		Yes	No		
Risk Factor	Yes	a	b	m_1
	No	c	d	m_2
		n_1	n_2	N

Then

$$\widehat{RR} = \frac{am_2}{cm_1}$$

$\widehat{P(F)} = \frac{m_1}{N}$, **an estimate**

$$\widehat{AR} = \frac{ad - bc}{n_1 m_2}$$

$\widehat{V} = \frac{cN(ad(N-c)+bc^2)}{n_1^3 m_2^3}$, **the asymptotic variance of** $\widehat{AR}$

$\left(\frac{ad-bc}{ad-bc+Nce^{u}}, \frac{ad-bc}{ad-bc+Nce^{-u}}\right)$, **gives the confidence interval where**

$$u = z_{\frac{\alpha}{2}} \sqrt{\frac{(a+c)(c+d)(ad(N-c)+bc^2)}{Nc(ad-bc)^2}}$$

Design 2

In this setting two random samples of hardware components are drawn from a population. One of the samples is exposed to the risk factor, and the other sample is not. The samples are then observed for a period of time. Notation for this model is as follows.

m_1 = **size of the sample of components exposed to the risk factor**
a = **number of components that are exposed and then fail**
m_2 = **size of the sample of components not exposed to the risk factor**
c = **number of components that are not exposed but do fail**

		Damage		
		Yes	No	
Risk Factor	Yes	a	b	m_1
	No	c	d	m_2
		n_1	n_2	N

$$\widehat{RR} = \frac{am_2}{cm_1}$$

$\theta = P(F)$, **value obtained from some other source of data**

$$\widehat{AR} = \frac{\theta(ad - bc)}{\theta(ad - bc) + cm_1}$$

$\widehat{V} = (\frac{am_2}{ad - bc})^2 (\frac{b}{am_1} + \frac{d}{cm_2})$, **obtained by Walter (1976)**

$(\frac{\theta(am_2 - cm_1)}{\theta(am_2 - cm_1) + cm_1 e^u}, \frac{\theta(am_2 - cm_1)}{\theta(am_2 - cm_1) + cm_1 e^{-u}})$, **the confidence interval, where**

$$u = z_{\frac{\alpha}{2}} (\frac{am_2}{ad - bc}) \sqrt{\frac{b}{am_1} + \frac{d}{cm_2}}$$

Design 3

Here, two random samples of hardware components are drawn. One of the samples consists of failed/damaged hardware components, and the other sample has no failed/damaged components. Damaged and undamaged components are not matched. This is a case-control study. The notation accompanying this model follows.

n_1 = **number of components with damage**
n_2 = **number of components without damage**
a = **number of damaged components exposed to the risk factor**
b = **number of undamaged components exposed to the risk factor**

		Damage: Yes	Damage: No	
Risk Factor	Yes	a	b	m_1
	No	c	d	m_2
		n_1	n_2	N

$$\widehat{RR} = \frac{ad}{bc}$$

$$\widehat{AR} = \frac{ad - bc}{dn_1}$$

$$\widehat{V} = \left(\frac{ad + d^2}{ad - bc}\right)^2 \left(\frac{a}{cn_1} + \frac{b}{dn_2}\right)$$

$$\left(\frac{ad - bc}{ad - bc + c(b + d)e^{u}}, \frac{ad - bc}{ad - bc + c(b + d)e^{-u}}\right)$$ **, the confidence interval, where**

$$u = z_{\frac{\alpha}{2}} \frac{db + d^2}{ad - bc} \sqrt{\frac{a}{c(a + c)} + \frac{b}{d(b + d)}}$$

Design 4

Design 4 is the same as Design 3 except that a failed component is matched with one that has not failed. This is a case-control study. The notation follows. Note that the table is not the same as that for the Designs 1, 2, and 3.

N **= the total number of damaged or (matched) undamaged components**
a **= number of matched pairs where both are exposed to the risk factor**
b **= number of matched pairs where the damaged component is exposed to the risk factor and the undamaged component is not exposed to the risk factor**
c **= number of matched pairs where the undamaged component is exposed and the damaged component in the pair is not**
d **= number of matched pairs where neither the damaged nor undamaged component is exposed to the risk factor**

		Undamaged	
		Exposed	Not Exposed
Damaged	Exposed	a	b
	Not Exposed	c	d
			N

$\widehat{RR} = \frac{b}{c}$

$P(F|D) \approx \frac{m_1}{N}$, **an estimate**

$\widehat{AR} = \frac{(a+b)(b-c)}{bN}$, **using Miettinen's result, (3)**

$\widehat{V} = (\frac{1}{bN})^2 (a(b-c)^2 + \frac{(b^2+ac)^2}{b} + c(a+b)^2 - \frac{(a+b)^2(b-c)^2}{N})$, **Kuritz and Landis (1987)**

$\widehat{SE} = \sqrt{\widehat{V}}$ **allows for the construction of desired confidence intervals**

USING BAYES THEOREM

Introduction and Preliminaries

In case-control studies one begins with a damaged set of components and an undamaged set. From that biased data one is not able to estimate $P(D|F)$ **nor** $P(D|\overline{F})$**. And thus one cannot estimate** RR **nor then** AR**. However, by the formula of Bayes we can write** $P(D|F)$ **in terms of** $P(F|D)$ **by**

$$P(D|F) = \frac{P(F|D)\,P(D)}{P(F)}$$

Now

$$odds(F|D) = \frac{P(F|D)}{P(\overline{F}|D)}$$

and with

$$odds(F|\overline{D}) = \frac{P(F|\overline{D})}{P(\overline{F}|\overline{D})}$$

and the so-called odds ratio, OR**, defined by**

$$OR = \frac{odds(F|D)}{odds(F|\overline{D})}$$

which is equivalent to $\dfrac{odds(D|F)}{odds(D|\overline{F})}$

we obtain the formula:

$$RR = OR\,\frac{P(\overline{D}|F)}{P(\overline{D}|\overline{F})} = \frac{(1-P(D))\,OR + P(D)\dfrac{P(F|D)}{P(F|\overline{D})}}{1-P(D)+P(D)\dfrac{P(F|D)}{P(F|\overline{D})}}$$

Conclusion

We observe that $RR \approx OR$ **when either the probability of damage,** $P(D)$**, is low, or when** $P(F|D)$ **is very much smaller than** $P(F|\overline{D})$**. Especially noteworthy regarding the applicability of the above methods to undertake case-control studies in the NASA space program is this. It is, in fact, the popular occurrence to have the probability of damage/failure be low, for that is a characteristic built into the design of the hardware components in the space program.**

GENERALIZATIONS AND RESEARCH

Logistic Regression

Logistic regression provides an avenue for assessing the probability of failure in hardware components when one or more causal variables is known to lead to failure. In what has been presented thus far in this paper, we speak of the probability of failure due to the exposure to just one risk factor. Using logistic regression the above methods can be generalized to include the consideration of more than one causal variable. In fact, the theory can be generalized to allow for one or more of the risk factors to be polychotomous, i.e., take on finitely many different values. Further generalizations as exposed in [2] show that the theory is

developed along lines that allow for risk factors to be continuous variables. The attributable risk due to any one risk factor can be singled out.

Censored Data

Research is presently being undertaken to further develop the theory of attributable risk as described in the latter paragraph. And beyond that, as well as what is exposed in [2], are efforts to develop the theory of attributable risk so that it will accommodate the inclusion of data that has been censored.

SOFTWARE

According to [2], "S-PLUS software has been developed for estimation of attributable risk and the standard error of the estimate in these settings." However, as of this writing portions of it will not operate within the Windows operating system, but instead requires the UNIX version of S-PLUS as well as, perhaps, a C compiler depending upon what version of the software is used. "A shell archive containing the software and related materials can be accessed via anonymous ftp from ftp.stolaf.edu in the directory pbu/kahn/atrisk." The latter is reported in [2].

REFERENCES

1. Encyclopedia of Biostatistics, Vol. 1, John Wiley and Sons, 1998.

2. Kahn, M.J., W.M. O'Fallon and J.D. Sicks. Generalized Population Attributable Risk Estimation. Technical Report #54, Mayo Clinic, Rochester, Minnesota, 1998.

3. S-PLUS 4, MathSoft, Inc., Seattle, Washington, 1997.

4. Stata 5, Stata Press, College Station, Texas, 1997.

MATHEMATICAL FOUNDATION FOR PLANE COVERING USING HEXAGONS

(13)

IN-64

Final Report

NASA/ASEE Summer Faculty Fellowship Program 1998

Johnson Space Center

Prepared by:	Gordon G. Johnson
Academic Rank:	Professor
University and Department:	University of Houston Department of Mathematics Houston, Texas

Directorate:	Information Systems
Division:	Information Technology
Branch:	
JSC Colleague:	Dr. Robert Shelton
Date Submitted:	August 7, 1998
Contract Number	NAG 9-867

Development and Mathematical Foundation
For
Two Dimensional Hexagon Plane Covering
With Addressing

This work is to indicate the development and mathematical underpinnings of the algorithms previously developed for covering the plane and the addressing of the elements of the covering.

The algorithms are of interest in that they provides a simple systematic way of increasing or decreasing resolution, in the sense that if we have the covering in place and there is an image superimposed upon the covering, then we may view the image in a rough form or in a very detailed form with minimal effort. Such ability allows for quick searches of crude forms to determine a class in which to make a detailed search. In addition, the addressing algorithms provide an efficient way to process large data sets that have related subsets.

The algorithms produced were based in part upon the work of D. Lucas "A Multiplication in N Space" [1] which suggested a set of three vectors, any two of which would serve as a bases for the plane and also that the hexagon is the natural geometric object to be used in a covering with a suggested bases.

The second portion is a refinement of the eyeball vision system, the globular viewer.

The work is confidential and proprietary.

/N-20

DYNAMIC ALTITUDE SIMULATION SYSTEM PERFORMANCE MODELING

Final Report

NASA/ASEE Summer Faculty Fellowship Program - 1998

Johnson Space Center

Prepared By:	Leo J. LaFrance
Academic Rank:	Associate Professor
University & Department:	New Mexico State University Mechanical Engineering Department Las Cruces, NM 88003-8001

NASA/JSC

Directorate:	Lyndon B. Johnson Space Center
Division:	White Sands Test Facility
Branch:	Propulsion Test Office
JSC Colleague:	David B. Harris
Date Submitted:	March 3, 1999
Grant Number:	NAG9-867

ABSTRACT

The “Dynamic Altitude Simulation Prediction Program,” DASSPP, is a program to predict the transient response of an engine, test cell, ejector system under engine shutdown conditions. These transients are important to know so that corrective modifications can be adapted to prevent any damage to the engine or test cell.

The “Dynamic Altitude System Simulation Prediction Program,” DASSPP, is a major rewrite of the existing program “RL-1000” written in BASIC. The RL-1000 program was written to analyze the transients of the RL-10 system only. The new program is written to run in Excell 97 and utilizes the Visual BASIC language in Excell. The program has many added features not included in the original “Rl-1000’ program. The program utilizes the ejector models developed during the summer of 1997. The new program is very user friendly and utilizes a dialog box for data input.

INTRODUCTION

WSTF tests rocket engines in a simulated high altitude environment. There are several test stands for doing these tests in the 300 and 400 area of WSTF. The test stands consist of a chamber, where the rocket engine is fired, that is kept at the high altitude condition by a steam ejector system. The ejector systems keeps the test stands under a vacuum or very low pressure to simulate the high altitude environment that the engine sees when it operates in space. For a given engine and flight condition, the technicians want to be able to predict how a test stand will perform a test on an engine given the engine mass flow rate, chamber pressure, and nozzle geometry. They also want to know of any adverse transients that may occur during engine shutdown. This work describes the performance modeling of several ejector systems and the subsequent incorporation of the performance models into a program for predicting the transient performance of a combination of test stand and ejector system during engine shutdown.

DYNAMIC ALTITUDE SYSTEM SIMULATION PREDICTION PROGRAM

The Dynamic Altitude System Simulation Prediction Program, DASSPP, is a major rewrite of the existing BASIC language "RL-1000" program. The user of the RL-1000 program sometimes had to go in and change the code for each run because the code did not have all the necessary features. A goal of this work was to generate a user friendly program that would be easy to use and have all the necessary features. Excell 97 was readily available at WSTF therefore it was used for the DASSPP program. The DASSPP program utilizes the Visual BASIC features of the Excell program.

Overview of Calculation Procedure

Most of the calculations in the RL-1000 program were retained in the new DASSPP code. The calculation procedure consists of keeping track of the conditions in the control volume. The control volume consists of the volume of the test stand system from the exit of the diffuser around the elbow to the entrance to the steam ejector system.

The input data to the program consists of steady state engine performance data and chamber pressure vs. time data. The steady state data consists of the chamber pressure, exhaust gas specific heat, exhaust gas molecular weight, exhaust gas mass flow rate, chamber temperature, and injected water mass flow rate. The chamber pressure vs. time data is data for the chamber pressure of an engine as it is shut down. Figure 1 shows a typical plot of chamber pressure vs. time.

The first calculations are for the steady state conditions during firing. The steady state conditions are calculated based on the ejector used. There are three available. The

Figure 1: Measured Chamber Pressure for OME Series 4 Test 8

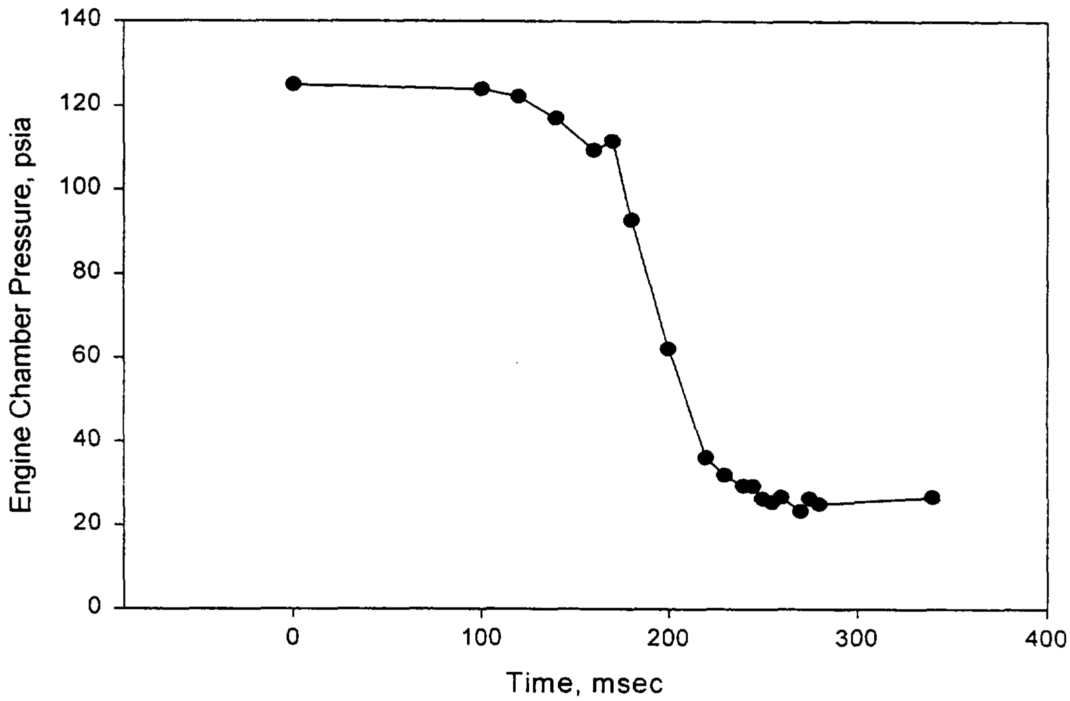

one, two, or three module design curves. The values calculated are the injected water free dry air equivalent, the total free dry air flow, the specific heat of the mixture, the temperature of the mixture, the ejector suction pressure, and the molecular weight of the mixture.

The next stage of the calculations is to keep track of the conditions in the control volume as the engine shuts down. The program increments in time and uses the chamber pressure vs. time information to calculate the engine mass input, the free dry airflow of the ejector based on y-stage pressure. Then the control volume parameters are calculated. They are the total enthalpy of control volume mass, specific heat of control volume mass, temperature of control volume mass, molecular weight of control volume mass, mass extracted by ejectors, and secondary gas flow.

Added Features in the DASSPP

Several features were added to the final DASSPP code to make the program more useful and user friendly. The main input is now accomplished by using a dialog box. All of the program input is contained on the dialog box.

Figure 2: 400 Area LASS Ejector Performance

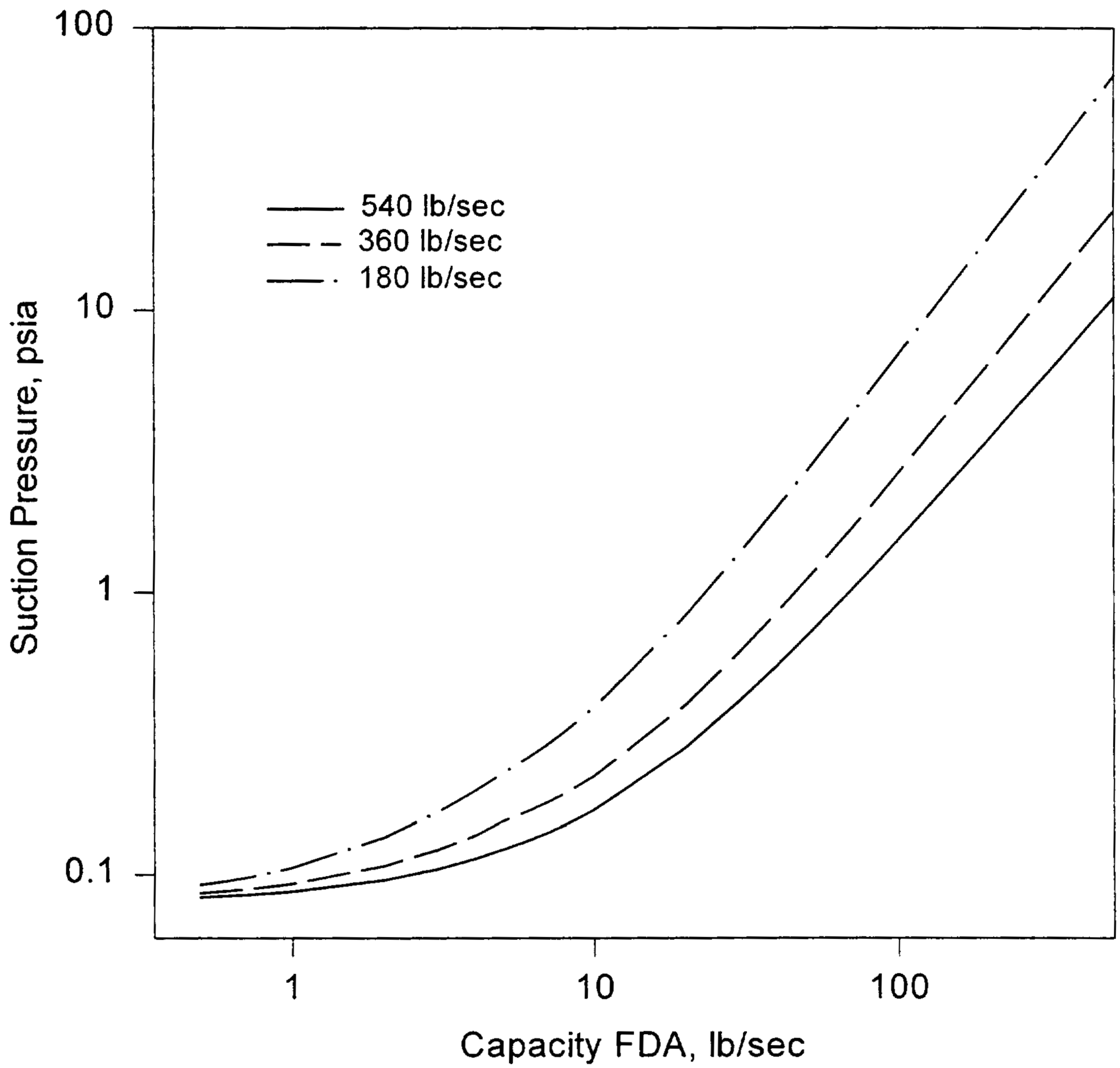

The DASSPP program uses the ejector models developed in the summer of 1997[1] for the steady state operating conditions during firing. They are shown in Figure 2. These models are also used in the transient calculation portion of the program. The transient part of the program required the calculation of the free dry airflow as a function of y-stage pressure. The original models developed were y-stage pressure as a function of free dry airflow. The equation is given as: $SP = A + B \times FDA^{C}$. Where A, B, and C are the curve fit values. SP is suction pressure and FDA is free dry air. The model was modified at low flow rates so that the models would have the proper blank off pressure. The inverse function was developed and is of the form: $FDA = \left[\dfrac{SP - A}{B}\right]^{\frac{1}{C}}$ and at low flow

rates and pressures the Newton's [2] method was used to find the free dry air flow as a function of y-stage pressure. The first initial guess for the Newton method came from the inverse function.

A curve fit of the one module air load curve was developed so that a complete choice was available for the program. The model developed was similar to those

Figure 3: One Module Air Load Curve

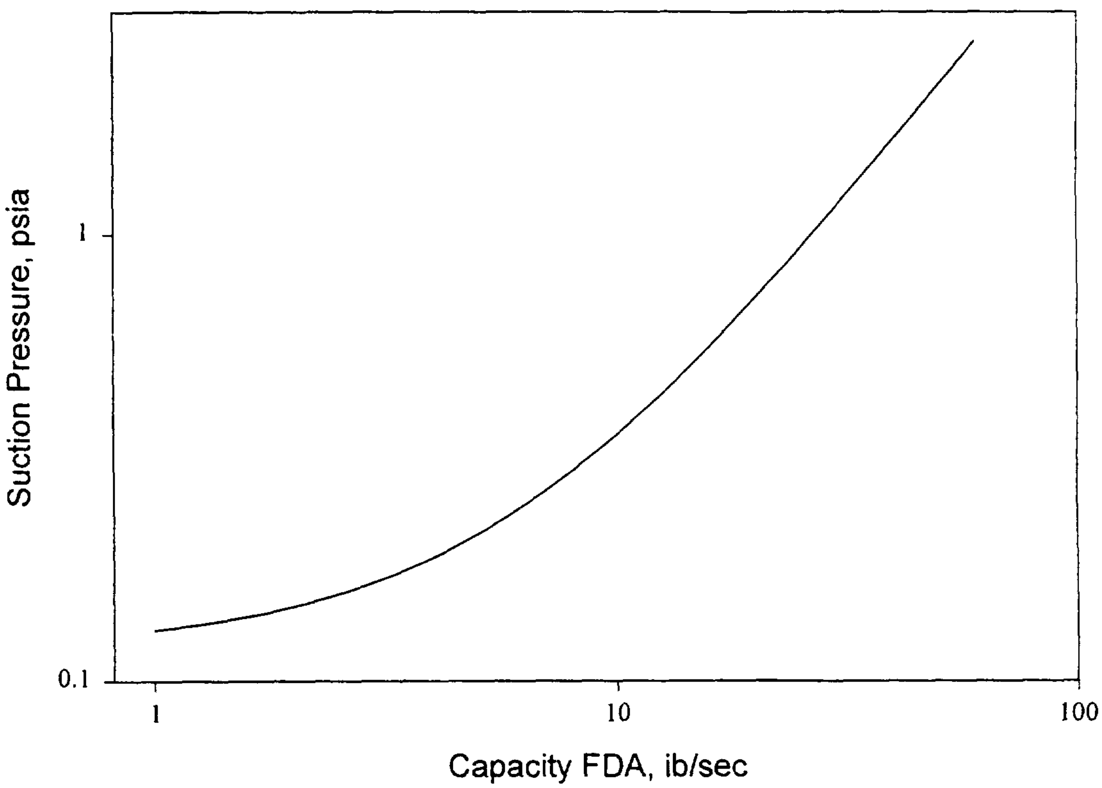

described above The curve fit is shown in Figure 3.

Figure 4: DASSPP Predicted Pressures

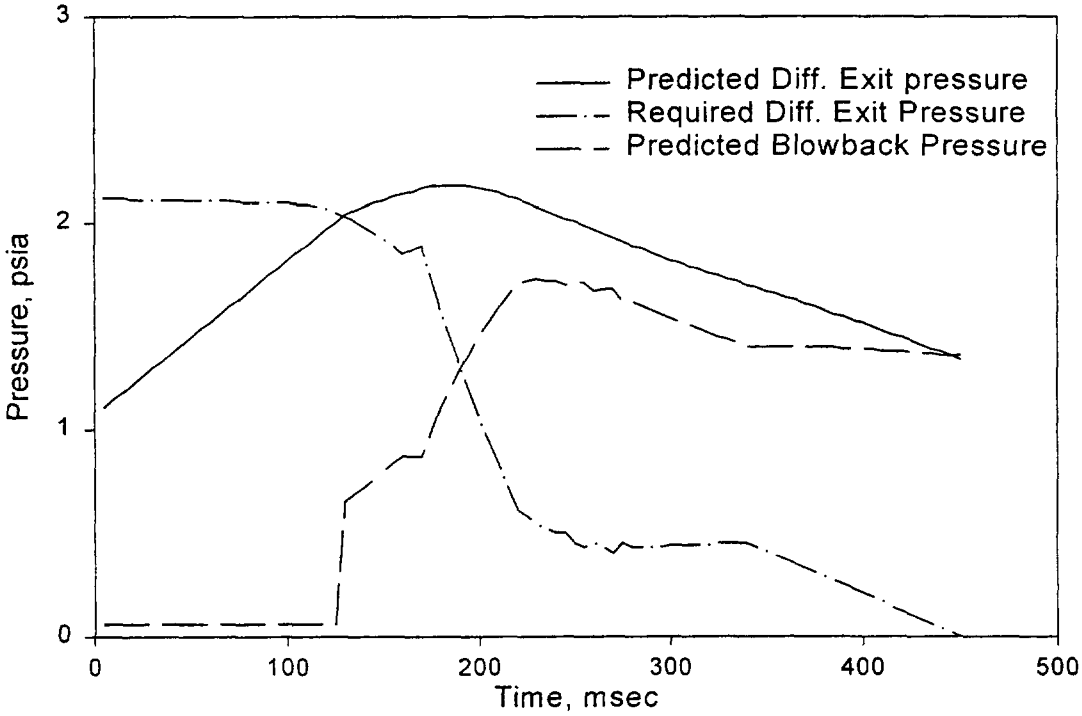

An example run of the DASSPP code is shown in the appendix. The dialog box is included with the typical output produced by the program. Figure 4 shows a plot of the resulting pressures calculated using the program.

CONCLUSIONS AND RECOMMENDATIONS

The program worked well and was very enthusiastically accepted at WSTF. There was a real need for such a program.

The curve fits for the two and three-module air load curves and the alternate Croll Reynolds three module design curve should be analyzed. The curves should be modified to produce smooth curves.

REFERENCES

1. LaFrance, L. J., "Altitude Simulation System Modeling", NASA 1997 Summer Faculty Fellow final report

2. Conte, S. D., "Elementary Numerical Analysis," 1965, McGraw-Hill Inc.

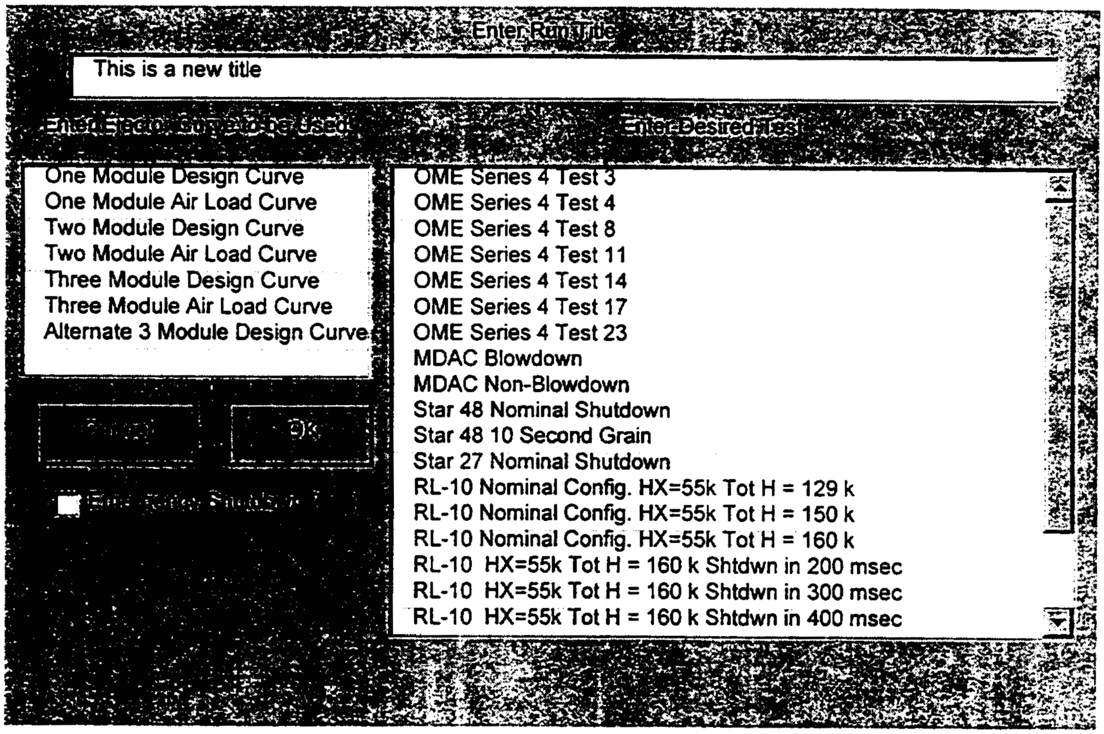
Enter Run Title
This is a new title
Enter Desired Test
One Module Design Curve
One Module Air Load Curve
Two Module Design Curve
Two Module Air Load Curve
Three Module Design Curve
Three Module Air Load Curve
Alternate 3 Module Design Curve
OME Series 4 Test 3
OME Series 4 Test 4
OME Series 4 Test 8
OME Series 4 Test 11
OME Series 4 Test 14
OME Series 4 Test 17
OME Series 4 Test 23
MDAC Blowdown
MDAC Non-Blowdown
Star 48 Nominal Shutdown
Star 48 10 Second Grain
Star 27 Nominal Shutdown
RL-10 Nominal Config. HX=55k Tot H = 129 k
RL-10 Nominal Config. HX=55k Tot H = 150 k
RL-10 Nominal Config. HX=55k Tot H = 160 k
RL-10 HX=55k Tot H = 160 k Shtdwn in 200 msec
RL-10 HX=55k Tot H = 160 k Shtdwn in 300 msec
RL-10 HX=55k Tot H = 160 k Shtdwn in 400 msec

This is a new title

For the OME Series 4 Test 8 Three Module Design Curve

Test Input Data

Chamber Pressure = 125.0
Specific Heat of Exhaust gas = 0.50
Exhaust Molecular Weight = 20.60
Exhaust Mass Flow = 18.30
Combustion Chamber Temperature = 5490.00
Heat Exchanger Pressure Drop at Max Thrust = 0.00
Heat Exchanger Enthalpy Extraction at Max Flow = 0.00 BTU/SEC
Duct Pressure Loss = 0.00
The Pressure vs Time data appears at the end of the report

Steady State Conditions Before Shutdown

Mass in the Elbow = 8.55
Control Volume = 4550.0
Steam Free Dry Air = 49.46
Exhaust Equivalent FDA = 23.50
Total Free Dry Air = 72.96
Injected H2O Mass = 35.55
Y Stage Temperature = 539.8
Y Stage Pressure = 1.071
Mix Specific Heat = 0.5
Mix Molecular Weight = 18.81
Differential exhaust pressure = 1.07

Time mSec.	Y Stg. PsiA	DifX PsiA	Req. DifX	Eng. PChamb.	Nozz. Amb. P.	Mass Int. L.	Mass Lve. L.	Elb. Mass	FDA Out	Elb. Temp.	Static Cell P.	Tsat. YStg.	Sec. Mass
5	1.11	1.11	2.12	124.94	0.06	60.47	54	8.84	72.75	539.8	0.1	105	6.63
10	1.15	1.15	2.12	124.89	0.06	60.45	55.6	9.15	74.92	539.7	0.1	106.1	6.62
15	1.18	1.18	2.12	124.83	0.06	60.43	57.19	9.45	77.06	539.6	0.099	107.2	6.60
20	1.22	1.22	2.11	124.78	0.06	60.41	58.77	9.75	79.18	539.5	0.099	108.3	6.59
25	1.26	1.26	2.11	124.72	0.06	60.39	60.34	10.05	81.29	539.4	0.099	109.4	6.58
30	1.3	1.3	2.11	124.67	0.06	60.37	61.9	10.35	83.39	539.3	0.099	110.4	6.56
35	1.33	1.33	2.11	124.61	0.06	60.34	63.44	10.66	85.46	539.2	0.099	111.4	6.55
40	1.37	1.37	2.11	124.56	0.06	60.32	64.97	10.96	87.52	539	0.098	112.4	6.54
45	1.41	1.41	2.11	124.5	0.06	60.3	66.5	11.26	89.57	538.9	0.098	113.3	6.52
50	1.45	1.45	2.11	124.45	0.06	60.28	68.01	11.56	91.6	538.7	0.098	114.3	6.51
55	1.49	1.49	2.11	124.4	0.06	60.26	69.51	11.86	93.62	538.5	0.098	115.2	6.50
60	1.52	1.52	2.11	124.34	0.06	60.24	71	12.16	95.63	538.4	0.098	116.1	6.48
65	1.56	1.56	2.11	124.29	0.06	60.22	72.49	12.46	97.62	538.2	0.097	116.9	6.47
70	1.6	1.6	2.11	124.23	0.06	60.2	73.96	12.76	99.6	538	0.097	117.8	6.46
75	1.63	1.63	2.1	124.18	0.06	60.17	75.43	13.07	101.57	537.8	0.097	118.6	6.44
80	1.67	1.67	2.1	124.12	0.06	60.15	76.88	13.37	103.53	537.6	0.097	119.4	6.43

85	1.71	1.71	2.1	124.07	0.06	60.13	78.33	13.67	105.48	537.3	0.097	120.2	6.42
90	1.75	1.75	2.1	124.01	0.06	60.11	79.77	13.97	107.41	537.1	0.096	121	6.41
95	1.78	1.78	2.1	123.96	0.06	60.09	81.21	14.27	109.33	536.9	0.096	121.8	6.39
100	1.82	1.82	2.1	123.9	0.06	60.07	82.63	14.57	111.24	536.7	0.096	122.5	6.38
105	1.86	1.86	2.09	123.47	0.06	59.99	84.05	14.87	113.14	536.4	0.096	123.3	6.37
110	1.89	1.89	2.09	123.05	0.06	59.92	85.45	15.17	115.02	536	0.096	124	6.35
115	1.93	1.93	2.08	122.63	0.06	59.84	86.84	15.47	116.88	535.5	0.095	124.7	6.34
120	1.97	1.97	2.07	122.2	0.06	59.77	88.22	15.77	118.71	534.9	0.095	125.3	6.33
125	2	2	2.05	120.9	0.06	59.56	89.58	16.07	120.52	534.2	0.095	126	6.31
130	2.04	2.04	2.03	119.6	0.65	59.36	90.91	16.36	122.28	533.1	0.095	126.6	6.30
135	2.06	2.06	2.01	118.3	0.69	36.46	91.91	16.57	123.59	531.9	0.099	127.1	-16.41
140	2.08	2.08	1.98	117	0.72	35.42	92.67	16.75	124.56	530.3	0.103	127.4	-17.26
145	2.1	2.1	1.95	115.08	0.76	34.18	93.39	16.92	125.47	528.4	0.107	127.7	-18.21
150	2.11	2.11	1.92	113.15	0.8	32.95	94.05	17.09	126.28	526.2	0.112	128	-19.17
155	2.13	2.13	1.89	111.23	0.84	31.75	94.66	17.25	127.02	523.6	0.117	128.3	-20.08
160	2.14	2.14	1.85	109.3	0.87	30.6	95.22	17.41	127.68	520.6	0.122	128.5	-20.95
165	2.15	2.15	1.87	110.4	0.87	30.6	95.75	17.56	128.29	517.7	0.127	128.7	-21.12
170	2.17	2.17	1.89	111.5	0.87	30.75	96.3	17.72	128.94	515.1	0.132	128.9	-21.12
175	2.18	2.18	1.73	102.15	0.99	27.04	96.79	17.86	129.48	511.5	0.138	129.1	-23.47
180	2.18	2.18	1.57	92.8	1.11	20.59	97.1	17.98	129.73	506.7	0.144	129.2	-26.27
185	2.18	2.18	1.44	85.15	1.2	14.4	97.26	18.07	129.8	502.4	0.151	129.2	-28.59
190	2.18	2.18	1.31	77.5	1.29	8.39	97.31	18.13	129.74	498.5	0.159	129.2	-30.74
195	2.18	2.18	1.18	69.85	1.37	2.44	97.25	18.15	129.54	495.1	0.167	129.1	-32.83
200	2.17	2.17	1.05	62.2	1.46	-3.45	97.08	18.15	129.2	492	0.176	129	-34.85
205	2.16	2.16	0.94	55.7	1.52	-8.43	96.8	18.12	128.74	489.3	0.185	128.8	-36.55
210	2.15	2.15	0.83	49.2	1.59	-13.3	96.44	18.06	128.17	486.9	0.195	128.6	-38.13
215	2.13	2.13	0.72	42.7	1.65	-18.1	95.98	17.98	127.49	484.8	0.205	128.4	-39.65
220	2.12	2.12	0.61	36.2	1.71	-22.8	95.43	17.88	126.71	483	0.215	128.2	-41.13
225	2.1	2.1	0.58	34.1	1.72	-24.3	94.82	17.76	125.84	481.3	0.226	127.9	-41.55
230	2.08	2.08	0.54	32	1.73	-25.5	94.18	17.64	124.94	479.8	0.237	127.5	-41.71
235	2.06	2.06	0.52	30.7	1.72	-26.2	93.52	17.51	124.02	478.3	0.248	127.2	-41.68
240	2.04	2.04	0.5	29.4	1.72	-26.7	92.86	17.37	123.09	476.9	0.259	126.9	-41.60
245	2.02	2.02	0.5	29.4	1.7	-26.4	92.18	17.24	122.16	475.5	0.27	126.6	-41.21
250	2.01	2.01	0.45	26.4	1.72	-28.1	91.51	17.1	121.22	474.2	0.281	126.2	-41.44
255	1.99	1.99	0.43	25.4	1.71	-28.5	90.81	16.96	120.26	473	0.292	125.9	-41.38
260	1.97	1.97	0.45	26.8	1.67	-27.1	90.11	16.82	119.29	471.7	0.304	125.5	-40.65
265	1.95	1.95	0.43	25.1	1.68	-27.8	89.43	16.69	118.35	470.5	0.314	125.2	-40.50
270	1.93	1.93	0.4	23.4	1.68	-28.7	88.74	16.54	117.4	469.3	0.325	124.9	-40.52
275	1.91	1.91	0.45	26.4	1.62	-26.1	88.04	16.41	116.45	468.1	0.336	124.5	-39.48
280	1.89	1.89	0.43	25.1	1.62	-26.5	87.39	16.28	115.54	466.8	0.347	124.2	-39.16
285	1.88	1.88	0.43	25.24	1.6	-26	86.73	16.14	114.63	465.6	0.358	123.8	-38.77
290	1.86	1.86	0.43	25.38	1.58	-25.5	86.08	16.01	113.74	464.3	0.368	123.5	-38.30
295	1.84	1.84	0.43	25.52	1.56	-24.9	85.44	15.89	112.86	463.1	0.379	123.2	-37.84
300	1.82	1.82	0.44	25.67	1.54	-24.4	84.81	15.77	111.99	461.8	0.389	122.8	-37.39
305	1.81	1.81	0.44	25.81	1.52	-23.9	84.2	15.64	111.14	460.5	0.399	122.5	-36.94
310	1.79	1.79	0.44	25.95	1.51	-23.4	83.59	15.53	110.31	459.2	0.41	122.2	-36.50
315	1.78	1.78	0.44	26.09	1.49	-22.9	83	15.41	109.49	457.9	0.42	121.8	-36.07
320	1.76	1.76	0.44	26.23	1.47	-22.4	82.42	15.3	108.68	456.5	0.43	121.5	-35.65
325	1.75	1.75	0.45	26.38	1.45	-21.9	81.84	15.19	107.89	455.2	0.44	121.2	-35.23

330	1.73	1.73	0.45	26.52	1.44	-21.4	78.54	15.08	103.5	453.8	0.449	120.9	-34.83
335	1.72	1.72	0.45	26.66	1.42	-20.9	77.89	14.97	102.6	452.4	0.459	120.6	-34.42
340	1.7	1.7	0.45	26.8	1.4	-20.4	77.24	14.87	101.71	451	0.469	120.3	-34.03
345	1.69	1.69	0.43	25.58	1.4	-21	76.6	14.77	100.84	449.7	0.478	120	-33.95
350	1.67	1.67	0.41	24.36	1.4	-21.6	75.95	14.66	99.95	448.4	0.488	119.7	-33.94
355	1.66	1.66	0.39	23.15	1.4	-22.2	75.29	14.55	99.05	447.1	0.498	119.3	-33.93
360	1.64	1.64	0.37	21.93	1.4	-22.8	74.62	14.44	98.13	446	0.507	119	-33.92
365	1.63	1.63	0.35	20.71	1.4	-23.4	73.94	14.32	97.21	444.8	0.517	118.7	-33.89
370	1.61	1.61	0.33	19.49	1.4	-24	73.24	14.2	96.27	443.8	0.526	118.3	-33.87
375	1.6	1.6	0.31	18.27	1.4	-24.6	72.54	14.08	95.32	442.8	0.536	118	-33.84
380	1.58	1.58	0.29	17.05	1.4	-25.1	71.82	13.96	94.36	441.8	0.546	117.6	-33.80
385	1.56	1.56	0.27	15.84	1.4	-25.7	71.1	13.83	93.38	440.9	0.555	117.3	-33.76
390	1.55	1.55	0.25	14.62	1.39	-26.3	70.36	13.7	92.4	440.1	0.565	116.9	-33.71
395	1.53	1.53	0.23	13.4	1.39	-26.9	69.62	13.56	91.4	439.3	0.575	116.5	-33.66
400	1.52	1.52	0.21	12.18	1.39	-27.4	68.86	13.43	90.39	438.6	0.584	116.2	-33.61
405	1.5	1.5	0.19	10.96	1.39	-28	68.09	13.29	89.37	438	0.594	115.8	-33.55
410	1.48	1.48	0.17	9.75	1.38	-28.5	67.32	13.15	88.33	437.4	0.604	115.4	-33.48
415	1.46	1.46	0.14	8.53	1.38	-29.1	66.53	13	87.29	436.9	0.613	114.9	-33.41
420	1.45	1.45	0.12	7.31	1.38	-29.6	65.73	12.86	86.23	436.4	0.623	114.5	-33.34
425	1.43	1.43	0.1	6.09	1.37	-30.2	64.92	12.71	85.16	436	0.632	114.1	-33.26
430	1.41	1.41	0.08	4.87	1.37	-30.7	64.11	12.55	84.08	435.7	0.642	113.7	-33.18
435	1.39	1.39	0.06	3.65	1.37	-31.2	63.28	12.4	82.99	435.5	0.652	113.2	-33.09
440	1.38	1.38	0.04	2.44	1.36	-31.8	62.44	12.24	81.89	435.3	0.661	112.8	-33.00
445	1.36	1.36	0.02	1.22	1.36	-32.3	61.6	12.08	80.78	435.2	0.671	112.3	-32.90
450	1.34	1.34	0	0	1.36	-32.8	60.74	11.92	79.66	435.1	0.68	111.8	-32.80

The maximum blowback pressure was 1.73 at time 230 msec

(15)
IN-27

A STUDY OF ABERRANT GLYCOSYLATION IN SIMULATED MICROGRVITY USING LASER INDUCED AUTOFLUORESCENCE AND FLOW CYTOMETRY

Final Report

NASA/ASEE Summer Faculty Fellowship Program - 1998
Johnson Space Center

Prepared by:	B. DeSales Lawless, PhD
Academic Rank:	Professor
University and Department	Fordham University Department of Science and Mathematics New York, N.Y., 10023
Rockefeller University	Adjunct Professor Department of Immunology and Cell Physiology New York, N.Y., 10021
NASA/JSC Directorate Division:	 Space and Life Sciences Medical Sciences
Branch:	SD12/Biotech Cell Science Office
JSC Colleague:	Dennis R. Morrison, Ph.D.
Date submitted	August 7, 1998
Contract Number	NAG 9-867

ABSTRACT

A number of pathologies and cellular dysfunctions including neoplasms have been correlated with autofluorescence. The complications of aging and diabetes have been associated with the accumulation of non-enzymatic glycosylations of tissue macromolecules. These products are known as the Advanced Glycosylated End Products (AGEs). A physical property associated with AGEs is the emission of 570 nm or 630 nm light energy (autofluorescence) following the absorption of 448 nm energy associated with the argon laser. This investigation sought to assess the induction of argon-laser induced autofluorescence in a variety of in vitro culture systems. Different fluorescence intensities distinguished tumor lines from normal cell populations. Laser-stimulated autofluorescence discriminated primary cultures of lymphocytes grown in the presence of excess glucose as opposed to normal glucose concentrations. The effects of deglycosylating agents upon laser-induced autofluorescence were also assessed. The studies included studies of cell cycle analysis using Propidium Iodide stained DNA of cells grown in simulated microgravity using NASA Bioreactor Vessels in media of normal and elevated glucose concentrations.

INTRODUCTION

These investigations were prompted by our deep interest in both normal and aberrant glycosylation. In earlier carbohydrate studies we found the flow cytometer and its argon laser of great value.

The complications of aging and diabetes are largely the result of accumulation of Advanced Glycosylation End Products (AGEs) which result from the non-enzymatic glycosylation of proteins (Brownlee, M) Long-term hyperglycemia is considered to be an important factor contributing to the accumulation of these glycoconjugates on tissue The age-related changes in tissue proteins are thought to result from the non-enzymatic reactions between proteins and reducing sugars. Several factors are believed to influence the extent of glycation , one of which is the ambient glucose concentration. This work was largely based on this premise. The interaction between the carbonyl group of a reducing sugar results in a Schiff base adduct, which can undergo an Amadori rearrangement to form a ketoamine adduct. (Sharon) The process is known as glycation, and these products can undergo multiple rearrangements over time to become the irreversibly bound, chemically-reactive Advanced Glycosylated End Products (AGEs). Tumor antigens and numerous cancers are characterized by altered glycoproteins and there is increasing evidence that the plaques characteristic of Alzheimer's disease are also the result of aberrant glycosylation.

A physical property associated with AGEs is the emission of 570 nm or 630 nm light energy (autofluorescence) following the absorption of 448 nm energy associated with the argon laser. In these investigation we observed the induction of Laser Induced Fluorescence (LIF) on cell cultures in vitro. In earlier studies with murine lymphocyte populations we assessed the induction of autofluorescence following the supplementation of growth medium with exogenous glucose. Our results demonstrated that cells cultured with exogenous glucose (400 mg%) increased autofluorescence when compared to cultures grown in conventional growth medium (100 mg% glucose). The intensity of fluorescence was proportional to the glucose concentration and time duration of exposure.

The present studies introduced a new variable --..simulated microgravity. In these studies Human Peripheral Blood Mononuclear Cells (PBMCs) were used. Cells were cultured in flasks at 37° C. at unit gravity served as controls. One cell population was suspended in media containing normal glucose and another population in normal media at elevated glucose. Similar experiments were performed NASA bioreactors which simulate an environment of microgravity. In these studies laser induced autofluorescence discriminated primary cultures of lymphocytes grown in excess glucose as opposed to normal glucose concentrations. Differences in fluorescence intensities distinguished tumor cell lines from normal cell populations. The effects of deglycosylating agents upon laser-induced autofluorescence were also assessed.

MATERIALS AND METHODS

Cells and media

Normal human blood was obtained from the Gulf Coast Regional Blood Center (Houston, Texas). The peripheral blood mononuclear cells (PBMC) were isolated on a Ficoll-Hypaque gradient (Pharmacia LKB, Piscataway, N.J.), washed three times in PBS and resuspended in complete RPMI-1640 (GIBCO-BRL, Grand Island, NY) supplemented with 10% heat-inactivated fetal bovine serum (Hyclone Labs, Logan, Utah) and penicillin (100 U/ml-streptomycin (100 ug/ml. GIBCO-BRL). Cell counts were determined with a hemacytometer and cell viability determined by trypan blue exclusion. Glucsose, Na+, K+ Cl- concentrations in the media were checked using the Portable Clinical Analyzer, I-State, from I-Stat Corporation, Princeton, N.J.

RWV Bioreactor

There are two types of NASA rotating wall vessels (RWV) Bioreactors used in simulating some aspects of microgravity. The HARV (High Aspect Ratio Vessel) with a volume of 10 ml and a rotation speed of 14 rpm was used in these studies.

Flow Cytometry Analysis

Cell data were acquired on a Becton Dickinson FACS-Calibur Flow Cytometer and analyzed with the Becton-Dickinson ModFit Software program. 10,000 events were recorded as dot plots with side scatter vs forward scatter ordinates. In all experiments, cells exhibiting 90 degree scatter were eliminated as dead and large granular cells were excluded from analysis by gating.

Laser Induced Autofluorescence

Cell concentrations were adjusted to 1 x 10^6/ml. In control studies cells were cultured in complete medium which contained approximately 100 mg% glucose. The glucose concentration was adjusted to 400 mg% in the test cells. These cell suspensions in the HARV were maintained at 37°C in 5% CO_2 atmosphere. Data were collected from aliquots using side scatter vs log FL1 (FITC) green emitted fluorescence. Overlay histogram plots of FL1 values for control vs test indicated cells absorbing the laser energy and retransmitting it as light in the green spectrum.

In cell cycle determinations, we followed the procedure of Shapiro for DNA staining. Cells were pelleted, washed and resuspended in 70% cold ethanol overnight. Ethanol fixative was removed and 100 ul Propidium Iodide in buffer was added for ten minutes. Residual RNA was eliminated by ribonuclease contained in the PI buffer. The cells ewere then stimulated by the argon laser of the flow cytometer. Fluorescence was recorded as histogram graph s of side scatter vs linear FL2. The linear scale permitted us to read 2N (diploid) and 4N (tetraploid- dividing) cells. Cells undergoing apoptosis (programmed cell death appeared as hypodiploid. Software statistical analysis gave the cell cycle percentages including those in the S-phase.

RESULTS

Distinguishing malignant cells from normal cells

This part of our investigation was completed at the FDA Laboratory of Dr. MaryAnn Principato. We did not repeat it here since our cancer cell lines were not available to us.

When Jurkat Cance Cells (Clone E6-1, Acute T-cell Leukemia, human) were stimulated by the argon laser of the flow cytometer, they emitted fluorescent light in the FITC (green) spectral region. The cells were suspended in HBSS (Hanks Balanced Salt Solution) with 3% FCS (fetal calf serum). The cytometer was set at side scatter vs log FL1 (green fluorescence) and data were recorded in histograms. Normal mrine splenocytes and bone marrow cells showed no appreciable fluorescence and served as conrols. The results confirmed our hypothesis that LIF could be used as an early assay for malignancy and aberrant glycosylation. The conclusion was based on the assumption that a tumor glycoconjugate antigen was responsible for the autofluorescence. It was furter indication that LIF can be used in some instances in determining malignancy and aberrant glycosylation.

Other cancer cell lines that were found to asutofluoresce under LIF were Daudi (B-Lymphoblast from Human Burkitts Lymphoma), Raji, (Human lymphoblast-like line), K-560, Human myelogenous leukemia), and HL-50 cell lines.

Cell Separation using LIF

Several invstigators have reported data that LIF can serve as a separation and fractionation protocol if some of the cells of a heterogeneous mixture autofluoresce under LIF more than others. In this instance LIF is a procedure for depleting or recovering a specific cell line from a suspension mixture. It has the added advantage of not adding extraneous materials to the culture which might functionally or morphologically affect the cells. (Carin, et al) Separation of alveolar macrophages and dendritic cells have been separated by this procedure. (Carin, et al).

A Fluorescence Activated Cell Sorter was not available to us at Johnson Space Center. We plan to study cell fractionation and separations using LIF in our home facility.

Histogram data from our laser stimulation studies appear in Fig 5. The Mean Fluorescence Intensity (MFI) of PBMC gown in unit gravity in the laboratory and in microgravity in the Bioreactor are compared in the graphs.

Cell cycle alterations in hyperglycemia.

A yet to be explained phenomenon in the JSC investigations is that a tetraploid peak of cells was found after several days in HARV culture. These 4N cells we re evident in both the 100 mg% glucose media and in the elevated glucose. One postulate is that a yet to be defined mitogen appears in the media when the cells are grown in the Rotating Wall Vessel (HARV). The reputed mitogen may possibly be a response to the stress of rotation or to the reduced microgrvity environment. Also to be identified is the cell that produces the postulated mitogen. We have found that a similar response is present when PBMCs are grown in high concentrations, e.g., 10^7cells/ml rather than 10^6cells/ml.

Cell cycle alterations in hyperglycemia.

A yet to be explained phenomenon in the JSC investigations is that a tetraploid peak of cells was found after several days in HARV culture. These 4N cells we re evident in both the 100 mg% glucose media and in the elevated glucose. One postulate is that a yet to be defined mitogen appears in the media when the cells are grown in the Rotating Wall Vessel (HARV). The reputed mitogen may possibly be a response to the stress of rotation or to the reduced microgrvity environment. Also to be identified is the cell that produces the postulated mitogen. We have found that a similar response is present when PBMCs are grown in high concentrations, e.g., 10^7cells/ml rather than 10^6cells/ml.

Cell cycle analysis of PBMC grown in unit gravity in our laboratory are depicted in Fig 1 and Fig 2. The cells grown in simulated microgravity are shown in Fig 3 and 4. The tetraploid (4N) peak which identify dividing cells appears only in the cells grown in the HARV in simulated microgravity. The data was collected using the Becton-Dickinson ModFit software program.

Figure #1 PBMC in flask and cultured at unit gravity in normal glucose

G2-M = 0.00% (dividing cells)
Apoptosis = 4.95% (programmed cell death)

Figure #2 PBMC in flask at unit gravity in high glucose.

G2-M = 0.57%
Apoptosis = 6.89%

Figure #3 PBMC in HARV - simulated microgravity - normal glucose

G2-M = 13.92%
Apoptosis = 0.312%

Figure #4 PBMC in HARV - simulated microgravity - high glucose.

G2-M = 14.99%
Apoptosis = 27.04%

DISCUSSION

The objective of this research is to demonstrate that LIF is an efficient assay for early detection of cancer and dysfunctions associated with aberrant glycosylation. When the assays show positive autofluorescence, the sugars on the glycoconjugates can be characterized by a panel of fluorescinated lectins. Cells that autofluoresce by absorbing the laser energy can be separated from cells that do not; therefore, LIF becomes a valuable technique. Researchers have separated dendritic cells from macrophages in this manner. (Carin) splenic macrophages and murine Kuppfer cells have also been seprated (ten Hagen). Early detection of colon cancer cells has been detected by LIF on in situ tissues. (Dus) Bladder cancer has likewise been recognized. (Koenig). These assays were performed histochemically. Cellular biopsies could be performed on in vitro cell suspensions as well by a single investigation with flow cytometry. Glycosylation is a frequently encountered posttranslational modification in cells. (Nigel) Altered glycosylation patterns have been found in most types of cancer cells. (Taylor) Aberrant glycosylation usually occurs on cell surface compounds but is alsos common in secreted mucins. (Dabelsteen).

Aberrant glycosylation in the formation of AGEs has been firmly implicated in the symptomology of diabetes and the aging process. (Brownlee) Vlassara) The presence of AGE formation is readily detected with LIF. The effectiveness of methodologies which prevent or reverse glycosylations can likewise be monitored. We have successfully used hyperbaric oxygenation treatment to reverse this formation; others have used aminoguanidine or butyrate. (Kimbrell) (Jacob)

All cells autofluoresce to some degree when stimulated by appropriate electromagnetic energy. In addition to cell surface compounds, LIF is observed in some degree by flavins, aromatics and various granules. The coenzyme $NADH_2$ absorbs the argon laser energy and can be used to appraise the oxidative state of the cell. Its excess is an indication of oxidative activity which is characteristic of cancerous cells. In LIF, fluorochromes absorb light at a characteristic wave length and then transmits it at a lower energy and longer wave length. The fluorochrome FITC (fluoroisothiocyanate) absorbs the argon light wave length 488 nm and emits light of 525 nm (green). . The energy is absorbed and excites electrons. When these electrons return to a lower energy level they transmit light of a lower energy and a longer wave length.

SUMMARY

Single exposure of cells to the argon laser can provide significant information . LIF can identify cancerous cells and aberrantly glycosylated cells. After the initial observations are obtained, the cells may be stained with propidium iodide and cell cycle data can be determined. LIF positive cells can be separated for LIF negative cells by the fluorescence activated cell sorter or they can be gated and separated by other protocols. In combination with lectin chemistry, LIF can provide additional information. Various protocols which prevent or enhance glycosylation can be evaluated and cell responses in conditioned media can be assessed. As a procedure for early detection of cancer LIF is a valuable and inexpensive time-saving procedure.

This research project produced some unexpected results in our studies with LIF and simulated microgravity. We learned that human PBMCs proliferate in an environment that simulates some aspects of microgravity. Furthermore, the proliferation takes place in microgavity in a medium containing normal glucose concentrations. This data will be meaningful for those research scientists who are doing studies which involve simulated microgravity. It will also be of Importance for those involved in the well-being of our astronauts undertaking long term space missions.

Cell Cycle Analysis of PBMCs at unit gravity and simulated microgravity

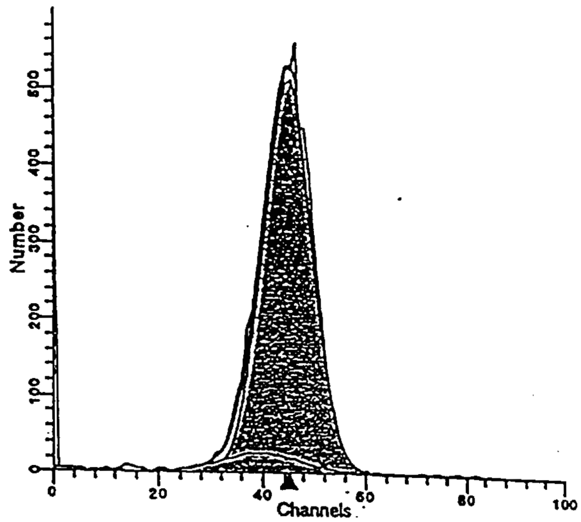

Fig 1
Cells in unit gravity - high glucose

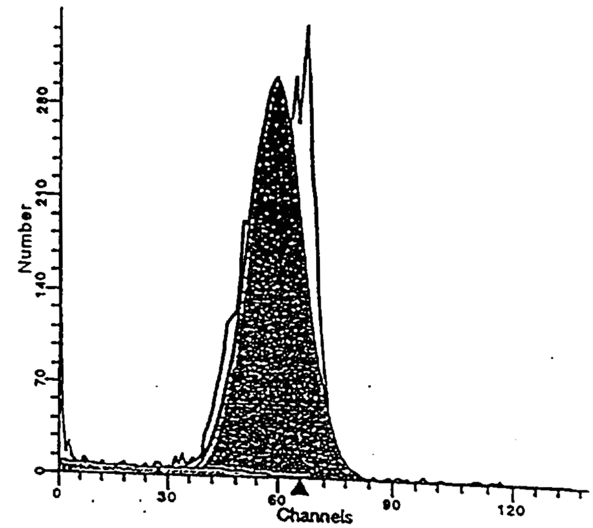

Fig 2
Cells in unit gravity - normal glucose

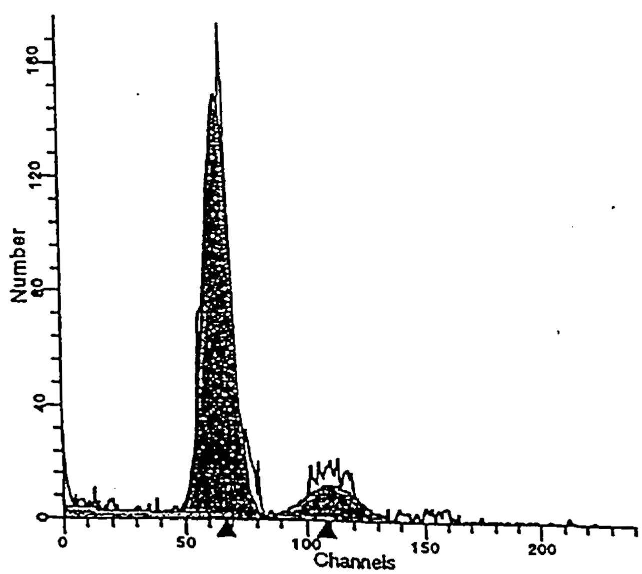

Fig 3
Cells in simulated microgravity - normal glucose

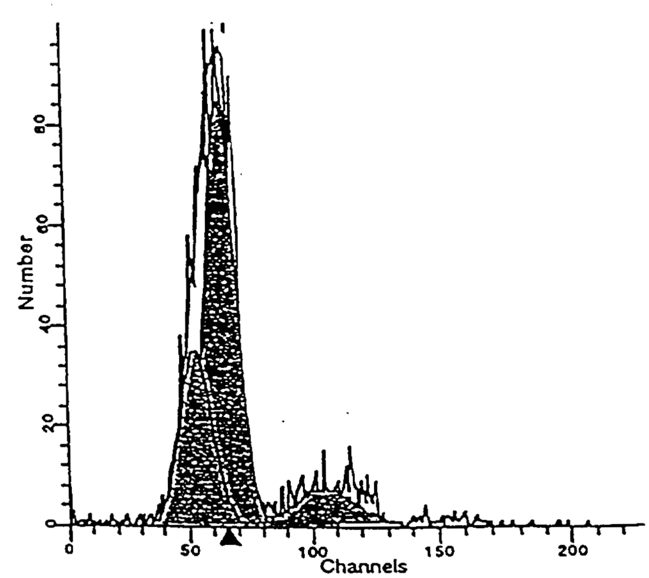

Fig 4
Cells in simulated microgravity - high glucose

Argon Laser Stimulation of cells at unit gravity and simulated microgravity

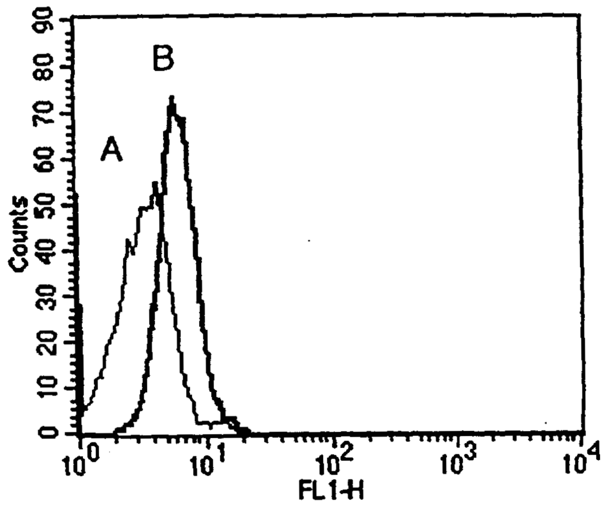

PBMC in flask

MFI for A = 3.5
MFI for B = 6.1

A = normal glucose

B = elevated glucose

MFI = mean fluorescence intensity

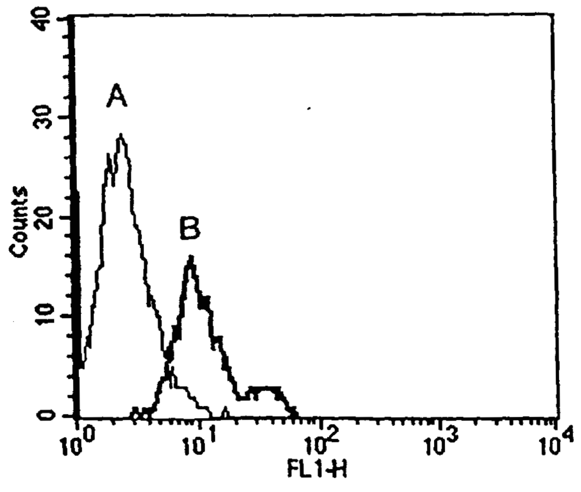

PBMC in HARV (High Aspect Ratio Vessel)

MFI for A = 1.6
MFI for B = 10.5

Fig 5 Histogram data of PBMCs from Flow Cytometer
(upper) unit gravity in flask (lower) simulated microgravity in HARV
(a) normal glucose (b) elevated glucose
There is a significant increase in FL1 fluorescence as shown by log scale x-axis

BIBLIOGRAPHY

Anidjar, M., et al., "Argon laser induced autofluorescence may distinguish between normal and tumor human urothelial cells." May, 1996. J. Urol., 155(5):1771-4

Bender, Armin, "Inactivated Influenza Virus, when Presented on Dendritic Cells, Elicits Human CD8+ Cytolytic T Cell Responses," J. Exp. Med., 182, Dec 1995, 1663-1671.

Boisteau, O., "Induction of apoptosis, in vitro and in vivo, on colonic tumor cells of the rat after sodium butyrate treatment.", Bulletin du Cancer. 83(3): 197-204, 1996, Mar.

Brockhausen, Inka and Huhns, W., "Glycoproteins and Human Disease." R.G.Landes Co, N.H.,1997

Brownlee, M., "Glycosylation of proteins and microangiopathy." Hosp Pract, 1992, Feb; 27(1):46-50

Brownlee, Michael, "Advanced Protein Glycosylation in Diabetes and Aging" annu. Rev. Med. 1995, 46:223-34

Carin, E.G.., et al., "Separation of Alveolar Macrophages and Dendritic Cells via autofluorescence: phenotypical and functional characterization." J. Leukoc. Biol. 53: 504-510; 1993

Cooper, David. Dissertation: 1998, Houston, Texas. "Suppression of T Lymphocyte Activation in Simulated Microgravity. " Graduate School of Biomedical Sciences, University of Texas

Dabelsteen, E., "Carbohydrate antigens and cancer." Ugeskr Laeger, 1993 Apr 26; 155(17): 1270-1275/

Dennis, J.W., "Swainsonine, prototype for a new class of anticancer agents." Clinical Cancer Research, 1:935-944, 1995

Fang, S.Y., "Assessment of cell ssurface glycoconjugates in normal, benign and malignant human nasal mucosa." Rhinology, 1997 Ded; 35(4): 166-170

Galustian C., "Swainsonine, a glycosylation inhibitor, enhances both lymphocyte efficacy and tumour susceptibility in LAK and NK cytotoxicity." Immunopharmacology, 1994, Mar; 27(2): 165-172.

Glinsky, G.V., "Antigen presentation, aberrant glycosylation and tumor progression" Critical Reviews in Oncology/Hemastology, 17, 1994 27-51, 1994.

Hakomori, S., "Tumor malignancy defined by aberrant glycosylation." Cancer Res, 1996, 56(23):5309-18

Jacob, G.S., "Glycosyslation inhibitors in biology and medicine." Curr. Opin. Struct. Biol., 1995 Oct: 5(5): 605-6

Kim, YS., "Mucin glycoproteins in colonic neoplasia" Keio J Med, 1998, Mar 47(1):10-18

Kimbrell, P.N., Lawless, B.D., et al., "Hyperbaric Oxygenation Treatment alters Immune Response in Non-Healing Wounds of Patients with Diabetes." Aviation, Space and Envioronmental Medicine, 66(5):488, 1995.

Koenig, K and Schneckenburger, H., "Laser-Induced Autofluorescence for Medical Diagnosis." Journal of Fluorescence, Vol 4, No. 1, 1994 (17-25)

Koscielak, J., "Diseases of Aberrant Glycosylation." Acta Biochim Pol, 42(1):1-10, 1995

Lewis, ML., Lawless, BD., et al. "Spaceflight alters microtubules and increases aoptosis in human lymphocytes (Jurkat)". FASEB J. 12, 1007-1018 (1998)

McIntyre, KM, "The Influence of hyperbaric oxygenation on leukocyte viability and surface protein expression." Aviat Space Environ Med, 1997, Dec; 68 (12): 1129-1133.

Monici, M., "Natural Fluorescence of White Blood Cells: Spectroscopic and Imaging Study, J. Photochem Photobiol 1995 Sept: 30(1)29-37.

Principato, M.A., Lawless, B.D., Reese, K., Roth, G. Foreman,A. "Glycoconjugate Distribution in Mouse Peripheral and Gut-associated :Lymphocytic Populations. " Abstract G-12, FORUM ON REGULATORY BIOSCIENCES, FDA, Washington, D.C.v., 1996, Dec

Roberts, J., "Role of Protein Glycosyslation Inhibitors in the Prevention of Metastasis and Therapy of Cancer." Cancer Detect Prevent., 1996; 20 (5).

Shapiro, Howard M., Practical Flow Cytometry, Wiley-Liss, New York, 1995.

Sharon, Nathan and Halina Lis, "Carbohydrates in Cell Recognition", Scientific American, Jan, 1993, 822-89.

Taylor-Papadimitriou, J., Epenetos, A.A. Exploiting altered glycosylation patterns in cancer. TRENDS IN BIOTECHNOLOGY, 12(6): 227-33, 1994, June.

tenHagen, T.L., "Isolation and characterization of murine Kupffer cells and splenic macrophages. J. Immunol. Meth., 1996, June 14(1):81-91.

Thom, S.R., et al., "Inhibition of human neutrophil beta-.1-integrin-dependent adherence by Hyperbaric Oxygen." Am J. Physiol, 272(3 Pt1): C770-777, 1997

Thome J., et al., "Advanced glycation endproducts-associated parameters in the peripheral blood of patients with Alzheimer's disease." Life Sci, 1996; 59(8):679-685.

Tuan Vo-Dinh, et al., "Laser-Induced Differential Fluorescence for Cancer Diagnosis without Biopsy." Appl. Spec. V51, (2), Jan 1997

Zimra, Y, et al., "Butyric acid and pivaloyloxymethyl butyrate, AN-9, a novel butyric acid derivative, induce apoptosis in HL-60 cells. J. Cancer Res. Clin. Oncol, 1997, 123(3): 152-160

PREDICTION OF FATIGUE CRACK GROWTH USING REGULARIZED NUMERICAL MODELS

Final Report

NASA/ASEE Summer Faculty Fellowship Program–1998

Johnson Space Center

Prepared By:	Andrew J. Meade, Jr., Ph.D
Academic Rank:	Associate Professor
University & Department	Rice University Department of Mechanical Engineering and Materials Science Houston, Texas 77005-1892

NASA/JSC	
Directorate:	Safety, Reliability and Quality Assurance Office
Division:	Technology Division
JSC Colleague:	Alice Lee
Date Submitted:	August 31, 1998
Contract Number:	NAG 9-867

ABSTRACT

Though it is known in the engineering community that successful analyses rest upon the proper balance of 1) theoretical analysis of mathematical models, 2) physical experimentation and 3) computational simulation, this balance is currently handled in a sometimes unwieldy and inefficient manner. It is proposed to investigate and develop a rigorous and computationally efficient method to effectively combine all available information, from both experimental measurements and mathematical models, in the emulation of physical systems. This will be specifically applied to fatigue crack growth in metallic structures of interest to NASA.

NOMENCLATURE

Symbols	**Explanation**
a	crack length
$B(\cdot)$	boundary operator of the mathematical model
$b\langle\cdot,\cdot\rangle$	symmetric form associated with the boundary operator B
c_m	basis expansion coefficients
$\overline{c}$	vector with components c_m
$E[\cdot]$	mathematical expectation operator
F	response of the physical system
f	arbitrary function satisfying the boundary operator B exactly / empirically derived constant
$\tilde{f}$	hypersurface that gives the global minimum of Eq. (5)
f_0	response of the mathematical model
$\overline{f_0}$	vector with components $f_0(x_j)$
f_a	numerical approximation of $\tilde{f}$
f_{cor}	correction of f_0 using experimental data
$f_e(x_i)$	experimental measurements of $F(x_i)$
$\overline{f_e}$	vector with components $f_e(x_i)$
$G(\cdot,\cdot)$	Green's function of the mathematical model
$\mathbf{G}$	matrix with components $G(x_k, x_m)$
g	algebraic function
ΔK	stress intensity factor range
$\mathbf{I}$	identity matrix
$L(\cdot)$	linear self-adjoined differential operator
$l\langle\cdot,\cdot\rangle$	quadratic symmetric energy form associated with L
N	number of applied fatigue cycles
p	weighting function / empirically derived constant
q	Lagrange multiplier function / empirically derived constant
R	stress ratio
R^d	d-dimensional Euclidian space
$\mathcal{R}(\alpha)$	residual of Eq. (19)
s	parameter related to the operator L where $s > 0$
$Var[\cdot]$	variance of a random variable
$x = (x_1, ..., x_d)$	d-dimensional spatial coordinate

Symbols	Explanation
$\Vert \cdot \Vert_{H^s(\Omega)}$	norm in the Sobolev space of order s
$\langle \cdot , \cdot \rangle$	inner product
α	regularization parameter where $\alpha \geq 0$
$\overline{\beta}$	set of basis function parameters and basis expansion coefficients
Δ_k	basis function parameter
$\delta(\cdot)$	Dirac delta function
δ_{ji}	$\delta(x - x_j\ ,\ x - x_i)$
$\epsilon(\cdot)$	objective function
η_k	basis function parameter
κ	positive constant
$\Lambda(\cdot)$	smoothness based Tikhonov regularization functional
μ	noise of measurement
ξ	arbitrary variable
ρ	positive constant
σ	basis function
$\Phi(\cdot)$	energy functional of the mathematical model
ϕ	arbitrary function
ψ	arbitrary function
Ω	spatial domain of the mathematical model
$\partial\Omega$	spatial boundary of the mathematical model

INTRODUCTION

The goal of engineering analysis is to obtain a comprehensive description of a physical system of interest. Three approaches to this goal exist: 1) theoretical analysis of mathematical models, 2) physical experimentation and 3) computational simulation. None of these approaches is superior and they are typically used in combination [1].

For example, utilizing only mathematical models for engineering analysis can yield general results which can then provide the foundation for parametric studies. However, even the most sophisticated mathematical model can only approximate a physical system. In this regard, the fidelity of mathematical models and their applicability for describing system behavior ultimately requires model validation using experimental measurements. In addition, the majority of sophisticated mathematical models do not have analytical solutions and must be simplified (low-fidelity) or solved by high performance computers combined with accurate numerical algorithms. Unfortunately, even with the use of numerical computation only a limited number of parameter combinations can be investigated and, like the experimental approach, the computational approach loses its generality. In fact, high fidelity computational studies are often

referred to as computational experiments.

Though it is known in the engineering community that successful analyses rest upon the proper balance of all three approaches, currently, this balance is handled in a sometimes unwieldy and inefficient manner. It is proposed to investigate and develop a rigorous and computationally efficient method to effectively combine all available information, from both experimental measurements and mathematical models, in the emulation of physical systems. This will be specifically applied to fatigue in metallic structures of interest to NASA.

The technical approach developed in this report utilizes a common tool borrowed from artificial neural network (ANN) applications, the theory of Tikhonov regularization of ill-posed problems [2]. Specifically, the problem of mathematical analysis of experimental data is treated as an ill-posed problem. Its regularization involves the introduction of additional information regarding the physical system. It is proposed to utilize a-priori mathematical models of physical systems, at appropriate degrees of fidelity, for regularization [3]. The example problem considered in this report is used to illustrate two major benefits of the approach. First, to show the benefit of employing a-priori mathematical models of moderate fidelity for extrapolation from sparse data. Second, to show the usefulness of incorporating a-priori mathematical models in the processing of experimental data corrupted by noise. The B_1 spline expansion is used as the numerical approximation tool in the developed method.

REGULARIZATION BY A-PRIORI MATHEMATICAL MODELS

The popular Tikhonov regularization method was originally adopted for ANN systems by Poggio and Girosi [4] and extensively used in ANN applications [5], [6]. In this case a set of constraints on the network approximation $f_a(x, \overline{\beta})$ is introduced through the Tikhonov regularization functional $\Lambda\left(f_a(x, \overline{\beta})\right)$ which specifies the penalty given to the oscillatory behavior of $f_a(x, \overline{\beta})$; the network parameters can be determined by minimizing the objective function

$$\epsilon(f_a) = \sum_{i=1}^{NN} \left| f_e(x_i) - f_a(x_i, \overline{\beta}) \right|^2 + \alpha\Lambda\left(f_a(x, \overline{\beta})\right) \quad . \tag{1}$$

Unfortunately, conventional smoothness based Tikhonov regularization of Poggio and Girosi may not be consistent with the smoothness required in emulating a physical system and so would be unable to properly approximate with noisy experimental data. Instead, the author believe that the regularization should be based on an a-priori mathematical model of some level of fidelity. This regularized model can then be approximated by more conventional computational methods.

A large class of mechanics problems can be described by the equations

$$Lf_0(x) = g(x) \ , \ x \in \Omega \quad \text{and} \quad Bf_0(x) = 0 \ , \ x \in \partial\Omega \quad , \tag{2}$$

The solution to Eq. (2) can also be determined by minimizing the following quadratic (energy) form

$$\Phi(f) = \frac{1}{2} l\langle f, f\rangle - \langle g, f\rangle \quad . \tag{3}$$

Since for any f that satisfies the boundary conditions satisfies

$$l\langle f_0, f\rangle = \langle g, f\rangle \quad , \tag{4}$$

then substituting Eq. (4) into Eq. (3) yields

$$\Phi(f) = \frac{1}{2} l\langle f - f_0, f - f_0\rangle - \frac{1}{2} l\langle f_0, f_0\rangle = \frac{1}{2} l\langle f - f_0, f - f_0\rangle + \text{constant} \quad .$$

From a physical perspective, the functional $\Phi(f)$ penalizes the mechanical energy of the discrepancy between the function f and the response of a mathematical model f_0.

With the use of f and the energy functional of Eq. (3), regularized modeling can be formulated as the minimization of the objective function,

$$\epsilon(f) = \sum_{i=1}^{NN} |f_e(x_i) - f(x_i)|^2 + \alpha \left(\frac{1}{2} l\langle f, f\rangle - \langle g, f\rangle \right) \quad , \tag{5}$$

which combines information from experimental data and the a-priori mathematical model. Note that α represents the degree of reliance on the a-priori mathematical model of the physical system relative to the reliability of the experimental data.

Analytical Approximation of Regularized Mechanical Systems

The formation of a regularized model of a mechanical system is identical to approximating the hypersurface $\tilde{f}(x)$ that gives the global minimum of Eq. (5). In this context, analytical study of $\tilde{f}(x)$ is essential for evaluating the properties of the regularized model.

Since $\tilde{f}(x)$ is the global minimum of Eq. (5),

$$L\tilde{f} = g + \frac{2}{\alpha} \sum_{i=1}^{NN} \left(\tilde{f}(x_i) - f_e(x_i) \right) \delta(x - x_i) \ , \ x \in \Omega$$
$$\text{and} \quad B\tilde{f} = 0 \quad , x \in \partial\Omega \quad . \tag{6}$$

From Eq. (6) it can be deduced that $\tilde{f}$ contains two components

$$\tilde{f}(x) = f_0(x) + f_{cor}(x) \quad . \tag{7}$$

These components can be determined by the equations

$$f_0(x) = \int_\Omega G(x, \xi) g(\xi) \mathrm{d}\xi$$

and

$$f_{cor}(x) = \frac{2}{\alpha} \sum_{i=1}^{NN} \left(f_e(x_i) - \tilde{f}(x_i) \right) G(x, x_i) \tag{8}$$

where the Green's function $G(x, \xi)$ satisfies the boundary value problem

$$LG(x,\xi) = \delta(x - \xi) \ , \ x \in \Omega \quad \text{and} \quad BG(x,\xi) = 0 \ \ , \ x \in \partial\Omega \quad .$$

Substituting Eq. (8) into Eq. (7) yields

$$\tilde{f}(x) = f_0(x) + \sum_{i=1}^{NN} c_i G(x, x_i) \quad , \tag{9}$$

where the coefficients are defined as

$$c_j = \frac{2}{\alpha} \left(f_e(x_j) - \tilde{f}(x_j) \right) \quad . \tag{10}$$

The coefficients can be evaluated by substituting Eq. (9) into Eq. (10), resulting in

$$c_j = \frac{2}{\alpha} \left(f_e(x_j) - f_0(x_j) - \sum_{i=1}^{NN} c_i G(x_j, x_i) \right) \quad , \ j = 1, ..., NN \tag{11}$$

with which $\bar{c}$ can be isolated. With the substitution of $\bar{c}$ into Eq. (9), $\tilde{f}$ can be written as

$$\tilde{f}(x) = f_0(x) + \sum_{i=1}^{NN} G(x, x_i) \left[\left(\mathbf{G} + \frac{\alpha}{2} \mathbf{I} \right)^{-1} \left(\overline{f_e} - \overline{f_0} \right) \right]_i \quad . \tag{12}$$

It is noted that the matrix $\mathbf{G}$ of Eq. (12) is positive definite since for an arbitrary function $\phi(x)$

$$\int_\Omega \int_\Omega G(x,\xi)\phi(\xi)\phi(x) \mathrm{d}\xi \ \mathrm{d}x = \int_\Omega \psi(x)\phi(x)\mathrm{d}x = \int_\Omega \psi(x) L\psi(x) \mathrm{d}x = l\langle \psi, \psi \rangle \quad ,$$

where $\psi(x)$ is the solution to Eq. (2), for $g(x) = \phi(x)$, and satisfies the boundary condition. Therefore, since the quadratic form $l\langle \cdot, \cdot \rangle$ is strictly elliptic,

$$\int_\Omega \int_\Omega G(x,\xi)\phi(\xi)\phi(x) \mathrm{d}\xi \ \mathrm{d}x \geq \kappa \|\psi\|^2_{H^s(\Omega)} > 0 \ . \tag{13}$$

Substituting $\phi(x) = \sum_{i=1}^{NN} c_i \delta(x - x_i)$ into Eq. (13) yields

$$\int_\Omega \int_\Omega G(x,\xi)\phi(\xi)\phi(x) \mathrm{d}\xi \ \mathrm{d}x = \bar{c}^T \mathbf{G} \bar{c} > 0 \ .$$

Because $\mathbf{G}$ is a positive definite matrix the matrix $(\mathbf{G} + \alpha \mathbf{I}/2)$ is also positive definite for any positive value of the parameter α. As a result, the vector $\bar{c}$ can be evaluated in a computationally stable manner.

Since the range of the regularizing parameter α is the set of all positive numbers, it is prudent to obtain qualitative results for the limits of α. Equation (12) indicates that as $\alpha \to \infty$ then $\tilde{f}(x) \to f_0(x)$, as expected, since with $\alpha \to \infty$ experimental data becomes less relevant and $\tilde{f}$ emulates more of the a-priori mathematical model.

For $\alpha \to 0$, the a-priori model of the mechanical system is assumed to be increasingly unreliable compared to the experimental data. Equation (12) gives

$$\tilde{f}(x) \to f_0(x) + \sum_{i=1}^{NN} G(x, x_i) \left[\mathbf{G}^{-1}\left(\overline{f_e} - \overline{f_0}\right)\right]_i$$

so that the regularized solution interpolates the data $f_e(x_j)$ exactly since

$$f_0(x_j) + \sum_{i=1}^{NN} G(x_j, x_i) \left[\mathbf{G}^{-1}\left(\overline{f_e} - \overline{f_0}\right)\right]_i = f_0(x_j) + \sum_{i=1}^{NN} \delta_{ji} \left[\overline{f_e} - \overline{f_0}\right]_i = f_e(x_j) \quad .$$

As a result, the a-priori mathematical model of mechanical system does not contribute to $\tilde{f}$ in the region of adequate data. However, the mathematical model is not eliminated from the modeling procedure; it is used by $\tilde{f}$ to extrapolate the data to the regions lacking data. In an alternate perspective, as $\alpha \to 0$ the function $\tilde{f}$ can be thought of as a response of the a-priori model "attached" to the data points.

Numerical Approximation of Regularized Mechanical Systems

The basis expansion used to approximate $\tilde{f}$ can be described by the equation,

$$f_a(x, \overline{\beta}) = \sum_k c_k \sigma\left(\frac{|x - \eta_k|}{\Delta_k}\right) \quad \text{where } \sigma(\xi) \text{ is the } B_1 \text{ spline.} \tag{14}$$

Since the basis expansion of Eq. (14) does not satisfy the boundary conditions of the mathematical model for arbitrary $\overline{\beta}$, the objective function of Eq. (5) is augmented to incorporate the boundary conditions. Specifically,

$$\epsilon(f_a) = \sum_{i=1}^{NN} \left|f_e(x_i) - f_a(x_i, \overline{\beta})\right|^2 + \alpha\left(\frac{1}{2} l\langle f_a, f_a\rangle - \langle g, f\rangle + b\langle f_a, q\rangle\right) \quad , \tag{15}$$

where $b\langle \cdot, \cdot \rangle$ may be defined as $b\langle f, q\rangle = \int_{\partial\Omega} \left(Bf(\xi)\right) q(\xi) d\xi$.

Preselecting the distribution and localization properties of the basis functions, Eq. (15) is minimized with respect to the remaining unknowns, c_k, resulting in

$$\sum_j^M \left(\alpha l\langle \sigma_j(x), \sigma_k(x)\rangle + 2\sum_{i=1}^{NN} \sigma_j(x_i)\sigma_k(x_i)\right) c_j + \alpha b\langle \sigma_k(x), q\rangle =$$

$$\alpha\langle g, \sigma_k(x)\rangle + 2\sum_{i=1}^{NN} f_e(x_i)\sigma_k(x_i) \quad , \text{ for } \; k = 1, ..., M \tag{16}$$

$$\text{and} \quad \sum_j^M c_j b\langle \sigma_j(x), p\rangle = 0 \tag{17}$$

where p and q belong to an appropriate finite dimensional subspace. Equations (16) and (17) are known as the Galerkin method [7]. This observation provides a useful link between the proposed method of data analysis and methods in computational mechanics. Also, rather than using a variational form of the a-priori mathematical model, which may be inconvenient, Eq. (16) suggests the regularization technique will work equally well by equating the equation residual of the a-priori mathematical model to the function residual of the $f_e - f_a$. This approach will be taken in the numerical example problems.

The use of Eq. (16) for regularization should suppress oscillations of the experimental data that are dissimilar to the oscillatory behavior of the a-priori model. Consequently, the approximation of a regularized mechanical system should filter the data noise. Assume the data noise μ is statistically independent of location and uniformly distributed between $\pm d/2$, with variance $Var[\mu] = d^2/12$. The value of the regularization parameter α can be determined such that Eq. (12) and the constraint

$$\sum_{i=1}^{NN} |f_e(x_i) - f(x_i)|^2 = E\left[\sum_{i=1}^{NN} {\mu_i}^2\right] = NN \cdot Var[\mu] = \rho \tag{18}$$

are satisfied for $f = \tilde{f}$. More specifically, α minimizes the magnitude of the equation residual $\mathcal{R}(\alpha)$ where,

$$\sum_{k=1}^{NN} \left| f_e(x_k) - f_0(x_k) - \sum_{i=1}^{NN} G(x_k, x_i) \left[\left(\mathrm{G} + \frac{\alpha}{2}\mathrm{I} \right)^{-1} \left(\overline{f_e} - \overline{f_0} \right) \right]_i \right|^2 = \mathcal{R}(\alpha) + \rho \,. \tag{19}$$

Use of Eq. (19) requires a-priori knowledge regarding the intensity of the random noise in measurements. This is usually available in engineering applications. The optimal α, which acts as a Lagrange multiplier, can be determined through any search technique [8].

EXAMPLE PROBLEMS

Consider the empirical differential equation modeling crack growth in a material, the NASGRO 2.0 equation (p. 5, reference [9]),

$$\frac{\mathrm{d}a}{\mathrm{d}N} = \frac{C(1-f)^n \Delta K^{(n-p)} (\Delta K - \Delta K_{\mathrm{th}})^p {K_c}^q}{(1-R)^{(n-q)}((1-R)K_c - \Delta K)^q} \,. \tag{20}$$

For these example problems, the value of the empirically derived constants (i.e., C, f, n, p, q, and K_c) will be taken for CDA 630 (C63000) Al Bronze. Experimental data is taken at a stress ratio $R = 0.4$ (p. 166, reference [9]).

In the first example, we imagine we only have experimental data for $R = 0.4$ but wish to produce a data-driven approximation of the crack-growth rate $\mathcal{A} = \mathrm{d}a/\mathrm{d}N$, as a function of $x = \Delta K$, for the stress ratio $R = 0.1$. This is equivalent to data-driven

extrapolation of the a-priori model. The a-priori mathematical model is produced by rewriting Eq. (20) as the following algebraic equation,

$$(\xi - x)^q \mathcal{A} = \tau x^{(n-p)}(x - \Delta K_{\text{th}})^p \tag{21}$$

where

$$\tau = \frac{C(1-f)^n K_c{}^q}{(1-R)^{(n-q)}} \quad \text{and} \quad \xi = (1-R)K_c \ .$$

In the second example, we again imagine we only have experimental data for $R = 0.4$, but wish to produce a data-driven approximation of the number of applied fatigue cycles N as a function of $x = \Delta K$ for the stress ratio $R = 0.1$. The a-priori mathematical model can be produced by rewriting Eq. (20) as a first-order ordinary differential equation,

$$\zeta x^{(n-p)}(x - \Delta K_{\text{th}})^p \frac{\mathrm{d}N}{\mathrm{d}x} = (\xi - x)^q \quad \text{where} \quad \zeta = \tau \frac{\mathrm{d}x}{\mathrm{d}a} \ . \tag{22}$$

Results for Example 1

Assuming $\mathcal{A}(x) = \sum_j^M \mathcal{A}_j \sigma_j(x)$ and using the Galerkin method, the matrix form of Example 1 is

$$\sum_j^M \left(\alpha \langle (\xi - x)^q \sigma_j(x), \frac{\mathrm{d}\sigma_k}{\mathrm{d}x} \rangle + 2 \sum_{i=1}^{NN} \sigma_j(x_i) \frac{\mathrm{d}\sigma_k(x_i)}{\mathrm{d}x} \right) \mathcal{A}_j =$$

$$\alpha \langle \tau x^{(n-p)}(x - \Delta K_{\text{th}})^p, \frac{\mathrm{d}\sigma_k}{\mathrm{d}x} \rangle + 2 \sum_{i=1}^{NN} \mathcal{A}_e(x_i) \frac{\mathrm{d}\sigma_k}{\mathrm{d}x}(x_i) \quad , \text{ for } \; k = 1, ..., M \tag{23}$$

$$\text{where} \quad \mathcal{A}_1 = 0 \text{ at } x_1 = \Delta K_{\text{th}} \text{ and } M = 201.$$

Figure (1) compares the response of the a-priori model and the 60 experimental data points ($NN = 60$). Figure (2) shows the resultant merging of numerical and experimental data through regularization with an $\alpha = 7 \times 10^3$. Results seem satisfactory between the experimental data and the regularized response using the a-priori model of moderate fidelity. The optimal curve passes through the data points while the curvature in the region between data matches the curvature of the a-priori mathematical model. This can be shown by noting that the function $f_{cor}(x)$, mentioned earlier, is a piece-wise linear function in the regions between data points.

Results for Example 2

Assuming $N(x) = \sum_j^M N_j \sigma_j(x)$, the matrix form of Example 2 is

$$\sum_j^M \left(\alpha \langle \zeta x^{(n-p)}(x - \Delta K_{\text{th}})^p \frac{\mathrm{d}\sigma_j}{\mathrm{d}x}, \sigma_k(x) \rangle + 2 \sum_{i=1}^{NN} \frac{\mathrm{d}\sigma_j(x_i)}{\mathrm{d}x} \sigma_k(x_i) \right) N_j =$$

$$\alpha \langle (\xi - x)^q, \sigma_k(x) \rangle + 2 \sum_{i=1}^{NN} N_e(x_i) \sigma_k(x_i) \quad , \text{ for } \; k = 1, ..., M \tag{24}$$

where $N_1 = 1$ at $x_1 = \Delta K_{th}$ and $M = 201$.

Figure (3) compares the response of the a-priori model and the 13 experimental data points ($NN = 13$). Figure (4) shows the resultant merging of numerical and experimental data through regularization with an $\alpha = 1.0 \times 10^{-4}$. Results seem satisfactory between the experimental data and the regularized response using the a-priori model of moderate fidelity.

SUMMARY

A method of combining experimental data and physical models is presented. Specifically, physical models of engineering interest can be expressed in the form of empirical, differential and/or integral equations of varying degrees of fidelity. These model equations can be incorporated in the form of a regularizing functional for a robust matching of experimental data. The method can be viewed as the adjustment of a low fidelity, and computationally inexpensive, mathematical model response by experimental data. The developed method can also be viewed as an efficient procedure for interpolating experimental data by utilizing physically motivated criteria. Specifically, work has concentrated on the use of an empirical fatigue crack-growth model and experimental data. Further, it has been shown how the developed method can be used to successfully extrapolate the physical system response at unmeasured coordinates and filter noisy experimental measurements. The basis expansion has been examined as the computational apparatus of the developed method. However, the developments of the report retain a sufficient level of generality and can be implemented in conjunction with any of the commonly used methods including finite difference.

REFERENCES

[1] Doebelin, E.O., *Engineering Experimentation: Planning, Execution, Reporting*, McGraw-Hill, New York, 1995.

[2] Tikhonov, A.N., and Arsenin, V.Y., *Solution of Ill-Posed Problems*, W.H. Winston, Washington, D.C, 1977.

[3] Zeldin, B.A. and Meade, A.J. Jr., "Integrating Experimental Data and Mathematical Models in Simulation of Physical Systems," *AIAA Journal*, Vol. 35, No. 11, 1997, pp. 1787-1790.

[4] Poggio, T., and Girosi, F., "Networks for Approximation and Learning," *Proceedings of the IEEE*, Vol. 78, No. 9, Institute of Electrical and Electronics Engineers, Washington, DC, 1990, pp. 1481-1497.

[5] Girosi, F., Jones, M., and Poggio, T., "Regularization Theory and Neural Network Architectures," *Neural Computation*, Vol. 7, 1995, pp. 219-269.

[6] Bishop, C.M., "Curvature-Driven Smoothing: A Learning Algorithm for Feedforward Networks," *IEEE Transactions on Neural Networks*, Vol. 4, No. 5, 1993, pp. 882-884.

[7] Fletcher, C.A.J., *Computational Galerkin Methods*, Springer, New York, 1984.

[8] Stoecker, W.F., *Design of Thermal Systems*, McGraw-Hill, New York, 1989, pp. 189-190.

[9] Forman, R.G., Shivakumar, V., Newman, J.C., De Koning, A.U., Henriksen, T.K., Chang, C., Mear, M., Beek, J.M., Henkener, J.A., Lawrence, V.B., Mettu, S.R., Piotrowski, S.M., Rivera, T., Williams, L.C., and Yeh, F., *Fatigue Crack Growth Computer Program "NASA/FLAGRO" Version 2.0*, JSC-22267A, Structures and Mechanics Division, Lyndon B. Johnson Space Center, 1994.

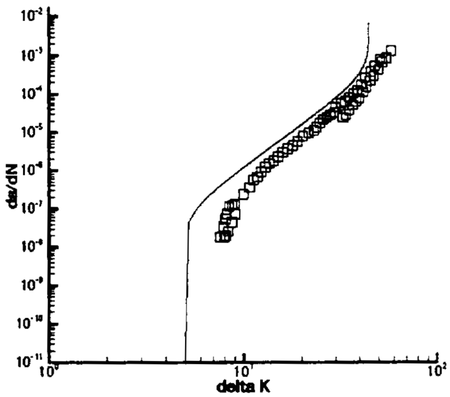

Figure 1: Comparison of a-priori mathematical model for the rate of crack-growth at $R = 0.1$ and experimental data from $R = 0.4$.

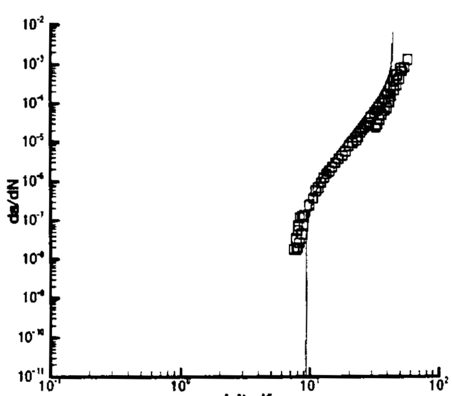

Figure 2: Comparison of regularized response for the rate of crack-growth and experimental data using $\alpha = 7 \times 10^3$.

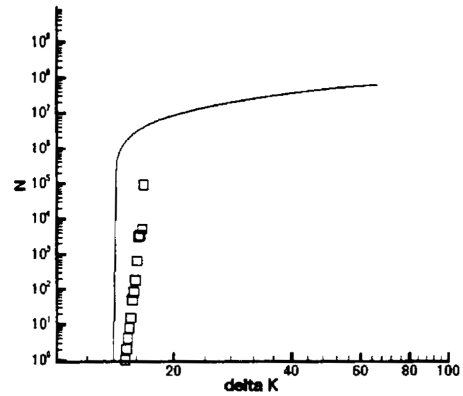

Figure 3: Comparison of the a-priori mathematical model for the number of applied fatigue cycles N at $R = 0.1$ and experimental data from $R = 0.4$.

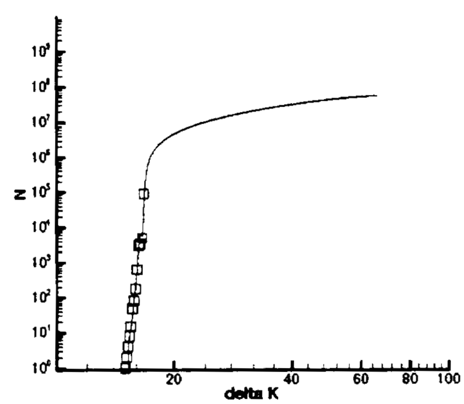

Figure 4: Comparison of the regularized response for the number of applied fatigue cycles N and experimental data using $\alpha = 1.0 \times 10^{-4}$.

ARCHEAN AGE FOSSILS FROM NORTHWESTERN AUSTRALIA (~3.3 TO 3.5GA, WARRAWOONA GROUP, TOWERS FORMATION)

/11

IN - 51

Final Report

NASA/ASEE Summer Faculty Fellowship Program-1998

Johnson Space Center

Prepared by:	Penny A. Morris Smith, Ph.D.
Academic Rank:	Lecturer
University & Department:	University of Houston-Downtown Department of Natural Science Houston, Texas 77002

NASA/JSC	
Directorate:	Space and Life Sciences
Division:	Earth Science and Solar System Exploration
Branch:	Earth Science
JSC Colleague:	David S. McKay
Date Submitted:	
Contract Number:	NAG 9-867

ABSTRACT

Archean aged rocks from the Pilbara Block area of western Australia (Warrawoona Group, Towers Formation, ~3.3-3.5 Ga) contain microfossils that are composed of various sizes of spheres and filaments. The first descriptions of these microfossils were published in the late 1970's (Dunlop, 1978; Dunlop, et. al., 1978). The authenticity of the microfossils is well established. The small size of the microfossils prevents isotope dating, at least with the present technology. Microbiologists, however, have established guidelines to determine the authenticity of the Archean aged organic remains (Schopf, Walter, 1992).

Historically, most studies of Archean aged fauna have used optical microscopy rather than scanning electron microscopy (SEM) and energy dispersive x-ray analysis (EDS) for morphological and mineralogical descriptions. Optical microscopy limits magnification and the ability to discern intricate morphological detail. By using all three instruments, it was found that the spheres from the Towers were composed of at least 4 rather than the 2 types previously described. The coccoid forms ranged from 2 μm to 40 or possibly 50 μm in diameter. Some were solitary coccoid shaped forms, some of which were apparently colonial, while others may have represented sheath enclosed bacteria, and still other may have been solitary coccoid forms. In addition, a possible intricate external morphology and distinctive chemical signature were detected. Filaments were long and narrow, 2 μm wide and over 100 μm long. The distinctive chemical signature, i.e., higher carbon levels in the microfossils, is possibly an additional biomarker that may be used to distinguish microfossils from "dubiofossils". These methods also allowed for comparison of these microfossils with those described from Formations immediately underlying and overlying the Towers, namely the Apex and Duffer.

In inclusion, it was found that the microfossils from the Towers Formation may be one of the earliest indications of a diverse microfauna that included filaments and a variety of spheres.

INTRODUCTION

The paleontologists and geologists of preceding centuries, and indeed most of this century, considered rocks older than 600 million years to be devoid of fossils. This idea began to change with two important discoveries. First, the discovery of a diverse soft bodied fauna called the Ediacara that predated the traditional 600 million year old date for the base of the Cambrian (Cloud, 1988). Second, the discovery of rod-shaped bacteria and filamentous strands from the 3.5 billion year old Fig Tree Formation of South Africa (Barghoorn, Schopf, 1966; Barghoorn, 1971; Prashnowsky, Oberlies, 1972). These discoveries, along with advances in technology, has enabled scientists to look for fossils in the oldest rocks on Earth, develop baselines and establish criteria for determining the authenticity of these oldest fossils. As we look for signs of life on other planets, these types of studies will serve as guides to determine organic authenticity and promote collecting sites.

This study represents a continuation of a 1997 NASA Summer Faculty Fellowship. In the previous study a diverse Archean community from the Pilbara Block of western Australia was identified from a stromatolitic carbonaceous chert. The community included bacterial and cyanobacterial remains that were identified by SEM, and EDS (Morris Smith, 1997, Morris, 1998). In the present study additional information includes element mapping, optical microscopy of petrographic thin sections, SEM imaging of HF (hydrofluoric acid) etched thin sections, and comparisons with other Archean forms from the Pilbara Block. The goals of this study are as follows: 1. To demonstrate that the ancient microfauna left unique biomarkers, 2. To demonstrate that the microfauna is not only syngenetic to the original rock matrix, but meets the criteria for establishing authenticity (Schopf, Walter, 1992), and 3. To compare stratigraphically the Towers Formation fauna with other Archean units.

METHODS

The sample, PPRG 002 from the Towers Formation was collected by J. W. Schopf and the Precambrian Paleobiology Research Group (PPRG). E. K. Gibson (NASA Johnson Space Center) obtained the sample from J. W. Schopf. In addition, F. Westall (NASA Johnson Space Center) has shared her knowledge of other Archean aged Formations and their microfauna, including the Duffer Formation.

Freshly broken chips from the stromatolitic chert were mounted on aluminum studs with aluminum paint and coated with either gold palladium or platinum using a Hummer X. A Phillips SEM XL 40 FEG scanning electron microscope and an Oxford ISIS energy dispersive x-ray spectrometry system was used to analyze the surface morphology and the chemical composition of both the fossils and the surrounding rock. In addition, thin sections were etched for 45 minutes in the fumes of hydrofluoric acid, rinsed with triple distilled water, and coated for 30 seconds with carbon.

EVIDENCE FOR BIOGENIC STRUCTURES

It was only relatively recently that stromatolitic domical structures and their associated microbiota were discovered within the Warrawoona (Dunlop, 1977; Dunlop, et. al., 1978; Walter et. al., 1980; Lowe, 1980). In the ensuing years filaments, rosette-shaped ?microfossils, and spheroids were found (Awramik, et. al., 1983, 1988; Schopf, Packer, 1986, 1987; Buick, 1988; Schopf, Klein, 1992; Schopf, 1993). In order to establish the authenticity of these microfossils, it was necessary to establish guidelines or criteria (Schopf, Walter, 1992). The criteria are as follows: 1. The rocks must be of unquestionable Archean age, 2. The microfossils must be indigenous to Archean sediments, 3. The microfossils must occur in clasts that are assuredly syngenetic with the deposition of the sedimentary unit. In the case of the Towers Formation, the fossils must be shown to pre-date deposition of the bedded cherts. 4. The microfossils must be biogenic, and 5. Replicate sampling of the fossiliferous outcrops should firmly demonstrate the provenance of the microfossils. The fossils that are discussed in the following paragraphs occur in fractured chips, thin sections, and many of the fossils have been accepted by other authors as microfossils (Schopf, Packer, 1987; Schopf, Klein, 1992).

Spheres

There are several sizes of spheres, and all are present in both fractured chips and petrographic thin sections. All of the spheres meet the criteria that are listed in the preceding paragraph. In addition, there are higher levels of carbon within the fossils than in the surrounding chert matrix (Fig. 1, 2).

SEM images indicates that the largest sphere is unique because of its rough, ropy exterior, and its size and complexity (Fig. 3, 4). It appears to be composed of numerous cells that are pressed together. As indicated in the optical thin sections, a sheath appears to surround the sphere (Fig. 5). Most specimens measure from 16 to 27 µm, although one or two are nearly 50 µm in diameter. The size and presence of a sheath indicate that it may be a chroococcalean cyanobacteria (Schopf, Packer, 1986, 1987).

Earlier investigators found only a single specimen of this organism from the Apex Formation, which immediately overlies the Towers Formation (Schopf, Packer, 1986, 1987). I have found a number of specimens in both fractured chips and petrographic thin sections (Morris, et. al., 1987). Analysis of material from the Duffer Formation, which immediately underlies the Towers, indicates the absence of these large, chroococcalean forms. Mineralogically the spheres are primarily composed of carbon and iron, while the surrounding matrix is high in chert (Fig. 1, 2, 3, 6).

Other spheres and ellipsoids averaging 5 to 12 μm in diameter have a similar minerological composition (Fig. 7). That is, iron and carbon are concentrated within the spheres, while silica is located in the surrounding chert matrix. In addition, optical microscopy of the petrographic thin sections indicate the possible presence of a sheath (Fig. 5). The spheres are similar to sheath enclosed forms assigned to the genus *Archaeospheroides*, while the ellipsoid shapes appear to resemble unnamed forms described from the North Pole barite deposits (Pilbara Block). (Dunlop, et. al., 1978; Awramik, et. al., 1983). The North Pole barite deposits are older than the Towers Formation, and are laterally equivalent to the underlying Duffer Formation. Spheres and ellipsoids within the 5 to 12 μm size range appear to be absent from the Duffer Formation.

The smallest spheres are 2 μm in diameter, possess a smooth surface, are linearly arranged, and are found in close association with a filament (Fig. 8). The spheres are similar in size to modern coccoid bacteria. Equatorial girdling and possible splitting of the outer wall is apparent in some of the coccoids. The splitting indicates a relatively thin (100 nm) covering. This could indicate the beginnings of cell division, or the beginnings of cell wall shedding due to excessive mineral nucleation sites (Fortin et. al. 1997). In addition, similarly sized coccoids can be found within petrographic thin sections that are linearly arranged in a series, and include pairing. These are similar to forms described from the Barberton of South Africa (Westall, et. al. in press). Oval to round impressions, including molds, are found in HF etched petrographic thin sections. These impressions and molds are similar in size and shape to the coccoid shaped fossils found within the fractured chips.

The chemistry of these 2 μm forms is different from the other spheres. In addition to high levels of carbon, there are also high levels of oxygen, aluminum, and silica. There is very little iron and calcium present. The surrounding matrix appears to be composed of calcite, siderite and dolomite in a quartz or chert ground mass as indicated by the presence of Ca, Mg., Al, Si, O, C.

Filaments

There are a variety of filaments that have been reported from the Warrawoona. Some are septate, that is, the filament appears to be divided into sections by cell walls, while others are nonseptate. Unfortunately it is not possible to distinguish between the two forms with a scanning electron microscope. Many of the filaments found with an optical microscope in the petrographic thin sections appear to be long, sinuous, and stained reddish brown. Subsequent analysis of the same thin sections with the SEM (both unetched and HF etched) failed to indicate the presence of these filaments. Therefore they were probably abiogenic mineral deposits.

The long, narrow filaments that are associated with the 2 μm spheres measure over 100 μm long, and average 2.0 μm in width. The filaments twist and curve over and under

parts of the rock (Fig. 8). Schopf believed that this particular size range represented the remains of filamentous bacteria (Schopf, 1983). If this is indeed the case, the presumed coccus shaped bacteria that are described above, and are closely associated with the filaments, may have originally been enclosed within the filament. Additionally, the filament chemistry is identical to that described for the 2 μm coccoid-shaped spheres. The long, narrow filament is similar in size and shape to *Eoleptonema* (Awramik, et. al., 1983). This filament, although it is also present in the Apex, has not been found in either the North Pole barite deposits or Duffer Formation.

DISCUSSION

Earlier investigators have described the rock from the Tower Formation as carbonaceous chert, and various forms of carbon, including kerogens, are considered organic derivatives (Schopf, 1983). The EDS analysis of the rock and its associated microfossils indicate that the carbon is primarily contained within the microfossils, in what optically might be considered clots (Dunlop et. al., 1978; Lowe, 1980; Walter, et. al., 1980).

The biogenicity of the fossils described above is based on several lines of evidence. First, with the exception of the 2 μm spheres, all of the fossils compare with previously described and accepted Archean organic remains (Schopf, 1983; Schopf, Klein, 1992). The 2 μm spheres are comparable to forms described from the Barberton Group of South Africa (Westall, et. al., in press). The Barberton forms, like those described above, form chains, appear in pairs, and are believed to be coccoid bacterial fossils. Second, the evidence presented in the previous paragraphs indicates that all of the forms have elevated carbon levels, and with the exception of *Eoleptonema* and its associated coccoid forms, also have elevated iron levels. Iron is important in microbial preservation, and in association with carbon and oxygen (siderite) can be evidence of microbially induced mineralization (Fortin, et. al., 1997; Liebig, et. al. 1996).

Stratigraphically the Towers is the oldest formation in the Warrawoona Group, and it is within this Formation that several different forms of microfossils have been found. Although the Duffer Formation and North Pole barite deposits are older, possibly 3.6 Ga, the microbial fauna appears to be scarce. Fossils from these older Formations include some possible coccoid or bacilli bacteria forms from the former, and an ellipsoid form from the latter formation. With the limited evidence at hand, it appears that the Towers may represent the earliest example of a diverse, complex microfauna, in which some representatives may have been colonial.

CONCLUSIONS

The study has produced the following contributions to Archean paleontology:

1. Although the rock is primarily chert (Si,O), the putative fossil remains are identified by

higher carbon levels in association with oxides that include varying amounts of metallic ions, including iron. The presence of metallic ions, particularly iron, enhance the chances of fossilization (Fortin, et. al. 1997).

2. Within the Australian group of Archean formations, the Towers Formation may represent the earliest assemblage of a well preserved, complex microfauna.

ACKNOWLEDGMENTS

I wish to thank D. McKay, C. Allen, K. Keprta-Thomas, S. Wentworth, F.Westall, for their help and suggestions and E. K. Gibson for obtaining the rock samples. In addition, my thanks to L. Hulse for the many hours of help with the SEM.

LITERATURE CITED

Awramik, S. M., Schopf, J. S., Walter, M. R. 1983. Filamentous fossil bacteria from the Archean of western Australia. Precambrian Research 20: 357-374.

Awramik, S. M., Schopf, J. S., Walter, M. R. 1988. Carbonaceous filaments from North Pole, western Australia: are they fossil bacteria in Archean stromatolites: A discussion: Precambrian Research 39: 303-309.

Barghoorn, E. S. 1971. The oldest fossils. Scientific American 224: 30-42.

Barghoorn, E. S., Schopf, J. W. 1966. Microorganisms three billion years old from the Precambrian of South Africa. Science 152: 758-763.

Buick, R. 1988. Carbonaceous filaments from North Pole, western Australia: are they fossil bacteria in Archaean stromatolites? A reply. Precambrian Research 39: 311-317.

Cloud, P. 1988. Oasis in Space. Earth History from the Beginning. W. W. Norton & Co., New York. 508 p.

Dunlop, J. S. R. 1978. Shallow water sedimentation at North Pole, Pilbara, western Australia. *In:* J. E. Glover, D. I. Groves, eds., Archean Cherty Metasediments: Their Sedimentology, Micropaleontology, Biochemistry, and Significance to Mineralization. Pert, Western Australian Spec. Publications. 2: 30-38.

Dunlop, J. S. R., Muir, M. D., Milne, V. A., Groves, D. L. 1978. A new microfossil assemblage from the Archean of western Australia: Nature 274: 676-678.

Fortin, D, Ferris, F. G., Beveridge, T. J. 1997. Surface-mediated mineral development by bacteria. *In:* Banfield, J. F., Nealson, K. H., eds., Geomicrobiology: Interactions between microbes and minerals. Reviews in Mineralogy 35: 161-180.

Liebig, K., Frey, E., Theobald, G., Willis, P. M. A., 1996. Taphonomy of crocodilians from the Eocene Lake Messel (Darmstadt, Germany) with implications for the sedimentary environments. N. Jb. Geol. Palaeont. Abh. 199: 269-293.

Lowe, D. R. 1980. Stromatolites 3,400-Myr old from the Archean of western Australia. Nature 284: 441-443.

Morris, P. A., Allen, C. C., Gibson, E. K., McKay, D. S., Thomas-Keprta, K. 1998. Reexamination of the Warrawoona Group fossils (Towers Formation, western Australia, 3.3 to 3.5 Ga): Analogs of Mars meteorite fossils? 27th Lunar and Planetary Conference, Houston, Tx.

Morris Smith, P. A. 1997. Evidence of early life forms. Final Report, NASA/ASEE Summer Faculty Fellowship Program - 1997. Johnson Space Center.

Prashnowsky, A. A., Oberlies, F. 1972. Uber Lebenszeugnisse im Prakambrium Afrikas und Sudamerikas. *In:* H. R. von Gaertner and H. Wehner, eds., Advances in Organic Geochemistry 1971. New York, Pergamon, 683-698.

Schopf, J. W. 1983. Earth's earliest biosphere. Princeton Univ. Press, New Jersey. 543 p.

Schopf, J. W. 1993. Microfossils of the Early Archean Apex Chert: New evidence of the antiquity of life. Science 260: 640-646.

Schopf, J. W., Klein, C. 1992. The Proterozoic biosphere: A multidisciplinary study. Cambridge Univ. Press. N. Y. 1348 p.

Schopf, J. W., Packer, B. M. 1986. Newly discovered early Archean (3.4-3.5 Ga old) microorganisms from the Warrawoona Group of western Austrralia. Abstracts of the 5th meeting of the International Society for the Study of the Origins of Life and the 8th International Conference on the Origin of Life (ISSOL). P. 163-164.

Schopf, J. W., Packer, B. M. 1987. Early Archean (3.3 billion to 32.5 billion year old) microfossils from Warrawoona Group, Australia. Science 237:70-72.

Schopf, J. W., Walter, M. R. 1992. Archean microfossils: new evidence of ancient microbes. *In*: The Proterozoic Biosphere. A Multidisciplinary Study. Cambridge Univ. Press, N. Y., 1348 p.

Walter, M. R., Buick, R, Dunlop, J.S. R, 1980. Stromatolites 3,400-3,500 Myr old from the North Pole area, western Australia. Nature 284: 443-445.

Westall, F., deWit, M., Dann, J., van der Gaast, S., de Ronde, C., Gerneke, D. In Press. Early Archean fossil bacteria and biofilms in hydrothermally-influenced, shallow water sediments, Barberton Greenstone Belt, South Africa. Precambrian Research.

FIGURE DESCRIPTIONS

Figure 1. This is an iron element map of the SEM image of Figure 3. The iron is concentrated in the spheroids indicated by arrows in Figure 3.

Figure 2. This is a silicon element map of the SEM image of Figure 3. The silicon is concentrated in the matrix surrounding and partially enclosing the spheroids.

Figure 3. An SEM image of a fractured chip from the Towers Formation that has been coated with gold-palladium. Several of the probable colonial chroococcalean (cyanobacteria) spheres are indicated by arrows.

Figure 4. This is the same areas as Figure 3, but the magnification has been increased. The chroococcalean cyanobacteria (as indicated by arrows) appears to be colonial and possess a rough, ropy texture. In this image some forms are completely exposed, while others are partially buried.

Figure 5. An optical thin section with various sized spheres indicated by arrows and letters. A. The largest sphere, measuring close to 50 µm, is probably a chroococcalean cyanobacteria. It appears to be enclosed by a sheath. C. Same as A, except it is one of the smaller colonial forms that averages 16 to 30 µm in diameter. D. Above the arrow and to the left at about 11 o'clock there are smaller coccoid shaped spheres that can occur in chains, pairs, or singly. They are usually 2 µm in diameter. E. These spheres average between 5 to 12 µm in diameter, and also appear to be sheath enclosed. They are probably assignable to the genus *Archaeospheroides*.

Figure 6. A low kv energy dispersive x-ray analysis (EDS) of the large chroococcalean cyanobacteria. Carbon, oxygen, and iron (L line) are present at higher levels than silicon. The specimen is coated with gold-palladium.

Figure 7. Low kv EDS of the 5 to 12 µm spheres (*Archaeospheroides*). This is similar to the chemistry of the chroococcalean forms.

Figure 8. SEM of a long filament that may be *Eoleptonema* with 2 µm coccoid spheres that appear to be closely associated. A. The long, narrow filament that can be seen twisting over and under rock fragments. B. Coccoid spheres that measure approximately 2 µm in diameter. C. 2 µm spheres with equatorial splitting or girdling that may indicate either early stages of cell division or a shedding of the exterior wall.

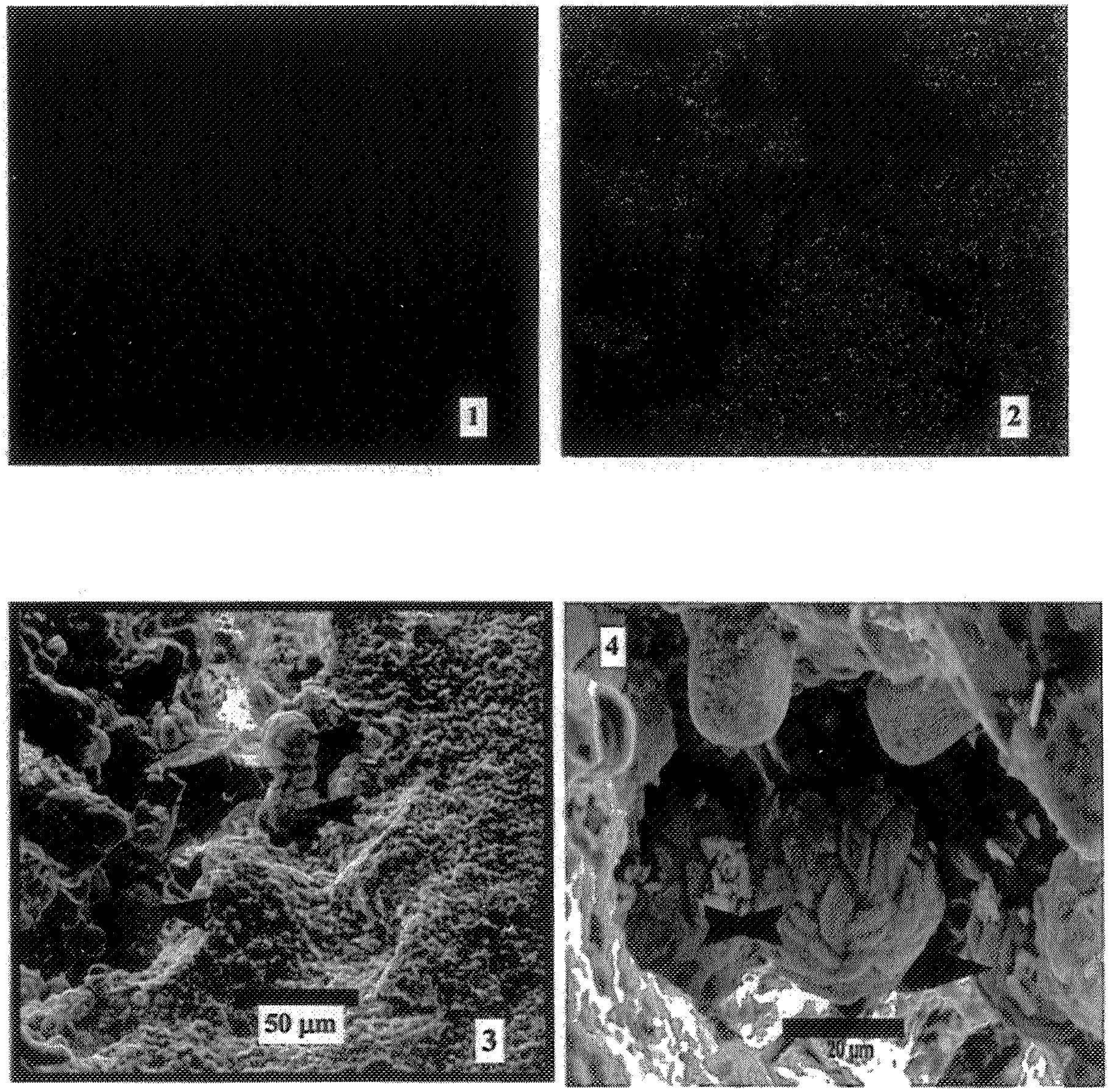
1
2
50 µm
3
4
20 µm

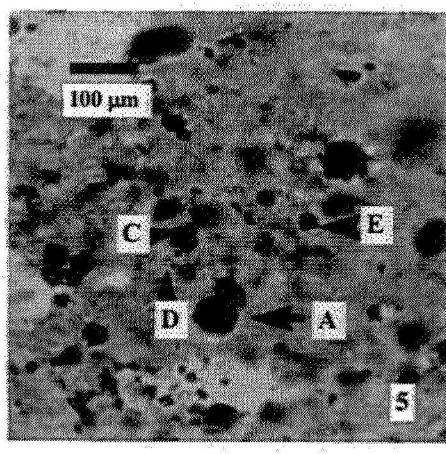
100 µm
C
E
D
A
5

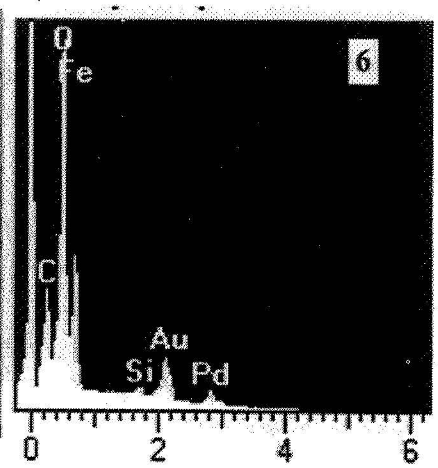
O
Fe
6
C
Au
Si
Pd
0
2
4
6

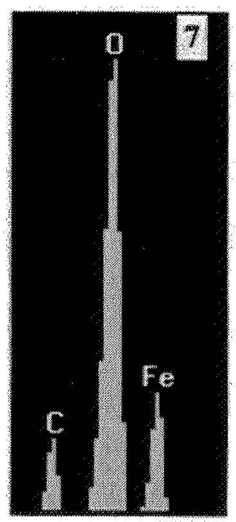
O
7
Fe
C

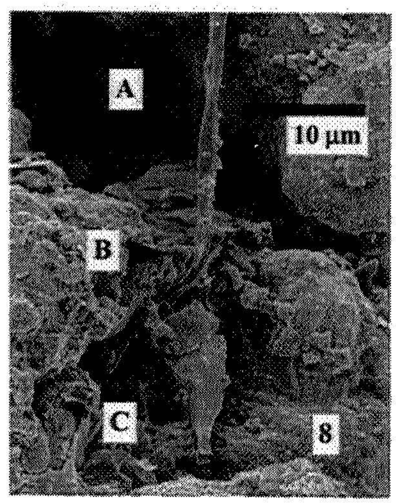
A
10 µm
B
C
8

( )9

IN-61

Virtual Manufacturing Techniques
Designed and Applied to Manufacturing Activities
In the Manufacturing Integration and Technology Branch

Final Report

NASA/ASEE Summer Faculty Fellowship Program –1998

Johnson Space Center

Prepared by:	Charles A. (Chip) Shearrow, Ph.D.
Academic Rank:	Associate Professor
Student:	Blake W. Ludban
Student:	Anthony W. Roth
University & Department	Ohio Northern University
	Department of Technology
	Ada, Ohio 45810

NASA/JSC

Directorate:	Engineering
Division:	Manufacturing, Materials, and Process Technology
Branch:	Manufacturing Integration and Technology Branch
JSC Colleague:	Charles L. Salkowski
Date Submitted:	August 7, 1998
Contract Number:	NAG 9-867

Abstract

One of the identified goals of EM3 is to implement virtual manufacturing by the time the year 2000 has ended. To realize this goal of a true virtual manufacturing enterprise the initial development of a machinability database and the infrastructure must be completed. This will consist of the containment of the existing EM-NET problems and developing machine, tooling, and common materials databases. To integrate the virtual manufacturing enterprise with normal day to day operations the development of a parallel virtual manufacturing machinability database, virtual manufacturing database, virtual manufacturing paradigm, implementation/integration procedure, and testable verification models must be constructed.

Common and virtual machinability databases will include the four distinct areas of machine tools, available tooling, common machine tool loads, and a materials database. The machine tools database will include the machine envelope, special machine attachments, tooling capacity, location within NASA-JSC or with a contractor, and availability/scheduling. The tooling database will include available standard tooling, custom in-house tooling, tool properties, and availability. The common materials database will include materials thickness ranges, strengths, types, and their availability. The virtual manufacturing databases will consist of virtual machines and virtual tooling directly related to the common and machinability databases.

The items to be completed are the design and construction of the machinability databases, virtual manufacturing paradigm for NASA-JSC, implementation timeline, VNC model of one bridge mill and troubleshoot existing software and hardware problems with EMNET. The final step of this virtual manufacturing project will be to integrate other production sites into the databases bringing JSC's EM3 into a position of becoming a clearing house for NASA's digital manufacturing needs creating a true virtual manufacturing enterprise.

Current Manufacturing
Flow Chart

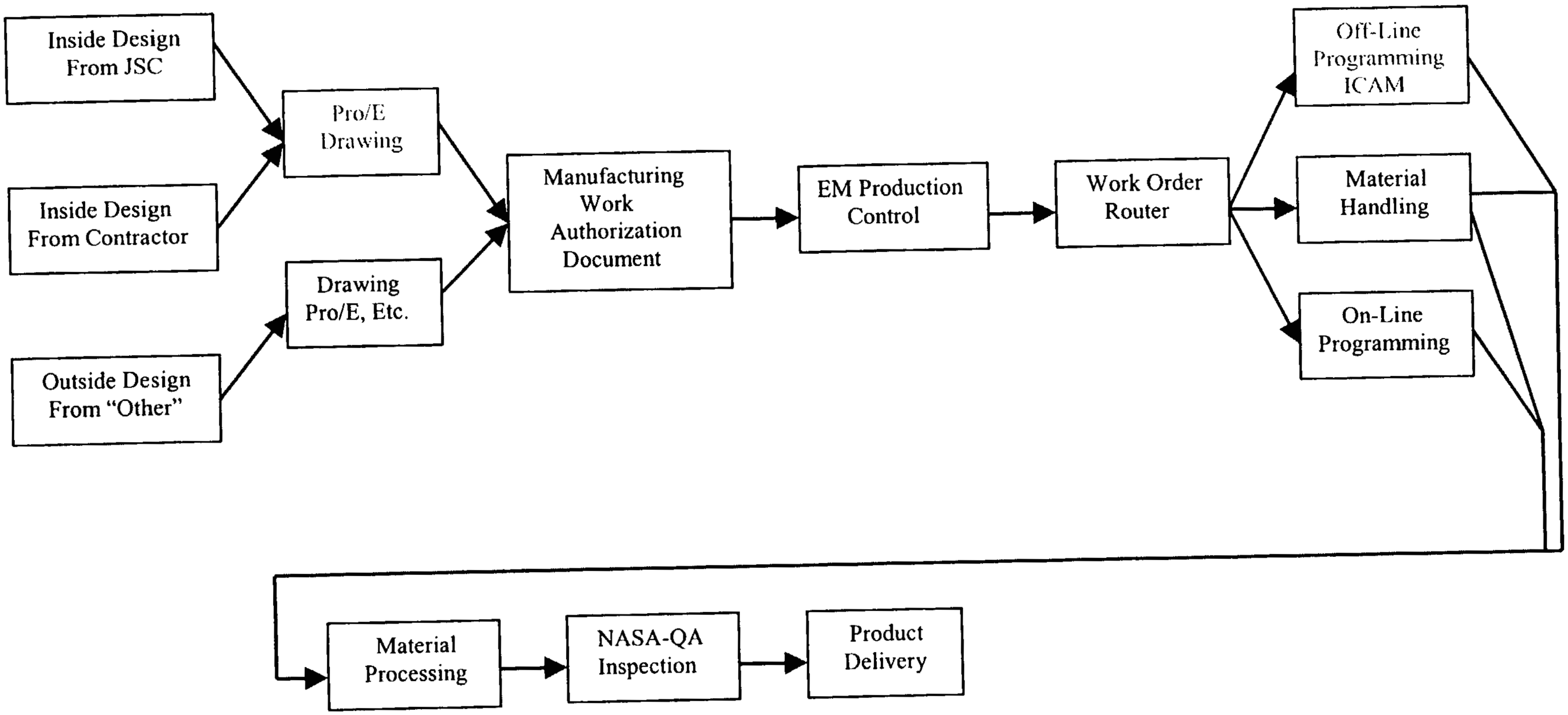

Discovery

Literature Review:

Virtual manufacturing has come of age by using the virtual environment which was first was implemented into video games. The virtual environment can be implemented into a company in many different forms to fit their needs. An example is that "Rolls-Royce has used a virtual environment to replace costly mock-ups for aero-engine maintenance and verification." (Carpenter, 1997) One of the unique features in a virtual simulation environment is the openness of the software's architecture. Virtual simulation software typically allows a company or an organization to develop a virtual manufacturing environment to fit their needs. The development of a complete virtual manufacturing enterprise will include tracking of cost reductions; development of a integrated environment for manufacturing and design process; common databases to insure communication between development and manufacturing; assured accurate assembly; verified numerical control programs with machining details delivered to the production floor; assistance to micro-machining procedures and processes; and cost effective off-line training.

Carpenter notes that "... few have begun to appreciate the potential of VR for exploitation in the commercial and industrial areas." (1997) The companies that have started implementing virtual simulation have found that " Optimizing a system before you build it should cut the time it takes to introduce a new product and should cut the cost of that product 40-60%" (Owen, 1997) On the other hand Ford motor company discovered that in a month a development team was able to produce a rough model and prototype of a forge for training purposes. This development was successful because "the technology (virtual simulation) lets manufactures transfer training for complex or dangerous jobs to virtual environments." (Owen, 1997) According to a presentation by Deneb Robotics at NASA-JSC, major aerospace and defense organizations that have bought into the application of virtual manufacturing techniques are Bell Helicopter, Boeing, British Aerospace, General Dynamics, Jet Propulsion Laboratories, Lockheed Martin Corp., McDonnell Douglas, NASA, Saab Aircraft, U.S. Army, U.S. Navy, U.S. Airforce and Westinghouse. (July, 1998)

Virtual reality applied in manufacturing has the ability to integrate the design process and the manufacturing process causing great savings in rework and manufacturing time. Coyle shares the same view in that "The virtual environment provides a visual guide to bridge the communication gaps between engineering and manufacturing." (1997) Coupled with the view of better communications is the belief that "The efficient flow of information shortens the design and build cycle and improves first time quality." (Coyle, 1997)

To achieve a good virtual environment within an organization it is necessary to develop databases that can be accessed by all the people who must handle the product from design, processing and final assembly. For JSC-EM it is necessary to develop the virtual machinability databases and machinability databases which include machines, tooling, fixtures, and materials that will support future virtual simulation. This is supported by Coyle in that he believes that "An integrated product database is a key

enabler which allows the effective use of the DMAPS (virtual manufacturing system) integrated toolset for developing new product design and existing product redesign." (Coyle, 1997)

When virtual manufacturing is used in assembly processes it is possible for the system to predict problems not only in the assembly but future servicing of the product. "A virtual assembly system is a set of computer-based models that capture the design, physical system—including 3-d solid models of equipment geometry, mass properties, and material properties." (Conrad, 1997) An example of this is when parts need to be moved in and out of the X-38 without skinning the structure or causing damage that may need to be replaced so the vehicle can be used for flight. Conrad supports this use of assembly software (Envision) in that "Any given product may employ more than one set of possible assembly processes, and each set of processes may use multiple possible operational sequences. Users must choose those feasible (or economically viable) to automate."(Conrad, 1997)

Virtual manufacturing has its immediate applications in miniature machining at JSC-EM3. There are times when the verification of a tool path or a measurement need to confirmed in a manner that can be used by the developers and operators of the equipment.

> "The approach implemented to perform positioning feedback by an external measurement, uses a model with a representation as detailed as possible with an a-priori- knowledge of the scene that is to be analyzed. The combination of prediction/verification techniques between the real worlds (i.e. the worlds as viewed by the microscope and that contained by the knowledge representation model) provides the necessary information required to carry out positioning." (Ramanowicz, 1996)

A good example of this process is using the virtual simulation software to check a tool path that has been developed to test a new five-axis machine to do micro machining. Where the round end of a workpiece intersects with a square protrusion it is difficult to see if the tool will penetrate the previously machined surface without virtual software.

Another application of virtual manufacturing is in the area of training personnel for jobs where loss of life or limb, manufacturing time and material loss is unacceptable. It has been found that a "... significant drop in learning curves and reduced cost under the curve for the virtual and physical factory has been validated for McDonnell Douglas Production products." (Coyle, 1997) With confirmed reductions in employee training, virtual simulation is a cost-effective way to train employees on manufacturing processes without drastically disrupting everyday operations.

In conclusion it appears that that EM is positioned to quickly move into a virtual manufacturing environment with the development of common databases such as standard tool loads, tools, fixtures, machine tool models, and materials. The cooperation between designers and the production facilities will provide the interface needed to insure the success of the virtual manufacturing enterprise.

Data Transfer:

Between 1995 and 1998, EM3 moved towards computer integrated manufacturing (CIM) by creating a method to deliver Numerical Control (NC) to the Direct Numerical Control (DNC) machines on the floor of building 10 at Johnson Space Center (JSC). A network was installed so data could be transferred to all the DNC machines. To facilitate the delivery of the data and give the machine operators an interface with the job being received an NT station was strategically placed so two machine operators and machines could share it. Post processors were developed to allow the NC files to be transmitted directly into a machine in its unique language. It was found that the CIMNET software purchased to regulate file transfer was too taxing on the network and it was replaced by EMnet developed by a programmer in EM3. The sections of EMnet that are complete are delivering data to and from the machines as designed.

The design of items in EM is done in Pro/E and can be accessed by the designer and the programming office. When the work order router is issued the job is transferred to the programmers. The programmers then use Pro/E to create the cutter location file (.CL) which then is converted by ICAM a post-processor, into a .tap file. The .tap file which is made of G and M codes is then delivered to the machines on the facility floor by network where available or by 3.5 disk.

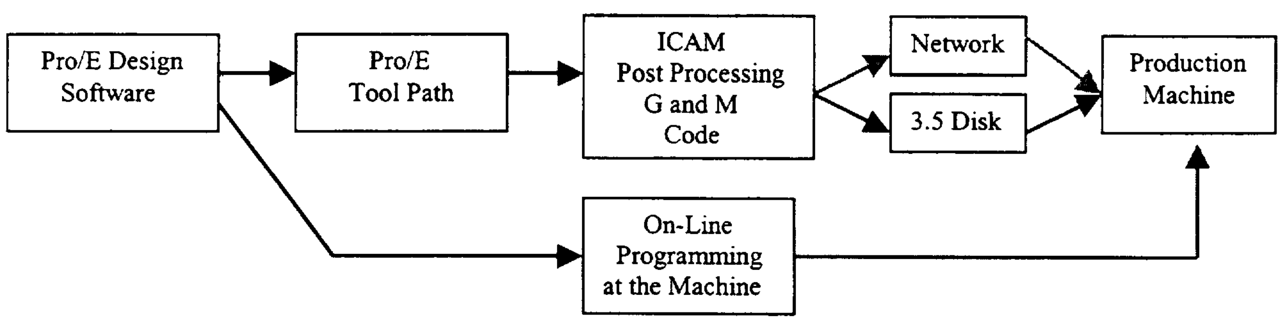

The problem with this manufacturing procedure diagram is that there are serious non-conformities to the original plan to integrate computer integrated manufacturing (CIM) into the manufacturing operations at JSC. The blue and green lines represent the flow of data that was presented to EM in 1995. The red line represents data flow that is costing EM fiscally due to the inefficiencies of the processes. For virtual manufacturing to be successful the infrastructure must be completed.

Initial Issues to be Addressed Before Virtual Manufacturing is Implemented:

The new software (Emnet) transfers the data efficiently but has some user interface problem. The software allows the machine operator access to all the NC files in a directory. This freedom of access allows the same file/part to be run more than one

time and allows the operator to run the wrong part producing waste and lost production time.

Not all of the NT stations have been located on the production floor between the machines. This means for the EMnet to be complete the stations will have to be installed and communications between the NT station and the machine must be established.

Integration between the designers and the production areas of EM must become integrated for a virtual manufacturing enterprise to be successfully implemented.

No paradigm for virtual manufacturing exists in EM3 to guide the implementation of the virtual manufacturing enterprise. The Paradigm must be developed at JSC then expanded to cover other NASA locations to streamline production costs.

Only a partial time line has been developed with virtual manufacturing identified as a goal for the year 2002. Not all aspects of EM are listed in the timeline and the order of implementation does not follow existing virtual manufacturing models and or research.

Machinability databases must be developed to promote efficient use of the virtual manufacturing paradigm. The databases consist of the machines available, standardized tooling, machine tooling and materials available.

Virtual databases must be developed to support the virtual manufacturing enterprise paradigm. The databases include modeled machines, virtual tools, virtual machine tooling, and virtual material blanks.

Development

EMnet is locally developed software used to transfer files from the programming area to the production floor. Since all the NC programs are post-processed to each machine it is recommended that the following action be taken to eliminate the problems of wrong and/or multiple parts being made. First, each machine should be given its own folder on the appropriate computer. Full access to the folder should be limited to the programming office. One solution to this problem would be making the file read only so access was limited to the programmers. The machine operator should be able to load the job once into the machine. After the job is loaded the file should "disappear" by changing the file extension in the Emnet code. This will leave the file available to the programmer if there was a problem with the job being processed. This should eliminate the multiple parts production by choosing the wrong part. To confirm the job and part number the operator should login with the job identification number (ID) (new field on the router identifying the machine) and have to use the same number to verify the download. This should insure the proper job being done at the right machine. The maintenance of these parts files and folders should be the programmer's responsibilities. This way only the programmer is responsible for the program and the machinist is responsibility for production.

NT stations need to be purchased so there is no more than two machines per station. This will allow adequate access to data transfer and allow virtual molds to be displayed at the workstations. Once the stations are installed the network needs to be extended to the workstations and the interface cabling needs to be developed to hook the machines to the stations. This will complete the infrastructure.

Machinability database is a general term used to describe the sum of the databases developed to implement integrated manufacturing. These databases must be redesigned and updated to reflect the change from manufacturing to virtual manufacturing. Additionally, these databases will need to be duplicated on common software across the NASA and contractor sites that wish to participate in the virtual manufacturing enterprise (VME).

Machine Tool Database includes 32 machines in buildings 9 and 10 that have the ability to be programmed off-line and connected to the network. The characteristics of each machine and their location at JSC were documented. This is in preparation of the plans to be able to farm out work to other sites such as White Sands to alleviate down time to customers due to the machines being busy. This would also enable JSC to rapidly respond to the need for parts in the case of an emergency by utilizing all the resources available at NASA proper before farming out work to other contractors. The data collected included the manufacturer, type of machine, model, controller type, owner location, facility location, network capabilities, media used for transfer, scheduling availability, auxiliary tooling available, auxiliary fixtures available, work envelope, number of tool stations, maximum travel for the machine, maximum feed rate, maximum rapid feed rate, maximum spindle speed, tool change time, rapid feed units, spindle feed rate, spindle horse power and table weight maximum.

Tooling Database is very extensive in nature at JSC with the number of cutting tools custom and off the shelf in the hundreds. A database has been developed for this research effort that includes only the off the shelf end mills available for use. The database will need to be completed to finish the machinability database. The type of cutter information that needs to be collected is the tool identification from InFiSy, tool type, tool length units, cutter diameter, corner radius, side angle, tool length, number of teeth, material, the JSC tool comment code and shank diameter. These attributes are necessary for ordering the tools and can be used by engineers in the design process. When a engineer designs to a stock cutter number the production time for the requested part will be shorter than if cutters have to be ordered.

Another way to standardize production is to develop a standardized tool load for each machine. If the first half of the tool magazine is loaded with standardized tools and the engineers and programmers use these tools then production will become more efficient. Only using the first half of the magazine will permit the flexibility needed to produce one-of-a-kind products one after another. A virtual standardized tool load has been developed by the VNC programmers as a demonstration of how efficient it will be to pull the same tools from one simulation to another.

Materials Database at JSC was unobtainable during the scope of this research effort. There is no standard stock of machinable materials with the nature of the specialized products being produced. In a "normal" manufacturing situation there would

be a standardized material list that would need to be adhered to by the designers to expedite production down time due to material not in stock.

Virtual Manufacturing Database will consist of all the DNC machines located in EM. Each machine will need to be modeled because the work envelope will differ from one machine to another even if they are the same machine. To improve the efficiency of the production facilities the lead machines need to be modeled first. Once the machines are built then tooling and clamping devices must be modeled to run simulations. Special tooling can be constructed as needed but designers need to be encouraged to use the common tool loads to speed production time.

Virtual manufacturing paradigm for NASA-JSC

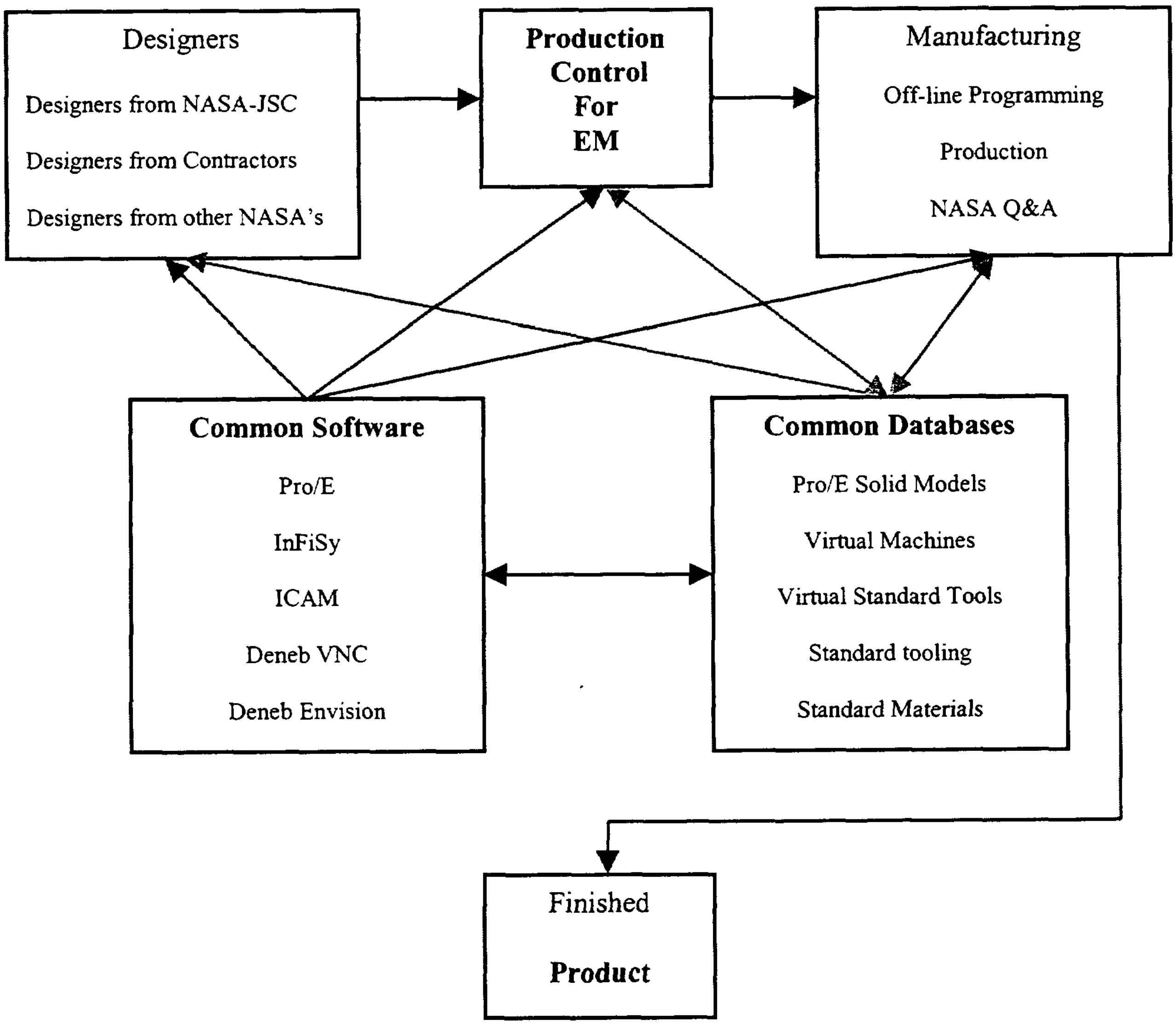

The virtual manufacturing paradigm depicted above is designed to be implemented as a prototype paradigm to be distributed throughout NASA. All designers whether employed by or working for NASA need adhere to the common software and procedures needed for the success of this paradigm. The common databases will have to be made available to all the persons involved with the design through the production and inspection of the parts. Some of the access to the files will have to be limited to a read only status to maintain the security of the data.

Once production control has the plans to the part to be manufactured the plans need to be distributed to off-line programming and Q&A. Having the distribution to both organizations/departments at the same time will enable timely off-line programming and verification. When the part is ready to be made, production can go into action and when production is done the Q&A people will be ready for the part cutting overall time from start to finish by as much as fifty percent.

Virtual manufacturing will provide a savings in the amount of materials ordered; machine time and employee time saved due to chips made; damage done to machines and their tooling; and in the overall throughput time factor. The success of virtual simulation will be bases in the use of the system avoiding the use of on-line programming and ordering duplicate materials. If designers and their organizations are penalized financially they will think twice about their design procedures.

NASA's Virtual Manufacturing Enterprise Paradigm shown below, is designed to promote centralization the management of materials processing for the NASA organization. The paradigm promotes the nine manufacturing facilities located across the United States to centralize and accelerate the manufacturing process by doing the machine code development and verification at NASA-JSC to more fully utilize the enterprise resources.

To develop a virtual enterprise such as this it will be necessary to have one common database that all of the facilities can access to perform design functions, manufacturing and inspection for quality. The common databases and software is essential to the success of the paradigm. With all the organizations communicating with the same software and using the same databases common design data can be collected and in turn be implemented into future designs. By centralizing the off-line programming and verification the confidence level of "good" parts being produce will rise due to the standardization of procedures and programming techniques.

NASA's Virtual Manufacturing Enterprise Paradigm

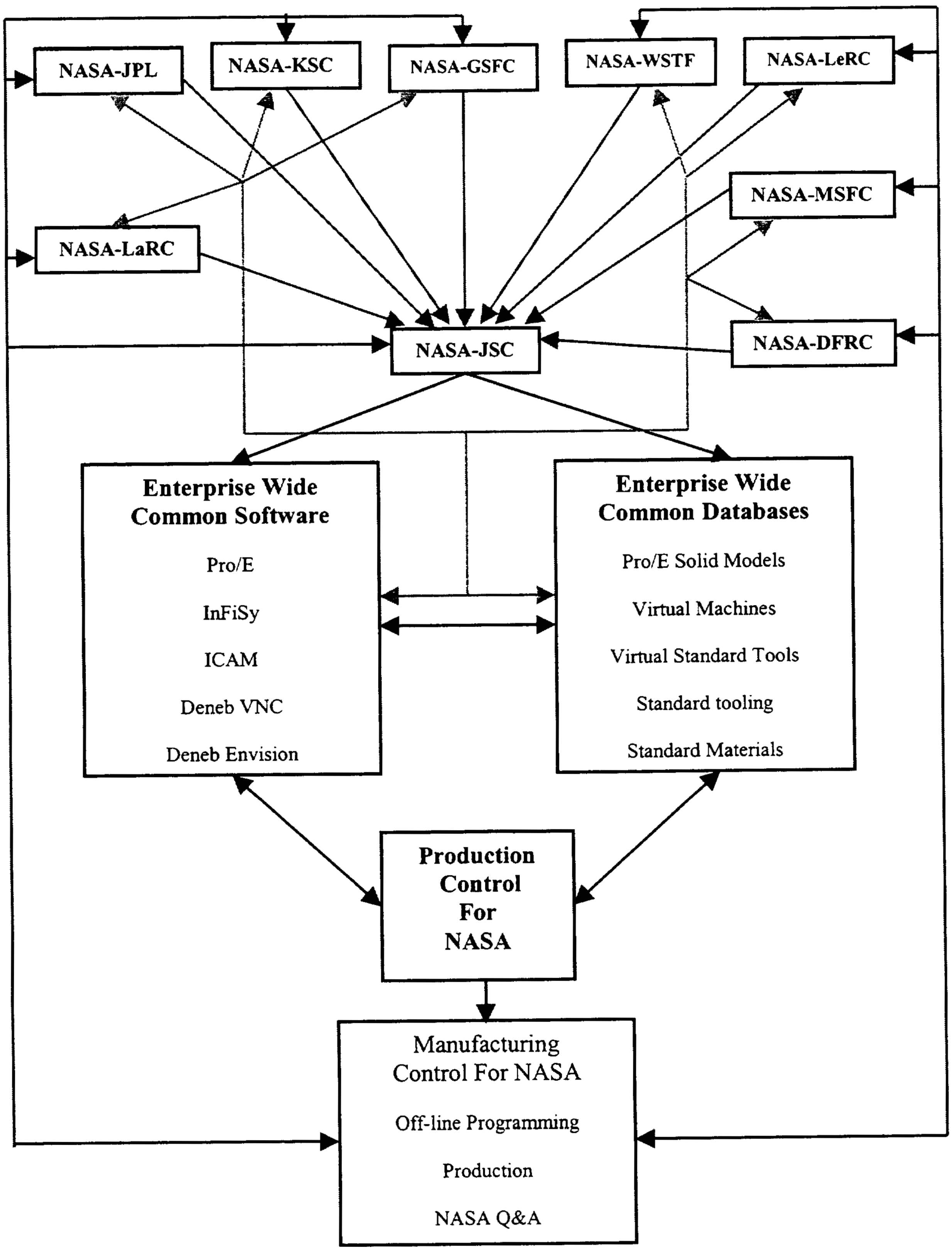

Virtual Manufacturing Implementation Timeline for EM

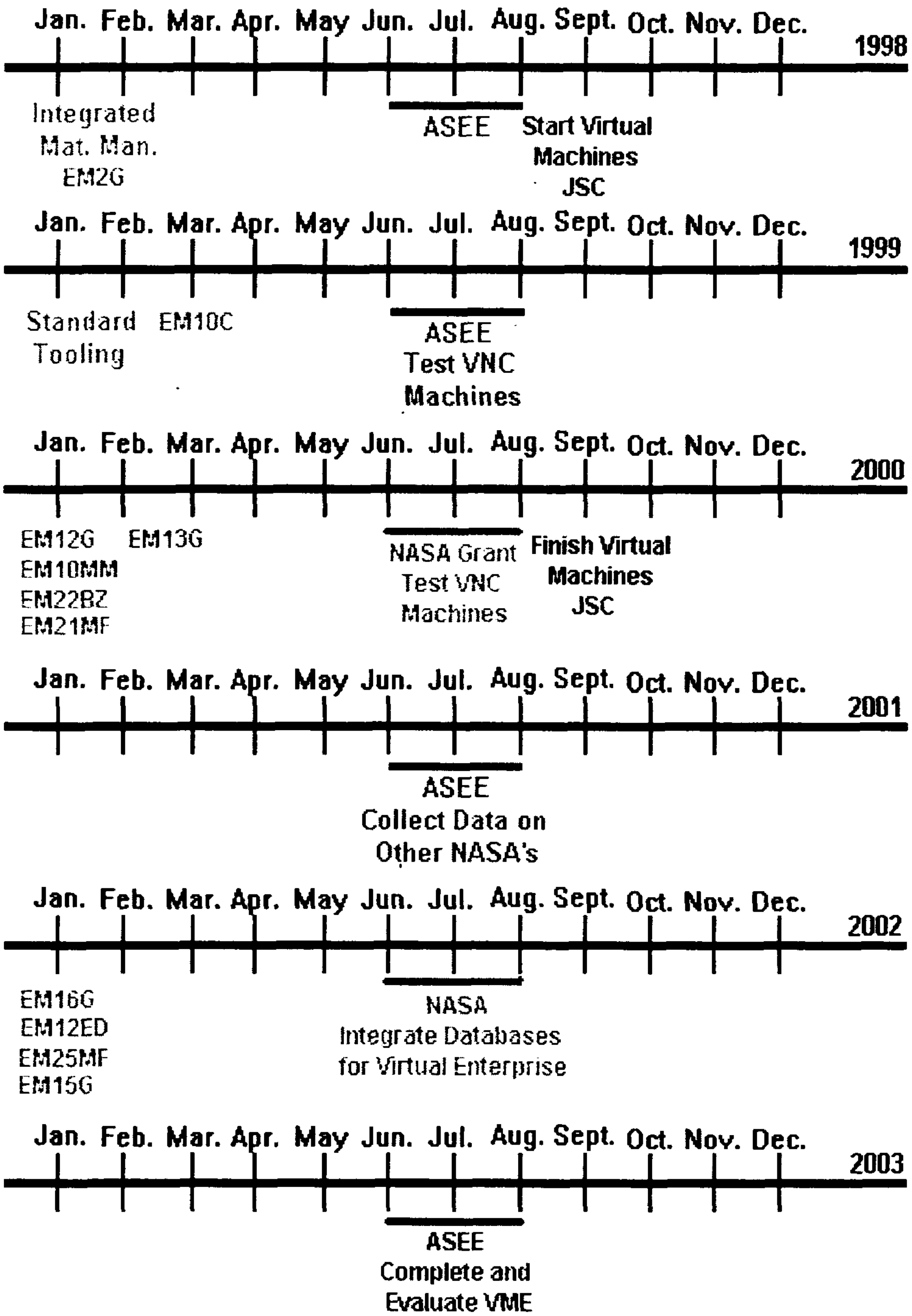

Virtual Manufacturing Implementation Timeline for EM includes the planned development of virtual manufacturing in EM at JSC and includes assistance from outside sources as partnerships. During 1998, the integration of manufacturing will have to be completed. This means that EMnet and the machinability database must be completed before virtual manufacturing can be fully implemented. In 1999, it will be necessary as more of the DNC machines come on line with virtual manufacturing to mandate that the first ten tools in each tool changer have the same cutters mount in them. If the machine has less than twenty tool positions then one half the positions should be held open for custom tooling needs. By the end of the year 2000, it is possible to have a virtual manufacturing facility that can be duplicated in concept and applied to all of NASA's manufacturing facilities. During the year 2001, it will be necessary to collect data on the other NASA sites to start their transformation using JSC as a model. The prospect of saving as much as fifty percent on manufacturing costs nationally makes this paradigm and timeline a necessity for survival. In 2002, the databases will have to be integrated from cost to cost. This will include the constructed virtual machines and tooling availability. Scheduling of the machines will have to be posted so other facilities can use a machine. By 2003, the virtual manufacturing enterprise can be fully implemented and an efficient NASA will have the potential to handle any manufacturing needed for the agency while maintaining a good confidence of quality.

Conclusion

With elimination of current manufacturing problems and the implementation of virtual manufacturing databases are completed, it will be possible to fully integrate JSC's EM into the next level of manufacturing. Once the paradigm is complete it will be easily duplicated at the other manufacturing facilities across the United States with a possible saving on manufacturing cost of as much as fifty percent. Yes, the front end load with virtual manufacturing software is heavy and the implementation of common software will be challenging but the rewards will be dramatic. JSC and NASA is ready to move in to the virtual realm of manufacturing.

Bibliography

Anelle, J., 1998. "Simulation Enhanced Work Instructions for Aircraft Assemblies", Society of Automotive Engineers, Aerospace Manufacturing Conference, The Boeing Company.

Carpenter I. D., June 1997. "Virtual Manufacturing", Manufacturing Engineer, Vol. 76, Issue 3, Page 113-116.

Conrad, C. J., Sept. 1997. "Assembly automation: the virtual and the physical", MANagement ENGineering, Vol. 119, Issue 3, Page 62-66.

Coyle, J., ND. "An Overview of DMAPS Virtual Product Definition", Presented by Virginia Vasey-Glandon, McDonnell Douglas Aerospace, St. Louis, Missouri.

Gulli, M. A., Oct. 1995. "Virtual Collaborative Simulation Environment for Integrated Product and Process Development", Deneb Robotics, Auburn Hills, Michigan.

JSC-EM, 1997. "EM Roadmap", Objective and Goals, EM/Manufacturing, Materials, & Processes Technology Division, National Aeronautics and Space Administration-Johnson Space Center; Manufacturing, Materials, & Processes Technology Division; Manufacturing Processes Development Branch, Houston, Texas.

Lin, E., Minis, I., Nau, D. S., Regli, W. C., May 1995. "Contribution to Virtual Manufacturing Background Research", Institute for Systems Reaearch, University of Maryland, College Park, MD 20742, Prepared for: Manufacturing Technology Directorate, Air Force Wright Laboratory, Air Force Systems Command, Wright-Patterson Air Force Base, Ohio 45433-6533

Nau, D. S., Herrmann, J. W., Regli, W. C., ND. "Virtual Factories" Institute for Complex Engineered Systems, Carnegie Mellon, Institute for Systems Research University of Maryland.

Owen, J. V., Oct. 1997. "Virtual Manufacturing", Manufacturing Engineering, Pg. 84-90.
Shearrow, Charles A., 1995. " Design and Implementation of a Windows NT Network to Support CNC Activities", Final Report NASA/ASEE Summer Faculty Fellowship Program--1995 Johnson Space Center; Engineering Directorate; Manufacturing, Materials, & Processes Technology Division; Manufacturing Processes Development Branch, Contract Number NGT-44-001-800, Houston, Texas.

Ramanowicz R., 1996. "Towards an Integrated Frame Work for Data Exchange", SPIE Proceedings (Microrobotics: Components and Applications), Vol. 2906, Pg.96-108.

Shearrow, Charles A., 1995. " Computer Integrated Manufacturing Proposal for EM/Manufacturing, Materials, & Processes Technology Division, National Aeronautics and Space Administration- Johnson Space Center; Manufacturing, Materials, & Processes Technology Division; Manufacturing Processes Development Branch, Houston, Texas.

Upton, D. M., McAfee, A., 1996. "The Real Virtual Factory", Harvard Business Review, July-August 1996, Pg. 123-133.

Yamazaki Mazak Co., 1993. "Programming Manual for MAZATROL T-32 EIA/ISO" Manual Editional Section of Engineering Generalization Section, Publication Number H712PB0501E.

TIPS AND SUGGESTIONS FOR USING DENEB'S VIRTUAL NC SOFTWARE

BLAKE W. LUDBAN
ANTHONY W. ROTH

ASEE/NASA SUMMER FACULTY FELLOWSHIP
JOHNSON SPACE CENTER
EM3
SUMMER, 1998

METHODS OF CUTTING

All methods of cutting are found in **CAD → MODIFY → CUT**

3-Point Cutting Method

Steps

1. Select three points on a single object using the LMB (or MMB to select a vertex).
2. These three points will define angle and orientation of the cutting plane.
3. The created plane encompasses the entire CAD world and can be applied to any object it can be extended through.

Polygon Cutting Method

All object surfaces are made up of one or more polygons.

Steps

1. Select a polygon on an object's surface to define the cutting plane.
2. As with the 3-Point method this plane extends through the whole CAD world.
3. Select any line, polygon, or object this plane intersects and it will be cut on that plane.

Frame Cutting Method

Any object or world coordinate system can be selected as the cutting plane frame.

Steps

1. Determine the X, Y, Z coordinates of a point in space.
2. A cutting plane will be created, at the point, that is perpendicular to the line from the origin to the point.
3. Select any object this plane intersects and it will be cut on that plane.

BOOLEAN METHODS OF MATERIAL REMOVAL

All Boolean functions are found in **CAD → MODIFY → (UNION, DIFF, MIDDLE, ALL)**

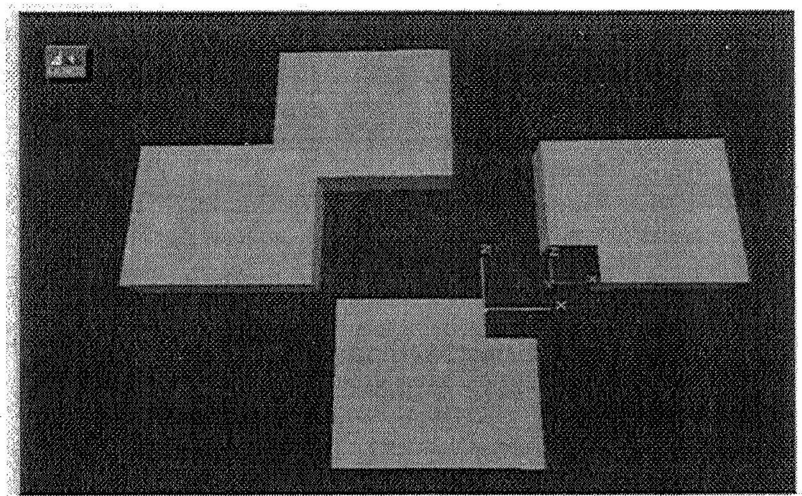

UNION Boolean Function

<u>Steps</u>

1. Select two overlapping objects and the UNION function will be performed.
2. The overlapping material will be removed from both objects, leaving each altered.

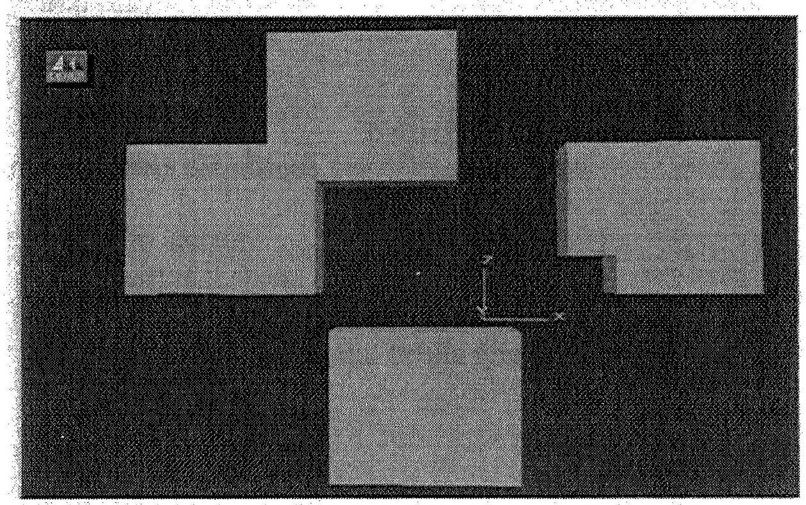

DIFF Boolean Function

<u>Steps</u>

1. The volume of the first selected object will be removed from the second object.
2. The first object will remain unchanged while the second loses the volume of the overlap

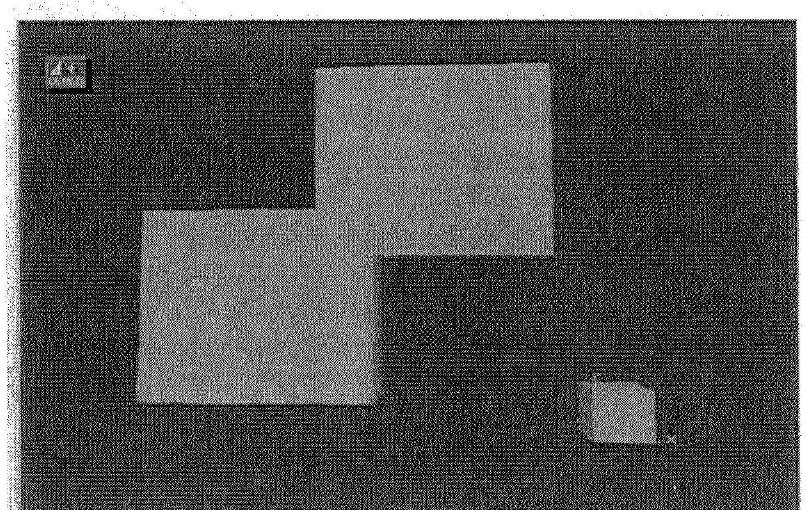

MIDDLE Boolean Function

<u>Steps</u>

1. Select two overlapping objects.
2. The objects will both be deleted leaving only the overlap volume.

ALL Boolean Function

Steps

1. ALL is a combination of UNION and MIDDLE.
2. After selecting both overlapping objects, each will be altered and the overlapping volume will become a separate object.

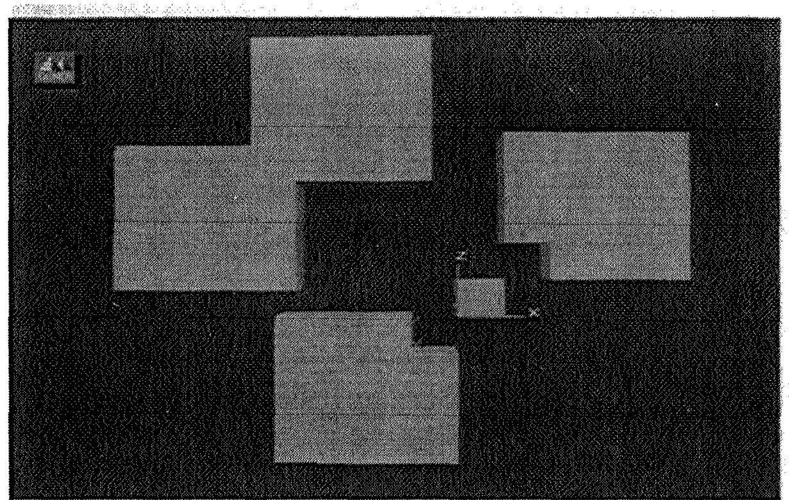

HOW TO CREATE SURFACES BETWEEN TWO OR MORE PARTS

At times a surface is needed to connect separate objects, but creating a new object is not a convenient method of doing so. Two methods of creating these surfaces are Meshing and creating Polygons.

Creating MESH

Mesh is a sheet of material with no thickness that can join co-planer surfaces. Mesh requires a closed wire frame to contain the material.

Steps

1. First a wire frame needs to be built to contain the mesh.
   a. **CREATE → LINE**
   b. The boundary lines will snap to a vertex.
   c. The last point selected must be the same as the first point so the boundary is closed.
2. Select **MESH**
   a. Select the boundary line that was just created.
   b. Select **DONE** in the lower right hand corner of the screen.

Creating Polygons

Polygons are useful in that they do no not require wire frames, existing vertexes and end-points can be selected. Another useful aspect of polygons is they can be made to be opaque or transparent.

Steps

1. **CREATE → POLYGON** or **MODIFY → POLYGON**
2. Select the co-planer, perimeter vertices where a surface is needed.
   -opaque → Counter-clockwise vertex selection
   -transparent → Clockwise vertex selection

MEASURING AND THE USE OF VARIABLE REGISTERS

Whenever an **ANALYSIS** function is performed, the data obtained is temporarily stored in a register that may then be used in other functions. Two examples of this will be performed below.

I. Selected **ANALYSIS** operations
II. **ANALYSIS** variables used to facilitate object construction
III. **ANALYSIS** variables used to facilitate object movement

Before beginning this section, create the following objects:

Block:

X origin	0
Y origin	0
Z origin	0
X length	10
Y length	10
Z length	2

Block:

X origin	5
Y origin	0
Z origin	2
X length	5
Y length	10
Z length	10

Cylinder:

X origin	20
Y origin	20
Z origin	20
Diameter	5
Eccentricity	1
Height	10
Start Angle	0
End Angle	360
Num Facets	12
Axis	Z-axis
Circumference	Inscribed
Lower Cap	Yes
Upper Cap	Yes
Center Point	Yes

Select **ROTATE** from the bottom menu, then **ABS** from the side window and enter the following values:

Yaw	40.000 deg
Pitch	-15.000 deg
Roll	20.000 deg

Vertex selections will be assumed to be selected from this view.

Note: *The object characteristics are kept simple so that the following functions may be easily checked by hand if so desired. These functions work equally as well with numbers which have more significant digits and VNC will store all appearing digits.*

I. Selected **ANALYSIS** operations

A. **ANALYSIS → MEASURE → DISTANCE MEASURE**

The first option available is the **GENERIC** measurement. Under this are 8 options:

1. Store Last Hit: This function is essentially unnecessary. It enables the user to reposition the world so that an entity can be selected which may not be currently seen. See the Button Help for more information on this item. As an alternative, select an item, select **CRUISE** so that the next entity may be seen. The dialog popup will disappear as you cruise. When the second entity may be seen, press the spacebar and the popup will reappear. This technique can be used in many applications and will usually make the previous popup reappear.
2. Centroid: The center of a selected polygon may be selected by clicking on the polygon.
3. Coorsys: Coordinate system
4. Edge:
5. Vertex:
6. Object: Measure between part origins of 2 objects
7. Curve:
8. Surface:

Note that Edge, Curve, and Surface measurements are done from the exact point of selection – there is no further snapping to an endpoint, midpoint, vertex, etc.

As an example, measure from the vertex identified below as "I" to "F".

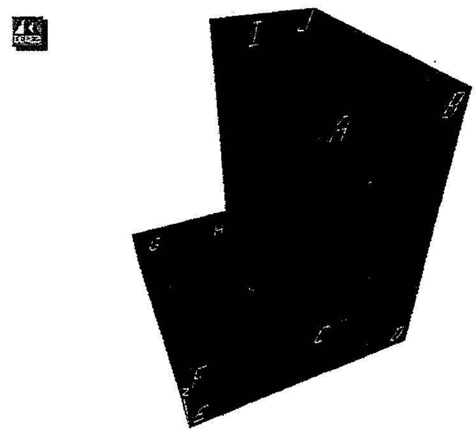

Notice that a series of 4 lines will appear: one along each of the 3 axes, and one directly from point to point. Also note in the "Distance Info" popup the information in bold below:

Distance **[d]**	15.000
Delta X **[dx]**	-5.000
Delta Y **[dy]**	-10.000
Delta Z **[dx]**	-10.000

The bold characters above correspond to the variable names which may be used in future calculations and data entries as well as to one of the green lines which appeared. All **ANALYSIS** functions performed will have such a variable associated with them and are retained until the world is cleared or until the function is performed again and the values are replaced.

B. The next three available options under **ANALYSIS → MEASURE → DISTANCE MEASURE** are shortcuts to the **GENERIC** measurement option in that it will measure between 2 vertices, objects, or coordinate systems.

C. The **ANALYSIS → MEASURE → ANGLE MEASURE** entity selection operates very similar to the distance measure selection but has fewer options and instead returns an angle measurement.

D. **ANALYSIS → PROPERTIES → IDENTIFY → VERTEX** is another useful function. It may be used to identify vertices for complex object location.

Experiment with the different buttons and options, measuring from the cylinder to the blocks, etc. to become familiar with the operation of this function as it will be used in sections II and III.

II. **ANALYSIS** variables used to facilitate object construction

A. The registers that these variables are stored into may be used in many combinations and formulas to facilitate object construction.

1. Select **ANALYSIS → PROPERTIES → VERTEX** and select "F".
2. Select **ANALYSIS → MEASURE → VERTS** and select "F" and then "I". By selecting the vertices in this order, a three dimensional volume may be defined by the **dx, dy,** and **dz** variables.
3. Create a block using the information gained from these operations: **CAD → CREATE → BLOCK**
   Enter the information below: Note that only the **bold** characters should be entered and then the information in (parentheses) will appear once the next cell is selected.

X origin	**X** (0)
Y origin	**Y** (0)
Z origin	**Z** (2)
X length	**Dx** (5)
Y length	**Dy** (10)
Z length	**Dz** (10)

B. All of the typical math operations, which VNC supports, may be performed on these variables as if they were numbers. For example, if a block to fill half of the height of the above were desired, **Dz/2** would be entered in the Z length cell instead of **Dz**.

III. **ANALYSIS** variables used to facilitate object movement

A. These variables may be used in object translation and rotation much like they are used in object construction.

1. Measure from the **centroid** of the bottom of the cylinder to the vertex identified as "A". Selecting in this order will return the correct signs to allow direct movement of the object. If they were selected in reverse orders, the signs of the variables would have to be changed by entering **–dx,** etc.
2. **CAD → CREATE → SELECT** and select the cylinder.
3. **CAD → CREATE → TRN OBJ**. With the LMB, select **Rel** which will appear at the bottom of the left-hand menu. Enter **dx** in the popup. (Note that it is case sensitive.)
4. Select **TRN OBJ** and **Rel** again using the MMB and entering **dy**, then with the RMB and entering **dz**. This should place the cylinder centered above vertex "A".

B. Once again, math operations may be performed on these variables.

SLIDING COVERS FOR MILL BEDS.

1. Many milling machines have sliding or telescoping covers over the moving devices to help protect them. These parts are complex in appearance but relatively simple to create.
2. In most cases, the operation of these covers is not hyper-critical to the operation of the machine and so some liberties may be taken. For example, it is assumed that the covers maintain a constant relationship to each other rather than bunching up as sometimes occurs in the real world.
3. Begin by creating solids to mimic the shape of the housing. In this example, a FULL WEDGE will be used. However, if more complex shapes are desired, the profile may be drawn and solids extruded from it.
   - **CAD → CREATE → WEDGE**
   - Create a wedge that will run in the proper orientation in the BUILD world. If the slider is to run along the X axis of the machine, it would make sense to build the slider in the same manner with the WIDTH of the WEDGE being along the X axis, as is the case here.
   - Begin by making Wedge1 from the chart below.

	Wedge1	Wedge2	Wedge3	Wedge4
X origin	0	0	0	0
Y origin	0	0	0	0
Z origin	0	0	0	0
Base 1	17	18	19	20
Base 2	0	0	0	0
Height 1	9	10	11	12
Height 2	7	8	9	10
Width	100	80	60	40
B-H-W axes	Y-Z-X	Y-Z-X	Y-Z-X	Y-Z-X
Type	Full	Full	Full	Full

4. Save this part as Wedge1 by selecting **CAD → CREATE → SAVE ALL**. You should be saving under the \Deneb\VNClib\Parts directory. Next select **CAD → CREATE → DEL ALL**
5. Make the parts Wedge2 and 3 as above.

6. The final slider piece (Wedge 4 in this case) should also contain the bed of the machine, or other moving part, if applicable. In this instance, before deleting the final piece, create a **BLOCK** with the following characteristics:

X origin	5
Y origin	-15
Z origin	0
X length	30
Y length	30
Z length	14

7. Save this final piece as Wedge4.
8. Next select **BUILD → DEVICES → CREATE**. Select Wedgel from the popup. In the following popup, change only the following properties:
   - Name: Slider (optional)
   - Defrees of Freedom: 1
9. Select **BUILD → DEVICES → COORSYS** and select All On from the popup. There should be a coordinate system at one end of the wedge. Cruise so you can see it.
10. Select **BUILD → PARTS → ATTACH**. You may either click on the wedge in the display or select Slider:Wedgel from the "Select Parent Part" popup. This second feature is useful in other situations when there are more parts on the screen. Select Wedge2 from the popup.
11. Use this same method to **Attach** Wedge3 to Wedge 2, and Wedge 4 to Wedge 3. You should now see all of the wedges, as below. (Note that the colors in this picture are for clarification purposes only – they will not appear like this on your screen)

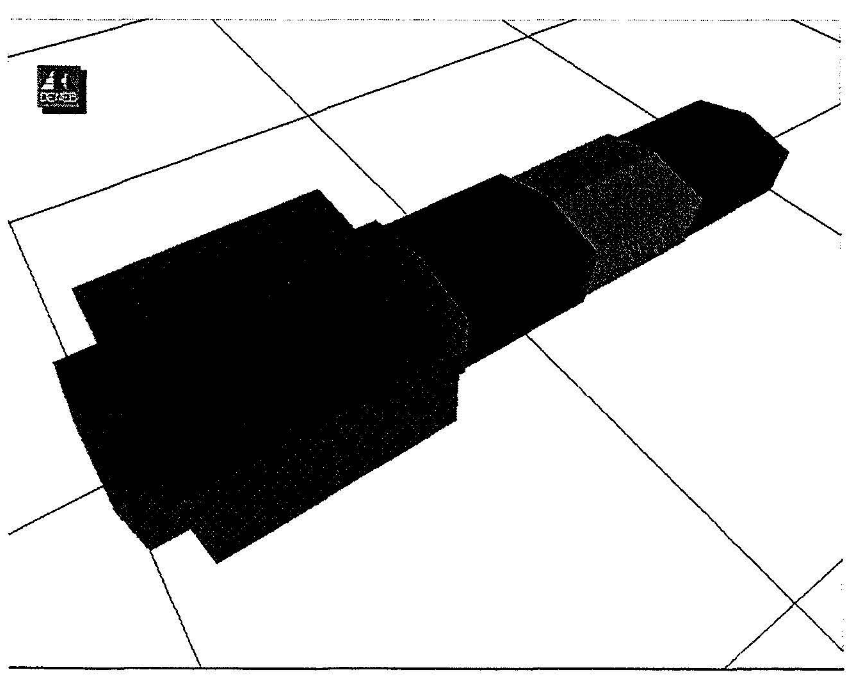

12. Next, select **BUILD → ATTRIB → TRANSFORMS → TX** Select Wedge2 from the "Select Part" popup. Click in the open portion of the "Translate X" window and type a "1" then click **OK**. Do the same procedure for Wedge3 and 4.
13. Select **BUILD → ATTRIB → AXIS LIMITS → TRAVEL** Enter 0 for the lower and 20 for the upper.
14. Select **RUN → PENDANT → JOG** A "jog pendant" popup will appear. You may select "step" to change the jog increment, click the + and – buttons next to step to do the same, or click the + and – buttons next to Axis 1 to move the sliders.

USE OF COORDINATE SYSTEMS IN BUILD

Many pieces that must be built would require rather complex orientations if they were to be brought into **BUILD** to a single origin. For example, one piece may actually sit in the middle of an angled surface of another. Getting this orientation exact in the **CAD** world is rather difficult. Therefore, the application of multiple coordinate systems in the **CAD** world may simplify the build process.

As a simple example, create a wedge, and place a square block in the middle of the angled surface. This may actually be done two ways: either by direct snaps, or through the use of coordinate systems. In this case, coordinate systems will be used.

1. Create a wedge with the following attributes:

X origin	1.25
Y origin	3.48
Z origin	2.07
Base 1	1
Base 2	.5
Height 1	1
Height 2	.5
Width	1
B-H-W axes	X-Y-Z
Type	Half

   This will simulate a surface to which another part must be attached.

2. Select **CAD → AUX → COORSYS → CREATE** and click on the wedge when prompted to select an object. Next select **CAD → AUX → ON SURF** and select "yes" for center on polygon. Click on the angled surface of the wedge and a coordinate system will appear in the middle of the surface.
3. Save this object as *tagwedge* and then delete all objects.
4. Create a block with the following attributes:

X origin	0
Y origin	0
Z origin	0
X length	1
Y length	1
Z length	1

5. Save this object as *tagblock* and delete all objects.
6. Select **BUILD → PARTS → ATTACH** and select the *tagwedge* as the file. Click OK in the "New Device" popup.

7. A popup will remain. You may either continue on using this popup, or click cancel to start again using the above prompt. In either case, select the *tagwedge* as the parent part. Select the coordinate system on the angled surface when prompted for the initial part position.
8. This is much simpler than trying to translate the block so that it will automatically come into the correct place without having to select a coordinate system.

CREATING A DEVICE AND ATTACHING PARTS IN BUILD

Once all of the parts are created, actually getting the machine together and the parts moving correctly is the next step.

Creating a device

Steps

1. **BUILD → DEVICE → CREATE**
   a. Select the main body of the machine from the parts menu.
   b. Name the device.
   c. Number of degrees of freedom (plus 1 for future additions).

Attaching parts

Steps

1. **BUILD → PARTS → ATTACH**
   a. Select the parent part. An existing part that the new part attaches to is its parent.
   b. If the parent part has any auxiliary coordinate systems select the coordinate system the part is to be attached to, otherwise the new part will attach to the parent's base coordinate system.
   c. Continue attaching parts to parents until all necessary parts are present.

PREPARATION FOR MOVEMENT

Once all of the parts are attached in Build, they can be made to move.

Change Device Type

When the first part was attached in the Build world and a name was assigned to it, a *Generic Device* was created. Before anything further can be done the device must be assigned a specific Device Type.

Steps

1. **BUILD → DEVICE → CHANGE DEV TYPE**
   - select **Machine**

Defining motion of a part

Each moving part must be assigned a specific axis (X, Y, or Z) on which its motion will be based, and the motion then defined as **Rotational** or **Translational**.

Steps

1. Defining Axis Types
   a. **BUILD → ATTRIB → AXIS TYPES**
   b. **Axis Name**
      - Choose a letter that is representative of the object.
        I.e. if axis 1 is the chuck, name it "C".
   c. **Axis Type**
      - Define the parts motion as **Rotational** or **Translational**.
   d. **Machine Coorsys Relationships**
      - Define which axis the part's rotation will be about or translation will be on.

2. Assigning motion to each moving part.
   a. **BUILD → ATTRIB → TRANSFORMS**
   b. **Rx, Ry,** and **Rz→** Rotational motion on specific axis.
   c. **Tx, Ty,** and **Tz→** Translational motion on specific axis.
   d. For an object that rotates on the Y axis, select **Ry**
   e. Select object
   f. **Rotate Y** menu comes up
      - The **Insert** number needs to match the number of the axis the object was assigned to in the Axis Types menu.

3. Home position
   a. **BUILD → ATTRIB → HOME POSITION**
   b. Select **Set Home**
   c. Select **Use Current**
      - Later on, when the machine can be jogged, the home position can be reset using the same steps on the new position.

4. Kinematics and Device Attributes

   a. **BUILD → KIN → BASE**
      - Select the main body as the Kinematics Base of the machine.

   b. **BUILD → KIN → MOUNT**
      - Select the part that holds the tool
      - Select **Pick Coordinate System**
      - A tag should be on the surface where the tool attaches

   c. **BUILD → ATTRIB → UTOOL**
      - Select "Pick" from pop-up
      - Choose coordinate system at base of tool mounts to define the gauge point

5. Travel

   a. **BUILD → ATTRIB → TRAVEL**

   b. Each axis will be displayed with an upper and lower limit.
      - Rotational motion will have limits in degrees
      - Translational motion will have limits in inches or millimeters.

JOGGING PARTS

If everything thus far has been done correctly, making the machine move should only take a couple minutes.

Positions of axis

Steps

1. **RUN → INFO → AXIS POSITIONS**
   - This menu shows the position of the parts on each of the axis that were defined in Axis Types.

Jogging

Steps

1. **RUN → PENDANT → JOG**
   - This menu allows you to move each axis.
   - Click on "Axis 1" and the object related to that axis will change color
   - The Plus (+) and Minus (-) buttons do the actual motion.
   - **Step** controls the increments of motion in both degrees for rotation and inches or millimeters for translation.

Note: By using the POSITION button on the JOG pop-up the axis limits or TRAVEL can be verified or adjusted.

SAMPLE CREATION OF A TOOLHOLDER

A virtual toolholder has 2 significant parts: The first is the standard CAT-50 style adapter and the second is any part of the toolholder that protrudes past that part. Therefore, toolholders may be built from a common CAT-50 holder and have any necessary additions made to it.

Standard CAT-50 holder	**EM100400 adapter**
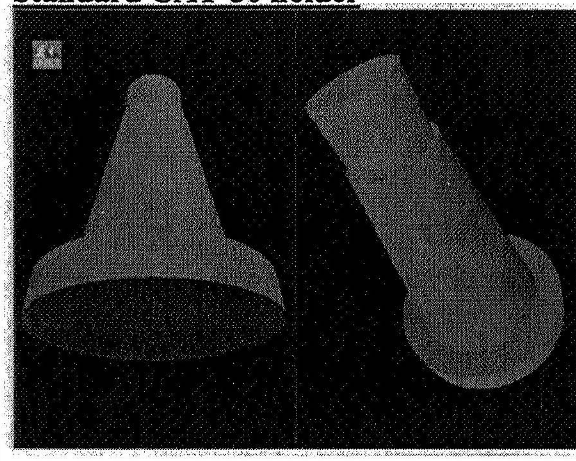	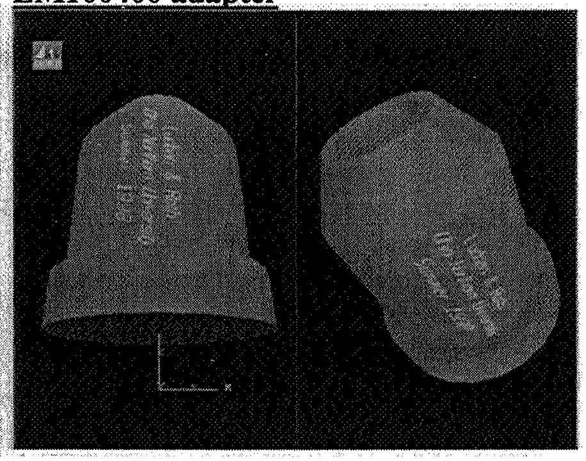

Creating the standard CAT-50 toolholder:

1. **CAD → CREATE → CONE**

X origin	0
Y origin	0
Z origin	0
Lower Diameter	2.75
Upper Diameter	1.5625
Eccentricity	1
Height	4.125
Start Angle	0
End Angle	360
Num facets	48
Axis	Z
Circumference	INSCRIBED
Lower cap	YES
Upper cap	YES
Center point	YES

2. **CAD → CREATE → CYLINDER**

X origin	0
Y origin	0
Z origin	0
Diameter	3.81248
Eccentricity	1
Height	.625001
Start Angle	0
End Angle	360
Num facets	48
Axis	Z
Circumference	Inscribed
Lower cap	Yes
Upper cap	Yes
Center point	Yes

3. The final cylinder is meant to represent a general outline of the tool retention knob located at the top of the toolholder. Specific dimensions are not necessary so time was not spent modeling it. Instead, a cylinder is used to represent the general profile for interference recognition purposes.

   CAD → CREATE → CYLINDER

X origin	0
Y origin	0
Z origin	0
Diameter	1.4
Eccentricity	1
Height	1.4
Start Angle	0
End Angle	360
Num facets	48
Axis	V
Circumference	Inscribed
Lower cap	Yes
Upper cap	Yes
Center point	Yes

4. Merge these objects by selecting **CAD → MODIFY → MERGE** and Merge All from the popup. Finally, select **CAD → CREATE → SAVE** and Save All from the popup. In the file name box, enter CAT-50_top. Next, select **CAD → CREATE → DEL ALL**

Creating an End Mill adapter

The construction of the End Mill adapter is dependent upon the adapter being modeled, but similar steps may be taken to model other types.

1. Create a polygon that represents both the profile of the adapter and the opening in the center. This can be done in any manner that will yield polygons to represent the profile. In this case, the profile may be shown by a single wedge as follows:

X origin	.5
Y origin	0
Z origin	0
Base 1	.69
Base 2	.20
Height 1	3.375
Height 2	2.5263
Width	0
B-H-W axes	X-Z-Y
Type	Half

2. The resulting wedge has zero thickness and may be revolved to form a doughnut-like solid: **CAD → CREATE → REVOLVE**, → Polygon → select the wedge just created as the polygon to revolve → select the world origin as the origin to revolve about → select frame as the vector method → select the object frame at the world origin → select Z as the axis selection → in the revolve popup, enter 360 degrees and 48 facets (this may be adjusted for desired resolution – a lower number is lower resolution)

3. **CAD → CREATE → CYLINDER**

X origin	0
Y origin	0
Z origin	0
Diameter	2.75
Eccentricity	1
Height	.62
Start Angle	0
End Angle	360
Num facets	48
Axis	Z
Circumference	Inscribed
Lower cap	Yes
Upper cap	Yes
Center point	Yes

This will create the collar just in front of the V-flange of the tool holder.

4. Select **CAD → MODIFY → MERGE** and Merge All. Then select **CAD → CREATE → SAVE** and Save All. Name this object CAT-50_bottom.

Combining the parts

Now that the parts are created, they must be joined in the proper orientation to be brought into the **BUILD** world.

1. If the last part has been deleted, it must be retrieved: **CAD → CREATE → RETRIEVE** and select CAT-50_bottom
2. Move this object out of the way: Select **CAD → CREATE → SELECT** and click on the object. Select **CAD → CREATE → TRN OBJ** Hold down the Left Mouse button and drag the object out of the way.
3. Retrieve the top portion of the toolholder: **CAD → CREATE → RETRIEVE** and select CAT-50_top
4. Move the bottom piece so it is oriented to the top: **CAD → CREATE → SNAP OBJ** and select "surface" and "yes" in the next two popups. Click on the bottom surface of the "top" piece. The two pieces should now be face to face with the opening facing in the negative Z direction.
5. Join all of the pieces: **CAD → MODIFY → MERGE** and Merge All.
6. Rotate the pieces so they are ready to receive the tool in the **Build** world: **CAD → CREATE → ROT OBJ** Click the **Snp** button immediately below **Rot Obj** twice with the Left Mouse button. This function allows the object to snap 90 degrees about the axis which is designated by which mouse button is used to select the **Snp** button – Left is X, Middle is Y, and Right is Z. This same method may be used when selecting the **Rel** and **Abs** buttons which appear in the same general location when available.

INFLUENCE OF HIGH ASPECT RATIO VESSEL CELL CULTURE ON TNF-ALPHA, INSULIN SECRETION AND GLUCOSE HOMEOSTASIS IN PANCREATIC ISLETS OF LANGERHANS FROM WISTAR FURTH RATS

Final Report

NASA/ASEE Summer Faculty Fellowship Program - 1998

Johnson Space Center

Prepared by:	Brian W. Tobin, Ph.D.
	Sandra K. Leeper-Woodford, Ph.D.
Academic Rank:	Associate Professors
University & Department	Mercer University School of Medicine Division of Basic Medical Sciences

NASA / JSC

Directorate:	Space and Life Sciences
Division:	Medical Sciences
Branch:	Life Sciences Research Laboratories
JSC Colleague:	Clarence F. Sams, Ph.D.
JSC NSBRI Research Associate:	Brian B. Hashemi, Ph.D.
Date Submitted:	October 26, 1998
Contract Number:	NAG 9-867

ABSTRACT

The present studies were carried out to determine the influence of a ground based microgravity paradigm, utilizing the High Aspect Ratio Vessel (HARV) cell culture upon lipopolysaccharide (LPS) stimulated tumor necrosis factor alpha (TNF-alpha) production of pancreatic islets of Langerhans. An additional aim was to elucidate alterations in insulin secretion and glucose utilization using the HARV low shear, gravity averaged vector, cell culture technique. Islets were isolated (1726±117, 150 micron islet equivalent units) from Wistar Furth rats and assigned to four treatment groups: 1) HARV, 2) HARV plus LPS, 3) static culture, 4) static culture plus LPS. Following 48 hours of culture, insulin concentration was increased in both HARV and static cultures ($p<0.05$). Islet medium from HARV and static cultures were assayed for TNF-alpha (L929 cytotoxicity assay) and was measured at selected time points for 48 hours. TNF-alpha was significantly increased in LPS-induced HARV and static cultures, yet the increase was more pronounced in the static culture group ($p<0.05$). This is a novel observation and indicates that TNF producing cells are present in islets and that LPS stimulates TNF secretion in isolated islets. A decrease in insulin concentration was demonstrated in the islet medium of the LPS stimulated HARV culture ($p<0.05$). That TNF-alpha is associated with a decreased insulin secretion is intriguing, both as it relates to in-flight investigations, and as it may provide insight into the pathophysiology of Type I and Type II diabetes. Glucose concentration in islet medium was lesser throughout the experiment in static cultures, suggesting a decreased reliance upon glucose as a metabolic substrate in the islets cultured in HARVs. In conclusion, the present studies demonstrate alterations in LPS induced TNF-alpha production of pancreatic islets of Langerhans, favoring a lesser TNF production in the microgravity HARV paradigm. Additionally, alterations in fuel homeostasis may be promulgated by HARV culture. The clinical and physiological significance of these observations remains to be determined.

INTRODUCTION

Microgravity and Glucose Homeostasis

Simulated microgravity in ground-based studies (Lipman et al. 1972, Vernikos-Daniellis et al. 1976), as well as post-flight investigations of cosmonauts (Grigroiev 1990) demonstrate alterations of glucose and insulin homeostasis. These include increased plasma glucose, decreased glucose tolerance, hyperinsulinemia, and insulin resistance (Dolkas and Greenleaf 1977). These observations suggest that microgravity induces metabolic changes similar to those observed in the glucose intolerance of pre-diabetes, aging, physical inactivity or obesity. An exception is the D-2 mission, which was unable to validate abnormal oral glucose tolerance tests (MaaB et al. 1994). These studies, however, utilized measures of glucose homeostasis which are relatively insensitive for non-diabetic populations.

Factors which may modulate glucose tolerance and insulin secretion/sensitivity include pancreatic islet insulin secretory function and peripheral tissue insulin sensitivity (Defronzo 1982). An intriguing candidate peptide which has recently been implicated in the glucose intolerance of obesity, is the cytokine tumor necrosis factor-alpha (TNF-alpha). TNF-alpha is a potent modulator of insulin sensitivity in adipocytes (Argiles 1994, Hotamisligil 1994).

Increased TNF-alpha induces insulin resistance which can decrease glucose utilization. While it was once believed that macrophages and adipocytes were the primary sites of TNF-alpha production, we have recently demonstrated that purified pancreatic islets of Langerhans are a potent source of TNF-alpha (Leeper-Woodford 1997). This observation may explain altered glucose homeostasis in diabetes and microgravity induced alterations in fuel homeostasis.

A series of in vitro studies illustrate altered immune cell cytokine activity in microgravity which may favor increased TNF-alpha release and insulin resistance. The SL-3 mission demonstrated that immune responses may be altered by space flight (Sonnenfeld et al. 1988). On STS-56, MC3T3-E1 osteoblasts activated in microgravity utilized less glucose and had reduced prostaglandin E_2, a proposed regulator of cytokine production (Hughes-Fulford and Lewis 1996). As little as eight seconds of microgravity has been demonstrated to alter macrophage responses (Armstrong et al. 1995). Perhaps the most salient studies to the present proposal are experiments which demonstrate that lipopolysaccharide (LPS) activated macrophages secrete more IL-1 and TNF-alpha when stimulated in microgravity than on earth (Chapes et al. 1992).

Taken together, these observations demonstrate that microgravity favors an altered immune system which influences enhanced TNF-alpha secretion via LPS stimulation. Given that TNF-alpha is a known modulator of insulin sensitivity in adipocytes, such observations may provide a mechanistic link between the glucose and insulin alterations of spaceflight through putative cytokine modulations of insulin sensitivity.

Microgravity Paradigms for Cell Culture

While there is disagreement in the literature as to whether ground based paradigms truly simulate microgravity (Unsworth and Lelkes 1998), there are newly developed cell culture systems which provide a more germane paradigm than previously available. One such system is the High Aspect Ratio Vessel (HARV, Fig. 1) which was developed at the Johnson Space Center and is currently licenced to the Synthecon Corporation. The HARV is a self contained horizontally rotating cell culture system that allows for diffusion of oxygen and carbon dioxide across a semi permeable membrane. An advantage of the HARV system is a very low shear stress, estimated at 0.5 dynes/cm^2 for one or two mm cellular aggregates (Unsworth and Lelkes 1998).

In addition to providing for a low shear stress, the HARV also demonstrates a time-averaged gravity vector of 10^{-2} g (Schwarz et al. 1992) as compared to that of near-earth orbit which is 10^{-4} - 10^{-6} g. Thus, the HARV is a useful paradigm for studying cellular physiology in a ground based, gravity averaged cell culture system, which demonstrates both low shear stress and a gravity averaged free-fall paradigm.

Research Hypothesis

We hypothesize that microgravity is associated with an increased LPS-induced TNF-alpha secretion from purified pancreatic islets of Langerhans, and alterations in insulin and glucose homeostasis.

Proposed Studies

A) We propose to determine the influence of simulated microgravity per se upon TNF-alpha, insulin, glucose and lactate production of isolated pancreatic islets of Langerhans.

B) We propose to investigate the effects of LPS-induced TNF-alpha secretion by pancreatic islets of Langerhans in simulated microgravity.
C) We propose to determine the glucose stimulated insulin secretory capacity of microgravity simulated islets of Langerhans.

MATERIALS AND METHODS

Animal Care

Male Wistar Furth rats (Harlan Sprague-Dawley, Houston TX) were obtained at 9-10 weeks of age, approximately 220 grams body weight, and housed in shoebox cages (n=3 / cage) with cellulose bedding. Animals were maintained on a twelve hour light/dark cycle (lights on 0700 hr) and had access to food and water ad libitum. All procedures were carried out in accordance with the guidelines of the National Institutes of Health and were approved by JSC Animal Care and Use Committee.

Pancreatectomy and Islet Isolation: Day 1, 2

All animals were acclimatized to the laboratory for one to two weeks prior to beginning experiments. We removed food from the cages of donor male Wistar Furth rats at approximately 1800 h; at 0800 h the following morning (day 1, Fig. 2a) the rats were anesthetized with 55 mg/kg sodium pentobarbital i.p., and pancreatectomized. Animals exsanguinated under surgical anesthesia following pancreatectomy. Islets were isolated using established methods (Ballinger and Lacey 1972), with modifications previously described (Finegood et al. 1992). Purified islets were hand picked to obtain approximately 1700 islets per treatment group, using 25x magnification with a green illuminated background and white fiber optic side illumination.

Static Culture of Islets Following Islet Isolation: Day 1, 2

Freshly isolated islets of Langerhans were placed into Medium-199 (with additional 100 U/ml penicillin, 100 μg/ml streptomycin, 10% fetal bovine serum, 25 mmoles/l Hepes buffer, 0.68 mmoles/l L-glutamine) as previously described (Finegood and Tobin 1992). Islets were isolated over a two day period. The islets from two rats each (6 rats per day of isolation), were placed into 6-well polystyrene culture plates with 10 ml Medium-199 per well (approx. 1200 islets). Islets were isolated on two separate days, and introduced into static culture at approximately 1700 hrs. Thus, islets remained on static culture for 24 - 48 hours prior to being aliquoted into HARV cultures for subsequent experiments

HARV Cell Culture Techniques for Pancreatic Islets: Day 3, 4

Islets were aspirated from culture plates and cells were transferred to 15 ml conical vials using 10 ml islet medium for transfer and 2x, 2 ml Medium-199 for rinse. Islets were centrifuged at 1000 RPM and islet medium was aspirated to leave 2 ml remaining. The islets were transferred from all 6 conical vials into one 50 ml conical vial. Two ml islet medium was used for transfer and 2x, 2 ml Medium-199 was used to rinse. The tube was brought to 40 ml with Medium-199. The islets were aliquoted into 4, 15 ml conical vials and centrifuged at 1000 rpm. Supernatant was aspirated to a total remaining volume of 6 ml. The vials were vortexed

and mixed, and aliquots of 100 ul (3x) were removed for determination of islet diameter, which was estimated according to standards established by Ricordi and colleagues (1990). A one ml sample was obtained, designated as 0 HRS and frozen at -70° C. The conical vials were subsequently centrifuged at 1000 rpm and the volume was aspirated to 4 ml remaining.

Islets were aliquoted into 2, 10 ml High Aspect Ratio Vessels (HARV, Synthecon, Houston) and into culture plate wells by transferring 4 ml of islet medium, with 2x, 3 ml rinses. Culture plates and HARVS were placed into a 5% CO_2, 99% humidified, 37° C incubator. The initial HARV speed was set at approximately 12 revolutions per minute. All bubbles were carefully removed from the HARVS prior to initiating revolutions.

Preparation for LPS Stimulation: Day 5

Following 48 hours of HARV or static culture, a 5 ml sample was removed from all treatments and 1 ml was aliquoted for analysis and designated as 48 HRS. Both HARV and static cultures had 5 ml freshly prepared Medium-199 added to bring the total volume to 10 ml. All subsequent samples were taken by isovolumetric techniques, for both HARV and static cultures. This was accomplished by infusing 300 uL of cold (4° C) Medium-199 into the bottom port of a vertical, stationary HARV while removing 300 ul of sample from the upper port. A similar technique was used in static cultures to assure equal treatment perturbations.

LPS Stimulation, Samples for TNF, Insulin, Glucose, Lactate: Day 5, 6

Prior to LPS addition, a 300 ul sample was removed from all treatments and designated as 0 HRS post LPS stimulation. At time zero, 100 ul of a 100 μg/ml LPS (EColi 026:B6, Sigma, St. Louis) dissolved in Medium-199 were added to HARVs and static cultures. The pipette tip was carefully rinsed in and out of the HARV three times, to assure complete introduction of LPS; it was also rinsed three times in the static culture plate for control purposes.

Islet medium samples were obtained (300 ul) for TNF, glucose, insulin, and lactate analysis at 3, 6, 12, 24, and 48 hours post LPS stimulation. The samples were placed into 1.8 ml cryovials and stored at -70° C for subsequent analyses.

Glucose Stimulation for Determination of Insulin Secretion: Day 7

Following a 5 ml isovolumetric exchange of fresh Medium-199 into all treatment groups, samples were obtained to determine basal glucose and insulin levels prior to glucose addition. A 1 ml sample was withdrawn at time zero and frozen at -70° C. Immediately following this, 1 ml of 50% Dextrose (Abbott, Montreal) was added to HARV and static cultures. Samples for insulin and glucose (1000 ul) were obtained at one or two hours post glucose addition. In experiment #2, both a one and a two hour sample value were averaged to utilize one number for statistical analysis.

Islet and Cell Image Analysis: Day 14

Islets were obtained from HARV and static cultures for image analysis by phase contrast and confocal microscopy. Representative images of freshly isolated islets of Langerhans (experiment #2) and islet cells cultured in HARVs for an additional 7 days following addition of glucose (experiment #1) were obtained on a Nikon Diaphot inverted microscope equipped with phase contrast optics. For phase contrast imaging, islets were maintained in culture medium and

images were acquired using a Nikon 35mm camera and a 40x air objective (NA 1.0). For subsequent confocal image analysis, both HARV and static cultures were exchanged with fresh Medium-199 (5 ml, isovolumetrically) every two days post glucose stimulation (experiment #2). Optical segments of cell aggregates were obtained using the cellular autofluorescence and Confocal Fluorescence Microscopy. Aggregates were mounted in between a slide and a cover slip using the Prolong anti-fade reagent (Molecular Probes). Images were acquired on a Zeiss LSM 410 confocal microscope using a 100x oil objective (NA 1.3). Fluorescence optics consisted of a 568 nm excitation line of an argon laser, a 580 nm Diacroic, and a 590 long pass barrier filter. Images were acquired and analyzed using the Zeiss LSM software (v. 3.8).

Sample Analysis

Tumor Necrosis Factor Assay: The L929 mouse fibroblast assay, as previously described (Leeper-Woodford et al. 1991, Leeper-Woodford et al. 1993, Leeper-Woodford and Tobin 1994), was used to measure islet medium TNF activity. Briefly, L929 cells were grown to confluence overnight in 96 well culture plates, Actinomycin-D (5 μg/ml; Merck Sharp & Dohme, Weston, PA) was added to each well and serial dilutions of experimental islet medium were added to duplicate L929 wells. Following incubation, adherent L929 cells were stained with 0.5% crystal violet, optical density of each well was spectrophotometrically measured and % cytotoxicity of L929 cells was determined (Leeper-Woodford et al. 1991, Leeper-Woodford et al. 1993, Newman et al. 1996). TNF activity was then converted to Units/ml (U/ml); one unit of TNF activity was defined as equal to 50% L929 cytotoxicity in the appropriate dilution of islet medium (Leeper-Woodford et al. 1991, Newman et al. 1996). Dose-response inhibition of TNF activity using rat-specific TNF-alpha antibodies (Endogen Inc., Boston, MA) were performed (Leeper-Woodford et al. 1991, Leeper-Woodford et al. 1993) on islet medium samples to confirm that L929 cytotoxicity was due to TNF-alpha activity.

Insulin Analysis: Islet medium was diluted 1:500 in Medium-199, and insulin was determined by competitive binding radioimmunoassay (Linco, St.Charles, MO) with antibodies raised against rat insulin and using rat insulin standards (Morgan and Lazarow 1963). Prior determination of the within-assay coefficient of variation for 8 assays of pooled rat plasma was estimated at 6.2%.

Glucose and Lactate Analysis: Samples were analyzed in duplicate as is or diluted 1:10 with distilled water for glucose and lactate analysis using a YSI 2300 Stat Plus Analyzer (Yellow Springs Instruments, Yellow Springs OH). The instrument uses a silver/platinum electrode and a sandwich of cellulose acetate, immobilized oxidase enzyme in a membrane, and a polycarbonate membrane. Glucose diffuses though the outer membrane and is oxidized producing hydrogen peroxide and glucono-delta-lactone. The hydrogen peroxide is dissociated to H^+, O_2 and $2e^-$; the latter is measured by a platinum electrode. A standard curve is generated to determine concentrations of glucose and lactate. Glucose and lactate were expressed as mg/dl of supernatant.

Statistical Analysis: There were four complete replications of the experimental protocol. Thus, four separate islet populations were evaluated in separate trials (n=4) of the experimental paradigm. Experiment #1 had no O HRS sample taken, thus, n=6 per group for study A. Studies B and C contained n=4 different islet populations per group throughout. The experimental

paradigm included dependent variable analysis consisting of: A) determination of basal TNF, insulin, glucose, and lactate concentrations during 48 hours of cell culture, B) LPS stimulation of TNF-alpha secretion, and subsequent insulin, glucose, and lactate measures during 48 hours of cell culture, and, C) glucose stimulation of insulin secretion, and subsequent TNF, glucose, and lactate determination during 1 or 2 hours of cell culture. The independent variables used for statistical analysis included: HARV (HARV or static plate culture), LPS (LPS stimulated, or non-LPS stimulated), and TIME (0, 48 hours for study A; 0, 3, 6, 12, 24, 48 hours for study B; 0, 1 hours for study C).

Study A, was analyzed by two-way analysis of variance (ANOVA, HARV vs TIME, SAS ver. 6.11, Cary NC, Snedecor and Cochran 1989). Post-hoc differences between treatments, were determined by one-way ANOVA with a post-hoc Duncan's test. A value of $p<0.05$ was considered as statistically significant. Means with similar superscripts are not significantly different by post-hoc analysis ($p>0.05$).

Study B, was analyzed by three factor (between | between | within-subjects) repeated measures ANOVA (HARV vs LPS vs TIME) with full interaction to determine main effects and all possible interactions. Raw data was used for all analyses with the exception of the insulin data. Due to a twofold greater basal insulin concentration in experiment 4, all data were transformed and normalized to % baseline prior to statistical analysis. At discreet time points, a one-way analysis of variance was performed, and a post-hoc Duncan's test was used to determine statistical significance between groups ($p<0.05$). Means with similar superscripts are not significantly different by post-hoc analysis ($p>0.05$).

Study C, was analyzed by three-way ANOVA (HARV vs LPS vs TIME). Post-hoc differences between treatments were determined by one-way ANOVA with a post-hoc Duncan's test. A value of $p<0.05$ was considered as statistically significant. Means with similar superscripts are not significantly different by post-hoc analysis ($p>0.05$).

RESULTS

Pancreatectomy and Islet Isolation

Islets were isolated from living pancreas donors and were placed into cell culture within 5 hours following pancreatectomy. Four experiments were performed, which consisted of two days of islet isolations each, in which six animals per day were pancreatectomized and islets isolated. During the four weeks of separate experiments, there were no significant differences between treatment groups for the 150 micron islet equivalent mass ($p>0.05$, Fig 2b). The average number of islets per treatment group, was 1726 ± 117 islet equivalent units. All values as shown in figures are mean ± SEM.

LPS Stimulated TNF-alpha Production

Prior to LPS stimulation there were no significant differences in L929 TNF-alpha cytotoxicity for any treatment group for any statistical measure (Fig 3a).

Following stimulation with LPS there were significant increases in TNF-alpha of both static and HARV cultured cells (Fig 3b). Three-way repeated measures ANOVA indicated significant between-subjects effects for HARV ($p=0.0049$, static culture > HARV), LPS

(p=0.0001, LPS > non-LPS), and HARV*LPS (p=0.0046, static culture LPS > HARV LPS). Within-subjects effects were significant for HOURS (p=0.0001) and an interaction of HOURS*LPS (p=0.0001). Islets stimulated with LPS in static culture retained a significantly greater TNF-alpha concentration vs LPS stimulated HARV cultures throughout the entire 48 hours of the study. There were no significant changes in TNF-alpha among control cultures.

Following glucose stimulation, three-way ANOVA indicated a significant difference due to LPS as a main factor (Fig 3c, p=0.0062, LPS > non-LPS). At 0 HRS, the static culture LPS group had equivalent TNF concentration to other treatments. Post-hoc Duncan's test indicated that the static culture LPS group differed from the HARV non-LPS stimulated control at 1 HRS.

Insulin Concentration

At time zero, insulin concentrations were less than 100 nmoles/l, and were not significantly different between HARV and static culture treatment groups (Fig 4a). Two-way ANOVA indicated a significant effect of TIME (p=0.0001, 48 HRS > 0 HRS). Following 48 hours of culture, there was greater than a 6-fold increase in immunoreactive rat insulin concentrations. However, there were no significant differences between HARV and static cultures at 48 hours.

There was a marked linear increase in the insulin concentration of both HARV and static culture islets which were not stimulated with LPS (Fig 4b). Repeated measures ANOVA indicated no significant differences between-subjects; however, within-subjects effects of HOURS and HOURS*LPS were significant (p=0.0001, p=0.0001). In both HARV and static cultures which were stimulated with LPS, insulin secretion was attenuated relative to non-stimulated treatment paradigms. At 48 hours post-stimulation with LPS, both control groups were different from the HARV-LPS group. However, the static culture islets with LPS, although intermediate in value at 48 HRS, did not differ from any other group in their insulin content.

Following stimulation with glucose (Fig 4c), there were no significant differences in the concentration of insulin in the culture media.

Glucose Concentration

Prior to cell culture, there were no significant differences in the amount of glucose in islet medium between HARV or static culture groups (Fig 5a). Two-way ANOVA demonstrated significant effects of HARV (p=0.0230, HARV > static culture) and TIME (p=0.0026, 48 HRS < 0 HRS). Following 48 hours of culture, HARVs demonstrated a significantly greater glucose concentration than did static cultures (p<0.05). The static plate culture at 48 hours also differed from all other treatment groups.

Following stimulation with LPS, there were relatively minor differences in the media glucose concentration up to 12 hours of culture (Fig 5b). Repeated measures ANOVA indicated a significant effect of HARV (p=0.0203, HARV > static culture). The within-subjects effect of HOURS was also significant (p=0.0026). At 48 hours post LPS stimulation, the static culture group had metabolized the greatest amount of glucose from the media. The highest media glucose concentrations were observed in the non LPS-stimulated HARV cultures, which were significantly different from the LPS stimulated static culture islets.

Following stimulation with glucose there was a significant effect of TIME (p=0.0001, 1 HRS > 0 HRS) as is evidenced by the 1 HRS glucose concentration (Fig 5c). Post-hoc one-way

ANOVA with Duncan's test illustrated that media glucose was slightly higher in HARV LPS media, than in the control HARV at 1 HRS.

Lactate Concentration

Media lactate concentrations increased during the initial 48 hour culture period to a level which was significantly different from the zero hour value (Fig 6a). Two-way ANOVA illustrated a significant effect of TIME ($p=0.0001$, 48 HRS > 0 HRS). However, there were no significant differences between the lactate concentrations of HARV or static culture groups.

During the LPS stimulation studies, all treatment groups increased their lactate concentrations (Fig 6b). Repeated measures ANOVA indicated significant main effects only for HOURS ($p=0.0001$). At 48 hours of study, there were no significant differences between groups.

Following stimulation with glucose (Fig 6c) the islet medium lactate concentration increased with time although no discreet differences could be differentiated between individual groups. Three-way ANOVA indicated an overall significant effect of TIME ($p=0.0042$, 1 HRS > 0 HRS).

HARV Generated Islet Cell Aggregates (ICA)

Phase contrast microscopy of freshly isolated islets of Langerhans, illustrates intact islets with apparently intact collagen capsules, as well as freely circulating cells from certain islets which were likely over digested (Fig. 7).

Following two weeks of culture, islet cell aggregates were analyzed by phase contrast microscopy (Fig. 8). This image illustrates the cellular aggregate of islets of Langerhans, with distinct islets visible within the aggregate matrix.

Islet cell aggregates were also prepared for confocal microscopy, and an image was scanned from a focal plane approximately at the center of an islet cell aggregate which was stimulated with LPS (Fig. 9). This image illustrates aggregation of islet units, with an apparent intra-islet space. Comparison of three LPS stimulated sections (Fig. 10a, b, c) and one control image (Fig. 10 d) illustrate autofluorescence. The autofluorescence appears lesser in the non-stimulated aggregate.

DISCUSSION

The present studies were designed to investigate the influence of the HARV microgravity paradigm upon LPS stimulated TNF-alpha production of pancreatic islets of Langerhans and elucidate related changes in insulin and glucose homeostasis. Additional studies were conducted to determine the influence of microgravity per se upon hormonal production. Glucose was added to islets to determine if the glucose stimulated secretion of pre-packaged islet insulin remained intact following 7 days of cell culture. The current studies demonstrate four novel observations: 1) LPS induced TNF-alpha production is lesser in the HARV paradigm, than in static cultures, 2) the increase in TNF-alpha is associated with a lesser basal insulin secretion especially in HARV cultures, 3) islets cultured with the HARV paradigm are associated with a lesser glucose consumption, than are islets from static culture, and 4) islets cultured with HARVs, will re-aggregate into "tissue like units", which we will designate as "Islet Cell Aggregates" (ICA's).

A most interesting and novel result in our present study is that isolated islet preparations had increased TNF levels with exposure to LPS indicating that TNF-producing cells are present in islets and that LPS stimulates TNF secretion in isolated islets. Our present studies indicate possible involvement of TNF at the site of insulin secretion, the pancreatic islets of rats. Others have suggested that TNF gene expression may be located in the pancreas and may play a role in islet function. Norman et al. (1995) noted increased TNF messenger RNA expression and intrapancreatic TNF detectable 1-6 hours after onset of acute pancreatitis induced by infusion of a cholecystokinin analogue into mice. They attributed this TNF expression to acute infiltration of macrophages during the pancreatic inflammation. Toyoda et al. (1994) detected TNF-alpha in mouse islets during development of diabetes in the non-obese diabetic mouse strain NOD-Sansum. They noted that fewer than 1% of islet immune cells in this strain were macrophages and suggested that TNF-alpha may be produced by islet T cells during an autoimmune reaction in the islets of this diabetic mouse. Our data provides further evidence that islets can be sites of TNF secretion in rats. We believe this is an intriguing observation with respect to islet secretory function. The lesser LPS induced TNF-alpha production in the HARV paradigm was not expected, and is contrary to that which has been previously observed during in-flight studies of LPS stimulated macrophages (Chapes et al. 1992). The present investigations suggest three possibilities: 1) that islets behave differently from macrophages following LPS stimulation in a microgravity paradigm, 2) that the HARV paradigm is not directly comparable to in-flight experiments, or 3) that the aggregation of cells into ICA's differentially modulates the production of TNF-alpha, following stimulation with LPS. The direct applicability of these data to in-flight studies remains to be determined.

That TNF-alpha is associated with a decreased basal insulin secretion is intriguing, both as it relates to in-flight extrapolations, and as it suggests insight into the pathophysiology of Type I and Type II diabetes mellitus. In-flight studies during the Skylab mission (Leach and Rambut 1977) illustrated a consistent decrease in the plasma insulin concentration from 38 to 82 days. It is not possible to say if these data are comparable, as serum insulin values are affected by rates of insulin secretion, insulin sensitivity, and insulin clearance: factors which were not measured on Skylab. In addition, plasma glucose values were also decreased in Skylab crewmembers, suggesting improved glucose control. However, the present studies raise the possibility of an endogenously mediated decrease in insulin secretion, as a secondary consequence of altered cytokine production in the HARV microgravity paradigm. That a lesser basal insulin secretion was observed in LPS stimulated cultures, is a novel observation, and suggests that islet derived TNF has the capacity to down regulate islet insulin secretion. Others have suggested that TNF may play a direct role in islet cell function during the autoimmune response in the development of insulin-dependent diabetes mellitus. Dunger et al. (1996) found that direct TNF exposure inhibited insulin secretion and caused significant DNA strand breakage in isolated rat islets. Others reported that TNF attenuated islet cell function and proposed that direct stimulation by TNF may be involved in modulation of insulin secretion from alpha cells during the progressive autoimmune development of insulin-dependent diabetes mellitus. The pathophysiology of Type II diabetes mellitus is known to involve both a primary decrease in insulin sensitivity as well as a consequential amelioration of insulin secretion. When combined, these two mediators promulgate hyperglycemia. The influence of TNF-alpha in peripheral insulin resistance of adipose tissue has been implicated in the pathophysiology of Type II diabetes (Argiles et al.

1994, Hotamisligil et al. 1994). The present studies provide an additional mechanism by which islet derived TNF-alpha may contribute to the development of Type II diabetes by suppressing insulin secretion and promulgating hyperglycemia. The clinical relevance of these observations is, however, unknown. The consistent increase in media insulin concentration, however, demonstrates by bioassay one measure indicating cell viability for 7 days of the study. The lack of a glucose stimulated insulin response in islet preparations, suggests that while basal insulin secretion may be preserved in the present paradigm, glucose stimulated insulin secretion is lost. This may indicate a subsequent depletion of pre-packaged proinsulin granules in the cytosol of the cultured islets. Our previous studies illustrate that this response is present in cultured islets, at 48 hours post pancreatectomy (Leeper-Woodford and Tobin 1994).

It has been proposed by others that insulitis with inflammatory cell influx into islets is responsible for any islet expression of TNF which may then influence islet function. While macrophages are present in islets and may be producing TNF in response to LPS, we propose that other possible sites of TNF production may also exist in the islet infrastructure. The many endocrine cell types located in islets could be possible sources of TNF, but vascular smooth muscle cells of the complex intra-islet vasculature may also be secreting TNF. In previous studies (Newman et al. 1996), we have shown that human blood vessels can be a significant source of TNF. We found that when stimulated with LPS, the time-dependant release of TNF from human vascular tissue was significantly increased compared with time-matched non-stimulated control vascular tissue. In human smooth muscle cells cultured from both internal mammary arteries and saphenous veins, the release of TNF into the medium essentially mimicked that seen in the intact vascular segments. Our experiments showed that TNF release occurred from both intact blood vessels and smooth muscle cells. Collectively, these findings suggested that at least one source of TNF may be the smooth muscle cell within vascular tissue. Since all islets have afferent arterioles that branch into numerous capillaries to form glomerular-like structures which then form an extensive network of peri-insular collecting venules, it is an intriguing possibility that cells, other than macrophages, located in or near such highly vascularized islet beds may also synthesize and secrete TNF.

The decrease in glucose utilization by pancreatic islets in HARV cultures is intriguing. That media lactate values did not differ between treatments, suggests that there were equivalent rates of glycolytic activity (anaerobic glucose metabolism) resulting in equivalent lactate production, regardless of the experimental paradigm. However, the lack of a change in media glucose concentration of HARV cultures during 48 hours of initial, and 48 hours of LPS culture, suggests that alternative fuel sources may have been utilized or that basal energy expenditure was significantly reduced in the microgravity paradigm. In the basal state 30% of islet metabolic energy requirements are met by the oxidation of the amino acid glutamine. The present culture media contained 0.68 mmoles/l L-glutamine, an amount sufficient to support basal energy expenditure. The possibility of altered glutamine metabolism in HARV cultures or alterations in energy metabolism are potential explanations for the present glucose data, however, verification of such hypotheses must await further data analysis.

The re-aggregation of isolated islets of Langerhans into ICA's was a serendipitous discovery. From the four experiments conducted herein, we observed that this re-aggregation occurs within 15 hours of HARV culture. That cells will re-aggregate within the HARV is a well know phenomenon, and has been documented elegantly in a recent review (Unsworth and Lelkes

1998). In addition, NASA currently collaborates with Dr. Donald Cameron on an MRD Program Task to develop islet beta cell / sertoli cell aggregates for transplantation (Cameron et al. 1998). The present studies illustrate that approximately 1700 whole islets will re-aggregate into ICA's that measure approximately 3 mm in diameter. The importance of such a large tissue mass may be salient to the success of pancreatic islet transplantation as a cure for Type I diabetes mellitus. At present, purified islets of Langerhans have been transplanted intraportally into the liver of Type I patients, resulting in normalization of plasma glucose concentrations (Warnock et al. 1992). The requirement for immunosuppresion is contraindicated to effective islet function, as most immunosuppresive agents decrease insulin sensitivity. Sertoli-islet cell aggregates may provide a cellularly induced immunoproviledged graft. However, these cells will still need to be transplanted into a highly vascularized organ site such as the liver. The potential of ICA's lies in the possibility of creating a greater tissue mass, with potential vascularization, which can be transplanted into a readily accessible vascularized organ such as the kidney capsule. Such an approach, if combined with sertoli cell technology, would provide a graft that is immunopriviledged and allow for removal of the graft in the presence of rejection. Such options are not currently available for intraportal islet transplants, and at present, recipients of purified islets require lifelong immunosuppresion. Such possibilities are encouraging for ultimate success in the search for a cure for Type I diabetes; a cure which ideally will ameliorate the need for daily exogenous insulin administration, and prevent the devastating secondary complications of this disease.

In conclusion, the present studies demonstrated alterations in LPS induced TNF-alpha production of pancreatic islets of Langerhans, favoring a lesser TNF-production in the microgravity HARV paradigm. We conclude that rat pancreatic islets are possible sources of TNF during exposure to bacterial LPS and that insulin secretion may be altered by LPS-induced TNF secretion. Our results are most interesting since TNF has been implicated as possibly playing a significant role in the obesity-related development of insulin resistance, glucose intolerance and non-insulin-dependent diabetes mellitus. If one proposes that an infectious agent or even increased levels of circulating lipoprotein or glucose could stimulate TNF secretion within the islet which then may alter insulin secretion, intriguing hypotheses could be developed as to the local production of islet-derived TNF and its action on islet cell function in the whole animal. The present studies also illustrated that basal insulin secretion was suppressed concomitant with an increase in TNF-alpha, and may be implicated in hormonal alterations of spaceflight and the pathophysiology of Type II diabetes. Fuel homeostasis appears to be different in the HARV culture, as virtually no glucose was utilized in this paradigm, suggesting an alternative fuel source for ICA's. Finally, islets which are cultured in HARVs will re-aggregate into ICA's. A limited number of biochemical/physiological characteristics of these aggregates have been documented in the present studies. The clinical significance of these observations, however, remains to be determined.

ACKNOWLEDGMENTS

The authors would like to acknowledge the important advice and assistance of Dr. Neal Pellis and Dr. Judith Campell-Washington (NASA-JSC, SD) for discussing microgravity paradigms with the authors, and advocating the HARV system as appropriate for these studies. Dr. Diana Risen (NASA-JSC, SD) gave timely advice and guidance in the use of HARV techniques for cell culture work. Dr. Peter Farrell, Professor of Physiology at The Pennsylvania State University, was most helpful in sharing his personal expertise and unpublished data on islet secretory function in free fall and microgravity paradigms. Without the gracious interdisciplinary assistance of these individuals, these studies would not have been carried to successful completion. Kimberly Welch-Holland, MUSM laboratory research assistant, performed the analysis of insulin, glucose and lactate in islet medium.

REFERENCES

Argiles, J.J., J. Lopez-Soriano and F. Lopez-Soriano. The role of cytokines in diabetes: update 1994. Edocrin Rev 2:76-80, 1994.

Armstrong, J.W., R.A. Gerren and S.K. Chapes. The effect of space and parabolic flight on macrophage hematopoiesis and function. Exp Cell Res 216:160-168, 1995.

Ballinger, W.F and P.E. Lacey. Transplantation of intact pancreatic islets in rats. Surgery 72:175-186, 1972.

Cameron, D.F., Selawry, H.P., Heller, R. and J. Becker. Development of an insulin secreting, immunopriviledged cell-cell aggregate utilizing the NASA rotating wall vessel. NASA MRD Program Task - Ground Based, 1998.

Chapes, S.K., et al. Cytokine secretion by immune cells in space. J Leukoccyte Biol 52:104-110, 1992.

DeFronzo, R.A., D. Simonson and E. Ferrannini. Hepatic and peripheral insulin resistance: a common feature of Type 2 and Type 1 diabetes mellitus. Diabetologia 23:313-319, 1982.

Dolkas, C.B. and J.E. Greenleaf. Insulin and glucose responses during bed rest with isotonic and isometric exercise. J Appl Physiol 43:1033-1038, 1977.

Dunger, A., J.M. Cunningham, C.A. Delaney, J.E. Lowe, M.H.L. Green, A.J. Bone, and I.C. Green. Tumor necrosis factor-alpha and gamma interferon inhibit insulin secretion and cause DNA damage in unweaned-rat islets. Diabetes 45:183-189, 1996.

Finegood, D.T., B.W. Tobin and J.T. Lewis. Dynamics of glycemic normalization following islet transplantation with sub-optimal islet mass. Transplantation 53:1033-1037, 1992.

Grigoriev, A.J. Man in space flight. Presentation on the 3rd Nihon University International Symposium on Aerospace Science. Tokyo, Japan, 1990.

Hughes-Fulford, M. and M.L. Lewis. Effects of microgravity on osteoblast growth activation. Exp Cell Res 224:103-109, 1996.

Leach, C.S. and P.C. Rambaut. Biochemical responses of the Skylab crewman: an overview. In: Biomedical Results from Skylab. NASA Lyndon B. Johnson Space Center. Johnson, R.S.. and L.F. Dietlein. Scientific and Technical Information Office. National Aeronautics and Space Administration. Washington D.C., 1977.

Leeper-Woodford, S.K., D. Carey, K. Byrne, B. Fisher, C. Blocher, H. Sugerman and A. Fowler. Ibuprofen attenuates plasma tumor necrosis factor activity during sepsis-induced acute lung injury. J. Appl. Physiol. 71:915-923, 1991.

Leeper-Woodford, S.K., B. Fisher, H. Sugerman and A. Fowler. Pharmacologic reduction in tumor necrosis factor activity of pulmonary alveolar macrophages. Am. J. Respir. Cell Mol. Biol. 8:169-175, 1993.

Leeper-Woodford, S.K. and B.W. Tobin. Tumor necrosis factor activity of pancreatic islets. Am J Physiol 273:E433-E437, 1997.

Lipman, R.L. et al. Glucose intolerance during decreased physical activity in man. Diabetes 21:101-107, 1972.

Maaβ. H., W. Raabe and H.M. Wegman. Effects of microgravity on glucose tolerance. Proceedings of the Norderney Symposium on Scientific Results of the German Spacelab Mission D-2, March 14-16, 1994, Norderney, Germany.

Morgan, C.R. and A. Lazarow. Immunoassay of insulin: Two antibody system. Plasma insulin levels in normal, subdiabetic, and diabetic rats. Diabetes 12:115, 1963.

Newman, W.H., L. Zhang, S.K. Leeper-Woodford, and M.R. Castresana. Human blood vessels release tumor necrosis factor-alpha from a smooth muscle cell source. Crit. Care. Med 24:294-297, 1996.

Norman, J.G., G.W. Fink, and M.G. Franz. Acute pancreatitis induces intrapancreatic tumor necrosis factor gene expression. Arch. Surg 130:966-970, 1995.

Ricordi, C. et al. Islet isolation assessment in man and large animals. Acta. Diabetol. Lat. 27:185-195, 1990.

Schwarz, R.P., Goodwin, T.J. and D.A. Wolf. Cell culture for three dimensional modeling in rotating-wall vessels: an application to simulated microgravity. J. Tiss. Culture Meth. 14:51-58, 1992.

Sonnenfeld, G., C.L. Gould, J. Williams and A.D. Mandel. Inhibited interferon production after space flight. Acta Microbiol Hung 35:411-416, 1988.

Toyoda, H., B. Formby, D. Magalong, A. Redford, E. Chan, and M.A. Charles. In situ islet cytokine gene expression during development of type I diabetes in the non-obese diabetic mouse. Immunol. Letters 39:283-288, 1994.

Unsworth, B.R. and P.I. Lelkes. Growing tissues in microgravity. Nature Medicine 4:901-907, 1998.

Warnock, G.L., N.M. Kneteman, E.A. Ryan, A. Rabinovitch, and R.V. Rajotte. Long-term follow-up after transplantation of insulin-producing pancreatic islets into patients with Type 1 (insulin dependent) diabetes mellitus. Diabetologia 35:89-95, 1992.

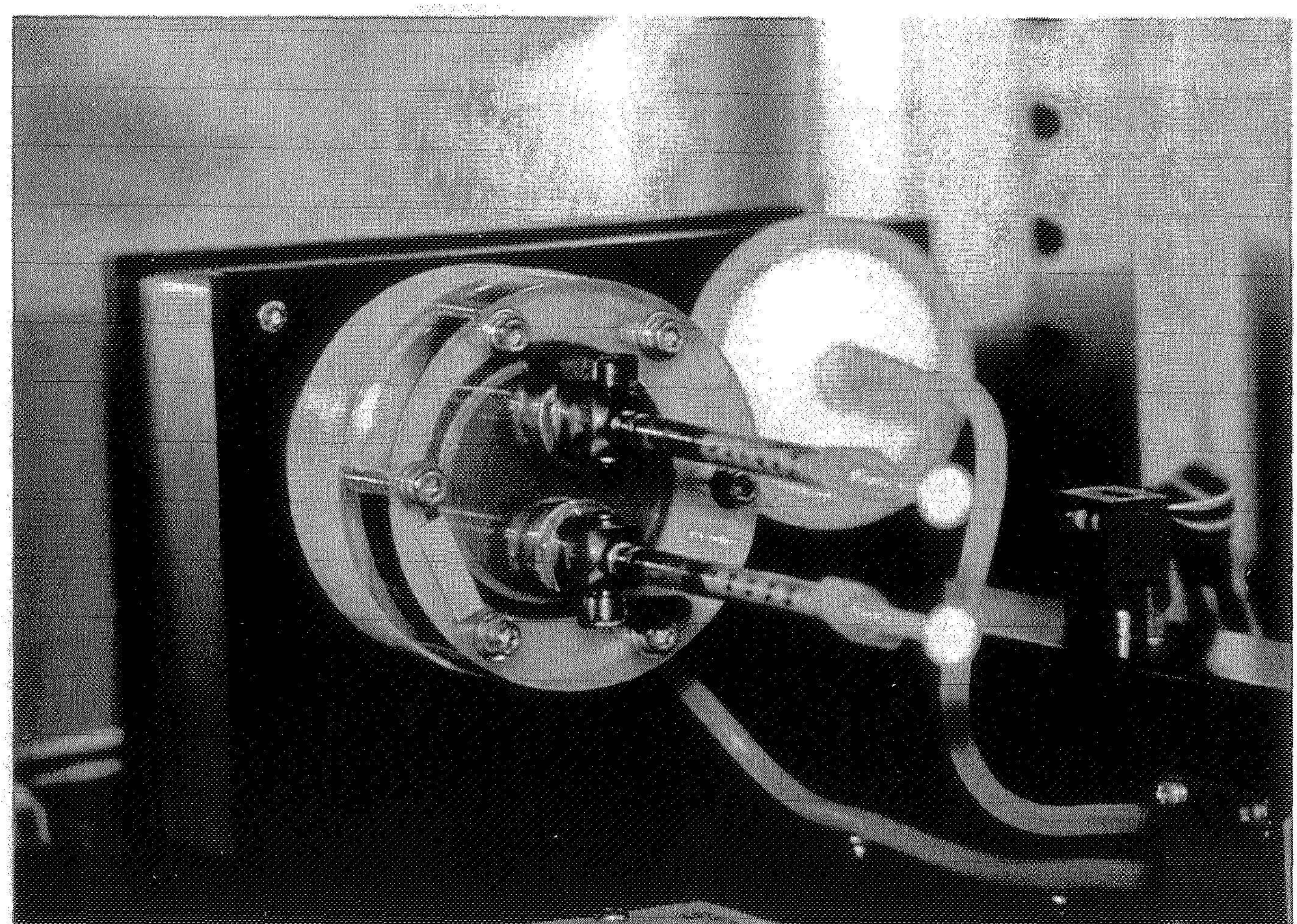

FIGURE 1. The NASA-developed High Aspect Ratio Vessel (HARV) cell culture system manufactured by the Synthecon corporation.

a

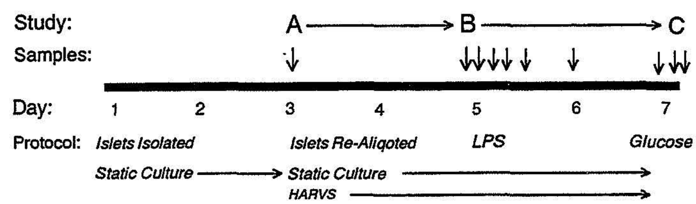

b

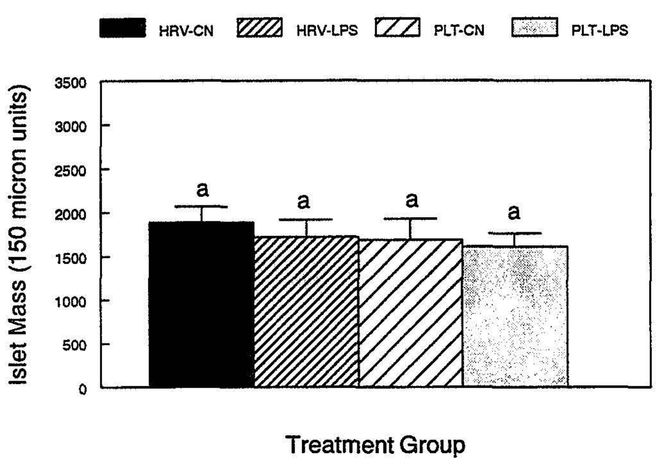

FIGURE 2. The experimental design (2a) and the islet equivalent units per treatment group (2b). HRV-CN, HARV control; HRV-LPS, HARV LPS-stimulated; PLT-CN, static culture plate control; PLT-LPS, static culture plate stimulated with LPS.

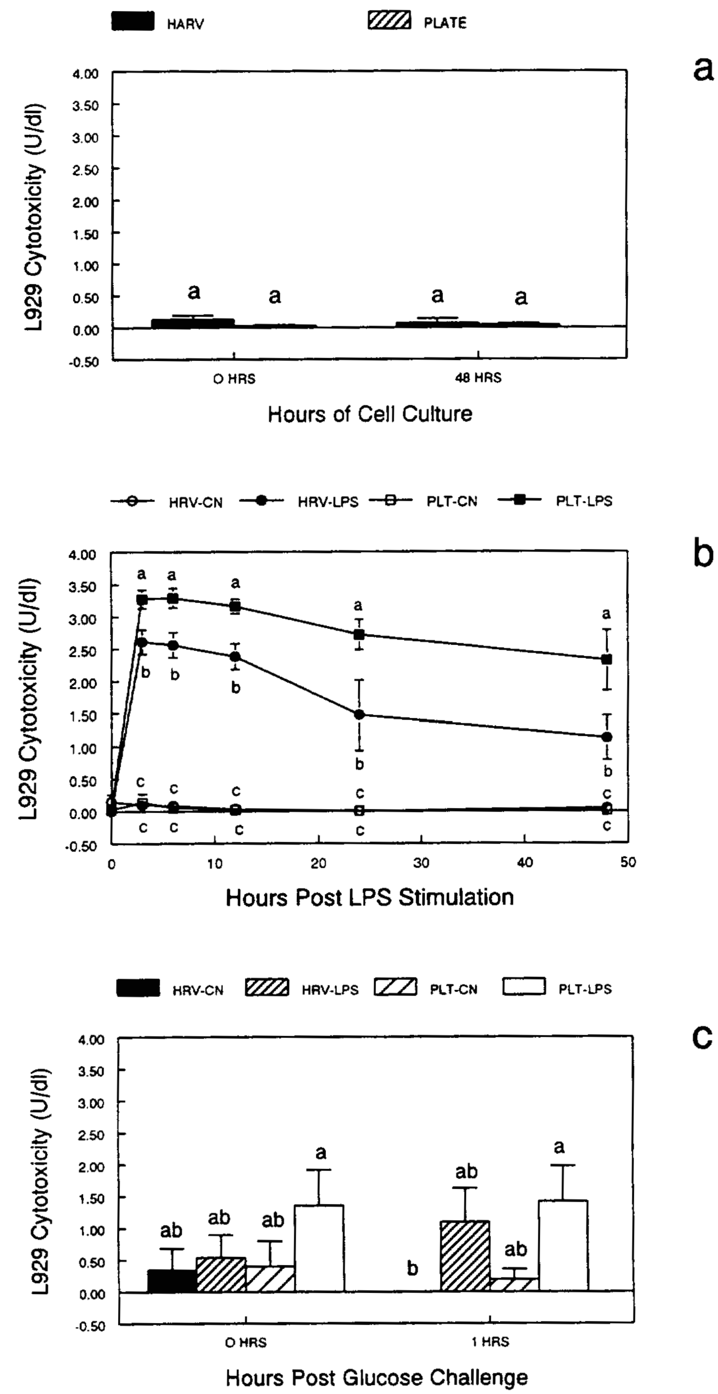

FIGURE 3. TNF-alpha in islet medium: a) during 48 hours culture, b) post LPS stimulation, c) post glucose addition. HRV-CN, HARV control; HRV-LPS, HARV LPS-stimulated; PLT-CN, static culture plate control; PLT-LPS, static culture plate stimulated with LPS.

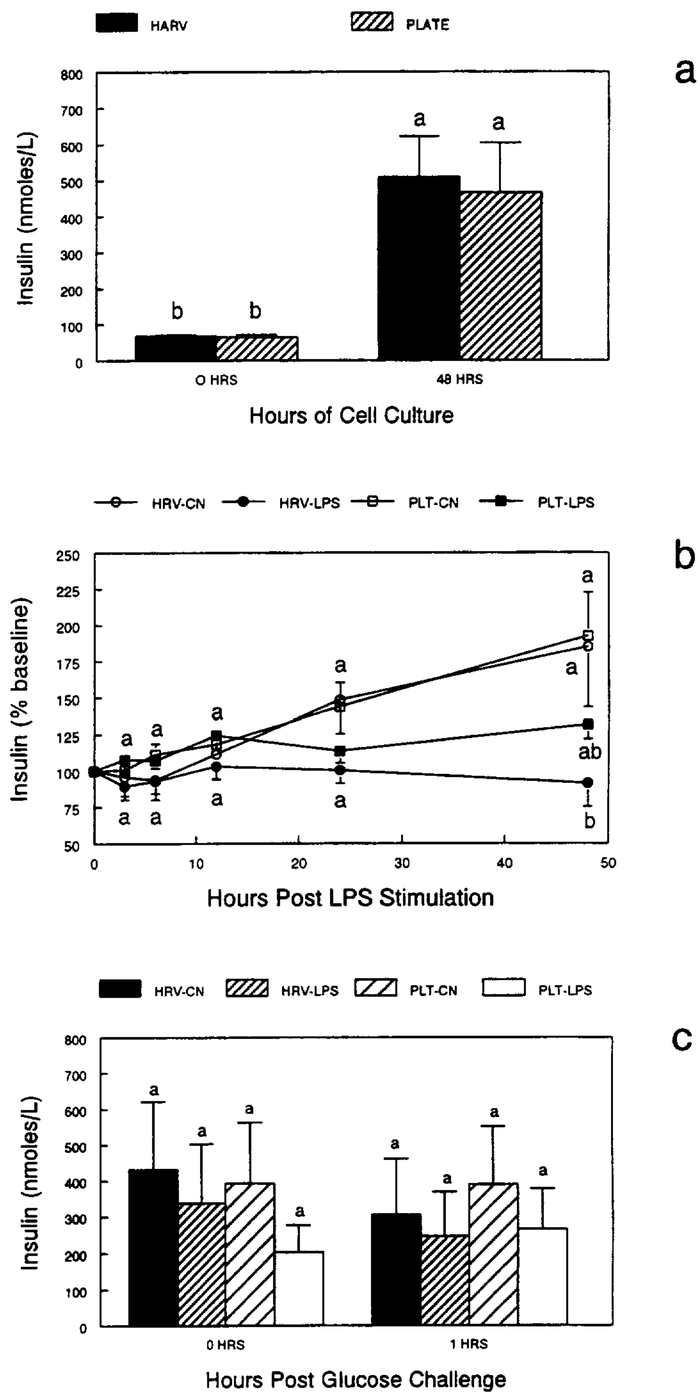

FIGURE 4. Insulin in islet medium: a) during 48 hours culture, b) post LPS stimulation, c) post glucose addition. HRV-CN, HARV control; HRV-LPS, HARV LPS-stimulated; PLT-CN, static culture plate control; PLT-LPS, static culture plate stimulated with LPS.

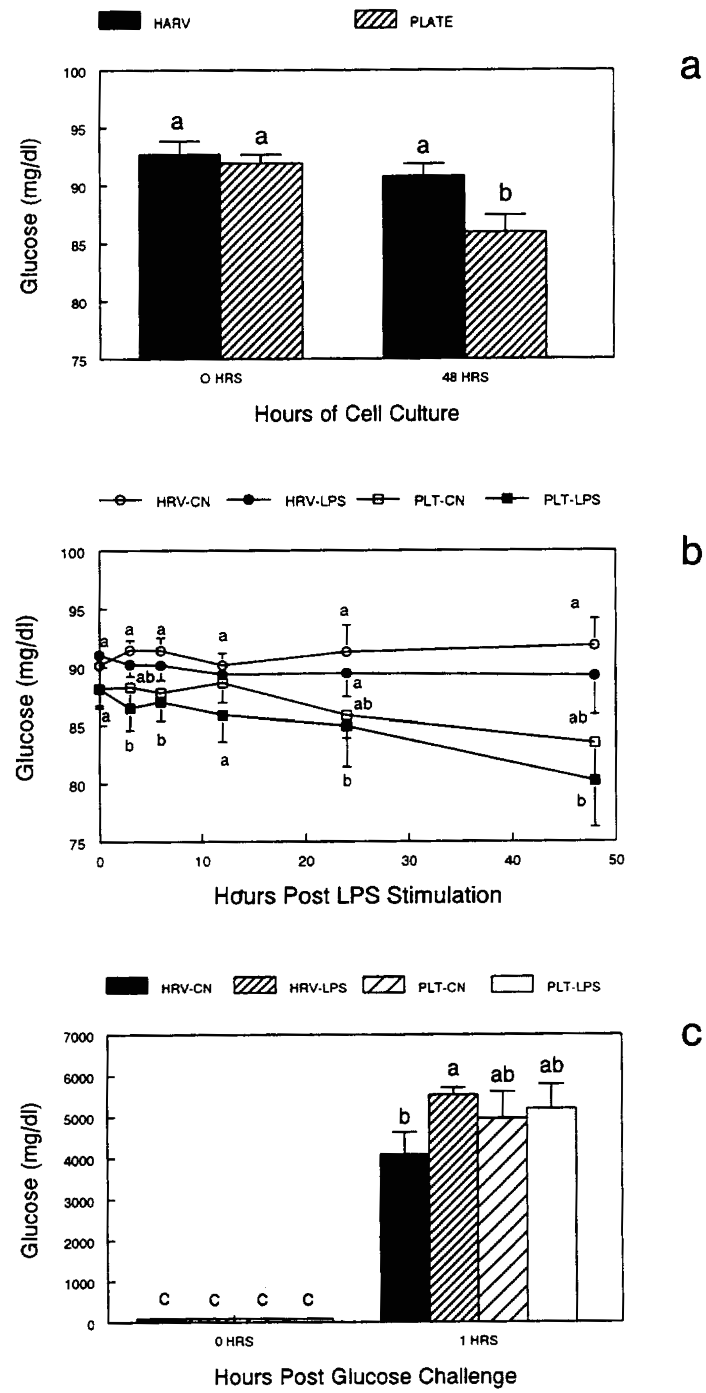

FIGURE 5. Glucose in islet medium: a) during 48 hours culture, b) post LPS stimulation, c) post glucose addition. HRV-CN, HARV control; HRV-LPS, HARV LPS-stimulated; PLT-CN, static culture plate control; PLT-LPS, static culture plate stimulated with LPS.

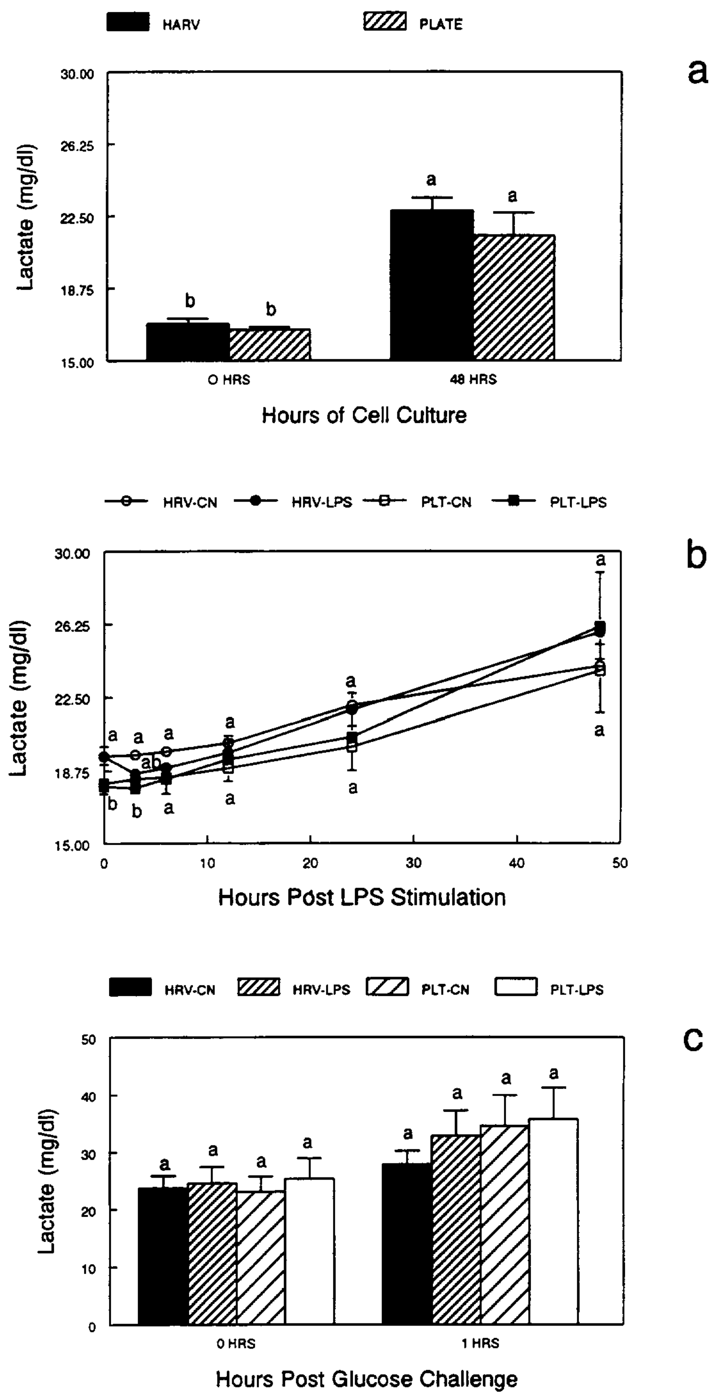

FIGURE 6. Lactate in islet medium: a) during 48 hours culture, b) post LPS stimulation, c) post glucose addition. HRV-CN, HARV control; HRV-LPS, HARV LPS-stimulated; PLT-CN, static culture plate control; PLT-LPS, static culture plate stimulated with LPS.

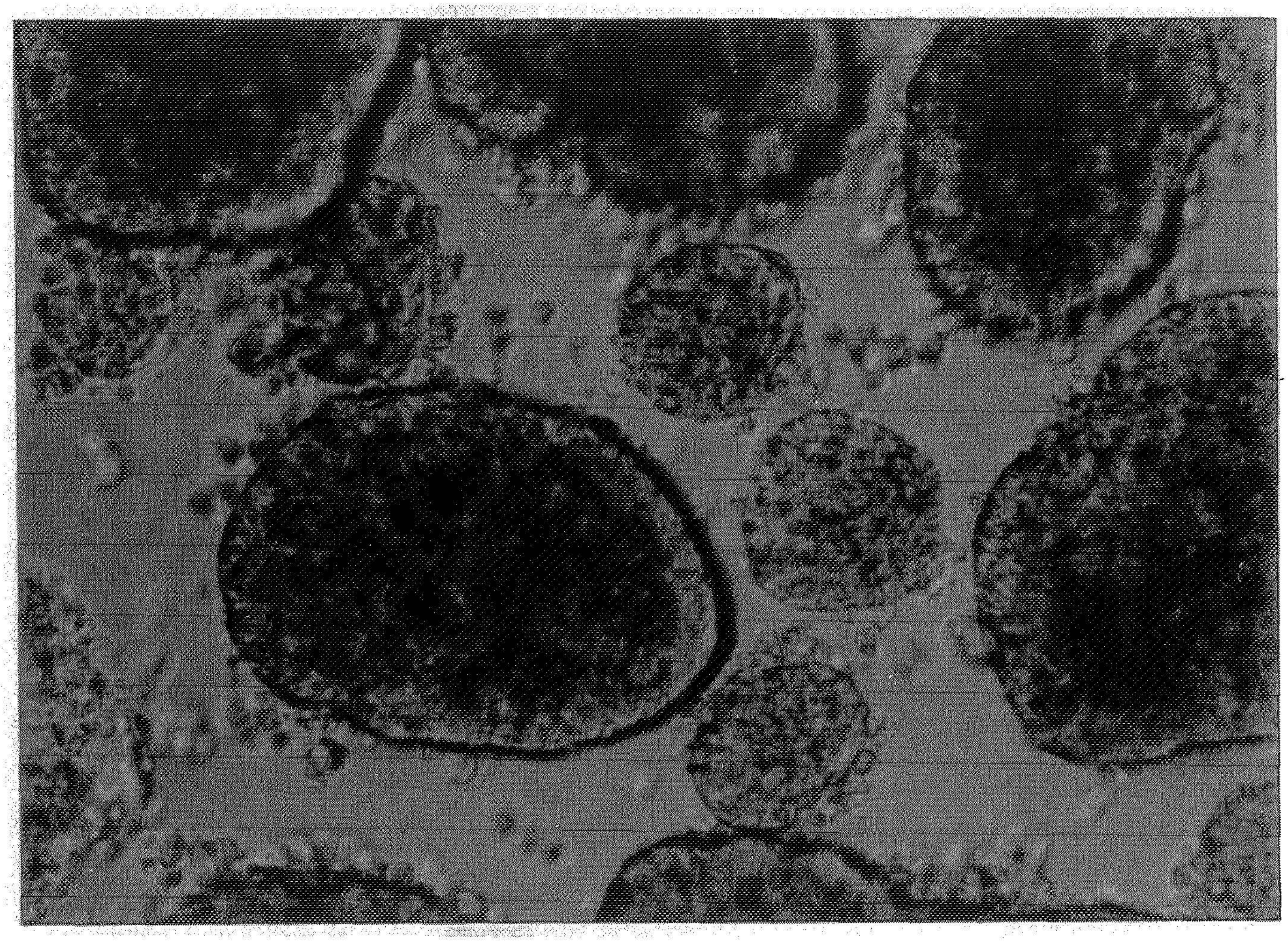

FIGURE 7. Photomicrograph of freshly isolated islets of Langerhans from male Wistar Furth rats. This phase contrast image was obtained using a 40x air objective.

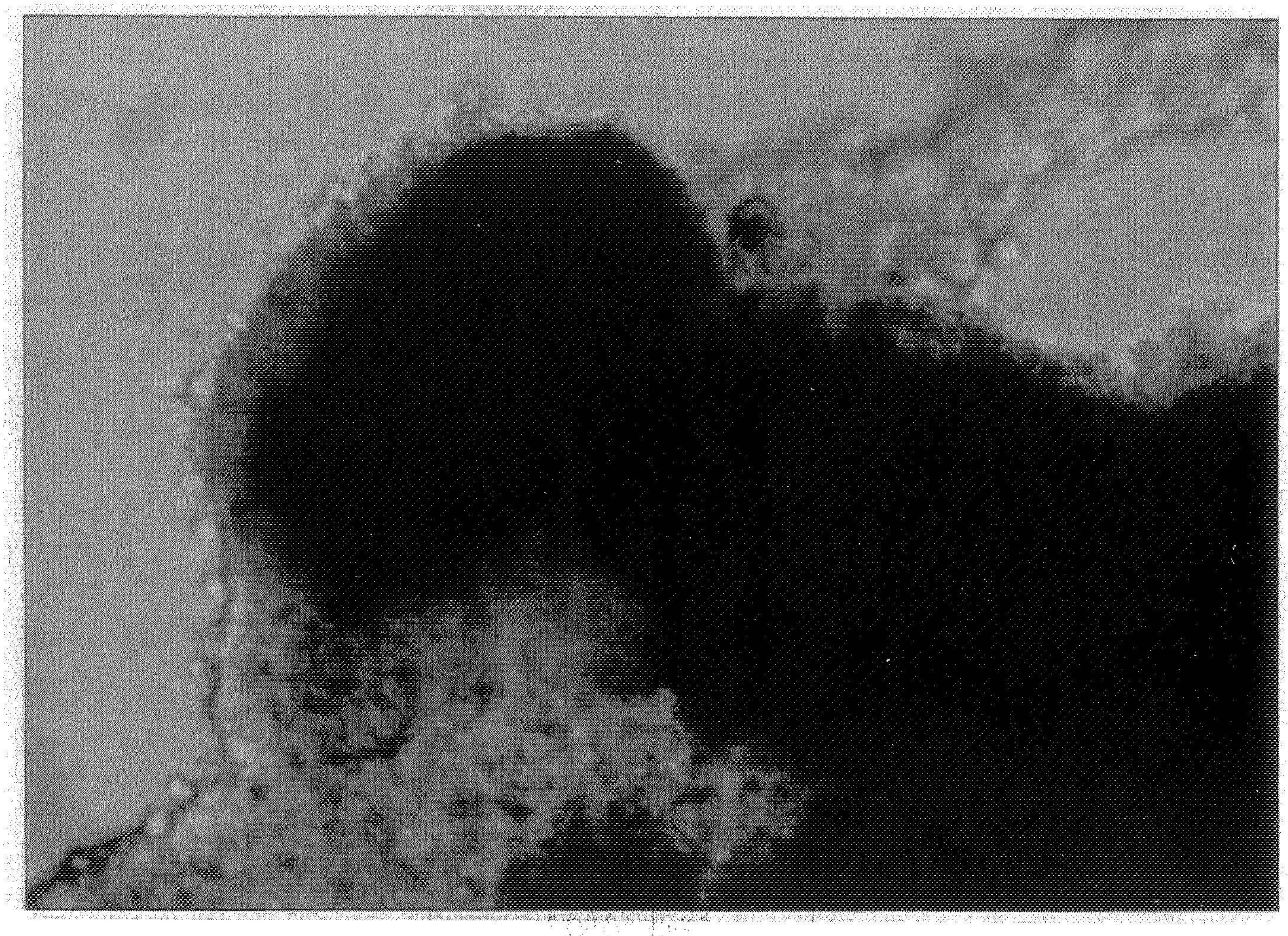

FIGURE 8. Photomicrograph of the edge of an islet cell aggregate (ICA) produced by HARV culture. This phase contrast image was obtained following 14 days of HARV culture using a 40x air objective.

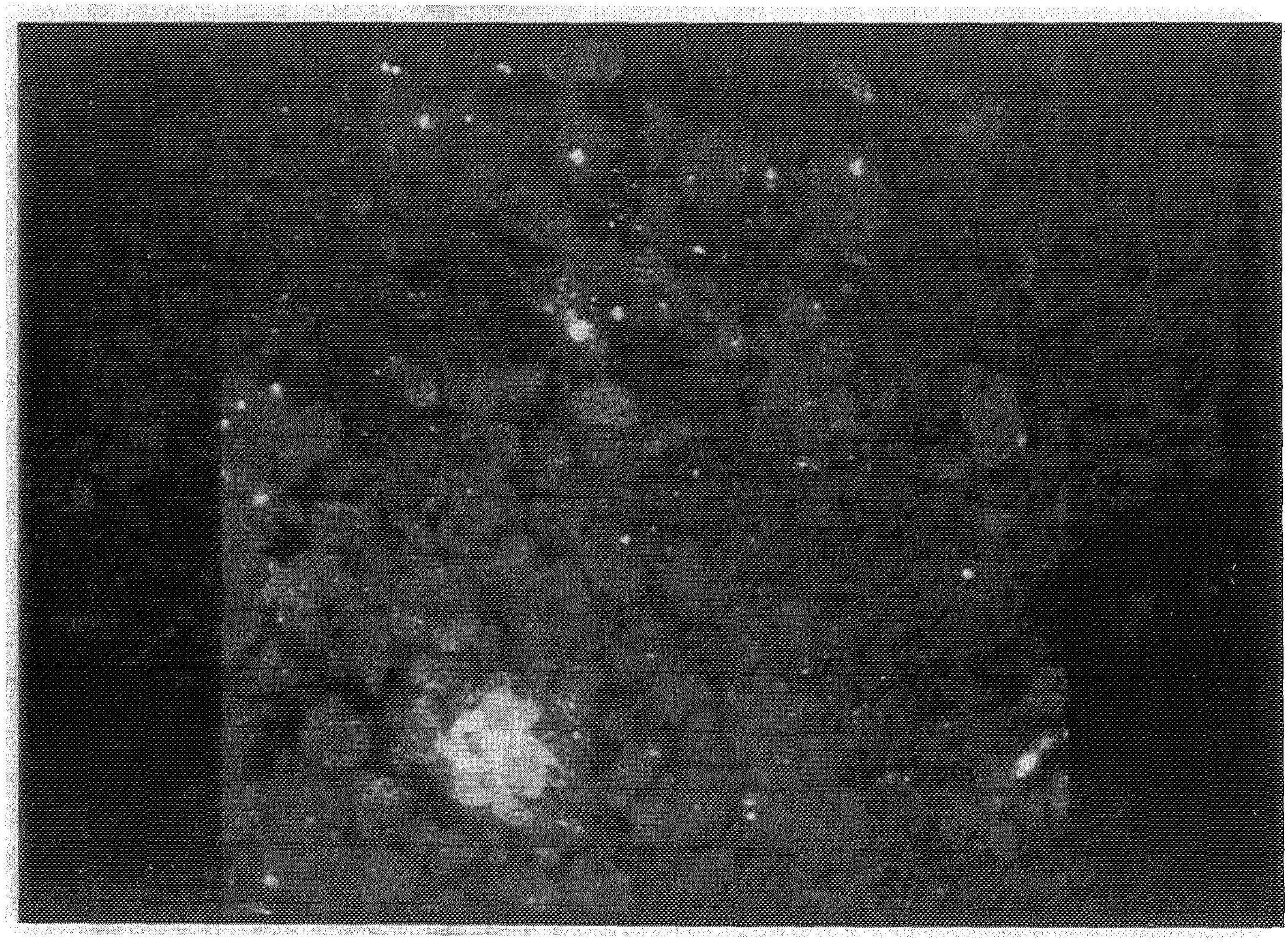

FIGURE 9. Confocal photomicrograph of an islet cell aggregate (ICA) produced by 14 days of HARV culture. Image was obtained using a 100x oil immersion objective, and is a representative image of the core of an ICA stimulated with LPS.

a b

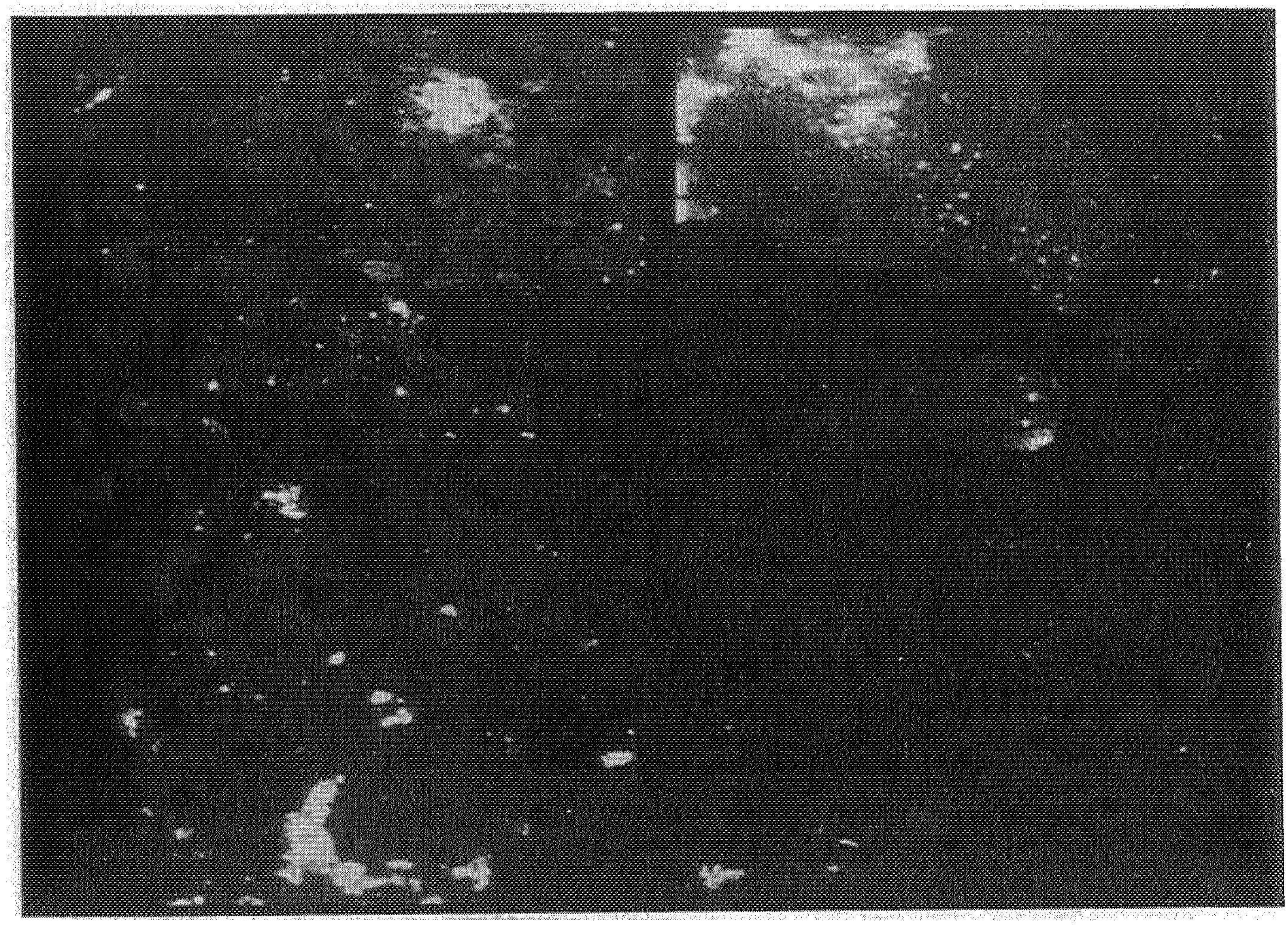

c d

FIGURE 10. Confocal photomicrographs of islet cell aggregates (ICAs) produced by 14 days of HARV culture. Images were obtained using a 100x oil immersion objective, and are representative images of the core of three ICAs stimulated with LPS (10a, b, c) and one non-LPS stimulated control (10d).

CHANGES IN BODY INERTIA DURING BED REST STUDIES

Final Report

NASA/ASEE Summer Faculty Fellowship Program – 1998

Johnson Space Center

IN-52

Prepared by: Beth A. Todd, Ph.D.

Academic Rank: Associate Professor

University & Department: The University of Alabama
Department of Mechanical Engineering
Tuscaloosa, AL 35487-0276

NASA/JSC

Directorate: Space and Life Sciences

Division: Medical Sciences

Branch: Life Sciences Research Laboratories

JSC Colleague: Linda C. Shackelford, M.D.

Date Submitted: August 7, 1998

Contract Number: NAG 9-867

ABSTRACT

Development of effective exercise countermeasures is crucial for long duration human space flight. To analyze the mechanical effects of a particular exercise on the musculoskeletal system, the inertial properties of segments of the body must be quantified. Since bone mineral density loss is related to the lack of mechanical stress and strain on the skeletal system, physical analysis can be very useful for countermeasure evaluation.

Bed rest is commonly used as a ground based method for studying the impact of microgravity. Three subjects who participated in a 17 week bed rest study where exercise was used as a countermeasure were analyzed to determine their body segment parameters.

The GEnerator of BODy data (GEBOD) software was developed by the Air Force and automotive industry for dynamic modeling of the human body. Two different calculation methods within GEBOD were used to evaluate the mass, center of gravity, and principal moments of inertia of the torso, head and neck, thighs, shanks, and feet of the three bed rest subjects. The Adult Male portion of the code uses standing height and total body weight as inputs and proportions the segment results to a data set within the program. The User-Supplied Data portion of the code uses 32 anthropometric measurements of the body to more precisely evaluate the segment inertial properties.

A table of results of the segment properties of the three bed rest subjects is available to interested persons, but these numbers are not included in the report. A potential discrepancy between the two methods was found when comparing the results for an individual subject. This discrepancy will be further investigated. Until then, more precise segment properties may be obtained if the 32 anthropometric measurements are collected on each subject.

INTRODUCTION

As NASA moves to long duration missions on Space Station and eventually to Mars, development of effective countermeasures for the physiological effects of long-term space flight becomes crucial. Currently bed rest is used to create the physiological effects of weightlessness in ground-based studies. The Horizontal Exercise Machine (HEM) has been developed to investigate the use of exercise countermeasures during bed rest, particularly for prevention of bone and mineral density (BMD) loss. Instrumentation on the HEM provides force and position data for dynamic analysis of the exercises. The results of the dynamic analyses will provide information leading to countermeasure selection.

To complete the dynamic analysis of HEM exercises, inertia properties including mass, center of mass, and principal moments of inertia of body segments are needed. The segments of interest include the torso, head and neck, both thighs, both shanks, and both feet. Only the lower extremities and spine undergo significant BMD loss in microgravity, so the inertial properties of upper extremities are not needed for the analysis [1]. A variety of techniques have been developed to determine inertia properties of body segments, including experimental techniques, mathematical models, and imaging and video methods [2-5]. Results from experimental techniques have been compiled into a number of tables and charts which are used to scale segment properties from stature and total body weight [6-7]. Mathematical models and video methods have been combined into computer software packages which can provide greater detail than the experimental tables [8-9].

The U.S. Air Force and automotive industries have worked together in conjunction with NASA to develop the application software GEBOD, ATB, and VIEW for modeling the dynamic motion of the human body [10-12]. ATB uses the Articulated Total Body Model to determine the body inertia, position, and movement under a variety of load situations [11]. Graphical results from ATB can be plotted with VIEW [12]. The segment inertia properties which ATB uses as input are generated with GEBOD, GEnerator of BODy data [10]. GEBOD provides the user with several different options for determining the segment parameters. In this project, GEBOD was used to determine the segment inertia parameters for three bed rest subjects. Results from two different algorithms within GEBOD were used to determine the sensitivity of the results to the method of calculation.

A detailed description of the methods used for the calculations are described below in the section on GEBOD. Briefly one method for calculating segment inertia is dependent on stature, total body weight, and gender. The other method incorporates 32 anthropometric measurements in the determination of segment inertia calculations. A primary issue is whether on a case-by-case basis the resulting inertia is dependent on the calculation method.

Another issue, which is unique to the bed rest studies, is the variation in body measurements during the 17 week period. Does the total body weight decrease enough to significantly affect segment inertia calculations? Do other anthropometric measurements change in a significant manner. This work attempts to begin to address some of these issues.

GEBOD

The modeling approach chosen by the developers of GEBOD and ATB considers the body as being divided into either 15 or 17 rigid segments with links at the joints. This is a refinement of the rigid segment model proposed by Hanavan [3]. The model incorporated into GEBOD and ATB further refines the segments as ellipsoids as shown in Figure 1 [11]. The difference between the 15 and 17 segment models is related to the modeling of the hands. The 15 segment model was used for these calculations since the upper extremities were not of interest. GEBOD is a FORTRAN 77 program with approximately 3846 lines of code which can be run on a desktop computer in DOS mode. Since it was developed by the federal government, it is in the public domain and readily available to potential users.

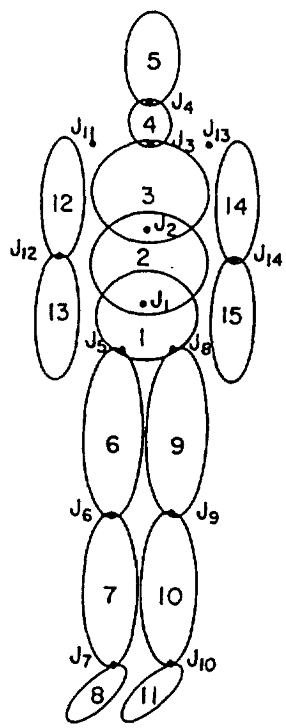

Figure 1.- Fifteen segment model of the human body [11]

There are a number of computational modes available in GEBOD for the adult male, adult female, children, anthropomorphic dummies, and user-supplied anthropometric data. The bed rest subjects of interest were adult males, so the two options used in this analysis were the Adult Male and User-Supplied Data modes.

In 1973 Calspan Corporation developed the GOOD (Generator Of Occupant Data) program to automate the generation of body segment data for input into a crash simulation program for modeling vehicle occupants in three dimensions [8]. GEBOD is a modification of GOOD. The Adult Male mode uses stereophotometric survey data to calculate the joint center locations and segment masses and inertial properties [10]. Input for the Adult Male mode consists of the Total body weight and Standing height. The User-Supplied Data mode uses the anthropometric measurements listed in Table 1 to develop a potentially more precise model.

Table 1.- Anthropometric Measurements for User-Supplied Data Mode [10]

--Total body weight	--Standing height	--Shoulder height
--Armpit height	--Waist height	--Seated height
--Head length	--Head breadth	--Head to chin height
--Neck circumference	--Shoulder breadth	--Chest depth
--Chest breadth	--Waist depth	--Waist breadth
--Buttock depth	--Hip breadth, standing	--Shoulder to elbow length
--Forearm-hand length	--Biceps circumference	--Elbow circumference
--Forearm circumference	--Waist circumference	--Knee height, seated
--Thigh circumference	--Upper leg circumference	--Knee circumference
--Calf circumference	--Ankle circumference	--Ankle height, outside
--Foot breadth	--Foot length	

To determine segment data for either of these options, four groups of regression equations are used [10]. There is a group of equations corresponding to each of the following: body measurements, joint locations, segment volumes, and segment principal moments of inertia. Note that each group of regression equations is independent of the other three groups. This leads to occasional inconsistencies in the output, and these inconsistencies could be potentially detrimental to the results as discussed below.

Segment output is given in terms of a local coordinate system with an origin at the segment centroid [10]. Output from the Adult Male mode consists of a repetition of the subject's weight and standing height, followed by estimates of the anthropometric measurements which are entered in the User-Supplied Data mode. Then the weight and principal moments of inertia about segment centroidal axes are given with the principal directions (yaw, pitch, and roll). The final section of data contains the locations of the joints at each end of the segment. Output from the User-Supplied Data mode is presented

in a similar manner beginning with a repetition of all of the anthropometric measurements, followed by inertia values and joint locations.

CALCULATION PROCEDURES

Since it is anticipated that the results of this report will be used in subsequent analyses, all of the calculations (including unit conversions) will be discussed so that there is no doubt as to how the values were obtained. The units used in GEBOD were not compatible with the units desired for the dynamic analysis, so several conversions were made. Also, the segment centroids in terms of a global coordinate system were calculated.

To convert the segment weights (lbs) into segment masses (slugs), the output segment values were divided by 32.2 [10]. To convert the moments of inertia from lb-sec^2-in to slug-in^2, the inertia values were multiplied by 386.4. The rotations were presented in degrees, and distances were given in inches.

The global coordinate system was chosen for the subject standing in the normal anatomical position with feet flat and toes forward [13] as shown in Figure 2. The +x-axis pointed from posterior to anterior, the +y-axis pointed from the subject's left to right, and the +z-axis pointed from superior to inferior. Thus a right-handed coordinate system was created. The origin of the global coordinate system was on the median plane at the bottom of the subject's feet. The yaw, pitch, and roll rotations are related to the rotations of an aircraft and related to a pilot in the seated position [10]. Thus, roll is rotation about the x-axis, pitch is rotation about the y-axis, and yaw is rotation about the z-axis.

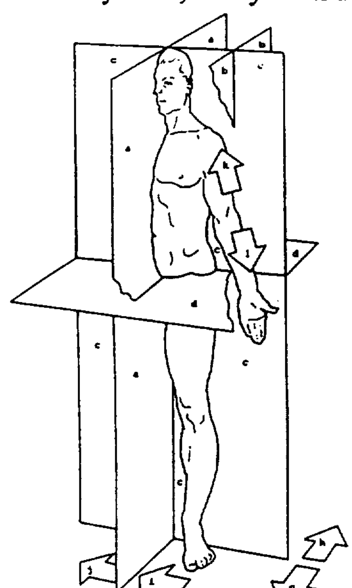

Figure 2.- Standard anatomical position [13]

To determine the location of each segment centroid in global coordinates, the joint output was used. It was assumed that the joint between the neck and thorax (upper torso) segments was located at shoulder height, so the global location of that joint was determined first from that measurement [10]. The location of this joint is given in the output both in terms of "neck coordinates" and "thorax coordinates". Through subtraction the location of the neck centroid and thorax centroid were located. Then the head-neck joint location was given in "neck coordinates" and "head coordinates". Again through subtraction, the head centroid was determined. Following a similar method, the centroids of the other body segments were located. For all of the calculations, GEBOD approximates all of the tissues in the body as having the same density: 0.00112287 slugs/in^3 [10].

GEBOD considers the feet in the model to be oriented with the toes downward. A coordinate rotation was used to place the feet in a toes forward position. Thus +x became –z, +y became +y, and +z became +x. For the lower extremities, calculations were duplicated for the left and right sides.

GEBOD considers the head and neck to be two separate segments and the torso to be three segments: pelvis, abdomen, and thorax (or sometimes lower torso, center torso, and upper torso) [10]. For the dynamic calculations to be performed on the bed rest subjects, the head and neck needs to be treated as one segment and the torso needs to be treated as one segment. The combined segment masses were determined through addition, and the combined segment centroids were determined through the calculation of composite shapes which is taught in a typical Statics course [14]. Calculation of the principal moments of inertia for the combined segments was more challenging.

For the head and neck, the parallel axis theorem was used to determine the new principal moment of inertia with respect to the combined segment centroid. Calculations for the torso were less straightforward. While the pelvis and abdomen were oriented with a yaw, pitch, and roll of zero degrees, the thorax had a pitch of 14.4 degrees. First the thorax was rotated so that its axes were also at a (0,0,0) orientation. In doing this, the inertia tensor of the thorax was calculated. According to Downey and Smith, [15]

$$I_x = l_{xx'}^2 I_{x'} + l_{xy'}^2 I_{y'} + l_{xz'}^2 I_{z'}$$

$$I_y = l_{yx'}^2 I_{x'} + l_{yy'}^2 I_{y'} + l_{yz'}^2 I_{z'}$$

$$I_z = l_{zx'}^2 I_{x'} + l_{zy'}^2 I_{y'} + l_{zz'}^2 I_{z'}$$

where I are the moments of inertia and l are direction cosines such that $l_{xx'} = i \cdot i'$, etc.,
i, j, and k are unit vectors for the x, y, z coordinates,
i', j', and k' are unit vectors for the x', y', z' coordinates, and
the primed system are the principal axes.

Likewise for the products of inertia, P_{xy}

$$P_{xy} = -l_{xx'} l_{yx'} I_{x'} - l_{xy'} l_{yy'} I_{y'} - l_{xz'} l_{yz'} I_{z'}$$

$$P_{xz} = -l_{xx'} l_{zx'} I_{x'} - l_{xy'} l_{zy'} I_{y'} - l_{xz'} l_{zz'} I_{z'}$$

$$P_{yz} = -l_{yx'} l_{zx'} I_{x'} - l_{yy'} l_{zy'} I_{y'} - l_{yz'} l_{zz'} I_{z'}$$

Once the inertia tensor for the thorax at (0,0,0) orientation was obtained, the moments of inertia were combined with the parallel axis theorem. Note that the resulting inertia tensor has non-zero products of inertia. The principal moments of inertia of the torso were determined by solving the eigenvalue problem [16]. After the eigenvalues were determined, the eigenvectors were found through the use of an adjoint matrix, and they were normalized so that the sum of the squares of the direction cosines was unity. After the direction cosines were found, a final rotation was made about the y-axis to determine the pitch angle for the principal moments of inertia.

As mentioned previously, the three bed rest subjects considered were all adult males. The available anthropometric measurements for the subjects are given in Table 2. For the User-Supplied Data option, values were taken from the Adult Male option output if individual measurements were not available.

Table 2.- Bed rest subject anthropometric measurements

Subject	53	54	52
Standing height	67.5 in.	73 in.	176 cm
Total body weight	56.5 kg	67 kg	69.5 kg
Foot length	23.1 cm	27.3 cm	25.8 cm
Heel width	4.7 cm	5.6 cm	5.6 cm
Foot width	8.6 cm	10.5 cm	8.7 cm
Medial malleolus - 1st metatarsal head	17.6 cm	14.4 cm	14.5 cm
Medial malleolus - heel	7.8 cm	8.3 cm	7.4 cm
Sphyrion height	5.4 cm	6.0 cm	9.7 cm
Shank length	42.3 cm	43.0 cm	42.7 cm
Ankle width	6.3 cm	7.2 cm	7.1 cm
Knee width	8.8 cm	9.9 cm	9.4 cm
Thigh circumference	44.8 cm	49.2 cm	55.5 cm
Thigh width	10.9 cm	12.6 cm	14.9 cm
Thigh length	42.0 cm	53.2 cm	37.6 cm
ASIS-ASIS distance	22.2 cm	22.0 cm	20.7 cm

RESULTS AND FUTURE WORK

The resulting values of segment mass, centroid location, and principal moment of inertia are available to colleagues on request. Results have been calculated for Subject #53 in both the Adult Male and User-Supplied Data modes. Results have been calculated for Subject #52 in the Adult Male mode. Other results will be available shortly.

RECOMMENDATIONS

One issue which arose in looking at the resulting segment values is the significance of the different parameters, including Seated height. As noted previously, GEBOD assumes a constant density, and Total body weight is entered as one of the first parameters. It appears that certain assumptions are made about the distribution of the body weight, based on data from catalogued subjects, such that the Total body weight divided by the body volume will lead to the correct density. Several of the parameters, such as Seated height appear to be used to determine the relative length of the various segments. It was curious that in the Adult Male option, the Seated height is calculated as being several inches below Waist height. When a more realistic value was used in the User-Supplied Data option, the size of the thigh and torso changed significantly. This issue of the seated height needs to be explored further, and may lead to the need for taking 32 anthropometric measurements on the bed rest subjects.

REFERENCES

1. Shackelford, L., Feiveson, A., Spector, E., LeBlanc, A., Oganov, V. "Prediction of Femoral Neck Bone Mineral Density Change in Space". *12th Man in Space Symposium: The Future of Humans in Space*, June 8-13, 1997, Washington, D.C., pp. 78-79.

2. Clauser, C.E., McConville, J.T., Young, J.W. *Weight, Volume and Center of Mass of Segments of the Human Body*, Report No. AMRL-TR-69-70, 1969.

3. Hanavan, E.P. *A Mathematical Model of the Human Body*, Report No. AMRL-TR-64-102, 1964.

4. Brown, G.A., Tello, R.J., Rowell, D., Mann, R.W. "Determination of Body Segment Inertial Properties", *RESNA 10th Annual Conference*, June 1987, San Jose, CA, pp. 289-301.

5. Todd, B.A., Woods, H.C., Shackelford, C. "Mass Centers of Body Segments". *Proceedings of the 16th Annual International Conference of the IEEE Engineering in Medicine and Biology Society Conference*, November 1994, Baltimore, MD, pp. 335-336.

6. NASA *Anthropometric Source Book—Volume I: Anthropometry for Designers*, NASA Reference Publication 1024, pp. IV.1-IV.75.

7. Winter, D.A. "Ch. 3. Anthropometry". *Biomechanics and Motor Control of Human Movement*, 2nd Ed. Wiley, 1990.

8. Bartz, J.A. *A Three Dimensional Computer Simulation of a Motor Vehicle Crash Victim, Phase I – Development of the Computer Program*, VJ-2979-V-1, 1971.

9. Bartz, J.A., Gianotti, C.R., *A Computer Program to Generate Input Data Sets for Crash Victim Simulations*, Calspan Report ZQ-5167-V-1, 1973.

10. Cheng, H., Obergefell, L., Rizer, A. *Generator of Body Data (GEBOD) Manual*, AL/CF-TR-1994-0051, March 1994.

11. Obergefell, L.A., Gardner, T.R., Kaleps, I., Fleck, J.T., *Articulated Total Body Model Enhancements; Volume 2: User's Guide*, Report No. AAMRL-TR-88-043, 1988.

12. Leetch, B.D., Bowman, W.L., *Articulated Total Body (ATB) "VIEW" Program Software Report, Part II, User's Guide*, AFAMRL-TR-81-111 Volume II, 1983.

13. Profio, A.E. *Biomedical Engineering,* Wiley, 1993.

14. Beer, F.P., and Johnston, E.R., *Vector Mechanics for Engineers: Statics and Dynamics*, 5th Ed., 1988.

15. Downey, G.L., Smith, G.M., *Advanced Dynamics for Engineers*, International Textbook Company, 1960.

16. Thompson, W.T. *Theory of Vibration with Applications*, Prentice-Hall, 1972, pp. 173, 425-426.

Establishing A Distance Learning Plan for International Space Station (ISS) Interactive Video Education Events (IVEE)

(21)
IN-18

Final Report

NASA Summer Faculty Fellowship Program

Johnson Space Center

Prepared by:	Clint Wallington, Ph.D.
Academic Rank:	Professor
University, Department, and Program	Rochester Institute of Technology School of Food, Hotel, and Travel Management Instructional Technology Program

NASA/JSC	
Program:	International Space Station
Unit:	Management Operations
Group:	Communications and Information Management
JSC Colleague:	Lyn Gordon-Winkler
Data Submitted:	26 August 1998
Contract Number:	NAG 9-867

Abstract

Educational outreach is an integral part of the International Space Station (ISS) mandate In a few scant years, the International Space Station has already established a tradition of successful, general outreach activities. However, as the number of outreach events increased and began to reach school classrooms, those events came under greater scrutiny by the education community. Some of the ISS electronic field trips, while informative and helpful, did not meet the generally accepted criteria for *education* events, especially within the context of the classroom.

To make classroom outreach events more acceptable to educators, the ISS outreach program must differentiate between communication events (meant to disseminate information to the general public) and education events (designed to facilitate student learning).

In contrast to communication events, education events:

- are directed toward a relatively homogeneous audience who are gathered together for the purpose of learning
- have specific performance objectives which the students are expected to master
- include a method of assessing student performance
- include a series of structured activities that will help the students to master the desired skill(s)

The core of the ISS *education* events is an interactive videoconference between students and ISS representatives. This interactive videoconference is to be preceded by and followed by classroom activities which help the students attain the specified learning objectives. Using the interactive videoconference as the centerpiece of the education event lends a special excitement and allows students to ask questions about what they are learning and about the International Space Station and NASA.

Whenever possible, the ISS outreach education events should be congruent with national guidelines for student achievement. ISS outreach staff should recognize that there are a number of different groups that will review the events, and that each group has different criteria for acceptance. For example, school administrators are more likely to be concerned about an event meeting national standards and the cost of the event. In contrast, a teacher's acceptance of an education event may be directly related to the amount of extra work the event imposes upon that teacher. ISS education events must be marketed differently to the different groups of educators, and must never increase the workload of the average teacher.

Introduction

Background

For the past few years, the International Space Station (ISS) Program has been conducting outreach activities through a variety of delivery systems–including traveling exhibits, informational and educational materials, sites on the World Wide Web, and interactive videoconferencing to both the general public and to schools. The interactive videoconferencing (dubbed "educational field trips") which reaches students in the classroom has been exceptionally popular. Content, however, has been somewhat limited and often involves a presenter at Johnson Space Center (JSC) simply conducting a tour of the International Space Station mock-up and telling students about NASA and the Space Station. While beneficial, these electronic field trips did not meet the more rigorous criteria usually applied by educators to *learning activities*. The aim of this project was to develop a long-range plan for the future outreach *education activities* of International Space Station.

Project Focus and Scope

After the International Space Station is completed, one of its assigned tasks is to "...act as a virtual classroom for students on earth." The activities leading to the is goal should start now.

The focus of this project was to develop an integrated master plan for the next three to five years (while Space Station is being built) for outreach activities which would:

- reach out to learners at all levels, especially from kindergarten through high school (K-12)
- build on the established success of other ISS outreach activities, especially interactive videoconferences
- be based (at least, in the beginning) primarily on existing ISS and NASA materials
- meet the criteria for an "educational" (as opposed to informational) activity
- link directly to the missions of NASA and ISS
- appeal to (and be accepted by) a range of education professionals, from teachers to superintendents
- offer a plan for the ongoing development of lessons that would be the basis for ISS education outreach

While International Space Station has been conducting a variety of outreach activities reaching the classroom, interested parties, and the general public, the plan would reflect a move toward more structured learning experiences.

Missions: NASA and Space Station

From its inception, NASA has been committed to the discovery and dissemination of new knowledge. NASA's *Strategic Plan for Education* (1st edition, 1992) commits the agency to the development of instructional materials, providing enrichment experiences for students, and using advanced technologies for education. A primary mission of the International Space Station is to "...serve as a virtual classroom in space to the benefit or teachers and students alike" (ISS *Factbook*).

Other ISS objectives include

> "...inspir[ing] in a new generation a sense of wonder and inquisitiveness about the world and the universe in which they live"

and

> "...aid[ing] teachers in stimulating young people in the study of science, math, technology, and engineering."

International Space Station's mission is congruent with the NASA *Education Framework* (April 1, 1997). International Space Station's endeavors can clearly be identified as falling in the several cells of the *Education Framework*. The issue is not a question of Space Station's mandate for educational outreach, but one of making that outreach truly world class. (Or, in this case, moving it past world class to *space class*.)

International Space Station Outreach: Current Configuration

Currently, International Space Station (ISS) uses a variety of delivery modes for its outreach programs. These delivery modes range from the more traditional printed material (brochures and teacher's guides) and traveling exhibits to electronic videoconferencing with students and virtual reality models of the Space Station. Each has been successful and has been developed to meet a particular need. As might be expected, there is some overlap in content and audience. Content has often been determined by the delivery method—as opposed to the having the content *drive* the delivery medium. The same message and delivery method would reach different audiences. The outreach event became categorized by the audience it reached rather than by the purpose of the outreach or the structure and content of the message. This caused special problems with regards to education.

Education–that is, formal education–is a specialized field. It has its own purpose, standards, regulations, methods of conduct, profession(s), and terminology. For educators to consider an event as educational, that event must be more than an isolated occurrence in classroom. Thus, ISS outreach to the classroom was not considered to be education by some educators. The deciding characteristic was definitely *not* the venue of the event.

Communication or Education?

Educators do not always agree on the details of what constitutes education. Most will agree, however, on some of the common characteristics that separate education from communication, especially mass communication. Education's basic characteristics include:

- a clearly defined, relatively homogeneous set of learners
- an objective (or set of objectives), usually based on a skill or performance which the learner must master
- a way of assessing whether or not the learner has mastered the desired skill or performance
- planned, structured activities or experiences that will aid the learner in mastering the desired performance

In contrast, communication is often more generic than education, In mass communication, messages are often directed at a broader, more heterogeneous audience. The objective may be less clear, and an assessment of the performance may not be required. (Most advertising, interestingly enough, meets the criteria for education.)

For ISS endeavors to be considered as education, especially by educators, these endeavors *must* meet (at minimum) the four criteria listed above.

The closest that ISS currently comes to a direct education event is the electronic field trip. (There are other educational activities, but these are usually suggested experiments in the teacher's guides.) The electronic field trip is an interactive videoconference with students in a classroom setting. The electronic field trip usually features a NASA host showing the mock-up(s) of the International Space Station. The host also tells about NASA and serves as a role model for students who aspire to a technical career.

It should be pointed out that anecdotal evidence–written and oral responses from the students and their teachers, along with observations of the classes by the NASA outreach team–indicate a high measure of success. Still, each electronic field trip had to be considered as an idiosyncratic event rather than a portion of an integrated curriculum. Moving into the mainstream of formal education requires that the electronic field trips be consistent with each other as well as be congruent with the standards of the education community. Meeting the criteria laid out above ensures that consistency and congruency.

Most current ISS outreach meets the more general and varied information needs of the lay public. This is *communication*.

When the outreach endeavor is a structured set of activities to help the audience master specific skills–skills which could and might well be tested–the result is *education*.

Categories within the Areas of Communications and Education

Communication and education are very broad categories. The outreach work that International Space Station currently conducts and will continue to conduct needs to be more precisely defined in order to set crisp, well defined goals. Accordingly, for ISS outreach events, communication and education are broken down into categories–two categories for communication and four categories for education. Details of the categories for communication and for education follow.

Communication Categories (2)

There are two categories of communication events. Events in **Communication Category 1** encompass communication with a fairly homogenous audience that has *gathered specifically for the outreach event.* A virtual tour of the Space Station for a PTA group is an example of Category 1 Communication. Other examples of Communications Category 1 include:

- a presentation to senior citizens of the benefits of medical research to be conducted on the International Space Station
- a demonstration of how foods are stored in the International Space Station for an American Dietetics Association workshop
- a sample tour for school district administrators
- a walk-through of the habitat module delivered to a middle school class

Notice that the last example (a walk-through for students) is communication, not education. The students are simply given a walk-through and allowed to ask questions. No objectives, tests, or pre- and post-presentation activities are indicated for the walk-through; hence, it remains a communication event.

Note, too, that in Communication Category 1, we know *before* the event takes place who the audience is and why they are present.

Events in **Communication Category 2** reach a broader audience who might participate in the outreach activities only in the context of a larger meeting–for example, visitors to a conference or visitors to a large public event where a Space Station exhibit is present. Most of the visitors come primarily for the meeting, rather than for the ISS exhibit. In this case, the audience is heterogeneous; anyone attending the conference (including friends and family) might stop by the exhibit. We know in general whom the conference might draw, but not who will come to the exhibit and a related communication event.

Category 1 Communication events are usually limited in duration (rarely more than an hour or so) and the group remains intact throughout the event. Category 2 Communication events might stretch through most of a day, depending on the exhibit hours and the resources to support to exhibit and the communication. The audience comes though a few at a time.

Education Categories (4)

The format of the education event is roughly the same in each education category. The process used to develop the education event is also the same for each category. The four education categories differ primarily in scope, in their congruence to curriculum guidelines, and by the amount of energy and resources required to develop the events for each category.

Education Category 1 is a temporary, transitional category in which currently existing electronic field trips would be quickly converted into relatively simple education events. This means working with currently existing presentation content and materials. The advantage of this approach is a relatively rapid start-up. The number of Education Category 1 events that could be developed is limited. Category 1 events would be replaced by Category 2, 3, and 4 events as soon as events in those categories were developed.

Education Category 2 includes events developed mostly from existing NASA curriculum materials. The topics for Category 2 are chosen primarily because most of the resources are readily at hand. Topics for Education Category 2 events may stem from teacher requests or from International Space Station (or NASA) special events. For example, the completion of the X-38 and its deployment to the Station might be the occasion for a lesson on lifting bodies. One special point to be made about Category 2 events is that they are *ad hoc* topics rather than directly linked to curriculum guidelines. As the ISS education outreach program matures, it is likely that Education Category 2 events will be supplanted by Category 3 events.

Education Category 3 is almost identical to Category 2 *except* that Category 3 events are always linked to curriculum guidelines, like the National Science Education Standards (NSES) or the guidelines from the National Council of Teachers of Mathematics (NCTM). Education events linked to guidelines (or to standardized tests) enjoy a certain acceptance because they more closely match existing curriculum recommendations. There is an implication is that Category 3 events might be more difficult (or costly) to produce simply because of a lack of existing resources that are already a close fit to guidelines.

Education Category 4 events are essentially the same as Category 2 and Category 3 with one major exception–*extended pre-release testing.* Education 4 events meet industry training standards–rigorous field testing (one-on-one, alpha test, beta test) rather than peer review. Category 4 events will have been proven effective, and have research data to support their effectiveness. Category 4 events will mostly likely be rare, because the required testing and revision is generally more resource-intensive than the actual development.

Having separate categories, each with its own appeal to different education groups and with its own demand on resources assists decision-makers in setting priorities for ISS outreach events.

ISS Outreach Events in the Education Categories

The ISS outreach *events* referred to in the four Education Categories are derivatives of the current electronic field trip. However, the term *electronic field trip* does not adequately reflect the new emphasis on education. Because the key activity in the event remains the interactive videoconference with an ISS presenter, the complete event is dubbed (at least, pro tem) an Interactive Video Education Event (IVEE) or, for simplicity's sake, an IVEE lesson. (The final terminology should be chosen on the basis of acceptance by teachers and educators.)

Under whatever name, IVEE lessons are composed of three parts (hereafter called units). The core unit is the interactive videoconference in which students communicate with ISS representatives. The interactive videoconferencing unit is the second of three units in an IVEE lesson. This interactive videoconference *must directly link* to the student activities/projects done *before* and *after* the videoconference. The activities in the videoconference unit must directly support the stated performance objectives. The other two units in the three-unit set are (not surprisingly) a pre-conference unit and a post-conference unit.

Thus, the three units in an IVEE lesson are:

- **pre-interactive videoconference** activities focused on the topic and learning objective(s), and leading to the learners discussing their activities with the ISS presenter
- an **interactive videoconference** in which the presenter discusses the students' pre-interactive videoconference activities; the presenter may also show related materials; the presenter can also relate student activities to current ISS and NASA projects, and will most certainly include some other information about NASA and the International Space Station
- **post-interactive videoconference** activities in which the teacher reinforces the learning and assesses learner proficiency

This three-unit lesson is the *standard template* for any outreach event that is to be considered an *education* event.

Although they are similar, each of the three units has its own elements. The following sections describe what would be required to support a complete IVEE lesson–all three units. *All* of the materials would be distributed to the teacher before the pre-interactive-videoconference unit. The materials are here separated into sections to give a better example of what support is needed for each unit. The notion of distributing all materials before the start of the process is ***to make the IVEE lesson as light a load as possible for the teacher.*** *The teacher should be concentrating on student needs rather than developing materials.* The success of IVEE lessons is predicated on *making the IVEE lesson as much a turnkey operation as possible.*

Key Elements (Best Case) Required to Support a Pre-Interactive Videoconference Unit

The best-case support for the unit preceding the interactive videoconference includes:

- an overview of the entire lesson with overall objectives and any information which supports the lesson's effectiveness
- a step-by-step lesson plan
- any teacher background information (as needed)
- a test or assessment plan to measure the desired learner performance
- any student handouts and difficult-to-obtain materials (commonly available materials would be provided by the teacher)

These support materials could be distributed in a number of ways–for example, on CD-ROM, through the Internet, or through professional associations. The distribution method should *never* drive the content or objectives. The distribution method should make a teacher's work easier, not harder.

As mentioned earlier, *all* materials (i.e., materials for all three units in the lesson) should be given to the teacher *before* the lesson starts. In this report the materials are listed unit by unit in order to show how they support each unit.

Key Elements (Best Case) Required to Support an Interactive Videoconference Unit

The best-case support for the interactive videoconference unit includes:

- background information about the class; this is gathered prior to the videoconference in order to personalize the contact with the learners
- a script for the presenter; the script covers the essentials of the lesson and allows the presenter to
    - include new material to reinforce the learning
    - add new events related to the topic
    - add motivational information and related ISS information
- a script for technical director to use as the presenter calls up video clips, graphics, websites, and other related material
- presentation support materials referred to above (e.g., slides, video clips)
- step-by-step lesson plan and outline of presenter's script
- student handouts and difficult-to-obtain materials

The teacher receives all of the above materials with the exception of the technical director's script. As mentioned above, support materials could be distributed in a number of ways, and the distribution channel should *never* drive the content or objectives.

Key Elements (Best Case) Required to Support a Post-Interactive Videoconference Unit

The best-case support for the unit following the interactive videoconference includes:

- a step-by-step lesson plan for follow-on activities
- a test or learner assessment materials or a description of ways to assess the learning
- student handouts and any difficult-to-obtain materials
- data collection instruments to gather information for ISS and for NASA

The teacher is not obliged to assess the students in the manner suggested. However, having a test (or method of assessment) keeps the test congruent with the stated objectives, and relieves the teacher of developing a separate test. In the case of Education Category 3 IVEE lessons, the assessment methods would conform to national guidelines. A worthy ISS goal would be to secure the approval of the assessment method and any tests from the professional group endorsing the guidelines.

Developing an IVEE Lesson: A Condensed Process Overview

The process used to develop an IVEE lesson follows the general instructional design model used both in education and in business/industry/organization training. While generic, the process below relates to *Criterion Referenced Instruction* (Mager), a widely accepted instructional design/development process. Not indicated in the process below (but highly recommended) is the use of a learning psychology taxonomy (Gagne preferred, Bloom or Guilford acceptable).

The key steps in a greatly simplified process to develop an IVEE Lesson include:

- select topic/goals; this may come from a number of sources–for example, from teachers' requests, from national guidelines, from existing NASA materials, from special events
- review currently existing NASA resources related to the objectives; if there is resources are scarce and/or the ROI for the lesson is low, the project may be set aside until adequate resources are available
- write objective(s)
  NOTE: the first three steps may occur in a different sequence, depending on the rationale and process for topic selection
- *write assessment (test);* this is italicized to emphasize its position in the development process; writing the test before the writing the lesson insures that the lesson stays in sync with the test and the objectives

- develop subobjective list (hierarchy format); in this step the skills or performances are analyzed and any subskills to be learned are identified
- outline units (pre-interactive videoconference, the interactive videoconference, post-interactive videoconference)
- review the outline, identify any existing resources (for example, student activities, materials, visual materials) and insert them into the outline
- start the scripting activity by writing any bridges to tie together the existing resources; also, make any modifications in the existing resources
- complete the lesson by writing and producing any missing segments of the lesson

At each step, there must be a review and revision process. This is a normal protocol for quality assurance. In Education Category 4, units are extensively tested with the appropriate learner group(s) before the revisions are made. Revisions are also tested until the learner performance matches the desired performance.

The desighn/development process will undoubtedly be adapted to fit International Space Station's specific needs. Three points are worth repeating.

First, the objectives should be clearly stated and stated *as learner performances*–overt, measurable actions that the students will (or should be able to) perform.

Second, the assessment method and/or any assessment instruments should be developed immediately after the objectives are determined and before the units are written. This forces "teaching to the test." Teaching to the test is not a bad thing. More often than not, objections to teaching to the test indicate a bad test–rather than a bad approach to teaching. For example, when we teach students to drive, we teach them to pass the driving test. If the driving test is too easy, the training will be too easy. In this case, the test should be improved–then, the training would improve to match the test.

Third, the development process should be focused on helping students learn without creating an additional burden on the teacher. The more the burden of information presentation and materials development is lifted from the teacher, the more opportunity the teacher has to coach students and assist them as individuals. *The goal of the IVEE lessons should be to free teachers for the very difficult task of classroom management and meeting the needs of each student.*

The success of outreach (of any form) into the education community lies with *reducing*–not increasing–the workload of busy teachers.

Selecting Topics for Interactive Videoconferencing Educational Event (IVEE) Lessons

Assuming that International Space Station does go forward with the development of IVEE lessons, the next question is "Where to begin?"

The answer depends on International Space Station's goals, policy, *and resources*. The key to developing the IVEE lessons lies with the availability of instructional designers, already produced materials, and media producers (in that order).

For example, if the goal is to get started quickly, develop modules which require the minimum amount of resources (especially instructional designers) and utilize already developed activities and projects. This jump-starts the development process and gets lessons into the pipeline. However, as more lessons are developed, the pool of available materials will inevitably dwindle.

After those easy-to-select lessons are done, International Space Station will be obliged to develop a process to examine other potential sources of topics, for example:

- teacher guides from other content areas
- national (and regional or large-state) curriculum guidelines
- requests from clients (teachers, administrators, et al.)

At some point (better sooner than later), ISS needs to identify the customer groups and to gather the *Voice of the Customer* for each customer group. Customer requirements will vary from customer group to customer group.

Do not treat customers as though they all belonged to the same group.

It is also worth using special information-gathering techniques (like Kano analysis) to discover what excites each client group; then, set priorities.

The Education Community as Customers

International Space Station is creating materials to supplement school curriculum. As a group outside of the schools (i.e., not directly responsible for operating schools) ISS must regard those who use the IVEE lessons as customers. ISS outreach staff must understand that while the learner is ultimately the user of the materials, learners do not select the curriculum nor the lessons taught to them. A variety of education professionals–each with different needs and agendas–chooses what reaches the learners. Those education professionals include:

- superintendents and administrators
- curriculum supervisors
- teachers

Curriculum materials will appeal to each group for distinctly different reasons.

For example, superintendents (and principals with curriculum authority) may select materials on the basis of budget, ease of integration into an existing curriculum, pressures from parents and the school board, and *contribution to improved scholastic measures* (with students considered as groups rather than as individuals).

While curriculum specialists have many of the concerns that line administrators do, curriculum specialists may not have the direct authority to mandate use of curriculum materials. Hence, their choices may be affected more by peer and administrative recognition, as well as teacher acceptance. Curriculum specialists may focus on a specific area (for example, math) to the exclusion of other areas (like technology).

When considering new curriculum, teachers probably favor ease of use (almost a turnkey operation), improved student attention and participation, improved student performance (for the group *and* for individual students).

Students, who have no intrinsic power over curriculum decisions, want something interesting and fun.

To have materials accepted and used, International Space Station must treat the audiences as different, and market to each on a different basis at different venues–all without forgetting the true consumer, the learner.

Summary

It is time for the International Space Station outreach to take the next step–to develop true education events, i.e., performance-based, learner-centered lessons. At the same time, ISS outreach should continue its general communications which inform the public at large.

ISS education events are structured around an interactive videoconference between ISS staff and learners. The interactive videoconference is preceded by activities that prepare learners for the videoconference. The videoconference is followed by wrap-up and evaluation activities.

ISS education events must conform to the standards used in the education profession and appeal to a variety of educators.

Lesson Plan Prototype for International Space Station's Interactive Video Education Events

22
IN-18

Final Report

NASA Summer Faculty Fellowship Program

Johnson Space Center

Prepared by:	Thomas Zigon
Academic Rank:	Assistant Professor
University & Department:	Rochester Institute of Technology Biomedical Photographic Communications

NASA/JSC

Program:	International Space Station
Unit:	Management Operations
Group:	Communications and Information Management - OA13
JSC Colleague:	Lyn Gordon-Winkler
Date Submitted:	August 20, 1998
Contract Number:	NAG 9-867

Abstract

The outreach and education components of the International Space Station Program are creating a number of materials, programs, and activities that educate and inform various groups as to the implementation and purposes of the International Space Station.

One of the strategies for disseminating this information to K-12 students involves an electronic class room using state of the art video conferencing technology. K-12 classrooms are able to visit the JSC, via an electronic field trip. Students interact with outreach personnel as they are taken on a tour of ISS mockups. Currently these events can be generally characterized as:

- Being limited to a one shot events, providing only one opportunity for students to view the ISS mockups
- Using a "one to many" mode of communications
- Using a transmissive, lecture based method of presenting information
- Having student interactions limited to Q&A during the live event
- Making limited use of media
- Lacking any formal, performance based, demonstration of learning on the part of students

My project involved developing interactive lessons for K-12 students (specifically 7th grade) that will reflect a 2nd generation design for electronic field trips. The goal of this design will be to create electronic field trips that will:

- Conform to national education standards
- More fully utilize existing information resources
- Integrate media into field trip presentations
- Make support media accessible to both presenters and students
- Challenge students to actively participate in field trip related activities
- Provide students with opportunities to demonstrate learning

This lesson plan prototype has been prepared for delivery to educators on a CD-ROM. Word processing text, HTML versions of the plan, and digital copies of all still and motion media that would be used in the proposed videoconference are included on the disc. The following screen captures are indicative of how the lesson plan would be presented as an HTML document.

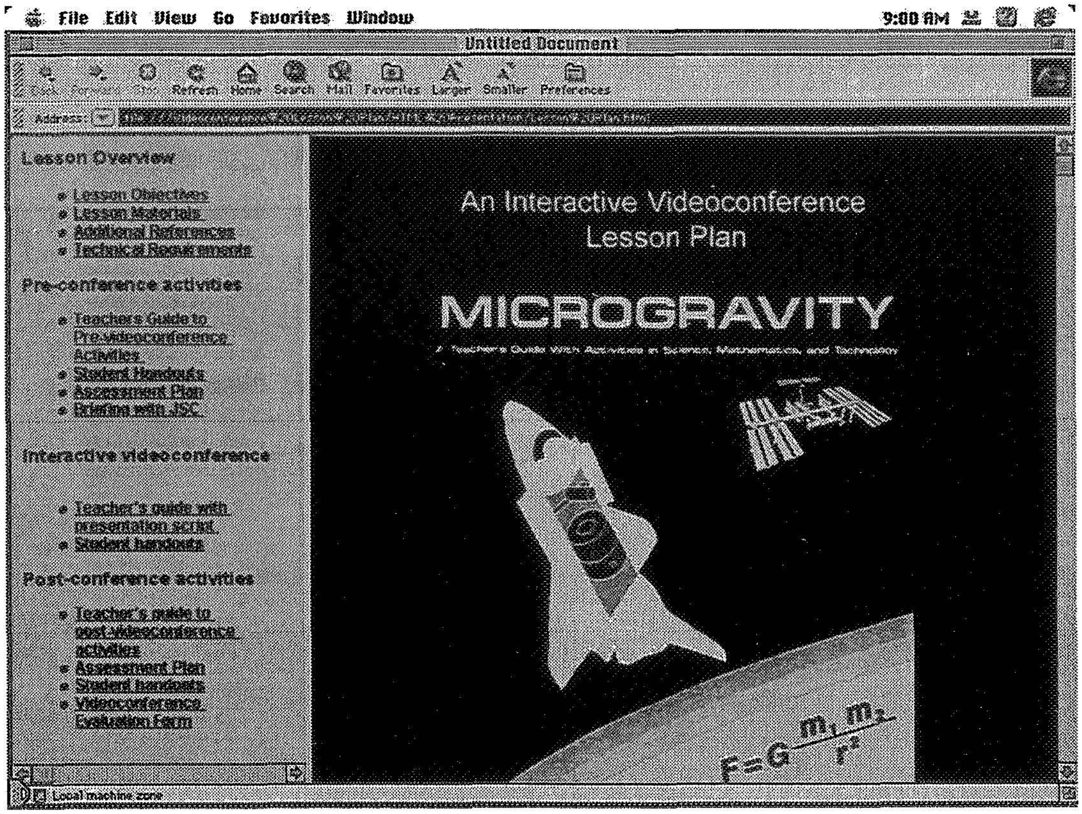

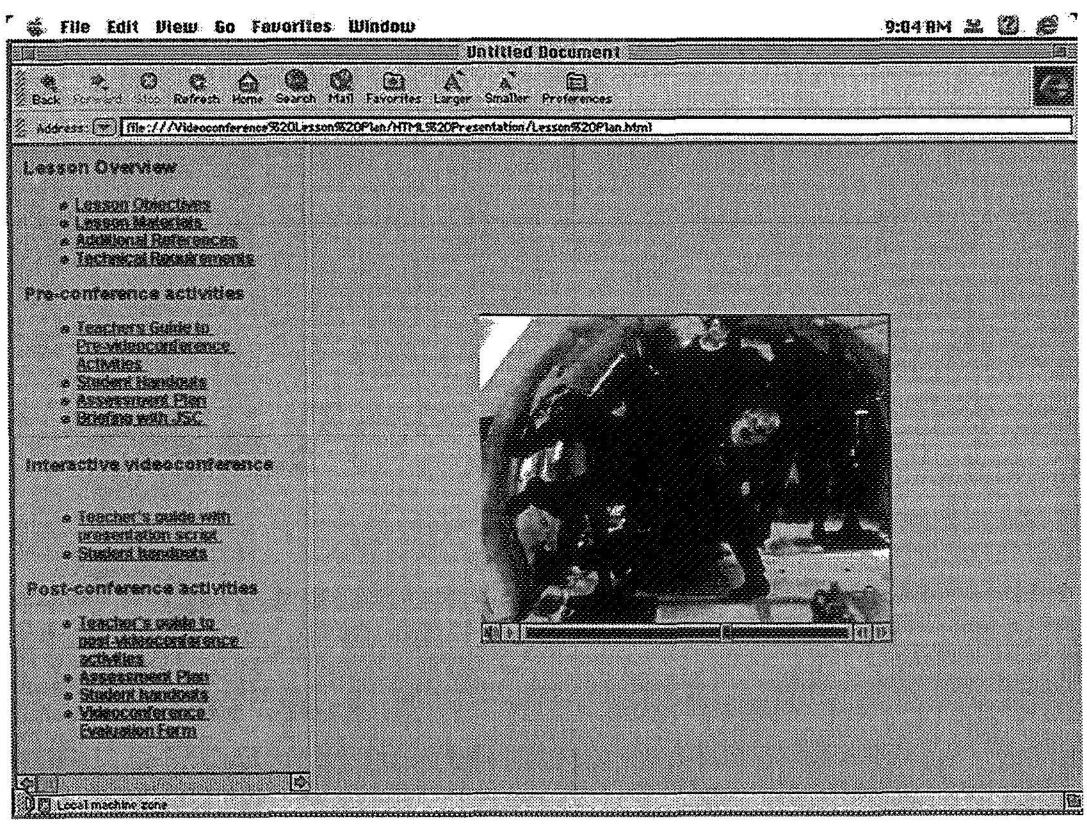

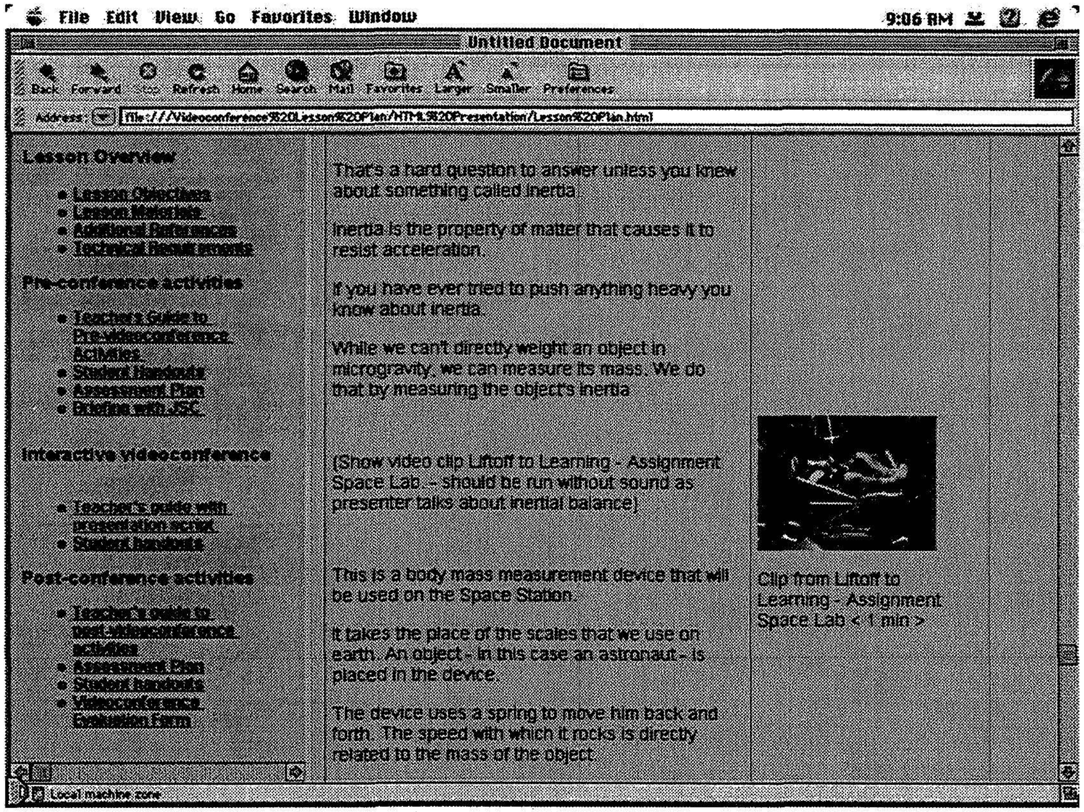

The pages that follow represent most of the components of the lesson plan's content. The aspect of the lesson plan not represent in this final report would be the fully scripted program (with appropriate media support,) that would be used by the Johnson Space Center presenter during the interactive videoconference.

Interactive Video Education Event Lesson Plan
Microgravity Environments

Overview

These materials are intended to support the learning activities associated with an interactive videoconference available from the Johnson Space Center. Designed for 6th and 7th grade students, the videoconference offers an exciting opportunity for you and your students to discuss principles of microgravity with scientists, engineers and technicians currently work in the International Space Station Program.

Lesson objectives

As a result of the information and activities presented in this lesson, your students, if successful, will be able to:

- Describe ways in which scientists create microgravity environments here on earth.
- Use an accelerometer to measure the effects of gravity in free fall
- Describe in their own words how a spacecraft stays in orbit
- Describe how a microgravity environment is created on an orbiting spacecraft
- List the advantages of microgravity in orbit compared to the "microgravity-like" environments that can be created on earth
- Describe in their own words how mass is measured in microgravity
- Calculate the mass of an object using an inertia balance

Lesson materials:

"Microgravity Teacher's Guide with Activities in Science Mathematics and Technology" (EG-1997-08-110-HQ) pages 1-12, 15-16

Liftoff to Learning Video Series
    Space Basics (videotape and resource guide)

Student Activities
    "Microgravity in the Classroom" (Microgravity Teacher's Guide pg. 79)
    "Around the World" (Microgravity Teacher's Guide pg. 95)
    "Accelerometers" (Microgravity Teacher's Guide pg. 88)
    "Inertial Balance" (Microgravity Teacher's Guide pg. 101)

Additionalreferences:

As you prepare for this lesson on Microgravity you may want to consider the following references for yourself and your students:

Books for the student

1. Ardley, N. "The Science Book of Gravity," Gulliver Books, Harcourt Brace Jovanovich, San Diego, 1992.

2. McKay, David W. and Smith, Bruce G. "Space Science: Projects for Young Astronauts." Franklin Watts, New York, 1986.

3. Sumners, Carolyn. "Toys in Space: Exploring Science with the Astronauts," TAB Books, Division of McGraw-Hill Inc., Blue Ridge Summit, PA 17294-0850, 1994.

4. Skurzynski, Gloria. "Almost the Real Thing: Simulation in Your High-Tech World," Bradbury Press, New York, 1991, pp. 25-30.

5. Skurzynski, G. Zero Gravity, Bradbury Press, New York, 1994.

6. VanCleave, J. Janice VanCleave's Gravity, John Wiley & Sons, Inc., New York, 1993.

Books for the teacher

1. Antar, Basil N., and Nuotio-Antar, Vappu S. "Fundamentals of Low Gravity Fluid Dynamics and Heat Transfer," CRC Press, Boca Raton, Florida, 1993.

2. Craft, Cathy, and Hernandez, Judy, "Mars: A Simulation of Human Exploration of Our Solar System's Fourth Planet," Interaction Publishers, Inc., Lakeside, California, 1992. 3. Eddington, A. Space, Time and Gravitation, Cambridge University Press, 1920, p.93-109.

4. Gonick, Larry, and Huffman, Art, "The Cartoon Guide to Physics," Harper Collins Publishers, New York, 1990, Chapters 1-5.

5. Wheeler, J. A Journey into Gravity and Spacetime, Scientific American Library, New York, 1990.

Technical Requirements

Electronic field trips to NASA's Johnson Space Center are made possible through the use of low bandwidth video-conferencing technology using ISDN data lines.

To participate you must have the following:

- Access to a 2B+D ISDN line. This is a 2-bearer channel at 56Kb/s or 64Kb/s per line and one 16Kb/s data channel. ISDN service can be obtained from your local telephone company
- One Network Terminator Adapter (NT1). Available from your local phone company
- One H.320 compatible videoconference system. The video conferencing system may be either a:
    - Fully integrated desktop system available from manufacturers such as Picture Tel or VTEL
    - A component system built around an existing Pentium class personal computer with an installed video conferencing kit. These kits are also available from manufacturers such as Picture Tel or VTEL
- Your school or sponsoring organization will have to initiate and fund the call to the Johnson Space Center

Once you confirm that your organization has access to the appropriate low bandwidth videoconferencing equipment, you will need to make a test call to the Johnson Space Center several days before the event to test the system's compatibility.

Please contact Sheila Bass at (281) 244 7325 or E-mail at sbass@ems.jsc.nasa.gov with any questions or concerns.

Pre-videoconference Activities

Teachers Guide to Pre-videoconference Activities

Obtain a copy of the "Liftoff to Learning: Space Basics" videotape and resource guide (item 077.6-25V). For more information about obtaining NASA CORE materials, call (440) 774 - 1051 or visit the CORE website at www.teacherlink.usu.edu/nasa/accessnasa/core.html.

Review the following background information on Microgravity:

"Microgravity Teacher's Guide with Activities in Science Mathematics and Technology" (EG-1997-08-110-HQ) pages 1-12, 15-16

"Liftoff to Learning Video Series - Space Basics" resource guide pages 2-5

Review the student readings, gather the needed materials, construct the apparatus, and familiarize yourself with the procedures necessary to help your class do the following activities.

- "Around the World" (Microgravity Teacher's Guide pg. 95-100)
- "Microgravity in the Classroom" (Microgravity Teacher's Guide pg. 79-87)

Have your class break up into small groups and do the "Around the World" activity as outlined on pages 97 - 100 of "Microgravity Teacher's Guide with Activities in Science Mathematics and Technology."

Coach student and answer questions as needed.

Collect student worksheets at the end of the activity.

Distribute the videotape study questions (as an advanced organizer to the showing of "Space Basics") Ask students to think about how they would answer the study questions as they watch the tape.

Show "Liftoff to Learning - Spaces Basic" video.

Review the student's answers to the videotape study questions.

Split the class into three groups and assign one of the following demonstrations to each group:

"Falling Weight Apparatus" (Microgravity Teacher's Guide pg. 84-85)
"Falling Water" (Microgravity Teacher's Guide pg. 86)
"Can Throw" (Microgravity Teacher's Guide pg. 87)

Ask each group to practice their demonstration and prepare to present it to the other groups.

Supervise student preparations and provide help as needed.

Have each group explain what they will be doing in their demonstration and ask the rest of the class to predict what will happen based on what they learned from the Liftoff to Learning video.

Assessment Plan

Collect the Around the World worksheet. Check item five to make sure students can accurately describe, in their own words, how a spacecraft stays in orbit.

Give the class an essay assignment (see student handouts) in which they are asked to explain how a microgravity environment is created on an orbiting spacecraft. The assignment asks the students to make reference to diagrams depicting the concepts acceleration's effect on weight and the falling path of an orbiting body.

Key points that should be included in the essay are:

- The cannon diagram series shows that a combination of forward velocity and the pull of gravity cause the cannonball to fall in an arc path.
- The greater the velocity of the cannonball, the further it will travel in an arc path before it falls back to earth
- With enough velocity, the cannonball will travel all the way around the earth in a continuously falling path
- Like the cannonball, a spacecraft in orbit is really in a continuous free fall path around the earth.
- In the elevator diagram, the apparent weight of an object will change depending on the direction of movement. The mass of an object remains the same.
- In free fall all objects fall at the same rate and appear to be floating
- On a spacecraft in free fall orbit around the earth, all objects on board are falling at the same rate and appear to be floating. This is known as a microgravity environment.

The primary indicators of student learning for these pre-videoconference activities will be the Student Worksheet for the "Around the World" activity and the essay assignment. Additionally, you may wish to have your students answer and turn in the Liftoff to Learning study questions as well as submit written predictions of what will happen in the "Microgravity in the Classroom" activities.

Background Report to JSC

In order to personalize this experience for your students, it is recommended that prior to the event you contact the Johnson Space Center. Please contact Sheila Bass at (281) 244 7325 or E-mail at "sbass@ems.jsc.nasa.gov". She will gather some background information from you, and if possible, she will arrange for you to speak with the presenter who will host the videoconference.

The goal of this background report is to help the presenter relate to you and your class in a more personal way and encourage greater two-way communication during the actual event.

You may want to discuss such things as:

Microgravity related discussions or activities that you've already covered with your students
Students that you'd like to recognize
School events
Sports team accomplishments
Community current events

Interactive Videoconference

Teacher's Guide

During the videoconference the presenter will be talking about the relationship between acceleration and apparent weight. He or she will mention the Accelerometer activity that is outlined on pages 88-94 of "Microgravity Teacher's Guide with Activities in Science Mathematics and Technology" (EG-1997-08-110-HQ). You may want to build one of the devices illustrated and have it available to pass around as the presenter talks about it.

The presenter will also be introducing the concept of weighing objects (measuring their mass) in a microgravity environment. He or she will be referring to the Inertial Balance activity outlined on pages 101-108 of "Microgravity Teacher's Guide with Activities in Science Mathematics and Technology" (EG-1997-08-110-HQ). You may want to build an example of the device illustrated on page 102 and have it available to show in class as the presenter talks about it.

The videoconference has been designed for a 50-minute interchange. The goal of this event is a meaningful, two-way exchange between the presenter and your class. To that end, the presenter will limit his or her comments to approximately 30 minutes. Please encourage your class to feel comfortable asking questions at any point in the presentation and remember that there will be about 20 minutes allotted for open discussion and questions.

Students should be encouraged to jot down ahead of time any questions they'd like to ask.

You may want to talk with your students about the fact that this will be a two-way videoconference. It won't be like watching television at home. You and your students will see and hear a presenter speaking from the Johnson Space Center at the same time that presenter sees and hears everything that is happening at your location.

Post-videoconference Activities

Teacher's Guide to Post Videoconference Activities

Review the student readings, gather needed materials, construct several inertial balances (depending on class size), and familiarize yourself with the procedures necessary to facilitate your class doing the following activities.

- "Accelerometers" (Microgravity Teacher's Guide pg. 88-94)
- "Inertial Balance" (Microgravity Teacher's Guide pg. 101-108)

During the videoconference the presenter talked about acceleration. Review that discussion with your class.

Have each student construct and calibrate an accelerometer as outlined in the activity guide. Ask your students to list two or three situations, outside of school, where they may experience gravitational forces less than or greater than 1G. For homework ask the students to conduct an investigation using their accelerometers to measure the gravitational forces in the situations they identified.

Ask your students to be prepared to report their findings to the class.

During the videoconference the presenter talked about inertia and how mass is measured in a microgravity environment. Review that discussion with your class.

Have the class breakup into smaller groups, calibrate their balances and measure the mass of several small objects. Have the students list (on their worksheet) each object they measured.

Assessment Plan

Collect the student worksheets for the "Measuring Mass With Inertia" activity. Check to see that the students had accurately constructed and interpreted their calibration graph and that the masses they were calculating were reasonable (given the objects they were measuring) Check their answers to the questions on Student Work Sheet - 3.

Collect the accelerometer homework assignment. Ask for several volunteers to report their findings to the class. Note any unique situations that were measured.

Give the class an essay assignment (see student handouts) in which they are asked to describe ways that microgravity environments can be created on earth, and how scientists measure the mass of an object in a microgravity environment.

Key points that should be included in the essay are:

- True microgravity requires sustained free fall outside the drag of earth's atmosphere. Technically therefore microgravity cannot be created on earth.
- However, on earth, reduced gravity environments can be sustained for brief periods of time
- Use of drop towers, sub-orbital rockets, and aircraft flying parabolic patterns are ways in which reduced gravity can be created on earth.
- Aircraft flying parabolic patterns offer the longest period of reduced gravity (up to 15 seconds
- While students may cite some of the ways weightlessness is simulated at the Johnson Space Center (eg. the neutral buoyancy lab or the precision air-bearing floor), technically these are not microgravity environments. Students should be aware of the difference between a simulation and actual microgravity.
- Scientists measure the mass of an object in microgravity indirectly by measuring the object's inertia
- Inertia is the property of matter to resist acceleration
- Objects are placed in spring measurement device that will vibrates the object back and forth
- The greater the mass, the slower the object will vibrate.

Videoconference Evaluation Form

Lesson Topic: "Microgravity Environments"

JSC Video Host:

Presentation Date:

School:

Grade Level:

Number of Students Participating:

Indicate the degree to which you agree with the following statements:

- This interactive video education event (IVEE) has been a positive learning experience for my students

  Strongly Agree Agree Neutral Disagree Strongly Disagree

- My students were generally able to demonstrated the learning performances outlined in the IVEE lesson plan

  Strongly Agree Agree Neutral Disagree Strongly Disagree

- I will be able to fulfilled specific curriculum requirements by participating in this interactive video education event.

  Strongly Agree Agree Neutral Disagree Strongly Disagree

- The lesson plans for this interactive video education event provided me with enough direction and support to adequately facilitate student learning.

  Strongly Agree Agree Neutral Disagree Strongly Disagree

- The lesson plans provided adequate testing recommendations for assess my student's learning.

  Strongly Agree Agree Neutral Disagree Strongly Disagree

- The videoconference content and presentation length were appropriate for my grade level

  Strongly Agree Agree Neutral Disagree Strongly Disagree

- There was enough time allotted for my students to ask questions.

  Strongly Agree Agree Neutral Disagree Strongly Disagree

- Where there learning objectives that were clearly more difficult than others for your students to master

  Strongly Agree Agree Neutral Disagree Strongly Disagree

What modifications, if any, would be needed for this lesson to fully comply with your curriculum requirements?

What features of the IVEE lesson plans did you find most helpful?

How can we make the IVEE support materials more effective for you?

How much time was allotted for pre and post event activities?

What other hands-on activities, that relate to lesson objectives, would you like to see included in this lesson plan

Does your classroom have access to the Internet?

SUPPORT FOR ASTRONAUT'S VIEW OF MEXICAN/CENTRAL AMERICAN FIRES AND ON-LINE EARTH OBSERVATIONS TRAINING MANUAL

Final Report

NASA/ASEE Summer Faculty Fellowship Program - 1998

Johnson Space Center

23

IN-43

Prepared by:	Charles F. Kaminski, Jr.
Academic Rank:	Undergraduate Student
University & Department:	University of Nebraska at Kearney Department of Physics Kearney, NE 68849

NASA/JSC

Directorate:	Life Science
Division:	Earth Science and Solar System Exploration Division
Branch:	Office of Earth Science
JSC Colleague:	Dr. Kamlesh Lulla
Date Submitted:	September 14, 1998
Contract Number:	NAG 9-867

ABSTRACT

A small project to compile remote sensing and in-site data to review the processes leading to the May 1998 Mexican/Central American fires was undertaken. A web page based on this project was assembled. The second project initiated involved an interactive and on-line program that will replace the paper version of the Earth Observations Preflight Training Manual. Technical support was provided to Prof. Marvin Glasser as needed.

SUPPORT FOR ASTRONAUT'S VIEW OF MEXICAN/CENTRAL AMERICAN FIRES

Introduction

The smoke that entered the southern states of the US during the Spring and Summer of 1998 originated from thousands of wildfires in Mexico and Central America. This was a continuation of seasonal burning practices that has accelerated since the early 1980's. Astronauts have been photographing fires in this region for more than 20 years. To better inform the scientific community and the general public about the fires and their effects, a web site was developed. Assistance was necessary to publish the web page to the public in a timely fashion.

Purpose

To assist and provide technical support to Prof. Glasser. This comprised of assisting in the search through uncataloged remote sensing data for pertinent information, analyzing air-quality data, converting analog video into Quicktime format, searching internet resources for secondary information, and building of the actual web site. A full report of the project can be found in section eight of this publication.

Conclusion

The end result of this project was a web site that can be found at "http://eol.jsc.nasa.gov/newsletter/Mexico_Burning/".

On-line Earth Observations Training Manual

Introduction

JSC's manned platform imagery database contains more than 300,000 photos spanning over a 30 year period. These photos are used to study such things as deforestation, soil an land degradation, coastal erosion an build-up, desertification, soil salinization, long-range dust transport, volcanic activity, hydrologic changes, and stream and reservoir sedimentation. The astronauts must train before each mission to be able to identify specific sites to photograph. They must also learn to optimizes the value of each photograph taken by studying specific photographic techniques.

The Earth Science Branch prepares a training manual before each mission with terrestrial and water sites chosen for that mission. The large paper-bound manual is not portable or indexed.

Purpose

To create an electronic version of the Earth Observations Training Manual that is portable and searchable. Mission Leads must be able to change and update new versions of the electronic manual efficiently. The electronic manual must also allow astronauts to quickly gain more information about a topic of interest if more information is available. The site data should also be in a standardized format to be shared with other JSC computer programs, but this is not a requirement.

Requirements and Limitations

Requirements:
- System must be searchable by keyword
- System must support hyperlinked text
- Sites must be easily added and removed
- System must be easy to maintain

Limitations:
All required information, pictures, and programs must fit on to one CD with a current capacity of 650 MB.

Files cannot be added or deleted to the hard drive of the astronaut's laptop.

The system must function properly from a CD on an astronaut-issued laptop with a screen of 800 / 600 pixels, running Windows 95.

Platform Analysis

Four platforms were considered for the system.

Visual Basic

Pros Visual Basic offers a completely self-contained system. There are no version conflicts as with HTML or JAVA and Visual Basic allows the programmer almost complete control when building the interface. The system interface could be updated dynamically according to what sites are available in the data files. Also, a simple keyword search could easily be programmed into the system.

Cons Visual Basic has no hyperlink function and requires a work-around to be programmed into the interface. Visual Basic also does not have a widely know and standardized format for reading data files and incorporating pictures. This would require specific training for the mission leads who would be ultimately responsible for maintaining the system. Incorporating the text and pictures for a terrestrial or water site directly in the program is not an option because the system must be dynamic. Finally, Visual Basic sometimes requires files to be installed in the system folder especially when plugins are used. This is not an option for the astronaut laptops.

Microsoft Word

Pros Microsoft Word allows a user to quickly organize text and pictures into a paper-like layout. A Microsoft Word based system would be easy to maintain and change. All Earth Science Branch employees are familiar with Microsoft Word; eliminating the need for more training. Also, version conflicts would not be a problem because of Microsoft's track record of maintaining backward compatibility. Microsoft Word would also enable a users to easily print out terrestrial or water sites if a hard copy is needed.

Cons Microsoft Word has an extremely poor on-line interface for studying data stored in multiple files and on multiple pages. Microsoft Word's find function does not support keyword indexing.

Windows Helpfile Format

Pros With the Helpfile format, indexing and searching is automatic. Creating a helpfile simple as well. Helpfiles are written in RTF format using Microsoft Word.

<u>Cons</u> Incorporating pictures is difficult with Helpfiles. Compiling also requires training. Finally, the Helpfile interface cannot be customized to suit the system's needs.

<u>HTML / JAVA</u>

<u>Pros</u> Internet Explorer 3.02 is already loaded onto the astronaut laptops. HTML provides a standardized format for the data that is supported by many programs. Using HTML would allow the astronauts to utilized a web browser with a well known interface.

<u>Cons</u> The mission leads within the Earth Science Branch may not be able to easily update the system interface. Updating the interface would fall to an employee familiar with HTML and JAVA. Also, a large, self-contained search engine that supports HTML would need to be loaded onto the CD unless a JAVA based solution can be found. Finally, Microsoft Internet Explorer Version 3.02 does not fully support JAVA. This is a major problem that will need to be worked around.

An HTML / JAVA solution was chosen for the system. HTML provides a standardized interface through Microsoft Internet Explorer that the astronauts are already familiar with. HTML supports hyperlinking and a JAVA based search engine was also found to incorporate into the system; thus eliminating the need for a self-contained search engine. Finally, other departments will benefit from the data to be incorporated into their systems because HTML is so widely supported and standardized. Some Earth Science Branch Mission Leads are already familiar with HTML and HTML editors which may increase the maintainability of the system.

JAVA Search Engine Analysis

JObjects Indexer was chosen to index the On-line Earth Observations Training Manual. The JAVA program automatically indexes specified web sites and also provides an IE 3.02 compatible applet interface.

Conclusion and Discussion

A web interface and two template terrestrial sites were built and indexed. The interface also includes a clickable map of the world, a JAVA-script based listing of all available sites, and the search engine interface. Documentation was also included to explain how to install the JAVA indexer,

build the search index, and configure the astronaut laptops.

Three training session were also given to Earth Science Branch Mission leads. The training sessions included using the system, going over the system documentation, building terrestrial and water sites, and tips for keeping the system modular.

The primary difficulty with the project was ensuring that all necessary JAVA commands were IE 3.02 compatible. Those that were not, required work arounds.

COMPUTER AIDED MODELING TO DETERMINE THE EFFECTIVENESS OF RESISTIVE EXERCISES AS COUNTERMEASURES FOR BONE MINERAL DENSITY LOSS

(34)

IN-52

Final Report

NASA/ASEE Summer Faculty Fellowship Program - 1998

Johnson Space Center

Prepared by:	Benjamin M. Murphy
Academic Rank:	Master's Level Graduate Student
University & Department:	The University of Alabama Department of Mechanical Engineering Box 870276 Tuscaloosa, AL 35487-0276

NASA/JSC

Directorate:	Space and Life Sciences
Division:	Medical Science
Branch:	Life Sciences Research Laboratories
JSC Colleague:	Linda C. Shackelford, M.D.
Date Submitted:	August 7, 1998
Contract Number:	NAG9-867

ABSTRACT

Due to the loss of gravitational loading, astronauts have a tendency to lose bone mineral density in their lumbar spine and lower extremities on orbit. NASA requires astronauts to perform exercises during space flight to help reduce the amount of demineralization. To test these exercises on earth, 17 week bed rest studies are conducted that consist of specific diet and exercise regimes. Developing a finite element model of these exercises will help to quantify the stress distribution imposed by of each of these exercises.

To help develop this model, MRI images are acquired from individuals participating in the bed rest studies. The MRIs can be used to create a subject specific model of each individual for testing. The MRIs are processed in the Magnetic Resonance Imaging Data Transfer System program to develop a three-dimensional finite element model of the femur for evaluation.

Modifications were made to the MRIDTS that simplified the model creation process. These modifications made it possible to construct two separate models of different portions of a bone simultaneously and then later connect them manually. This helped alleviate the warping problem associated with the drastic changes in geometry found in some body parts, such as the joints. The code was also modified to incorporate material properties of various bone components into the model. Interior meshing was also incorporated into the program to allow for both the cortical shell and the entire bone to be modeled.

A prototype model of the right femur of an adult female is being constructed and tested to determine the feasibility of finite element analysis as a tool for evaluating exercise effectiveness. The model is being run through the ANSYS finite element program on the Alabama Super Computer Network. After the model is validated, models of bedrest subjects can be genereated to investigate exercise countermeasures.

INTRODUCTION

In recent years, more and more engineering calculations are done using computer software. The finite element method has greatly decreased the time required to perform stress analysis on objects with highly complex geometry, including problems related to the human body [1]. As the performance of computer hardware and software has increased, the accuracy of the models has improved. With today's software, models from internal combustion engines to human bone can be more easily processed.

Astronauts face the problem of bone demineralization and muscle atrophy, which becomes more significant with increased mission length [2]. According to Wolff's Law, bone remodels to the stresses placed on it [3]. Since astronauts on orbit do not have continuous gravitational loads placed on their lower extremities and lumbar spine, they tend to show noticeable mineral loss in these regions. To counteract muscle atrophy and bone demineralization, NASA requires astronauts to exercise during their time in space. By performing these exercises, stress is placed on the bone, which should decrease the rate of demineralization.

To develop more effective countermeasures, the different stress distributions induced by different exercises can be compared to the distribution of stress due to weight-bearing. To properly perform these analyses, a subject specific model needs to be developed for each participant in the testing program. Producing a model of human bone is challenging due to the complex geometry and the difficulty involved in gathering data. Most models are developed in a generalized manner using cadaver samples. To develop a model specific to an individual, a non-invasive technique must be used. This can be accomplished using computer tomography (CT) scans or magnetic resonance imaging (MRI) [4-5]. NASA prefers to use MRI since it does not require the subject, often an astronaut, to be given multiple doses of radiation [5]. Astronauts are continually bombarded with radiation in space, and therefore minimizing their exposure during testing is very important.

The MRI Data Transfer System (MRIDTS) was developed by Todd and Wang [6] to facilitate the generation of finite element models from MRI data provided in bitmap format. This computer program provided the basis for generating the model in this project.

The two goals of this project are to 1) modify the software to increase efficiency when developing a subject specific model and 2) develop a prototype model to be tested with a weight-bearing load.

SOFTWARE DEVELOPMENT

The MRIDTS software was developed in Visual Basic to run on a standard desktop computer using Windows 95 or higher operating system [6]. Consecutive serial transverse MRIs in bitmap format are used to develop a three dimensional model of a body component.

The model is developed by taking the area of interest in each slide, meshing that area, and then extruding the two-dimensional meshes into the third dimension. The images used to develop the prototype model were taken from a 41-year-old female who is approximately 66 in. tall and weighs approximately 128 lbs.

Using the MRIDTS

The MRIDTS has a graphical user interface (GUI) which is very familiar to any user of WINDOWS software [6]. After executing the program, the user opens the first bitmap MRI file. Selected points are then chosen around the outer edge of the area of interest. A cubic spline is fit to the selected points, forming an enclosed area. The user then inputs the number of divisions (essentially the number of nodes per spline) for the spline. (Note that the number of divisions needs to be divisible by four in order for the new "solid" model code to function properly.) Points along the interior edge of the area are then selected, a second spline is fit, and the spline is divided into the same number of sections. These two subdivided splines are then connected together to form a two-dimensional mesh of the selected area. The process is continued with the next slide in the same fashion. As each slice is meshed in two dimensions, it is stacked on top of the previous mesh. Once the two-dimensional meshes are connected, they form a three-dimensional model with 3-D SOLID64 anisotropic brick elements. The node and element information can be written into ASCII files in either NASTRAN or ANSYS format. This technique is very efficient for modeling the diaphysis of a long bone, such as the femur. Regions such as the femoral head, which have significant changes in geometry on adjacent images require significant manual intervention. To create models with fewer manual modifications of node and element information, additional features were added to the program.

MRIDTS Modifications

The MRIDTS program has difficulty handling complex changes in geometry that are often found in components of the body. Although the images used in this project were taken at 3mm intervals, the geometry still changes very rapidly in certain areas, specifically around the joints as shown in Figure 1.

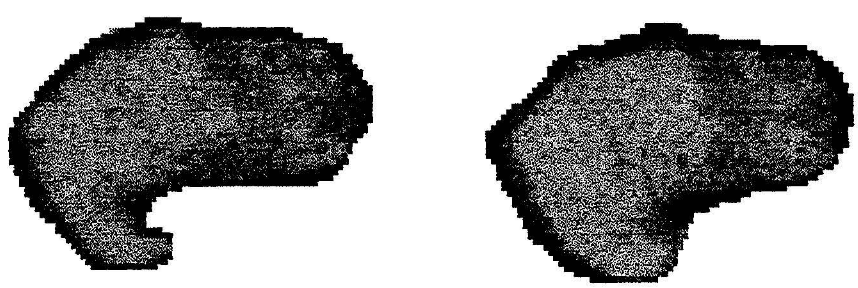

Figure 1.- Geometric Change between 3mm slices

To increase the flexibility of the model in each image, the ability to develop two separate splines per level was added to the program. This allowed the slice to be split so that

each spline handled one complex area. Later, these splines could be joined as described in a later section. To facilitate node numbering, the first node in spline one is 1 and the first node in spline two is 5001. The program, if the user requests, shows node numbers on the screen as they are created. The next algorithm that was added allowed one mesh to be started (cubic spline 2), and second spline to begin on a later image in the model (cubic spline 1). The two splines were continued until spline 1 was no longer needed in the model. This was done by continually increasing the size of cubic spline 2 while continually decreasing the size of spline 1 as seen Figure 2. Due to the geometry of the human femur, spline 1 can be phased out before reaching the diaphysis.

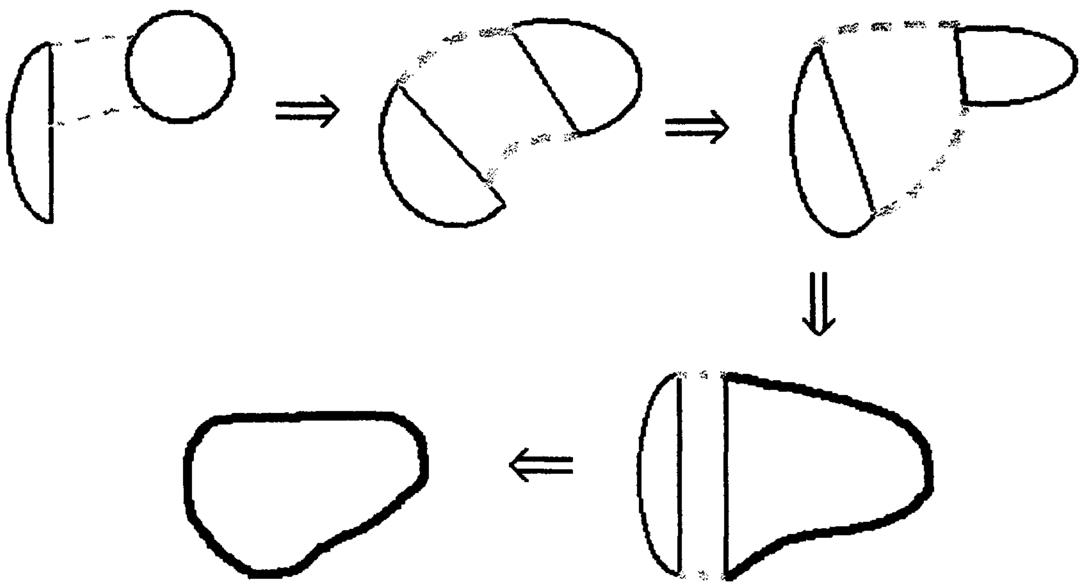

Figure 2.- Reduction Process to Single Spline

Code was added to the program to allow the area inside the interior spline to be meshed. This allowed for both a model of a shell in the diaphysis with a solid cross section in the epiphysis, all developed in the same program. This was accomplished by finding the center of the spline and then connecting each node of the spline with the center. This process formed the triangular cross-section elements. inside the interior spline. In ANSYS, these elements are a version of the 3-D SOLID64 anisotropic bricks used in modeling the cortical bone. It is very important to note that the shape of the interior spline must be such that there will be no overlapping of interior and exterior elements. This is easily done in circular regions, but much harder in the complex geometries of the joints as seen in Figure 3.

To facilitate the different materials found in human bone, a material selection form was added to the program. This form allows the user to select one of three types of bone: cortical, trabecular, or marrow. For the program to properly incorporate these materials, it is important that the interior spline also be meshed. This allows the model to be completely solid in regions, such as around the joints, and a shell in others, such as in the diaphysis.

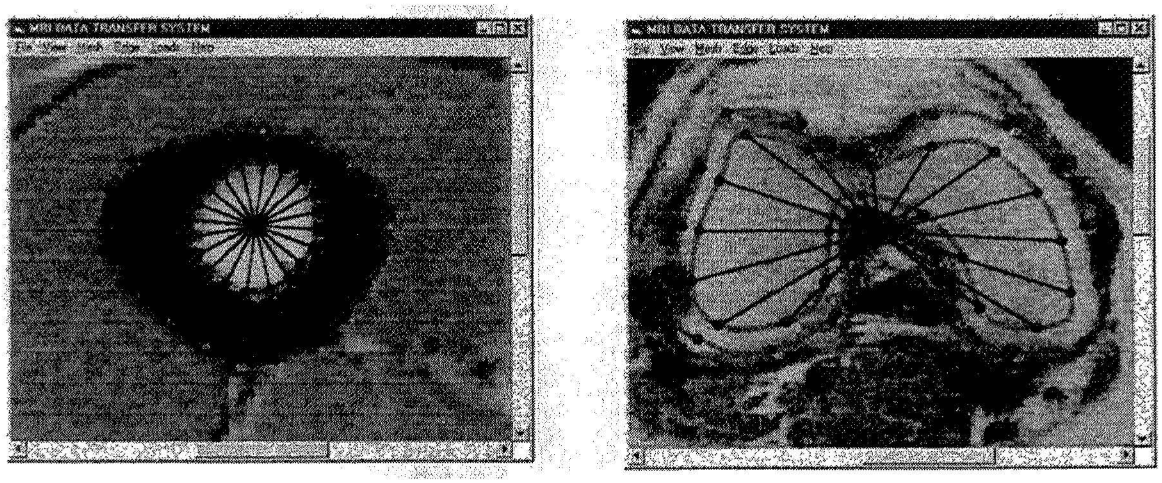

Figure 3.- Good Interior Mesh and Bad Overlapping Interior Mesh

Once the algorithm for the dual splines was completed, the hidden line removal section had to be modified to handle both splines. A new algorithm was implemented to produce the visual effect of a solid model, instead of the original wire-frame code. This code actually paints the areas of interest in a fashion that builds a "solid" model. This new code, however, does have some limitations that will be addressed in future modifications. The main limitation is the range of the viewing angles, which are 0° to 90° for x-rotation and 0° to 90° for y-rotation. Looking at Figure 3, the horizontal direction is the x-axis, the vertical direction is the y-axis, and the z-axis is coming out of the plane of the paper forming a left-handed coordinate system. Once the model is entered into a finite element program, such as ANSYS, the model follows a right handed coordinate system. As seen in Figure 4, the new "solid" model code is easier to visualize than the original wire-frame model. The two spline mesh overlaps in some places and this causes areas to be covered that should remain visible.

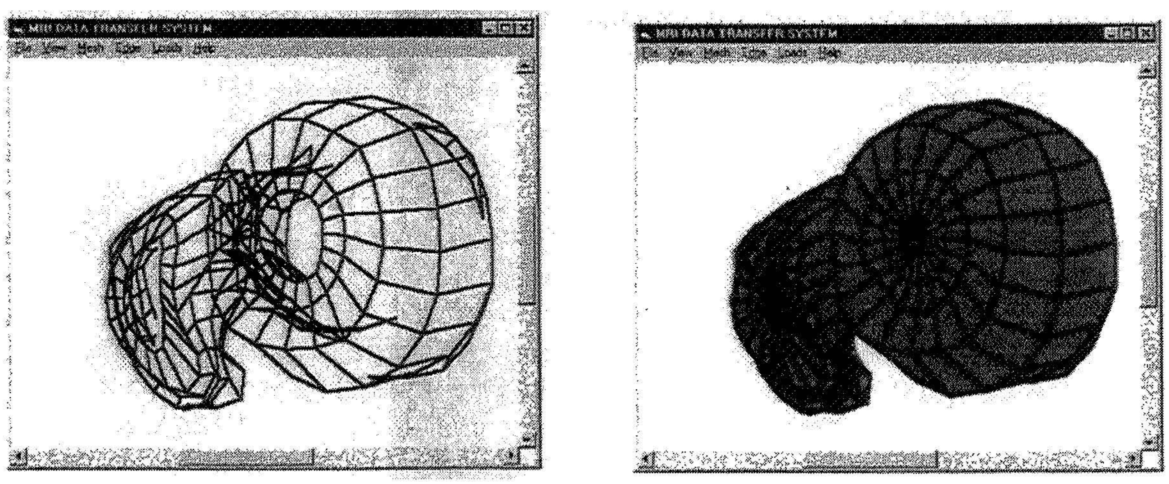

Figure 4.- Old Wire-Frame Model and New "Solid" Model

Joining the Two Splines

The two splines were joined in most cases using simple 8 node brick elements or 6 node wedge elements. Joining related nodes between the two slides (see Figure 5) created connecting elements.

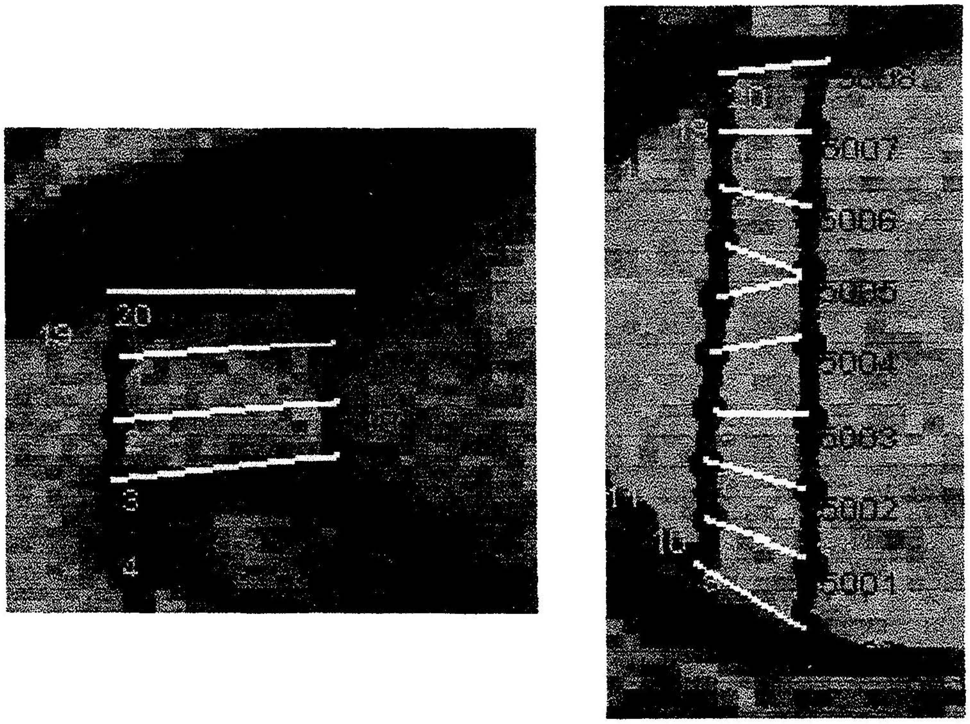

Figure 5.- Joining the Two Splines Together

By working with the images being used in model production, the appropriate number of divisions per spline can be chosen to have nodes that coincide between the two splines. This is seen in the first image of Figure 5, where each node connects to the coinciding node on the opposite spline. Even if the same pattern does not work on the next slide, the previous pattern must still be completed. Often these elements might have a warped face that will cause them to appear as error elements. This problem can usually be corrected by changing the brick elements into 6 tetrahedrals [2].

Once the pattern is completed, a new pattern can be created on the same slice and then completed on the following slice as seen in Figure 6. It is important that the top of the slice pattern must be smaller or the same size as the next slice. Therefore, once the connection area begins decreasing in size, the later slice becomes the top slice. These connections must be written by hand, and therefore it is advantageous to have a set of dot plots, much like Figure 6, to record the appropriate node numbers.

Data File Conversion

When the ASCII file written for ANSYS is run with the graphical interface version,

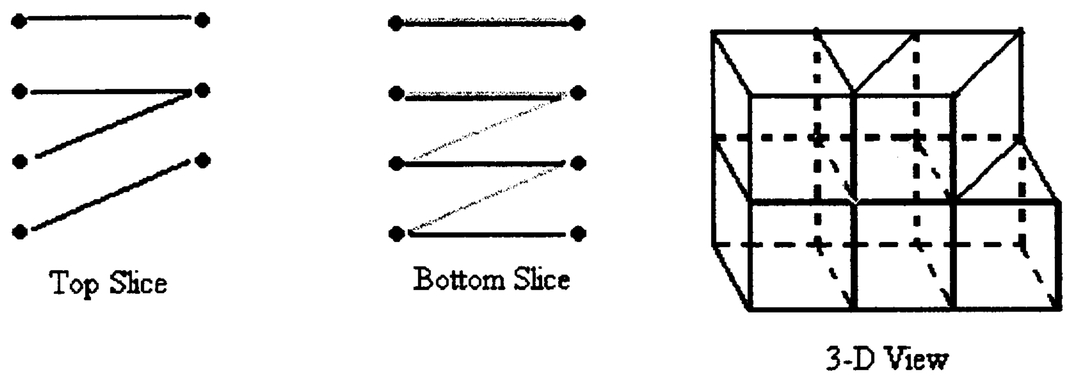

Figure 6.- Connection Patterns

such as ANSYS/ED Ver. 5.3, the ASCII file can be entered without modification. Unfortunately, the only graphical version of ANSYS available had sever limits on the problem size that it could handle. Therefore a batch version of ANSYS was used on the Alabama Super Computer Network. The batch input was entered with the command:

runansys inputfile.F5 outputfile.F27

and an appropriate queue was selected on the CRAY C94A. The filename *inputfile.F5* is the input ASCII file. The file named *outputfile.F27* is the output ASCII file. To run ANSYS in batch mode, several modifications must be made to the *inputfile.F5*. All of the following commands can be accessed using the ANSYS Online Help Manual [9].

At the very beginning of the input file, the *PREP7* command must be inserted. This command tells ANSYS that this input is to be used in the pre-processing module, where the model is built. *PREP7* is the pre-processor for a static structural model.

Once the model is completed in the MRIDTS, and the data is output, the information about the two splines must be combined into one input file. The nodal information is output in the following format:

N, *Node number, X-coordinate, Y-coordinate, Z-coordinate*

The element information was output in the following format:

E, *Node 1, Node 2, Node 3, Node 4, Node 5, Node 6, Node 7, Node 8*

where the node numbers are defined as seen in Figure 7.

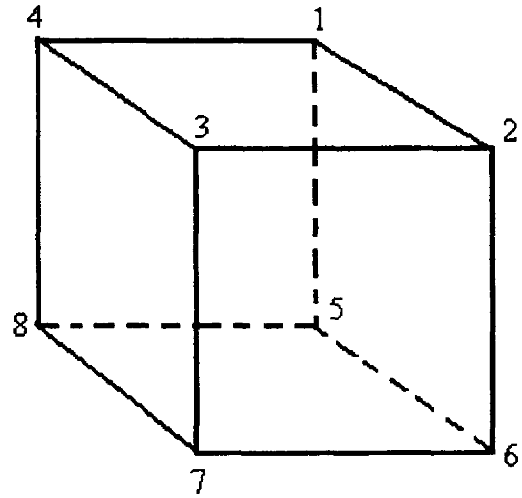

Figure 7.- Node Numbering Scheme

The loads and boundary conditions were then added to the input file created by the model. Future modification will be made to the code to allow the user to select boundary conditions while preprocessing the model. The load was applied to the model using the following format:

F, *Node number, Label, value*

where the label is FX, FY, or FZ for a force in the X, Y, or Z direction or MX, MY, or MZ for a moment about the X, Y, or Z-axis. The boundary conditions were added to the model input file using the following format:

D, *Node number, Label, , , End node number*

where the label is ALL, or RX, RY, or RZ for fixed rotation about the X, Y, or Z-axis, or UX, UY, or UZ for fixed displacement along the X, Y, or Z-axis. Note: the commas and spaces are required for the *D* command to function properly.

The MRIDTS program adds the required material properties to the end of the ANSYS input file. This command uses the following format:

MP, *Label, Material Number, Value*

where the label is, EX, EY, or EZ for Young's Modulus in the X, Y, or Z-direction or DENS for the density of the material. The values used in the MRIDTS were taken from data collected by Cowin [8]. The material number was the number associated with each different material.

These material property values are shown in Table 1. These numbers for the MRIDTS were 1 for cortical bone and 2 for trabecular bone. The value was the associated numerical value with the preceding applied label. In order for an element to be created with a certain material, the following command was added before each section of elements created by the MRIDTS program:

MAT, *Material Number*

where the material number is the number described above.

TABLE 1.- MATERIAL PROPERTIES

MATERIAL	EX (psi)	EY (psi)	EZ (psi)	DENSITY (lb/in^3)
Cortical Bone	1,600,00	1,300,000	2,500,000	0.0134
Trabecular Bone	1,850,000	1,850,000	1,850,000	0.0119

When using ANSYS without a GUI, it is necessary to add solution commands and output commands to the input file. These commands are as follows:

```
/COM END PREPROCESSING
FINISH
/COM SOLUTION
SOLVE
FINISH
/POST PROCESSING
ETABLE, STR1, S, 1
ETABLE, STR2, S, 2
ETABLE, STR3, S, 3
SET, 1, 1
ESORT, ETAB, STR1, 0
PRETAB, STR1, STR2, STR3
CONTINUOUS
ESORT, ETAB, STR3, 1
PRETAB, STR1, STR2, STR3
CONTINUOUS
PRNSOL, U, COMP
CONTINUOUS
FINISH
```

The *FINISH* command tells ANSYS that the mode (pre-processing, solution, or post-

processing) it is presently in is complete. The *SOLVE* commands tells ANSYS to move into solution mode and solve the input information. The *ETABLE* command tells ANSYS to fill a table with values for display. It has the following format:

ETABLE, *Label, Item, Component*

where the label is a user defined label (e.g. STR1 represents the 1st principal stress). The item is the corresponding ANSYS label for the appropriate requested value (e.g. S represents the principal stresses) and the component is the specific part of the item (e.g. 1 represents the 1st principal stress). Other item commands can be found in tables in the ANSYS User Online Help Reference. The *SET* command tells ANSYS which load set to retrieve. For the static modeling described above, there will only be one load set with only one subset, therefore the SET command will always be SET,1,1. *ESORT* is used to sort the elements placed in the table by the *ETABLE* command. The *ESORT* command has the following format:

ESORT, *Item, Label, Order*

where the item is the item requested (at this time *ETAB* is the only available command), label is the user labeled requested data (e.g. the previously named information, e.g. STR1), and order is either 0 for descending or 1 for ascending. The *PRETAB* command prints the element table information and has the following format:

PRETAB, *Label 1, Label 2, Label 3*

where the labels are the user defined names for the requested output. The *CONTINUOUS* command tells ANSYS not to ask for user input, but to print out all requested information continuously.

PROTOTYPE MODEL

At this time, a prototype model is being tested to determine the required time for model construction and modification. As described previously, the model is being run in batch mode on the Alabama Supercomputer Network in association with The University of Alabama. Since the Supercomputer network is used by more than The University of Alabama, computer time is very demanding and not always available. With each run, the model must be modified to correct errors. These errors are often caused by warping, but usually can be corrected by converting the elements into tetrahedrals.

A new command was discovered that helped to reduce the time for error modification. Using the EN command numbers the elements instead of allowing ANSYS to auto-number the elements. In this manner, the user can quickly identify the problem elements and make those corrections. The EN command has the following format:

EN, *Element Number, Node 1, Node 2, Node 3, Node 4, Node 5, Node 6, Node 7, Node 8*

where the element number is user defined and the node numbers are the same as described above. Once the model is complete and error free and output is obtained, it will be examined to determine the value of the model for stress calculation.

FUTURE WORK

The MRIDTS needs to be modified to correct the problems encountered during this project. The first modification that should be made is to incorporate the new *EN* command into the output algorithm. The next modification that needs to be completed is the limited rotation angles of the new "solid" model. Once this problem is completed, the overlapping effect of the new "solid" model code needs to be addressed. By correcting these problems, the user will get a better view of the model they are creating by being able to view the model from all directions.

If possible, the MRIDTS needs an algorithm that will allow the user to manually build the connecting sections as they go. This will also help the user visualize their model and determine if they have any elemental warping. If this algorithm is written, the "solid" model code will need to be manipulated to include the new element information.

If the prototype model is able to simulate the analytical stress calculations previously performed, the models needed for the exercise evaluation will be created and tested. Once the force application data is received from another colleague working with this project, the femur models will be loaded and analyzed. This information will be used to compare the gravitational load stress distribution to the stress distribution created by specific exercises. This information will be compared with the results of 17 week bed rest studies being performed at Methodist Hospital in association with JSC. If the finite element analysis of the femur exhibits approximately the same results of the bed rest study, then it may be possible to test new exercises without using bed rest to simulate microgravity.

REFERENCES

1. Zienkiewicz, O.C., "Finite elements – a unified problem solving and information transfer method". *Finite Elements in Biomechanics, International Conference Proceedings*, 1, pp. 3-5, 1980

2. Shackelford, L., Fieveson, A., E. LeBlanc, A., and Oganov, V., "Prediction of femoral neck bone mineral density change in space". *12th Man in Space Symposium: The Future of Humans in Space*, June 8-13, 1997, Washington, D.C., pp. 78-79.

3. Fung, Y.C., *Biomechanics: Mechanical Properties of Living Tissue*, Springer-Verlag, 1981.

4. Cunningham, I. A. and Judy, P.F., "Computed Tomography". *The Biomedical Engineering Handbook*, pp. 990-1005, CRC Press, 1995.

5. Conolly, S., Macovski, A., Pauly, J., Schenck, J., Kwong, K., Chesler, D., Hu, X., Chen, W., Patel, M., and Ugurbil, K., "Magnetic Resonance Imaging". *The Biomedical Engineering Handbook*, pp. 1006-1045, CRC Press, 1995.

6. Todd, B. A., and Wang, H., "A Visual Basic program to pre-process MRI data for finite element modeling". *Computing in Biology and Medicine*. 26: 489-495, 1996.

7. Zienkiewicz, O.C. and Taylor, R.L., *The Finite Element Method*, Vol. 1, 4th Ed., pp. 97, McGraw-Hill,1989.

8. Cowin, S. C., *Bone Mechanics*, pp. 139-141, CRC Press, 1989.

9. ANSYS, INC., (1998.) "ANSYS/ED User's Online Help – Command Index." *ANSYS/ED* [Computer program]. Upper Saddle River, NJ: Prentice-Hall, Inc. Version 5.3.

25
IN-54

Hydroponics Database and Handbook for the Advanced Life Support Test Bed

Final Report
NASA/ASEE Summer Faculty Fellowship Program – 1998
Johnson Space Center

Prepared by:	Allen J. Nash
Status:	student assistant
University & Department:	Cornell University Agricultural and Biological Engineering Department Ithaca, NY 14850

NASA/JSC

Directorate:	Engineering
Division:	Crew and Thermal Systems
Branch:	Life Support Systems
JSC Colleague:	Dr. Daniel J. Barta
Date Submitted:	August 14, 1998
Contract Number:	K-8-50547

Abstract

During the summer 1998, I did student assistance to Dr. Daniel J. Barta, chief plant growth expert at Johnson Space Center – NASA. We established the preliminary stages of a hydroponic crop growth database for the Advanced Life Support Systems Integration Test Bed, otherwise referred to as BIO-Plex (Biological Planetary Life Support Systems Test Complex). The database summarizes information from published technical papers by plant growth experts, and it includes bibliographical, environmental, and harvest information based on plant growth under varying environmental conditions. I collected 84 lettuce entries, 14 soybean, 49 sweetpotato, 16 wheat, 237 white potato, and 26 mix crop entries. The list will grow with the publication of new research. This database will be integrated with a search and systems analysis computer program that will cross-reference multiple parameters to determine optimum edible yield under varying parameters.

Also, we have made preliminary efforts to put together a crop handbook for BIO-Plex plant growth management. It will be a collection of information obtained from experts who provided recommendations on a particular crop's growing conditions. It includes bibliographic, environmental, nutrient solution, potential yield, harvest nutritional, and propagation procedure information. This handbook will stand as the baseline growth conditions for the first set of experiments in the BIO-Plex facility.

Introduction

In response to NASA's plans to create a fully self-sufficient life support system for future long-term moon and Mars habitation, the Advanced Life Support Integration Test Bed (otherwise known as BIO-Plex, Biological Planetary Life Support System Complex) is under development. With modules similar to what might be available on Mars, BIO-Plex will be used to perform long duration human testing of integral regenerative physicochemical and biological technology with a high degree of mass closure. It is presently scaled to support 4-8 people for this testing. To provide proper nutrition, specific plants like wheat, soybean, white potato, sweet potato, lettuce, tomato, and peanut will need to be grown within the confines of a module called the Biomass Production Chamber (BPC).

Maximum constraints restrict the height of the growth bays within the BPC, energy to support the nutrient delivery systems and lighting banks, and the environmental conditions that can be provided to the plants. To optimize the growth area, large amounts of data are being assimilated to obtain statistically supported choices of the proper cultivars to use for each crop type, proper growing conditions, and correct arrangements of the crops within the BPC. The summer has been spent organizing articles written by plant production experts from around the country which support the methods of plant growth that will be implemented in the BIO-Plex. This collection of data in spreadsheet form will be linked to a computer analysis program. This program will be a search engine that cross-references several plant growth parameters (i.e. lighting and growing area requirements) and will provide statically supported recommendations based on optimum growing conditions.

BIO-Plex Background

In preparation for human exploration our solar system, it will be necessary to place scientists and astronauts at their particular sights of research for longer periods of time. For instance, the preliminary long-duration exploration of Mars will consist of a six-month journey to the Red Planet, an eighteen-month stay on the surface, and a six-month journey returning to Earth. The BIO-Plex will evaluate a ground-based habitat where near complete self-sufficiency is necessary. Therefore, present research for this facility includes development of both biological and physicochemical technologies to maintain food and atmospheric requirements for human life and to recycle the human byproducts into usable resources. BIO-Plex is a five-chambered unit (see fig 1) with separate areas for laboratory experiments, plant growth, and life support, habitation.

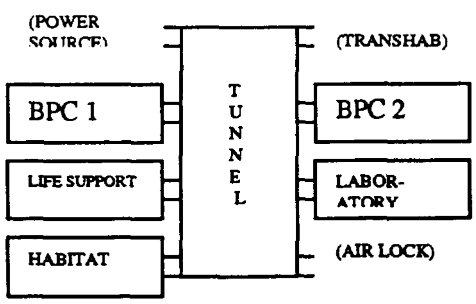

FIG 1. BIO-Plex Floor Layout in Bldg. 29 Rotunda. Power source transhab, and air lock, are merely access locations to the tunnel.

Human ecology studies have deduced general proportions of the chosen crop mix (crops that will be used in the Biomass Production Chamber) that can help maintain proper nutrition. The astronauts will have to bring all that is necessary to grow these crops with them in cargo. Traveling with the passengers will be many seed and asexual propagules (as is the case with sweet potato where a plant may be generated from a

particular part of another) which may be grown into mature plants. Referring to the plant growth and processing procedures listed in figure 2 and the many drawings of the components in figure 3, a propagule (seed or stem cutting) is placed in a wick (fig 3b – a piece of cloth or other object that draws nutrient solution from a tray immediately below). Then several wicks/propagules will be placed in each growing tray (fig 3a). These trays will support the plant through maturity allowing the roots to reach into the nutrient solution and the stems to grow toward the light. Upon maturity, the trays will be transported out of the BPC by means of a conveyor and elevator, Traybot (fig 3c). Once out of the BPC and into the tunnel (fig 1), certain crops like wheat and soybean will need immediate separation of the edible and inedible parts. Separation is performed by a harvester tentatively designed like in figure 3d. Lastly, the harvest may have to be eaten within a few days of harvest, or it may be dried (fig 3e) and stored much longer. The harvested plant products will undergo an undetermined series of steps to prepare it for storage or immediate preparation for consumption.

Fig 2. Crop handling procedure flowchart from propagation to final storage.

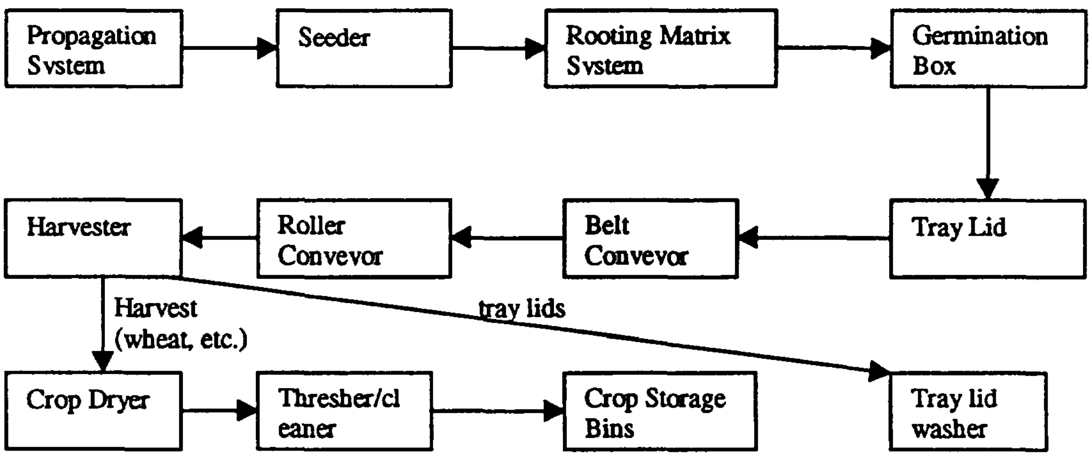

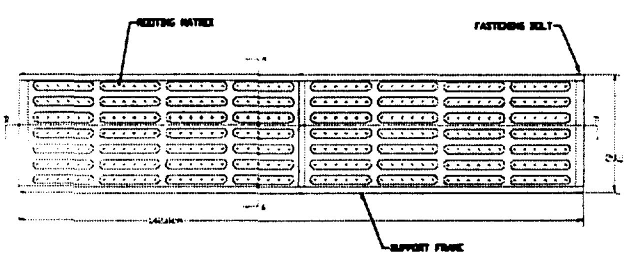

Fig 3a. Plant Growth Tray Lid

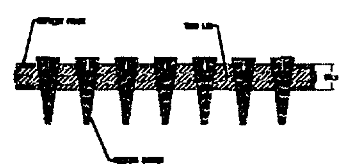

Fig 3b. Wicks for Tray Lid

Fig 3c. Conveyor System
And Elevator (Traybot)

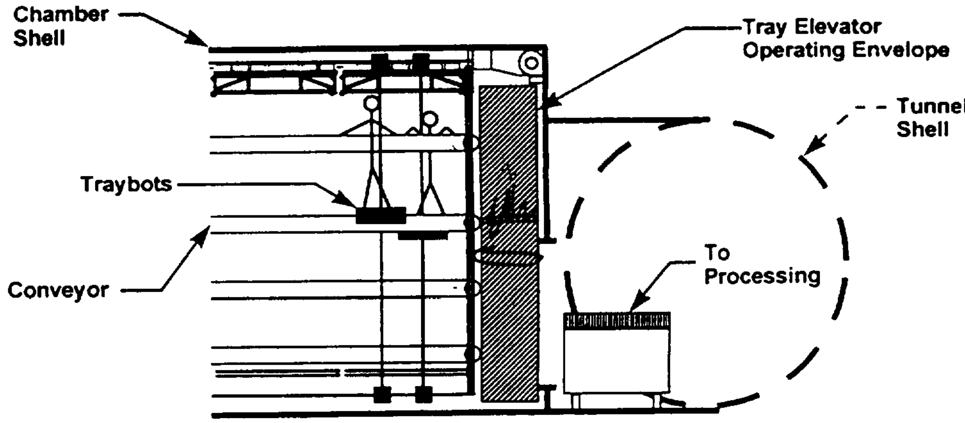

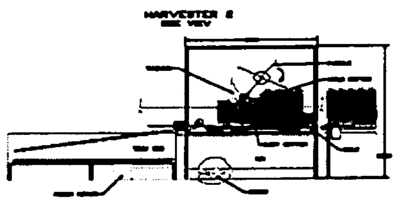

Fig 3d. Harvester (side view)

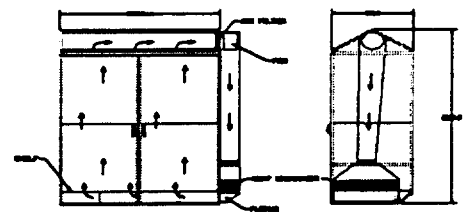

Fig 3e. Crop Dryer, front (left) and side right)

Figure 4 depicts the dimensions that are presently recognized for the inside of the BPC. As is described in the chart to the right, there are very specific growing volumes for each crop. These proportions may change by rearranging the crops' locations for each test depending on test requirements (such as nutritional requirements, degree of closure, etc.). Therefore, a database has been inspired that includes multiple growth characteristics for all crop mix scenarios.

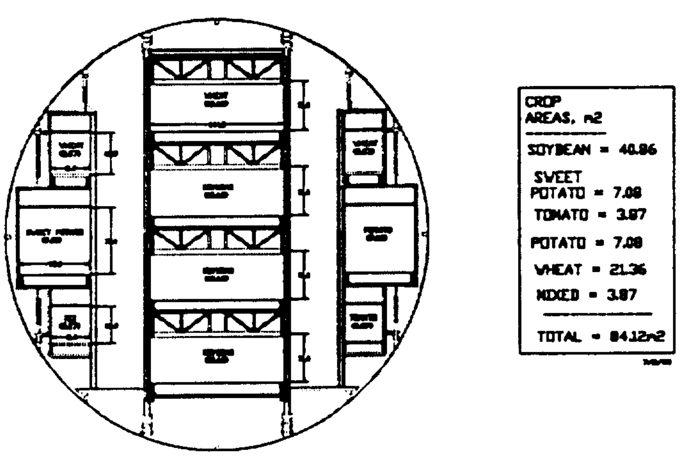

Fig 4. Crop Mix by Bay.

Summer 1998

Hydroponic Crop Database

Under the instruction of my mentor, Dr. Daniel J. Barta, I set out to create a database of plant growth research data from published articles, dating back as far as the seventies and written by scientists supported by NASA grants. I focused the compilation to the major crops listed in figure 4; "mix" crops include lettuce, cabbage, kale, chard, radish, carrot, green bean, mustard, and spinach; and potentially corn, sugar beet, and peanut. I was able to collect yield data at 84 different environmental conditions for lettuce, 14, soybean, 49 sweetpotato, 16 wheat, 237 sweet potato, and 26 others including several cultivars of each. In the future, this list will grow as more research is reported, and as this occurs, the effectiveness of the database as an analysis tool will increase.

The information that I attained from the many articles included the bibliographic information, environmental conditions, and crop harvest. More specifically, biographical information included crop name, crop cultivar, published article citing, and the type of crop it is (i.e. staple, grain, salad, etc.). Environmental information included day and night temperature, day and night relative humidities, light irradiance (the intensity of the light banks at the canopy height within the photosynthetic range), lamp type, photoperiod (the number of hours the lights are on each light/dark cycle), dark period (the number of hours the lights are off), carbon dioxide concentration, nutrient solution type, type of nutrient solution delivery system, and whether or not the growth chamber crop was grown as individual plants or full canopy. The harvest information was the fresh and dry weights of the total, edible and inedible, root, and shoot harvests. Finally, I found the number of days after planting the seed that the plant was harvested, the edible harvest productivity per day, the total growth area, planting density, harvest index (grams of edible yield per grams of total yield), and canopy height.

After it has been completed, this database will be provided to scientists at the NJ-NSCORT to be incorporated into on-line systems analysis tools on the internet. Furthermore, this program will be able to link the many data sets and determine the optimum balance of all the crops in the list mentioned before. In this manner, if a plant growth researcher attempts to experiment with a certain crop to attain a certain result, they will have an easier way to attain the knowledge learned by former research.

Crop Handbook

Though in its early stages, a handbook will serve as a "cookbook" of crop growth. For simplicity's sake, this handbook will specify the baseline of proper environmental conditions under which specific crops that the crop mix crops should be grown. From this baseline, slight modifications will be made based on observed experimental results.

The handbook information has been solicited from NASA funded scientists who are considered one of the top experts on their particular crop or crops. Once the handbook is fully established, it will be the base for BPC and related BIO-Plex specifications.

Additional Activities

First and foremost, I had the great opportunity to work with this JSC Advanced Life Support Program within the Engineering directorate and with the Advanced Life Support Test Bed (BIO-Plex) team. Experimentation on various concepts for the Biomass Production Chamber included growing bay lighting strategies in the "Lighting Test Stand", preliminary AutoCAD design of the many pieces of equipment mentioned earlier (i.e. harvester, crop dryer, conveyor, etc.). I assisted in the AutoCAD design drawings, which were then sent for official configuration and documentation in the Engineering records. Also, the engineers allowed me to join them in the brainstorming phase of preliminary design on the harvester and other machines, and I had the gratification to see some of my ideas put to paper.

With the Summer Faculty Fellowship Program, I was able to visit many departments and see many NASA sites. The educational experience of this summer has been enormous, and for the first time, I have the thrills that accompany engineering in action. Coming upon my senior year at Cornell University, I now have the background to know what to expect and what to look for in my search for employment.

SIGNAL PROCESSING SYSTEM FOR PRESSURE RATE DATA OF THE AUXILIARY POWER UNITS ON THE SPACE SHUTTLE

Final Report

NASA/ASEE Summer Faculty Fellowship Program - 1998

Johnson Space Center

(26) IN-16

Prepared by:	Monica R. Sharpnack
Academic Rank:	Senior, Undergraduate
University & Department:	University of Houston Department of Natural Sciences and Mathematics Houston, Texas 77004

NASA/JSC

Directorate:	Information Systems Directorate
Division:	Information Technology Office
JSC Colleague:	Robert O. Shelton
Date Submitted:	August 7, 1998
Contract Number:	NAG 9-867

ABSTRACT

For the positioning of engines during launch and operation of flight control surfaces during launch and re-entry, each of three auxiliary power units on the space shuttle use hydrazine to power a turbine. If a leak occurs in one of these units, significant problems can arise on the space shuttle. The pressure and temperature of the tank where the hydrazine is stored are obtained via signals provided by sensors. These signals need to be filtered and processed in order to develop graphics that show, and data that monitors the status of the system at all times. This paper addresses the problem of developing a filtering system for those signals based on state models and filters, such as the Kalman filter, that will accurately filter the noise and account for data jumps and gaps, without resulting in misinterpretations of the data. Although no definite system will be shown to solve the problem, suggestions for the attributes of such a system will be provided.

INTRODUCTION

As part of the mechanics of the space shuttle, there are three auxiliary power units each using hydrazine to power a turbine. Among other things, these units are used for positioning of engines during launch and operation of flight control surfaces during launch and re-entry. The auxiliary power unit, as shown in Figure 1 below, has a holding tank

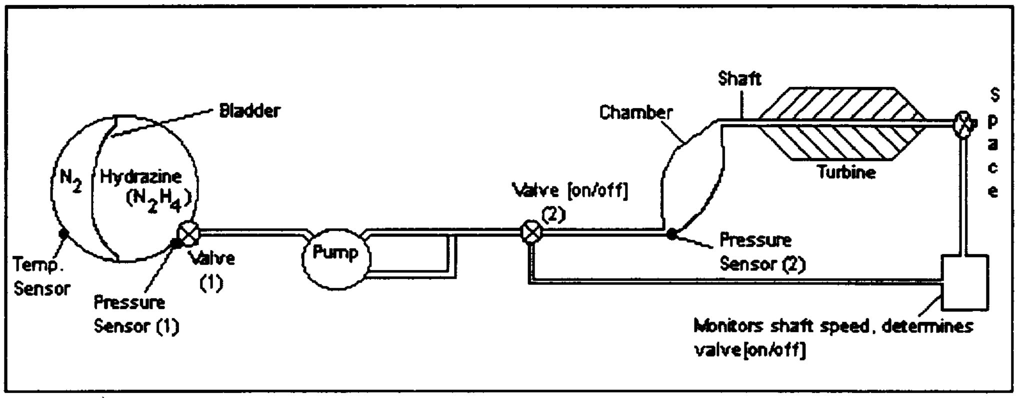

Figure 1.- Auxiliary Power Unit

which contains nitrogen (N_2) and hydrazine, separated by a bladder. The N_2 expands as needed to create pressure in order to push the hydrazine out of the tank and into the system. The hydrazine then flows through the pump to valve (2), which is a "bang, bang", or on/off, switch. If the valve is "on", the hydrazine flows into the chamber where it combusts and the gas flows out to turn the turbine. In Figure 1, there is a box below the turbine. This box measures the shaft speed and determines whether or not to switch valve (2) on or off based on the nominal speed of the turbine rotor. When valve (2) is turned "off", the pump (Figure 1) continues to cycle the hydrazine in order to maintain pressure in the system.

In addition to the components that make up the auxiliary power unit, there are also various sensors that detect pressure and temperature in the system. There is a temperature sensor in the hydrazine/N_2 tank, as well as pressure sensors at valve (1) and in the chamber. These send back data signals that will be processed and analyzed by a computer program in order to detect leaks in the system. If a leak occurs in one of the hydrazine tanks, problems can arise on the space shuttle. Examples of such problems are: due to the nature of the hydrazine, it would more than likely combust once it was exposed to the air outside the tank causing fire to occur, and, if not that, then there would be an inability to use the hydraulics upon re-entry in order to operate flight control surfaces for a proper landing.

THE KALMAN FILTER

Characteristics Of The Kalman Filter

Vector modeling of the random processes under consideration and recursive processing of the noisy measurement (input) data are the main features of the Kalman formulation that lead to the solution of a particular problem. The Kalman filter takes the incoming data and uses vector models in a recursive process in order to arrive at a solution. Essentially, the filter starts with an estimation of the signal at time t_0. Using this data, the Kalman filter then goes through four steps in order to project ahead to a new estimate. The first step is to compute the Kalman gain, the next is to update the estimate with a measurement (observation) of the process at discrete time intervals, then the error covariance for the updated estimate is computed, and the final step is to project ahead. The filter continues through this process of estimation until it reaches the time at which the programmer has told it to stop.

The Conditions Needed For A Solution

In order to set up the equations for the Kalman filter, the programmer needs to know a few essential formulas and equations. The first equation is that of the Kalman gain, the factor that yields an updated, optimal estimate. Another necessary equation is for the error covariance matrix which is a measure of the range of the error estimation. One also needs to know how to determine the observation or measurement of the process, which is assumed to occur at discrete points in time, according to a linear equation. Other important factors include the matrix of the noise signal that is entering the system, and a process to describe how the ideal noiseless signal should appear (an example of the last would be a Gauss-Markov process, which is the process assumed for the signal from the auxiliary power unit). It is essential that the programmer knows what the end signal should look like, i.e. the process of that signal, because the Kalman filter uses this information in order to help shape the signal that is read from the filtering process.

Programming Into The Computer

The steps in the recursive process can be programmed into a computer with indications as to what the matrix variables represent, given the process to be analyzed. The graph of the data signals thus filtered can be displayed on the screen so that the programmer can use them as necessary. In the case of the data signals coming from the sensors in the auxiliary power unit, noise is filtered out of the system and then a signal is plotted to show the pressure of the system and its derivative. The data from these graphs are then used in formulas to determine the mass of the hydrazine and its derivatives which are used in determining the occurrence of leaks in the system. The information obtained from the data and graphs is then analyzed.

CURRENT SIGNAL PROCESSING SYSTEM

The sensors in the auxiliary power unit monitor the pressure and temperature of the gas in the tank, as well as pressure in the chamber (see Figure 1). The data received from the sensors in the tank is then plotted to show the pressure of the hydrazine versus time. From this data, the derivative of the pressure curve is taken and plotted as the rate of change in pressure. The pressure sensor located in the chamber plots a graph of the chamber pressure; this pressure, however, is not used to determine what is happening in the tank.

In the process of plotting the pressure in the hydrazine tank, a Kalman filter is currently being used. The filter takes the noisy data it receives from the sensors in the hydrazine tank and plots the pressure, then that graph is used to plot the rate of change of the pressure. Through manipulation of a non-ideal gas law, a formula of pressure, volume, temperature, and their respective derivatives can be formed as ($P'/P + V'/V = T'/T$). The Kalman filter is used to determine the derivative of the pressure in the tank, and that information along with the temperature of the N_2 and its derivative are used to find the volume of the N_2 in the tank. Knowing the volume of the entire tank, and also the volume of the N_2 in the tank, the volume of the hydrazine can be found. The volume of the hydrazine is then used to find the mass of the hydrazine. The mass, and its first and second derivatives are plotted in order to help determine when leaks occur. The filter should take into account that not all of the data being fed to it is an accurate measure of the process. It should adjust itself around erroneous data and data gaps so that a smooth and accurate curve of the change in pressure can be plotted. This, in turn, will lead to an appropriate graph of the mass of the hydrazine and its derivatives.

PROBLEMS WITH THE KALMAN FILTER

General Problems

There are several problems that may be encountered when using a Kalman filter. First, the programmer has to tell the computer what type of process is to be observed when setting up the filter. If this information is incorrect, the filter will continually try to fit the measurement data to the wrong curve. This is a problem if the programmer is unsure of exactly what type of process is to be modeled, or if the process tends to change state.

The Kalman filter also tends to begin to ignore new data when it has found a common "theme" to the information it has been given. It will oftentimes continue on its current path based on what it knows from before and ignore data that does not coincide with that curve, even if the new data suggests that the curve should start changing shape. This act of "ignoring" incoming data is partly due to the error covariance of the system. The error covariance is the amount of leeway the system has for error in its estimates. If a data point lies outside the error covariance range, then the filter ignores it, considering it to be erroneous. Along this same line, and for much of the same reason, the Kalman filter also

is slow in adjusting to incoming information that is different from the information it has been previously receiving. It can not adjust fast enough to large changes in data, therefore it does not consistently plot an accurate graph of the signal. In essence the filter tends to start believing itself and prior data rather than the actual information currently coming into the system.

Problems For Use In Hydrazine Leak Detection

Due to the environment of the space shuttle (i.e. vibrations, periods when a signal cannot be received, etc.), data being received from the sensors is often jumpy and sometimes there are gaps in the signal. Having to sort through erroneous data and data gaps is difficult for the Kalman filter. Since it tends to start trusting prior knowledge of the data filtering through the system, the Kalman filter does not adjust quickly when what appear to be data jumps end up being changes in the process curve. Sometimes when the graph should indicate a rapid change in pressure (when turning the system on/off, or in the event of a leak), the filter is slow in recognizing that it should change, and instead of the observer noticing a large change, or sudden drop, they can only see a slow decrease on the graph.

The main problem with the filter in the case of this system, is that the model fails where the simplifying assumptions fail. When designing the filter, assumptions as to certain aspects of the system must be made. One assumption is that the system is slowly changing. If a leak occurs, there will be a fast change in incoming data, but since the original assumption is that of a slow changing system, it takes a long time to adjust to the fast-changing data. Essentially, it is precisely when the system needs to be the most accurate that it tends to fail.

SOLUTIONS

Altering The Filter System

If there is a problem with the Kalman filter due to inaccurate modeling of the process being estimated, changes need to be made in the program to account for this. Not all processes are constant, and if the programmer is trying to model a constant process, this could lead to a problem with the end result. A possible solution is to insert some process noise into each of the state variables to give them more flexibility to work with the incoming signal and for the system to estimate more appropriately. This may result in some degree of sub optimality but it makes for a much safer filter.

Avoidance of fixed-point arithmetic will help in the calculations of estimates by the filter, because it will minimize round off error in the data being calculated. In addition to accounting for round off error, the programmer must be wary of making too many steps between measurements when data is sparse. This will insure that the system is not taking measurements where there is not enough data to be used. Finally, the filter does not work well with deterministic, undriven processes in the filter modeling because these usually

lead to a situation in which the matrix of the error covariance approaches a semi-definite condition as the number of steps becomes large. When this occurs, even a small error in expected measurement will trip the system into a divergent path.

Running A Parallel Filter

Even if the program is written correctly and the process modeled adequately, the Kalman filter may still have some difficulty in accurately plotting and adjusting to incoming data. Thus, it may be necessary to introduce another filter into the system to take over when large amounts of erroneous data and data gaps are occurring. Having another filter begin when the Kalman filter gets off course is not enough, though, because determining when the Kalman filter gets off course is a difficult problem to handle. Instead of having to pinpoint when divergence occurs in order to find a starting point for a second filter, the second filter should instead run parallel with the Kalman filter. The second filter would not use its data to plot a graph alongside the graph of the Kalman filter, but would only be running through its process so that data between the two filtering systems can be compared. The Kalman filter is a "tight" filter, meaning that it tracks within a relatively small range of error covariance. This means that the filter only takes into account data that is within a certain range of error, ignoring the data that falls outside of this range. The second filter would need to be a "looser" filter that would allow for a larger range of covariance, and thus would accept data that might be outside the range of the Kalman filter. Then the second filter would be able to tell when the Kalman filter was not plotting a curve within the proper range of the incoming data, and an addition to the program would need to be written to tell the Kalman filter to adjust in order to graph the new, more accurate curve.

The second filter would be like a parent filter and would monitor the progress of the Kalman filter, only interrupting it when there were large changes in data, or data gaps which the Kalman filter could not handle. It would essentially put the Kalman filter back on a more appropriate course, making the graph of the pressure more accurate. This would lead to a more appropriate graph of the rate of change in pressure which is used to find the mass of the hydrazine needed for checking if the system has a leak.

The problem with implementing this solution is that we have to find a way to tell the program which filter is correct. A process of determining the correct signal needs to be found so that this solution may be beneficial.

Using The Kalman Filter To Check Itself

Instead of programming an additional filter into the computer, it may prove more beneficial and more cost effective to use the Kalman filter as a check against itself. In order to do this, the computer program would need to be set up so that there is one original Kalman filter tracking the system. As this filter is tracking, another filter begins at a certain moment, for a certain period of time. This would serve as a check, because each new run of the Kalman filter starts from scratch without knowledge of the previous data

being plotted. The alternate filter will not be influenced by prior estimations that may cause the original filter to get off track. If the graph of the additional filter is different then that of the original filter, a means of determining which filter is correct will need to be used so that, if need be, a proper adjustment may be made in the original Kalman filter.

The Kalman filter overlapping the original filter will begin with fresh data and will be better able to follow a path that is off the course of the original filter, thus tracking the more accurate path for the graph. It will help keep the filter on the correct path, helping to alter the original filter when it tends to get off track.

Knowing when to start the overlapping filters may prove troublesome, though there may be a sufficient way of doing so. There is a certain amount of error between what the filter actually graphs and the noisy signal entering the filter. On a graph of the second derivative, you can see that there is a variance of this error. When the difference between what the filter expects the signal to be and what the signal actually is becomes larger than the given variance, this may be an indicator that the Kalman filter is running off course. At this point, it would be useful to start a new filter and check to see if the new filter continues along the course of the "error" from the original filter. When it becomes apparent that the graph has indeed changed, then the original Kalman filter can be reset to follow the more accurate path.

As in the case of running a parallel filter, there may be problems in knowing which of the filters to believe, and in the implementation of a program in the computer that will be able to assess which filter is "true."

Determining Which Filter To Believe

By looking at the probability distribution curves of the signals being graphed, one might be able to find a way of determining which filter is the most accurate approximation of the given process. When there are two filters running, their distribution curves should be plotted. Then the normalization of the product of these two curves, the product distribution, should be graphed as well. The product distribution curve will tend to look like the distribution of the more accurate filter. By comparing the product distribution curve to the two probability distribution curves one will be able to see whether or not the original filter is graphing the most accurate measurements. If the product distribution curve tends toward the probability distribution curve of the parallel or second Kalman filter, then one would necessarily assume that the additional filter was the more accurate approximation of the process. Going back to the graph of the pressure, which the original filter is generating, one would then want to restart the Kalman filter at the point where the product distribution curve began to look like the probability distribution curve of the parallel or second Kalman filter.

To start the Kalman filter at any particular point in time, the program needs to know the initial value of the derivative of the pressure at that point. The program would have to know the derivative of the pressure at the point where the product distribution curve began to look most like the probability distribution curve of the parallel or second Kalman filter. Fortunately, this derivative has already been calculated through the running of the

additional filter. Using the data given by the parallel or second Kalman filter, the derivative of the pressure at the new point in time, where we would want to restart the original Kalman filter, could be determined.

CONCLUSION

The filtering system currently being used to plot a graph of the pressure in the auxiliary power units of the space shuttle is not completely accurate. Due to erroneous data and data gaps, the Kalman filter is not able to plot an appropriate graph that can be used for the automatic detection of leaks in the system. It is therefore necessary to develop a system that will be more accurate. First, the Kalman filter that has been written into the computer program has to be looked at to ensure that the process being modeled is correct, and that there are no errors within the actual programming of the filtering system. Second, another filter may need to be added - whether it be a looser filter in parallel, or an additional Kalman filter - in order to keep the original Kalman filter from misreading the data it receives so that an accurate curve may be plotted. This analysis of the problem does not give definite solutions, but it gives a starting point for determining how to alter the present filter system in order to make it adjust appropriately given the signals it receives.

In the process of gathering background information on Kalman filters and the characteristics of the auxiliary power units and filtering system currently in use, I referred to Robert G. Brown's book, Introduction to Random Signal Analysis and Kalman Filtering [1], along with personal communication with Mr. David Hammen, the programmer involved with setting up the system for leak detection.

REFERENCES

1. Brown, Robert Grover. Introduction to Random Signal Analysis and Kalman Filtering. New York: John Wiley & Sons, Inc., 1983.

NUTRITIONAL ASPECTS OF CREWMEMBERS' CARDIOVASUCULAR HEALTH INDICATED BY DIETARY LIPIDS

27

IN-54

Final Report

NASA/ASEE Summer Faculty Fellowship Program – 1998

Johnson Space Center

Prepared by: Marcelle A. Thurston

Academic Rank: Graduate Student

University & Department: Bowling Green State University

Department of Family and Consumer Sciences

Bowling Green, OH 43402

NASA/JSC

Directorate: Space and Life Sciences

Division: Medical Sciences

Branch: Life Sciences Laboratories

JSC Colleague: Scott M. Smith

Date Submitted: September 1998

Contract Number: NAG 9-867

ABSTRACT

This summer's project examined the relationships between dietary and physiological factors on serum lipoproteins using data from past United States astronauts. Nutritional assessment was required to determine whether a relationship existed between dietary intake and risk of cardiovascular disease (CVD) in crewmembers. Risk for CVD was assessed by the measurement of preflight, inflight, and postflight serum lipoproteins. The purpose of this project was to evaluate the dietary practices of past crewmembers before and during flight, and to examine their relationship with blood indicators of lipid status. Because of mortality and morbidity associated with CVD, such assessments are critical for the maintenance of astronaut health before, during, and after space flight. It was anticipated that the results from this project would assess the effects space flight and diet have on cardiovascular health, thus, defining the adequacy of the current dietary recommendations during space travel. It was hypothesized that the mean preflight serum lipoproteins compared to mean postflight serum lipoproteins would not be statistically different and that the current inflight diet is adequate in nutrient content, having little or no effect on lipoprotein levels.

INTRODUCTION

In order to assure that future long-term missions will be productive, it is imperative that the deleterious effects of space flight on the human body are known and can be limited and/or avoided. Nutrition is one of several factors that provide for the success of extended duration missions. The effects dietary factors have on the human body before, during, and after space flight is essential to understand in order for manned missions to continue in a metabolically safe way.

Cardiovascular disease (CVD) is the number one cause of death in the United States among men aged 45 years and older and for women aged 55 years and older.[1] There are many factors that influence the level of risk for heart disease; diet, lipid profile, physical activity, age, gender, tobacco, and genetics are the primary variables.

Generally speaking, individuals in the astronaut corps are healthy subsets of the population. They are likely to be at risk, not because of adverse dietary habits, but because of the physiological effects of space flight. Gender, age, and stress are also critical factors and are important for any health assessment for crewmembers. By assessing the risk level of astronauts and discovering ways to prevent or delay the onset of heart disease in crewmembers, it is hoped that this research can be applied to the general public and benefit them as well.

LITERATURE REVIEW

Diet

The National Health and Nutrition Examination Surveys (NHANES) reported that the general public consumes approximately 33% of calories as fat and 12-14% of calories as saturated fat.[2] To reduce the risk of heart disease, the American Heart Association (AHA) recommends less than 30% of total calories as fat, 8%-10% of total calories as saturated fat, 50%-60% of total calories as carbohydrates, and dietary cholesterol less than 300 mg per day. The current diet provided for crewmembers during flight is within these guidelines. However, crewmembers often consume a significantly higher amount of carbohydrates and a significantly lower fat intake. This is often the result of a variety of factors, primarily due to space motion sickness, changes in appetite due to microgravity, and change in energy expenditure.[3]

Lipids

Cholesterol screening involves the examination of total cholesterol and low density lipoprotein (LDL) levels when assessing risk for heart disease. Total serum cholesterol should be less than 200 mg/dL and LDL levels should be less than 135 mg/dL to reduce risk of heart disease. A decrease in LDL by 10-20 mg/dL can decrease CVD risk by 10-20%.[4] However, recent studies[5] show that low high density lipoprotein (HDL) levels are a better indicator for risk of heart disease for both men and women compared to LDL levels. HDL levels should be at 35 mg/dL or higher to be considered low risk for heart disease. The National Cholesterol Education Program (NCEP) recently added the measurement of HDL cholesterol as part of the initial screening for hypercholesterolemia.[6] An increase in HDL by 10 mg/dL can decrease CVD risk by 50%.[4] According to Leach, normal lipoprotein ranges for astronauts are; total serum cholesterol 125-239 mg/dL; LDL 52-216; HDL 21-85 mg/dL.[7]

The ratio of apolipoprotein A to apolipoprotein B (apo A:B) is also indicative of heart disease. As dietary fat and cholesterol intake decreases, apolipoprotein A-1 decreases, in turn, decreasing the ratio. Apo A:B is now examined instead of the ratio of LDL to HDL and total cholesterol to HDL, which were ratios used in the past. Leach[7,8] studied the effects of space flight on serum lipoproteins in 1988 and 1994 and found that postflight HDL levels were significantly different than preflight HDL levels. Results showed that postflight levels were 12.8% lower or 5.8 mg/dL, but were not considered clinically significant. Within 23 days of landing, LDL and cholesterol levels had decreased significantly compared to preflight values. Apo A:B did not change and remained at a value above 1.5. Leach reports that it was not likely HDL levels decreased as a result of diet during space flight since HDL levels continued to decrease after flight and further cites several studies that have failed to demonstrate a change in HDL cholesterol after changes in diet, such as a low cholesterol diet. Leach suggests space flight and decreased levels of activity during flight compared to preflight regimens may be the cause for changes in lipoprotein levels.

Gender

Men are typically at a higher risk for heart disease compared to women.[1] In women, LDL cholesterol levels are 7-10 mg/dL lower and HDL cholesterol levels are 10-13 mg/dL higher than those in men.[9] As men and women age, their cholesterol levels change. In men, LDL cholesterol levels increase with age as do women's, especially around the age of 50 years. However, HDL levels continue to increase for women only. Current research[8] although limited, appears to show that space flight has the same effect on lipoprotein levels in both male and female crewmembers.

Age

As mentioned previously, risk for heart disease for men begins at 45 years whereas women lag behind approximately 10 years. The present project examined astronauts aged approximately 30 to 70 years old. However, the average age of a crewmember is becoming older over time. The effect space flight has on older individuals remains to be seen.

METHODS AND PROCEDURES

Data was gathered from astronauts who flew in shuttle missions in 1981-1998. Each crewmember had blood data from annual medical exams (AME's), less than 10 days before launch (average of L-10, L-2) and on landing day (R+0). Diet data was only recorded for preflight and during flight. Gender, diet and age statistics were also available. Crewmembers that had flown more than one mission were not repeated in any of the data sets. Leach also used this method to avoid any immunity to space motion sickness a crewmember may have developed from a previous mission. AME's were compiled into three-year blocks beginning with 1981 and were examined for a trend over time using a one way repeated measure analysis of variance. A second data set was compiled consisting of three data points for each crewmember; AME two years preflight, the average of ten days before launch and two days before launch, and landing day. This data set was statistically analyzed using a one way repeated measure analysis of variance to examine significant changes in lipid levels preflight compared to postflight. Paired t-tests and multiple linear regression models were also used for data sets that were compiled to examine any effects age, gender, or diet may have had on lipoproteins.

RESULTS AND DISCUSSION

Annual Medical Exams (first data set)

There was no apparent trend with the AME's from 1981-1998; 1984-1998; 1987-1998; 1990-1998; 1993-1998 (Table 1-Table 5). There were significant differences between certain 3-year blocks, but no apparent trend (see superscripts). These AME data sets were compiled by using astronauts who had consecutive AME's in these and were not repeated twice. Also, when examining comparisons, methods of collecting serum samples and analyzing lipid data have changed over time. Therefore, comparison may not be entirely equal. It is important to note that apo A:B was not measured until 1987.

TABLE 1. - SERUM LIPOPROTEIN LEVELS OF CREWMEMBERS FROM 1981-1998

Serum Lipoproteins	1981-1983 (n = 33) Means ± SD	1984-1986 (n = 33) Means ± SD	1987-1989 (n = 33) Means ± SD	1990-1992 (n = 33) Means ± SD	1993-1995 (n = 33) Means ± SD	1996-1998 (n = 33) Means ± SD
HDL (mg/dL)	46.1 ± 8.7^{acd}	41.9 ± 8.9^{e}	49.1 ± 12.7^{bc}	49.8 ± 12.8^{b}	45.8 ± 13.6^{acd}	48.6 ± 11.8^{bd}
LDL (mg/dL)	137.6 ± 33.9^{a}	152.6 ± 34.7^{bc}	142.1 ± 36.1^{ac}	129.7 ± 29.3^{a}	136.5 ± 29.5^{a}	134.2 ± 29.2^{a}
Chol (mg/dL)	202.9 ± 38.1	211.9 ± 39.8	209.4 ± 42.1	200.2 ± 31.7	201.3 ± 30.8	202.9 ± 31.9

Values with different superscripts are significantly different ($p < 0.05$)

TABLE 2. - SERUM LIPOPROTEIN LEVELS OF CREWMEMBERS FROM 1984-1998

Serum Lipoproteins	1984-1986 (n = 73) Means ± SD	1987-1989 (n = 73) Means ± SD	1990-1992 (n = 73) Means ± SD	1993-1995 (n = 73) Means ± SD	1996-1998 (n = 73) Means ± SD
HDL (mg/dL)	42.3 ± 12.2	48.3 ± 10.7	49.9 ± 11.7	46.5 ± 10.6	48.7 ± 10.9
LDL (mg/dL)	137.9 ± 33.2	130.5 ± 26.7	122.0 ± 25.9	129.8 ± 25.7	132.1 ± 26.5
Chol. (mg/dL)	197.3 ± 38.5	196.1 ± 32.4	192.6 ± 32.4	194.3 ± 31.8	199.2 ± 33.4

Values with different superscripts are significantly different ($p < 0.05$)

TABLE 3. - SERUM LIPOPROTEIN LEVELS OF CREWMEMBERS FROM 1987-1998

Serum Lipoproteins	1987-1989 (n = 25) Means ± SD	1990-1992 (n = 25) Means ± SD	1993-1995 (n = 25) Means ± SD	1996-1998 (n = 25) Means ± SD
HDL (mg/dL)	47.2 ± 10.1^{a}	47.2 ± 8.1^{a}	44.0 ± 8.9^{bc}	46.8 ± 10.4^{ac}
LDL (mg/dL)	125.9 ± 28.9^{a}	114.7 ± 28.3^{b}	127.9 ± 32.5^{a}	127.9 ± 38.2^{a}
Chol. (mg/dL)	189.8 ± 33.2^{bc}	181.1 ± 32.0^{ac}	190.1 ± 35.9^{bc}	194.8 ± 44.2^{b}
Apo A/B Ratio	1.9 ± 0.5^{a}	1.6 ± 0.3^{c}	1.4 ± 0.3^{b}	1.5 ± 0.4^{bc}

Values with different superscripts are significantly different ($p < 0.05$)

TABLE 4. - SERUM LIPOPROTEIN LEVELS OF CREWMEMBERS FROM 1990-1998

Serum Lipoproteins	1990-1992 (n = 36) Means ± SD	1993-1995 (n = 36) Means ± SD	1996-1998 (n = 36) Means ± SD
HDL (mg/dL)	51.5 ± 12.6	49.4 ± 12.7	50.8 ± 12.9
LDL (mg/dL)	108.6 ± 32.4	115.0 ± 29.4	114.4 ± 31.4
Chol. (mg/dL)	177.8 ± 34.2	179.9 ± 32.4	182.0 ± 34.2
Apo A/B Ratio	1.8 ± 0.6	1.7 ± 0.6	1.7 ± 0.6

Values with different superscripts are significantly different ($p < 0.05$)

TABLE 5. - SERUM LIPOPROTEIN LEVELS OF CREWMEMBERS FROM 1993-1998

Serum Lipoproteins	1993-1995 (n = 32) Means ± SD	1996-1998 (n = 32) Means ± SD
HDL (mg/dL)	45.3 ± 10.5	47.3 ± 10.8
LDL (mg/dL)	117.8 ± 29.9	120.1 ± 28.7
Chol. (mg/dL)	179.0 ± 32.2	183.4 ± 30.7
Apo A/B Ratio	1.5 ± 0.5	1.5 ± 0.5

Values with different superscripts are significantly different ($p < 0.05$)

Effect of Space Flight on Lipoproteins (second data set)

HDL levels preflight 2 years, < 10 days launch, and R+0 were all significantly different (Table 6). LDL levels significantly increased post flight < 10 days compared to preflight two years. However, LDL levels had also significantly increased since two years pre launch. Total serum cholesterol levels also differed significantly only between preflight two years and preflight < 10 days. For apo A:B, preflight two years, preflight < 10 days, and R+0 all differed significantly from one another.

TABLE 6. - SERUM LIPOPROTEIN LEVELS IN CREWMEMBERS TWO YEARS BEFORE FLIGHT, BEFORE LAUNCH, AND AT LANDING

Serum Lipoproteins	**Preflight 2 yrs (n = 176) Means ± SD**	**Preflight < 10d (n = 176) Means ± SD**	**R+0 (n = 176) Means ± SD**
HDL (mg/dL)	49.9 ± 12.6^{a}	49.6 ± 11.5^{a}	44.5 ± 11.0^{b}
LDL (mg/dL)	121.2 ± 33.7^{a}	126.4 ± 35.6^{b}	130.2 ± 41.9^{b}
Cholesterol (mg/dL)	187.7 ± 36.8^{a}	194.3 ± 38.2^{b}	$191.8 \pm 44.5^{a,b}$
Apo A:B	1.8 ± 0.6^{a}	1.7 ± 0.5^{b}	1.5 ± 0.4^{c}

Values with different superscripts are significantly different ($p < 0.05$)

It is apparent that all lipids were adversely skewed after space flight. HDL and apo A:B levels decreased, and LDL and total serum cholesterol levels increased. This was in concurrence with data compiled by Leach.[8] However, these adverse changes are not considered clinically significant according to the American Heart Association.[8] Possible explanations for changes in lipoprotein levels include, modified diet, different lengths of fasting time before blood was drawn, stress during flight, decreased physical activity relative to preflight activity, and effects of weightlessness.

Effect of Diet on Lipids (third data set)

Studies[3] have proven that dietary intake decreases when in orbit. Our data, using a paired t-test, similarly showed a significantly decreased intake of fat and percent calories as fat during flight compared to preflight intake (Figure 1-2).

Figure 1. - Preflight vs. Inflight Fat Intake

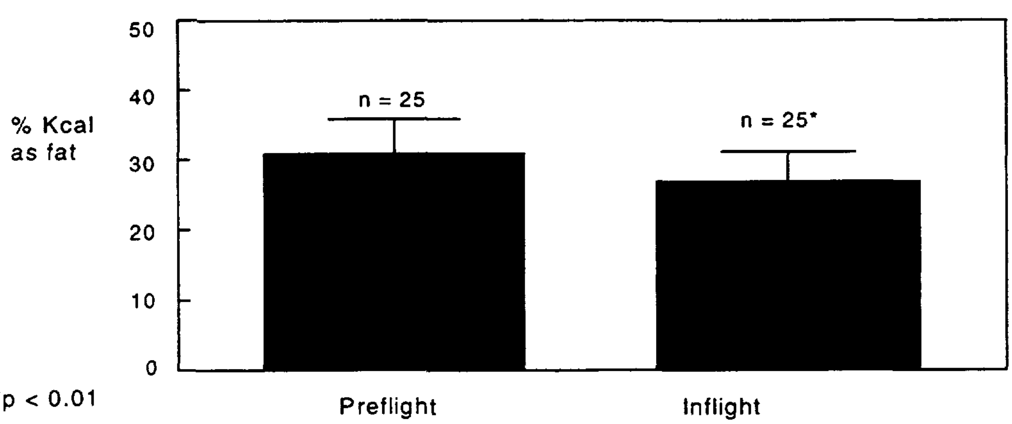

Figure 2. - Preflight vs. Inflight; Percent Kilocalories as Fat

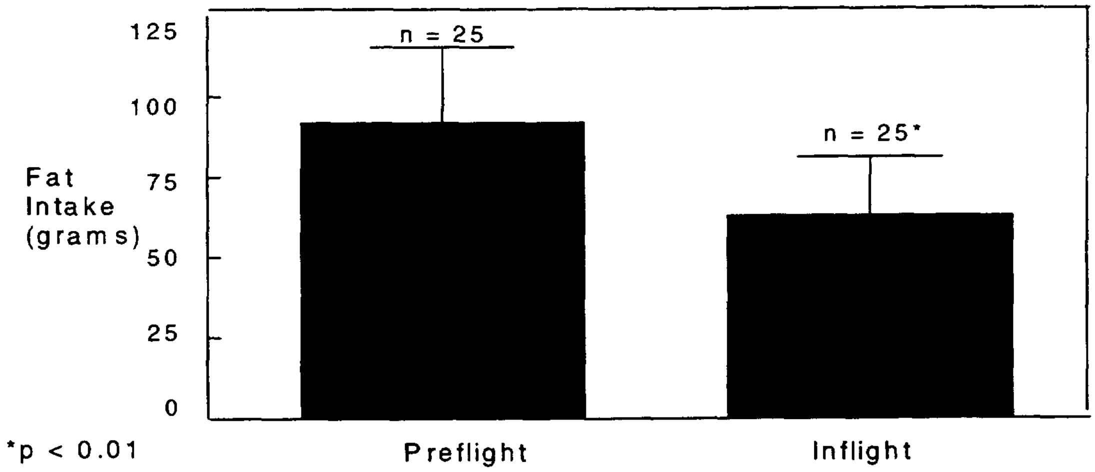

According to the American Heart Association, a low fat diet improves serum lipoprotein levels, decreasing risk of heart disease.[10] Therefore, the astronaut's lipoprotein levels should be improving as well, when in fact, they are doing the opposite. This solidifies Leach's argument that inflight diet is not the catalyst for skewed lipid profiles. Studies[4,13-14] have shown that compliance to a low fat diet, not only decreases total and LDL cholesterol, but also decreases HDL levels, thus, increasing risk for heart disease. Since astronauts typically increase their carbohydrate intake and decrease their fat intake during flight, this may be the cause for undesirable lipid profiles after space flight. The decrease in dietary intake during flight compared to preflight intake may be due to several factors, including preoccupation with work or space motion sickness within the first few days of flight. A multiple linear regression model and scatter plot (Figure 3) was used to examine if there was relationship between diet and lipoproteins, both before and during flight. There was a significant relationship between LDL and preflight fat intake, only. All other lipids compared to preflight and inflight diet intake were not significantly different.

Figure 3. - Effect of Preflight Fat Intake on Low Density Lipoproteins

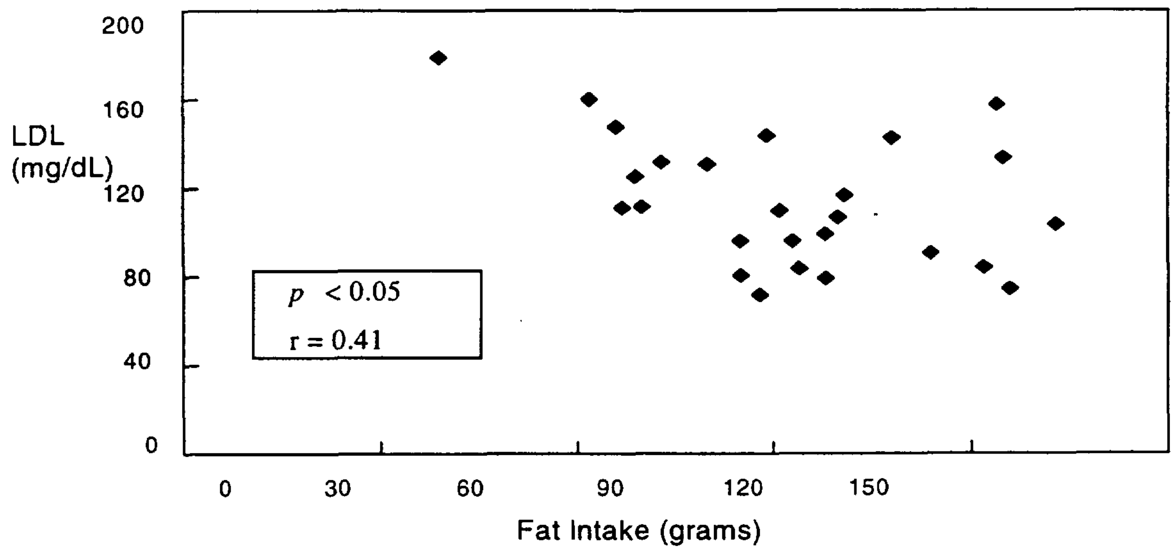

Effect of Gender on Lipids (fourth data set)

The effect of gender on lipids was only preliminary data. Time allowed for statistical analysis using two way repeated measure analysis of variance for the data set of AME from 1981-1998, only. There was only a significant difference between men and women for HDL and total cholesterol when broken down by years. HDL values differed between the two genders in 1993-1995 and 1996-1998 , only. Cholesterol values differed significantly in 1996-1998, only. There were no significant differences in LDL between the two genders even when divided by years.

Effect of Age on Lipids (fifth data set)

Due to time restraints, statistical analysis was not run on this data set. We were simply looking to see if there was a trend of age on lipid levels. According to the literature,[1] as age increases, lipid profiles become less desirable. LDL increases in both men and women as they age and HDL continues to increase in women only. Our data showed a visual increase in LDL and cholesterol levels. It appeared that HDL levels remained relatively unchanged and apo A:B ratio decreased. It would be interesting to see what this data set would look like once broken down by gender, as well as age.

LIMITATIONS AND FUTURE RECOMMENDATIONS

Diet intake was only recorded before and during flight and only calories, percent calories as fat, and total fat intake was available. Studies[11,12] show that saturated fat and specific fatty acids are important to examine in regards to risk for heart disease. Records of a controlled diet post flight would allow researchers to accurately compare lipid levels as a result of diet during space flight.

Although it appears that lipid levels are not a primary concern with short-term space travel, it is questioned what effects long-term missions may have. If there is a larger drop in HDL levels or a larger increase in LDL values with longer missions, it is then questioned what the period of time would be in order for lipid levels to return to preflight values. Research needs to continue in this area, especially as the duration of missions increase.

REFERENCES

1. Posner BM, Cobb JL, Belanger MA, et al. Dietary lipid predictors of coronary heart disease in men. The Framingham Study. *Arch Intern Med.* 1991;151:1181-1188.

2. Daily dietary fat and total food-energy intakes – Third National Health and Nutrition Examination Survey, Phase 1, 1988-1991. *Morbidity and Mortality Weekly Report.* 1994;43:116-125.

3. Lane HW. Energy requirements for space flight. *J Nutr.* 122:13-18, 1992.

4. Sonnenberg LM, Quatromoni PA, Gagnon DR, et al. Diet and plasma lipids in women. II. Macronutrients and plasma triglycerides, high-density lipoprotein, and the ratio of total to high-density lipoprotein cholesterol in women: The Framingham Nutrition Studies. *J Clin Epid.* 1996;49:665-672.

5. Bass KM, Newschaffer CJ, Klag MJ, Bush TL. Plasma lipoprotein levels as predictors of cardiovascular death in women. *Arch Intern Med.* 1993;153:2209-2216.

6. Expert panel on detection, evaluation, and treatment of high-blood cholesterol in adults. Summary of the second report of the National Cholesterol Education Program (NCEP) expert panel on detection, evaluation, and treatment of high blood cholesterol in adults (Adult Treatment Panel II). *JAMA.* 1993;269:3015-3023.

7. Leach CS, Lane HW, Krauhs JM. Short-term space flight on nitrogenous compounds, lipoproteins, and serum proteins. *J Clin Pharmacol.* 1994;34:500-509.

8. Leach CS, Johnson PC, Krauhs JM, et al. Cholesterol in serum lipoprotein fractions after spaceflight. *Aviat Space Environ Med.* 1988;59:1034-1037.

9. Denke MA. Individual responsiveness to a cholesterol lowering diet in postmenopausal women with moderate hypercholesterolemia. *Arch Intern Med.* 1994; 154:1977-1982.

10. Krauss RM, Deckelbaum RJ, Ernst N, et al. Dietary guidelines for healthy adults: A statement for health professionals from the Nutrition Committee, American Heart Association. *Circulation.* 1996;94:1795-1800.

11. Howard BV, Hannah JS, Heiser CC, et al. Polyunsaturated fatty acids result in greater cholesterol lowering and less triacylglycerol elevation than do monounsaturated fatty acids in a dose-response comparison in a multiracial study group. *Am J Clin Nutr.* 1995;62:392-402.

12. Ginsberg HN, Kris-Etherton P, Dennis B, et al. Effects of reducing dietary saturated fatty acids on plasma lipids and lipoproteins in healthy subjects; The delta study, protocol I. *Arterioscler Thromb Vasc Biol.* 1988;18:441-449.

13. Jeppesen J, Schaaf P, Jones C, Zhou MY, Chen YDI, Reaven GM. Effects of low-fat, high-carbohydrate diets on risk factors for ischemic heart disease in postmenopausal women. *Am J Clin Nutr.* 1997;65:1027-1033.

14. Denke MA. Effects of continuous combined hormone-replacement therapy on lipid levels in hypercholesterolemic postmenopausal women. *Am J Med.* 1995;999:29-35.

SPECTROSCOPIC PROPERTIES OF METAMORPHOSED MAFIC ROCKS: REMOTE SENSING APPLICATIONS ON MARS

Final Report

NASA / ASEE Summer Faculty Fellowship Program - 1998

Johnson Space Center

IN-46

Prepared by:	Trevor G. Graff
Academic Rank:	Undergraduate Student
University and Department:	Youngstown State University Department of Geology and Environmental Science One University Plaza Youngstown, Ohio 44555

NASA / JSC

Directorate:	Space and Life Sciences
Division:	Earth Science and Solar System Exploration
Branch:	Space Science
JSC Colleague:	Richard V. Morris
Date Submitted:	September 4, 1998
Contract Number:	NAG 9-867

ABSTRACT

Reflectance spectroscopy in the visible and near-infrared wavelengths, between 420 nm to 2588 nm, was utilized on a suite of hydrothermally metamorphosed mafic rocks from the Smartville complex in the northern Sierra Nevada mountains in California. A detailed data base of 102 samples was compiled in order to distinguish differences in mineralogy, petrology and degree of metamorphism for remote sensing applications. Study was limited to metaigneous and metasedimentary rocks in an attempt to spectrally characterize terrestrial rocks analogous to the possible surface of Mars, for a better understanding and possible detection of the geologic features on the remote surface.

Diagnostic absorption bands of iron, water and hydroxyl produced the majority of discernible features in this study. Mössbauer spectroscopy was performed in order to determine specific iron sites. The resulting spectral data base along with thin section mineral identification, metamorphic zone, rock type and location were recorded and available for future application and research.

Continued exploration of Mars in the advancing years, will further advance our understanding of the geology of Mars. Spectroscopic techniques will undoubtedly be integral parts of these future missions. Work on terrestrial analogs to the Martian surface must continue, in order to produce extensive data bases and broaden our knowledge of spectral features.

INTRODUCTION

With the growing interest for Martian exploration and the search for evidence of life, numerous techniques must be examined for their observation potential as remote sensors on Mars. Spectroscopic methods have the ability to be powerful tools in this exploration and further examination of the Martian surface and geology.

Highly diversified, spectroscopic techniques can be utilized from Earth based telescopes, orbiters and planetary rovers. This allows spectral features to be gathered over broad regions characterizing different environments, or on single samples in order to determine specific mineralogy and other distinct features.

Spectral complexity, due to subtle changes in crystal structure or chemistry, is rapidly becoming a powerful means of studying the structure and composition of minerals (Clark, 1995). Variations found in the visible and near-infrared spectra (VNIR) with reflectance spectroscopy are key for remotely determining and mapping the composition of planetary surfaces (Allen et al., 1995). These features in the VNIR range are generally controlled by crystal-field electronic transition within transition series cations (most commonly iron), electronic charge transfers between cations and electronic charge transfers between both cations and anions (Burns, 1970; Clark, 1995). Further into the near-IR, overtone absorption of vibrational fundamentals begin to dominate reflectance spectra, with diagnostic absorption features for water, the hydroxyl ion and various carbonates (Allen et al., 1995; Clark, 1995).

Distinguishing spectral changes recognized in terrestrial samples, analogous to Martian rocks, allows for a better understanding and detection of the geologic features on the remote surface of Mars. In this study, metamorphosed mafic rocks were analyzed in order to distinguish differences in mineralogy, petrology and degree of metamorphism, utilizing reflectance spectroscopy. A detailed data base of 102 optical reflectance measurements in the VNIR (420-2588 nm) was generated. This potential spectroscopic detection of metamorphism and mineralogic changes on Mars would be a considerable asset in remote sensing and understanding the red planet.

SAMPLES

A suite of hydrothermally metamorphosed mafic rocks, from the Smartville complex in the northern Sierra Nevada mountains in California were analyzed using reflectance spectroscopy. The Jurassic metaigneous and metasedimentary rocks are interpreted to represent a rifted volcanic arc (Beiersdorfer, 1992). Previous work on these samples indicates that changes in pressure, temperature, and chemical characteristics can result in large scale changes in mineralogy (Beiersdorfer, 1992). Those mineralogical changes were examined by thin section analysis in order to determine the mineral assemblages. The metamorphic minerals identified in the Smartville Complex include:

albite, amphibole, calcite, epidote, garnet, magnetite, mica, plagioclase feldspar, prehnite, pumpellyite, pyrite and quartz (Beiersdorfer, 1992).

The Smartville region can be divided into two distinct metamorphic zones; a Prehnite-pumpellyite zone marked by the presents of these two minerals and a Greenschist zone which is absence of prehnite and pumpellyite bearing rocks. Areas of intense hydrothermal alteration are also present within the Smartville Complex, indicated by massive sulfide mineralization and epidosites (Beiersdorfer, 1992). Degree of hydrothermal alteration and metamorphic zone changes, if indicated by reflectance spectroscopy, would prove to be a great resource and a possible key to searching for life on Mars.

The samples chosen in this study were from an extensive collection of rocks used to perform thin section analysis. The resulting spectral data base along with thin section mineral identification, metamorphic zone, rock type and location were recorded and available for future application and research.

INSTRUMENTATION AND EXPERIMENTAL PROCEDURES

Utilizing spectral reflectance features over the solar region of the spectrum (420-2588 nm), with a SpectroReflectometer (Model LPSR-300) was the primary technique explored to distinguish differences in terrestrial analogs of Martian metamorphosed mafic rocks. The instrumentation by AZ Technology Corporation utilizes a 115 mm integrating sphere with lead sulfide (1100-2800 nm) and silicon detectors (420-1100 nm). Measuring total hemispherical reflectance in the solar range with a monochromatic light source, spectral data was obtained by 4nm steps. Raw data was then normalized with an optically black paint and Halon, an optically white material (Weidner, 1981). Smoothing was executed by a Fast Fourier Transform program, by Microcal Origin software, in which band position was assigned and further graphical enhancement was performed.

Mössbauer spectroscopy was performed on two chosen samples in order to determine the specific iron sites. Sample preparation included an approximate 160mg of powered sample passed through a 150 micron sieve, this power was then set in an epoxy mold. A ^{57}Co source was then activated for transmission Mössbauer spectra.

Research was performed in the Spectroscopy and Magnetics Laboratory in building 31, Johnson Space Center, National Aeronautics and Space Administration.

SPECTRAL FEATURES

Diagnostic absorption bands of iron, water and hydroxyl produced the majority of discernible features in this study. Understanding their absorption process allows further

study on the net effect of the reflectance features obtained.

Ferrous ion, Fe^{2+} - Only one spin allowed transition gives rise to features in the VNIR spectra of minerals for a ferrous ion in a perfectly octahedral site. Distortion of the octahedral site allows for the levels to be split further, so additional transitions may occur (Hunt, 1977). The spectral features for ferrous iron occur at different wavelengths for differing minerals. The nature of the site conveys important information, useful in many remote sensing applications, concerning the bulk structure of the mineral (Hunt, 1977).

Ferric ion, Fe^{3+} - Ferric iron has a symmetric ground state that is not split in any crystal field. Most sites arise in visible wavelengths, the most firmly assigned at 440 nm (Hunt, 1977). Absorption bands can also be caused between iron in the different valence states; a charge transfer absorption feature is recognized at ~700 nm.

Water, H_2O - Spectral features in minerals due to the presence of water occur in the near-IR due to overtones and combinations. Water can be physically absorbed on the surface of mineral grains, occupy specific lattice sites, or be a part of the crystal structure. The bands produced may be sharp, indicating well ordered sites, or broad, due to multiple or poorly ordered sites (Clark et al., 1990). The presence of a 1900 nm band indicates molecular water, occurring with a 1400 nm hydroxyl band. The absence of the 1900 nm band, but the presence of the 1400 nm, band indicates that only the hydroxyl is present (Hunt, 1977; Clark et al., 1990).

Hydroxyl, OH - There is only one vibration of OH^- and it is active in the IR at ~2750 nm (Hunt, 1977; Clark, 1995). The first overtone position of the OH stretch is responsible for the common band at 1400 nm (Hunt, 1977). Hydroxyls linked to metals produce a metal-OH bend whose position is typically in the 2200-2400 nm region (Clark et al., 1990).

RESULTS AND DISCUSSION

Reflectance Spectroscopy

Features observed in this study will be characterized according to representative samples shown in the following figures (Figures 1 and 2). Detailed identification of the selected samples, including; rock type, geologic unit, metamorphic zone and mineral assemblage, are recorded in table 1.

TR89-48 - The ferrous iron present in the recorded spectra occurs most commonly as broad bands centered between 1000 and 1100 nm. This sample displays an ~1100 nm Fe^{2+} band, with the distinctive reflective maximum at ~530 nm producing the green color of the sample. The large Fe^{2+} band is believed to be from chlorite, and possibly the presence of prehnite and pumpellyite. The FeOH stretch, at ~2368 nm, in this sample displays a shift to a higher wavelength from the most common placement observed in this study. This is believe to be due to a high Fe^{2-} concentration resulting in a difference in the hydrogen bond strength.

TR89-20 - This epidosite (hydrothermal epidote deposit) sample has two Fe^{3+} bands occurring in the visible region. A charge transfer band at ~700 nm, and Fe^{2-} feature at ~900 nm also occur. Molecular water at ~1920 nm and its accompanying OH stretch at ~1408 nm indicate water in the crystal lattice. The strong FeOH metal OH-bend at ~2344 nm and shoulder at ~2280 nm are intriguing features and will be discussed further. The band at ~1560 nm is believed to be associated with the FeOH stretch, as a combination/overtone of the FeOH group.

TR80-11b - Strong reflectance also characterizes this epidosite, and a similar spectra results. However, this sample displays the distinct Fe^{3+} sites described by Clark et al. The Fe^{3-} feature at ~1060 nm is at a longer wavelenght then in most ferric material.

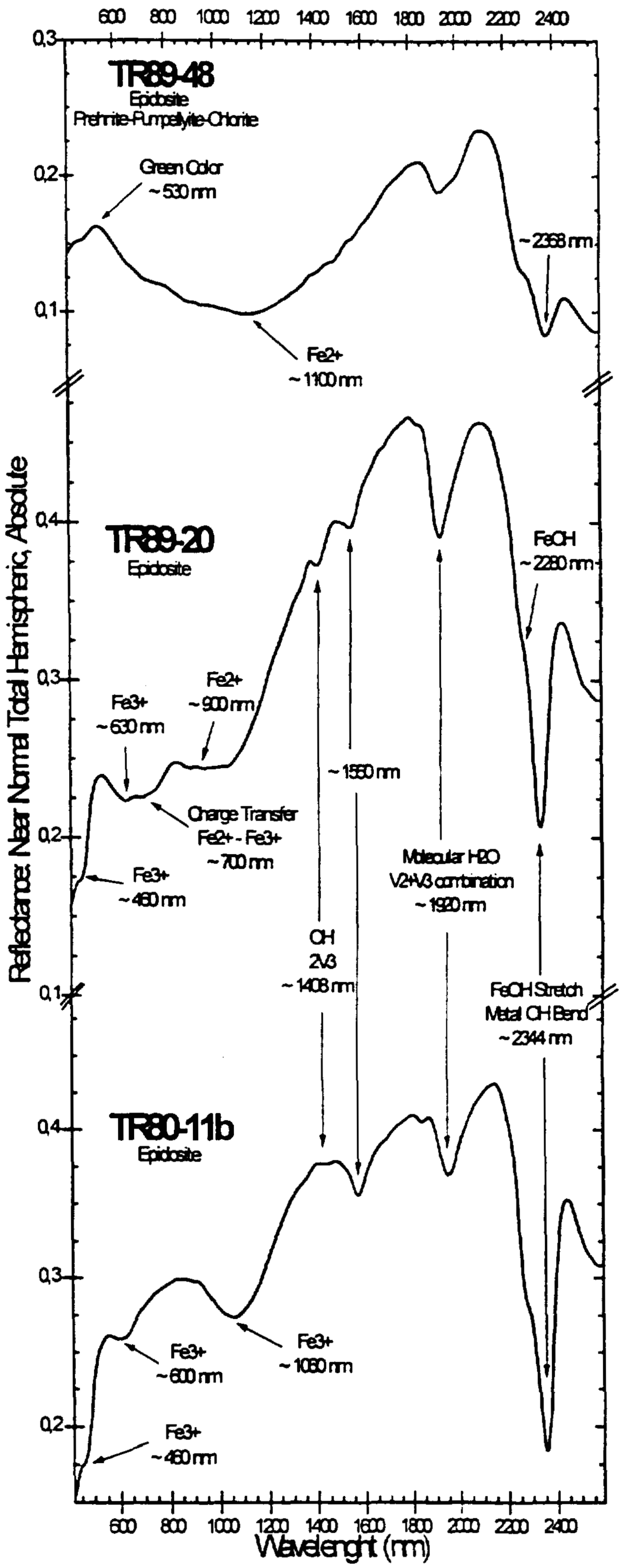

Figure 1.- Reflectance spectra of three representative samples. Table 1 displays detailed sample identification.

TR90-19 - This Bassite, like the Epidosite in TR89-48, has the characteristic broad Fe^{2+} band, the spectra band in this case it is centered at ~1030 nm. Broadening the water band in this sample is a feature located at ~2000 nm, which we can not currently assign.

TR91-6 - This volcaniclastic specimen has numerous spectral differences. The band at ~1484 nm was the only spectral feature observed in this location. It is believed to be a result of the unique mineral assemblage containing prehnite. and absence of amphibole, chlorite and epidote (Table 1). The spectrum of this sample also contains a broad Fe^{2+} band, centered near 1080 nm, the unassigned 2000 nm band and a shifted FeOH stretch.

TR90-26 - This highly reflective Bassite spectra again displays the Fe^{3+} features due to epidote. A pure epidote sample from southern Idaho was scanned by the SpectroReflectometer in order to correlate band position and determine the occurrence of the ~1560 nm band. This procedure confirmed the band positions and related the ~1560 nm feature to the FeOH stretch.

The effects on total reflectance and the iron bands. with the presence of chlorite and possibly prehnite and pumpellyite, are displayed in the following figures (Figures 3 and 4).

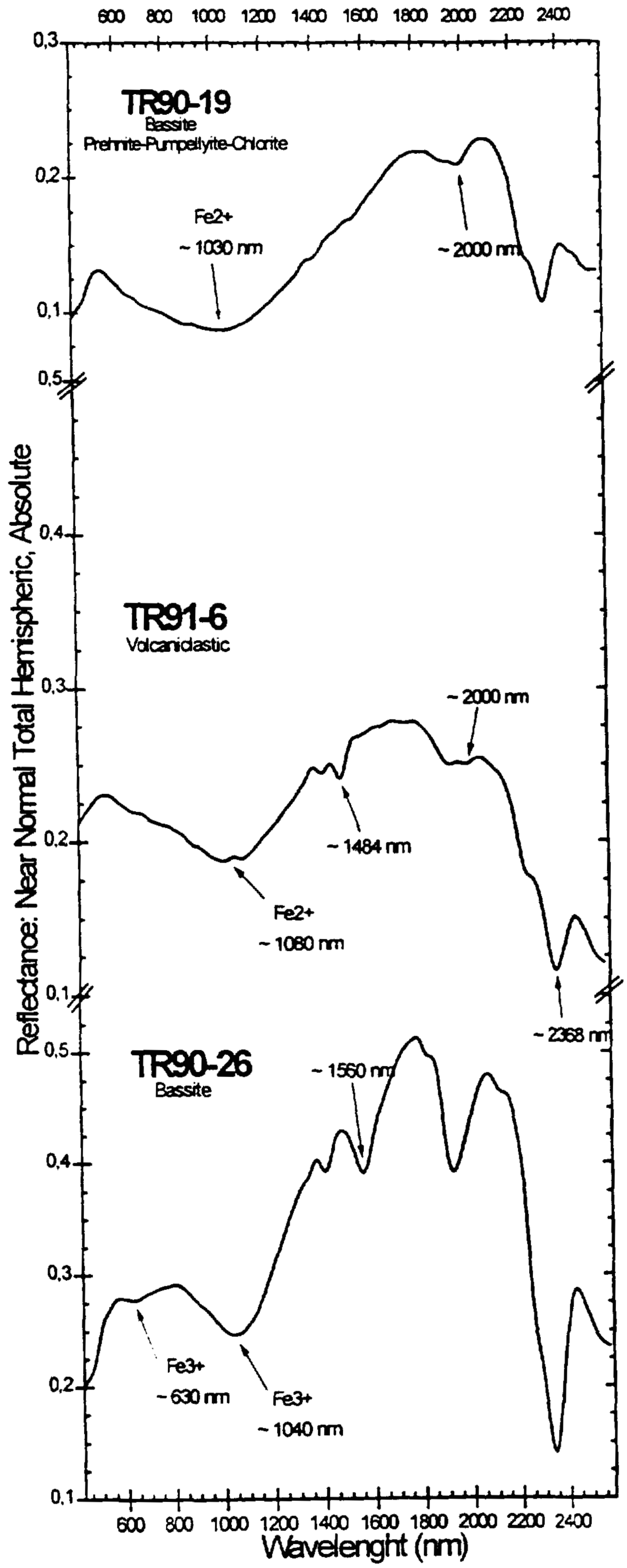

Figure 2.- Reflectance Spectra of selected samples. Scale varies slightly on the vertical axis. Table 1 displays detailed sample identification.

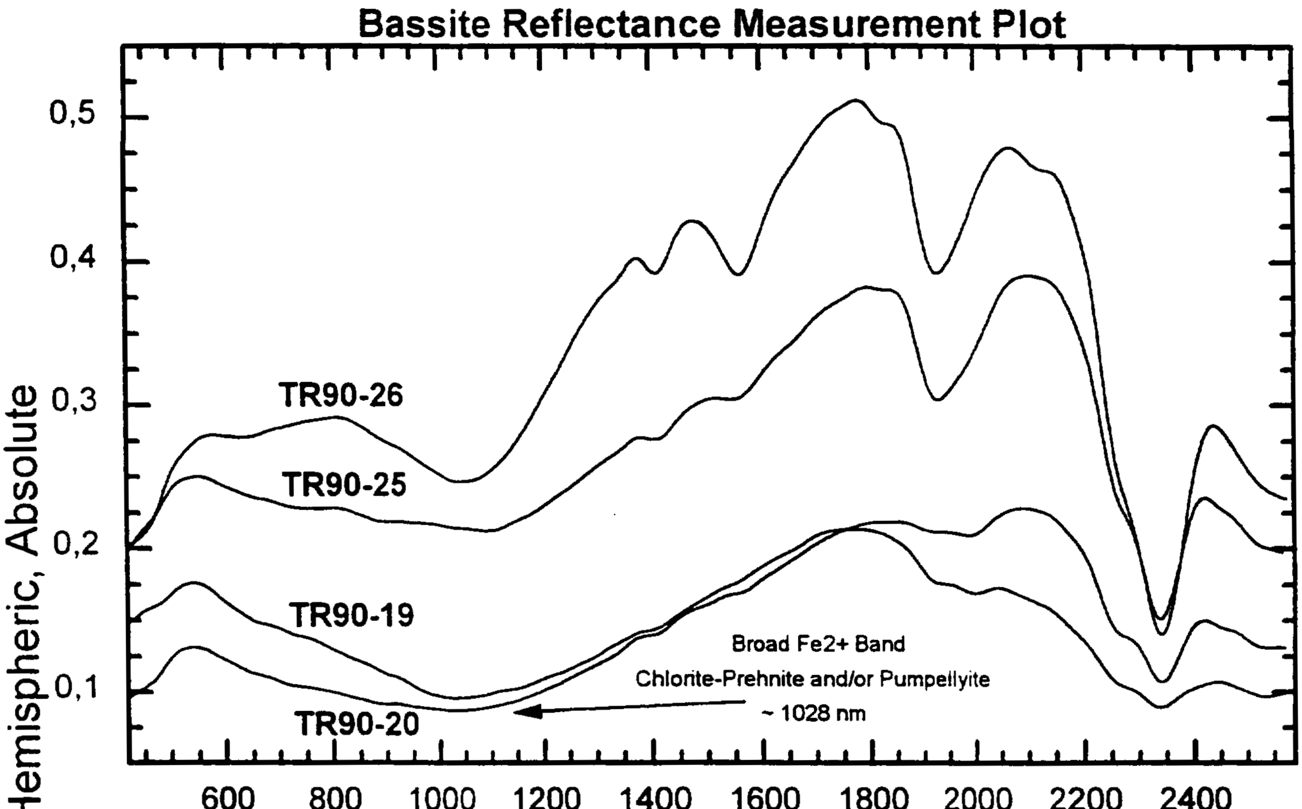

Figure 3.- Bassite reflectance plot of four samples, demonstrating the broad Fe2+ band associated with Chlorite-Prehnite and/or Pumpellyite occurence in the mineral assemblage. Fe2+ band centered at ~1028 nm.

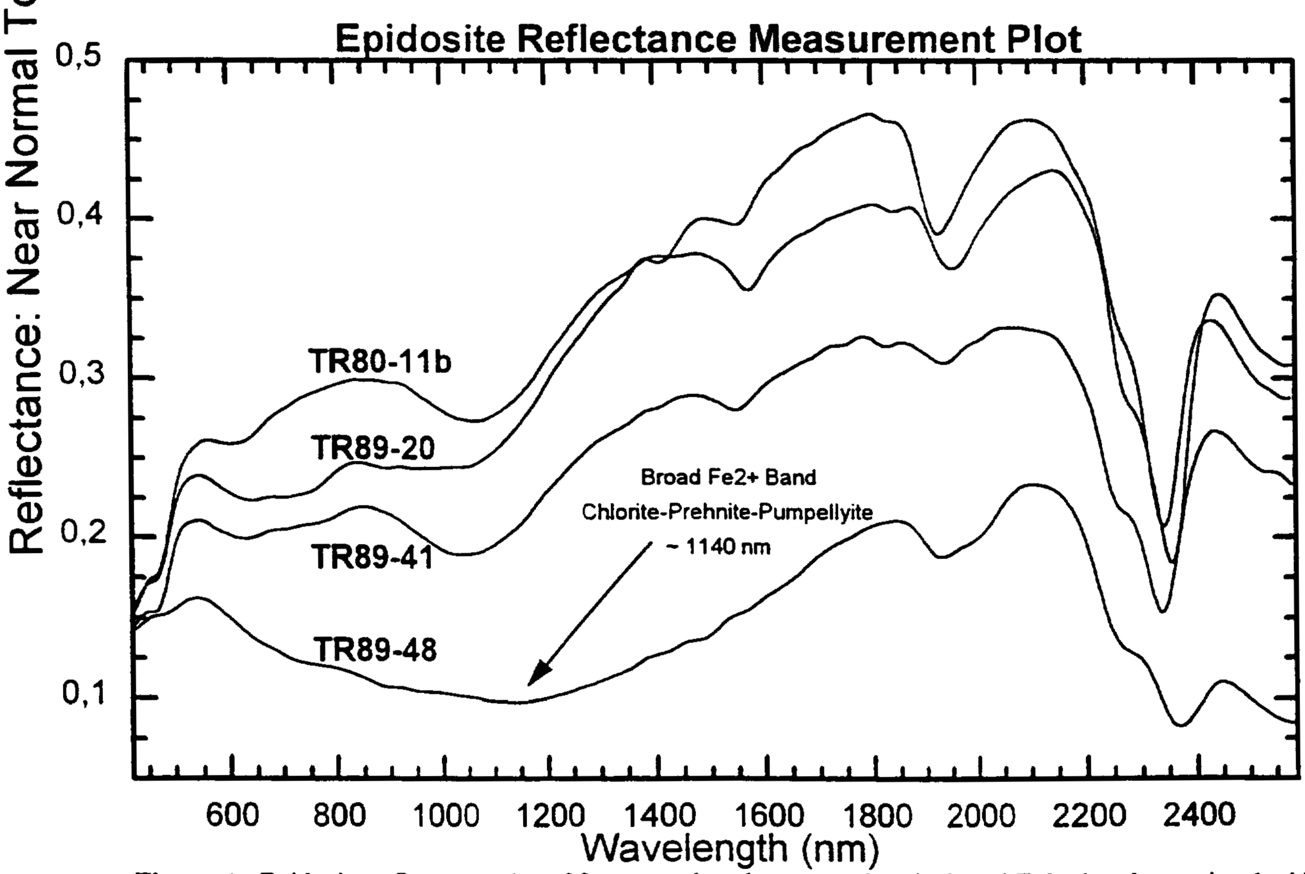

Figure 4.- Epidosite reflectance plot of four samples, demonstrating the broad Fe2+ band associated with Chlorite-Prehnite-Pumpellyite occurence in the mineral assemblage. Fe2+ band centered at ~1140 nm.

SAMPLE#	ROCKTYPE	UNIT	ZONE	AMP	CHL	AB	EP	PMP	PRH	BT	QTZ	TTN	OPQ	CAL	CPX	MS
TR80-11B	Epidosite	UV	PP				XXG				AVX					
TR89-20	Epidosite	UV	GS				XXG				XXG		XXG			
TR89-41	Epidosite	UV	PP	XXG		XXG	AVG				XXG	XXG	XXG	XXG		
TR89-48	Epidosite	UV	PP		AXG	XXG	AXX	AXG	AXG		XXG	XXG	XXG		I	
TR90-19	Bassite	LV	PP		AXG	XXG	AXX	XXG	XVG		AVG	XXG	XXG		I	
TR90-20	Bassite	LV	PP		AXG	XXG	AXG	AXG			AXG	XXG	XXG		I	
TR90-25	Bassite	SD	GS	XXG		XXG	XXG				XXG	XXG	XXG			
TR90-26	Bassite	SD	GS				XXG									
TR91-6	Volcaniclastic	UV	PP						XVG		XVG	XXG	XXG	XVG	I	

Table 1.- Sample identification; UNIT: UV-Upper Volcanic. LV-Lower Volcanic, SD-Sheeted Dike Complex, ZONE: PP-Prehnite-Pumpellyite, GS-Greenschist, MINERALS: AMP-Amphibole. CHL-Chlorite. AB-Albite. EP-Epidote, PMP-Pumpellyite, PRH-Prehnite, BT-Biotite, QTZ-Quartz, TTN-Titanite(Sphene), OPQ-Opaques(Magnetite/Pyrite), CAL-Calcite, CPX-Clinopyroxene, MS-Muscovite, OCCURRENCE: A-Amygdule, G-Groundmass, I-Relict Igneous Phase, X or blank-No Occurrence.

The entire collected data base displays the FeOH stretch as described in the representative samples. This feature, ranging between ~2328 nm to ~2368 nm, is believed to be variable do to the strength of the hydrogen bonding in relation to other iron sites. Its most common center was observed at ~2344 nm and its accompanying shoulder at ~2280 nm. The interesting application of this feature is related to the spatially resolved spectra of Mars in the 2200 nm to 2400 nm region. using an Earth based IR telescope (Clark et al., 1990). Band positions in this region have been observed on Mars and have been attributed to the mineral scapolite, due to HCO_3^- and HSO_4^- ions in its structure (Clark et al., 1990). Further study in the region, without the complications of CO in the Martian atmosphere, need to be performed in order to determine the true origin of these features.

Continued research on the samples in this study may assist in the assigning of the spectral features in this region. The FeOH stretch can be better understood by observing the vibrational behavior of the fundamental hydroxyl in the IR, at ~2750 nm. The position of the fundamental band allow for the calculations of its overtones, the FeOH and the presumed related ~1560 nm band. If the ~1560 nm band is indeed related, it then could be then used as an indicator of the bands in the region in question. Further calculations of overtones also may reveal the ~2000 nm feature.

Mössbauer Spectroscopy

Two representative samples were chosen to confirm the iron location utilizing Mössbauer spectroscopy. Spectrum of TR89-48 (Figure 5) displays a large octahedral Fe^{2+} doublet due to the abundance of chlorite. The minor octahedral Fe^{3+} features displayed in this spectrum results from an unknown ferric-bearing phase.

Mössbauer spectrum of sample TR89-20 (Figure 6) shows high epidote content, displayed by the octahedtal Fe^{3+} doublet with large splitting. The Fe^{2+} octahedral is believed to represent possible chlorite traces in the sample.

The result of the Mössbauer measurements coincide with the findings of the reflectance spectroscopic scans and thin section analysis. Future application of these two spectroscopic techniques together will be extremely useful in complex assemblages.

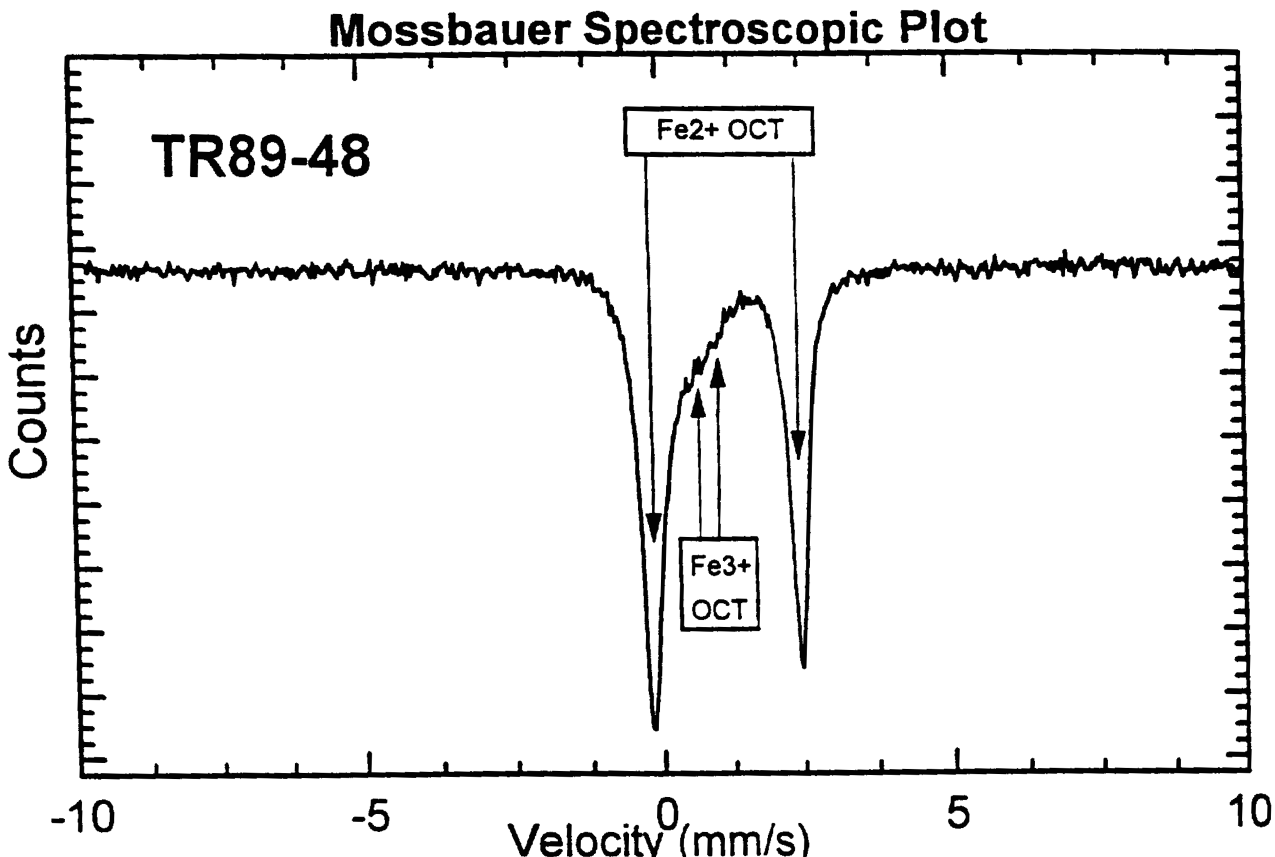

Figure 5.- Mossbauer spectra of TR89-48. Large octahedral Fe2+ doublet due to chlorite. Minor octahedral Fe3+ features are displayed, believed to be from the presence of minor Fe3+ bearning mineral.

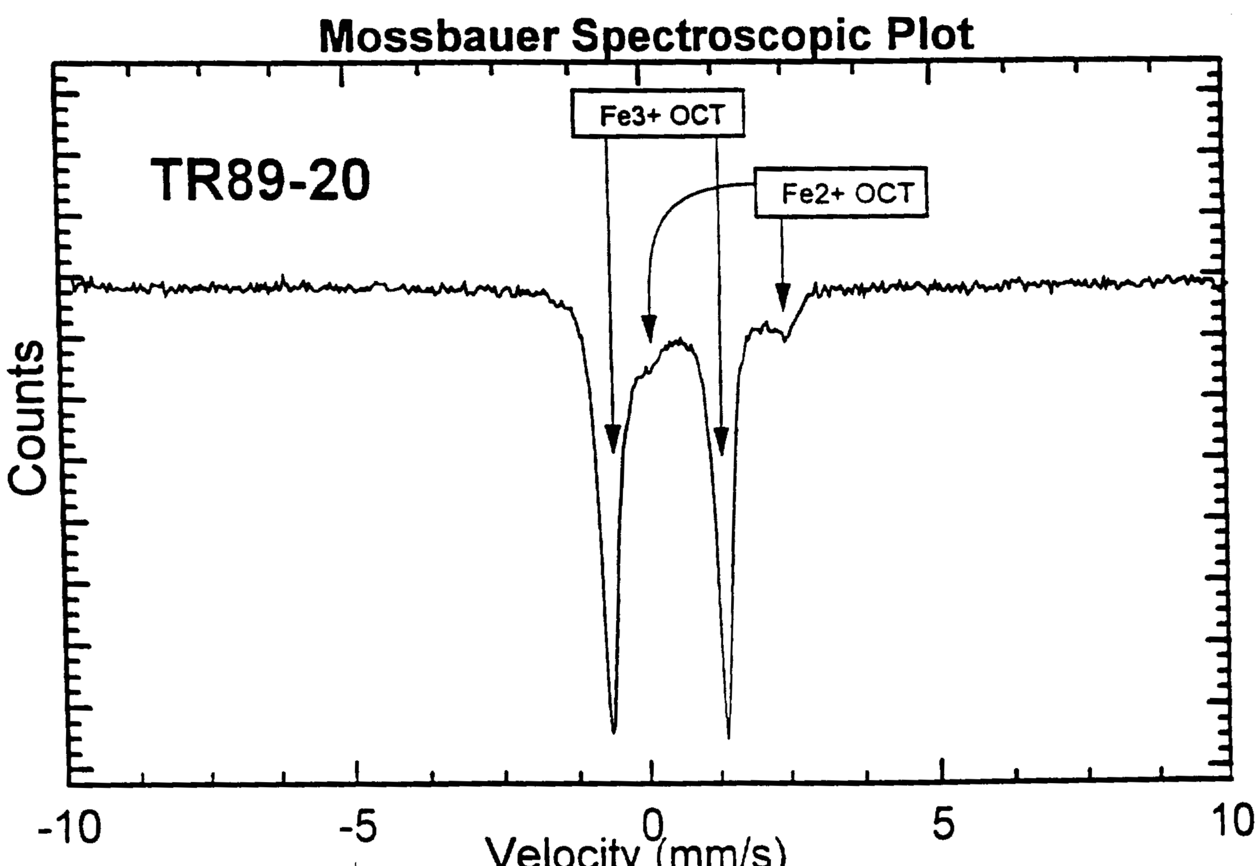

Figure 6 - Mossbauer spectra of TR89-20. High epidote content is displayed by the tetrahedral Fe3+ doublet. Octahedral Fe2+ displayed as a doublet is believed to be a possible result of chlorite traces in the sample.

APPLICATION

The Mars Surveyor 2001 Rover (Rocky 7), together with the 2001 Lander, are scheduled for launch on April 3, 2001. On Jan. 27, 2002, if launched on schedule, they will land on the surface Mars. After landing, the long-range Rover, carrying the Athena instrument payload, will be deployed for a 365-Earth-day mission to investigate the geological record of the ancient terrain of Mars, collecting samples at sites where evidence of life might be preserved (Mars Surveyor 2001). As part of the Athena payload a point reflectance spectrometer, with an operating wavelength of 440-1000 nm (primarily the VNIR), will be incorporated in the rovers sampling arm. A Mössbauer spectrometer is also to be a part of the rovers payload, in order to identify Fe-bearing mineral phases, detect nanophase and amorphous hydrothermal Fe minerals, and determine oxidation state of those Fe minerals.

Continued exploration of Mars, with the planned 2003 orbiter and lander, will further advance our understanding of the geology of Mars. All missions are part of the National Aeronautics and Space Administrations long-term, systematic exploration of Mars in which two missions are launched to the planet approximately every 26 months (Mars Surveyor 2001).

Spectroscopic techniques will undoubtedly be integral parts of these future missions. Work on terrestrial analogs to the Martian surface must continue in order to produce extensive data bases and broaden our knowledge of spectral features.

CONCLUSIONS

The reflectance spectra collected in this study have certain characteristic features that are believed to represent functional data for remote sensing on Mars and other planetary surfaces. Extensive study of spectroscopic methods has shown that they can indicate a wealth of information about mineralogy. However, minimal work has been conducted on mineral assemblages using these techniques. Research is still needed to better understand the subtle changes in absorption features before reflectance spectroscopy reaches its full potential. Spectral databases documenting all the absorption features and trends must then be compiled before these techniques can be widely used.

The data base and results acquired on the suite of metamorphosed mafic rocks observed in this research are preliminary. Further in-depth study in reflectance and Mössbauer spectroscopy, aided by major elemental analysis data and fundamental band positions, may prove beneficial in future applications on Mars and beyond.

REFERENCES

Allen, C., Jakes, P., Jaumann, R., Marshall, J., Moses, S., Ryder, G., Saunders, S., Singer, R., 1995, Field Geology: Processes, Lunar and Planetary Institute, Tech. Rep. 95-05.

Beiersdorfer, R.E., 1992, Metamorphism of the Smartville Complex and Contiguous Rocks, Northern Sierra Nevada and Klamath Mountains, California, Doctorate Dissertation.

Burns, R.G., 1970, Mineralogical Applications of crystal Field Theory, Cambridge Earth Science Series.

Clark, R.N., 1995, Reflectance Spectra, Rock Physics and Phase Relations: A Handbook of Physical Constants, American Geophysical Union, p. 178-188.

Clark, R.N., King, T.V., Klejwa M., Swayze, G.A., 1990, High Spectral Resolution Reflectance Spectroscopy of Mineral, Journal of Geophysical Research, vol. 95, no. B8, pp. 12,653-12,680.

Clark R.N., Swayze G.A., Singer, R.B. and Pollack J.B., 1990, High-Resolution Reflectance Spectra of Mars in the 2.3-µm Region: Evidence for the Mineral Scapolite, J. Geophysical Research, vol. 95, no. B9, pp. 14463-14480.

Hawthorne, F.C. ed., 1988, Spectroscopic Methods in Mineralogy and Geology, Reviews in Mineralogy, vol. 18.

Hunt, G.R., 1977, Spectral Signatures of particulate Mineral in the Visible and Near Infrared, Geophysics, vol. 42, no. 3, pp. 501-513.

Hunt, G.R. and Salisbury, 1970, Visible and Near-Infrared Spectra of Minerals and Rocks: I Silicates Minerals, Modern Geology, vol.1, pp. 283-300.

Mars Surveyor 2001, Internet, September 2, 1998, Available: http://www.jpl.nasa.gov/

Weidner V.R. and Hsia J.J.. 1981, Optical Society of America, vol 71, pp.856-861.

39

IN-16

Crystal Chemistry of Melanite Garnet

Final Report

NASA/ASEE Summer Faculty Fellowship Program - 1998

Johnson Space Center

Prepared by:	Dawn Marie Nguyen
Academic Rank:	Undergraduate - Senior
University & Department:	Youngstown State University Department of Geoscience Youngstown, Ohio 44555

NASA/JSC

Directorate:	Space and Life Sciences
Division:	Earth Science and Solar System Exploration
Branch:	Planetary Science
JSC Colleague:	Douglas W. Ming
Date Submitted:	
Contract Number:	NAG 9 - 867

ABSTRACT

This original project resulted in a detailed crystal chemical data map of a titanium rich garnet (melanite) suite that originates from the Crowsnest Volcanics of Alberta Canada. Garnet is typically present during the partial melting of the earth's mantle to produce basalt. Prior studies conducted at Youngstown State University have yielded questions as to the crystal structure of the melanite.

In the Studies conducted at Youngstown State University, through the use of single crystal x-ray diffraction, the c-axis appears to be distorted creating a tetragonal crystal instead of the typical cubic crystal of garnets. The micro probe was used on the same suite of titanium rich garnets as used in the single crystal x-ray diffraction.

The combination of the single crystal x-ray research and the detailed microprobe research will allow us to determine the exact crystal chemical structure of the melanite garnet. The crystal chemical data was gathered through the utilization of the SX100 Electron Probe Micro Analyzer. Determination of the exact chemical nature may prove useful in modeling the ultramafic source rock responsible for the formation of the titanium rich lunar basalts.

INTRODUCTION

Titanium rich garnets are known to have a very complex crystal chemical structure (Schwartz *et al.* 1980). Through microprobe analysis chemical data maps have been produced, defining the chemical composition melanite garnet. Qualitative analysis has allowed for assumptions to be made as to the exact position of the elements within the tetragonal, octagonal and dodecahedral sites (Deer *et al.* 1966). More experimental analysis is required to determine to with further certainty the position and ratio of Fe^{3+} to Fe^{2+}.

A detailed crystal chemical history of the garnet samples, inclusions, twinning and zoning were gathered. Inclusions in the garnet samples cause fluctuations in the amounts of silica and aluminum found along the line of analysis. Zoning and twinning occur in most samples analyzed. Zoning is apparent in the chemical bands of titanium and aluminum.

EXPERIMENTAL TECHNIQUES

Electron microprobe analysis

Garnet crystals where manually separated from source rock using the binocular microscope to choose pure samples. Highly polished samples where glued to glass slides and then carbon coated. The five garnet melanites where scanned using the Cameca SX100 Electron Probe Micro Analyzer at 15 kV and a 20nA beam current. Ten elements where scanned for. Sample sm3b was scanned on a line of 20 points. Samples sm3c and sm3d were scanned along a line of 40 points. Samples sm3e and sm3f were scanned on a line of 30 points. National Institute of Standards and Technology mineral standards were used for calibration.

Loss on Ignition

To determine if the samples were hydrogarnets, thus influencing the weight percents, loss on ignition was conducted. 0.7802 g of garnet sample was dried overnight at 80 degrees Celsius. The garnet sample was also then heated to 800 degrees Celsius for two hours. A desiccater was used during cooling times to prevent the addition of water back into the samples.

Description of samples

Five melanite garnet samples where analyzed in this experiment. The samples originated from unconsolidated sandstone in the Crowsnest Volcanics of Alberta Canada. The samples consisted of subhedral crystals (2-3mm). Physical mineralogy included dark color, glassy luster, no cleavage, and occasional twinning. Within the samples were high inclusions of Al and Si and low inclusions of Ti. All samples were clearly zoned except for sample sm3b. Samples sm3c and sm3d also show twinning.

RESULTS AND DISCUSSIONS

Electron microprobe experiments

Qualitative data is presented in Table 1. Points scanning non-sample material were discarded in calculations. Points less than 95 total weight percent were not considered valuable data. Ten significant elements were measured by the microprobe. Iron was measured as FeO and converted entirely to Fe_2O_3. There was no distinction made between Fe^{3+} and Fe^{2+} by the microprobe. Mössbauer would have been a possible choice for determining the ferrous versus ferric ration; however, Mössbauer does not present valuable results when working with zoned garnets (Huggins *et al.* 1980).

Table 1. - Electron micro probe chemical analysis

Specimen	sm3b	sm3c	sm3d	sm3e	sm3f
			Analyses, wt %		
SiO2	35.11	35.41	33.13	33.53	34.44
TiO2	2.62	3.00	3.34	5.16	3.57
Al2O3	6.46	6.43	5.97	3.70	5.84
Cr2O3	0.01	0.01	0.01	0.01	0.01
Fe2O3	21.91	20.90	21.18	22.86	21.23
MnO	0.89	0.83	0.77	0.63	0.81
MgO	0.25	0.44	0.24	0.27	0.26
CaO	31.19	31.08	31.36	32.04	32.20
Na2O	0.07	0.11	0.10	0.18	0.09
K2O	0.01	----	0.01	0.01	----
Total	98.50	98.23	96.10	98.40	98.45
		Number of metal ions on basis of 12 oxygen			
Si	2.907	2.927	2.830	2.821	2.865
Ti	0.163	0.187	0.214	0.328	0.223
Al	0.631	0.628	0.600	0.365	0.571
Cr	----	----	----	----	----
Fe3+	1.365	1.302	1.362	1.448	1.331
Mn	0.062	0.058	0.055	0.045	0.057
Mg	0.031	0.053	0.031	0.034	0.032
Ca	2.767	2.757	2.871	2.889	2.872
Na	0.011	0.018	0.016	0.029	0.015
K	----	----	----	----	----

To calculate the cation assignment, the oxide weight percentage data was first reduced on a formula bases assuming eight cations per formula unit (X_3, Y_2, Z_3: O_{12}). Cation to anion ratios were adjusted to 8:12, through regular garnet stoichiometry, to arrive at the garnet formulae in Table 2. By reduction of ferric iron to ferrous iron the formulae were balanced close to 3:2:3. Four of the five samples fit the garnet formula adequately with only sm3c 0.064 away from 3.00 required of the site. This can be explained by the oxidation loss of a Fe^{3+} as ferrous changes to ferric.

Table 2. - Garnet formulae

Si	2.919	2.937	2.832	2.821	2.866
Ti	0.164	0.187	0.214	0.327	0.223
Al	0.633	0.629	0.601	0.367	0.573
Cr	0.001	0.001	0.001	0.001	0.001
Fe 3+	1.284	1.247	1.352	1.447	1.330
Fe 2+	0.078	0.052	0.010	0.000	0.000
Mg	0.031	0.055	0.031	0.034	0.032
Mn	0.063	0.058	0.055	0.045	0.057
Ca	2.779	2.762	2.872	2.888	2.871
Na	0.011	0.018	0.016	0.029	0.015
K	0.001	0.000	0.001	0.001	0.000

*All iron as Fe2O3

Loss on ignition

Water being present in the garnet (Huggins *et al.*, 1977) was explored as another possible explanation of low totals in both wt% and cation assignment. After the garnet was heated to 800 degrees Celsius, a loss of 0.0029 g was measured. This is not a significant amount of loss to be a hydrogarnet. The volatiles given off were less than 1 percent. This also rules out error of low totals due to the presence of unmeasured volatiles.

Zoning, twinning, and inclusions

All crystals except sm3b have zoning evident by "growth rings" visible in images collected with the microprobe. Inclusion composition has also been determined from these chemical data maps. Chemical zoning was also determined from these chemical data maps.

(1) Crystal sm3c has an interesting growth history (Figure 1). It has high amounts of Si and Al inclusions. Ti and Al are the primary elements zoning this crystal. The growth pattern indicates a twinning that must have began early in its history, due to the distortion of the geometry starting at its core.

(2) Crystal sm3d has high amounts of Si and Al inclusions and low amounts of Ca and Fe inclusions. Ti zones this crystal primarily. In the crystals core it is zoned by low amounts of Ti, Fe, and Al. This crystal has undergone several stages in which twinning has occurred (Figure 1). This is obvious in distortion in the core and at the outer edge of the crystal.

(3) Crystal sm3e has high amounts of Si, Ca, Ti, and Al inclusions. Primarily Ti and Al zone this crystal, with the core being zoned by Fe.

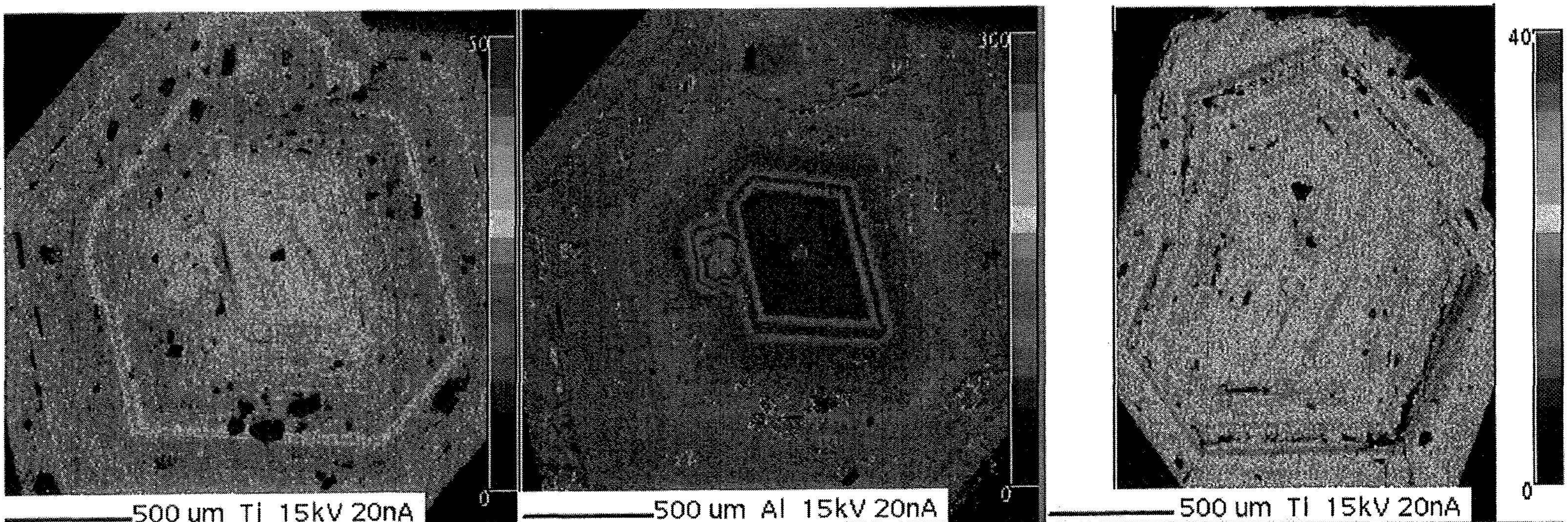

Figure 1. - left to right: sm3d showing high zoning and twinning; sm3d showing distorted-zoned core; sm3c showing high zoning and twinning.

(4) Crystal sm3f has high amounts of Si, Ca, and Al inclusions. Ti and Al zone this crystal. This crystal appears to have cracked early in its growth history at the core allowing a mirror image of it to form opposite the crack.

Summary of crystal chemistry

Had the ferrous to ferric ratios been know, all other positions could have been accurately filled according to site preference of the elements. The only exceptions would be the distribution of Al and Ti in the octahedral and tetragonal sites (Huggins *et al.* 1980). All iron was calculated as ferric. Excess ferric was converted to ferrous to fill the dodecahedral site. The remaining cations were distributed under the following assumptions (table 3):

1. Si was placed in the tetragonal site only.
2. Ca was placed in the dodecahedral site only.
3. Fe^{3+} was placed in the octagonal sites with Ti, Al, and Cr. An excess amount of Fe^{3+}, over 2.0, was placed in the tetragonal site.
4. Fe^{3+} excess not accommodated in the octagonal and tetragonal sites was converted to Fe^{2+} and placed in the dodecahedral with the Mg, Mn, Na, and K (Schwartz *et al.* 1980; Huggins *et al.* 1977).

Table 3. - Cation locations

Specimen	sm3b	sm3c	sm3d	sm3e	sm3f
			Tetragonal Cations		
Si	2.919	2.937	2.832	2.821	2.866
Fe 3+	0.081	0.063	0.168	0.142	0.126
sum Z	3.000	3.000	3.000	2.963	2.992
			Octahedral Cations		
Ti 4+	0.164	0.187	0.214	0.327	0.223
Al 3+	0.633	0.629	0.601	0.367	0.573
Fe 3+	1.203	1.183	1.184	1.306	1.204
Cr	0.001	0.001	0.001	0.001	0.001
sum Y	2.000	2.000	2.000	2.000	2.000
			Dodecahedral Cations		
Ca	2.779	2.762	2.872	2.888	2.871
Fe 2+	0.078	0.052	0.010	0.000	0.000
Mg	0.031	0.055	0.031	0.034	0.032
Mn	0.063	0.058	0.055	0.045	0.057
Na	0.011	0.018	0.016	0.029	0.015
K	0.001	0.000	0.001	0.001	0.000
sum X	2.962	2.946	2.985	2.997	2.975

Conclusions

The chemical data maps gathered define the areas of zoning and the inclusions. When zoning was present the elements titanium and aluminum primarily caused it. Inclusions consisted primarily of silica and aluminum. Oxidation of ferrous to ferric caused weight loss. Replacement of silica by titanium caused variations in the total weight percent.

Introduction of titanium into a garnet system causes extreme complication in the structure. More experimental analysis is required to determine to with further certainty the position and ratio of Fe 3+ to Fe2+. With further research the cation distribution can be perfected and an exact distribution know. This data in combination with past single crystal x-ray diffraction work will allow us to learn the exact crystal and chemical structure of titanium rich garnets.

References

Deer, W.A., Howie, R.A., and Zussman, J., 1966. "Garnet Group," *An Introduction to the Rock Forming Minerals*, pp. 21-31.

Huggins, F. E., Virgo, D., and Huckenholtz, G., 1977. "Titanium-containing silicate garnets. II. The crystal chemistry of melanites and schorlomites," *The American Minerologist: Journal of the Mineralogical Society of America,* Vol. 62, No. 7 and 8, pp. 647-665.

Schwartz, K.B., Nolet, D.A., and Burns, R.G., 1980. "Mõssbauer spectroscopy and crystal chemistry of natural Fe-Ti garnets," *The American Mineralogist: Journal of the Mineralogical Society of America,* Vol. 65, No. 1 and 2, pp. 142-153.

REPORT DOCUMENTATION PAGE

Form Approved
OMB No. 0704-0188

1. AGENCY USE ONLY *(Leave Blank)*	
2. REPORT DATE	May 1999
3. REPORT TYPE AND DATES COVERED	NASA Contractor Report
4. TITLE AND SUBTITLE	CR-1999-208923, National Aeronautics and Space Administration (NASA)/American Society for Engineering Education (ASEE) Summer Faculty Fellowship Program - 1998, Volume 1
5. FUNDING NUMBERS	
6. AUTHOR(S)	Richard B. Bannerot* & Donn G. Sickorez, editors
7. PERFORMING ORGANIZATION NAME(S) AND ADDRESS(ES)	Lyndon B. Johnson Space Center Houston, Texas 77058
8. PERFORMING ORGANIZATION REPORT NUMBERS	
9. SPONSORING/MONITORING AGENCY NAME(S) AND ADDRESS(ES)	National Aeronautics and Space Administration Washington, DC 20546-0001
10. SPONSORING/MONITORING AGENCY REPORT NUMBER	CR-1999-208923
11. SUPPLEMENTARY NOTES	*University of Houston, Houston, Texas
12a. DISTRIBUTION/AVAILABILITY STATEMENT	Available from the NASA Center for AeroSpace Information (CASI) 7121 Standard Hanover, MD 21076-1320
12b. DISTRIBUTION CODE	

13. ABSTRACT *(Maximum 200 words)*

The 10-week JSC NASA/ASEE Summer Faculty Fellowship Program was conducted by the University of Houston and JSC, under the auspices of the ASEE. The objectives of the program are to further the professional knowledge of qualified engineering and science members; stimulate an exchange of ideas between participants and NASA; enrich and refresh the research and teaching activities of participants' institutions; and contribute to the research objectives of the NASA Centers.

Each faculty fellow spent at least 10 weeks at JSC engaged in a research project commensurate with his/her interests and background and worked in collaboration with a NASA/JSC colleague. This document is a compilation of the final reports on the fellows' research projects performed during the summer of 1998. Volume 1 contains the first reports, and volume 2 contains the remaining reports.

14. SUBJECT TERMS	15. NUMBER OF PAGES	16. PRICE CODE
information transfer, research, research projects, urban research, engineering science, universities, university program	453	

17. SECURITY CLASSIFICATION OF REPORT	18. SECURITY CLASSIFICATION OF THIS PAGE	19. SECURITY CLASSIFICATION OF ABSTRACT	20. LIMITATION OF ABSTRACT
Unclassified	Unclassified	Unclassified	Unlimited